Neuromodulation of Sex-Specific Pheromone-Mediated Behaviors

A Dissertation

Submitted to the Faculty of

WORCESTER POLYTECHNIC INSTITUTE

in partial fulfillment of the requirements for the degree of

Doctor of Philosophy

in

Biology and Biotechnology

By

Douglas K. Reilly

_____

10 April 2020

APPROVED BY:

_____

Jagan Srinivasan, PhD
Associate Professor
Department of Biology and Biotechnology
Worcester Polytechnic Institute

_____

Joseph B. Duffy, PhD
Associate Professor, Department Head
Department of Biology and Biotechnology
Worcester Polytechnic Institute

_____

Inna V. Nechipurenko, PhD
Assistant Professor
Department of Biology and Biotechnology
Worcester Polytechnic Institute

_____

Dirk R. Albrecht, PhD
Associate Professor
Department of Biomedical Engineering
Worcester Polytechnic Institute

This dissertation is dedicated to my wife Nichole, my daughter Lucy, and my cat Whisper. Without you three, I would have given up on my dreams long ago.

This is for you.

Thank you.

There is no struggle to vast,

no odds too overwhelming,

for even should we fail…

we will know that we have lived.

-Steven Erikson, Toll the Hounds

Abstract

The ability of organisms to sense – and properly respond to – their environment is crucial to their survival. Higher organisms communicate with conspecifics to ensure the survival of the species. Nematodes, such as the roundworm *Caenorhabditis elegans*, are ubiquitous across all biomes, and rely on chemical communication to convey information with one another. The small molecules they utilize in this communication are called ascarosides. These modular pheromones are employed by all taxa, ranging from *Caenorhabditis* to *Ascaris*. The ascaroside, ascr#8, is release by hermaphroditic *C. elegans* to attract potential mates. Previous work has shown that a class of male specific neurons are required for sensation of this pheromone. Here, we show that these neurons initiate a neural circuit modulated by the FMRFamide-like neuropeptide, *flp-3*. This neuropeptide is sensed by a set of G protein-coupled receptors (GPCRs), NPR-10 and FRPR-16. Together, these components determine the behavioral valence of males to ascr#8. Within the male-specific sensory neurons, the CEM, we show that another group of GPCRs sense the ascr#8. Two of these receptors, DMSR-12 and SRW-97, are expressed in the cilia, suggesting their involvement in direct sensation of the cue. As a targeted approach to identifying and confirming receptors for ascr#8, we have developed a bioactive photoaffinity probe. We have also confirmed that the ability of ascr#8 to attract males is conserved across the genus. Together, these studies coalesce to deepen our understanding of sex-specific chemosensation and neuronal processing. These results can be used to better understand the defects that are seen in neurodegenerative diseases – many of which exhibit sex-specific defects in neuronal processing.

Preface

Deciding to start a graduate career while undergoing chemotherapy treatments for Hodgkin's Lymphoma is not something many people would consider a "rational" decision. Graduate school is notorious for being extremely taxing: physically, mentally, and emotionally. Chemotherapy treatments are also known for being taxing: physically, mentally, and emotionally.

So, I figured: *why not?*

I had always dreamed of doing research since childhood. My oncologist was extremely optimistic, and I'm always one to have a light-hearted and optimistic attitude as well. I was already working through my treatments, and only had two to three treatments left in my regiment once the school year started.

I need to thank my advisor, Dr. Jagan Srinivasan, for being willing to take me into his lab as a new graduate student with such a drastically different personal situation from everyone else. At the same time: he was running a new lab, with only one other graduate student, and was still years away from applying for tenure. Taking me was a risk.

But I have to say: it paid off.

Since then, I am glad to say that I've been in remission – and just hit the 5-year-cancer-free mark around the same time I began to put together this dissertation.

Jagan and I have worked rather brilliantly together, and thanks to his mentorship, I'm leaving WPI with a rather impressive publication record. He pushed me to do more, but never too much – exactly what I needed to succeed.

I've taken his post-doctoral research project investigating the nematode mating pheromone, ascaroside #8, to the next stage. Jagan has always been glad to follow the data where it leads, as opposed to where we want to go when we first start out. As such,

the whole tail end of my time at WPI is the result of a side-project gone too far. But it's an exciting story, and awesome things have come of it.

It's niche – I know not everyone cares about nematode mating pheromones – but still exciting. I've developed new tools to help people outside of my field. I've honed my presentation skills, and I've made great contacts.

I hope anyone reading this dissertation finds that one line of information that they need for that reference they've been searching for.

Acknowledgments

I always thought it odd that every acknowledgments section I've read starts off with, "It's impossible to thank everyone," but now that I'm trying to do the same, I understand. It truly is impossible. But here we go:

First off, I have to thank my advisor, Dr. Jagan Srinivasan. You've been a great mentor, pushing me not only to do well, but to strive to do well. You help me do *good science* and let me follow random tangents as they worked. You also kept me on track and are sending me off into the real world with a solid publication record. You also let me follow my desires to teach, and I have to thank you extra for that. You understood that not everyone wants to be a PI – and let me do what needed to be done to set myself up for a good career following here. Thank you.

Life in the lab is tough, full of ups and downs. A lot of downs, actually. Without good people surrounding you in the lab, research would be impossible. So, I have to thank the members of the Srinivasan Lab who helped me get through graduate school. In particular: Chris Chute, the lab's "first-born" doctor, for the scientific discussions that were just as common as random conversations about our favorite fantasy novel series; Laura (Aurilio) Innarelli, the lab's former lab manager, for all of the work you did keeping the lab running, and keeping Chris and I on track with the daily crosswords; Elizabeth DiLoreto, the lab's current lab manager (and no longer "the new Laura", but her own person), for keeping the lab from falling apart, but for also taking a huge stab at your own research, and propelling the lab forward into new collaborations; and all of the undergraduates I've mentored – especially Emily McGlame, Haylea Northcott, Lily Randle, and Annalise Robidoux – without whom my research would never be done, and papers left unsubmitted.

I want to extend a special thanks to Dr. Jill Rulfs, for all your help in best preparing myself for a career in college education. Instead of simply assigning my TA courses, you allowed me to partake in the design of a new CURE lab and acting as my mentor for my mentored teaching experience. Thank you for giving me the opportunity to present on the course's first iteration at the local PKAL meeting. Thank you for all of the lunch discussions on arbitrary things that kept me sane. I'll do my best to take what you've taught me and succeed in that regard.

In a similar vein, I want to thank Dr. Mike Buckholt for all the advice over the years as your TA, and for your help in preparing myself for my career after WPI. Being a fellow Whovian doesn't hurt either.

I want to thank my advisory committees. First, my qualifying exam committee, comprised of (along with Jagan): Dr. Dirk Albrecht, Dr. Kwonmoo Lee, and Dr. Robert Gegear. Outside of the standard qualifying exam grilling session, you helped hone the focus of my research, preventing me from fizzling out and drowning in too many research questions. Secondly, my thesis committee, comprised again of Jagan and Dirk, but also Dr. Joseph "Duff" Duffy, and Dr. Inna Nechipurenko. Duff, it means a lot that you were willing to serve on my committee, despite the demands of running an entire department. Your insights into my research and target journals has proven invaluable. Inna, thank you for sitting on my committee within your first few months at WPI.

It is impossible to do science in isolation. Collaborations are a necessity – now, more than ever. Jagan has connected me with collaborators who not only do complimentary research, but who have provided valuable insights, recommendations, and conversations. I want to thank Dr. Frank Schroeder (Cornell), for all your help in my time here, resulting in a co-first author publication with Ying "Kitty" Zhang, as well as all the ascr#8 I used.

I also want to thank Dr. Erich Schwarz. While the transcriptomic work you assisted with never made it to fruition in the form of a publication while I was here at WPI, your

help, conversations, and recommendations made my first few years of graduate school more bearable. It was a relief to be able to send personable, not-super-formal emails about my research – especially during Quals – it was an odd form of stress relief. Thank you for that.

I want to thank Dr. Stephan von Reuss, from all the way over in Switzerland, for giving me the opportunity as a new graduate student to work on the hydroxylated ascaroside project. That was an awesome opportunity to see collaboration in action early on in graduate school – and it paid off with a paper!

Lastly among collaborators, I want to thank Dr. Isabel Beets – also across the pond – for your help in determining EC_{50}s of all the FLP-3 peptides. Without this, my paper would be much less than its final product. Thank you.

I want to extend a quick thanks to Dr. Sonia Hall for her work at the Genetics Society of America, and in starting the GENETICS Peer Review Training Program. This has been a valuable experience that I couldn't have gotten anywhere else. I don't know how you convinced editors to give feedback to all of the mentees but thank you for that. I hope your time at BioKansas is just as successful.

There are countless graduate students and staff in the building that have contributed to my research success and mental sanity. (Again, now I get the "I can't thank everyone" thing). I want to at least thank (the now doctors) Toni Delorey and Todd Alexander. You two provided me with not only scientific help, but the *completely* necessary coffee runs away from lab that accomplished little else besides extra caffeinating, gossip sharing, and FitBit steps. But importantly, on a personal level, we developed friendships which I think will last well past our time at WPI. I hope you guys the best, and I'm sure I'll see you again soon.

My thank-yous would be complete without thanking my family: Mom and Dad, because while you never understood the science (which is why my explanation for a bad day in lab was always "the DNA wasn't working"), you were always supportive. To my

sister, Brianna, who had a better idea than they did as to what was going on – thanks for the support. As a seemingly random thank you: my cousin Dr. Colleen Harris, for inspiring me to do this whole grad-school thing by getting not one, but TWO doctoral degrees.

And last, but certainly not least, I want to thank my wife, Nichole, for bearing with me through this. I know it was a massive pay cut going back to school – but I think we're doing okay. Thank you for always understanding random extra days in the lab, and late nights that I wasn't even working on my own stuff but helping someone else with a presentation. Thank you for just innately knowing that when I texted "I'll be done in lab in 15 minutes", that that meant, "I have about an hour left until I'm in my car." The end is in sight, I promise: Only 15 more minutes. Thank you for giving me a beautiful and perfect daughter to come home to. Lucy makes all this worth it. I love you both and thank you.

Sorry for anyone that feels I skipped over them. Just know that I remember everything you did, and you're not forgotten. Your help was equally invaluable. I could write an entire dissertation length thank you. But at the same time, alas, I can't.

Thank You.

Inclusion of Previously Published Works

Multiple chapters and sub-chapters in this thesis have previously been published in peer-reviewed journals. All of the works included in this dissertation are not included in any other thesis dissertations. I also hold first or co-first author positions on all of the manuscripts in this dissertation.

These previously published chapters and sub-chapters are:

- **Chapter 1C**, published as: Reilly DK, Srinivasan J (2017). *Caenorhabditis elegans* Olfaction. *Oxford Research Encyclopedia of Neuroscience*. doi: 10.1093/acrefore/9780190264086.013.191
- **Chapter 2B**, published as: Reilly DK, Srinivasan J. (2019) Chemical Communication: Linking Behavior and Physiology. *Current Biology*. doi: 10.1016/j.cub.2019.10.031
- **Chapter 4B**, published as: Reilly DK, Lawler DE, Albrecht DR, Srinivasan J (2017). Using an Adapted Microfluidic Olfactory Chip for the Imaging of Neuronal Activity in Response to Pheromones in Male *C. elegans* Head Neurons. *J. Vis. Exp.* (127), E56026, doi:10.3791/56026
- **Chapter 5**, published as: Zhang YK*, Reilly DK*, Yu J, Srinivasan J, Schroeder FC. (2019). Photoaffinity probes for nematode pheromone receptor identification. *Journal of Organic and Biomolecular Chemistry*. doi: 10.1039/C9OB02099C
- **Chapter 6**, published as: Reilly DK*, Randle LJ*, Srinivasan J (2019). Evolution of Hermaphroditism Decreases Efficacy of Ascaroside#8-Mediated Mate Attraction in *Caenorhabditis* Nematodes. *microPublication Biology*. doi: 10.17912/micropub.biology.000134

Not included in this manuscript directly, I have been listed as a co-author on multiple publications which act towards the furthering of this dissertation or act tangentially to it. These other manuscripts include:

- **Reilly DK**, Srinivasan J (2015). Reproductive Evolution: Pulling the Plug on Selection. *Current Biology* (25), R980-R1001. doi:10.1016/j.cub.2015.09.008
- Narayan A, Venkatachalam V, Durak O, **Reilly DK**, Bose N, Schroeder FC, Samuel ADT, Srinivasan J, Sternberg PW (2016). Contrasting response within a single neuron class enable sex-specific attraction in *C. elegans*. PNAS Plus. (113), E1392-E1401. doi:10.1073/pnas.1600786113
- Dong C, **Reilly DK**, Bergame C, Dolke F, Srinivasan J, von Reuss SH (2018). Comparative Ascaroside Profiling of *Caenorhabditis* Exometabolomes Reveals Species-Specific (ω) and (ω – 2)-Hydroxylation Downstream of Peroxisomal β-Oxidation. Journal of Organic Chemistry. doi: 10.1021/acs.joc.8b00094
- Chute CD, DiLoreto EM, Zhang YK, **Reilly DK**, Rayes D, Coyle VL, Choi HJ, Alkema MJ, Schroeder FC, Srinivasan J (2019). Co-option of neurotransmitter signaling for inter-organismal communication in *C. elegans*. Nature Communications. doi:10.1038/s41467-019-11240-7

Table of Contents

Table of Figures

Table of Tables

Table of Schemes

Table of Supplementary Figures

Table of Supplementary Tables

List of Abbreviations

OR: Olfactory Receptor

VNO: Vomeronasal Organ

GPCR: G protein-coupled Receptor

°C: Degrees Celsius

him: high incidence of males mutation

CRISPR: clustered regularly interspaced short palindromic repeats

GFP/RFP: Green/Red Fluorescent Protein

RNA: ribonucleic acid

dsRNA: double stranded RNA

RNAi: RNA interference

GECI: genetically encoded calcium indicator

GCaMP: GFP-Calmodulin M13-Peptide

gof: gain of function mutation

lof: loss of function mutation

CEM: male-specific cephalic neurons

ascr: ascaroside

icas: indolated ascaroside

osas: octopamine succinylated ascaroside

ascr#8: ascaroside #8

5-HT: serotonin

nM: nanomolar

μM: micromolar

SDS: sodium dodecyl sulfate

mL: milliliter

s/h: seconds/hours

$\Delta F/F_0$: change in fluorescence compared to baseline

ins: insulin-like peptide

flp: FMRFamide-like peptide

nlp: non-insulin/non-FLP peptide

npr: neuropeptide receptor

CEM: cephalic male neurons

Chapter 1 Olfaction and Nematodes

Chapter 1A Mechanisms of Olfaction

Summary

The ability of an animal to sense and respond to its environment is critical to its own survival – and that of the species as a whole. The most ancient form of environmental sensation is chemosensation. From bacteria to humans, all life can sense chemicals in the environment. The integration of the nervous system into chemosensation has given rise to olfaction. The organs which contribute to olfaction vary greatly between species and across taxa, although the mechanisms controlling the neural functions related to olfaction are strongly conserved. Deepening our understanding of the mechanisms of olfaction will allow for better diagnoses and therapies surrounding neurodegenerative diseases, such as Alzheimer's Disease and Parkinson's Disease, both of which often exhibit anosmia prior to impairments in motor control and cognitive function. This chapter provides a review of the olfactory organs observed in nature, and a primer on G protein-coupled receptor-mediated ligand sensation.

What is Olfaction?

The ability to sense and respond to the surrounding environment is essential for the survival. The "five senses" that allow an organism to perceive their surroundings include mechanosensation (touch), vision (optic sensation), hearing (auditory/aural sensation), taste (gustation), and smell (olfaction). However, research has revealed that these senses are only a portion of how we perceive our surroundings, with studies revealing magneto- (Clites & Pierce, 2017; Frankel & Bazylinski, 2009), gravi- (Matsuo & Kamikouchi, 2013; Pouliquen et al., 2017), and aerosensation (Frankel & Bazylinski, 2009; Taylor, Zhulin, & Johnson, 1999).

The most ancient of these sensations, however, is olfaction, or chemosensation. In this, receptors on the surface of a cell bind to a ligand in the space surrounding the cell, and initiate an intra-cellular cascade responding to that binding. In more complex organisms, olfaction plays a role in recognition of conspecifics (Lightfoot et al., 2019), mating and pheromone sensation (Choe et al., 2012), and locating food (Hughes, Price, & Banks, 2010).

Olfactory Organs in Nature

The human olfactory system, while complex, is simple compared to many other olfactory systems (Liberles, 2014; Walliczek-Dworschak & Hummel, 2017). The olfactory receptor neurons (ORNs) within the nasal epithelium near the top of the nasal cavity detect odorants and project axons onto the Mitral cells within the olfactory bulb (Branigan & Tadi, 2019; Pinto, 2011; Walliczek-Dworschak & Hummel, 2017). The Mitral cells then project onto the 1100-1200 glomeruli located in the olfactory bulb (Pinching & Powell, 1971), before projecting to higher order processing centers in the brain.

More well-detailed and studied olfactory systems are found in the mouse (*Mus musculus* (Liberles, 2014)), the fruit fly, (*Drosophila melanogaster* (Couto, Alenius, & Dickson, 2005)), and the nematode (*Caenorhabditis elegans* (See **Chapter 1C**) (Reilly &

Srinivasan, 2017)). These olfactory systems range from the relatively "simple" (the entirety of the *C. elegans* nervous system is comprised of only 302 neurons) (White, Southgate, Thomas, & Brenner, 1986)), to complex (as in the mouse olfactory system (Liberles, 2014)).

The Mouse Olfactory System

Olfaction in mice offers a strong model of study. With the genetic tools available for study, mice offer a mammalian model of olfaction outside of human study. Not a perfect model, as humans lack most of the olfactory organs present in mice, *Mus musculus* offers a model for a larger grouping of animals that contain the same organs (**Figure 1**).

Main Olfactory Epithelium

The largest olfactory structure in mice is the main olfactory epithelium (MOE) (Liberles, 2014). Responsible for the detection of airborne odorants and pheromones, the MOE projections eventually converge on the hypothalamus, amygdala, and BNST (bed nucleus of the stria terminalis) (**Figure 1**) to influence stress, aggression, and reproduction (Liberles, 2014).

Main and Accessory Olfactory Bulbs

The main olfactory bulb (MOB), wherein mitral cells project from to innervate multiple regions of the brain, is located downstream of the MOE (Harvey & Heinbockel, 2018). Individual glomeruli integrate inputs from neurons containing the same olfactory receptor (the one-neuron-one-receptor rule translates here to a one-glomeruli-one-receptor rule) (**Figure 1**) (Liberles, 2014).

Likewise, the accessory olfactory bulb (AOB) also contains individual glomeruli comprised of mitral cells, related to specific V1R and V2R receptor expressing olfactory neurons (Ma, 2010). However, while the MOB will project to multiple brain regions, the AOB often projects to limbic circuits (Liberles, 2014).

Vomeronasal Organ

The most prominently studied olfactory organ is the vomeronasal organ (VNO) (also known as Jacobson's organ). The VNO, while absent in humans, is present in mice, many other mammals, snakes, lizards, and birds (Taniguchi & Taniguchi, 2014). A pair of cylindrical structures connected to the nasal cavity by a water-filled duct, the VNO detects pheromones (Silva & Antunes, 2017) and other water-soluble molecules (Liberles, 2014; Wirsig-Wiechmann, Houck, Feldhoff, & Feldhoff, 2002). The VNO projects onto the AOB, hypothalamus, and limbic system to affect sex, aggression, and other behaviors (**Figure 1**) (Liberles, 2014).

Grueneberg Ganglion

A relatively tiny olfactory structure, the Grueneberg Ganglion (GG) is comprised of approximately 300-500 cells (Fleischer & Breer, 2010). Expressing only a handful of receptors and a single guanylyl cyclase, the exact function of the GG largely remains an enigma. There have been a few reports of the GG being activated by alarm pheromones, playing a role in detecting cold temperatures, as well as suckling behaviors (Liberles, 2014).

Septal Organ

The septal organ (SO) is a thin layer of ciliated neurons that resemble MOE neurons. However, due to its location in the nasal septum, and no correlation to pheromone response, the SO is a unique organ from the MOE (Liberles, 2014). However, the expression of a large number of olfactory receptors and the three-layer organization of sensory neurons pose the SO as a more definitive olfactory organ than the GG (Breer, Fleischer, & Strotmann, 2006; Ma et al., 2003; Wackermannova, Pinc, & Jebavy, 2016).

These structures are not limited to mice, however. As with the VNO, which is present in mammals, bird, reptiles, and amphibians, (Taniguchi & Taniguchi, 2014; Wirsig-

Wiechmann et al., 2002), the septal organ can be found throughout mammals (Ma et al., 2003), while the Greuneberg ganglion is present only in rodents (Fleischer & Breer, 2010).

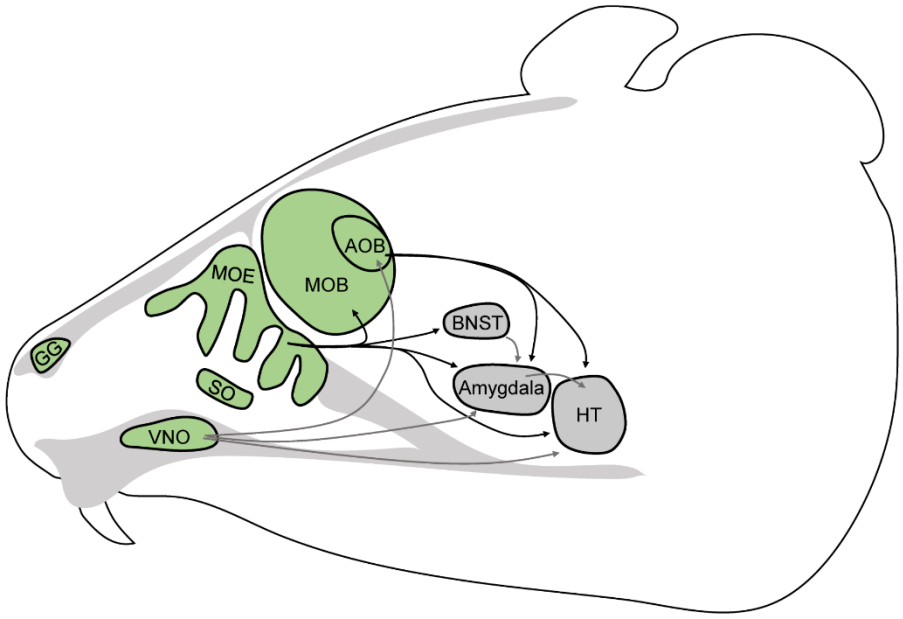

Figure 1. The Mouse Olfactory System.
The Main Olfactory Epithelium, located within the nasal cavity, projects to the BNST, amygdala, and hypothalamus (HT), as well as on the Main Olfactory Bulb (MOB). The MOB integrates inputs, and with the Accesory Olfactory Bulb (AOB), projects to the limbic system. The vomoernasal organ (VNO) sends projections into the AOB, HT, and limbic system. The Greuneberg Ganglion and Septal Organ projects are not mapped. In general, the olfactory organs (green), project onto the limbic system (grey). Adapted from Asaba et al. (Asaba, Hattori, Mogi, & Kikusui, 2014).

Insect Olfaction

Insects detect a large variety of volatile and soluble odorants which can signal the location of food and its quality, mates, and even oviposition sites (Dahanukar, Hallem, & Carlson, 2005). The sensilla which sense these cues are innervated by olfactory receptor neurons (ORNs), which project to the antennal lobe from two olfactory organs on the head, the antennae, and maxillary pulps. In insects, olfaction is extremely closely linked with gustation, as odorant (OR) and gustatory (GR) receptors are present in these sensilla.

As in mammalian olfactory systems, the ORNs of insects follow a one-neuron-one-receptor rule, as well as the subsequent one-receptor-one-glomerulus structural

organization (Carlson, 1996; Couto et al., 2005; Vosshall, 2000). Eventually, these circuits project to the mushroom body and lateral horn of *Drosophila* (Couto et al., 2005).

The functional components of the Drosophila olfactory system are complex, relying on integration of multiple networks, synaptic and peptidergic neurotransmission, physiological state, sex, and live stage (Guven-Ozkan & Davis, 2014; Joseph & Carlson, 2015; Martin, Boto, Gomez-Diaz, & Alcorta, 2013; Nassel & Zandawala, 2019; Smith, 1996, 2007).

Non-Drosophila Olfaction Models

The well-studied *Drosophila* constitutes a holometabolous model, as they progress through a pupal stage of development (Callier, Hand, Campbell, Biddulph, & Harrison, 2015). Many aquatic insects, however, are hemimetabolous, and have no pupal stage of development, instead progressing from egg to nymph to imago (Crespo, 2011).

Of these hemimetabolous, three orders of insects have well studied olfactory systems: Ephemeroptera, Odonata, and Plecoptera – the latter having very little anatomical study to date. Ephemeroptera and Odonata lack the glomerular antennal lobes necessary for sensation of volatile cues and are often considered anosmic (see **GPCRs, Olfaction, and Public Health** below) (Crespo, 2011). The higher order organization in these insects is also varied, with the mushroom body calyx being absent – those glomeruli projecting to the pedunculus instead (Crespo, 2011). While Ephemeroptera are considered anosmic, there is doubt as to the existence of an actual olfactory system in Odonata (Plotnikova & Isavnina, 2006). The massive mushroom bodies of these insects receive inputs from the optic lobes, but not from any olfactory sensilla (Crespo, 2011).

Aquatic Olfaction

Fish offer an interesting model for studying olfaction. Living the entirety of their lives in aquatic environments, there are no volatile cues to be sensed, and pockets of odorant concentrations rapidly diffuse across massive regions, making detectable levels extremely important in olfaction.

Despite this, the olfactory system of zebrafish is comprised of two peripheral olfactory organs called rosettes, which project to corresponding olfactory bulbs (Calvo-Ochoa & Byrd-Jacobs, 2019). Despite such a deceptively "simple" olfactory system, the olfactory bulbs of migratory coastal-pelagic shark species are the largest known olfactory bulbs to date (Nosal, Chao, Farrara, Chai, & Hastings, 2016). This massive increase in olfactory bulb size has been shown to play a role in linking physical location to olfactory space within the brain (Yopak, Lisney, & Collin, 2015), furthering our understanding as to how olfaction contributes to pelagic, or open-sea, navigation.

Nematode Olfaction

Nematodes, such as *Caenorhabditis elegans*, navigate an ever-changing environment utilizing an extremely limited number of neurons. With only 302 neurons in hermaphrodites, and 385 in males, *C. elegans* expertly navigate and respond to complex cues (Sammut et al., 2015; White et al., 1986).

> A more detailed description of *C. elegans* olfactory mechanisms is presented as **Chapter 1C** of this thesis dissertation (Reilly & Srinivasan, 2017).

Molecular Mechanisms of Olfaction

In olfaction, olfactory receptors (ORs) bind these volatile and water-soluble molecules and propagate signals down the olfactory neurons (ORNs) to higher regions of the brain where integration and perception occur (Pinto, 2011). Olfactory receptors, or chemoreceptors, have undergone expansion in specific taxa. In a study by Kahn and colleagues, investigating two reptile species, the number of identified ORs approached 1,000 in each species. Meanwhile, when analyzing forty-eight avian genomes, they found that the number of OR genes only spanned between 182 and 688 genes per species (Khan et al., 2015).

The neural circuits which govern the integration of olfactory inputs vary in form and complexity (Calvo-Ochoa & Byrd-Jacobs, 2019; Liberles, 2014; Walliczek-Dworschak &

Hummel, 2017; Wicher, 2015). While this makes generalizations easy to identify, finding homologous processes and organs is more difficult.

The molecular mechanics of olfaction are remarkably conserved. G protein-coupled receptors (GPCRs) function as olfactory receptors (ORs) in both vertebrates and invertebrates. The signaling cascades may vary in the identity of molecular components, but again, the overall processes are remarkably conserved across taxa.

In short, G protein-coupled receptors (GPCRs) are seven-transmembrane proteins with their N-terminus in the extracellular space, and the C-terminus in the cytoplasm (**Figure 2A**). Upon binding a ligand, GPCRs undergo a conformation change, allowing them to interact with heterotrimeric G protein complexes (G$\alpha\beta\gamma$), and displace a GDP molecule bound to the Gα subunit (Bastiani & Mendel, 2006). This GDP is readily replaced with a GTP, the binding of which displaces Gα from both the GPCR and the G$\beta\gamma$ complex. Following this, GTP-Gα and G$\beta\gamma$ interact with respective effector proteins

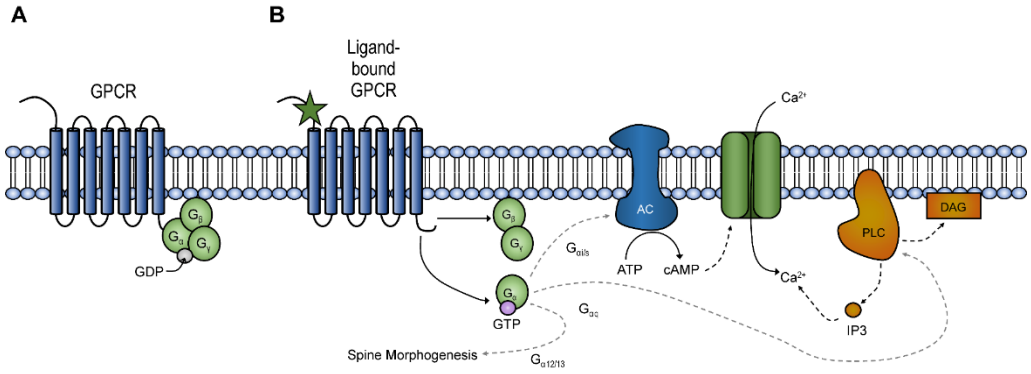

Figure 2. G protein-Coupled Receptor Signaling Cascades.
(A) A ligand-free GPCR interacts with heterotrimeric G protein complexes, comprised of G_β, G_γ, and G_α subunits bound to GDP. **(B)** Following GPCR-ligand binding, GDP is replaced by GTP, which dissaciates the receptor from the G protein complex. The complex further dissociated into a G_β-G_γ complex, and a GDP-G_α complex. Dependent on the type of Gα protein involved in singaling, one of three major signaling cascades are initiatied. If $G_{\alpha i/s}$ signaling is involved, the transmembrone protein, adenylyl cyclase (AC), is made to convert ATP to cAMP, which in turn causes ion channels to open, allowing ions such as Ca^{2+} to flow into the cell. In $G_{\alpha q}$ signaling, the inner-membrane bound phosolipase C (PLC) is signlaed to activate DAG or IP3 related pathways, similar resulting in caclium flux within the cell. $G_{\alpha 12/13}$ signaling results in spine morphogensis downstream of Rho signaling cascades. Adapted from Frooninckx et al. (Frooninckx et al., 2012).

to initiate a signaling cascade which results in ion flux and/or transcriptional changes (**Figure 2B**) (Bastiani & Mendel, 2006).

Chemosensory Receptors are present in variable amounts between species

The human genome encodes nearly 400 ORs – GPCRs specific to olfactory functions (Block, 2018). The total number of GPCRs in the human genome is nearly double that number (Sriram & Insel, 2018). There are multiple classes of receptors that contribute to olfaction among this large number of GPCRs. Along with the 400 ORs, six trace amine-associated receptors (TAARs), and three Formyl Peptide Receptors (FPRs) (Migeotte, Communi, & Parmentier, 2006) also contribute to olfactory diversity along with the gustatory 25 bitter (TAS2Rs), 2 sweet, and 2 umami taste receptors (TAS1Rs) receptors (Di Pizio, Behrens, & Krautwurst, 2019).

Many mammals also express two families of GPCRs in the vomeronasal organ: the V1R and V2R receptors (Silva & Antunes, 2017). A unique, enigmatic subsystem of the olfactory epithelium has recently been discovered in mice, termed the "necklace" subsystem. Located within the "cul-de-sac" regions of the olfactory epithelium, these OSNs project onto a specific set of glomeruli that encircle the caudal olfactory bulb "like beads on a necklace" (Greer et al., 2016). The necklace OSNs have been found to sense gases, pheromones, plant odors, and urinary peptides. Recent analysis of murine olfactory systems has uncovered a novel class of chemosensory proteins specific to the "necklace" subsystem (Greer et al., 2016). These unique, four-pass transmembrane receptors (MS4A) sense pheromones and fatty acids.

Insects express a variable number of GCPRs, with *Drosophila melanogaster* encoding approximately 100 GPCRs, but *Anopheles gambiae* encoding 276. (Brody & Cravchik, 2000; Hill et al., 2002). Ionotropic receptors (IRs) also play a major role in insect chemosensation. Unlike ORs, IRs are not seven-transmembrane proteins, and are instead more closely related to inotropic glutamate receptors (iGluR) (Gomez-Diaz, Martin, Garcia-Fernandez, & Alcorta, 2018). Insects also express class of proteins known as

odorant binding proteins (Obps), which build on the array of ORs present (Sun, Xiao, & Carlson, 2018). However, structural elucidation of Obps has determined that they are not GPCRs, nor are they membrane bound. Instead, they are found in sensillum lymph, and serve to solubilize and transport odorants to the ORs (Gonzalez et al., 2019; Sun et al., 2018).

A massive expansion of GPCRs occurred at some point in *Caenorhabditis elegans*' evolutionary history, resulting on over 1200 GPCRs being expressed – about half of which are chemosensory receptors (Cornelia I. Bargmann, 1998). Despite the large variation in number of genomic ORs, the mechanism of action remains the same across taxa.

Variation in C. elegans Receptor Function

C. elegans add a vast amount of functional variation to its already large number of GPCRs in that it expresses 21 Gα proteins, 2 Gβ proteins, and 2 Gγ proteins. The Gα proteins exhibit homologies to mammalian Gα proteins (specifically Gs, Gi/o, Gq, and G12 proteins) (Bastiani & Mendel, 2006). This vast array allows for GPCRs to mix-and-match G proteins, with some complexes activating neurons, and other inhibiting neuronal activity. Also, by not adhering to the one-receptor-one-neuron rule, *C. elegans* allow neurons to play singular roles in generating behavior or developmental outcomes, by sensing multiple stimuli. For example, the neuron ASH can sense multiple noxious stimuli via various GPCRs and G protein complexes, each eliciting specific downstream effects (C. I. Bargmann, 2006; Bastiani & Mendel, 2006).

GPCRs, Olfaction, and Public Health

The ability to manipulate GPCR activity is a major front of modern drug development: approximately 35% of approved drugs affect GPCR activity in one way or another (Di Pizio et al., 2019). Because of the vast array of GPCRs in the human genome, many avenues have been followed in determining the therapeutic potentials of targets specific GPCRs with drugs (Shore & Reggio, 2015).

Neurodegenerative disease (ND) diagnoses are on the rise. Analysis of the 2010 United States census has determined that while there were 4.7 million patients with Alzheimer's Disease (AD) dementia, by 2050, this number is projected to rise to 13.8 million (Hebert, Weuve, Scherr, & Evans, 2013). The second most common ND is Parkinson's Disease (PD) (630,000 patients in 2010), projected to double between 2030-2040 (Kowal, Dall, Chakrabarti, Storm, & Jain, 2013; Marras et al., 2018). While the pathologies vary drastically, there are similarities in some of the symptomatic expressions of NDs. For example, anosmia is a common symptom – although many people do not even notice a loss of smell (Hawkes, 2003). The loss of smell often precedes motor and cognitive impairments in these disorders (Hüttenbrink, Hummel, Berg, Gasser, & Hähner, 2013).

Opposite to that seen in PD and AD – and nowhere near as worrisome – is the advent of hyperosmia during pregnancy. Reports of pregnancy-related hyperosmia are largely anecdotal, going back over 100 years (Cameron, 2014). Studies have found however, that increased sense of smell may be odor-specific, as patient performance depended on specific odors (Cameron, 2014). As Cameron notes in their review, future studies should: *(1)* assay traits such as recognition threshold and odor identification across a broader range of odorants, *(2)* determine if there are odors which are unpleasant to pregnant women in particular, *(3)* identify odors which are smelled at lower concentrations, and *(4)* confirm that these odors are purely olfactory, and do not include gustatory sensation (Cameron, 2014).

Conclusions

Chemosensation is a complicated biological process that is vital for all forms of life to survive. In higher order eukaryotes containing nervous systems, olfaction drives aspects related to survival, such as reproduction, development, food location, predatory avoidance, and many other behaviors.

Study of the mechanisms relating olfactory sensation (i.e. OR-ligand binding (Gonzalez et al., 2019)) to behavioral outputs (i.e., predator avoidance (Vernet-Maury, Polak, & Demael, 1984)) will deepen our understanding of how we smell. Proper and specific olfaction is essential for normal development and survival. Olfactory dysfunction may be a natural part of life (i.e., pregnancy-related hyperosmia), but is also a warning sign of deeper problems (i.e., neurodegenerative disease).

The specifics of olfaction vary from species to species. While most mammals contain a vomeronasal organ contributing to pheromone sensation, humans are lacking this order. Even in smaller organisms however, such as nematodes, the basic mechanisms governing olfaction are conserved. The sensory machinery can be found across taxa (i.e. GPCRs are conserved across higher order eukaryotes), and understanding the laws governing neural sensation will assist in designing future therapies for those suffering anosmia or hyperosmia.

This thesis dissertation will investigate the molecular mechanisms regulating the sensation of a nematode mating pheromone, ascaroside #8 (See **Chapter 2C**), at both the sensory level (see Chapter 4C**, Chapter 5A** (Zhang, Reilly, Yu, Srinivasan, & Schroeder, 2019)**, Chapter 6A** (Reilly, Randle, & Srinivasan, 2019)) and the neuromodulatory level (see Chapter 3B).

References

Asaba, A., Hattori, T., Mogi, K., & Kikusui, T. (2014). Sexual attractiveness of male chemicals and vocalizations in mice. *8*(231). doi:10.3389/fnins.2014.00231

Bargmann, C. I. (1998). Neurobiology of the *Caenorhabditis elegans* Genome. *Science, 282*(5396), 2028. doi:10.1126/science.282.5396.2028

Bargmann, C. I. (2006). Chemosensation in *C. elegans*. *WormBook*, 1-29. doi:10.1895/wormbook.1.123.1

Bastiani, C., & Mendel, J. (2006). Heterotrimeric G proteins in C. elegans. *WormBook*, 1-25. doi:10.1895/wormbook.1.75.1

Block, E. (2018). Molecular Basis of Mammalian Odor Discrimination: A Status Report. *J Agric Food Chem, 66*(51), 13346-13366. doi:10.1021/acs.jafc.8b04471

Branigan, B., & Tadi, P. (2019). Physiology, Olfactory. In *StatPearls*. Treasure Island (FL): StatPearls Publishing.

Breer, H., Fleischer, J., & Strotmann, J. (2006). The sense of smell: multiple olfactory subsystems. *Cell Mol Life Sci, 63*(13), 1465-1475. doi:10.1007/s00018-006-6108-5

Brody, T., & Cravchik, A. (2000). Drosophila melanogaster G protein-coupled receptors. *J Cell Biol, 150*(2), F83-88. doi:10.1083/jcb.150.2.f83

Callier, V., Hand, S. C., Campbell, J. B., Biddulph, T., & Harrison, J. F. (2015). Developmental changes in hypoxic exposure and responses to anoxia in Drosophila melanogaster. *J Exp Biol, 218*(Pt 18), 2927-2934. doi:10.1242/jeb.125849

Calvo-Ochoa, E., & Byrd-Jacobs, C. A. (2019). The Olfactory System of Zebrafish as a Model for the Study of Neurotoxicity and Injury: Implications for Neuroplasticity and Disease. *Int J Mol Sci, 20*(7). doi:10.3390/ijms20071639

Cameron, E. L. (2014). Pregnancy and olfaction: a review. *Frontiers in psychology, 5*, 67-67. doi:10.3389/fpsyg.2014.00067

Carlson, J. R. (1996). Olfaction in Drosophila: from odor to behavior. *Trends Genet, 12*(5), 175-180. doi:10.1016/0168-9525(96)10015-9

Choe, A., Chuman, T., von Reuss, S. H., Dossey, A. T., Yim, J. J., Ajredini, R., . . . Edison, A. S. (2012). Sex-specific mating pheromones in the nematode Panagrellus redivivus. *Proc Natl Acad Sci U S A, 109*(51), 20949-20954. doi:10.1073/pnas.1218302109

Clites, B. L., & Pierce, J. T. (2017). Identifying Cellular and Molecular Mechanisms for Magnetosensation. *Annu Rev Neurosci, 40*, 231-250. doi:10.1146/annurev-neuro-072116-031312

Couto, A., Alenius, M., & Dickson, B. J. (2005). Molecular, anatomical, and functional organization of the Drosophila olfactory system. *Curr Biol, 15*(17), 1535-1547. doi:10.1016/j.cub.2005.07.034

Crespo, J. G. (2011). A review of chemosensation and related behavior in aquatic insects. *Journal of insect science (Online), 11*, 62-62. doi:10.1673/031.011.6201

Dahanukar, A., Hallem, E. A., & Carlson, J. R. (2005). Insect chemoreception. *Curr Opin Neurobiol, 15*(4), 423-430. doi:10.1016/j.conb.2005.06.001

Di Pizio, A., Behrens, M., & Krautwurst, D. (2019). Beyond the Flavour: The Potential Druggability of Chemosensory G Protein-Coupled Receptors. *Int J Mol Sci, 20*(6). doi:10.3390/ijms20061402

Fleischer, J., & Breer, H. (2010). The Grueneberg ganglion: a novel sensory system in the nose. *Histol Histopathol, 25*(7), 909-915. doi:10.14670/hh-25.909

Frankel, R. B., & Bazylinski, D. A. (2009). Magnetosomes and magneto-aerotaxis. *Contrib Microbiol, 16*, 182-193. doi:10.1159/000219380

Frooninckx, L., Van Rompay, L., Temmerman, L., Van Sinay, E., Beets, I., Janssen, T., . . . Schoofs, L. (2012). Neuropeptide GPCRs in C. elegans. *frontiers in Endocrinology, 3*, 167. doi:10.3389/fendo.2012.00167

Gomez-Diaz, C., Martin, F., Garcia-Fernandez, J. M., & Alcorta, E. (2018). The Two Main Olfactory Receptor Families in Drosophila, ORs and IRs: A Comparative Approach. *Front Cell Neurosci, 12*, 253. doi:10.3389/fncel.2018.00253

Gonzalez, D., Rihani, K., Neiers, F., Poirier, N., Fraichard, S., Gotthard, G., . . . Briand, L. (2019). The Drosophila odorant-binding protein 28a is involved in the detection of the floral odour ss-ionone. *Cell Mol Life Sci*. doi:10.1007/s00018-019-03300-4

Greer, P. L., Bear, D. M., Lassance, J. M., Bloom, M. L., Tsukahara, T., Pashkovski, S. L., . . . Datta, S. R. (2016). A Family of non-GPCR Chemosensors Defines an Alternative Logic for Mammalian Olfaction. *Cell, 165*(7), 1734-1748. doi:10.1016/j.cell.2016.05.001

Guven-Ozkan, T., & Davis, R. L. (2014). Functional neuroanatomy of Drosophila olfactory memory formation. *Learn Mem, 21*(10), 519-526. doi:10.1101/lm.034363.114

Harvey, J. D., & Heinbockel, T. (2018). Neuromodulation of Synaptic Transmission in the Main Olfactory Bulb. *Int J Environ Res Public Health, 15*(10). doi:10.3390/ijerph15102194

Hawkes, C. (2003). Olfaction in neurodegenerative disorder. *Mov Disord, 18*(4), 364-372. doi:10.1002/mds.10379

Hebert, L. E., Weuve, J., Scherr, P. A., & Evans, D. A. (2013). Alzheimer disease in the United States (2010-2050) estimated using the 2010 census. *Neurology, 80*(19), 1778-1783. doi:10.1212/WNL.0b013e31828726f5

Hill, C. A., Fox, A. N., Pitts, R. J., Kent, L. B., Tan, P. L., Chrystal, M. A., . . . Zwiebel, L. J. (2002). G Protein-Coupled Receptors in *Anopheles gambiae*. *Science, 298*(5591), 176. doi:10.1126/science.1076196

Hughes, N. K., Price, C. J., & Banks, P. B. (2010). Predators are attracted to the olfactory signals of prey. *PLoS One, 5*(9). doi:10.1371/journal.pone.0013114

Hüttenbrink, K.-B., Hummel, T., Berg, D., Gasser, T., & Hähner, A. (2013). Olfactory dysfunction: common in later life and early warning of neurodegenerative disease. *Deutsches Arzteblatt international, 110*(1-2), 1-e1. doi:10.3238/arztebl.2013.0001

Joseph, R. M., & Carlson, J. R. (2015). Drosophila Chemoreceptors: A Molecular Interface Between the Chemical World and the Brain. *Trends Genet, 31*(12), 683-695. doi:10.1016/j.tig.2015.09.005

Khan, I., Yang, Z., Maldonado, E., Li, C., Zhang, G., Gilbert, M. T., . . . Antunes, A. (2015). Olfactory Receptor Subgenomes Linked with Broad Ecological Adaptations in Sauropsida. *Mol Biol Evol, 32*(11), 2832-2843. doi:10.1093/molbev/msv155

Kowal, S. L., Dall, T. M., Chakrabarti, R., Storm, M. V., & Jain, A. (2013). The current and projected economic burden of Parkinson's disease in the United States. *Movement Disorders, 28*(3), 311-318. doi:10.1002/mds.25292

Liberles, S. D. (2014). Mammalian pheromones. *Annu Rev Physiol, 76*, 151-175. doi:10.1146/annurev-physiol-021113-170334

Lightfoot, J. W., Wilecki, M., Rödelsperger, C., Moreno, E., Susoy, V., Witte, H., & Sommer, R. J. (2019). Small peptide–mediated self-recognition prevents cannibalism in predatory nematodes. *Science, 364*(6435), 86. doi:10.1126/science.aav9856

Ma, M. (2010). The Neurobiology of Olfaction. In A. Menini (Ed.). Boca Raton (FL): CRC Press/Taylor & Francis.

Ma, M., Grosmaitre, X., Iwema, C. L., Baker, H., Greer, C. A., & Shepherd, G. M. (2003). Olfactory signal transduction in the mouse septal organ. *The Journal of Neuroscience, 23*(1), 317-324. doi:10.1523/JNEUROSCI.23-01-00317.2003

Marras, C., Beck, J. C., Bower, J. H., Roberts, E., Ritz, B., Ross, G. W., . . . Tanner, C. M. (2018). Prevalence of Parkinson's disease across North America. *NPJ Parkinsons Dis, 4*, 21. doi:10.1038/s41531-018-0058-0

Martin, F., Boto, T., Gomez-Diaz, C., & Alcorta, E. (2013). Elements of olfactory reception in adult Drosophila melanogaster. *Anat Rec (Hoboken), 296*(9), 1477-1488. doi:10.1002/ar.22747

Matsuo, E., & Kamikouchi, A. (2013). Neuronal encoding of sound, gravity, and wind in the fruit fly. *J Comp Physiol A Neuroethol Sens Neural Behav Physiol, 199*(4), 253-262. doi:10.1007/s00359-013-0806-x

Migeotte, I., Communi, D., & Parmentier, M. (2006). Formyl peptide receptors: a promiscuous subfamily of G protein-coupled receptors controlling immune responses. *Cytokine Growth Factor Rev, 17*(6), 501-519. doi:10.1016/j.cytogfr.2006.09.009

Nassel, D. R., & Zandawala, M. (2019). Recent advances in neuropeptide signaling in Drosophila, from genes to physiology and behavior. *Prog Neurobiol, 179*, 101607. doi:10.1016/j.pneurobio.2019.02.003

Nosal, A. P., Chao, Y., Farrara, J. D., Chai, F., & Hastings, P. A. (2016). Olfaction Contributes to Pelagic Navigation in a Coastal Shark. *PLoS One, 11*(1), e0143758-e0143758. doi:10.1371/journal.pone.0143758

Pinching, A. J., & Powell, T. P. (1971). The neuropil of the glomeruli of the olfactory bulb. *J Cell Sci, 9*(2), 347-377.

Pinto, J. M. (2011). Olfaction. *Proceedings of the American Thoracic Society, 8*(1), 46-52. doi:10.1513/pats.201005-035RN

Plotnikova, S. I., & Isavnina, I. L. (2006). [Possible olfactory function of the antennal nerve and the lateral protocerebrum of dragonfly (Aeschna grandis) larva]. *Zh Evol Biokhim Fiziol, 42*(3), 269-272.

Pouliquen, O., Forterre, Y., Berut, A., Chauvet, H., Bizet, F., Legue, V., & Moulia, B. (2017). A new scenario for gravity detection in plants: the position sensor hypothesis. *Phys Biol, 14*(3), 035005. doi:10.1088/1478-3975/aa6876

Reilly, D. K., Randle, L. J., & Srinivasan, J. (2019). Evolution of hermaphroditism decreases efficacy of Ascaroside#8-mediated mate attraction in *Caenorhabditis* nematodes. *microPublication Biology*. doi:10.17912/micropub.biology.000134

Reilly, D. K., & Srinivasan, J. (2017). *Caenorhabditis elegans* Olfaction. doi:10.1093/acrefore/9780190264086.013.191

Sammut, M., Cook, S. J., Nguyen, K. C. Q., Felton, T., Hall, D. H., Emmons, S. W., . . . Barrios, A. (2015). Glia-derived neurons are required for sex-specific learning in C. elegans. *Nature, 526*(7573), 385-390. doi:10.1038/nature15700

Shore, D. M., & Reggio, P. H. (2015). The therapeutic potential of orphan GPCRs, GPR35 and GPR55. *Front Pharmacol, 6*, 69. doi:10.3389/fphar.2015.00069

Silva, L., & Antunes, A. (2017). Vomeronasal Receptors in Vertebrates and the Evolution of Pheromone Detection. *Annu Rev Anim Biosci, 5*, 353-370. doi:10.1146/annurev-animal-022516-022801

Smith, D. P. (1996). Olfactory mechanisms in Drosophila melanogaster. *Curr Opin Neurobiol, 6*(4), 500-505.

Smith, D. P. (2007). Odor and pheromone detection in Drosophila melanogaster. *Pflugers Arch, 454*(5), 749-758. doi:10.1007/s00424-006-0190-2

Sriram, K., & Insel, P. A. (2018). G Protein-Coupled Receptors as Targets for Approved Drugs: How Many Targets and How Many Drugs? *Molecular pharmacology, 93*(4), 251-258. doi:10.1124/mol.117.111062

Sun, J. S., Xiao, S., & Carlson, J. R. (2018). The diverse small proteins called odorant-binding proteins. *Open Biol, 8*(12), 180208. doi:10.1098/rsob.180208

Taniguchi, K., & Taniguchi, K. (2014). Phylogenic studies on the olfactory system in vertebrates. *The Journal of veterinary medical science, 76*(6), 781-788. doi:10.1292/jvms.13-0650

Taylor, B. L., Zhulin, I. B., & Johnson, M. S. (1999). Aerotaxis and other energy-sensing behavior in bacteria. *Annu Rev Microbiol, 53*, 103-128. doi:10.1146/annurev.micro.53.1.103

Vernet-Maury, E., Polak, E. H., & Demael, A. (1984). Structure-activity relationship of stress-inducing odorants in the rat. *J Chem Ecol, 10*(7), 1007-1018. doi:10.1007/bf00987509

Vosshall, L. B. (2000). Olfaction in Drosophila. *Curr Opin Neurobiol, 10*(4), 498-503.

Wackermannova, M., Pinc, L., & Jebavy, L. (2016). Olfactory sensitivity in mammalian species. *Physiol Res, 65*(3), 369-390.

Walliczek-Dworschak, U., & Hummel, T. (2017). The Human Sense of Olfaction. *Facial Plast Surg, 33*(4), 396-404. doi:10.1055/s-0037-1603828

White, J. G., Southgate, E., Thomas, J. N., & Brenner, S. (1986). The structure of the nervous system of the nematode Caernorhabditis elegans. *Phil Trans Royal Soc Lon, 314B*. doi:10.1098/rstb.1986.0056

Wicher, D. (2015). Olfactory signaling in insects. *Prog Mol Biol Transl Sci, 130*, 37-54. doi:10.1016/bs.pmbts.2014.11.002

Wirsig-Wiechmann, C. R., Houck, L. D., Feldhoff, P. W., & Feldhoff, R. C. (2002). Pheromonal activation of vomeronasal neurons in plethodontid salamanders. *Brain Research, 952*(2), 335-344. doi:10.1016/S0006-8993(02)03369-3

Yopak, K. E., Lisney, T. J., & Collin, S. P. (2015). Not all sharks are "swimming noses": variation in olfactory bulb size in cartilaginous fishes. *Brain Struct Funct, 220*(2), 1127-1143. doi:10.1007/s00429-014-0705-0

Zhang, Y. K., Reilly, D. K., Yu, J., Srinivasan, J., & Schroeder, F. C. (2019). Photoaffinity probes for nematode pheromone receptor identification. *Journal of Organic & Biomolecular Chemistry*, 10.1039/c1039ob02099c. doi:10.1039/c9ob02099c

Chapter 1B *Caenorhabditis elegans*

Summary

The roundworm, *Caenorhabditis elegans*, is an ideal model for studying multiple facets of life. From studies investigating developmental pathways, to behavior, to aging, to mating, *C. elegans* offers many advantages and tools which make it extremely useful. A sexually dimorphic species, *C. elegans* is an ideal tool for studying sex differences in development and behavior. Here, a brief overview of *C. elegans* biology, ranging from its ecological niche to its genomic structure and mating system is provided, as well as an introduction into the genetic tools and advantages of *C. elegans*. More in-depth summaries on relevant topics are provided in later chapters, namely **Chapter 1C, Chapter 2A**, **Chapter 3A**, and **Chapter 4A**.

Caenorhabditis elegans

The free-living roundworm, *Caenorhabditis elegans*, was first introduced to the scientific community as a model for studying genetics in 1974 by Sydney Brenner. With adults that grow to be 1 mm in length, *C. elegans* is a transparent, sexually dimorphic, eutelic animal (Brenner, 1974). Because of this trait in which there are the exact same number of somatic cells in every individual (959 cells in hermaphrodites) the developmental lineage of every cell has been mapped – from a fertilized zygote to a fully developed adult (Sulston & Horvitz, 1977). There are 302 neurons present in the *C. elegans* nervous system which, using electron-microscopy, has been mapped at the synaptic level (White, Southgate, Thomas, & Brenner, 1986) to generate an entire physical "connectome" of the worm. In contrast, the male nervous system is comprised of 385 neurons, 294 of which are shared between the sexes (Sammut et al., 2015). Recent analyses have led to the full mapping to the connectomes of both sexes (Cook et al., 2019).

C. elegans Life Cycle

C. elegans have a rapid life cycle in the lab, cycling from laid egg to egg-laying adult in approximately 3-days under standard laboratory conditions (Corsi, Wightman, & Chalfie, 2015). Post-hatching, the nematode develops through four larval stages (denoted as L1, L2, L3, and L4), before entering its final stage as an adult (conventionally divided into "young adult" [YA] and "adult").

Under unfavorable conditions, such as cover-crowding, lack of food, or increased temperature, the secreted pheromone cocktail of *C. elegans* changes (Butcher, 2017; Ludewig & Schroeder, 2013; Srinivasan et al., 2008), altering the developmental path of conspecifics in the L2 larval stage to enter what is known as the dauer state (Cassada & Russell, 1975). The worm can remain in this environmentally persistent state for up to six months. Within that time, if conditions improve and the right signals are sensed, the worm can exit dauer, and proceed to the L4 stage, bypassing the L3 stage (Ludewig & Schroeder, 2013).

The Ecological Niche of *Caenorhabditis* Nematodes

This 3-day life cycle is considered specific to laboratory conditions, wherein worms are exposed to a constant temperature of ~20 °C. In a natural habit, temperatures fluctuate wildly, resulting in slower generation times (A. D. Cutter, 2010; A. D. Cutter, Yan, Tsvetkov, Sunil, & Felix, 2010). In its natural environment, where *C. elegans* spends the majority of its life in the dauer stage, the generation time is often closer to 60-days, rather than the 3-days observed in lab settings (Asher D. Cutter, Wasmuth, & Washington, 2008). Originally described as a "soil-dwelling nematode" (Caswell-Chen et al., 2005; Gershon & Gershon, 2002; Hope, 1999; W. Wood, 1988), *C. elegans* has since been shown to instead thrive within rotting fruits and other vegetation (Caswell-Chen et al., 2005; Félix, Braendle, & Cutter, 2014; Kiontke & Fitch, 2005).

C. elegans are one of three *Caenorhabditis* nematode species that are contain hermaphrodites. These species (*C. elegans*, *C. briggsae*, and *C. tropicalis*) all employ uniquely evolved androdiecious mating systems: they are largely hermaphroditic, with an extremely small proportion of males present (Ellis & Lin, 2014; Wei, Zhao, et al., 2014). As such, *C. elegans* is largely self-fertile, with each hermaphrodite containing the ability to fertilize its own eggs with its own sperm. The remainder of the *Caenorhabditis* genus employs a gonochoristic, or male-female, mating mode (Wei, Zhao, et al., 2014).

The Genetic and Genomic Structure of *C. elegans*

The genome of *C. elegans*, which was completely mapped in 1998, is organized into five autosomes and one sex chromosome, X (Nigon, 1949). These chromosomes encode approximately 20,191 protein coding genes (Wormbase, Assembly WBcel235, Dec 2012). In order to more efficiently understand how genes are linked, each chromosome has been divided into, on average, 50 centiMorgans (cM) (Fay, 2006). A centiMorgan is a genetic "map unit" of the genome representing a 1% meiotic recombination frequency. Therefore,

genes on opposite ends of each chromosome will separate during meiosis 50% of the time, and therefore, appear genetically unlinked (Fay, 2006).

As in other nematode species, the sex of *C. elegans* is controlled by XX determining hermaphrodites and XO resulting in males (Albritton et al., 2014; Gupta, Johnsen, & Chen, 2007; Hodgkin, Horvitz, & Brenner, 1979; Pires-daSilva & Sommer, 2004; Redman et al., 2008). In males, only one sex chromosome is present, due to non-disjunction of the chromosome during meiosis. It is this imbalance of X dosage, along with the sex determination proteins HER-1, TRA-2, and TRA-1, that shapes the gene expression profile of the chromosome (Albritton et al., 2014; Zarkower, 2006). TRA-1 is the transcription factor controlling sex determination, with one of its downstream targets being the male sexual regulator, MAB-3, which is considered across arthropods and vertebrates as well (Zarkower, 2006).

C. elegans Nomenclature

Given the widespread use of *C. elegans* as a genetic model, conventions for nomenclature have been adopted by the research communicate at large (Horvitz, Brenner, Hodgkin, & Herman, 1979). The initial suggestions were presented by Horvitz et al. in 1979, with more recent additions being added via *The Worm Breeder's Gazette*. The *Gazette* (http://wbg.wormbook.org/) offers a compilation of up-to-date methods, findings, etc. which may not be relevant to published data, but is still of use to the research community as a whole. A brief explanation of the nomenclature naming systems employed by *C. elegans* researchers will make an understanding of the subsequently described research in this dissertation significantly easier.

Novel genes are given names using a system of three letters (italicized), followed by a hyphen, and a number (e.g., *unc-13*) (Richmond, Davis, & Jorgensen, 1999). If the name of the gene is due to a mutant phenotype, the letters denote the "most easily scored

phenotype", so that *unc* mutants are uncoordinated, *dpy* mutants are dumpy, and *rol* mutants are "rollers" (Brenner, 1974).

Cloned genes, or genes which have a known homolog, are named based on their roll, such as *mlc* genes, which encode Myosin Light Chain components (Anderson, 1989). Genes that encode G Protein-Coupled Receptors (GPCRs) are named based on the family of serpentine receptors to which they initially belong (i.e., *srr-7* encodes a serpentine receptor class R gene, while *srbc-64* encodes a serpentine receptor class bc gene) (Jansen et al., 1999).

Homologs of *C. elegans* genes found in species within the Rhabditis subclass – especially within the *Caenorhabditis* genus – are denoted by a two- to –three letter prefix to the gene, such that the *C. elegans* gene for *daf-22* would be specified as either *Cel-* or *Ce-daf-22*, while the *Haemonchus contortus* homolog would be *Hc-daf-22* (Y. Huang et al., 2017).

Because there are multiple alleles of each gene studied, a system to maintain consistency of alleles has been implemented. In parentheses following the gene name, the allele is presented as one or two italicized letters (denoting the lab which isolated and

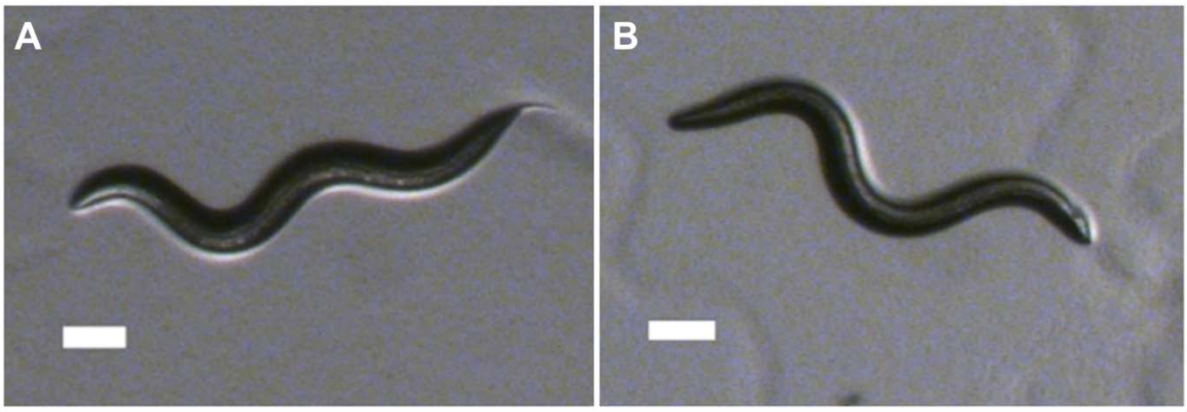

Figure 3. The sexually dimorphic morphologies of *Caenorhabditis elegans*

A. A *C. elegans* adult hermaphrodite. An adult is 1 mm in length, with a tapering tail structure. Two gonadal arms meet in the center of the animal's body length, where eggs are deposited through the vulva. **B.** A *C. elegans* adult male. Slightly shorter than an adult hermaphrodite, males are thinner, having only one gonadal arm, and no eggs within. The most distinctive feature is the male's tail, which develops as a fan-shaped structure innervated with the majority of the male-specific nervous system. Scale bars denote 0.1 mm.

registered the allele with the *Caenorhabditis* Genetics Center) and a number (e.g., *unc-13(e51)* (Richmond et al., 1999). All wild-type alleles refer to those present in the N2 wild-type strain isolated from Bristol, England, in Brenner's seminal paper (Brenner, 1974).

While genes are written in lowercase italics, the proteins they encode are written in full capitals (e.g., *unc-13* encodes UNC-13) (Richmond et al., 1999).

Nematode strains are again named according to which lab generated and isolated them. A set of letter prefixes denoted the laboratory, and the numbers denote that lab's strain ID (e.g., the strain CB4088 is a *him-5(e1490)* strain isolated in the MRC Laboratory of Molecular Biology (Hodgkin et al., 1979).

Using this nomenclature system, *C. elegans* researchers are able to consistently describe and convey information regarding the components of the systems they study. Sharing of information and reagents between labs is hereby fluid, which unvarying naming techniques making mistakes rare.

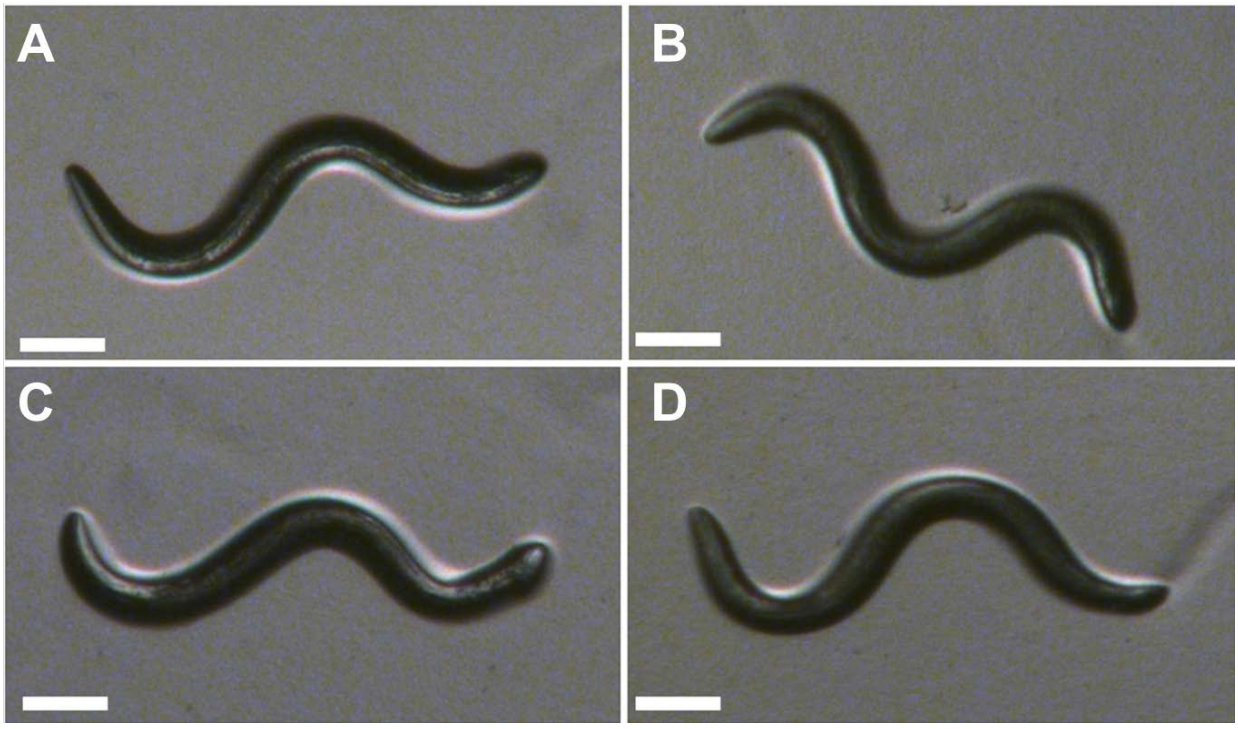

Figure 4. *Caenorhabditis* nematodes are morphologically cryptic.
. Males *Caenorhabditis* species are visually identical. **A.** *C. briggsae (him-8).* **B.** *C. tropicalis (him-8).* **C.** *C. nigoni.* **D.** *C. wallacei.* Scale bars denote 0.1 mm.

C. elegans Employs an Androdiecious Mating System

Unlike most other *Caenorhabditis* nematodes found in similar ecological niches, *C. elegans* employs an androdiecious mating system. As such, while mostly hermaphroditic, *C. elegans* does produce males (**Figure 3**). Only 0.01-0.02% of wild-type *C. elegans* populations are males, a probability dependent on the non-disjunction rate of the sex chromosome (Hodgkin et al., 1979). Within the *Caenorhabditis* genus, there are only three species that are androdiecious (*C. elegans, C. briggsae*, and *C. tropicalis*). Each evolved their hermaphroditic traits separately and uniquely (Fierst et al., 2015; Gupta et al., 2007; Poullet, Vielle, Gimond, Ferrari, & Braendle, 2015; Rodelsperger et al., 2018; Stewart & Phillips, 2002). The remainder of the genus employs a gonochoristic mating strategy, with both males and females being present (Félix et al., 2014). The nematodes of *Caenorhabditis* are morphological cryptic, with genomic analyses needed to determine species identity (**Figure 4**).

A notable exception to this rule is *C. inopinata* (formerly *C. sp. 34*), the newly characterized "sister-species" to *C. elegans* (Kanzaki et al., 2018). While *C. elegans* is the closest relative of *C. inopinata*, there is an ancient divergence between the two. *C. inopinata* is gonochoristic, and most strikingly, is nearly twice as long as *C. elegans*. (**Figure 5**).

Two Non-disjunction Mutants, *him-5* and *him-8*, Allow for Increased Amounts of Males in Populations

With such a low rate of male production, the study of males in wild-type *C. elegans* becomes tedious. As such, *him* mutant strains (high incidence of males) have been generated for the study of males. These strains are developmentally, morphologically, and behaviorally similar – if not identical – to the wild-type N2 strain, allowing their use as a wild-type background in male-based research. The two *him* strains used in this thesis dissertation are *him-5(e1490)* and *him-8(e1489)*, which generate 25% and 39% males, respectively (Hodgkin et al., 1979; Phillips et al., 2005).

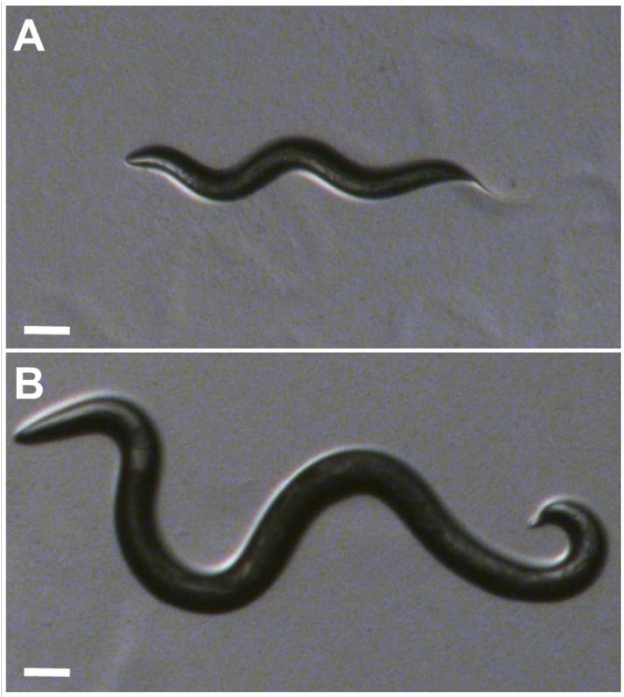

Figure 5. *C. inopinata* adults are twice as long as *C. elegans* and other *Caenorhabditis* adults.
A. A *C. elegans* adult hermaphrodite. **B.** A *C. inopinata* adult female. The adult female not proportionally wider, only longer than *C. elegans* hermaphrodites. Scale bars denote 0.1 mm.

Both recessive alleles, *him-5* and *him-8* were first discovered in a screen to identify non-disjunction mutations (Hodgkin et al., 1979). Both genes play pivotal roles in regulating X chromosome crossover during meiosis (Broverman & Meneely, 1994), with *him-5* being able to initiate double strand breaks (DSBs (Chung et al., 2015; Meneely, McGovern, Heinis, & Yanowitz, 2012)). Meneely et al. propose that the role of *him-5* (located on chromosome V) is to promote meiotic DSBs in order to rescue nondisjunction events (Meneely et al., 2012). When *him-5* is mutant, this cannot occur, and the nondisjunction rate is increased, leading to a higher proportion of male progeny. *him-8* (located on chromosome IV) encodes a zinc-finger protein that binds to the meiotic pair center of the X chromosome (Phillips et al., 2005). Similarly, in *him-8* mutants, the pairing of the X chromosomes is destabilized, resulting in more male progeny.

Throughout this thesis dissertation, both *him-5* and *him-8* strains are used as wild-type backgrounds. The use of each is dependent on the genomic location of the genes studied. For projects in which crosses are necessary to incorporate males (see **Chapter 3, Chapter**

4), the chromosomal location was crucial, and worms were crossed in a manner that avoided chromosome co-residence. For example, the gene *flp-6* is present on chromosome V, as is *him-5*. Therefore, the *flp* genes tested were all crossed into a *him-8* background, as this gene resides on chromosome IV (see **Chapter 3B**).

C. elegans is a Powerful Genetic Tool

The genome of *C. elegans* is readily accessible – the worm being the first multicellular organism to have its genome completely mapped (Consortium, 1998) – and with the advent of genome editing technologies, the generation of mutants has become commonplace in nearly every *C. elegans* laboratory (Friedland et al., 2013; Sugi, 2016; A. J. Wood et al., 2011). Taking advantage of these many traits, researchers have used *C. elegans* to propel our understanding of both basic and complicated biological systems forward at a rapid pace.

Initially mutants were generated by EMS screens (Brenner, 1974; Hodgkin et al., 1979), and uncovered a fair portion of the nematode's genome. However, more targeted approaches to genetic manipulations require directed techniques. As such, the advent of zinc-finger nucleases (ZFNs) into *C. elegans* research shortly after the new millennium (Morton, Davis, Jorgensen, & Carroll, 2006; A. J. Wood et al., 2011) saw an explosion of gene editing in both *C. elegans* and *C. briggsae*, both of which exhibited heritable genome edits (Morton et al., 2006; Wei, Shen, Chen, Shifman, & Ellis, 2014).

TALENs (transcription activator-like effector nucleases) were incorporated into *C. elegans* biology around the same time, allowing for editing with few limitations – barring an upfront, laborious design phase (Lo et al., 2013; Sugi, 2016; Wei, Shen, et al., 2014; A. J. Wood et al., 2011).

The more recent revolution of CRISPR/Cas9 based editing (Vinci Au et al., 2019; Dickinson & Goldstein, 2016; Farboud, 2017; Friedland et al., 2013; Gaj, Gersbach, & Barbas Iii, 2013; Lo et al., 2013; H. T. Schwartz & Sternberg, 2014; Silas et al., 2016) allows

for, not only, the generation of targeted mutations within the genes themselves, but the incorporation of rescue alleles and markers, such as GFP (Sugi, 2016). While TALENs were initially able to generate mutations in 1.1% of F1 progeny, current CRISPR techniques generate upwards of 85% success in generating homozygous, targeted deletions within three generations of injection (V. Au et al., 2019).

As a whole, development of transgenic animals is now a simple process. In 1986, Fire et al. showed injection of extrachromosomal material into maturing oocytes within the gonadal arms of *C. elegans* results in heritable transfer of the novel genetic material (Andrew Fire, 1986). In 1991, Mello et al. released a seminal paper expanding on that technique, including co-injection markers and analyzed the formation and heritability of transgenic extrachromosomal arrays (Mello, Kramer, Stinchcomb, & Ambros, 1991). It was this technique that lead to the Nobel Prize winning elucidation of double-strand RNA (dsRNA) mediated genetic interference (RNAi) (A. Fire et al., 1998), which is now an indispensable technique not only in *C. elegans*, but all fields of biological research.

Using injection techniques to create transgenic animals, *C. elegans* researchers have been able to produce rescue strains, marker strains (using GFP to examine expression profiles of gene promoters), and imaging strains. These imaging strains utilize genetically encoded calcium indicators (GECIs) to visualize neuronal activity in real-time, in live animals (Akerboom et al., 2012; Chronis, 2010; Chronis, Zimmer, & Bargmann, 2007; Sun et al., 2013). The most common GECI utilized is GCaMP, although red-shifted indicators are also commonly used. A more in-depth overview of GECIs is provided in **Chapter 4B** (Reilly, Lawler, Albrecht, & Srinivasan, 2017).

***C. elegans* Behavior**

C. elegans have been found to exhibit robust behaviors, taxis to and from odorants and also socially driven interactions (Hart, 2006). Among the earliest quantifications of nematode behavior was their ability to navigate up the concentration gradient of an

attractive cue (Ward, 1973). As the analysis of this behavior was optimized, the now-canonical chemotaxis assay was developed (Bargmann, Hartwieg, & Horvitz, 1993). Avoidance behaviors have been quantified using modified versions of the same assay, drop tests, and holding assays (Chute et al., 2019; Hilliard, Bergamasco, Arbucci, Plasterk, & Bazzicalupo, 2004). A more in-depth description of *C. elegans* behaviors analyzed by such assays is provided in **Chapter 1C** (Reilly & Srinivasan, 2017) of this thesis dissertation.

The natural behaviors observed in *C. elegans* are inherent to the wild-type strain to which they are compared. Unless noted otherwise, the wild-type strain utilized in *C. elegans* research is the N2 strain, isolated from Bristol, UK (Brenner, 1974). N2 are relatively solitary animals, while worms of the wild isolate CB4856 from Hawaii, USA are considered more "social" animals (Thompson et al., 2015). These worms will aggregate in large clumps of conspecifics, as opposed to N2 animals that roam the plate. Notably, this aggregation can be attributed to a polymorphism in CB4856's *npr-1* gene locus. This gene has been shown (in an N2 background) to regulate dispersal versus aggregation on the edges of bacterial lawns (Andersen, Bloom, Gerke, & Kruglyak, 2014).

While the *npr-1* gene drives the noticeable behavioral difference between N2 and CB4856 (Andersen et al., 2014), there a remarkable number of differences in the genomes of each strain that are not visible as obvious behavioral phenotypes (Thompson et al., 2015; Vergara et al., 2014). For example, the Hawaii isolate is resilient against RNAi, compared to N2's susceptibility to dsRNA-meditated knockdown. This can be attributed to a polymorphism in the *ppw-1* gene of Hawaii animals (Tijsterman, Okihara, Thijssen, & Plasterk, 2002).

However, both the Bristol and Hawaii strains are wild isolates, neither being a "mutant" strain. It is therefore to take the background isolate into consideration when making any claims as to the "natural state" on species.

Neuromodulation of C. elegans Behavior

The ability of *C. elegans* to interact with its environment, in a manner that best ensures survival, is affected via neuromodulation of the neural networks governing behaviors (Williams et al., 2017). Classical neurotransmitters and neuropeptides play a variety of roles in regulating neural circuits (Huang, Sun, Zhang, Deng, & Peng, 2017). Alongside dopamine and serotonin, the *C. elegans* nervous system employs tyramine and octopamine as monoaminergic analogs of the mammalian epinephrine and norepinephrine (Bauknecht & Jekely, 2017). Glutamate has likewise been shown to regulate the behavioral responses of nematodes (R. Y. Lee, Sawin, Chalfie, Horvitz, & Avery, 1999).

A much broader array of neuromodulatory signals is found in *C. elegans*' peptidergic system. There are over 130 genes encoding nearly 400 neuropeptide sequences within the nematode genome (Li & Kim, 2008; Van Bael, Edwards, Husson, & Temmerman, 2018; Sven Van Bael et al., 2018). This results in an extremely complex and fascinating array of modulatory networks, with many peoples acting in synergy (Serrano-Saiz et al., 2017).

The three main classes of neuropeptides are the insulin-like peptides (INS), the FMRFamide-like peptides (FLP), and the non-insulin/non-FLP-like peptides (NLP) (Li & Kim, 2008). The INS system signals through the DAF-2 receptor, as both antagonists and agonists (Zhang, Gao, Chen, & Tu, 2018). Still, the INS system is able to affect the physiological responses of sensory neurons to olfactory cues, learning, behavior, synapse formation, and more (**Chapter 3A**). The FLP and NLP families of neuropeptides are more intertwined in their biology and outcomes than the INS system, affecting locomotion, reproduction, olfaction, sleep, and lipid metabolism through related receptors and neural circuits (**Chapter 3A**).

Chapter 3B of this dissertation focuses on role of FLP genes in the behavioral response of adult male *C. elegans* to a mating pheromone. Multiple *flp* genes have been shown to play a role in regulating the physical aspect of mating, namely the turning behavior

stereotypical of a male *C. elegans* locating the vulva of its potential mate (Liu, Kim, Li, & Barr, 2007). In **Chapter 3B**, we elucidate the role of *flp-3*, a gene encoding a precursor product with ten unique processed peptide sequences (S. Van Bael et al., 2018). We show that the peptides function to control the male-specific behavioral response. Interestingly, only two of the ten peptides are shown to be involved in regulating the behavior (**Chapter 3B**).

C. elegans Development

The eutelic nature of *C. elegans* drives many of its advantageous features. Because the lineage of every cell has been traced (both pre- and post- hatching), genes which control the proper development of *C. elegans* are easily studied (Sulston & Horvitz, 1977; Sulston, Schierenberg, White, & Thomson, 1983).

Among the first genes isolated in Brenner's first EMS screen were "dumpy" (*dpy*), "small" (*sma*), and "long" (*lon*) mutants (Brenner, 1974). These gene names are descriptive of the morphological phenotype observed in these mutants. One of the most common, and widely utilized, "class" of mutations in *C. elegans* are the "uncoordinated", or *unc*, mutants. Mutants that result in uncoordinated animals may be due to improper development, or a nervous system malfunction (i.e., the inability to communicate via synaptic transmission).

In the decades since Brenner's introduction of *C. elegans* a model organism, a plethora of studies have uncovered vast amounts of detail concerning the worm's development. Summaries of these can be found in the peer-reviewed, open-access resource, WormBook (www.wormbook.com). Focusing on the material needed to fully understand this thesis dissertation, a brief overview will be provided in regard to neuronal development and sex-determination.

Neuronal Development

The hermaphroditic nervous system of *C. elegans* invariably has 302 neurons (and 385 in a male) (Sammut et al., 2015; White et al., 1986). The developmental programming for this system must therefore be extremely specific and error-proof. This becomes even more astounding when one realizes that neurons are, as Hobert, when looking at Sulston's cell lineages (Sulston et al., 1983) points out: "are largely non-clonally derived from many different lineages" (O. Hobert, 2010). Because cells are not committed until the "terminal cell division", the transcriptional regulators controlling cell-fate are unique to each cell class (Horvitz & Sulston, 1980).

The 302 adult neurons are organized into 118 neuron classes, based on the electron microscopy studies of White and colleagues in 1986 (White et al., 1986). Among these, there are many neurons that exhibit left-right symmetry (e.g. the amphid sensory neurons). The neurons that comprise these pairs do not often share common ancestral cells. Instead, the development split between "left" and "right" occurs extremely early in development, as opposed to immediately prior to the terminal cell division (Horvitz & Sulston, 1980; Sulston et al., 1983).

Transcription factors have been isolated (through genetic screens) which, when mutated, result in incomplete – or failed – differentiation into the terminal neuronal identity (**Table 1**). These transcription factors play a role as "master regulators" and have been termed "terminal selectors" because of their prominent roles in determining final differentiation of these neurons (Oliver Hobert, 2008; O. Hobert, 2016).

There are, of course, other transcriptional regulators that function in these cells throughout development that steer the course of differentiation. For example, the transcription factors *zag-1* and *ceh-28* work in conjunction to lead to proper differentiation of the pharyngeal M4 neuron (Ramakrishnan & Okkema, 2014).

Male-Specific Neuronal Development

Male *C. elegans*, with their imbalanced X chromosome dosage, develop under a unique set of transcription factors. This results in 91 male-specific neurons (along with another 116 somatic cells) (Emmons, 2005). In addition to male-specific neurons, the developmental sex-deterministic transcriptional profile in the male results in sex-shared neurons exhibiting unique profiles in the male (Fagan et al., 2018).

The majority of these male-specific neurons develop in the tail, forming the sensory sensilla involved in mating. This structure is comprised of "hook," "ray," "spicule," and "post-cloacal" sensilla (Emmons, 2005). Each ray no longer develops as a left-right pair, but an A-B pair, developing into a total of 36 sensory cells. A host of transcription factors that are involved in the proper development of the male sensory sensilla have been determined.

Table 1. Transcription factors involved in development of the male-tail sensilla.

Transcription Factor	Role in Cell-Fate Determination	References
lin-32	Ray development	**1, 2, 3**
mab-5	Separates Ray 1 from Ray 2	**4**
hlh-2	Functions alongside *lin-32*	**5**
mab-3	Male-specific Regulatory Transcription Factor	**6, 7**
egl-5	Promotes Ray 3 identity	**8, 9, 10, 11**
mab-18	Differentiations Ray 6	**12**

Transcription factors regulating male sensilla development shown with corresponding facets of differentiation and determination of cell identity. References: **1** (Ferreira et al., 1999); **2** (Kenyon, 1986); **3** (Zhao & Emmons, 1995); **4** (Salser & Kenyon, 1996); **5** (Portman & Emmons, 2000); **6** (Shen & Hodgkin, 1988); **7** (Yi et al., 2000); **8** (Chow & Emmons, 1994); **9** (Chow et al., 1995); **10** (Lints & Emmons, 1999); **11** (Lints & Emmons, 2002); **12** (Zhang & Emmons, 1995).

There are six neurons in the head of the male which are sex-specific as well. Two of these are glial derived interneurons that play a role in learning (Sammut et al., 2015). The remaining four neurons comprise a single class of radially symmetric neurons. These CEM neurons are born embryonically in both sexes and die off during larval development in the hermaphrodite. Through gain-of-function (*gof*) and loss-of-function (*lof*) mutations, two independent groups simultaneously uncovered the role of the BarH

homeodomain protein encoded by *ceh-30* in protecting the CEM neurons during male development (Peden, Kimberly, Gengyo-Ando, Mitani, & Xue, 2007; Hillel Tsvi Schwartz, 2009; H. T. Schwartz & Horvitz, 2007). They were able to prevent these neurons from undergoing apoptosis during hermaphroditic development, as well as cause them to die off during male development (Peden et al., 2007; H. T. Schwartz & Horvitz, 2007). Using the promoter for the mechanosensory protein, *pkd-2*, the CEM neurons (along with neurons in the tail), can be labeled using GFP (**Figure 6A**).

We have shown, in our own lab, that these male-specific neurons are involved in pheromone sensation. When expressed in hermaphrodites using a *gof* mutation, hermaphrodites no longer ignore mating pheromone ascr#8, but are instead attracted, similar to males (**Figure 6B**). Males exhibiting a *lof* mutation show a decrease in sensation, not a total loss (**Figure 6B**). However, this is likely due to the incomplete penetrance of the mutation, as well as the role of other sensory neurons in responding to the pheromone.

Conclusions

The nematode *Caenorhabditis elegans* is a powerful biological tool. Not only is its entire genome mapped and well annotated, but the genomes of related species within the genus are growing increasingly annotated. This allows for high powered comparative studies, construction of strong phylogenies for genes of interest, and follow-up studies (A. D. Cutter, 2010; Fierst et al., 2015; Gupta et al., 2007; Kanzaki et al., 2018; Thompson et al., 2015; Vergara et al., 2014). Insights into the mechanisms driving the evolution of self-fertilization are able to be gleaned from comparisons between androdiecious nematodes and their gonochoristic kin (Asher D. Cutter et al., 2008; Ellis & Lin, 2014; Fierst et al., 2015; Kanzaki et al., 2018; Kiontke & Fitch, 2005; Pires-daSilva & Sommer, 2004). Even variations among *C. elegans* isolates provide novel clues into how the biological systems function within the nematode (Thompson et al., 2015).

Outside of evolutionary insights, *C. elegans* offers the opportunity to rapidly develop novel techniques aiding in the study of basic biologic mechanisms, from the discovery of RNAi, even microRNAs, (another ode to *C. elegans*) (A. Fire et al., 1998; R. C. Lee & Ambros, 2001) to GECI and microfluidic tools for imaging live neurons (Akerboom et al., 2012; Chronis et al., 2007; Reilly et al., 2017). Recent advances have even developed

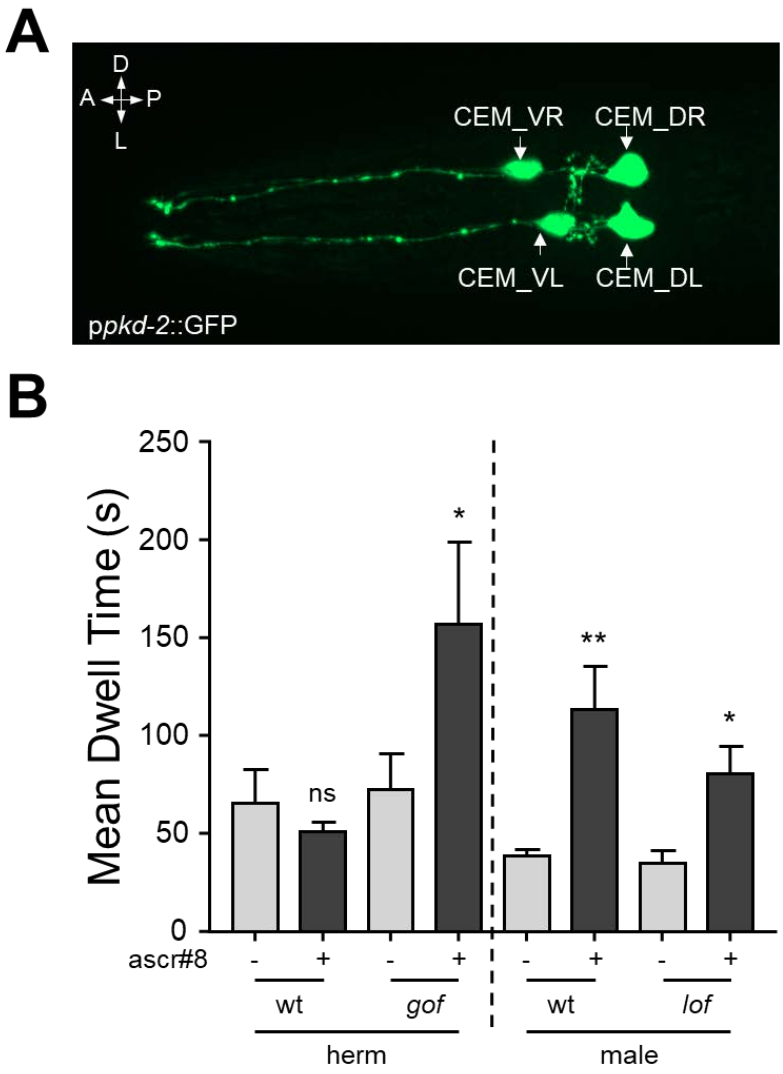

Figure 6. The CEM neurons play a role in mating pheromone response.
A. The CEM neurons can be labeled using a promoter for *pkd-2* (p*pkd-2*::GFP). Radially symmetric neurons can be visualized, with each dorsal-ventral pair containing a left-right member. **B.** *ceh-30* controls CEM development and affects pheromone response. In hermaphrodites, expression a *gof* mutation for *ceh-30*, wherein the CEM neurons are still present, hermaphrodites response attractively to a mating pheromone, ascr#8, which wild-type animals seem to ignore. Wild-type males are attracted to the cue, while *lof* males show a slight decrease in response. Error bars denote SEM. n ≥ 9. Paired t-tests of "-" vs "+" ("-" being solvent control and "+" being the pheromone ascr#8). * $p < 0.05$, ** $p < 0.01$.

techniques for imaging calcium transients in freely moving animals, thereby bypassing any effects that may be inherent to trapping of animals within microfluidic devices (Hums et al., 2016; Skora, Mende, & Zimmer, 2018; Venkatachalam et al., 2016).

Utilizing all of the advantages offered by the powerful nematode *Caenorhabditis elegans*, this thesis dissertation will aim to elucidate some facets governing neuromodulation of a network responsible for the sensation and behavioral response to the sex-specific mate recognition pheromone, ascaroside #8 (Narayan et al., 2016; Pungaliya et al., 2009). This work will combine:

- Genetic tools (such as *lof* mutants, transgenics, and CRISPR – **see Chapter 1** and **Chapter 4**)
- Imaging techniques (see **Chapter 4B** (Reilly et al., 2017))
- Phylogenic analyses (see **Chapter 4C**)
- Comparative studies (see **Chapter 6** (Reilly, Randle, & Srinivasan, 2019))

Together, these studies build a strong foundation for studying sex-specific sensation and neuromodulation.

References

Akerboom, J., Chen, T.-W., Wardill, T. J., Tian, L., Marvin, J. S., Mutlu, S., . . . Looger, L. L. (2012). Optimization of a GCaMP calcium indicator for neural activity imaging. *The Journal of Neuroscience, 32*(40), 13819-13840. doi:10.1523/JNEUROSCI.2601-12.2012

Albritton, S. E., Kranz, A. L., Rao, P., Kramer, M., Dieterich, C., & Ercan, S. (2014). Sex-biased gene expression and evolution of the x chromosome in nematodes. *Genetics, 197*(3), 865-883. doi:10.1534/genetics.114.163311

Andersen, E. C., Bloom, J. S., Gerke, J. P., & Kruglyak, L. (2014). A Variant in the Neuropeptide Receptor npr-1 is a Major Determinant of Caenorhabditis elegans Growth and Physiology. *PLOS Genetics, 10*(2), e1004156. doi:10.1371/journal.pgen.1004156

Anderson, P. (1989). Molecular genetics of nematode muscle. *Annu Rev Genet, 23*, 507-525. doi:10.1146/annurev.ge.23.120189.002451

Au, V., Li-Leger, E., Raymant, G., Flibotte, S., Chen, G., Martin, K., . . . Moerman, D. G. (2019). CRISPR/Cas9 Methodology for the Generation of Knockout Deletions in *Caenorhabditis elegans*. *G3 (Bethesda), 9*(1), 135-144. doi:10.1534/g3.118.200778

Au, V., Li-Leger, E., Raymant, G., Flibotte, S., Chen, G., Martin, K., . . . Moerman, D. G. (2019). CRISPR/Cas9 Methodology for the Generation of Knockout Deletions in *Caenorhabditis elegans*. *G3: Genes|Genomes|Genetics, 9*(1), 135. doi:10.1534/g3.118.200778

Bargmann, C. I., Hartwieg, E., & Horvitz, H. R. (1993). Odorant-selective genes and neurons mediate olfaction in C. elegans. *Cell, 74*(3), 515-527. doi:10.1016/0092-8674(93)80053-H

Bauknecht, P., & Jekely, G. (2017). Ancient coexistence of norepinephrine, tyramine, and octopamine signaling in bilaterians. *BMC Biol, 15*(1), 6. doi:10.1186/s12915-016-0341-7

Brenner, S. (1974). The Genetics of *Caenorhabditis elegans*. *Genetics, 77*(1), 71-94.

Broverman, S. A., & Meneely, P. M. (1994). Meiotic mutants that cause a polar decrease in recombination on the X chromosome in Caenorhabditis elegans. *Genetics, 136*(1), 119-127.

Butcher, R. A. (2017). Small-molecule pheromones and hormones controlling nematode development. *Nat Chem Biol, 13*(6), 577-586. doi:10.1038/nchembio.2356d

Cassada, R. C., & Russell, R. L. (1975). The dauerlarva, a post-embryonic developmental variant of the nematode Caenorhabditis elegans. *Developmental Biology, 46*(2), 326-342. doi:10.1016/0012-1606(75)90109-8

Caswell-Chen, E. P., Chen, J., Lewis, E. E., Douhan, G. W., Nadler, S. A., & Carey, J. R. (2005). Revising the standard wisdom of C. elegans natural history: ecology of longevity. *Science of aging knowledge environment : SAGE KE, 2005*(40), pe30-pe30. doi:10.1126/sageke.2005.40.pe30

Chronis, N. (2010). Worm chips: Microtools for C. elegans biology. *Lab on a Chip, 10*(4), 432-437. doi:10.1039/B919983G

Chronis, N., Zimmer, M., & Bargmann, C. I. (2007). Microfluidics for in vivo imaging of neuronal and behavioral activity in *Caenorhabditis elegans*. *Nat Meth, 4*(9), 727-731. doi:10.1038/nmeth1075

Chung, G., Rose, A. M., Petalcorin, M. I., Martin, J. S., Kessler, Z., Sanchez-Pulido, L., . . . Boulton, S. J. (2015). REC-1 and HIM-5 distribute meiotic crossovers and function redundantly in meiotic double-strand break formation in Caenorhabditis elegans. *Genes Dev, 29*(18), 1969-1979. doi:10.1101/gad.266056.115

Chute, C. D., DiLoreto, E. M., Zhang, Y. K., Reilly, D. K., Rayes, D., Coyle, V. L., . . . Srinivasan, J. (2019). Co-option of neurotransmitter signaling for inter-organismal communication in *C. elegans*. *Nat Commun, 10*(1), 3186. doi:10.1038/s41467-019-11240-7

Consortium, T. C. e. S. (1998). Genome Sequence of the Nematode *C. elegans*: A Platform for Investigating Biology. *Science, 282*(5396), 2012. doi:10.1126/science.282.5396.2012

Cook, S. J., Jarrell, T. A., Brittin, C. A., Wang, Y., Bloniarz, A. E., Yakovlev, M. A., . . . Emmons, S. W. (2019). Whole-animal connectomes of both Caenorhabditis elegans sexes. *Nature, 571*(7763), 63-71. doi:10.1038/s41586-019-1352-7

Corsi, A. K., Wightman, B., & Chalfie, M. (2015). A Transparent window into biology: A primer on Caenorhabditis elegans. *WormBook*, 1-31. doi:10.1895/wormbook.1.177.1

Cutter, A. D. (2010). Molecular evolution inferences from the *C. elegans* genome. *WormBook*, 1-14. doi:10.1895/wormbook.1.149.1

Cutter, A. D., Wasmuth, J. D., & Washington, N. L. (2008). Patterns of molecular evolution in Caenorhabditis preclude ancient origins of selfing. *Genetics, 178*(4), 2093-2104. doi:10.1534/genetics.107.085787

Cutter, A. D., Yan, W., Tsvetkov, N., Sunil, S., & Felix, M. A. (2010). Molecular population genetics and phenotypic sensitivity to ethanol for a globally diverse sample of the nematode *Caenorhabditis briggsae*. *Mol Ecol, 19*(4), 798-809. doi:10.1111/j.1365-294X.2009.04491.x

Dickinson, D. J., & Goldstein, B. (2016). CRISPR-Based Methods for Caenorhabditis elegans Genome Engineering. *Genetics, 202*(3), 885. doi:10.1534/genetics.115.182162

Ellis, R. E., & Lin, S. Y. (2014). The evolutionary origins and consequences of self-fertility in nematodes. *F1000Prime Rep, 6*, 62. doi:10.12703/p6-62

Emmons, S. W. (2005). Male development. *WormBook*, 1-22. doi:10.1895/wormbook.1.33.1

Fagan, K. A., Luo, J., Lagoy, R. C., Schroeder, F. C., Albrecht, D. R., & Portman, D. S. (2018). A Single-Neuron Chemosensory Switch Determines the Valence of a Sexually Dimorphic Sensory Behavior. *Curr Biol, 28*(6), 902-914.e905. doi:10.1016/j.cub.2018.02.029

Farboud, B. (2017). Targeted genome editing in Caenorhabditis elegans using CRISPR/Cas9. *Wiley Interdiscip Rev Dev Biol, 6*(6). doi:10.1002/wdev.287

Fay, D. (2006). Genetic mapping and manipulation: chapter 1--Introduction and basics. *WormBook*, 1-12. doi:10.1895/wormbook.1.90.1

Félix, M.-A., Braendle, C., & Cutter, A. D. (2014). A Streamlined System for Species Diagnosis in *Caenorhabditis* (Nematoda: Rhabditidae) with Name Designations for 15 Distinct Biological Species. *PLoS One, 9*(4), e94723. doi:10.1371/journal.pone.0094723

Fierst, J. L., Willis, J. H., Thomas, C. G., Wang, W., Reynolds, R. M., Ahearne, T. E., . . . Phillips, P. C. (2015). Reproductive Mode and the Evolution of Genome Size and Structure in Caenorhabditis Nematodes. *PLoS Genet, 11*(6), e1005323. doi:10.1371/journal.pgen.1005323

Fire, A. (1986). Integrative transformation of Caenorhabditis elegans. *The EMBO Journal, 5*(10), 2673-2680.

Fire, A., Xu, S., Montgomery, M. K., Kostas, S. A., Driver, S. E., & Mello, C. C. (1998). Potent and specific genetic interference by double-stranded RNA in *Caenorhabditis elegans*. *Nature, 391*. doi:10.1038/35888

Friedland, A. E., Tzur, Y. B., Esvelt, K. M., Colaiacovo, M. P., Church, G. M., & Calarco, J. A. (2013). Heritable genome editing in C. elegans via a CRISPR-Cas9 system. *Nat Meth, 10*(8), 741-743. doi:10.1038/nmeth.2532

Gaj, T., Gersbach, C. A., & Barbas Iii, C. F. (2013). ZFN, TALEN, and CRISPR/Cas-based methods for genome engineering. *Trends in Biotechnology, 31*(7), 397-405. doi:10.1016/j.tibtech.2013.04.004

Gershon, H., & Gershon, D. (2002). Caenorhabditis elegans--a paradigm for aging research: advantages and limitations. *Mech Ageing Dev, 123*(4), 261-274.

Gupta, B. P., Johnsen, R., & Chen, N. (2007). Genomics and biology of the nematode Caenorhabditis briggsae. *WormBook*, 1-16. doi:10.1895/wormbook.1.136.1

Hart, A. C. (2006). Behavior. *WormBook*. doi: doi/10.1895/wormbook.1.87.1

Hilliard, M. A., Bergamasco, C., Arbucci, S., Plasterk, R. H. A., & Bazzicalupo, P. (2004). Worms taste bitter: ASH neurons, QUI-1, GPA-3 and ODR-3 mediate quinine avoidance in *Caenorhabditis elegans*. *The EMBO Journal, 23*(5), 1101-1111. doi:10.1038/sj.emboj.7600107

Hobert, O. (2008). Regulatory logic of neuronal diversity: Terminal selector genes and selector motifs. *Proceedings of the National Academy of Sciences, 105*(51), 20067. doi:10.1073/pnas.0806070105

Hobert, O. (2010). Neurogenesis in the nematode Caenorhabditis elegans. *WormBook*, 1-24. doi:10.1895/wormbook.1.12.2

Hobert, O. (2016). A map of terminal regulators of neuronal identity in Caenorhabditis elegans. *Wiley Interdiscip Rev Dev Biol, 5*(4), 474-498. doi:10.1002/wdev.233

Hodgkin, J., Horvitz, H. R., & Brenner, S. (1979). Nondisjunction Mutants of the Nematode *Caenorhabditis elegans*. *Genetics, 91*(1), 67-94.

Hope, I. A. (1999). *C. elegans: a practical approach* (Vol. 213): OUP Oxford.

Horvitz, H. R., Brenner, S., Hodgkin, J., & Herman, R. K. (1979). A uniform genetic nomenclature for the nematode Caenorhabditis elegans. *Mol Gen Genet, 175*(2), 129-133. doi:10.1007/bf00425528

Horvitz, H. R., & Sulston, J. E. (1980). Isolation and genetic characterization of cell-lineage mutants of the nematode Caenorhabditis elegans. *Genetics, 96*(2), 435-454.

Huang, T., Sun, Y., Zhang, Z., Deng, S., & Peng, R. (2017). Monoamine and neuropeptide connections significantly alter the degree distributions of the Caenorhabditis elegans connectome. *Neuroreport, 28*(16), 1071-1077. doi:10.1097/wnr.0000000000000875

Huang, Y., Zheng, X., Zhang, H., Ding, H., Guo, X., Yang, Y., . . . Du, A. (2017). Site-Directed Mutagenesis Study Revealed Three Important Residues in Hc-DAF-22, a

Key Enzyme Regulating Diapause of Haemonchus contortus. *Front Microbiol, 8*, 2176. doi:10.3389/fmicb.2017.02176

Hums, I., Riedl, J., Mende, F., Kato, S., Kaplan, H. S., Latham, R., . . . Zimmer, M. (2016). Regulation of two motor patterns enables the gradual adjustment of locomotion strategy in Caenorhabditis elegans. *eLife, 5*. doi:10.7554/eLife.14116

Jansen, G., Thijssen, K. L., Werner, P., van derHorst, M., Hazendonk, E., & Plasterk, R. H. A. (1999). The complete family of genes encoding G proteins of *Caenorhabditis elegans*. *Nat Genet, 21*(4), 414-419. doi:10.1038/7753

Kanzaki, N., Tsai, I. J., Tanaka, R., Hunt, V. L., Liu, D., Tsuyama, K., . . . Kikuchi, T. (2018). Biology and genome of a newly discovered sibling species of *Caenorhabditis elegans*. *Nature Communications, 9*(1), 3216-3216. doi:10.1038/s41467-018-05712-5

Kiontke, K., & Fitch, D. H. (2005). The phylogenetic relationships of Caenorhabditis and other rhabditids. *WormBook*, 1-11. doi:10.1895/wormbook.1.11.1

Lee, R. C., & Ambros, V. (2001). An extensive class of small RNAs in Caenorhabditis elegans. *Science, 294*(5543), 862-864. doi:10.1126/science.1065329

Lee, R. Y., Sawin, E. R., Chalfie, M., Horvitz, H. R., & Avery, L. (1999). EAT-4, a homolog of a mammalian sodium-dependent inorganic phosphate cotransporter, is necessary for glutamatergic neurotransmission in *Caenorhabditis elegans*. *J Neurosci, 19*(1), 159-167.

Li, C., & Kim, K. (2008). Neuropeptides. *WormBook*. doi:10.1895/workbook.1.142.1

Liu, T., Kim, K., Li, C., & Barr, M. M. (2007). FMRFamide-like neuropeptides and mechanosensory touch receptor neurons regulate male sexual turning behavior in *Caenorhabditis elegans*. *J Neurosci, 27*(27), 7174-7182. doi:10.1523/JNEUROSCI.1405-07.2007

Lo, T. W., Pickle, C. S., Lin, S., Ralston, E. J., Gurling, M., Schartner, C. M., . . . Meyer, B. J. (2013). Precise and heritable genome editing in evolutionarily diverse nematodes

using TALENs and CRISPR/Cas9 to engineer insertions and deletions. *Genetics, 195*(2), 331-348. doi:10.1534/genetics.113.155382

Ludewig, A. H., & Schroeder, F. C. (2013). Ascaroside signaling in *C. elegans*. *WormBook*, 1-22. doi:10.1895/wormbook.1.155.1

Mello, C. C., Kramer, J. M., Stinchcomb, D., & Ambros, V. (1991). Efficient gene transfer in *C.elegans*: extrachromosomal maintenance and integration of transforming sequences. *The EMBO Journal, 10*(12), 3959-3970. doi:10.1002/j.1460-2075.1991.tb04966.x

Meneely, P. M., McGovern, O. L., Heinis, F. I., & Yanowitz, J. L. (2012). Crossover distribution and frequency are regulated by him-5 in Caenorhabditis elegans. *Genetics, 190*(4), 1251-1266. doi:10.1534/genetics.111.137463

Morton, J., Davis, M. W., Jorgensen, E. M., & Carroll, D. (2006). Induction and repair of zinc-finger nuclease-targeted double-strand breaks in Caenorhabditis elegans somatic cells. *Proc Natl Acad Sci U S A, 103*(44), 16370-16375. doi:10.1073/pnas.0605633103

Narayan, A., Venkatachalam, V., Durak, O., Reilly, D. K., Bose, N., Schroeder, F. C., . . . Sternberg, P. W. (2016). Contrasting responses within a single neuron class enable sex-specific attraction in *Caenorhabditis elegans*. *Proc Natl Acad Sci U S A, 113*(10), E1392-1401. doi:10.1073/pnas.1600786113

Nigon, V. (1949). Les modalites de la reproduction et le determinisme due sexe chez quelques nematodes libres. *Ann. Sci. Nat., 11*, 1-132.

Peden, E., Kimberly, E., Gengyo-Ando, K., Mitani, S., & Xue, D. (2007). Control of sex-specific apoptosis in *C. elegans* by the BarH homeodomain protein CEH-30 and the transcriptional repressor UNC-37/Groucho. *Genes Dev, 21*(23), 3195-3207. doi:10.1101/gad.1607807

Phillips, C. M., Wong, C., Bhalla, N., Carlton, P. M., Weiser, P., Meneely, P. M., & Dernburg, A. F. (2005). HIM-8 binds to the X chromosome pairing center and

mediates chromosome-specific meiotic synapsis. *Cell, 123*(6), 1051-1063. doi:10.1016/j.cell.2005.09.035

Pires-daSilva, A., & Sommer, R. J. (2004). Conservation of the global sex determination gene tra-1 in distantly related nematodes. *Genes Dev, 18*(10), 1198-1208. doi:10.1101/gad.293504

Poullet, N., Vielle, A., Gimond, C., Ferrari, C., & Braendle, C. (2015). Evolutionarily divergent thermal sensitivity of germline development and fertility in hermaphroditic Caenorhabditis nematodes. *Evol Dev, 17*(6), 380-397. doi:10.1111/ede.12170

Pungaliya, C., Srinivasan, J., Fox, B. W., Malik, R. U., Ludewig, A. H., Sternberg, P. W., & Schroeder, F. C. (2009). A shortcut to identifying small molecule signals that regulate behavior and development in *Caenorhabditis elegans*. *Proceedings of the National Academy of Sciences of the United States of America, 106*(19), 7708-7713. doi:10.1073/pnas.0811918106

Ramakrishnan, K., & Okkema, P. G. (2014). Regulation of C. elegans neuronal differentiation by the ZEB-family factor ZAG-1 and the NK-2 homeodomain factor CEH-28. *PLoS One, 9*(12), e113893. doi:10.1371/journal.pone.0113893

Redman, E., Grillo, V., Saunders, G., Packard, E., Jackson, F., Berriman, M., & Gilleard, J. S. (2008). Genetics of mating and sex determination in the parasitic nematode Haemonchus contortus. *Genetics, 180*(4), 1877-1887. doi:10.1534/genetics.108.094623

Reilly, D. K., Lawler, D. E., Albrecht, D. R., & Srinivasan, J. (2017). Using an Adapted Microfluidic Olfactory Chip for the Imaging of Neuronal Activity in Response to Pheromones in Male *C. Elegans* Head Neurons. *Journal of Visualized Experiments*(127), e56026. doi:doi:10.3791/56026

Reilly, D. K., Randle, L. J., & Srinivasan, J. (2019). Evolution of hermaphroditism decreases efficacy of Ascaroside#8-mediated mate attraction in *Caenorhabditis* nematodes. *microPublication Biology*. doi:10.17912/micropub.biology.000134

Reilly, D. K., & Srinivasan, J. (2017). *Caenorhabditis elegans* Olfaction. doi:10.1093/acrefore/9780190264086.013.191

Richmond, J. E., Davis, W. S., & Jorgensen, E. M. (1999). UNC-13 is required for synaptic vesicle fusion in C. elegans. *Nature Neuroscience, 2*(11), 959-964. doi:10.1038/14755

Rodelsperger, C., Roseler, W., Prabh, N., Yoshida, K., Weiler, C., Herrmann, M., & Sommer, R. J. (2018). Phylotranscriptomics of Pristionchus Nematodes Reveals Parallel Gene Loss in Six Hermaphroditic Lineages. *Curr Biol, 28*(19), 3123-3127.e3125. doi:10.1016/j.cub.2018.07.041

Sammut, M., Cook, S. J., Nguyen, K. C. Q., Felton, T., Hall, D. H., Emmons, S. W., . . . Barrios, A. (2015). Glia-derived neurons are required for sex-specific learning in C. elegans. *Nature, 526*(7573), 385-390. doi:10.1038/nature15700

Schwartz, H. T. (2009). *The genetics of the sexually dimorphic deaths of the C. elegans CEM neutrons.* Massachusetts Institute of Technology,

Schwartz, H. T., & Horvitz, H. R. (2007). The *C. elegans* protein CEH-30 protects male-specific neurons from apoptosis independently of the Bcl-2 homolog CED-9. *Genes Dev, 21*(23), 3181-3194. doi:10.1101/gad.1607007

Schwartz, H. T., & Sternberg, P. W. (2014). Transgene-free genome editing by germline injection of CRISPR/Cas RNA. *Methods Enzymol, 546*, 441-457. doi:10.1016/B978-0-12-801185-0.00021-0

Serrano-Saiz, E., Pereira, L., Gendrel, M., Aghayeva, U., Battacharya, A., Howell, K., . . . Hobert, O. (2017). A Neurotransmitter Atlas of the Caenorhabditis elegans Male Nervous System Reveals Sexually Dimorphic Neurotransmitter Usage. *Genetics, 206*(3), 1251-1269. doi:10.1534/genetics.117.202127

Silas, S., Mohr, G., Sidote, D. J., Markham, L. M., Sanchez-Amat, A., Bhaya, D., . . . Fire, A. Z. (2016). Direct CRISPR spacer acquisition from RNA by a natural reverse transcriptase-Cas1 fusion protein. *Science, 351*(6276), aad4234. doi:10.1126/science.aad4234

Skora, S., Mende, F., & Zimmer, M. (2018). Energy Scarcity Promotes a Brain-wide Sleep State Modulated by Insulin Signaling in *C. elegans*. *Cell Rep, 22*(4), 953-966. doi:10.1016/j.celrep.2017.12.091

Srinivasan, J., Kaplan, F., Ajredini, R., Zachariah, C., Alborn, H. T., Teal, P. E., . . . Schroeder, F. C. (2008). A blend of small molecules regulates both mating and development in *Caenorhabditis elegans*. *Nature, 454*(7208), 1115-1118. doi:10.1038/nature07168

Stewart, A. D., & Phillips, P. C. (2002). Selection and maintenance of androdioecy in Caenorhabditis elegans. *Genetics, 160*(3), 975-982.

Sugi, T. (2016). Genome Editing in C. elegans and Other Nematode Species. *Int J Mol Sci, 17*(3), 295. doi:10.3390/ijms17030295

Sulston, J. E., & Horvitz, H. R. (1977). Post-embryonic cell lineages of the nematode, Caenorhabditis elegans. *Dev Biol, 56*(1), 110-156. doi:10.1016/0012-1606(77)90158-0

Sulston, J. E., Schierenberg, E., White, J. G., & Thomson, J. N. (1983). The embryonic cell lineage of the nematode *Caenorhabditis elegans*. *Dev Biol, 100*. doi:10.1016/0012-1606(83)90201-4

Sun, X. R., Badura, A., Pacheco, D. A., Lynch, L. A., Schneider, E. R., Taylor, M. P., . . . Wang, S. S. H. (2013). Fast GCaMPs for improved tracking of neuronal activity. *Nature Communications, 4*, 2170. doi:10.1038/ncomms3170

Thompson, O. A., Snoek, L. B., Nijveen, H., Sterken, M. G., Volkers, R. J. M., Brenchley, R., . . . Waterston, R. H. (2015). Remarkably Divergent Regions Punctuate the Genome Assembly of the *Caenorhabditis elegans* Hawaiian Strain CB4856. *Genetics, 200*(3), 975. doi:10.1534/genetics.115.175950

Tijsterman, M., Okihara, K. L., Thijssen, K., & Plasterk, R. H. (2002). PPW-1, a PAZ/PIWI protein required for efficient germline RNAi, is defective in a natural isolate of C. elegans. *Curr Biol, 12*(17), 1535-1540. doi:10.1016/s0960-9822(02)01110-7

Van Bael, S., Edwards, S. L., Husson, S. J., & Temmerman, L. (2018). Identification of Endogenous Neuropeptides in the Nematode *C. elegans* Using Mass Spectrometry. *Methods Mol Biol, 1719*, 271-291. doi:10.1007/978-1-4939-7537-2_18

Van Bael, S., Zels, S., Boonen, K., Beets, I., Schoofs, L., & Temmerman, L. (2018). A *Caenorhabditis elegans* Mass Spectrometric Resource for Neuropeptidomics. *Journal of The American Society for Mass Spectrometry*. doi:10.1007/s13361-017-1856-z

Venkatachalam, V., Ji, N., Wang, X., Clark, C., Mitchell, J. K., Klein, M., . . . Samuel, A. D. (2016). Pan-neuronal imaging in roaming Caenorhabditis elegans. *Proc Natl Acad Sci U S A, 113*(8), E1082-1088. doi:10.1073/pnas.1507109113

Vergara, I. A., Tarailo-Graovac, M., Frech, C., Wang, J., Qin, Z., Zhang, T., . . . Chen, N. (2014). Genome-wide variations in a natural isolate of the nematode Caenorhabditis elegans. *BMC Genomics, 15*(1), 255. doi:10.1186/1471-2164-15-255

Ward, S. (1973). Chemotaxis by the Nematode Caenorhabditis elegans: Identification of Attractants and Analysis of the Response by Use of Mutants. *Proceedings of the National Academy of Sciences of the United States of America, 70*(3), 817-821. doi:10.1073/pnas.70.3.817

Wei, Q., Shen, Y., Chen, X., Shifman, Y., & Ellis, R. E. (2014). Rapid creation of forward-genetics tools for C. briggsae using TALENs: lessons for nonmodel organisms. *Mol Biol Evol, 31*(2), 468-473. doi:10.1093/molbev/mst213

Wei, Q., Zhao, Y., Guo, Y., Stomel, J., Stires, R., & Ellis, R. E. (2014). Co-option of alternate sperm activation programs in the evolution of self-fertile nematodes. *Nat Commun, 5*, 5888. doi:10.1038/ncomms6888

White, J. G., Southgate, E., Thomas, J. N., & Brenner, S. (1986). The structure of the nervous system of the nematode Caernorhabditis elegans. *Phil Trans Royal Soc Lon, 314B*. doi:10.1098/rstb.1986.0056

Williams, E. A., Veraszto, C., Jasek, S., Conzelmann, M., Shahidi, R., Bauknecht, P., . . . Jekely, G. (2017). Synaptic and peptidergic connectome of a neurosecretory center in the annelid brain. *eLife, 6*. doi:10.7554/eLife.26349

Wood, A. J., Lo, T.-W., Zeitler, B., Pickle, C. S., Ralston, E. J., Lee, A. H., . . . Meyer, B. J. (2011). Targeted Genome Editing Across Species Using ZFNs and TALENs. *Science (New York, N.Y.), 333*(6040), 307-307. doi:10.1126/science.1207773

Wood, W. (1988). The nematode Caenorhabditis elegans. *New York, NY, New York, NY*.

Zarkower, D. (2006). Somatic sex determination. *WormBook*, 1-12. doi:10.1895/wormbook.1.84.1

Zhang, X. M., Gao, J., Chen, C. H., & Tu, H. J. (2018). Progress in the mechanisms of neural modulation of innate immunity in *Caenorhabditis elegans*. *Yi chuan = Hereditas, 40*(12), 1066-1074. doi:10.16288/j.yczz.18-133

Chapter 1C *Caenorhabditis elegans* Olfaction

Published as:

Reilly DK, Srinivasan J (2017). *Caenorhabditis elegans* Olfaction. Oxford Research Encyclopedia of Neuroscience. doi: 10.1093/acrefore/9780190264086.013.191.

Summary

To survive, animals must properly sense their surrounding environment. The types of sensation that allow for detecting these changes can be categorized as tactile, thermal, aural, or olfactory. Olfaction is one of the most primitive senses, involving the detection of environmental chemical cues. Organisms must sense and discriminate between abiotic and biogenic cues, necessitating a system that can react and respond to changes quickly. The nematode, *Caenorhabditis elegans*, offers a unique set of tools for studying the biology of olfactory sensation.

The olfactory system in *C. elegans* is comprised of 14 pairs of amphid neurons in the head and two pairs of phasmid neurons in the tail. The male nervous system contains an additional 89 neurons, many of which are exposed to the environment and contribute to olfaction. The cues sensed by these olfactory neurons initiate a multitude of responses, ranging from developmental changes to behavioral responses. Environmental cues might initiate entry into or exit from a long-lived alternative larval developmental stage (dauer), or pheromonal stimuli may attract sexually mature mates, or repel conspecifics in crowded environments. *C. elegans* are also capable of sensing abiotic stimuli, exhibiting attraction and repulsion to diverse classes of chemicals. Unlike canonical mammalian olfactory neurons, *C. elegans* chemosensory neurons express more than one receptor per cell. This enables detection of hundreds of chemical structures and concentrations by a chemosensory nervous system with few cells. However, each neuron detects certain classes of olfactory cues, and, combined with their synaptic pathways, elicit similar responses (i.e., aversive behaviors). The functional architecture of this chemosensory system is capable of supporting the development and behavior of nematodes in a manner efficient enough to allow for the genus to have a cosmopolitan distribution.

Keywords

olfaction, chemosensation, connectomics, GPCRs, neural circuits

In its simplest form, olfaction requires a receptor to detect a chemical and transduce a signal within the cell detecting the cue. The evolution of eukaryotic nervous systems has led to the production of specialized cells, the olfactory neurons, which sense, process, and communicate chemical changes sensed in the environment and transmit information to the rest of the organism.

Studies of olfaction in humans and other mammals have found that the olfactory neurons are extremely specialized, and express only one odorant receptor per cell, following a "one neuron, one receptor" rule (Bargmann, 2006b; Bear, Lassance, Hoekstra, & Datta, 2016; Chess, Simon, Cedar, & Axel, 1994; Serizawa et al., 2003). However, these receptors are not specific themselves, and may detect multiple odorants. While much can be learned studying these systems, researchers also investigate evolutionarily distinct olfactory systems, using the fruit fly *Drosophila melanogaster* and the nematode *Caenorhabditis elegans*. Both species offer useful benefits, such as nervous systems that are easily manipulated. The nervous system of *Drosophila* contains approximately 150,000 neurons (Jenett et al., 2012), compared to approximately 86 billion neurons found in human brains (Azevedo et al., 2009). The *C. elegans* nervous system, meanwhile, has only 302 neurons (J. G. White, Southgate, Thomson, & Brenner, 1986) whose lineal origins and connectivity are known, and therefore is an extremely compact and experimentally tractable nervous system. In *C. elegans*, approximately 36 neurons contribute to olfaction, and the "one neuron, one receptor" rule is not followed; multiple olfactory receptors are present in individual neurons. Despite this, the molecular mechanisms of olfaction remain conserved, with G protein-coupled receptors, receptor guanylate cyclases, and intracellular signaling cascades sensing and initiating responses to many chemical cues in the environment (Bargmann, 2006a). Studying the *C. elegans* olfactory network will allow for generation of an in-depth understanding of a complex neural coding strategy: How does this small number of olfactory neurons sense and integrate a myriad of olfactory signals to generate the robust behaviors observed?

Caenorhabditis elegans

The nematode *Caenorhabditis elegans* is eutelic—every animal has the same number of somatic cells. As such, every cell lineage has been mapped, from fertilized zygote to fully developed adult (Sulston & Horvitz, 1977). As such, the structure of the entire nervous system, comprised of 302 neurons, has been determined using electron micrographs (Ward, Thomson, White, & Brenner, 1975; Ware, Clark, Crossland, & Russell, 1975; J. G. White et al., 1986). In recent years, researchers have started characterizing the network's functional connections (Azulay, Itskovits, & Zaslaver, 2016; Bargmann, 2012; Bargmann & Marder, 2013; Hong & Park, 2016; Rengarajan & Hallem, 2016; Sohn, Choi, Ahn, Lee, & Jeong, 2011; Towlson, Vertes, Ahnert, Schafer, & Bullmore, 2013).

A small proportion of *C. elegans* are male (0.01%–0.02%) (Hodgkin, 1983), which are morphologically distinct from hermaphrodites. Males do not carry eggs and exhibit a fan-shaped tail (Barr & Garcia, 2006). Besides these gross morphological differences, the male nervous system is comprised of 385 neurons, 89 of which are sex-specific (Sammut et al., 2015; Sulston, Albertson, & Thomson, 1980). Only a small number of these sex-specific neurons are thought to function in olfaction. How the addition of these sex-specific neurons changes the connectome of the nervous system has not yet been fully explained (Fagan & Portman, 2014; García & Portman, 2016; M. P. Hart & Hobert, 2015; Portman, 2017; Serrano-Saiz et al., 2017).

C. elegans has become a leading model for understanding olfactory nervous systems, as it has a fully mapped hermaphroditic nervous system, is transparent, and is amenable to genetic manipulations. The nematode allows for the study of mechanisms underlying olfaction using genetically encoded calcium indicators (GECIs) to measure real-time neural dynamics in live animals (Chokshi, Bazopoulou, & Chronis, 2010; Massimo A. Hilliard et al., 2005; Schrodel, Prevedel, Aumayr, Zimmer, & Vaziri, 2013; Tatro, 2014; Touhara & Vosshall, 2009). Combining the robust behavioral responses of nematodes

with the ease of generating genetic mutants, understanding olfactory mechanisms has dramatically increased through the use of this roundworm.

In their natural milieu—usually rotting fruits and vegetables (Félix & Braendle, 2010; Schulenburg & Félix, 2017; Teotonio, Estes, Phillips, & Baer, 2017)—*C. elegans* individuals are exposed to a large variety of chemical cues, which signal information about their environment. These cues range from gases and volatiles, to water-soluble compounds, and from abiotic to biogenic cues.

Olfactory Neuronal Anatomy

Although olfaction occurs at both ends of the nematode (M. A. Hilliard, Bargmann, & Bazzicalupo, 2002), most research has focused on the neurons within major anterior sensilla, the amphids. The amphids are a pair of channels that each contain sensory dendrites of 12 sensory neurons (Ward et al., 1975; Ware et al., 1975; J. G. White et al., 1986) (**Figure 7A**). Eleven of the amphid neuron-types are chemosensory. In addition to amphid olfactory neurons, the head contains other olfactory neurons: BAG and URX, which are involved in sensing carbon dioxide and oxygen, respectively (**Figure 7B**), with the aid of the AQR and PQR neurons (Gray et al., 2004).

The IL2 neurons, located anterior to the amphid olfactory neurons, are not present as a bilateral pair, but instead are present as a set of *six* neurons, with dorsal, ventral, and lateral pairs (**Figure 7B**). The lateral neurons display a connectivity different from that of the remaining four neurons, further complicating the elucidation of their role. (Juan Wang, Schwartz, & Barr, 2010). There are neurons in the tail (phasmids) that sense odorants, though the number of chemosensory neurons in the tail is drastically lower than that seen in the anterior, with only two pairs of phasmid neurons being present that contain cilia exposed to the external environment (**Figure 7C**).

The Male Nervous System

Of the 89 sex-specific neurons present in the male nervous system, only four located in the amphid region participate in olfaction: the cephalic male (CEM) neurons (J. Q. White et al., 2007). These radially symmetric neurons exhibit dorsal/ventral as well as left/right symmetry, with cilia exposed to the external environment alongside the hermaphroditic amphid olfactory neurons (**Figure 7A**). The clearly distinguishable male-tail is heavily involved in the mating process and includes the majority of the male-specific neurons. Thirty-six ray neurons innervate this structure (Liu, 1995; J. Q. White et al., 2007).

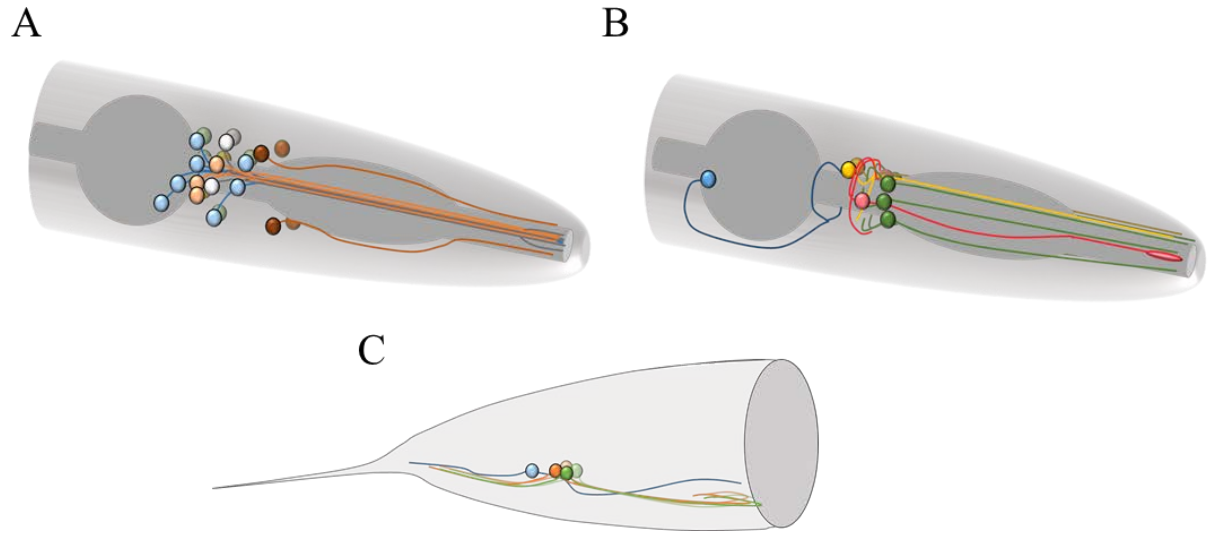

Figure 7. *C. elegans* Olfactory Anatomy.
(A) The Chemosensory Amphid Olfactory Sensilla: The ciliated amphid olfactory neurons develop as bilateral pairs with three distinct cilia morphologies: single-rod (blue), double-rod (white), and winged (orange). The dendritic extensions for the left-side neurons are shown in matching colors. The CEM (brown) are male-specific neurons that exhibit radial symmetry, with both dorsal and ventral left-right pairs. **(B)** The Oxygen and Carbon Dioxide Sensing Amphid Sensilla: The BAG neurons (pink) sense carbon dioxide and develop bag-shaped cilia (also shown in pink). The URX neurons (yellow) contribute to oxygen sensation, with dendrites that do not develop cilia and that terminate in the pseudocoelomic fluid. URX sensation of oxygen is aided by the AQR neuron (blue), which develops as a single neuron, with a dendrite that wraps around the pharyngeal tube. The IL2 neurons (green) develop as three bilateral pairs (dorsal, lateral, and ventral), with cilia exposed to the environment. **(C)** The Phasmid Olfactory Sensilla. The PQR neuron (blue) contributes to the gas sensing network, alongside the URX and AQR neurons located in the amphid region. The two chemosensory phasmid neurons, PHA (green) and PHB (orange), extend their cilia out to the external environment, and modulate turns initiated by amphid olfactory neurons.

The Nature of Amphid Olfactory Neurons

Winged Cilia Olfactory Neurons

Although not exposed to the external environment, winged ciliated neurons are involved in the sensation of volatile cues, which diffuse across the cuticle (Wes & Bargmann, 2001; J. G. White et al., 1986). *C. elegans* is able to distinguish between seven classes of these odors. Most of these volatiles were found to be products of bacterial metabolism, suggesting a biologically relevant role for AWA and AWC—food chemotaxis (Bargmann, Hartwieg, & Horvitz, 1993). Most neurons in *C. elegans* are present as anatomically symmetrical, bilateral pairs. However, AWC has been shown to exhibit stochastic asymmetry in its gene expression and sensing abilities (Cochella et al., 2014; Pierce-Shimomura, Morse, & Lockery, 1999; Troemel, Kimmel, & Bargmann, 1997; Wes & Bargmann, 2001; Yu, Avery, Baude, & Garbers, 1997).

One of the repulsion-driving olfactory neurons, AWB, also senses volatiles, such as 1-octanol (Troemel et al., 1997). The biological relevance of 1-octanol in natural environments can be debated, as it has only been found in the extracts from some enteric Gram negative bacteria (Elgaali et al., 2002). However, given that the volatile metabolites emitted by bacteria are complex mixtures (Hamilton-Kemp et al., 2005), and the natural food sources of nematodes are incompletely known, 1-octanol serves as a reliable stimulus for AWB in experimental conditions.

The Single- and Double-Rod Ciliated Amphid Neurons

Water-soluble attractants and repellents are sensed by the single- and double-rod ciliated amphid neurons (**Table 2**). These neurons contain rod-shaped cilia which extend through the amphid sheath and cuticle to sense odorants in the external environment (Bargmann, 2006a; Ward et al., 1975). Like AWC, ASE is asymmetric, but it is more consistent in its asymmetry than AWC, with the right neuron (ASER) always sensing Cl^- and K^+ ions, and ASEL sensing Na^+ (Pierce-Shimomura et al., 1999).

Table 2. Olfactory Neurons.

	Cilium	Role	Olfactory Cues Sensed	Intracellular Components
AWA	Winged	Attraction	Volatiles	*osm-9*, *ocr-2*
AWB	Winged	Repulsion	Volatiles	*tax-2*
AWC	Winged	Attraction	Volatiles	*tax-2*, *tax-4*, *osm-9*
ASE	Single Rod	Attraction	Water-Solubles	*tax-2*, *tax-4*, *osm-9*
ASG	Single Rod	Dauer Control	*Unknown*	*tax-2*, *tax-4*, *osm-9*
ASH	Single Rod	Nociceptive	Aversive Stimuli	*osm-9*, *ocr-2*
ASI	Single Rod	Dauer Control/Foraging	Daumone, Icas#9	*tax-2*, *tax-4*, *osm-9*
ASJ	Single Rod	Dauer Control	Icas#9	*tax-2*, *tax-4*, *osm-9*
ASK	Single Rod	Attraction	Icas, ascr#3	*tax-2*, *tax-4*, *osm-9*
ADF	Double Rods	Dauer Control	*Unknown*	*osm-9*, *ocr-2*
ADL	Double Rods	Repulsion	Water solubes, ascr#3, icas#9	*osm-9*, *ocr-2*
BAG	Bag	Aerotaxis	CO_2	*tax-2*, *tax-4*
URX	Non-Ciliated	Aerotaxis	O_2	*tax-4*
AQR	Non-Ciliated	Aerotaxis	O_2	*tax-2*
PQR	Non-Ciliated	Aerotaxis	O_2	*tax-2*
IL2	-	*Unknown*	*Unknown*	-
PHA/PHB	Single Rod	Repulsion	*Unknown*	*osm-9*, *ocr-2*
CEM	-	Male Attraction	ascr#3, ascr#8	-
Rays	-	Mating	*Unknown*	-
SPV/SPD	-	Mating	Vulval Pheromones	-

The cilium structures, as well as the chemicals detected by individual neurons, where known. While there is no overlap between cells expressing both *tax-2* and *tax-4*, and cells expressing both *osm-9* and *ocr-2*, there is some overlap between *tax-2*, *tax-4* and *osm-9* alone.

ASH is unique among the amphid sensilla in that it is polymodal and acts as the key nociceptor in *C. elegans* (Chatzigeorgiou, Bang, Hwang, & Schafer, 2013; de Bono & Maricq, 2005; Hukema, Rademakers, Dekkers, Burghoorn, & Jansen, 2006; Rick Komuniecki, Harris, Hapiak, Wragg, & Bamber, 2012; Walker et al., 2009). While most

neurons sense an odorant and elicit a general response downstream, ASH's response is more complex, as the downstream signaling exhibits specificity to the stimulus sensed. For example, while OCR-2 and OSM-9 (see *Downstream Ion Channels Involved in Olfaction* section) are required for all responses within the ASH Neurons, the g-proteins utilized for different GPCRs varies (i.e., either GPA-3 or ODR-3 can function to generate a neuronal response) (Massimo A. Hilliard, Bergamasco, Arbucci, Plasterk, & Bazzicalupo, 2004; Walker et al., 2009).

Largely involved in developmental processes, ASI assists in controlling entry into dauer. ASI is the sole source of DAF-7 and TGF-β in *C. elegans*, which act to prevent dauer entry (Meisel, Panda, Mahanti, Schroeder, & Kim, 2014; Ren et al., 1996; Schackwitz, Inoue, & Thomas, 1996). This signaling pathway is regulated by the availability of food, population density, carbon dioxide levels, the presence of dauer pheromone, and temperature, while more recent work has expanded this list to include mRNA decay pathways (Androwski, 2017; Borbolis et al., 2017). ASI is also required for proper dauer exit and resumption of normal development after stress conditions are mitigated (Ren et al., 1996), as well as being required for withdrawal from noxious stimuli (Mills et al., 2016). The olfactory regulation of dauer control arises through ASI sensation of the majority of daumone constituents: ascr#2, ascr#3, and ascr#5 (Kim et al., 2009; McGrath et al., 2011).

The double-ciliated neuron, ADL, has been shown to sense ascr#3 as well. However, instead of initiating dauer entry or avoidance behaviors, ADL regulates body fat content (Hussey et al., 2017).

The ASK neuron functions in driving both avoidance and attractive behaviors. Removal of ASH through laser ablation experiments results in ASK gaining the ability to sense many aversive stimuli (M. A. Hilliard et al., 2002; Hukema et al., 2006; Sambongi et al., 1999). ASK plays a major role in sensing attractive biogenic cues. Icas#1, #3, and #9, indolated derivatives of ascr#1, #3, and #9, respectively, were shown to attract *C. elegans*

of both sexes (Srinivasan et al., 2012). However, this attraction is extremely concentration-dependent across the sexes, with males no longer attracted to low concentrations. ASK has also been shown to sense ascr#3, which is repulsive to hermaphrodites at concentrations that attract males. This likely arises from the combined output of ASK in males with the chemoattraction that is driven by the male-specific CEM neurons (Narayan et al., 2016; Pungaliya et al., 2009; Srinivasan et al., 2008; Jamie Q. White & Jorgensen, 2012).

ADF is unique in that it is the only serotonergic sensory neuron in *C. elegans* hermaphrodites (Sze, Victor, Loer, Shi, & Ruvkun, 2000). Little is known about what ADF may be sensing in the surrounding environment, although it has been shown to contribute to dauer control, as animals lacking ADF display aberrant dauer repression (Schackwitz et al., 1996).

Little has been studied concerning the role of the ASG and ASJ neurons. ASJ is known to contribute to dauer entry and recovery, but what exactly it senses in the environment to initiate these developmental changes remains unknown. ASJ has also been shown to be involved in the sensation of pathogenic bacteria (Meisel et al., 2014). It is likely that, like ASI, these neurons sense a combination of pheromone cues, population density cues, and information about food availability. This, however, remains to be determined.

Male-Specific Ciliated Amphid Olfactory Neurons

Male *C. elegans* contain four extra ciliated neurons that function as olfactory neurons—the CEM neurons. Ascarosides #3 and #8, both of which contribute to the induction of dauer, also elicit repulsion of hermaphrodites, yet attract males, are sensed by these neurons (Jang et al., 2012; Macosko et al., 2009; Narayan et al., 2016; Pungaliya et al., 2009; Srinivasan et al., 2008).

Oxygen and Carbon Dioxide Sensing Neurons

Water soluble and volatile compounds are not the only stimuli sensed by olfactory neurons. Oxygen and carbon dioxide levels are sensed by a small subset of sensory neurons not included in the classical set of amphid olfactory neurons (Carrillo & Hallem, 2015).

The ciliated BAG neurons sense CO_2 levels (A. J. Bretscher, Busch, & de Bono, 2008; Andrew J. Bretscher et al., 2011; Busch et al., 2012; Zimmer et al., 2009), and drive avoidance behaviors in situations in which there are elevated levels of the gas (Hallem & Sternberg, 2008). With help from ASE, and the canonical thermosensory neuron AFD, BAG is the main sensor of CO_2 in the nematode (Andrew J. Bretscher et al., 2011).

The URX neurons, which are *not* ciliated, also develop in the amphid region and contain dendrites that are exposed to the pseudocoelomic fluid (Styer et al., 2008). In combination with the AQR and PQR neurons, URX helps *C. elegans* aerotax towards ideal O_2 levels (Chang, Chronis, Karow, Marletta, & Bargmann, 2006; Gray et al., 2004).

Other Amphid Olfactory Neurons

The IL2 neurons have cilia exposed to the external environment, but what they sense and what they communicate is unknown. In dauer larvae, IL2 cilia regulate a dispersal behavior, though it remains unknown how the cilia are activated to induce this output (Lee et al., 2012).

The Nature of Phasmid Olfactory Neurons

Although the roles of PHA and PHB have been determined (Barrios, Ghosh, Fang, Emmons, & Barr, 2012; M. A. Hilliard et al., 2002), what these neurons are sensing remains largely unknown. Many of the sex-specific neurons present in males are located in the tail, increasing the overall number of neurons exposed to the environment, increasing phasmid olfactory capability (J. Q. White et al., 2007). Three pairs of ray neurons also contribute to an increase in the number of serotonergic olfactory neurons (Jafari, Xie,

Kullyev, Liang, & Sze, 2011; J. Q. White et al., 2007). It has not been yet determined exactly what these olfactory neurons sense.

The distal tips of the copulatory spicules contain the exposed cilia of the SPD and SPV neurons. Given the spicules' role during mating, it is proposed that these neurons sense vulval pheromones to manage release of sperm into the correct location (LeBoeuf, Correa, Jee, & García, 2014; Liu, 1995; Schindelman, Whittaker, Thum, Gharib, & Sternberg, 2006). To date, there has been no identification of these proposed vulval pheromones.

Assays Used in the Study of *C. elegans* Olfaction

Behavioral Assays

The most ethologically relevant output of sensation to study is behavior. With obtainable results on short timescales, the effect of a stimulus on *C. elegans* behavior can be studied both in fine detail and in a high-throughput manner (Ghosh, Nitabach, Zhang, & Harris, 2017; Maruyama, 2016). The simplest of observable behaviors are attraction and repulsion. In fact, this chemotaxis was studied in *C. elegans* even before Brenner's initial push for the use of the nematode as a standard model system (Ward, 1973).

The eutelic and transparent nature of *C. elegans* allows for reliable identification and laser ablation of specific cells. In these ablations, a laser is focused and pulsed at the nucleus of a neuron of interest, effectively killing the cell (Fang-Yen, Gabel, Samuel, Bargmann, & Avery, 2012). Nematodes undergo this laser surgery as larvae, and are then allowed to develop in the absence of the ablated cell, after which, the animal can be assayed, and changes in outputs observed.

In 1973, Ward et al. showed that *C. elegans* are able to respond to attractants by moving up a concentration gradient, accumulating in the area of the cue, and then habituating to the cue (**Figure 8A**) (Ward, 1973). In the now-canonical population chemotaxis assay developed by the Bargmann lab, the number of *C. elegans* at selected

time points within specified attractant areas are counted to generate a chemotaxis index (**Figure 8A**) (Bargmann et al., 1993). Changes in this index amongst mutants or laser-ablated animals have helped identify neurons and neuromodulators that play roles in attractive olfaction.

C. elegans utilize two independent mechanisms to chemotax towards ideal concentrations of odorants: pirouettes (klinokinesis) and weathervaning (klinotaxis). Characterization of changes in the uses of these methods of chemotaxis in mutant animals has helped to identify the underpinnings of how *C. elegans* reach an ideal environment (Chalasani et al., 2007; Lockery, 2011; Luo, Gabel, Ha, Zhang, & Samuel, 2008). The pirouette mechanism is comprised of "bouts of sharp turns," usually including a reversal and/or ω turn (Iino & Yoshida, 2009). These sharp turns are initiated upon a sensation of a decrease in the concentration of an attractant, such as salt (Pierce-Shimomura et al., 1999), although they also utilize this method in response to volatile odorants (Chalasani et al., 2007).

In contrast to pirouettes, *C. elegans* also employ a more gradual curving towards an attractant, termed weathervaning (Iino & Yoshida, 2009). This behavior was first proposed in 1973, but there was no further evidence supporting this behavior until over three decades later (Iino & Yoshida, 2009; Ward, 1973). To generate this curve, the amphid sensory neurons were found to sense changes in odorant concentrations at each apex of the head swing during the sinusoidal movement of the worm (Izquierdo & Lockery, 2010; S. Kato, Xu, Cho, Abbott, & Bargmann, 2014; Johannes Larsch et al., 2015). Iino and Yoshida proposed that slightly larger head swings are then generated in the direction of an attractant, generating the curving motion (Iino & Yoshida, 2009).

Avoidance assays have also been established to aid in the understanding of how *C. elegans* senses chemical cues in its environment. A drop assay was developed by Hilliard

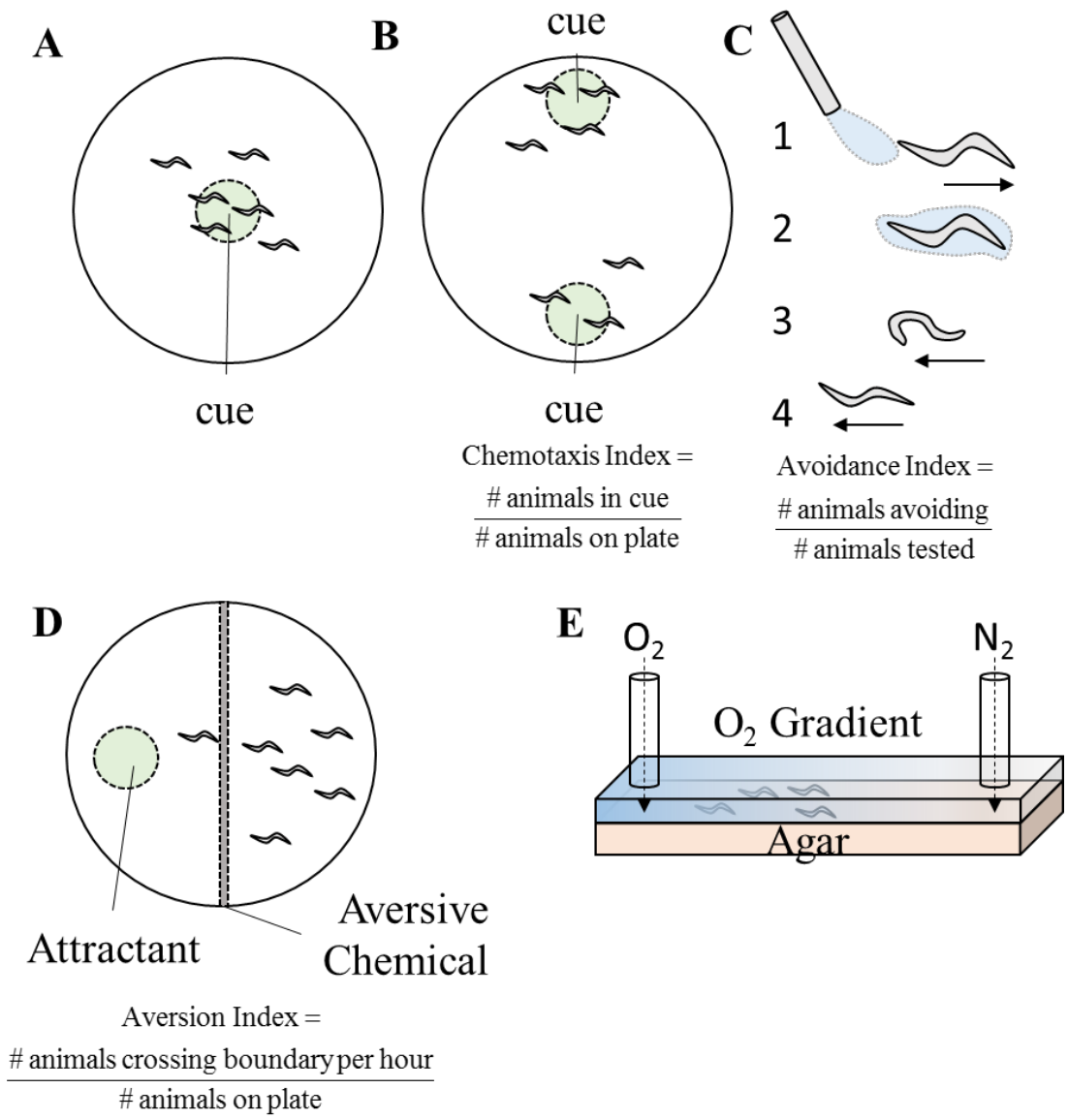

Figure 8. Behavioral Assays Used in Understanding Olfaction.
(A) Attractive Gradient Assay: *C. elegans* are placed in a drop of an attractant chemical (shaded area). As the chemical diffuses, creating a gradient, animals reside in the ideal concentration of the cue. **(B)** Chemotaxis Assay: *C. elegans* are placed in the center of plate, with two drops of attractant at either end of the plate (shaded area). The number of animals within this region are scored over time and divided by the total number of worms on the plate to generate an Attraction Index. **(C)** Drop Avoidance Assay: A drop of aversive chemical is placed on the tail of a forward moving nematode. Capillary action draws the solution up to the head of the animal where it is sensed and initiates a reversal, and ultimately, a change of direction. The number of drops that cause animals to avoid is divided by the total number of drops applied to generate an Avoidance Index. **(D)** Population Level Avoidance Assay: *C. elegans* are placed on one side of an aversive chemical barrier (darker region). In order to reach a volatile attractant (shaded area), they must cross the aversive barrier. **(E)** Aerotaxis Assay: An agar field containing *C. elegans* is placed in a chamber, which is connected to inputs for oxygen and nitrogen. The inflow of gases is controlled to create an oxygen gradient across the chamber. Nematodes can aerotax to the region with the preferred oxygen content.

et al., which exposes a forward moving animal to a drop of a soluble chemical cue (**Figure 8C**) (M. A. Hilliard et al., 2002; Massimo A. Hilliard et al., 2004). An avoidance index is then calculated by determining the fraction of worms that initiate reversals upon exposure to the cue. There is also a population-level aversion assay in which worms are placed on one side of a line of aversive chemical. A volatile attractant is then placed on the opposite side of the aversive chemical line (**Figure 8D**). An aversion index is calculated by dividing the number of worms that cross the boundary in one hour by the total number of worms on the plate (A. C. Hart, 2006).

C. elegans senses oxygen and carbon dioxide levels through olfactory neurons. Aerotaxis studies involve specialized devices, in which a gas gradient can be generated by pumping opposing gases into a chamber housing an agar arena (**Figure 8E**) (Gray et al., 2004). A score is given based upon where animals are found within the gradient, and mutants can easily be determined by changes in this distribution.

Assays allowing for the study of more complex behaviors (such as aggregation, foraging, and dispersal) have also been developed, as advancements in worm tracking and technological capabilities have been made (Greene et al., 2016b; Milward, Busch, Murphy, de Bono, & Olofsson, 2011; Sambongi et al., 1999). With greater software and coding capabilities, worm tracking is now common, and even a marketable process. Many labs have developed their own tracking software (Albrecht & Bargmann, 2011; Buckingham, Partridge, & Sattelle, 2014; Chalasani et al., 2007; Cronin, Feng, & Schafer, 2006; Faumont et al., 2011; Feng, Cronin, Wittig, Sternberg, & Schafer, 2004; Kawano et al., 2011; Leifer, Fang-Yen, Gershow, Alkema, & Samuel, 2011; Stirman et al., 2011; Swierczek, Giles, Rankin, & Kerr, 2011; Tsechpenakis, Bianchi, Metaxas, & Driscoll, 2008; Tsibidis & Tavernarakis, 2007), and companies exist that offer user friendly software for purchase, such as *WormLab[http://www.mbfbioscience.com/wormlab]*—developed by MBF Bioscience. There are options available for the tracking of single worms or populations of worms, either on agar plates, in suspension, and more. Analyses with

these trackers include parameters such as speed, turning frequencies, and bending angles, with multi-worm trackers even being able to distinguish between two worms that come into contact with each other. In-depth descriptions of available worm-trackers, with side-by-side comparisons are available (Husson, Costa, Schmitt, & Gottschalk, 2012).

Developmental Assays

As a result of processing information about their immediate environment and their developmental state, nematodes emit small molecules to communicate information to conspecifics. To do so, they utilize a class of biogenic, small-molecule pheromones, termed ascarosides. To date, ascarosides have been found to mediate entry into dauer, an alternative and environmentally persistent developmental state (the collective mix of ascarosides that signal dauer formation are termed "daumone" (Golden & Riddle, 1982)), foraging behavior, avoidance behavior, and mate recognition(Butcher, 2017a, 2017b; Chute & Srinivasan, 2014; Ludewig & Schroeder, 2013).

In dauer-formation assays (**Figure 9A**), worms are allowed to develop on plates containing chemicals that may induce dauer development. Since dauer worms survive harsh conditions, the worms surviving after treatment can be scored and compared to the pre-treatment population to calculate the fraction of induced dauer larvae (Jeong et al., 2005). Alternatively, dauers can also be identified "based on size, shape, and lack of pharyngeal pumping" (Butcher, Fujita, Schroeder, & Clardy, 2007).

In dauer recovery assays (**Figure 9B**), worms are cultured in liquid media and allowed to form dauers. Non-dauer worms are removed from the culture, and the dauers are then placed on an agar plate containing chemicals that may induce exit from dauer. After two days, dauer and non-dauer worms are visually scored (Butcher et al., 2007).

Imaging of Neural Activity in Olfactory Neurons

With the development of genetically encoded calcium indicators (GECIs), visualization of neuronal activity *in vivo* has become possible (Nakai, Ohkura, & Imoto, 2001). These

proteins allow for real-time readout of intra-cellular calcium levels. Original GECIs utilized Green Fluorescent Protein (GFP) as their fluorescent protein in the fusion (generating the GCaMP family of GECIs), although recent developments have incorporated red-shifted chromophores, such as RFP (RCaMPs) (Akerboom et al., 2012; Akerboom et al., 2009; Sun et al., 2013).

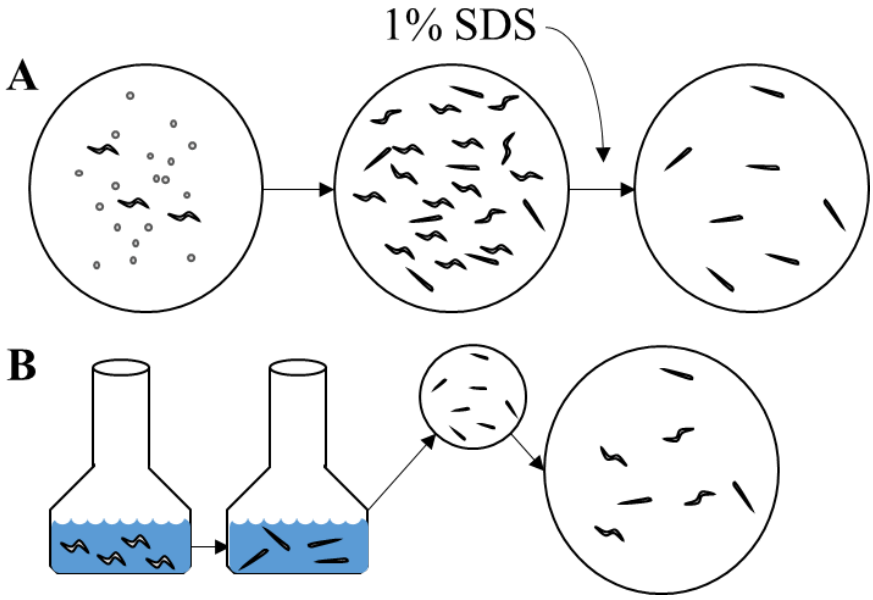

Figure 9. Dauer Development Assays.
(A) Dauer Formation Assay: A few adult *C. elegans* are allowed to lay eggs on a plate before being removed. These eggs are allowed to hatch and larvae grow under dauer promoting conditions (pheromone, temperature, etc.). The proportion of worms in the dauer state are determined in two ways: By visual scoring of worms that maintain dauer appearance and morphology, or by applying a solution of 1% SDS to the population, and scoring the animals still alive after as being in the dauer state. The number of animals that enter dauer are divided by the total number of animals on the plate to determine Percent Dauer Formation. **(B)** Dauer Recovery Assay: *C. elegans* are grown in liquid culture until entering dauer. Non-dauer animals are removed from the population, and dauer animals are plated. After three days, the number of nematodes that have exited dauer to resume normal development are scored and divided by the total number of plated animals to determine Percent Dauer Recovery.

By expressing GECIs in olfactory neurons, and exposing *C. elegans* to an olfactory stimulus, the depolarization and hyperpolarization of sensory neurons can not only be visualized, but measured (Massimo A. Hilliard et al., 2005). Microfluidic devices allow for the containment of nematodes in a manner that allows for capture of the fluorescent dynamics of GECIs upon exposure to olfactory cues (Reilly, Lawler, Albrecht, & Srinivasan, 2017). Animals can be assayed while "trapped" in devices or allowed to roam

in "arenas" (Chronis, Zimmer, & Bargmann, 2007; Lagoy & Albrecht, 2015; J. Larsch, Ventimiglia, Bargmann, & Albrecht, 2013).

Mechanisms of Olfaction

Molecular and Cellular Mechanisms

G Protein-Coupled Receptors

The *C. elegans* genome encodes approximately 1,200 G protein-coupled receptors (GPCRs), over half of which are proposed to be chemosensory in nature. Only a handful of receptors have been directly linked to sensation of specific cues (Bastiani & Mendel, 2006). This has likely arisen due to the redundancy of olfactory neurons in the nematode. With only approximately three dozen neurons participating in olfaction, there is a remarkable amount of GPCR co-expression within olfactory neurons. As such, the redundant nature of these receptors has caused genetic screens to be ineffective in linking receptors to biological roles. In the two decades since the finding that ODR-10 senses diacetyl (Sengupta, Chou, & Bargmann, 1996), only a handful of GCPRs have been linked to specific targets: SRBC-64 and -66, DAF-37 and -38, SRG-36 and -37 sense dauer inducing ascarosides (Kim et al., 2009; McGrath et al., 2011; Park et al., 2012), SRX-43 and SRX-44 sense icas#9 to control foraging behaviors (Greene et al., 2016b; Greene, Dobosiewicz, Butcher, McGrath, & Bargmann, 2016a), while SRI-14 senses high concentrations of diacetyl alongside the low-concentration sensing ODR-10 (Sengupta et al., 1996; Taniguchi, Uozumi, Kiriyama, Kamizaki, & Hirotsu, 2014).

GPCRs can bind ligands present in the worm's environment, and, in conjunction with associated G proteins, propagate signaling cascades. The remaining GPCRs, which are not expected to be chemosensory in nature, likely play other roles in neurotransmission (Bargmann, 1998; Bargmann, 2006a).

The original method of determining GPCR expression patterns was through the generation of transcriptional fusions, wherein the promoter of the GPCR gene of interest

drives expression of GFP. These first tests showed that GPCRs in *C. elegans* are expressed in either single or multiple neuronal classes (Taniguchi et al., 2014; Troemel, Chou, Dwyer, Colbert, & Bargmann, 1995). As expected, it was confirmed that GCPRs, which function as chemoreceptors in these olfactory neurons, are localized to the cilia of these neurons (Dwyer, Troemel, Sengupta, & Bargmann, 1998; Troemel et al., 1995).

This has continued to hold true with the advent of ascaroside receptor discoveries, using both fusions and immunostaining (Greene et al., 2016b; Greene et al., 2016a; Kim et al., 2009; McGrath et al., 2011; Park et al., 2012). GPCRs have been shown to function as heterodimers, with two unique receptors involved in the sensation of each cue. In this sensation method, some receptors function as primary binders of specific targets, while the other member may function as a partner for *multiple* primary receptors in the sensation of stimuli (Park et al., 2012). Despite the relatedness of ascarosides in terms of core structure, the receptors identified to date are widespread across the GPCR families present in *C. elegans*; genes have been discovered to be responsible for ascaroside sensation in the *srbc*, *srg*, *srw*, and *srx* families (Greene et al., 2016b; Greene et al., 2016a; Kim et al., 2009; McGrath et al., 2011; Park et al., 2012).

Stimuli sensed by GPCRs need not be as structurally complex as ascaroside pheromones, however. In fact, the ketone diacetyl was found to be sensed by two different GPCRs, dependent on the concentration of the stimuli: ODR-10 for low concentrations and SRI-14 for high concentrations. Diacetyl elicits an attractive response when sensed by the AWA neurons and bound to ODR-10 (Sengupta et al., 1996). However, high concentrations are sensed by SRI-14, expressed in the nociceptive ASH neuron, and produce aversive behaviors (Taniguchi et al., 2014).

G protein-coupled receptors would not function properly without the related G proteins and downstream intracellular signaling cascades. Within the *C. elegans* genome, there are twenty Gα, two Gβ, and two Gγ subunits (Jansen et al., 1999). Due to the presence of hundreds of GPCRs in the olfactory neurons, it is understandable that

multiple subunits may be expressed in individual neurons. Because of this, the roles of individual Gα subunits vary in importance (Bastiani & Mendel, 2006).

Downstream Ion Channels Involved in Olfaction

Downstream of GPCRs and their related G-protein complexes (Cuppen, van der Linden, Jansen, & Plasterk, 2003), *C. elegans* use two canonical intracellular signaling cascades to elicit depolarizations (Bargmann, 2006a): cyclic nucleotide-gated channels, and transient receptor potential (TRP) channels, which are utilized in two separate subsets of olfactory neurons (**Table 2**) (Coburn & Bargmann, 1996; Colbert & Bargmann, 1997; Komatsu, Mori, Rhee, Akaike, & Ohshima, 1996; Tobin et al., 2002).

Olfactory neurons utilizing cyclic nucleotide-gated channels to initiate depolarizations express TAX-2 and TAX-4 as a heterodimer in the cilia of the neuron (**Table 2**). This channel is downstream of receptor-type guanylate cyclases, which induce influxes of cGMP, and lead to a flood of sodium or calcium into the neuron (Ortiz et al., 2006). These channels are also functional in the oxygen and carbon dioxide sensing neurons, where they are activated by *soluble* guanylate cyclases (Andrew J. Bretscher et al., 2011; Carrillo, Guillermin, Rengarajan, Okubo, & Hallem, 2013; Cheung, Arellano-Carbajal, Rybicki, & de Bono, 2004; Gray et al., 2004; Hallem et al., 2011; Hallem & Sternberg, 2008; Yu et al., 1997).

While receptor-type guanylate cyclases (rGCs) are crucial toward generating cGMP flux downstream of GCPRs in TAX-2/TAX-4 neurons (Ortiz et al., 2006), there are a few instances wherein they act as chemoreceptors themselves. For example, GCY-9 functions to directly bind CO_2 in the BAG neurons, while GCY-14 serves as a pH indicator in the left ASE neuron (Takashi Murayama & Maruyama, 2013; T. Murayama, Takayama, Fujiwara, & Maruyama, 2013; Smith, Martinez-Velazquez, & Ringstad, 2013). The large, nematode specific expansion of rGCs (Fitzpatrick, O'Halloran, & Burnell, 2006) suggests that there are more playing as yet unknown but direct roles in chemosensation.

Conversely, olfactory neurons can utilize heterodimeric TRP channels to provoke depolarizations in the sensory cilia. OSM-9/OCR-2 form a heterodimeric channel in these TRP-utilizing cilia (**Table 2**). In this signaling cascade, G proteins regulate lipid metabolism which, in turn, activate the TRP channel, leading to the desired depolarization (Kahn-Kirby et al., 2004).

Circuit-Level Analysis

Integration of Olfactory Inputs

Unlike other known olfactory systems studied in neuroscience, such as that of the mouse, *C. elegans* olfaction relies on only a small subset of neurons, requiring co-expression of receptors within individual neurons. This is in juxtaposition to the one-neuron-one-receptor system observed in mammals (Bargmann, 2006b; Chess et al., 1994; Serizawa et al., 2003). The majority of this limited number of olfactory neurons converges onto a small subset of interneurons, largely responsible for integration of sensation. Without this integration, proper olfactory responses would be impossible. This layer of neuronal networks is critical when investigating olfactory mechanisms.

With the exception of ASJ and URX, all of the amphid olfactory neurons synapse onto at least one member of the "first-layer interneurons": AIA, AIB, AIY, and AIZ (Ward et al., 1975; Ware et al., 1975; J. G. White et al., 1986). It is these neurons that are speculated to integrate the information from the upstream neurons, and initiate proper behavioral or developmental responses. These "first-layer interneurons" are responsible for summing and integrating sensory input, before passing the information downstream onto either motor neurons or the command interneurons which control forward and reverse locomotory circuitries (**Figure 10**) (Chalfie et al., 1985). The complex and recurrent connectivity among these four neurons allows for fine-tuning and integration of sensory input prior to initiating downstream signaling.

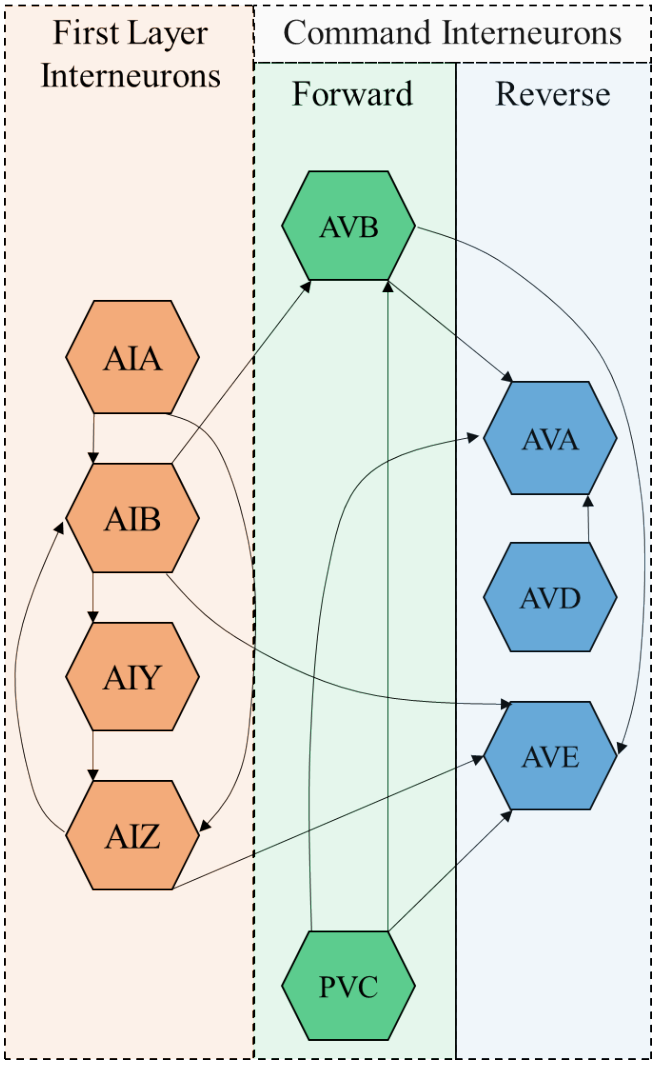

Figure 10. Network Regulation of Olfaction.
The first two layers of olfactory sensation integration: The majority of amphid olfactory neurons synapse onto at least one of the "First Layer Interneurons." These recurrently connected interneurons then synapse and transmit information onto motor neurons (not shown) and the Command Interneurons: AVB, PVC, AVA, AVD, and AVE. The Command Interneurons control the forward and reverse locomotory circuitries. Black arrows denote physical, not functional connections.

Interneurons such as RMG have are thought to serve as hubs for integration of olfactory input. RMG receives inputs from six amphid olfactory neurons, and modulates aggregation and other social behaviors (**Figure 11A**) (Macosko et al., 2009). Likewise, neurons such as AWA and ASH modulate the RIM interneuron to initiate backward and inhibit forward movements (**Figure 11B**) (Ghosh et al., 2016). While they are not directly responsible for sensing olfactory stimuli in the environment, it is critical to include these

A Functional Foraging Circuit

Icas#9, a weak inducer of dauer, promotes foraging behavior. Work by Greene, Dobosiewicz, et al. (2016a) unveiled a circuit that senses icas#9 through three olfactory neurons: ASI, ASJ, and ADL (**Figure 11C**) (Greene et al., 2016b; Greene et al., 2016a). ASI promotes roaming when sensing icas#9 in opposition to ADL (**Figure 11C**). ASJ senses icas#9 through a different receptor than that present in ASI, yet drives the same behavior (Greene et al., 2016a). ADL, utilizing the same receptor found in ASJ, represses the foraging behavior promoted by ASI and ASJ.

Responding to Volatile Odors

The AWC-AIA-AIY circuit is a complex circuit that tunes responses to volatile odors. AWC functions in an "odor-off" fashion; when odors are removed, AWC inhibition of the downstream interneuron AIY is relieved (**Figure 11D**) (Chalasani et al., 2007). Upon removal of the odor, glutamatergic inhibition of AIY resumes. In turn, the response of AWC to these odors is modulated by the AIA interneuron (**Figure 11D**) (Chalasani et al., 2010).

Nociception and Avoidance

ASI and ASH both sense copper to drive avoidance behaviors. The "reciprocal inhibition" observed in these neurons tunes this avoidance behavior. ASI activates ADF, which, in turn, functions to inhibit ASH (**Figure 11E**). ASH, meanwhile, activates the RIC interneuron, which then works to inhibit ASI signaling (Guo et al., 2015).

ASH has also been shown to sense 1-octanol and to activate the AIB interneuron and the AVA motor neuron, which drives backwards locomotion (**Figure 10**). AWC also contributes towards the rate of spontaneous reversals by activating the AIB interneuron (**Figure 11D**). However, AWC is inhibited by both 1-octanol and food, preventing it from activating the AIB interneuron. The removal of food alters internal 5-HT levels (G. Harris et al., 2011; G. P. Harris et al., 2009), which in turn also inhibits the AIB interneuron. This

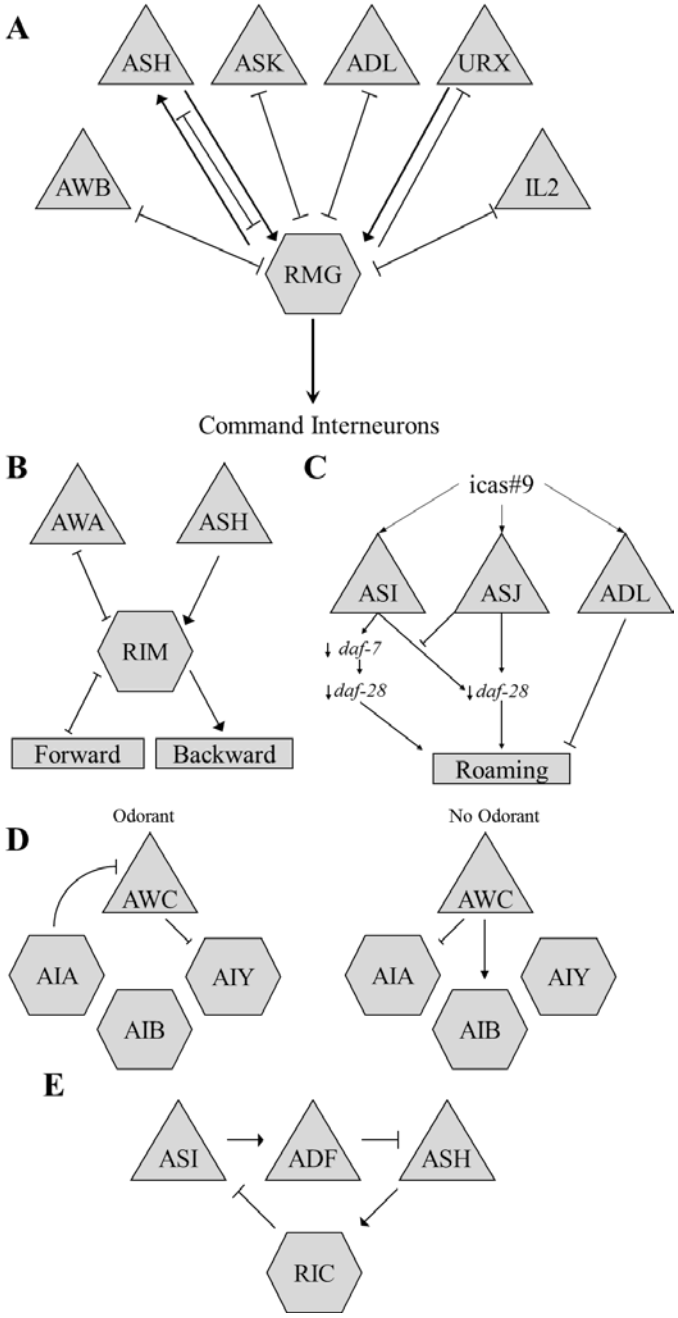

Figure 11. Functional Circuits Involved in *C. elegans* Olfaction.
(A) The RMG interneuron acts as a hub for olfactory input from four chemosensory neurons, the oxygen-carbon dioxide sensing URX neuron, and the IL2 neurons. Integrated input is them passed downstream onto the command interneuron. **(B)** The AWA and ASH neurons synapses onto the RIM interneuron to control initiation of forward and backwards locomotion. **(C)** Icas#9, an indolated ascaroside is sensed by three chemosensory neurons and two receptors to control roaming behavior. **(D)** The AWC-AIA-AIY circuit functions in an "Odor-OFF" fashion. When odor is present (left), the AWC neuron inhibits AIY, and is inhibited by AIA. When the odor is removed (right), the AWC neurons inhibit the inhibitory AIY, and activate AIB. The removal of AIY inhibition contributes to AIY activity as well. **(E)** Nociceptive avoidance is fine-tuned by ASI and ASH. A "reciprocal inhibition" is observed, with ASI activating ADF inhibition of ASH. Meanwhile, ASH activates RIC inhibition of ASI.

cumulative inhibition of the AIB interneuron results in inhibition of reversals and, upon completion of a reversal, re-initiation of forward movement (Summers et al., 2015).

Male Ascaroside Sensation

Many functional connectomes remain to be understood. Male-specific CEM neurons sense ascarosides #3 and #8 to attract males to receptive hermaphrodites (Srinivasan et al., 2008). However, while the class of neurons is required for proper response to these cues, not all four CEM neurons elicit the same changes in calcium levels (Narayan et al., 2016). A subset of CEM neurons depolarize, others hyperpolarize, and others seem to not respond at all. These subsets vary from animal to animal, suggesting that the cumulative output of the CEM neurons is more important than individual CEM neuron response. Given that the four neurons respond differently, it is likely that there is cross-talk occurring between the four neurons, possibly similar to the ASI-ASH "reciprocal inhibition."

Future Directions

Given the complexity of the olfactory system in *C. elegans*, genetic and molecular approaches need to be complemented with functional circuit studies. Identifying receptors responsible for the sensation of olfactory stimuli coupled with elucidating the *functional* connections of the nematode, will improve the understanding of the olfactory connectome.

Functional Connectomics

The initial wave of *C. elegans* neuronal circuit dissections focused heavily on understanding the physical connectome. Many studies have since shown that neurons communicate heavily outside of synaptic connections suggesting a much bigger picture of how neural circuits function (Bargmann, 2012; Bentley et al., 2016; Rajendran et al., 2014). Canonically, only neuropeptide signals have been known to function in a long-range, extra-synaptic fashion (Leinwand & Chalasani, 2014; Mills et al., 2012). However,

recent studies have shown that the monoaminergic nervous system communicates in context-dependent and extra-synaptic manners (Hardaway et al., 2015; R. Komuniecki, Hapiak, Harris, & Bamber, 2014). Also, extracellular vesicles are playing increasingly important roles in extra-synaptic cell-to-cell signaling and circuit regulation (Rajendran et al., 2014; J. Wang et al., 2015).

Increasingly, the physiological state or age of *C. elegans* is being found to influence the functional aspects of the connectome (Chao, Komatsu, Fukuto, Dionne, & Hart, 2004; Ghosh et al., 2016; Leinwand et al., 2015). To completely elucidate the functional connectome, factors such as age, sex, physiological state, and life history, must be taken into account and assayed independently. A likely outcome of these studies is that many overlapping functional connectomes will be generated providing deeper insights into the role of neuroregulators.

Receptor Identification

To fully understand olfaction, the mechanistic underpinnings of the process must be revealed. To do this, the receptors that physically sense and bind these cues need to be identified. Due to the inherent complexity that arises from co-expression (Hostettler et al., 2017; Troemel et al., 1995) and heterodimerization (Park et al., 2012) of GPCRs, fully identifying receptor complexes will require an immense amount of investigation. With multiple receptors being required for sensing different concentrations of the same cue, the mechanisms of olfaction have become even more complex than initially believed (Taniguchi et al., 2014).

There are many approaches currently available for identifying receptors, ranging from RNAi knockdowns to quantitative trait locus mapping for identification of chromosomal regions responsible for proper olfactory response (Greene et al., 2016b; Greene et al., 2016a; Taniguchi et al., 2014). The development of biochemical probes increases the scope by which identifying olfactory receptors can be achieved. These

probes are modified cues, containing functional groups that can be photo-activated to covalently bind to the receptor, allowing for direct confirmation of binding. These probes can also be constructed to allow for FRET analysis following covalent binding, removing the need for purification to identify the receptor (Park et al., 2012). Recently, genomic and transcriptomic investigations have been used to match receptor expression profiles with ligand targets (Greene et al., 2016b; Greene et al., 2016a; Greer et al., 2016).

While much has been discovered about molecular and circuit mechanisms of olfaction, much remains to be understood. *C. elegans'* experimental amenability and defined connectome offers an ideal tool for addressing these gaps by providing a "systems-level" analysis of olfaction. Increases in neuronal imaging capabilities allows for unrestrained live imaging with minimal alterations being made to the natural state of the animal. This allows for circuit-level read-outs to be deciphered. Recent studies have focused on understanding global control of olfaction (Saul Kato et al., 2015; Nguyen et al., 2016; Venkatachalam et al., 2016). Future work will likely focus on uncovering the regulation of olfactory circuits that integrate olfactory stimuli along with targeted identification of individual GPCRs necessary for olfactory sensation.

References

Akerboom, J., Chen, T.-W., Wardill, T. J., Tian, L., Marvin, J. S., Mutlu, S., . . . Looger, L. L. (2012). Optimization of a GCaMP calcium indicator for neural activity imaging. *The Journal of Neuroscience, 32*(40), 13819-13840. doi:10.1523/JNEUROSCI.2601-12.2012

Akerboom, J., Rivera, J. D. V., Guilbe, M. M. R., Malavé, E. C. A., Hernandez, H. H., Tian, L., . . . Schreiter, E. R. (2009). Crystal Structures of the GCaMP Calcium Sensor Reveal the Mechanism of Fluorescence Signal Change and Aid Rational Design. *The Journal of Biological Chemistry, 284*(10), 6455-6464. doi:10.1074/jbc.M807657200

Albrecht, D. R., & Bargmann, C. I. (2011). High-content behavioral analysis of Caenorhabditis elegans in precise spatiotemporal chemical environments. *Nat Meth, 8*(7), 599-605. doi:10.1038/nmeth.1630

Androwski, R. J. (2017). Phenotypic plasticity and remodeling in the stress-induced Caenorhabditis elegans dauer. *Wiley interdisciplinary reviews. Developmental biology*, e278.

Azevedo, F. A. C., Carvalho, L. R. B., Grinberg, L. T., Farfel, J. M., Ferretti, R. E. L., Leite, R. E. P., . . . Herculano-Houzel, S. (2009). Equal numbers of neuronal and nonneuronal cells make the human brain an isometrically scaled-up primate brain. *The Journal of Comparative Neurology, 513*(5), 532-541. doi:10.1002/cne.21974

Azulay, A., Itskovits, E., & Zaslaver, A. (2016). The *C. elegans* Connectome Consists of Homogenous Circuits with Defined Functional Roles. *PLoS Comput Biol, 12*(9), e1005021. doi:10.1371/journal.pcbi.1005021

Bargmann, C. I. (1998). Neurobiology of the *Caenorhabditis elegans* Genome. *Science, 282*(5396), 2028. doi:10.1126/science.282.5396.2028

Bargmann, C. I. (2006a). Chemosensation in *C. elegans*. *WormBook*, 1-29. doi:10.1895/wormbook.1.123.1

Bargmann, C. I. (2006b). Comparative chemosensation from receptors to ecology. *Nature, 444*(7117), 295-301. doi:10.1038/nature05402

Bargmann, C. I. (2012). Beyond the connectome: how neuromodulators shape neural circuits. *Bioessays, 34*(6), 458-465. doi:10.1002/bies.201100185

Bargmann, C. I., Hartwieg, E., & Horvitz, H. R. (1993). Odorant-selective genes and neurons mediate olfaction in C. elegans. *Cell, 74*(3), 515-527. doi:10.1016/0092-8674(93)80053-H

Bargmann, C. I., & Marder, E. (2013). From the connectome to brain function. *Nat Methods, 10*(6), 483-490.

Barr, M. M., & Garcia, L. R. (2006). Male mating behavior. *WormBook*, 1-11. doi:10.1895/wormbook.1.78.1

Barrios, A., Ghosh, R., Fang, C., Emmons, S. W., & Barr, M. M. (2012). PDF-1 neuropeptide signaling modulates a neural circuit for mate-searching behavior in *C. elegans*. *Nature Neuroscience, 15*(12), 1675-1684. doi:10.1038/nn.3253

Bastiani, C., & Mendel, J. (2006). Heterotrimeric G proteins in C. elegans. *WormBook*, 1-25. doi:10.1895/wormbook.1.75.1

Bear, Daniel M., Lassance, J.-M., Hoekstra, Hopi E., & Datta, Sandeep R. (2016). The Evolving Neural and Genetic Architecture of Vertebrate Olfaction. *Current Biology, 26*(20), R1039-R1049. doi:10.1016/j.cub.2016.09.011

Bentley, B., Branicky, R., Barnes, C. L., Chew, Y. L., Yemini, E., Bullmore, E. T., . . . Schafer, W. R. (2016). The Multilayer Connectome of *Caenorhabditis elegans*. *PLoS Comput Biol, 12*(12), e1005283. doi:10.1371/journal.pcbi.1005283

Borbolis, F., Flessa, C.-M., Roumelioti, F., Diallinas, G., Stravopodis, D. J., & Syntichaki, P. (2017). Neuronal function of the mRNA decapping complex determines survival of Caenorhabditis elegans at high temperature through temporal regulation of heterochronic gene expression. *Open Biology, 7*(3), 160313. doi:10.1098/rsob.160313

Bretscher, A. J., Busch, K. E., & de Bono, M. (2008). A carbon dioxide avoidance behavior is integrated with responses to ambient oxygen and food in *Caenorhabditis elegans*. *Proceedings of the National Academy of Sciences, 105*(23), 8044-8049. doi:10.1073/pnas.0707607105

Bretscher, Andrew J., Kodama-Namba, E., Busch, Karl E., Murphy, Robin J., Soltesz, Z., Laurent, P., & de Bono, M. (2011). Temperature, Oxygen, and Salt-Sensing Neurons in *C. elegans* Are Carbon Dioxide Sensors that Control Avoidance Behavior. *Neuron, 69*(6), 1099-1113. doi:10.1016/j.neuron.2011.02.023

Buckingham, S. D., Partridge, F. A., & Sattelle, D. B. (2014). Automated, high-throughput, motility analysis in Caenorhabditiselegans and parasitic nematodes: Applications in the search for new anthelmintics. *International Journal for Parasitology: Drugs and Drug Resistance, 4*(3), 226-232. doi:10.1016/j.ijpddr.2014.10.004

Busch, K. E., Laurent, P., Soltesz, Z., Murphy, R. J., Faivre, O., Hedwig, B., . . . de Bono, M. (2012). Tonic signaling from O2 sensors sets neural circuit activity and behavioral state. *Nat Neurosci, 15*(4), 581-591. doi:10.1038/nn.3061

Butcher, R. A. (2017a). Decoding chemical communication in nematodes. *Nat Prod Rep, 34*(5), 472-477. doi:10.1039/c7np00007c

Butcher, R. A. (2017b). Small-molecule pheromones and hormones controlling nematode development. *Nat Chem Biol, 13*(6), 577-586. doi:10.1038/nchembio.2356d

Butcher, R. A., Fujita, M., Schroeder, F. C., & Clardy, J. (2007). Small-molecule pheromones that control dauer development in *Caenorhabditis elegans*. *Nat Chem Biol, 3*(7), 420-422. doi:10.1038/nchembio.2007.3

Carrillo, M. A., Guillermin, M. L., Rengarajan, S., Okubo, R. P., & Hallem, E. A. (2013). O2-sensing neurons control CO2 response in C. elegans. *J Neurosci, 33*(23), 9675-9683. doi:10.1523/jneurosci.4541-12.2013

Carrillo, M. A., & Hallem, E. A. (2015). Gas sensing in nematodes. *Mol Neurobiol, 51*(3), 919-931. doi:10.1007/s12035-014-8748-z

Chalasani, S. H., Chronis, N., Tsunozaki, M., Gray, J. M., Ramot, D., Goodman, M. B., & Bargmann, C. I. (2007). Dissecting a circuit for olfactory behaviour in Caenorhabditis elegans. *Nature, 450*(7166), 63-70. doi:10.1038/nature06292

Chalasani, S. H., Kato, S., Albrecht, D. R., Nakagawa, T., Abbott, L. F., & Bargmann, C. I. (2010). Neuropeptide feedback modifies odor-evoked dynamics in *Caenorhabditis elegans* olfactory neurons. *Nat Neurosci, 13*(5), 615-621. doi:10.1038/nn.2526

Chalfie, M., Sulston, J. E., White, J. G., Southgate, E., Thomson, J. N., & Brenner, S. (1985). The neural circuit for touch sensitivity in Caenorhabditis elegans. *The Journal of Neuroscience, 5*(4), 956. doi:10.1523/JNEUROSCI.05-04-00956.1985

Chang, A. J., Chronis, N., Karow, D. S., Marletta, M. A., & Bargmann, C. I. (2006). A Distributed Chemosensory Circuit for Oxygen Preference in *C. elegans*. *PLoS Biology, 4*(9), e274. doi:10.1371/journal.pbio.0040274

Chao, M. Y., Komatsu, H., Fukuto, H. S., Dionne, H. M., & Hart, A. C. (2004). Feeding status and serotonin rapidly and reversibly modulate a Caenorhabditis elegans chemosensory circuit. *Proc Natl Acad Sci U S A, 101*(43), 15512-15517. doi:10.1073/pnas.0403369101

Chatzigeorgiou, M., Bang, S., Hwang, S. W., & Schafer, W. R. (2013). tmc-1 encodes a sodium-sensitive channel required for salt chemosensation in C. elegans. *Nature, 494*(7435), 95-99. doi:10.1038/nature11845

Chess, A., Simon, I., Cedar, H., & Axel, R. (1994). Allelic inactivation regulates olfactory receptor gene expression. *Cell, 78*(5), 823-834.

Cheung, B. H. H., Arellano-Carbajal, F., Rybicki, I., & de Bono, M. (2004). Soluble Guanylate Cyclases Act in Neurons Exposed to the Body Fluid to Promote C. elegans Aggregation Behavior. *Current Biology, 14*(12), 1105-1111. doi:10.1016/j.cub.2004.06.027

Chokshi, T. V., Bazopoulou, D., & Chronis, N. (2010). An automated microfluidic platform for calcium imaging of chemosensory neurons in Caenorhabditis elegans. *Lab on a Chip, 10*(20), 2758-2763. doi:10.1039/C004658B

Chronis, N., Zimmer, M., & Bargmann, C. I. (2007). Microfluidics for in vivo imaging of neuronal and behavioral activity in *Caenorhabditis elegans*. *Nat Meth, 4*(9), 727-731. doi:10.1038/nmeth1075

Chute, C. D., & Srinivasan, J. (2014). Chemical mating cues in *C. elegans*. *Semin Cell Dev Biol, 33*, 18-24. doi:10.1016/j.semcdb.2014.06.002

Coburn, C. M., & Bargmann, C. I. (1996). A Putative Cyclic Nucleotide–Gated Channel Is Required for Sensory Development and Function in C. elegans. *Neuron, 17*(4), 695-706. doi:10.1016/S0896-6273(00)80201-9

Cochella, L., Tursun, B., Hsieh, Y. W., Galindo, S., Johnston, R. J., Chuang, C. F., & Hobert, O. (2014). Two distinct types of neuronal asymmetries are controlled by the *Caenorhabditis elegans* zinc finger transcription factor die-1. *Genes Dev, 28*(1), 34-43. doi:10.1101/gad.233643.113

Colbert, H. A., & Bargmann, C. I. (1997). Environmental signals modulate olfactory acuity, discrimination, and memory in Caenorhabditis elegans. *Learn Mem, 4*(2), 179-191.

Cronin, C. J., Feng, Z., & Schafer, W. R. (2006). Automated imaging of C. elegans behavior. *Methods Mol Biol, 351*.

Cuppen, E., van der Linden, A. M., Jansen, G., & Plasterk, R. H. (2003). Proteins interacting with Caenorhabditis elegans Galpha subunits. *Comp Funct Genomics, 4*(5), 479-491. doi:10.1002/cfg.318

de Bono, M., & Maricq, A. V. (2005). Neuronal substrates of complex behaviors in C. elegans. *Annu Rev Neurosci, 28*, 451-501. doi:10.1146/annurev.neuro.27.070203.144259

Dwyer, N. D., Troemel, E. R., Sengupta, P., & Bargmann, C. I. (1998). Odorant Receptor Localization to Olfactory Cilia Is Mediated by ODR-4, a Novel Membrane-Associated Protein. *Cell, 93*(3), 455-466. doi:10.1016/S0092-8674(00)81173-3

Elgaali, H., Hamilton-Kemp, T. R., Newman, M. C., Collins, R. W., Yu, K., & Archbold, D. D. (2002). Comparison of long-chain alcohols and other volatile compounds emitted from food-borne and related Gram positive and Gram negative bacteria. *Journal of Basic Microbiology, 42*(6), 373-380. doi:10.1002/1521-4028(200212)42:6<373::AID-JOBM373>3.0.CO;2-4

Fagan, K. A., & Portman, D. S. (2014). Sexual modulation of neural circuits and behavior in Caenorhabditis elegans. *Semin Cell Dev Biol, 33*, 3-9. doi:10.1016/j.semcdb.2014.06.007

Fang-Yen, C., Gabel, C. V., Samuel, A. D., Bargmann, C. I., & Avery, L. (2012). Laser microsurgery in *Caenorhabditis elegans*. *Methods Cell Biol, 107*, 177-206. doi:10.1016/B978-0-12-394620-1.00006-0

Faumont, S., Rondeau, G., Thiele, T. R., Lawton, K. J., McCormick, K. E., Sottile, M., . . . Lockery, S. R. (2011). An Image-Free Opto-Mechanical System for Creating Virtual Environments and Imaging Neuronal Activity in Freely Moving Caenorhabditis elegans. *PLoS One, 6*(9), e24666. doi:10.1371/journal.pone.0024666

Félix, M.-A., & Braendle, C. (2010). The natural history of Caenorhabditis elegans. *Current Biology, 20*(22), R965-R969. doi:10.1016/j.cub.2010.09.050

Feng, Z., Cronin, C. J., Wittig, J. H., Sternberg, P. W., & Schafer, W. R. (2004). An imaging system for standardized quantitative analysis of C. elegans behavior. *BMC Bioinformatics, 5*. doi:10.1186/1471-2105-5-115

Fitzpatrick, D. A., O'Halloran, D. M., & Burnell, A. M. (2006). Multiple lineage specific expansions within the guanylyl cyclase gene family. *BMC Evolutionary Biology, 6*, 26-26. doi:10.1186/1471-2148-6-26

García, L. R., & Portman, D. S. (2016). Neural circuits for sexually dimorphic and sexually divergent behaviors in Caenorhabditis elegans. *Curr Opin Neurobiol, 38*, 46-52. doi:10.1016/j.conb.2016.02.002

Ghosh, D. D., Nitabach, M. N., Zhang, Y., & Harris, G. (2017). Multisensory integration in C. elegans. *Curr Opin Neurobiol, 43*, 110-118. doi:10.1016/j.conb.2017.01.005

Ghosh, D. D., Sanders, T., Hong, S., McCurdy, L. Y., Chase, D. L., Cohen, N., . . . Nitabach, M. N. (2016). Neural Architecture of Hunger-Dependent Multisensory Decision Making in C. elegans. *Neuron, 92*(5), 1049-1062. doi:10.1016/j.neuron.2016.10.030

Golden, J. W., & Riddle, D. L. (1982). A pheromone influences larval development in the nematode Caenorhabditis elegans. *Science, 218*(4572), 578. doi:10.1126/science.6896933

Gray, J. M., Karow, D. S., Lu, H., Chang, A. J., Chang, J. S., Ellis, R. E., . . . Bargmann, C. I. (2004). Oxygen sensation and social feeding mediated by a C. elegans guanylate cyclase homologue. *Nature, 430*(6997), 317-322. doi:10.1038/nature02714

Greene, J. S., Brown, M., Dobosiewicz, M., Ishida, I. G., Macosko, E. Z., Zhang, X., . . . Bargmann, C. I. (2016b). Balancing selection shapes density-dependent foraging behaviour. *Nature, 539*(7628), 254-258. doi:10.1038/nature19848

Greene, J. S., Dobosiewicz, M., Butcher, R. A., McGrath, P. T., & Bargmann, C. I. (2016a). Regulatory changes in two chemoreceptor genes contribute to a *Caenorhabditis elegans* QTL for foraging behavior. *eLife, 5*. doi:10.7554/eLife.21454

Greer, P. L., Bear, D. M., Lassance, J. M., Bloom, M. L., Tsukahara, T., Pashkovski, S. L., . . . Datta, S. R. (2016). A Family of non-GPCR Chemosensors Defines an Alternative Logic for Mammalian Olfaction. *Cell, 165*(7), 1734-1748. doi:10.1016/j.cell.2016.05.001

Guo, M., Wu, T. H., Song, Y. X., Ge, M. H., Su, C. M., Niu, W. P., . . . Wu, Z. X. (2015). Reciprocal inhibition between sensory ASH and ASI neurons modulates

nociception and avoidance in Caenorhabditis elegans. *Nat Commun, 6*, 5655. doi:10.1038/ncomms6655

Hallem, E. A., Spencer, W. C., McWhirter, R. D., Zeller, G., Henz, S. R., Ratsch, G., . . . Ringstad, N. (2011). Receptor-type guanylate cyclase is required for carbon dioxide sensation by Caenorhabditis elegans. *Proc Natl Acad Sci U S A, 108*(1), 254-259. doi:10.1073/pnas.1017354108

Hallem, E. A., & Sternberg, P. W. (2008). Acute carbon dioxide avoidance in Caenorhabditis elegans. *Proc Natl Acad Sci U S A, 105*(23), 8038-8043. doi:10.1073/pnas.0707469105

Hamilton-Kemp, T., Newman, M., Collins, R., Elgaali, H., Yu, K., & Archbold, D. (2005). Production of the long-chain alcohols octanol, decanol, and dodecanol by Escherichia coli. *Curr Microbiol, 51*(2), 82-86. doi:10.1007/s00284-005-4469-x

Hardaway, J. A., Sturgeon, S. M., Snarrenberg, C. L., Li, Z., Xu, X. Z., Bermingham, D. P., . . . Blakely, R. D. (2015). Glial Expression of the Caenorhabditis elegans Gene swip-10 Supports Glutamate Dependent Control of Extrasynaptic Dopamine Signaling. *J Neurosci, 35*(25), 9409-9423. doi:10.1523/jneurosci.0800-15.2015

Harris, G., Korchnak, A., Summers, P., Hapiak, V., Law, W. J., Stein, A. M., . . . Komuniecki, R. (2011). Dissecting the Serotonergic Food Signal Stimulating Sensory-Mediated Aversive Behavior in *C. elegans*. *PLoS One, 6*(7), e21897. doi:10.1371/journal.pone.0021897

Harris, G. P., Hapiak, V. M., Wragg, R. T., Miller, S. B., Hughes, L. J., Hobson, R. J., . . . Komuniecki, R. W. (2009). Three distinct amine receptors operating at different levels within the locomotory circuit are each essential for the serotonergic modulation of chemosensation in Caenorhabditis elegans. *J Neurosci, 29*(5), 1446-1456. doi:10.1523/jneurosci.4585-08.2009

Hart, A. C. (2006). Behavior. *WormBook*. doi: doi/10.1895/wormbook.1.87.1

Hart, M. P., & Hobert, O. (2015). Sexual Dimorphism: Mystery Neurons Control Sex-Specific Behavioral Plasticity. *Curr Biol, 25*(24), R1170-1172. doi:10.1016/j.cub.2015.11.002

Hilliard, M. A., Apicella, A. J., Kerr, R., Suzuki, H., Bazzicalupo, P., & Schafer, W. R. (2005). In vivo imaging of C. elegans ASH neurons: cellular response and adaptation to chemical repellents. *The EMBO Journal, 24*(1), 63-72. doi:10.1038/sj.emboj.7600493

Hilliard, M. A., Bargmann, C. I., & Bazzicalupo, P. (2002). C. elegans responds to chemical repellents by integrating sensory inputs from the head and the tail. *Curr Biol, 12*(9), 730-734.

Hilliard, M. A., Bergamasco, C., Arbucci, S., Plasterk, R. H. A., & Bazzicalupo, P. (2004). Worms taste bitter: ASH neurons, QUI-1, GPA-3 and ODR-3 mediate quinine avoidance in *Caenorhabditis elegans*. *The EMBO Journal, 23*(5), 1101-1111. doi:10.1038/sj.emboj.7600107

Hodgkin, J. (1983). Male Phenotypes and Mating Efficiency in *Caenorhabditis elegans*. *Genetics, 103*(1), 43-64.

Hong, J. H., & Park, M. (2016). Understanding Synaptogenesis and Functional Connectome in C. elegans by Imaging Technology. *Front Synaptic Neurosci, 8*, 18. doi:10.3389/fnsyn.2016.00018

Hostettler, L., Grundy, L., Kaser-Pebernard, S., Wicky, C., Schafer, W. R., & Glauser, D. A. (2017). The Bright Fluorescent Protein mNeonGreen Facilitates Protein Expression Analysis In Vivo. *G3 (Bethesda), 7*(2), 607-615. doi:10.1534/g3.116.038133

Hukema, R. K., Rademakers, S., Dekkers, M. P., Burghoorn, J., & Jansen, G. (2006). Antagonistic sensory cues generate gustatory plasticity in Caenorhabditis elegans. *Embo J, 25*(2), 312-322. doi:10.1038/sj.emboj.7600940

Hussey, R., Stieglitz, J., Mesgarzadeh, J., Locke, T. T., Zhang, Y. K., Schroeder, F. C., & Srinivasan, S. (2017). Pheromone-sensing neurons regulate peripheral lipid metabolism in Caenorhabditis elegans. *PLoS Genet, 13*(5), e1006806. doi:10.1371/journal.pgen.1006806

Husson, S. J., Costa, W. S., Schmitt, C., & Gottschalk, A. (2012). Keeping track of worm trackers. *WormBook*, 1-17. doi:10.1895/wormbook.1.156.1

Iino, Y., & Yoshida, K. (2009). Parallel Use of Two Behavioral Mechanisms for Chemotaxis in Caenorhabditis elegans. *The Journal of Neuroscience, 29*(17), 5370. doi:10.1523/JNEUROSCI.3633-08.2009

Izquierdo, E. J., & Lockery, S. R. (2010). Evolution and analysis of minimal neural circuits for klinotaxis in Caenorhabditis elegans. *J Neurosci, 30*(39), 12908-12917. doi:10.1523/jneurosci.2606-10.2010

Jafari, G., Xie, Y., Kullyev, A., Liang, B., & Sze, J. Y. (2011). Regulation of extrasynaptic 5-HT by serotonin reuptake transporter function in 5-HT-absorbing neurons underscores adaptation behavior in Caenorhabditis elegans. *J Neurosci, 31*(24), 8948-8957. doi:10.1523/jneurosci.1692-11.2011

Jang, H., Kim, K., Neal, S. J., Macosko, E., Kim, D., Butcher, R. A., . . . Sengupta, P. (2012). Neuromodulatory state and sex specify alternative behaviors through antagonistic synaptic pathways in *C. elegans*. *Neuron, 75*(4), 585-592. doi:10.1016/j.neuron.2012.06.034

Jansen, G., Thijssen, K. L., Werner, P., van derHorst, M., Hazendonk, E., & Plasterk, R. H. A. (1999). The complete family of genes encoding G proteins of *Caenorhabditis elegans*. *Nat Genet, 21*(4), 414-419. doi:10.1038/7753

Jenett, A., Rubin, Gerald M., Ngo, T.-T. B., Shepherd, D., Murphy, C., Dionne, H., . . . Zugates, Christopher T. (2012). A GAL4-Driver Line Resource for Drosophila Neurobiology. *Cell Reports, 2*(4), 991-1001. doi:10.1016/j.celrep.2012.09.011

Jeong, P.-Y., Jung, M., Yim, Y.-H., Kim, H., Park, M., Hong, E., . . . Paik, Y.-K. (2005). Chemical structure and biological activity of the *Caenorhabditis elegans* dauer-inducing pheromone. *Nature, 433*(7025), 541-545. doi:10.1038/nature03201

Kahn-Kirby, A. H., Dantzker, J. L. M., Apicella, A. J., Schafer, W. R., Browse, J., Bargmann, C. I., & Watts, J. L. (2004). Specific Polyunsaturated Fatty Acids Drive TRPV-Dependent Sensory Signaling In Vivo. *Cell, 119*(6), 889-900. doi:10.1016/j.cell.2004.11.005

Kato, S., Kaplan, Harris S., Schrödel, T., Skora, S., Lindsay, Theodore H., Yemini, E., . . . Zimmer, M. (2015). Global Brain Dynamics Embed the Motor Command Sequence of Caenorhabditis elegans. *Cell, 163*(3), 656-669. doi:10.1016/j.cell.2015.09.034

Kato, S., Xu, Y., Cho, C. E., Abbott, L. F., & Bargmann, C. I. (2014). Temporal responses of C. elegans chemosensory neurons are preserved in behavioral dynamics. *Neuron, 81*(3), 616-628. doi:10.1016/j.neuron.2013.11.020

Kawano, T., Po, Michelle D., Gao, S., Leung, G., Ryu, William S., & Zhen, M. (2011). An Imbalancing Act: Gap Junctions Reduce the Backward Motor Circuit Activity to Bias *C. elegans* for Forward Locomotion. *Neuron, 72*(4), 572-586. doi:10.1016/j.neuron.2011.09.005

Kim, K., Sato, K., Shibuya, M., Zeiger, D. M., Butcher, R. A., Ragains, J. R., . . . Sengupta, P. (2009). Two Chemoreceptors Mediate Developmental Effects of Dauer Pheromone in *C. elegans*. *Science, 326*(5955), 994-998. doi:10.1126/science.1176331

Komatsu, H., Mori, I., Rhee, J.-S., Akaike, N., & Ohshima, Y. (1996). Mutations in a Cyclic Nucleotide–Gated Channel Lead to Abnormal Thermosensation and Chemosensation in C. elegans. *Neuron, 17*(4), 707-718. doi:10.1016/S0896-6273(00)80202-0

Komuniecki, R., Hapiak, V., Harris, G., & Bamber, B. (2014). Context-dependent modulation reconfigures interactive sensory-mediated microcircuits in

Caenorhabditis elegans. *Curr Opin Neurobiol, 29*, 17-24. doi:10.1016/j.conb.2014.04.006

Komuniecki, R., Harris, G., Hapiak, V., Wragg, R., & Bamber, B. (2012). Monoamines activate neuropeptide signaling cascades to modulate nociception in C. elegans: a useful model for the modulation of chronic pain? *Invertebrate Neuroscience, 12*(1), 53-61. doi:10.1007/s10158-011-0127-0

Lagoy, R. C., & Albrecht, D. R. (2015). Microfluidic Devices for Behavioral Analysis, Microscopy, and Neuronal Imaging in Caenorhabditis elegans. *Methods Mol Biol, 1327*, 159-179. doi:10.1007/978-1-4939-2842-2_12

Larsch, J., Flavell, S. W., Liu, Q., Gordus, A., Albrecht, D. R., & Bargmann, C. I. (2015). A circuit for gradient climbing in C. elegans chemotaxis. *Cell Reports, 12*(11), 1748-1760. doi:10.1016/j.celrep.2015.08.032

Larsch, J., Ventimiglia, D., Bargmann, C. I., & Albrecht, D. R. (2013). High-throughput imaging of neuronal activity in Caenorhabditis elegans. *Proc Natl Acad Sci U S A, 110*(45), E4266-4273. doi:10.1073/pnas.1318325110

LeBoeuf, B., Correa, P., Jee, C., & García, L. R. (2014). *Caenorhabditis elegans* male sensory-motor neurons and dopaminergic support cells couple ejaculation and post-ejaculatory behaviors. *eLife, 3*, e02938. doi:10.7554/eLife.02938

Lee, H., Choi, M.-k., Lee, D., Kim, H.-s., Hwang, H., Kim, H., . . . Lee, J. (2012). Nictation, a dispersal behavior of the nematode Caenorhabditis elegans, is regulated by IL2 neurons. *Nat Neurosci, 15*(1), 107-112. doi:10.1038/nn.2975

Leifer, A. M., Fang-Yen, C., Gershow, M., Alkema, M. J., & Samuel, A. D. T. (2011). Optogenetic manipulation of neural activity in freely moving Caenorhabditis elegans. *Nature methods, 8*(2), 147-152. doi:10.1038/nmeth.1554

Leinwand, S. G., & Chalasani, S. H. (2014). From genes to circuits and behaviors: Neuropeptides expand the coding potential of the nervous system. *Worm, 3*, e27730. doi:10.4161/worm.27730

Leinwand, S. G., Yang, C. J., Bazopoulou, D., Chronis, N., Srinivasan, J., & Chalasani, S. H. (2015). Circuit mechanisms encoding odors and driving aging-associated behavioral declines in Caenorhabditis elegans. *eLife, 4*, e10181. doi:10.7554/eLife.10181

Liu, K., Sternberg, P. (1995). Sensory Regulation of Male Mating Behavior. *Neuron*.

Lockery, S. R. (2011). The computational worm: spatial orientation and its neuronal basis in C. elegans. *Curr Opin Neurobiol, 21*(5), 782-790. doi:10.1016/j.conb.2011.06.009

Ludewig, A. H., & Schroeder, F. C. (2013). Ascaroside signaling in *C. elegans*. *WormBook*, 1-22. doi:10.1895/wormbook.1.155.1

Luo, L., Gabel, C. V., Ha, H. I., Zhang, Y., & Samuel, A. D. (2008). Olfactory behavior of swimming C. elegans analyzed by measuring motile responses to temporal variations of odorants. *J Neurophysiol, 99*(5), 2617-2625. doi:10.1152/jn.00053.2008

Macosko, E. Z., Pokala, N., Feinberg, E. H., Chalasani, S. H., Butcher, R. A., Clardy, J., & Bargmann, C. I. (2009). A Hub-and-Spoke Circuit Drives Pheromone Attraction and Social Behavior in *C. elegans*. *Nature, 458*(7242), 1171-1175. doi:10.1038/nature07886

Maruyama, I. N. (2016). Receptor Guanylyl Cyclases in Sensory Processing. *Front Endocrinol (Lausanne), 7*, 173. doi:10.3389/fendo.2016.00173

McGrath, P. T., Xu, Y., Ailion, M., Garrison, J. L., Butcher, R. A., & Bargmann, C. I. (2011). Parallel evolution of domesticated *Caenorhabditis* species targets pheromone receptor genes. *Nature, 477*(7364), 321-325. doi:10.1038/nature10378

Meisel, J. D., Panda, O., Mahanti, P., Schroeder, F. C., & Kim, D. H. (2014). Chemosensation of bacterial secondary metabolites modulates neuroendocrine signaling and behavior of C. elegans. *Cell, 159*(2), 267-280. doi:10.1016/j.cell.2014.09.011

Mills, H., Ortega, A., Law, W., Hapiak, V., Summers, P., Clark, T., & Komuniecki, R. (2016). Opiates Modulate Noxious Chemical Nociception through a Complex

Monoaminergic/Peptidergic Cascade. *J Neurosci, 36*(20), 5498-5508. doi:10.1523/jneurosci.4520-15.2016

Mills, H., Wragg, R., Hapiak, V., Castelletto, M., Zahratka, J., Harris, G., . . . Komuniecki, R. (2012). Monoamines and neuropeptides interact to inhibit aversive behaviour in Caenorhabditis elegans. *Embo J, 31*(3), 667-678. doi:10.1038/emboj.2011.422

Milward, K., Busch, K. E., Murphy, R. J., de Bono, M., & Olofsson, B. (2011). Neuronal and molecular substrates for optimal foraging in Caenorhabditis elegans. *Proceedings of the National Academy of Sciences of the United States of America, 108*(51), 20672-20677. doi:10.1073/pnas.1106134109

Murayama, T., & Maruyama, I. N. (2013). Decision making in C. elegans chemotaxis to alkaline pH: Competition between two sensory neurons, ASEL and ASH. *Communicative & Integrative Biology, 6*(6), e26633. doi:10.4161/cib.26633

Murayama, T., Takayama, J., Fujiwara, M., & Maruyama, I. N. (2013). Environmental alkalinity sensing mediated by the transmembrane guanylyl cyclase GCY-14 in C. elegans. *Curr Biol, 23*(11), 1007-1012. doi:10.1016/j.cub.2013.04.052

Nakai, J., Ohkura, M., & Imoto, K. (2001). A high signal-to-noise Ca(2+) probe composed of a single green fluorescent protein. *Nat Biotechnol, 19*(2), 137-141. doi:10.1038/84397

Narayan, A., Venkatachalam, V., Durak, O., Reilly, D. K., Bose, N., Schroeder, F. C., . . . Sternberg, P. W. (2016). Contrasting responses within a single neuron class enable sex-specific attraction in *Caenorhabditis elegans*. *Proc Natl Acad Sci U S A, 113*(10), E1392-1401. doi:10.1073/pnas.1600786113

Nguyen, J. P., Shipley, F. B., Linder, A. N., Plummer, G. S., Liu, M., Setru, S. U., . . . Leifer, A. M. (2016). Whole-brain calcium imaging with cellular resolution in freely behaving Caenorhabditis elegans. *Proc Natl Acad Sci U S A, 113*(8), E1074-1081. doi:10.1073/pnas.1507110112

Ortiz, C. O., Etchberger, J. F., Posy, S. L., Frøkjær-Jensen, C., Lockery, S., Honig, B., & Hobert, O. (2006). Searching for Neuronal Left/Right Asymmetry: Genomewide Analysis of Nematode Receptor-Type Guanylyl Cyclases. *Genetics, 173*(1), 131. doi:10.1534/genetics.106.055749

Park, D., O'Doherty, I., Somvanshi, R. K., Bethke, A., Schroeder, F. C., Kumar, U., & Riddle, D. L. (2012). Interaction of structure-specific and promiscuous G-protein-coupled receptors mediates small-molecule signaling in *Caenorhabditis elegans*. *PNAS, 109*(25), 9917-9922. doi:10.1073/pnas.1202216109

Pierce-Shimomura, J. T., Morse, T. M., & Lockery, S. R. (1999). The fundamental role of pirouettes in Caenorhabditis elegans chemotaxis. *J Neurosci, 19*(21), 9557-9569.

Portman, D. S. (2017). Sexual modulation of sex-shared neurons and circuits in Caenorhabditis elegans. *J Neurosci Res, 95*(1-2), 527-538. doi:10.1002/jnr.23912

Pungaliya, C., Srinivasan, J., Fox, B. W., Malik, R. U., Ludewig, A. H., Sternberg, P. W., & Schroeder, F. C. (2009). A shortcut to identifying small molecule signals that regulate behavior and development in *Caenorhabditis elegans*. *Proceedings of the National Academy of Sciences of the United States of America, 106*(19), 7708-7713. doi:10.1073/pnas.0811918106

Rajendran, L., Bali, J., Barr, M. M., Court, F. A., Kramer-Albers, E. M., Picou, F., . . . Breakefield, X. O. (2014). Emerging roles of extracellular vesicles in the nervous system. *J Neurosci, 34*(46), 15482-15489. doi:10.1523/jneurosci.3258-14.2014

Reilly, D. K., Lawler, D. E., Albrecht, D. R., & Srinivasan, J. (2017). Using an Adapted Microfluidic Olfactory Chip for the Imaging of Neuronal Activity in Response to Pheromones in Male *C. Elegans* Head Neurons. *Journal of Visualized Experiments*(127), e56026. doi:doi:10.3791/56026

Ren, P., Lim, C. S., Johnsen, R., Albert, P. S., Pilgrim, D., & Riddle, D. L. (1996). Control of C. elegans larval development by neuronal expression of a TGF-beta homolog. *Science, 274*(5291), 1389-1391.

Rengarajan, S., & Hallem, E. A. (2016). Olfactory circuits and behaviors of nematodes. *Curr Opin Neurobiol, 41*, 136-148. doi:10.1016/j.conb.2016.09.002

Sambongi, Y., Nagae, T., Liu, Y., Yoshimizu, T., Takeda, K., Wada, Y., & Futai, M. (1999). Sensing of cadmium and copper ions by externally exposed ADL, ASE, and ASH neurons elicits avoidance response in Caenorhabditis elegans. *Neuroreport, 10*(4), 753-757.

Sammut, M., Cook, S. J., Nguyen, K. C. Q., Felton, T., Hall, D. H., Emmons, S. W., . . . Barrios, A. (2015). Glia-derived neurons are required for sex-specific learning in C. elegans. *Nature, 526*(7573), 385-390. doi:10.1038/nature15700

Schackwitz, W. S., Inoue, T., & Thomas, J. H. (1996). Chemosensory neurons function in parallel to mediate a pheromone response in C. elegans. *Neuron, 17*(4), 719-728.

Schindelman, G., Whittaker, A. J., Thum, J. Y., Gharib, S., & Sternberg, P. W. (2006). Initiation of male sperm-transfer behavior in *Caenorhabditis elegans* requires input from the ventral nerve cord. *BMC Biology, 4*(1), 26. doi:10.1186/1741-7007-4-26

Schrodel, T., Prevedel, R., Aumayr, K., Zimmer, M., & Vaziri, A. (2013). Brain-wide 3D imaging of neuronal activity in Caenorhabditis elegans with sculpted light. *Nat Methods, 10*(10), 1013-1020. doi:10.1038/nmeth.2637

Schulenburg, H., & Félix, M. A. (2017). The Natural Biotic Environment of Caenorhabditis elegans. *Genetics, 206*(1), 55-86. doi:10.1534/genetics.116.195511

Sengupta, P., Chou, J. H., & Bargmann, C. I. (1996). odr-10 encodes a seven transmembrane domain olfactory receptor required for responses to the odorant diacetyl. *Cell, 84*(6), 899-909.

Serizawa, S., Miyamichi, K., Nakatani, H., Suzuki, M., Saito, M., Yoshihara, Y., & Sakano, H. (2003). Negative feedback regulation ensures the one receptor-one olfactory neuron rule in mouse. *Science, 302*(5653), 2088-2094. doi:10.1126/science.1089122

Serrano-Saiz, E., Pereira, L., Gendrel, M., Aghayeva, U., Battacharya, A., Howell, K., . . . Hobert, O. (2017). A Neurotransmitter Atlas of the Caenorhabditis elegans Male

Nervous System Reveals Sexually Dimorphic Neurotransmitter Usage. *Genetics, 206*(3), 1251-1269. doi:10.1534/genetics.117.202127

Smith, E. S., Martinez-Velazquez, L., & Ringstad, N. (2013). A chemoreceptor that detects molecular carbon dioxide. *J Biol Chem, 288*(52), 37071-37081. doi:10.1074/jbc.M113.517367

Sohn, Y., Choi, M. K., Ahn, Y. Y., Lee, J., & Jeong, J. (2011). Topological cluster analysis reveals the systemic organization of the Caenorhabditis elegans connectome. *PLoS Comput Biol, 7*(5), e1001139. doi:10.1371/journal.pcbi.1001139

Srinivasan, J., Kaplan, F., Ajredini, R., Zachariah, C., Alborn, H. T., Teal, P. E., . . . Schroeder, F. C. (2008). A blend of small molecules regulates both mating and development in *Caenorhabditis elegans*. *Nature, 454*(7208), 1115-1118. doi:10.1038/nature07168

Srinivasan, J., von Reuss, S. H., Bose, N., Zaslaver, A., Mahanti, P., Ho, M. C., . . . Schroeder, F. C. (2012). A modular library of small molecule signals regulates social behaviors in *Caenorhabditis elegans*. *PLoS Biol, 10*(1), e1001237. doi:10.1371/journal.pbio.1001237

Stirman, J. N., Crane, M. M., Husson, S. J., Wabnig, S., Schultheis, C., Gottschalk, A., & Lu, H. (2011). Real-time multimodal optical control of neurons and muscles in freely-behaving Caenorhabditis elegans. *Nature methods, 8*(2), 153-158. doi:10.1038/nmeth.1555

Styer, K. L., Singh, V., Macosko, E., Steele, S. E., Bargmann, C. I., & Aballay, A. (2008). Innate Immunity in *Caenorhabditis elegans* Is Regulated by Neurons Expressing NPR-1/GPCR. *Science, 322*(5900), 460. doi:10.1126/science.1163673

Sulston, J. E., Albertson, D. G., & Thomson, J. N. (1980). The Caenorhabditis elegans male: postembryonic development of nongonadal structures. *Dev Biol, 78*. doi:10.1016/0012-1606(80)90352-8

Sulston, J. E., & Horvitz, H. R. (1977). Post-embryonic cell lineages of the nematode, Caenorhabditis elegans. *Dev Biol, 56*(1), 110-156. doi:10.1016/0012-1606(77)90158-0

Summers, P. J., Layne, R. M., Ortega, A. C., Harris, G. P., Bamber, B. A., & Komuniecki, R. W. (2015). Multiple Sensory Inputs Are Extensively Integrated to Modulate Nociception in C. elegans. *J Neurosci, 35*(28), 10331-10342. doi:10.1523/jneurosci.0225-15.2015

Sun, X. R., Badura, A., Pacheco, D. A., Lynch, L. A., Schneider, E. R., Taylor, M. P., . . . Wang, S. S. H. (2013). Fast GCaMPs for improved tracking of neuronal activity. *Nature Communications, 4*, 2170. doi:10.1038/ncomms3170

Swierczek, N. A., Giles, A. C., Rankin, C. H., & Kerr, R. A. (2011). High-throughput behavioral analysis in C. elegans. *Nat Meth, 8*(7), 592-598. doi:10.1038/nmeth.1625

Sze, J. Y., Victor, M., Loer, C., Shi, Y., & Ruvkun, G. (2000). Food and metabolic signalling defects in a Caenorhabditis elegans serotonin-synthesis mutant. *Nature, 403*(6769), 560-564. doi:10.1038/35000609

Taniguchi, G., Uozumi, T., Kiriyama, K., Kamizaki, T., & Hirotsu, T. (2014). Screening of odor-receptor pairs in Caenorhabditis elegans reveals different receptors for high and low odor concentrations. *Sci Signal, 7*(323), ra39. doi:10.1126/scisignal.2005136

Tatro, E. T. (2014). Brain-wide imaging of neurons in action. *Front Neural Circuits, 8*, 31. doi:10.3389/fncir.2014.00031

Teotonio, H., Estes, S., Phillips, P. C., & Baer, C. F. (2017). Experimental Evolution with Caenorhabditis Nematodes. *Genetics, 206*(2), 691-716. doi:10.1534/genetics.115.186288

Tobin, D. M., Madsen, D. M., Kahn-Kirby, A., Peckol, E. L., Moulder, G., Barstead, R., . . . Bargmann, C. I. (2002). Combinatorial Expression of TRPV Channel Proteins Defines Their Sensory Functions and Subcellular Localization in C. elegans Neurons. *Neuron, 35*(2), 307-318. doi:10.1016/S0896-6273(02)00757-2

Touhara, K., & Vosshall, L. B. (2009). Sensing odorants and pheromones with chemosensory receptors. *Annu Rev Physiol, 71*, 307-332. doi:10.1146/annurev.physiol.010908.163209

Towlson, E. K., Vertes, P. E., Ahnert, S. E., Schafer, W. R., & Bullmore, E. T. (2013). The rich club of the C. elegans neuronal connectome. *J Neurosci, 33*(15), 6380-6387. doi:10.1523/jneurosci.3784-12.2013

Troemel, E. R., Chou, J. H., Dwyer, N. D., Colbert, H. A., & Bargmann, C. I. (1995). Divergent seven transmembrane receptors are candidate chemosensory receptors in C. elegans. *Cell, 83*(2), 207-218. doi:10.1016/0092-8674(95)90162-0

Troemel, E. R., Kimmel, B. E., & Bargmann, C. I. (1997). Reprogramming chemotaxis responses: sensory neurons define olfactory preferences in C. elegans. *Cell, 91*(2), 161-169.

Tsechpenakis, G., Bianchi, L., Metaxas, D., & Driscoll, M. (2008). A novel computational approach for simultaneous tracking and feature extraction of C. elegans populations in fluid environments. *IEEE Trans Biomed Eng, 55*. doi:10.1109/tbme.2008.918582

Tsibidis, G. D., & Tavernarakis, N. (2007). Nemo: a computational tool for analyzing nematode locomotion. *BMC Neuroscience, 8*(1), 86. doi:10.1186/1471-2202-8-86

Venkatachalam, V., Ji, N., Wang, X., Clark, C., Mitchell, J. K., Klein, M., . . . Samuel, A. D. (2016). Pan-neuronal imaging in roaming Caenorhabditis elegans. *Proc Natl Acad Sci U S A, 113*(8), E1082-1088. doi:10.1073/pnas.1507109113

Walker, D. S., Vázquez-Manrique, R. P., Gower, N. J. D., Gregory, E., Schafer, W. R., & Baylis, H. A. (2009). Inositol 1,4,5-Trisphosphate Signalling Regulates the Avoidance Response to Nose Touch in Caenorhabditis elegans. *PLOS Genetics, 5*(9), e1000636. doi:10.1371/journal.pgen.1000636

Wang, J., Kaletsky, R., Silva, M., Williams, A., Haas, L. A., Androwski, R. J., . . . Barr, M. M. (2015). Cell-Specific Transcriptional Profiling of Ciliated Sensory Neurons

Reveals Regulators of Behavior and Extracellular Vesicle Biogenesis. *Curr Biol, 25*(24), 3232-3238. doi:10.1016/j.cub.2015.10.057

Wang, J., Schwartz, H. T., & Barr, M. M. (2010). Functional Specialization of Sensory Cilia by an RFX Transcription Factor Isoform. *Genetics, 186*(4), 1295. doi:10.1534/genetics.110.122879

Ward, S. (1973). Chemotaxis by the Nematode Caenorhabditis elegans: Identification of Attractants and Analysis of the Response by Use of Mutants. *Proceedings of the National Academy of Sciences of the United States of America, 70*(3), 817-821. doi:10.1073/pnas.70.3.817

Ward, S., Thomson, N., White, J. G., & Brenner, S. (1975). Electron microscopical reconstruction of the anterior sensory anatomy of the nematode caenorhabditis elegans. *The Journal of Comparative Neurology, 160*(3), 313-337. doi:10.1002/cne.901600305

Ware, R. W., Clark, D., Crossland, K., & Russell, R. L. (1975). The nerve ring of the nematode Caenorhabditis elegans: Sensory input and motor output. *The Journal of Comparative Neurology, 162*(1), 71-110. doi:10.1002/cne.901620106

Wes, P. D., & Bargmann, C. I. (2001). C. elegans odour discrimination requires asymmetric diversity in olfactory neurons. *Nature, 410*(6829), 698-701. doi:10.1038/35070581

White, J. G., Southgate, E., Thomson, J. N., & Brenner, S. (1986). The Structure of the Nervous System of the Nematode Caenorhabditis elegans. *Phil Trans of the Royal Soc of Lon, 314*(1165), 1. doi:10.1098/rstb.1986.0056

White, Jamie Q., & Jorgensen, Erik M. (2012). Sensation in a Single Neuron Pair Represses Male Behavior in Hermaphrodites. *Neuron, 75*(4), 593-600. doi:10.1016/j.neuron.2012.03.044

White, J. Q., Nicholas, T. J., Gritton, J., Truong, L., Davidson, E. R., & Jorgensen, E. M. (2007). The sensory circuitry for sexual attraction in C. elegans males. *Curr Biol, 17*(21), 1847-1857. doi:10.1016/j.cub.2007.09.011

Yu, S., Avery, L., Baude, E., & Garbers, D. L. (1997). Guanylyl cyclase expression in specific sensory neurons: a new family of chemosensory receptors. *Proc Natl Acad Sci U S A, 94*(7), 3384-3387.

Zimmer, M., Gray, J. M., Pokala, N., Chang, A. J., Karow, D. S., Marletta, M. A., . . . Bargmann, C. I. (2009). Neurons Detect Increases and Decreases in Oxygen Levels Using Distinct Guanylate Cyclases. *Neuron, 61*(6), 865-879. doi:10.1016/j.neuron.2009.02.013

Chapter 2 Ascarosides

Chapter 2A Chemical Communication in *C. elegans*

Portions of the work in this chapter contributed to published manuscripts.

Figure 2 is adapted from figures present in:

> Chute, C. D., DiLoreto, E. M., Zhang, Y. K., Reilly, D. K., Rayes, D., Coyle, V. L., . . . Srinivasan, J. (2019). Co-option of neurotransmitter signaling for inter-organismal communication in C. elegans. *Nat Commun, 10*(1), 3186. doi:10.1038/s41467-019-11240-7

Figures 3 B and C were present as Supp. Fig. 13 A and B in:

> Dong, C., Reilly, D. K., Bergame, C., Dolke, F., Srinivasan, J., & von Reuss, S. H. (2018). Comparative Ascaroside Profiling of *Caenorhabditis* Exometabolomes Reveals Species-Specific (ω) and (ω - 2)-Hydroxylation Downstream of Peroxisomal beta-Oxidation. *J Org Chem*. doi:10.1021/acs.joc.8b00094

Summary

Roundworms, including the nematode *Caenorhabditis elegans*, communicate with conspecifics chemically. The majority of these signals are comprised of a single class of small molecules called ascarosides. These chemicals, comprised of a core sugar and fatty-acid derived side chain, signal a plethora of information, ranging from the sender's age, maturity, sexual identity, and life-history, to environmental conditions. Ascarosides were first identified signaling the entry into, and exit from, the dauer stage. More recently, ascarosides have been found to elicit behavioral responses, ranging from foraging and starvation responses, to mating cues. Here, we describe the current stage of the field of ascaroside study, including how structural changes affect outcomes. We also touch on the new field of non-ascaroside small molecule pheromones that are only just beginning to be discovered as a tool in nematode communication.

Chemical Signaling in *C. elegans*

C. elegans are microscopic organisms, lacking eyes and ears. Their means of sensing their surroundings is limited to thermo-, magno-, aero-, mechano- (one of the canonical "five senses": touch) and chemo-sensations (two of the "five senses": taste and smell). Olfaction is one of the most critical sense that *C. elegans* rely on (See **Chapter 1C**), and chemical communication is the main mode of communication employed by the nematode (D. K. Reilly & Srinivasan, 2017).

The majority of *C. elegans* chemical communication occurs solely through an ever-expanding class of small-molecule pheromones termed ascarosides (McGrath & Ruvinsky, 2019), with a growing – albeit significantly smaller – number of non-ascaroside chemical cues being discovered in recent years (Artyukhin et al., 2018; Liu et al., 2018; Ludewig et al., 2019).

It is with this modular, yet complex set of social signals that *C. elegans* communicates with conspecifics information about (Srinivasan et al., 2012; Stephan H. von Reuss et al., 2012; Stephan H. von Reuss & Schroeder, 2015; Zhang, Sanchez-Ayala, Sternberg, Srinivasan, & Schroeder, 2017): an individual's life-stage (Butcher, 2017a, 2017b; Kaplan et al., 2011; Ludewig & Schroeder, 2013), history, and sex (Chute & Srinivasan, 2014); the environment's nutrient status (Dolke et al., 2019); population density; and a host of other signals (Butcher, 2017b; Kaplan et al., 2011; Pungaliya et al., 2009; Srinivasan et al., 2008). None of these cues are sensed in isolation, existing instead as a blend, or cocktail, (Chute & Srinivasan, 2014; Srinivasan et al., 2008), from which the nematode must integrate and decode the information signaled from their native environment.

Ascarosides

Ascarosides are small-molecule pheromones produced by nematodes. These glycosides are built around a sugar – specifically the 3,6-dideoxysugar, L-ascarylose –linked to fatty-acid side chains of varying lengths and saturation (**Figure 12**) (Butcher, 2017b; Ludewig

& Schroeder, 2013). The first ascaroside (**Figure 12, Structure1**) discovered was found in extracts of species of the parasitic genus, *Ascaris*, in 1957 by both Fairburn and Fouquey (Fairbairn, 1957; Fouquey, Polonsky, & Lederer, 1957). Since then, this class of compounds has expanded, with known structures numbering in the hundreds. However, the functions of these are limited to only a handful.

The synthetic pathways of ascarosides are modular, with the same building blocks being utilized (i.e., L-ascarylose, and fatty acids) (Stephan H. von Reuss et al., 2012; Stephan H. von Reuss & Schroeder, 2015). This allows for a multitude of similar, yet unique structures to be constructed. For example, ascaroside #3 (ascr#3) (**Figure 12, Structure 2**) and ascaroside #10 (ascr#10) (**Figure 12, Structure 3**) contain the same length fatty acid. The fatty acid in ascr#3 is unsaturated, while ascr#10 lacks the double bond.

However, differences in structure can be diverse. For example, ascr#7 (**Figure 12, Structure 4**) can be modified via a para-aminobenzoate group to produce ascr#8 (**Figure 12, Structure 5**) (Pungaliya et al., 2009), which can be further modified to produce ascr#81 (**Figure 12, Structure 6**) and ascr#82 (**Figure 12, Structure 7**) (Artyukhin et al., 2018). Common moieties employed in ascaroside signaling include indole and octopamine groups, producing ascarosides such as icas#9 (**Figure 12, Structure 8**) (Srinivasan et al., 2012) and osas#9 (**Figure 12, Structure 9**) (Artyukhin et al., 2013; Chute et al., 2019), respectively.

Daumone/Developmental Ascarosides

The initial push to identify the structures of *C. elegans* pheromones focused on those involved in dauer formation. This cocktail of pheromones was long known to induce dauer development (Golden & Riddle, 1982). Over two decades later, the structure of one of the dauer-inducing pheromones was elucidated by Jeong et al (Jeong et al., 2005).

At the time, as the only structure elucidated dauer inducing pheromone in *C. elegans*, the compound was termed daumone (Jeong et al., 2005). Soon thereafter, it was found

that there was more than one "daumone" that functioned synergistically to induce dauer formation. Given that they were based around the core L-ascarylose sugar, the naming

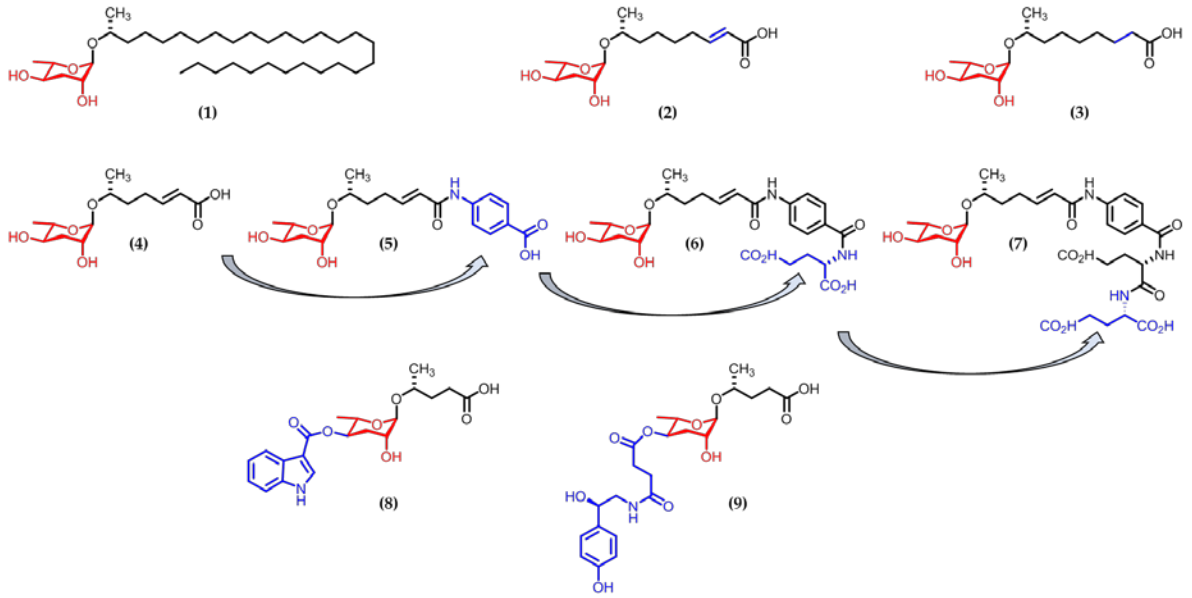

Figure 12. Structures of Ascarosides.
All ascarosides contain a core L-ascarylose sugar (red) attached to a fatty-acid derived side chain. The initially discovered ascaroside **(1)** contains an extraordinarily long sidechain. Ascarosides #3 **(2)** and #10 **(3)** differ only in the saturation o of a single double bond (blue). Ascaroside #7 **(4)** can be modularly modified via a PABA group to produce ascr#8 **(5)**, while glutamates can be added to generate ascr#81 **(6)** and ascr#82 **(7)** (unique additions shown in blue). Other moieties can also be added to the sugar, such as indole (blue) as in icas#9 **(8)** and octopamine (bule), as in osas#9 **(9)**.

convention changed from "daumone" to "ascaroside". As the first ascaroside elucidated, daumone was named ascaroside #1. It was Butcher and colleagues who soon determined the structures of ascr#2 and ascr#3 (Butcher, 2017b). After decades of no structural identity of *C. elegans* pheromones, the number of structurally elucidated ascarosides sky-rocketed from zero to into the hundreds (Butcher, 2017a, 2017b; McGrath & Ruvinsky, 2019). Those ascarosides that play a role in the dauer developmental switch also include indole-containing ascarosides, such as icas#9 (**Figure 12, Structure 8**) (Butcher, Ragains, & Clardy, 2009).

Reception of these dauer inducing pheromones has been determined as well. Neuronal involvement has been elucidated through laser ablation experiments, while

receptor identification has occurred through reverse genetic screens, quantitative trace locus analyses, and photo-affinity probe binding.

The major players in dauer-regulating pheromone sensation are the ASI amphid chemosensory neurons. ASI contributes heavily to dauer development, as the sole source of the TGF-β homolog, DAF-7, in the worm (Ren et al., 1996). DAF-7 functions to regulate the switch into and out of dauer development. ASI sensing dauer-inducing pheromones, which trigger transcriptional changes in ASI (as opposed to calcium transients) - these transcriptional changes then result in DAF-7 signaling (Ren et al., 1996; Schackwitz, Inoue, & Thomas, 1996).

Behavioral Ascarosides

Ascarosides have also been found to elicit not only developmental changes, but also behavioral outputs. The indole-containing ascaroside, icas#9, for example, which inhibits dauer formation at high concentrations (Butcher et al., 2009), also functions as an aggregation molecule at lower concentrations (Srinivasan et al., 2012). The dauer inhibitory concentration acts in 100 nM range, while attraction is seen in the fM-pM range.

Such multimodal distributions of behavioral responses are not uncommon in ascaroside signal. ascr#3 (**Figure 12, Structure 2**) functions to induce dauer (in synergy with ascr#1 and ascr#2) in the nM range (Butcher, Fujita, Schroeder, & Clardy, 2007), also serves as a mating cue (repelling hermaphrodites and attracting males) in the μM concentration range (Fagan et al., 2018; Narayan et al., 2016).

Again, changes in structure alter the behavior elicited by ascarosides. ascr#9 has been shown to elicit aggregation behavior, while its indole-containing derivative, icas#9 (**Figure 12, Structure 8)**, is found in a "dispersal blend" (Kaplan et al., 2012). Recently, an ascr#9 derivative has been identified, which contains an octopamine moiety attached to the 4-carbon instead of an indole group. Connected by a succinyl group, the octopamine

containing moiety is known as octopamine-succinylated ascaroside #9 (osas#9) (Artyukhin et al., 2013) (**Figure 12, Structure 9)**.

osas#9 Functions as a Dispersal Cue Under Starvation Conditions

osas#9 is produced solely by starved L1-arrest animals (Artyukhin et al., 2013), and elicits a strong avoidance response, but only in similarly starved animals (of all life stages) (**Figure 13A**) (Chute et al., 2019). Work performed by members of our lab elucidated that the reception machinery for osas#9 includes the chemosensory neurons ASK (as well as ASE and ASI to a lesser extent), the G protein-coupled receptor, TYRA-2, and the G protein, GPA-6 (Chute et al., 2019).

In order to evaluate the role of TYRA-2 in the osas#9 response further, we assayed two unique loss-of-function (*lof*) *tyra-2* mutants for their ability to respond to the pheromone. Neither allele responded to osas#9 over the solvent control at physiologically relevant levels but did avoid at extremely high concentrations (100 μM) (**Figure 13B**). This appearance of avoidance is likely due to non-specific binding of the pheromone to receptors at such a high concentration.

The osas#9 receptor, TYRA-2, functions as an endogenous receptor for tyramine in a synaptic function (Fu et al., 2018; Ghosh, Nitabach, Zhang, & Harris, 2017). Given that it has since been co-opted for a role in extra-organismal sensation of a related molecule, octopamine, we examined if tyramine completes with osas#9 for cilia-localized TYRA-2 in eliciting avoidance behaviors (**Figure 13C**).

We first examined a 0:1 ratio of tyramine:osas#9, as in the absence of exogenous tyramine, starved *C. elegans* can avoid osas#9 (**Figure 13C**). In a 1:1 ratio of the two chemicals, wild type animals avoided the mixture, while *tyra-2 lof* animals did not (**Figure 13C**). At this concentration (1 μM), tyramine does not elicit avoidance on its own (Chute et al., 2019). However, at a 1000:1 ratio of tyramine:osas#9, both wild-type and tyra-2 lof animals exhibited avoidance (**Figure 13C**). At this concentration of tyramine (1 mM), *C.*

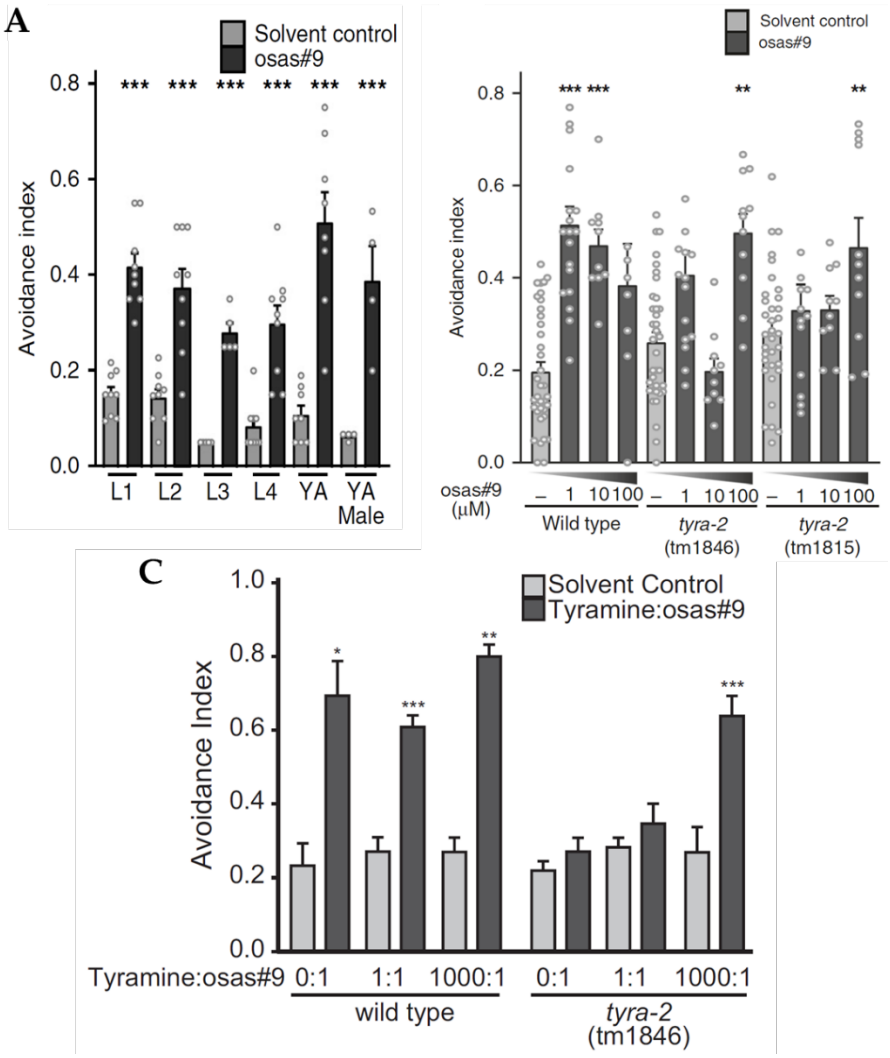

Figure 13. The Octopamine Containing Ascaroside, osas#9, Is Sensed by TYRA-2.
(A) All life-stages and sexes avoid 1 μM osas#9 when starved (See (Chute et al., 2019), Figure 1). **(B)** TYRA-2 senses osas#9 to drive avoidance behavior. In the loss-of-function mutants (*tm1846* and *tm1815*), no avoidance is observed at physiologically relevant levels. **(C)** Tyramine does not compete with osas#9 for TYRA-2 binding in avoidance of exogenous molecules. Ratios represent μM concentrations of tyramine to osas#9. All statistical comparisons are paired t-tests of osas#9 versus the respective solvent control. Error bars denote SEM. Trial counts are listed in (Chute et al., 2019). * $p < 0.05$, ** $p < 0.01$, *** $p < 0.001$. All panels adapted from: (Chute et al., 2019).

elegans can sense and avoid the neurotransmitter, sensing it through a distinct receptor and neuron than the ASK/TYRA-2 system utilized in osas#9 signaling (Chute et al., 2019). Therefore, the avoidance observed in *tyra-2 lof* mutants can be attributed to sensation of the extra-organismal neurotransmitter by another receptor/neuron pair.

A more in-depth investigation into the roles of the GPCR, TYRA-2, the chemosensory neuron, ASH, and the G protein, GPA-6, can be found in our laboratory's manuscript by

Chute et al., entitled, "Co-option of neurotransmitter signaling for inter-organismal communication in *C. elegans*". (Nature Communications, 2019, doi: 10.1038/s41467-019-11240-7).

Ascarosides Elicit Structure Specific Outcomes

The structure of each ascaroside is unique and offers nematodes the ability to convey a plethora of information. As stated earlier, ascr#3 (**Figure 12, Structure 2**) and ascr#10 (**Figure 12, Structure 3**) differ only in the saturation of a single carbon bond. Even with this ever so slight change in structure, there are vast differences. On one hand, ascr#10 is only produced by males, and serves to attract hermaphrodites (Aprison & Ruvinsky, 2017; Izrayelit et al., 2012). On the other hand, ascr#3 is produced by hermaphrodites, and: (1) attracts males (Srinivasan et al., 2008; Srinivasan et al., 2012), (2) repels other hermaphrodites (Fagan et al., 2018), and (3) contributes to dauer formation (Butcher et al., 2007; Butcher, Ragains, Kim, & Clardy, 2008). (A discussion on other roles of ascr#10 is provided in **Chapter 2B** of this thesis dissertation.)

Furthermore, each of these ascarosides is sensed through unique sets of amphid sensory neurons, with ascr#3 being sensed by ASK (Fagan et al., 2018; Narayan et al., 2016), ADL (Fagan et al., 2018; Jang et al., 2012), ADF (Fagan et al., 2018), ASJ (Aprison & Ruvinsky, 2017), AWB (Aprison & Ruvinsky, 2017), AWC (Aprison & Ruvinsky, 2017), and the male-specific CEM (Narayan et al., 2016); and ascr#10 being sensed by ADL (Aprison & Ruvinsky, 2017).

ω-Carbon Hydroxylation of ascaroside #3

In 2018, we – along with the group of Stephan H. von Reuss – showed that a male-female relative of *C. elegans*, *C. nigoni*, produces a novel class of ascr#3 derivatives (Dong et al., 2018). Examining the exometabolome extracts of *Caenorhabditis* species, a GC-EIMS-based comparative analysis (S. H. von Reuss, Dolke, & Dong, 2017) revealed three ascarosides that were uncharacterized. These compounds made up 10% of the *C. nigoni* exometabolome yet did not match any of the vast array of known ascarosides structures.

Via solid phase extraction, the structures of these novel ascarosides were determined to be ascr#3 (**Figure 14A, Structure 2**) derivatives. However, they contained a hydroxyl group added to either the ω (**Figure 14A, Structure 12**) or ω -2 (**Figure 14A, Structures 10 and 11**) carbons. We refer to these hydroxylated ascarosides as 9-HO-ascr#3, 7R-HO-ascr#3, and 7S-HO-ascr#3, respectively (Dong et al., 2018).

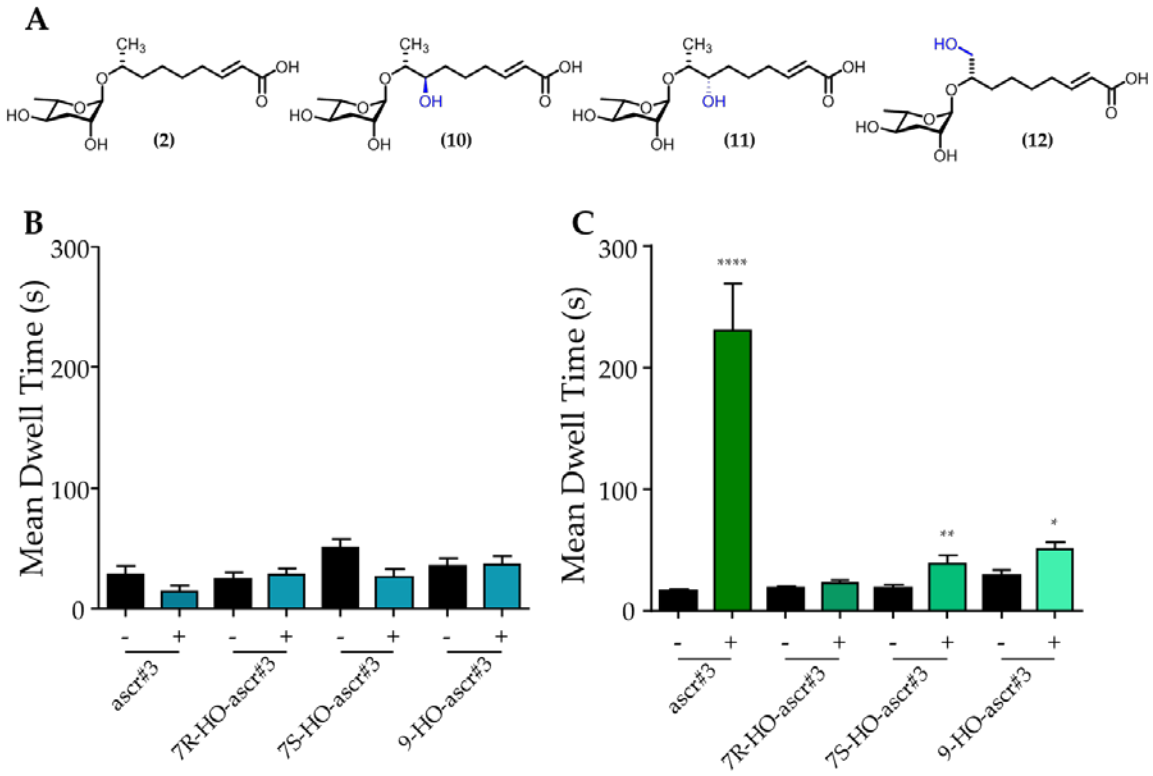

Figure 14. The Structures and Activity Profiles of Hydroxylated ascr#3 Derivatives.
(A) Additions of hydroxyl groups to the ω- **(12)** and ω-2 carbons **(10, 11)** of ascr#3 **(2)** are shown in blue. Both *R*- **(10)** and *S*- **(11)** configurations of the ω-2 hydroxlation were assayed. **(C)** *C. nigoni* females exhibit no attraction to ascr#3 or any of its derivatives. **(C)** Male *nigoni* animals are significantly attracted to the *S*-configuration (but not the *R*- configuration) of 7-HO-ascr#3, as well as the ω- hydroxylated 9-HO-ascr#3. Error bars denote SEM. n ≥10. Wilcoxon Matched-Pairs Signed Rank Test; control vs 1 μM ascaroside #3 derivative. * $p < 0.05$, ** $p < 0.01$, **** $p < 0.0001$. See (Dong et al., 2018), Supp. Fig, 13A and 13B.

In order to try and elucidate the biological function of these novel ascarosides, we employed a Spot Retention Assay previously used by our lab (Narayan et al., 2016; Pungaliya et al., 2009). In this assay, animals are placed on an NGM agar plate with two drops: one comprised of a vehicle control, and one containing a non-volatile attractant – usually an ascaroside. Worms are allowed to explore the plate, and their dwell time in

each drop is scored. In previous studies, both ascr#3 and ascr#8 have been shown to be extremely attractive to males using this assay (Narayan et al., 2016; Pungaliya et al., 2009). Given that ascr#3 elicits a strong male-specific attractive behavior (Pungaliya et al., 2009), we exposed both male and female *C. nigoni* worms to 1 μM concentrations of each hydroxlated-ascr#3 and assayed for any attraction to these compounds.

We found no attraction of female *C. nigoni* to any compound, including ascr#3 (**Figure 14B**) (Dong et al., 2018). We saw a statistically significant increase in the amount of time spent in 7S-HO-ascr#3 and 9-HO-ascr#3 over vehicle controls (**Figure 14C**). However, these dwell times were markedly decreased when compared to male *C. nigoni* attraction to ascr#3 (**Figure 14C**) (Dong et al., 2018).

Of note is that the more distant relative of *C. elegans*, *C. afra*, was also found to produce these compounds, suggesting that the ability to hydroxylate ascarosides is a new example of convergent evolution (Dong et al., 2018). While more experiments are needed to elucidate the biological function of hydroxylated-ascr#3 derivatives, their existence provides a precedent for species-specific modifications to "common" ascaroside structures. Exactly what these novel compounds are doing will likely be responses to variations in the individual ecological niches of these species.

Variations in the Structure of the Core Sugar Alters Behavioral Valences

While L-ascarylose is the main building block of ascarosides; other sugars have been identified in nematode exometabolomes. The dimorphic species *Pristionchus pacificus* has been found to employs an epimerization at the 2-position, resulting in the incorporation of an L-paratose over an L-ascarylose, such as in the production of part#9 (**Figure 15A, Structure 14**) from ascr#9 (**Figure 15A, Structure 13**) (Bose et al., 2012). There have recently been newly uncovered 3,6-dideoxy sugar which employs epimerization a the 4-position, named L-caenorhabdose. Recently discovered and synthesized by Stephan H. von Reuss' group, this pheromone is present in *C. nigoni*, acting as a species-specific

signal (**Figure 15A, Structure 15**) (Bergame, Dong, Sutour, & von Reuss, 2019). As with the hydroxylated ascr#3 derivatives (**Figure 15A, Structure 10**), L-caenorhabdose pheromones have also been identified in the distantly related *C. afra* (Bergame et al., 2019).

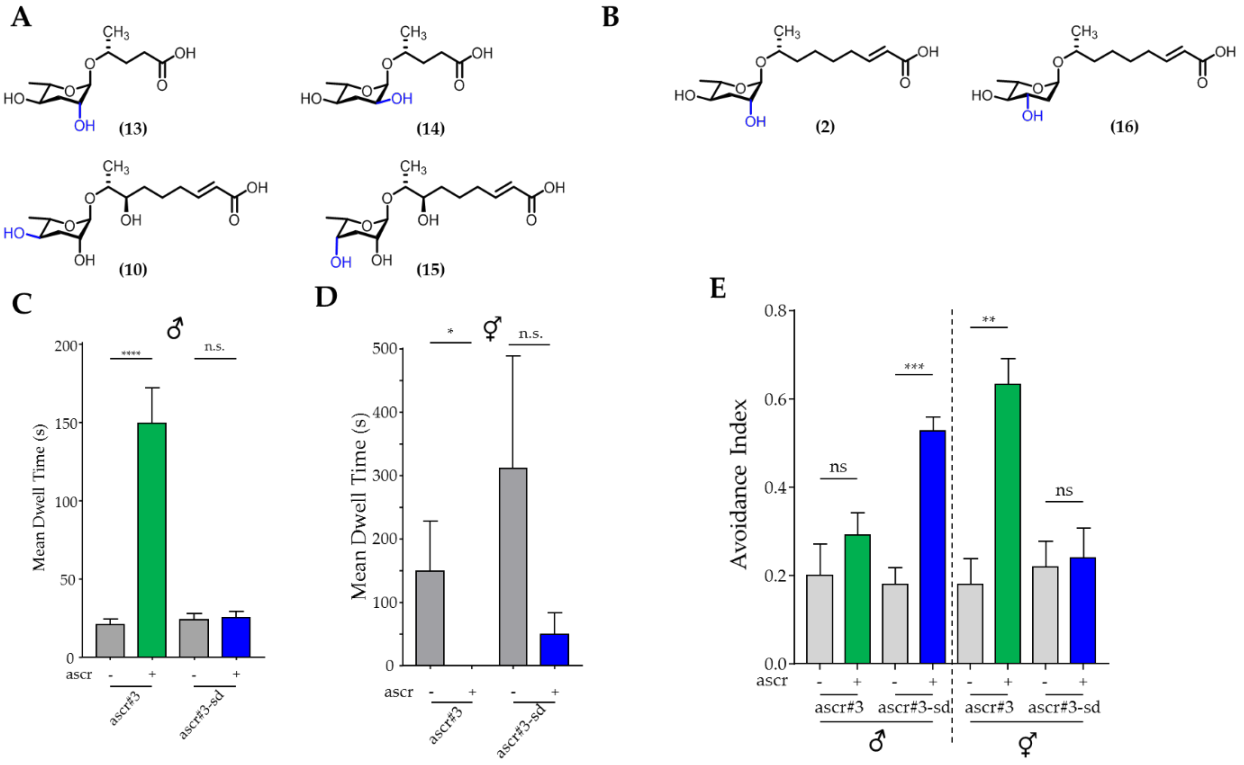

Figure 15. Sugar Epimerization Affects Behavioral Outputs.
(A) Examples of sugar epimerization in the literature include ascr#9 **(13)**, which can undergo a 2-epimerization to yield part#9, containing an L-paratose **(14)**. Meanwhile, 7R-HO-ascr#3 **(10)** can undergo a 4-epimerization to generate a pheromone containing an L-caenorhabdose sugar **(15)**. (B) An ascr#3 **(2)** sugar derivative **(16)**, in which a hydroxyl group has been moved from the 4- carbon to the 3-carbon, yielding ascr#3-sd. **(C)** Males are not attracted to ascr#3-sd, while they remain attracted to ascr#3. **(D)** Hermaphrodites are attracted to neither chemical. **(E)** Male *C. elegans* exhibit a behavioral valence flip between ascr#3 and ascr#3-sd, avoiding the novel cue, while hermaphrodites appear to not respond to the cue at all. Error bars denote SEM. n ≥ 5. Wilcoxon Matched-Pairs Signed Rank Test; control vs 1 μM ascaroside. * $p < 0.05$, ** $p < 0.01$, *** $p < 0.001$, **** $p < 0.0001$.

However, all these core building blocks are 3,6-dideoxy sugars, with hydroxyl groups being present in the 2- and 4- positions. Our collaborators in the Schroeder lab at Cornell University have recently uncovered a novel ascr#3 derivative in which the sugar contains the hydroxyl groups at the 3- and 4- positions (**Figure 15B, Structure 16**).

As male *C. elegans* are strongly attracted to ascr#3 (Pungaliya et al., 2009), we first assayed males for their respond to this ascr#3 sugar derivative (hereafter referred to as: ascr#3-sd). We again utilized the Spot Retention Assay previous employed by our lab (Narayan et al., 2016).

We found that males exhibited a stark decrease in the amount of time spent in ascr#3-sd compared to ascr#3 (**Figure 15C**). In fact, there was no discernable difference in the amount of time spent in the vehicle versus 1 μM ascr#3-sd.

However, given the flaws in the Spot Retention Assay (see **Chapter 3B**), specifically in regards to being unable to distinguish between "lack of attraction" and "avoidance" of the cues tested, we next tested male *C. elegans* against ascr#3 and ascr#3-sd using an avoidance drop test (Hilliard, Bergamasco, Arbucci, Plasterk, & Bazzicalupo, 2004). In this test, a drop of the chemical is placed on the tail of an animal. Capillary action wicks the cue to the amphid region, allowing the animal to sense the cue. If aversive, the compound will elicit an avoidance response, characterized as: (1) an omega-turn followed by a reversal; (2) a reversal of two body bends, or; (3) a change in direction of greater than 90 degrees. **Chapter 1C** of this thesis provides a more detailed description of this assay.

We found that male *C. elegans* do not avoid ascr#3, as expected – given the pheromone's attractive nature. However, when exposed to ascr#3-sd, males exhibited a strong avoidance to the novel cue (**Figure 15E**). This change in behavioral valence (i.e., switching from an attractive to aversive response) was unexpected, give the relatively small change to the structure of ascr#3.

The pheromone ascr#3 has been shown to function uniquely in each sex: attracting males and repelling hermaphrodites through unique pathways (Aprison & Ruvinsky, 2017; Fagan et al., 2018; Jang et al., 2012; Narayan et al., 2016). We therefore wondered whether this changing of behavioral valence was limited to males or was not a sex-specific change.

Hermaphrodites displayed no change in their response to ascr#3-sd over ascr#3 in the same assay (**Figure 15D**). We then assayed hermaphrodites for their ability to avoid ascr#3 (Fagan et al., 2018). While hermaphrodites did indeed avoid ascr#3 (**Figure 15E**), they no longer exhibited an avoidance when exposed to ascr#3-sd (**Figure 15E**).

There are a few hypotheses that can be drawn from this data. Given that males exhibited such a stark change in behavioral valence to ascr#3-sd over ascr#3, and that hermaphrodites avoided neither cue (nor were they attracted to either) (**Figure 15D, E**), it may be that the receptors necessary for response to ascr#3-sd are (1) only expressed in males, or (2) require masculinization of the nervous system to elicit a behavioral response (Fagan et al., 2018). It may also be that ascr#3-sd solely functions in males, and that hermaphrodites have no ecological reason to respond to the pheromone. However, given the strong avoidance observed in males, suggesting unfavorable conditions, this is unlikely. There may be transcriptional changes that ascr#3-sd elicits in hermaphrodites. Full-animal RNAseq should be performed on both males and hermaphrodites exposed to ascr#3 and ascr#3-sd, and genes which exhibit differential expression targeted for follow-up studies.

Future Work

Having observed a similar loss of attraction in ascr#3-sd as in the HO-ascr#3 derivatives isolated in *C. nigoni* exometabolomes (Dong et al., 2018)– both of which were assayed using the Spot Retention Assay – it would be prudent to examine the HO-ascr#3 pheromones for the ability to elicit avoidance responses in either sex. Similarly, females showed no different in their behavior to the HO-ascr#3 pheromone – as in their response to ascr#3-sd. However, a male-specific change is still possible.

Simply moving a hydroxyl group from the 2- to the 3- position of the sugar ring elicited a switch in male behavioral valence. Follow-up studies which investigate the mechanisms that result in these changes will be fascinating. Not only focused on why *C.*

elegans would employ another sugar in such a "common" ascaroside like ascr#3, these questions will seek to answer what are the differences in reception biology between the two pheromones: What neurons are involved in ascr#3-sd sensation? Are the receptors that sense ascr#3 the same as those that sense ascr#3-sd, and just expressed in unique neurons, or are they evolutionarily divergent? Are the male and hermaphroditic receptors the same between the sexes – and pheromones? What internal machinery does *C. elegans* employ to produce ascr#3-sd? What does it tell conspecifics about the environment, mating status, life history, etc.?

Expanding the signaling repertoire even further: non-ascarosides

Nematodes, lacking options in auditory and visual communication, are limited to chemical communication to describe the environment to conspecifics. While the ascaroside system is conserved and vast (McGrath & Ruvinsky, 2019), it is not the sole form of communication between nematodes.

Sulfated Small-Molecule Predator Signals

C. elegans are not the only animals in their environment. There are predatory nematodes, specifically the distant relative, *Pristionchus pacificus*, which inhabit overlapping ecological niches as *C. elegans*. *P. pacificus* provides an interesting dimorphic creature of study, as when starved, adult animals undergo a morphological change, developing an extra denticle, or tooth-like structure it its oral cavity (Bento, Ogawa, & Sommer, 2010). This allows the larger nematode to break through the cuticle of larval *C. elegans* and ingest them.

Naturally, any advantage to *C. elegans* that would allow it to detect and avoid predatory *P. pacificus* would be an enormous boon. As such, *C. elegans* has developed the ability to eavesdrop on *P. pacificus* secretions – namely compounds that are present in the secretions of starved *P. pacificus* (Liu et al., 2018). During development, *P. pacificus* can follow two paths: developing into a bacterivorous state, or a predacious state. One of the

outcomes of this switch is the massive sulfation of small molecules, specifically by the enzyme EUD-1 (Ragsdale, Muller, Rodelsperger, & Sommer, 2013). It is two of these sulfated compounds, sufac#1 (**Figure 16A, Structure 17**) and sufal#2 (**Figure 16A, Structure 18**), that *C. elegans* senses (Liu et al., 2018).

Unlike osas#9 (**Figure 12, Structure 9**), which requires a precise physiological state of *C. elegans* to elicit avoidance (Chute et al., 2019), sufac#1 and sufal#2 drive avoidance responses in *C. elegans* regardless of internal state. Liu et al. were able to show that the sensory machinery required for responding to these two compounds is redundant, involving four neuronal pairs, ensuring proper sensation and escape behavior (Liu et al., 2018).

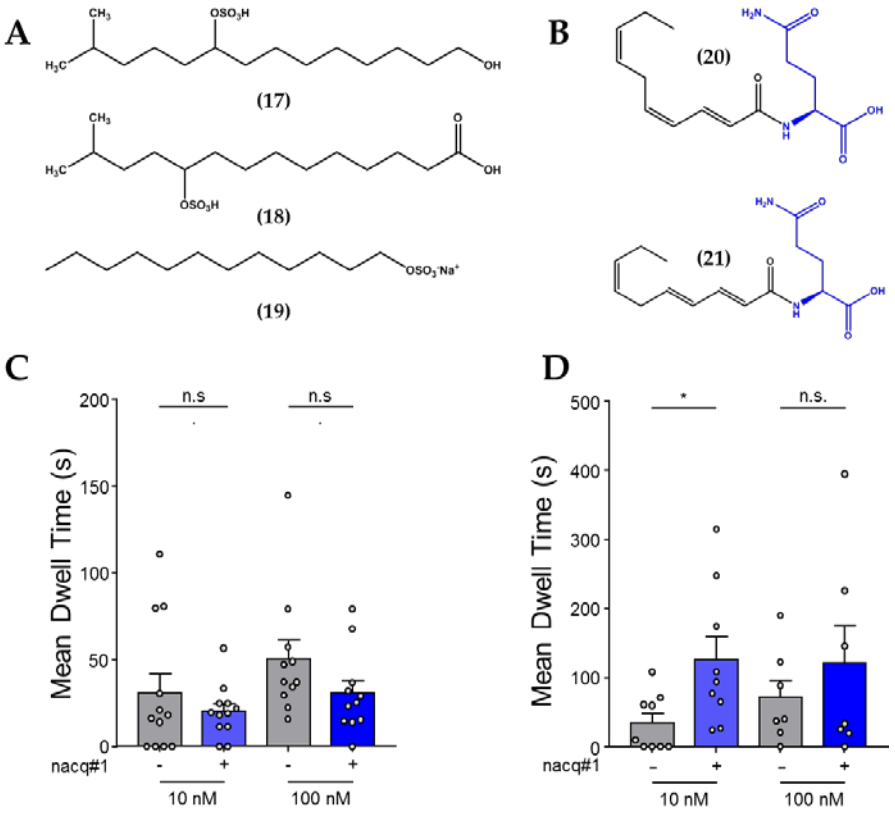

Figure 16. Non-ascaroside small molecule signaling in nematodes.
(A) Structures of sufac#2 (**17**) and sufal#1 (**18**), produced by *P. pacificus*. The structure of sodium dodecyl sulfact (SDS) is shown as well (**19**). **(B)** Structures of *cis* (**20**) and *trans* (**21**) configuration of *N*-acyl gluatamine (nacq#1 and nacq#2, respectively). **(C)** Male *C. elegans* exhibit no behavioral response to nacq#1. **(D)** Hermaphrodite behavioral response to nacq#1. Hermaphrodites are attracted to lower concentrations of nacq#1. Error bars denote SEM. n ≥ 8. Wilcoxon Matched-Pairs Signed Rank Test; control vs nacq#1. * p = 0.0391.

Interestingly, these two compounds share a striking similarity to the nematode repellent, sodium dodecyl sulfate (SDS) (**Figure 16A, Structure 19**) (Liu et al., 2018). SDS is a synthetic detergent (commonly found in toothpastes as sodium lauryl sulfate), and as such, *C. elegans* would never encounter this compound in its natural environment. Other than its role as a detergent, there was previously no known reason for *C. elegans* to exhibit such robust behavioral and neurophysiological responses to SDS (Hilliard et al., 2004; Zou et al., 2017). However, Liu et al. showed that the same neurons that sense sufac#1 and sufal#2 are required for the SDS response, suggesting that the same machinery is able to detect SDS (Liu et al., 2018).

Self-Recognition Peptides

Pristionchus secretes an exometabolome that includes non-ascaroside signals which *C. elegans* senses as predator cues. When starved, *P. pacificus* undergoes an irreversible morphological change, developing a second denticle allowing for the devouring of larval nematodes. In order to recognize their own progeny as "self" and not prey, *P. pacificus* utilizes a small peptide, SELF-1 (Lightfoot et al., 2019).

Lightfoot et al. showed that *P. pacificus* will even kill larvae from other *pacificus* strains, but not of self-progeny. The presence of a short peptide, 63-66 amino acids long, they found, is what determined "self". The first 57 amino acids are extremely conserved in the 38 *P. pacificus* strains tested, with a "hypervariable domain" being present on the C-terminus. This sequence varied greatly in length and composition and was found to be required for determining "self" (Lightfoot et al., 2019). A transcriptional reporter localized expression of *self-1* to the epidermis of the nematodes, although their attempts at epitope-tagging continually resulted in *self-1* mutant phenotype. There are cleavage sites (Lysine-Arginine residues as seen in in *C. elegans* PC2 cleavage enzyme, *egl-3* (Li & Kim, 2014)), suggesting that the final product may be cleaved and released into the environment, but this has yet to be determined (Lightfoot et al., 2019).

C. elegans Expanded Signaling Repertoire

In recent analysis of *C. elegans* exometabolomes, Ludewig et al. identified non-ascaroside signaling molecules. nacq#1 (**Figure 16B, Structure 20**) (*N*-acyl glutamine #1) and nacq#2 (**Figure 16B, Structure 21**) are comprised of *cis* and *trans* isomers of the same compound, respectively, with nacq#1 being the primary biosynthetic product (Ludewig et al., 2019).

nacq#1 is enriched in *him-5* cultures, which contain ~30% males in this mutant population (**see Chapter 1B**) (Hodgkin, 1983; Ludewig et al., 2019). The compound is sensed by hermaphrodites, which then undergo developmental acceleration. The functional range of nacq#1 is low, affecting development in the 10 pM – 1 nM range (Hodgkin, 1983; Ludewig et al., 2019). Ludewig et al. propose that nacq#1 shuttles *C. elegans* development into reproductive pathways, and is antagonized by ascarosides which promote dauer development (i.e., ascr#2 and ascr#3) (Butcher et al., 2007; Jeong et al., 2005; Ludewig et al., 2019; Shi, Runnels, & Murphy, 2017). While nacq#1 had little effect on likewise antagonizing dauer entry, it was able to signal dauer exit (Ludewig et al., 2019). Ludewig et al. propose that this is likely due to its transient production around the age of sexual maturity, functioning as a signal that conditions are no longer unfavorable.

Given that ascarosides can affect both development and behavior (i.e., ascr#3 (Butcher et al., 2007; Fagan et al., 2018; Narayan et al., 2016; Srinivasan et al., 2008)), we questioned whether nacq#1 could do the same. We first tested males for a behavioral response to nacq#1 using the Spot Retention Assay (Dong et al., 2018; Narayan et al., 2016; Pungaliya et al., 2009). Males exhibited no attractive behavior to either 100 nM or 10 nM concentrations of nacq#1 over a vehicle control (**Figure 16C**). Given that males produce the molecule, which affects reproductive development rates, there was little reason to expect an attraction.

We next assayed hermaphrodites for a behavioral response at the same concentrations. We found that while there was no significant increase in dwell time in

100 nM nacq#1 over a vehicle control, there was in 10 nM nacq#1 (**Figure 16D**). This trend matches with the lower concentration values of nacq#1 activity (10 pM – 1 nM) compared to ascaroside activity (e.g., ascr#3 affects male attractive behaviors from 100 nM – 1 mM) (Narayan et al., 2016).

Future Work

It will be interesting to see if the concentration curve for nacq#1 mediated hermaphrodite attraction matches the concentration range that affects reproductive development. Testing lower concentrations of nacq#1 for hermaphrodite attraction will also allow for identifying an ideal concentration for study in future studies (such as the 1 μM concentration used for osas#9 testing (Chute et al., 2019)).

nacq#1 exhibits strong similarity to compounds found in human sweat and maize. Fatty acylated glutamines have been implicated in both vertebrate and invertebrate signaling. Finding a similar molecule which is explicitly involved in inter-organismal signaling suggests that these molecules may likewise serve signaling functions (Ludewig et al., 2019).

Conclusions

Ascaroside structure-function relationships are complex, and specific. This "alphabet" of modular communicative cues allows nematodes to communicate nearly every aspect of their environment, physiological state, and life history to any and all conspecifics in the immediate vicinity. The effects can result in developmental changes (i.e., dauer) or behavioral responses (i.e. aggregation).

The octopamine-containing ascaroside, osas#9, offers a unique tool for studying how animals weigh their choices. The cue serves to signal starvation and lack of food in the environment. However, this signal can be immediately overridden upon sensation of food odors (Chute, 2018). Elucidation of the neuronal mechanisms underlying this

multisensory integration will provide interesting insights into how olfactory information is processed.

A promiscuous signal, ascr#3 poses a model to study a myriad of physiological effects and signals. This lone molecule can signal (1) entry into dauer (Butcher et al., 2007), (2) male attraction (Narayan et al., 2016; Pungaliya et al., 2009), or (3) hermaphroditic avoidance (Ryu et al., 2018), while also relying on (1) a host of sensory neurons (including ASK (Srinivasan et al., 2008), ADL (Ryu et al., 2018), ADF (Fagan et al., 2018), and the male-specific CEM (Narayan et al., 2016)), and (2) the sexual identity of those neurons (Fagan et al., 2018).

ascr#3 also functions – alongside ascr#10 – to signal the sex of the animal emitting the cocktail of ascarosides (Aprison & Ruvinsky, 2017). The two pheromones only differ in the presence of a double bond in ascr#3 yet signal completely different things. ascr#10 is enriched in male cultures, and it is the ratio of ascr#3 to ascr#10 that determines whether the sender is a male or hermaphrodite (Aprison & Ruvinsky, 2017). Interestingly, the ration of ascr#3 to ascr#10 also affects germline development (Aprison & Ruvinsky, 2016) and the ability of hermaphrodites to respond to heat stress (Aprison & Ruvinsky, 2015).

In **Chapter 2B** of this dissertation, the role of ascr#10 in relating sexually maturity of the hermaphrodite to its production of germline precursor cells and exploratory behaviors is elaborated on (Douglas K. Reilly & Srinivasan, 2019).

The focus of this dissertation is on the ascaroside, ascr#8 (**Figure 12, Structure 5**). A biosynthetic derivative of ascr#7 (**Figure 12, Structure 4**), ascr#8 is unique in that it contains a *p*-aminobenzoate group at the terminus of the fatty acid chain (Pungaliya et al., 2009). While some moieties are common additions to ascaroside structures [such as: indole (icas) octopamine (osas), tyramine (tsas), hydrobenzoyl (hbas), and methylbutenoyl (mbas)], *p*-aminobenzoate has only been observed in ascr#8. The notable exceptions are ascr#81 (**Figure 12, Structure 6**). and ascr#82 (**Figure 12, Structure 7**), which are biosynthetic successors to ascr#8 (**Figure 12, Structure 5**).

Meanwhile, **Chapter 2C** focuses on the mating ascaroside, ascr#8. This pheromone will be the focus on the remainder of this dissertation, namely the neuromodulation of the male behavioral response (**Chapter 3**), the sensation of the cue (**Chapter 4**), identification of the pheromone's receptors (**Chapter 5**), and the evolutionary conservation of the ability to behaviorally respond to the cue (**Chapter 6**).

References

Aprison, E. Z., & Ruvinsky, I. (2015). Sex Pheromones of *C. elegans* Males Prime the Female Reproductive System and Ameliorate the Effects of Heat Stress. *PLoS Genet, 11*(12), e1005729. doi:10.1371/journal.pgen.1005729

Aprison, E. Z., & Ruvinsky, I. (2016). Sexually Antagonistic Male Signals Manipulate Germline and Soma of *C. elegans* Hermaphrodites. *Curr Biol, 26*(20), 2827-2833. doi:10.1016/j.cub.2016.08.024

Aprison, E. Z., & Ruvinsky, I. (2017). Counteracting Ascarosides Act through Distinct Neurons to Determine the Sexual Identity of *C. elegans* Pheromones. *Curr Biol, 27*(17), 2589-2599.e2583. doi:10.1016/j.cub.2017.07.034

Artyukhin, A. B., Yim, J. J., Srinivasan, J., Izrayelit, Y., Bose, N., von Reuss, S. H., . . . Schroeder, F. C. (2013). Succinylated octopamine ascarosides and a new pathway of biogenic amine metabolism in *Caenorhabditis elegans*. *J Biol Chem, 288*(26), 18778-18783. doi:10.1074/jbc.C113.477000

Artyukhin, A. B., Zhang, Y. K., Akagi, A. E., Panda, O., Sternberg, P. W., & Schroeder, F. C. (2018). Metabolomic "Dark Matter" Dependent on Peroxisomal beta-Oxidation in *Caenorhabditis elegans*. *J Am Chem Soc, 140*(8), 2841-2852. doi:10.1021/jacs.7b11811

Bento, G., Ogawa, A., & Sommer, R. J. (2010). Co-option of the hormone-signalling module dafachronic acid-DAF-12 in nematode evolution. *Nature, 466*(7305), 494-497. doi:10.1038/nature09164

Bergame, C. P., Dong, C., Sutour, S., & von Reuss, S. H. (2019). Epimerization of an Ascaroside-Type Glycolipid Downstream of the Canonical β-Oxidation Cycle in the Nematode *Caenorhabditis nigoni*. *Organic Letters*. doi:10.1021/acs.orglett.9b03808

Bose, N., Ogawa, A., von Reuss, S. H., Yim, J. J., Ragsdale, E. J., Sommer, R. J., & Schroeder, F. C. (2012). Complex small-molecule architectures regulate phenotypic

plasticity in a nematode. *Angew Chem Int Ed Engl, 51*(50), 12438-12443. doi:10.1002/anie.201206797

Butcher, R. A. (2017a). Decoding chemical communication in nematodes. *Nat Prod Rep, 34*(5), 472-477. doi:10.1039/c7np00007c

Butcher, R. A. (2017b). Small-molecule pheromones and hormones controlling nematode development. *Nat Chem Biol, 13*(6), 577-586. doi:10.1038/nchembio.2356d

Butcher, R. A., Fujita, M., Schroeder, F. C., & Clardy, J. (2007). Small-molecule pheromones that control dauer development in *Caenorhabditis elegans*. *Nat Chem Biol, 3*(7), 420-422. doi:10.1038/nchembio.2007.3

Butcher, R. A., Ragains, J. R., & Clardy, J. (2009). An indole-containing dauer pheromone component with unusual dauer inhibitory activity at higher concentrations. *Org Lett, 11*(14), 3100-3103. doi:10.1021/ol901011c

Butcher, R. A., Ragains, J. R., Kim, E., & Clardy, J. (2008). A potent dauer pheromone component in Caenorhabditis elegans that acts synergistically with other components. *Proc Natl Acad Sci U S A, 105*(38), 14288-14292. doi:10.1073/pnas.0806676105

Chute, C. D. (2018). *Decoding Neural Circuits Modulating Behavioral Responses to Aversive Social Cues.* (PhD). Worcester Polytechnic Institute,

Chute, C. D., DiLoreto, E. M., Zhang, Y. K., Reilly, D. K., Rayes, D., Coyle, V. L., . . . Srinivasan, J. (2019). Co-option of neurotransmitter signaling for inter-organismal communication in *C. elegans*. *Nat Commun, 10*(1), 3186. doi:10.1038/s41467-019-11240-7

Chute, C. D., & Srinivasan, J. (2014). Chemical mating cues in *C. elegans*. *Semin Cell Dev Biol, 33*, 18-24. doi:10.1016/j.semcdb.2014.06.002

Dolke, F., Dong, C., Bandi, S., Paetz, C., Glauser, G., & von Reuss, S. H. (2019). Ascaroside Signaling in the Bacterivorous Nematode *Caenorhabditis remanei* Encodes the

Growth Phase of Its Bacterial Food Source. *Org Lett, 21*(15), 5832-5837. doi:10.1021/acs.orglett.9b01914

Dong, C., Reilly, D. K., Bergame, C., Dolke, F., Srinivasan, J., & von Reuss, S. H. (2018). Comparative Ascaroside Profiling of *Caenorhabditis* Exometabolomes Reveals Species-Specific (ω) and (ω - 2)-Hydroxylation Downstream of Peroxisomal beta-Oxidation. *J Org Chem*. doi:10.1021/acs.joc.8b00094

Fagan, K. A., Luo, J., Lagoy, R. C., Schroeder, F. C., Albrecht, D. R., & Portman, D. S. (2018). A Single-Neuron Chemosensory Switch Determines the Valence of a Sexually Dimorphic Sensory Behavior. *Curr Biol, 28*(6), 902-914.e905. doi:10.1016/j.cub.2018.02.029

Fairbairn, D. (1957). The biochemistry of *Ascaris*. *Exp Parasitol, 6*(5), 491-554.

Fouquey, C., Polonsky, J., & Lederer, E. (1957). [Chemical structure of ascarylic alcohol isolated from *Parascaris equorum*]. *Bull Soc Chim Biol (Paris), 39*(1), 101-132.

Fu, J., Zhang, H., Huang, W., Zhu, X., Sheng, Y., Song, E., & Xu, T. (2018). AIM interneurons mediate feeding suppression through the TYRA-2 receptor in C. elegans. *Biophysics Reports, 4*(1), 17-24. doi:10.1007/s41048-018-0046-2

Ghosh, D. D., Nitabach, M. N., Zhang, Y., & Harris, G. (2017). Multisensory integration in C. elegans. *Curr Opin Neurobiol, 43*, 110-118. doi:10.1016/j.conb.2017.01.005

Golden, J. W., & Riddle, D. L. (1982). A pheromone influences larval development in the nematode Caenorhabditis elegans. *Science, 218*(4572), 578. doi:10.1126/science.6896933

Hilliard, M. A., Bergamasco, C., Arbucci, S., Plasterk, R. H. A., & Bazzicalupo, P. (2004). Worms taste bitter: ASH neurons, QUI-1, GPA-3 and ODR-3 mediate quinine avoidance in *Caenorhabditis elegans*. *The EMBO Journal, 23*(5), 1101-1111. doi:10.1038/sj.emboj.7600107

Hodgkin, J. (1983). Male Phenotypes and Mating Efficiency in *Caenorhabditis elegans*. *Genetics, 103*(1), 43-64.

Izrayelit, Y., Srinivasan, J., Campbell, S. L., Jo, Y., von Reuss, S. H., Genoff, M. C., . . . Schroeder, F. C. (2012). Targeted metabolomics reveals a male pheromone and sex-specific ascaroside biosynthesis in *Caenorhabditis elegans*. *ACS Chem Biol, 7*(8), 1321-1325. doi:10.1021/cb300169c

Jang, H., Kim, K., Neal, S. J., Macosko, E., Kim, D., Butcher, R. A., . . . Sengupta, P. (2012). Neuromodulatory state and sex specify alternative behaviors through antagonistic synaptic pathways in *C. elegans*. *Neuron, 75*(4), 585-592. doi:10.1016/j.neuron.2012.06.034

Jeong, P.-Y., Jung, M., Yim, Y.-H., Kim, H., Park, M., Hong, E., . . . Paik, Y.-K. (2005). Chemical structure and biological activity of the *Caenorhabditis elegans* dauer-inducing pheromone. *Nature, 433*(7025), 541-545. doi:10.1038/nature03201

Kaplan, F., Alborn, H. T., von Reuss, S. H., Ajredini, R., Ali, J. G., Akyazi, F., . . . Teal, P. E. (2012). Interspecific nematode signals regulate dispersal behavior. *PLoS One, 7*(6), e38735. doi:10.1371/journal.pone.0038735

Kaplan, F., Srinivasan, J., Mahanti, P., Ajredini, R., Durak, O., Nimalendran, R., . . . Alborn, H. T. (2011). Ascaroside expression in Caenorhabditis elegans is strongly dependent on diet and developmental stage. *PLoS One, 6*(3), e17804. doi:10.1371/journal.pone.0017804

Li, C., & Kim, K. (2014). Family of FLP Peptides in *Caenorhabditis elegans* and Related Nematodes. *Front Endocrinol (Lausanne), 5*, 150. doi:10.3389/fendo.2014.00150

Lightfoot, J. W., Wilecki, M., Rödelsperger, C., Moreno, E., Susoy, V., Witte, H., & Sommer, R. J. (2019). Small peptide–mediated self-recognition prevents cannibalism in predatory nematodes. *Science, 364*(6435), 86. doi:10.1126/science.aav9856

Liu, Z., Kariya, M. J., Chute, C. D., Pribadi, A. K., Leinwand, S. G., Tong, A., . . . Chalasani, S. H. (2018). Predator-secreted sulfolipids induce defensive responses in *C. elegans*. *Nature Communications, 9*(1), 1128. doi:10.1038/s41467-018-03333-6

Ludewig, A. H., Artyukhin, A. B., Aprison, E. Z., Rodrigues, P. R., Pulido, D. C., Burkhardt, R. N., . . . Schroeder, F. C. (2019). An excreted small molecule promotes *C. elegans* reproductive development and aging. *Nat Chem Biol, 15*(8), 838-845. doi:10.1038/s41589-019-0321-7

Ludewig, A. H., & Schroeder, F. C. (2013). Ascaroside signaling in *C. elegans*. *WormBook*, 1-22. doi:10.1895/wormbook.1.155.1

McGrath, P. T., & Ruvinsky, I. (2019). A primer on pheromone signaling in *Caenorhabditis elegans* for systems biologists. *Curr Opin Syst Biol, 13*, 23-30. doi:10.1016/j.coisb.2018.08.012

Narayan, A., Venkatachalam, V., Durak, O., Reilly, D. K., Bose, N., Schroeder, F. C., . . . Sternberg, P. W. (2016). Contrasting responses within a single neuron class enable sex-specific attraction in *Caenorhabditis elegans*. *Proc Natl Acad Sci U S A, 113*(10), E1392-1401. doi:10.1073/pnas.1600786113

Pungaliya, C., Srinivasan, J., Fox, B. W., Malik, R. U., Ludewig, A. H., Sternberg, P. W., & Schroeder, F. C. (2009). A shortcut to identifying small molecule signals that regulate behavior and development in *Caenorhabditis elegans*. *Proceedings of the National Academy of Sciences of the United States of America, 106*(19), 7708-7713. doi:10.1073/pnas.0811918106

Ragsdale, E. J., Muller, M. R., Rodelsperger, C., & Sommer, R. J. (2013). A developmental switch coupled to the evolution of plasticity acts through a sulfatase. *Cell, 155*(4), 922-933. doi:10.1016/j.cell.2013.09.054

Reilly, D. K., & Srinivasan, J. (2017). *Caenorhabditis elegans* Olfaction. doi:10.1093/acrefore/9780190264086.013.191

Reilly, D. K., & Srinivasan, J. (2019). Chemical Communication: Linking Behavior and Physiology. *Current Biology, 29*(23), R1226-R1228. doi:10.1016/j.cub.2019.10.031

Ren, P., Lim, C. S., Johnsen, R., Albert, P. S., Pilgrim, D., & Riddle, D. L. (1996). Control of C. elegans larval development by neuronal expression of a TGF-beta homolog. *Science, 274*(5291), 1389-1391.

Ryu, L., Cheon, Y., Huh, Y. H., Pyo, S., Chinta, S., Choi, H., . . . Kim, K. (2018). Feeding state regulates pheromone-mediated avoidance behavior via the insulin signaling pathway in Caenorhabditis elegans. *Embo J, 37*(15). doi:10.15252/embj.201798402

Schackwitz, W. S., Inoue, T., & Thomas, J. H. (1996). Chemosensory neurons function in parallel to mediate a pheromone response in C. elegans. *Neuron, 17*(4), 719-728.

Shi, C., Runnels, A. M., & Murphy, C. T. (2017). Mating and male pheromone kill Caenorhabditis males through distinct mechanisms. *eLife, 6*. doi:10.7554/eLife.23493

Srinivasan, J., Kaplan, F., Ajredini, R., Zachariah, C., Alborn, H. T., Teal, P. E., . . . Schroeder, F. C. (2008). A blend of small molecules regulates both mating and development in *Caenorhabditis elegans*. *Nature, 454*(7208), 1115-1118. doi:10.1038/nature07168

Srinivasan, J., von Reuss, S. H., Bose, N., Zaslaver, A., Mahanti, P., Ho, M. C., . . . Schroeder, F. C. (2012). A modular library of small molecule signals regulates social behaviors in *Caenorhabditis elegans*. *PLoS Biol, 10*(1), e1001237. doi:10.1371/journal.pbio.1001237

von Reuss, S. H., Bose, N., Srinivasan, J., Yim, J. J., Judkins, J. C., Sternberg, P. W., & Schroeder, F. C. (2012). Comparative Metabolomics Reveals Biogenesis of Ascarosides, a Modular Library of Small-Molecule Signals in *C. elegans*. *Journal of the American Chemical Society, 134*(3), 1817-1824. doi:10.1021/ja210202y

von Reuss, S. H., Dolke, F., & Dong, C. (2017). Ascaroside Profiling of Caenorhabditis elegans Using Gas Chromatography-Electron Ionization Mass Spectrometry. *Anal Chem, 89*(19), 10570-10577. doi:10.1021/acs.analchem.7b02803

von Reuss, S. H., & Schroeder, F. C. (2015). Combinatorial chemistry in nematodes: modular assembly of primary metabolism-derived building blocks. *Nat Prod Rep, 32*(7), 994-1006. doi:10.1039/c5np00042d

Zhang, Y. K., Sanchez-Ayala, M. A., Sternberg, P. W., Srinivasan, J., & Schroeder, F. C. (2017). Improved Synthesis for Modular Ascarosides Uncovers Biological Activity. *Org Lett, 19*(11), 2837-2840. doi:10.1021/acs.orglett.7b01009

Zou, W., Cheng, H., Li, S., Yue, X., Xue, Y., Chen, S., & Kang, L. (2017). Polymodal Responses in C. elegans Phasmid Neurons Rely on Multiple Intracellular and Intercellular Signaling Pathways. *Sci Rep, 7*, 42295. doi:10.1038/srep42295

Chapter 2B Chemical Communication: Linking Behavior and Physiology

Published as:

Reilly DK, Srinivasan J. (2019) *Chemical Communication: Linking Behavior and Physiology*. Current Biology. doi: 10.1016/j.cub.2019.10.031

Summary

How does physiological state affect the reproductive behavior of an organism? Two new studies in *Caenorhabditis elegans* implicate an ancient serotonergic neuronal circuit in the link between these two outputs — reproductive behavior and physiology.

Main Text

Animals must constantly choose between long-term survival (reproduction) and short-term survival (behavior) strategies in their biological niches [1-3]. How this choice is made remains an enigma. Chemical signaling between members of the same species can help to direct these decisions [1]. Pheromones, a specialized form of chemical signal [2, 4], convey information between conspecifics regarding personal fitness [4, 5], environmental state [1], sexual receptivity [6], and life stage [2]. The neural networks that translate these signals often diverge into those regulating physiological responses [1, 2, 7] or behavioral responses [8, 9]. In this issue of Current Biology, two reports from Aprison and Ruvinsky elucidate a neuronal network connecting behavior and physiology [10, 11]. Their results implicate an ancient, serotonergic pathway — with strong homology to serotonergic signaling in mammalian raphe nuclei — that licenses both behavioral and physiological responses to a sex-specific pheromone in an age dependent manner.

Caenorhabditis elegans is predominantly hermaphroditic, with only a small proportion of the population being male (0.1–0.2%) [12] and uses chemical signals for communication. Previous studies have elucidated a class of small molecule pheromones called ascarosides that exhibit structure–function relationships eliciting both behavioral and physiological effects [1, 2, 8, 9, 13, 14]. The amount of each ascaroside in the pheromone profile of *C. elegans* is unique to each worm's life history, developmental stage, sex, and physiological state [2].

Aprison and Ruvinsky sought to understand a fundamental question regarding animal behavior: how does an animal integrate reproductive behavior with its internal physiological state? To address this question, they studied the responses of *C. elegans* to a sex-specific mating pheromone, ascaroside #10 (ascr#10), which is predominantly

produced by male *C. elegans* and elicits attractive behaviors in hermaphrodites at lower concentrations [14]. Structurally, ascr#10 is identical to ascr#3, except for a single carbon–carbon bond in the fatty acid-derived side chain (**Figure 17A**). However, these two pheromones are functionally divergent between the two sexes, with ascr#10 being a hermaphrodite attractant and ascr#3 eliciting hermaphroditic avoidance [9, 13] . The ratio of ascr#3 to ascr#10 in the pheromone profile describes the sexual identity of an individual [13].

Previous work from the Ruvinsky lab has shown that ascr#10 affects germline development, increasing the number of germline precursor cells (GPCs) [15]. Now, in the new studies, they show that two outputs—reproductive physiological changes in the GPCs, and changes in exploratory behavior — are linked via a single neuronal circuit (**Figure 17B, C**) [10, 11]. The initial finding that led to the elucidation of this circuit was the identification of a role for serotonin in ascr#10 responses [10]. After examining animals that lack the serotonin biosynthesis gene *tph-1* specifically in the NSM and hermaphrodite-specific HSN neurons, they discovered that the increase in GPCs in response to ascr#10 was abolished. A similar phenotype was seen in animals lacking the serotonin-gated chloride channel MOD-1. Rescuing the expression of this channel in specific interneurons (AIY and RIF) recapitulated the ascr#10-mediated GPC increase. Although the authors first noticed that the increase in GPCs was diminished in serotonin-deficient animals, they decided to investigate changes in behavior.

Serotonin is a neurotransmitter intricately tied to behavioral regulation [3]. Aprison and Ruvinsky demonstrated that the increase in attractive behavior of *C. elegans* exposed to ascr#10 is in fact due to decreased exploration [10]. They showed that ascr#10 induces a reduction of exploration in sexually mature hermaphrodites [16]. These findings contradict previous studies that argued that the increased attraction elicited by ascr#10 was due to an increase in the amount of time *C. elegans* were exposed to the ascaroside. In animals with defective serotonin signaling (*tph-1* or *mod-1* mutants), the decrease in

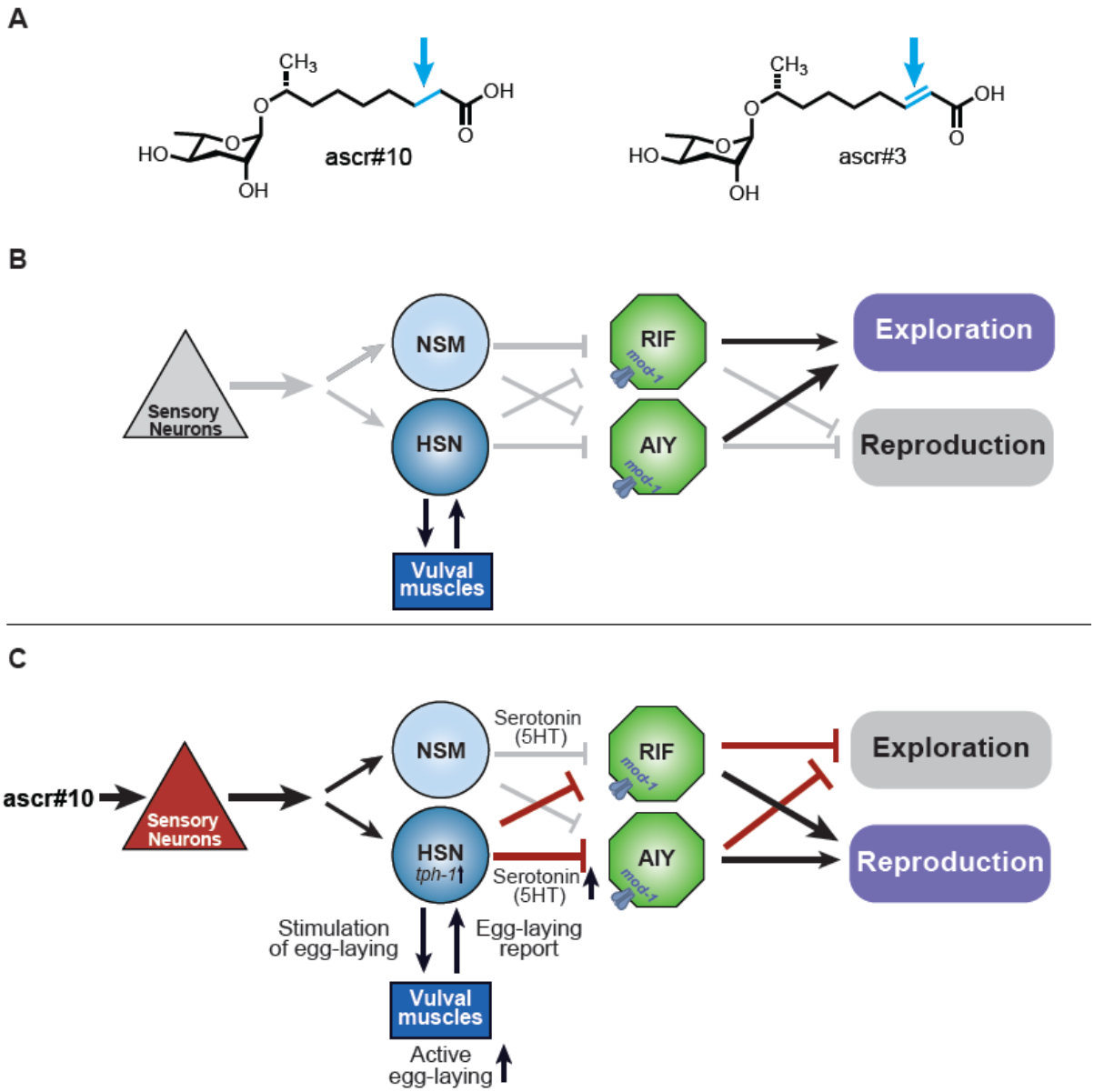

Figure 17. The HSN-vm2 circuit links the behavioral and physiological outputs of ascr#10 signaling. **(A)** The ascarosides ascr#10 and ascr#3 are structurally identical with the exception of a single carbon–carbon bond (blue arrow) within the fatty-acid-derived side chain. **(B)** In the absence of ascr#10, there is no upregulation of the serotonin biosynthesis gene *tph-1* in either NSM or HSN neurons, allowing the RIF and AIY neurons to remain active. This results in exploratory behavior and a slowing of germline development. **(C)** In the presence of ascr#10, after the HSN–vm2 network is completely formed, *tph-1* levels increase in the HSN neurons. This results in serotonin (5HT) release and inhibition of the RIF and AIY neurons via the serotonin-gated chloride channel MOD-1. Exploratory behavior decreases, and the rate of germ cell production is increased. The HSN–vm2 circuit (blue) is critical in linking the behavioral and physiological outputs of ascr#10. Upon forming synaptic connections during development, the HSN neurons stimulate the vm2 vulval muscle cells to initiate egg laying. Conversely, the vm2 cells then report back to the HSN neurons on the status of egg laying. This network allows ascr#10 sensation to initiate *tph-1* transcription in the HSN neurons

exploration upon ascr#10 sensation was lost. Surprisingly, the authors found that serotonin activity in the same neurons that are required for ascr#10-mediated GPC proliferation— NSM and HSN neurons—is also required for maintaining the behavioral response, suggesting a linkage between the two outputs [10]. They further found that the effects of the serotonergic signaling response to ascr#10 are countered by signaling mediated via the neuropeptide PDF-1 (pigment dispersing factor-1) [10, 17]. Aprison and Ruvinsky propose that the inclusion of PDF-1 signaling in the same circuit helps to maintain the balance between reproductive performance and exploration. By antagonizing serotonin signaling, the PDF-1 neuropeptide can therefore function to modulate this balance, preventing an all-or-none phenotype and allowing the organism to adapt quickly to its immediate environment.

In the second of the two studies, the authors investigated how HSN neurons relate the decrease in exploratory behavior to an increase in GPCs [11]. They discovered that HSN neurons communicate via a looped circuit with the vm2 vulval muscle cells, which report back to the HSN neurons on the egg-laying status of the animal [11] (**Figure 17B, C**). As worms begin to lay eggs, the vm2 cells communicate this information back to the HSN neurons, resulting in an increase in *tph-1* expression in these neurons (**Figure 17**). When ascr#10 is encountered during this state, HSN neurons are signaled to release serotonin, inhibiting AIY and RIF neurons and resulting in reduced roaming and exploration [10] (**Figure 17C**). In conjunction, this same network signals an increase in GPC proliferation, and thereby reproduction (*C. elegans* are self-fertile). Hence, the HSN– vm2 feedback circuit functions as a 'licensing' mechanism, limiting the ascr#10-mediated responses to sexually mature adults [11]. The HSN– vm2 connections aren't completely formed until the animal reaches sexual maturity [18], thereby 'licensing' ascr#10 signaling to elicit reduced exploration and increased GPC production [10, 11].

These findings lead to a unique and interesting model. They show that a sex-specific pheromone promotes an increase in GPCs (i.e., eggs), thereby allowing for an increased

chance of successful mating. However, a second signal is not required to affect reproductive behavior because this sex-specific pheromone also causes sexually mature mates to decrease their exploration [10]. This decrease in movement gives males a better chance at locating and reproducing with a mate. *C. elegans* takes advantage of the developmental timing of the HSN–vm2 circuit to allow this network to ensure that the effects desired by the ascr#10- releasing males only occur in animals that are mature enough to mate [11].

C. elegans may have a simple nervous system, but it is still a useful model for studying neuronal circuits that are similar to those found in humans. The serotonergic raphe nuclei in mammalian brains are known to modulate behavior— generally, mood regulation — and their malfunction can be involved in anxiety and depression [19]. However, they also have physiological functions, as they contribute to the regulation of the sleep– wake cycle and to stress resistance [19]. The HSN neurons have a similar function as the key player in a serotonergic neuronal circuit in *C. elegans*: they link the behavioral and physiological outputs of ascr#10 signaling, via their feedback loop with the vm2 muscle cells. Interestingly, the transcriptome of serotonergic HSN neurons in *C. elegans* resembles that of raphe serotonergic neurons found in mammals [20].

These findings beg the question: just how conserved is this circuit? It is tempting to propose that the coupling of behavior and physiology within a serotonergic circuit is an ancient system. The functional homology between HSN neurons and raphe nuclei is remarkable and, given the continued evidence that serotonin plays major roles in behavior and physiology across phyla [3, 16, 20], it may be that this ancestral linkage through a single neural circuit is as ancient as the origin of Metazoa [10].

Acknowledgments

We thank Elizabeth DiLoreto in the Srinivasan Lab for assisting in the editing of this manuscript. This work was supported in part by the NIH (R01DC016058, JS).

References

1. Butcher, R.A., Fujita, M., Schroeder, F.C., and Clardy, J. (2007). Small-molecule pheromones that control dauer development in *Caenorhabditis elegans*. Nat Chem Biol *3*, 420-422.
2. McGrath, P.T., and Ruvinsky, I. (2019). A primer on pheromone signaling in *Caenorhabditis elegans* for systems biologists. Current opinion in systems biology *13*, 23-30.
3. Pooryasin, A., and Fiala, A. (2015). Identified Serotonin-Releasing Neurons Induce Behavioral Quiescence and Suppress Mating in Drosophila. J Neurosci *35*, 12792-12812.
4. Liberles, S.D. (2014). Mammalian pheromones. Annu Rev Physiol *76*, 151-175.
5. Buesching, C.D., Stopka, P., and MacDonald, D.W. (2003). The Social Function of Allo-Marking in the European Badger (Meles meles). Behaviour *140*, 965-980.
6. Houck, L., Palmer, C., Watts, R., Arnold, S., Feldhoff, P., and Feldhoff, R. (2007). A new vertebrate courtship pheromone, PMF, affects female receptivity in a terrestrial salamander. Animal Behaviour *73*, 315-320.
7. Wilburn, D.B., Doty, K.A., Chouinard, A.J., Eddy, S.L., Woodley, S.K., Houck, L.D., and Feldhoff, R.C. (2017). Olfactory effects of a hypervariable multicomponent pheromone in the red-legged salamander, Plethodon shermani. PloS one *12*, e0174370-e0174370.
8. Chute, C.D., DiLoreto, E.M., Zhang, Y.K., Reilly, D.K., Rayes, D., Coyle, V.L., Choi, H.J., Alkema, M.J., Schroeder, F.C., and Srinivasan, J. (2019). Co-option of neurotransmitter signaling for inter-organismal communication in C. elegans. Nat Commun *10*, 3186.
9. Fagan, K.A., Luo, J., Lagoy, R.C., Schroeder, F.C., Albrecht, D.R., and Portman, D.S. (2018). A Single-Neuron Chemosensory Switch Determines the Valence of a Sexually Dimorphic Sensory Behavior. Curr Biol *28*, 902-914.e905.

10. Apirson, E.Z., and Ruvinsky, I. (2019). Coordinated behavioral and physiological responses to a social signal are regulated by a shared neuronal circuit. Curr Biol.
11. Apirson, E.Z., and Ruvinsky, I. (2019). Dynamic regulation of adult-specific functions of the nervous system by signaling from the reproductive system. Curr Biol.
12. Hodgkin, J., Horvitz, H.R., and Brenner, S. (1979). Nondisjunction Mutants of the Nematode *Caenorhabditis elegans*. Genetics *91*, 67-94.
13. Aprison, E.Z., and Ruvinsky, I. (2017). Counteracting Ascarosides Act through Distinct Neurons to Determine the Sexual Identity of C. elegans Pheromones. Curr Biol *27*, 2589-2599.e2583.
14. Izrayelit, Y., Srinivasan, J., Campbell, S.L., Jo, Y., von Reuss, S.H., Genoff, M.C., Sternberg, P.W., and Schroeder, F.C. (2012). Targeted metabolomics reveals a male pheromone and sex-specific ascaroside biosynthesis in *Caenorhabditis elegans*. ACS Chem Biol *7*, 1321-1325.
15. Aprison, E.Z., and Ruvinsky, I. (2016). Sexually Antagonistic Male Signals Manipulate Germline and Soma of C. elegans Hermaphrodites. Curr Biol *26*, 2827-2833.
16. Flavell, S.W., Pokala, N., Macosko, E.Z., Albrecht, D.R., Larsch, J., and Bargmann, C.I. (2013). Serotonin and the neuropeptide PDF initiate and extend opposing behavioral states in C. elegans. Cell *154*, 1023-1035.
17. Barrios, A., Ghosh, R., Fang, C., Emmons, S.W., and Barr, M.M. (2012). PDF-1 neuropeptide signaling modulates a neural circuit for mate-searching behavior in *C. elegans*. Nature Neuroscience *15*, 1675-1684.
18. Ravi, B., Garcia, J., and Collins, K.M. (2018). Homeostatic Feedback Modulates the Development of Two-State Patterned Activity in a Model Serotonin Motor Circuit in Caenorhabditis elegans. J Neurosci *38*, 6283-6298.

19. Walker, E.P., and Tadi, P. (2019). Neuroanatomy, Nucleus Raphe. In StatPearls. (Treasure Island (FL): StatPearls Publishing).

20. Lloret-Fernandez, C., Maicas, M., Mora-Martinez, C., Artacho, A., Jimeno-Martin, A., Chirivella, L., Weinberg, P., and Flames, N. (2018). A transcription factor collective defines the HSN serotonergic neuron regulatory landscape. Elife *7*.

Chapter 2C Ascaroside #8

A portion of the work in this chapter (Figure 1F, G) was included in Figure 6 of:

> Narayan, A., Venkatachalam, V., Durak, O., Reilly, D. K., Bose, N., Schroeder, F. C., . . . Sternberg, P. W. (2016). Contrasting responses within a single neuron class enable sex-specific attraction in *Caenorhabditis elegans*. *Proc Natl Acad Sci U S A, 113*(10), E1392-1401. doi:10.1073/pnas.1600786113

Summary

Of the two most potent mating cues, ascaroside #3 (ascr#3) and ascaroside #8 (ascr#8), the focus of this thesis dissertation will be on the ascr#8 response: the modulation of the ascr#8 behavioral circuit (Chapter 3), and the identification of receptors responsible for ascr#8 sensation (**Chapter 4**, **Chapter 5**, **Chapter 6**).

Ascaroside #8 Mate Recognition Signaling

The pheromone, ascr#8, is produced by sexually mature hermaphrodites, and serves as a mate recognition cue for males (Narayan et al., 2016; Pungaliya et al., 2009). Alongside ascr#3, ascr#8 is the most potent male attractant ascaroside, with a bimodal activity curve between 100 nM and 100 μM (Narayan et al., 2016). Interestingly, at concentrations of 1 mM or higher, *C. elegans* are no longer attracted to ascr#8 (Narayan et al., 2016).

Ascarosides #3 and #8 Are Sensed Via the CEM Neurons

Both ascr#3 and ascr#8 are sensed by the male specific CEM neurons, located in the head region. Laser ablations of the CEM neurons completely removed the male behavioral response to ascr#8, while a combination of CEM and ASK removal was required to ablate the ascr#3 response (Narayan et al., 2016) (**Figure 18A**). More recent studies have also confirmed that the ADF neurons play a significant role in the sex-specific response to ascr#3, as determined by the sexual identity of the neuron (Fagan et al., 2018).

The physiological responses with the CEM neurons to both ascr#3 and ascr#8 are extremely complex. The four neurons exhibit a seemingly stochastic array of responses, with depolarizing, hyperpolarizing, and even non-responding neurons contributing to the total response (Narayan et al., 2016; Reilly, Lawler, Albrecht, & Srinivasan, 2017) (**Figure 18B)**. Some neurons are even found to exhibit what has been termed as "complex responses", with specific regions of individual cells responding independently – exhibiting localized depolarizations and hyperpolarizations within the same cell. Making the CEM response to these cues even more complex is that while the behavioral output is consistent (males are attracted to ascr#3 and ascr#8), the responses between animals - and even pulses within the same animal – are not consistent **(Figure 18C)**.

In order to better investigate the responses of the CEM neurons, our lab, in collaboration with the Albrecht lab, worked to develop a male-adapted microfluidic device. This device features a narrower loading port, to more efficiently trap the smaller male *C. elegans*. The manuscript detailing this device is presented as **Chapter 4B** of this dissertation.

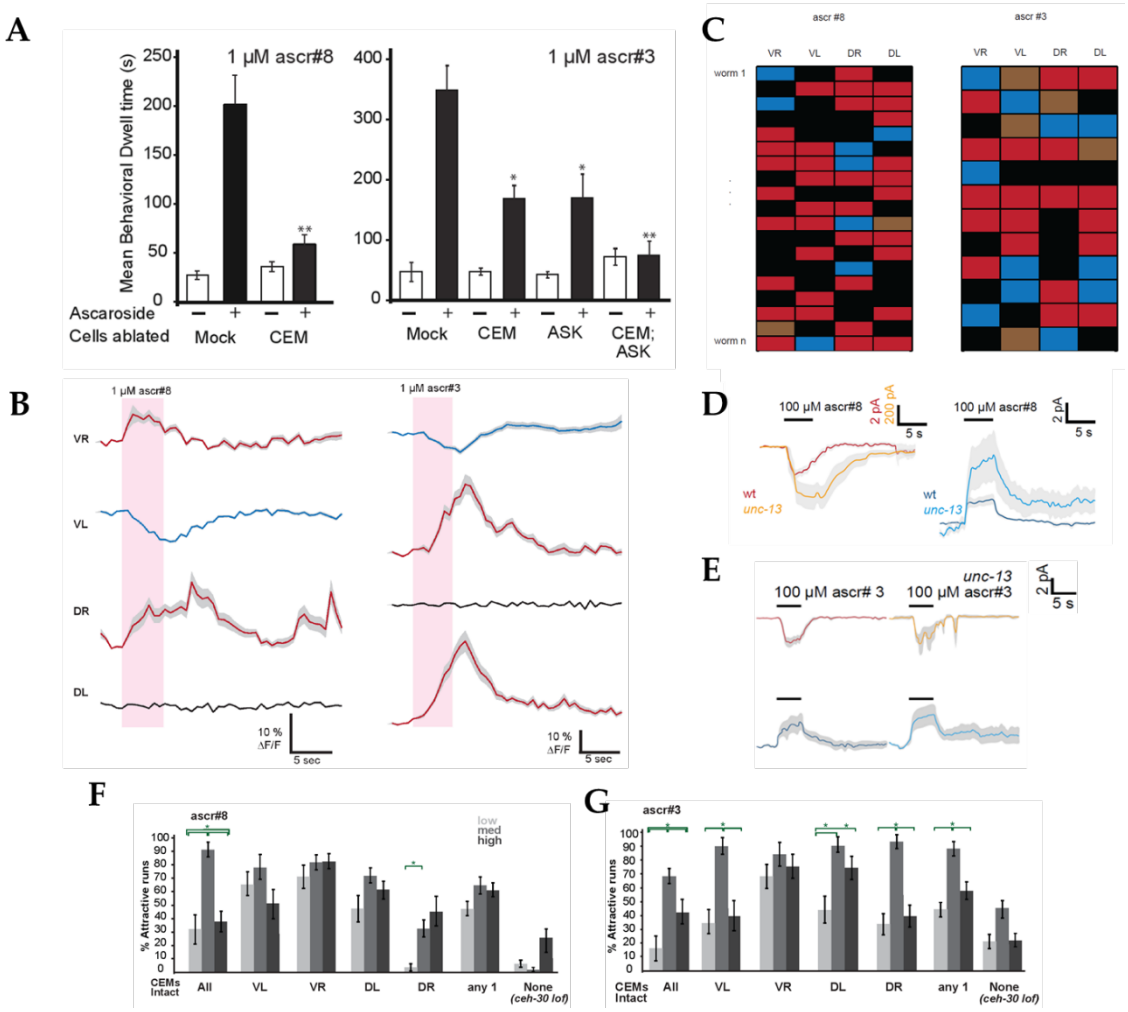

Figure 18. Ascaroside #8 Functions to Attract Males via the CEM neurons in a Separate Circuit from Ascaroside #3.

(A) The male specific CEM neurons are required for response to ascr#3 and ascr#8. The ASK neurons are also required for the ascr#3 male behavioral response. **(B)** The physiological response of the CEM class of male-specific neurons to ascr#8 (left) and ascr#3 (right). The responses within the class are variable. **(C)** The CEM responses to both cues are not consistent across animals. Each row represents an individual animal. Blue denotes a depolarizing response; red denotes a hyperpolarizing response; brown denotes a "complex" response; black denotes no-response. **(D, E)** Removal of synaptic transmission increases the magnitude of responses to ascr#8 **(D)**, and the shape of response to ascr#3 **(E)**. Statistics, *p*-values, and trial counts are listed in (Narayan et al., 2016). Adapted from (Narayan et al., 2016).

Although the CEM neurons are not synaptically connected, they form a complex sensory network. Removal of synaptic transmission via an *unc-13 lof* mutant results in changes in electrophysiological response to both cues. The magnitudes of both hyper- and de-polarizations of ascr#8 elicited responses are increased (**Figure 18D**), suggesting synaptic throttling of the responses. In contrast, the magnitude of ascr#3 responses remains unchanged with loss of synaptic transmission. Interestingly, however, the shape of the response changes (**Figure 18E**), indicating that fast synaptic transmission sculpts the neuronal response via a mixture of excitatory and inhibitory input (Narayan et al., 2016)

Adding to the evidence of an integrated network regulating the response of CEM neurons to ascr#3 and ascr#8 is that the loss of individual CEM neurons changes the attractiveness of the cues (**Figure 18F, G**). The presence of all four CEM neurons results in a natural "tuning-curve" towards an intermediate concentration of each ascaroside, centering at 1 μM, with higher (100 μM) and lower (100 nM) concentrations eliciting less attractive responses. When any three CEM neurons are ablated, the attractiveness of the extreme concentration changes, flattening the curve (**Figure 18F, G**). When all four CEM neurons are absent (a *ceh-30 lof* mutation in which the CEM neurons die off during male development (Peden, Kimberly, Gengyo-Ando, Mitani, & Xue, 2007; Schwartz & Horvitz, 2007)) the attraction to ascr#8 is completely lost (**Figure 18F**). The increased attraction at 100 μM is likely due to off-target binding at such high concentrations, although other sensory pathways cannot be excluded at this point. The tuning curve to 1 μM ascr#3 surprisingly remained intact, although diminished, when all four CEMs are absent (**Figure 18G**). This is likely due to the roles of ASK and ADF in ascr#3 sensation (Fagan et al., 2018; Narayan et al., 2016).

ascr#3 and ascr#8 Exhibit the Same Behavioral Output Via Unique Sensory Circuits

Our lab has generated some preliminary results which further suggest that the neural circuits which sense both mating cues are independent of each other. We assayed enzymes involved in neurotransmitter synthesis for roles in response to either ascr#3 or ascr#8. We also asked if the mechanosensory proteins *pkd-2* and *lov-1*, which function in

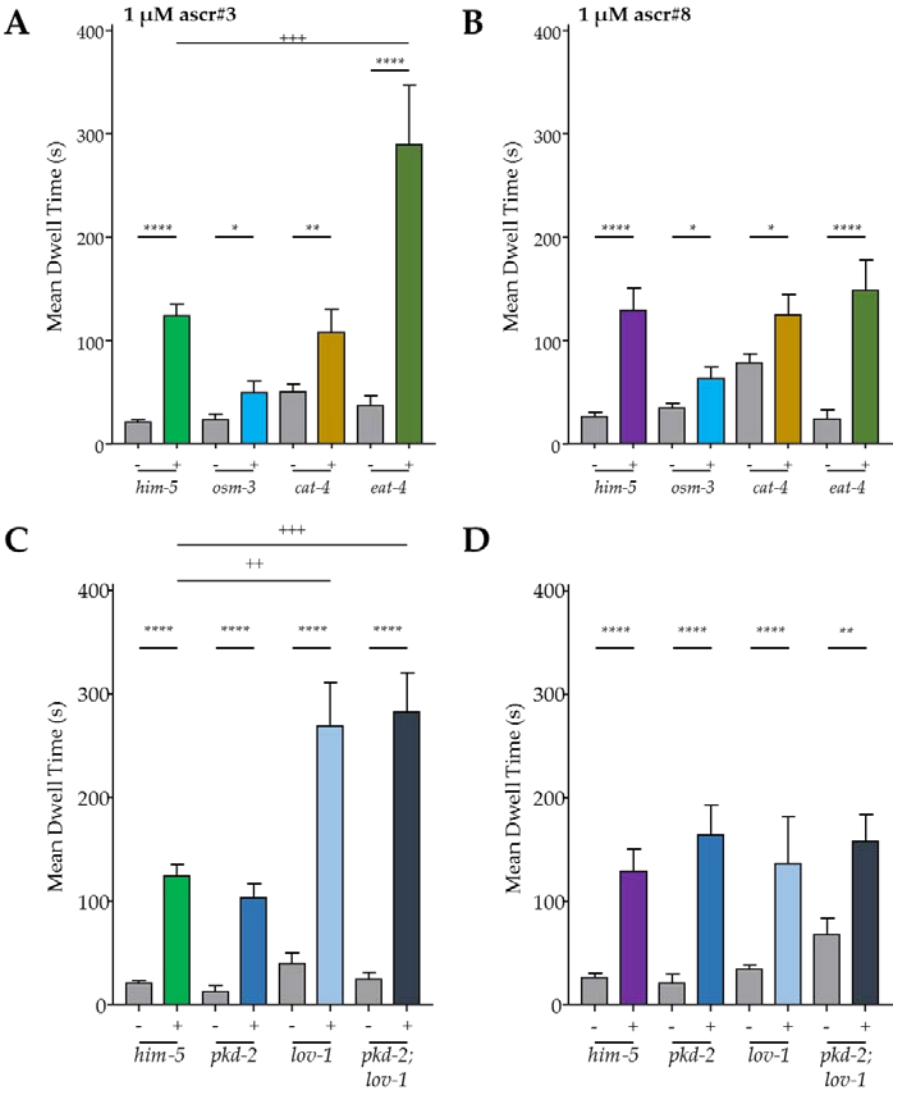

Figure 19. Different molecular mechanisms regulation the responses to ascr#3 and ascr#8.
(A, B) Loss of glutamatergic, but not bioaminergic signaling results in increased attraction to ascr#3 **(A)** but not ascr#8 **(B)**. **(C, D)** The mechanosensory protein *lov-1*, but not the associated *pkd-2*, functions in the ascr#3 response **(C)**, but not the ascr#8 response **(D)**. "-" and "+" denote the present of vehicle control (-) and ascaroside (+), respectively. Error bars denote SEM. n ≥ 15. Wilcoxon Matched-Pairs Signed Rank Test; control vs 1 μM ascaroside. * $p < 0.05$, ** $p < 0.01$, **** $p < 0.0001$. One-Way ANOVA ($p < 0.0001$) comparing fold-change increases in dwell time across strains. ++ $p < 0.01$, +++ $p < 0.001$.

the CEM neurons (Bae et al., 2006; Barr et al., 2001; Knobel, Peden, & Barr, 2008), play a role in CEM chemosensation.

We first examined the response of *osm-3* mutants as a second control. The *osm-3 lof* mutants tested *(mn391)* are deficient for a kinesin motor involved in cilium development (Snow et al., 2004), and exhibit defective attractive chemotaxis behaviors (Frøkjær-Jensen, Ailion, & Lockery, 2008). While we found that *osm-3 lof* animals still spent more time in both ascr#3 and ascr#8 (Wilcoxon Matched-Pairs Signed Rank tests comparing vehicle to ascr#3 or ascr#8 dwell times, $p = 0.0178$ and $p = 0.0175$, respectively), these dwell times were noticeably reduced compared to the *him-5* control (Mann-Whitney tests comparing transformed fold-change of *osm-3* to *him-5*, $p < 0.0001$ (ascr#3) and $p = 0.0130$ (ascr#8)) (**Figure 19A,B**).

We then assayed animals deficient in the synthesis of bioaminergic enzymes. The *cat-4* gene encode a GTP cyclohydrase enzyme, which acts as a cofactor for the TPH-1, CAT-2, and TBH-1 enzymes, contributing to the production of serotonin, dopamine, and octopamine, respectively (Loer & Kenyon, 1993; Sulston, Dew, & Brenner, 1975). Males lacking *cat-4* responded normally to both ascr#3 and ascr#8 (**Figure 19A, B**).

However, the role of tyramine in these responses cannot be determined, as *cat-4 lof* does not affect tyramine synthesis from tyrosine via TDC-1. The protein product of cat-4 is a co-factor, and as such, these results should not be viewed as pertaining to a complete lack of the subsequent neurotransmitters. A more accurate analysis would involve the assaying of animals lacking either *bas-1* (and therefore serotonin and dopamine), *tph-1* (producing the precursor to serotonin), *cat-2* (dopamine synthesis), *tdc-1* (tyramine synthesis), and *tbh-1* (octopamine synthesis from tyramine) (Chase & Koelle, 2007).

The gene *eat-4* provides a powerful tool for studying glutamatergic signaling, as *eat-4* animals are not deficient in glutamate production, but rather glutamate reuptake (Lee, Sawin, Chalfie, Horvitz, & Avery, 1999). So, while the neurotransmitter is still present, these animals are unable to use it in sustained synaptic transmission (Rankin & Wicks,

2000). We found that *eat-4* animals responded normally to ascr#8 but exhibited significantly increased attraction to ascr#3 (**Figure 19A, B**).

To date, ascr#8 has only been found to be sensed by the CEM neurons, while ascr#3 is also sensed by ASK and ADF neurons (Fagan et al., 2018; Narayan et al., 2016). Laser ablations of ASK revealed a major role of these neurons in regulating the response to ascr#3 (Narayan et al., 2016). The ASK neurons are also known to express *eat-4*, and signal via glutamate (Lee et al., 1999). Therefore, it is not surprising that the ascr#3 response would be affected by a mutation in the *eat-4* gene (**Figure 19A**).

A Single Polycystin plays a role in Ascaroside Response

We then tested mutants for *pkd-2* and *lov-1*. These two genes encode *C. elegans* homologs of the human genes *PDK2* (TRPP2) and *PDK1* (TRPP1), respectively (Bae et al., 2006). In both nematodes and human kidneys, these proteins localize to the cilia, suggesting an ancient, conserved mechanism. The mechanosensory roles of *pkd-2* and *lov-1* are dependent on male-tail neurons and their contact with a mate. However, outside of the tail, these two genes are also expressed in the male head: specifically, the CEM neurons (Bae et al., 2006). As *pkd-2* and *lov-1* are both required for response to mate contact and sensation of the mate's vulva - *pkd-2* mutants have been found to exhibit decreased mating efficiency (Bae et al., 2006) - we asked if they are also involved in the sensation of ascr#3 and ascr#8.

We found that *pkd-2* mutants were wild-type for their response to both ascr#3 and ascr#8 (**Figure 19C, D**). However, despite the fact that *lov-1* acts in the genetic pathway as *pkd-2* (Barr et al., 2001) we found that *lov-1* animals exhibited a significant increase in their attraction to ascr#3 (**Figure 19C**). This phenotype was limited to ascr#3, with no defect observed in the ascr#8 response, and a double mutant for *pkd-2; lov-1* recapitulated the *lov-1* phenotype (**Figure 19C**), suggesting its genetic dominance in the pathway.

The finding that only *lov-1* is active in the ascr#3 response, separate from *pkd-2*, is intriguing. To date, the two genes have been phenotypically indistinguishable. This finding offers an interesting tool to study the function of *lov-1* independently from *pkd-2* function.

Ascaroside #8 As A Target of Study

Together, these data show that, while both ascr#3 and ascr#8 result in similar behavioral outputs (**Figure 18A**) (Narayan et al., 2016; Pungaliya et al., 2009), the cellular and molecular machineries driving these responses are unique to each pheromone (**Figure 18, Figure 19**). While both ascr#3 and ascr#8 are sensed by the CEM neurons, ascr#3 sensation also involved ASK and ADF processing (Fagan et al., 2018; Narayan et al., 2016). Glutamatergic transmission is essential for the proper response to ascr#3, while ascr#8 seems to not require glutamate at all (**Figure 19A, B**). Synaptic transmission affects the magnitude of the ascr#8-elicited CEM calcium response, but the shape of the ascr#3-elicited response (Narayan et al., 2016). Furthermore, the polycystin *lov-1* functions to mediate the ascr#3 behavioral response (**Figure 19C**) (the first finding of *lov-1* functioning independently of *pkd-2*), with neither functioning in the ascr#8 response.

For these reasons, this dissertation research was focused on understanding the ascr#8 response by pursuing two avenues of inquiry:

(1) elucidating the neuromodulation of the ascr#8 response, and

(2) identifying receptors responsible for sensing ascr#8.

This was accomplished by investigating the neuromodulation *p*-aminobenzoate containing ascaroside, ascr#8, by an FMRFamide-like neuropeptide, *flp-3* (**Chapter 3B**). In the process of investigating this neuropeptide, a novel peptide-feeding rescue paradigm was developed (**Chapter 3B**). In studying ascr#8, a male-adapted microfluidic device was developed in collaboration with the Albrecht lab (**Chapter 4B**).

Identification of the receptors necessary for proper sensation of ascr#8 was the second spear of the research contributing towards this dissertation. Utilizing single-cell transcriptomes of individual CEM neurons, two G protein-coupled receptors were identified as partially defective in their ascr#8 response (**Chapter 4C**). Combined, they result in a complete loss of response. In order to more accurately identify ascaroside receptors in an unbiased manner, we worked with the Schroeder lab at Cornell University to develop a tri-functional probe which would bind native ascr#8 receptors (**Chapter 5**).

An interesting finding in the phylogenetic analyses performed on one of the candidate receptors lead to an exciting foray into assaying how the evolution of self-fertility in *Caenorhabditis* nematodes affects their ability to respond to mating cues like ascr#8 (**Chapter 6**).

Together, the following work contributing to this thesis builds a complex and interesting model of sex-specific pheromone behavioral responses. More frequently, studies are finding that receptors that function in these behaviors have been co-opted into these functions from a more ancient utilization. Therefore, it would not be surprising to find that the ligands and receptors investigated in this these are the products of ancient co-option events.

References

Bae, Y. K., Qin, H., Knobel, K. M., Hu, J., Rosenbaum, J. L., & Barr, M. M. (2006). General and cell-type specific mechanisms target TRPP2/PKD-2 to cilia. *Development, 133*(19), 3859-3870. doi:10.1242/dev.02555

Barr, M. M., DeModena, J., Braun, D., Nguyen, C. Q., Hall, D. H., & Sternberg, P. W. (2001). The *Caenorhabditis elegans* autosomal dominant polycystic kidney disease gene homologs *lov-1* and *pkd-2* act in the same pathway. *Curr Biol, 11*. doi:10.1016/S0960-9822(01)00423-7

Chase, D. L., & Koelle, M. R. (2007). Biogenic amine neurotransmitters in *C. elegans*. *WormBook*, 1-15. doi:10.1895/wormbook.1.132.1

Fagan, K. A., Luo, J., Lagoy, R. C., Schroeder, F. C., Albrecht, D. R., & Portman, D. S. (2018). A Single-Neuron Chemosensory Switch Determines the Valence of a Sexually Dimorphic Sensory Behavior. *Curr Biol, 28*(6), 902-914.e905. doi:10.1016/j.cub.2018.02.029

Frøkjær-Jensen, C., Ailion, M., & Lockery, S. R. (2008). Ammonium-Acetate Is Sensed by Gustatory and Olfactory Neurons in Caenorhabditis elegans. *PLoS One, 3*(6), e2467. doi:10.1371/journal.pone.0002467

Knobel, K. M., Peden, E. M., & Barr, M. M. (2008). Distinct protein domains regulate ciliary targeting and function of *C. elegans* PKD-2. *Experimental Cell Research, 314*(4), 825-833. doi:10.1016/j.yexcr.2007.10.017

Lee, R. Y., Sawin, E. R., Chalfie, M., Horvitz, H. R., & Avery, L. (1999). EAT-4, a homolog of a mammalian sodium-dependent inorganic phosphate cotransporter, is necessary for glutamatergic neurotransmission in *Caenorhabditis elegans*. *J Neurosci, 19*(1), 159-167.

Loer, C. M., & Kenyon, C. J. (1993). Serotonin-deficient mutants and male mating behavior in the nematode *Caenorhabditis elegans*. *J Neurosci, 13*.

Narayan, A., Venkatachalam, V., Durak, O., Reilly, D. K., Bose, N., Schroeder, F. C., . . . Sternberg, P. W. (2016). Contrasting responses within a single neuron class enable sex-specific attraction in *Caenorhabditis elegans*. *Proc Natl Acad Sci U S A, 113*(10), E1392-1401. doi:10.1073/pnas.1600786113

Peden, E., Kimberly, E., Gengyo-Ando, K., Mitani, S., & Xue, D. (2007). Control of sex-specific apoptosis in *C. elegans* by the BarH homeodomain protein CEH-30 and the transcriptional repressor UNC-37/Groucho. *Genes Dev, 21*(23), 3195-3207. doi:10.1101/gad.1607807

Pungaliya, C., Srinivasan, J., Fox, B. W., Malik, R. U., Ludewig, A. H., Sternberg, P. W., & Schroeder, F. C. (2009). A shortcut to identifying small molecule signals that regulate behavior and development in *Caenorhabditis elegans*. *Proceedings of the National Academy of Sciences of the United States of America, 106*(19), 7708-7713. doi:10.1073/pnas.0811918106

Rankin, C. H., & Wicks, S. R. (2000). Mutations of the caenorhabditis elegans brain-specific inorganic phosphate transporter eat-4 affect habituation of the tap-withdrawal response without affecting the response itself. *J Neurosci, 20*(11), 4337-4344.

Reilly, D. K., Lawler, D. E., Albrecht, D. R., & Srinivasan, J. (2017). Using an Adapted Microfluidic Olfactory Chip for the Imaging of Neuronal Activity in Response to Pheromones in Male *C. Elegans* Head Neurons. *Journal of Visualized Experiments*(127), e56026. doi:doi:10.3791/56026

Schwartz, H. T., & Horvitz, H. R. (2007). The *C. elegans* protein CEH-30 protects male-specific neurons from apoptosis independently of the Bcl-2 homolog CED-9. *Genes Dev, 21*(23), 3181-3194. doi:10.1101/gad.1607007

Snow, J. J., Ou, G., Gunnarson, A. L., Walker, M. R. S., Zhou, H. M., Brust-Mascher, I., & Scholey, J. M. (2004). Two anterograde intraflagellar transport motors cooperate to

build sensory cilia on *C. elegans* neurons. *Nat Cell Biol, 6*(11), 1109-1113. doi:10.1038/ncb1186

Sulston, J., Dew, M., & Brenner, S. (1975). Dopaminergic neurons in the nematode *Caenorhabditis elegans*. *J Comp Neurol, 163*. doi:10.1002/cne.901630207

Chapter 3 Neuromodulation of Behavior

Chapter 3A Peptidergic Regulation of the *C. elegans* Nervous System

Summary

The nematode, *Caenorhabditis elegans*, relies on a compact, yet extremely complex nervous system of 302 neurons to sense, integrate, and respond to their environment. Aside of gap junctions and classic neurotransmitter signaling, *C. elegans* employs peptidergic signaling to modulate their physiology and neuronal function. Three main classes of neuropeptides have been identified to date in the *C. elegans* genome: the insulin-like peptides (INS), FMRFamide-like peptides (FLP), and non-insulin/non-FLP peptides (NLP). Here, we discussion the current progress into the elucidation of neuropeptide function, as well as deorphanization of neuropeptide receptors. **Chapter 3B** of this dissertation investigates the role of the FMRFamide-like peptide, *flp-3*, using the techniques discussed in **this chapter**, alongside the development of a novel and robust rescue paradigm.

Introduction

The ability to interact with the world is inherently dependent on an individual's ability to sense and respond to its environment. The nervous system allows for both of these assets, by sensing stimuli, integrating a plethora of information, and activating muscles or physiological cascades to react to those stimuli. The nervous system is comprised of individual units, called neurons. These specialized cells communicate to other neurons via three methods: neurotransmitter signaling [1], peptidergic signaling [2], and electrical signaling through gap junctions [3].

Neurotransmitters - GABA [4] and glutamate [5], acetylcholine [6], and bioamines (dopamine, tyramine, octopamine, and serotonin [1]) – are used to communicate between neurons, eliciting hyper- or de-polarizing effects in post-synaptic neurons [7]. Gap junctions allow for electrical communication by directly connecting the intracellular spaces of two adjacent cells [3].

However, these forms of communication tend to skew towards all-or-none activations and network regulation. The environment in which an animal must survive however, is not black-and-white, instead requiring fine-tuned responses for long-term survival. To accomplish this, the nematode, *Caenorhabditis elegans* employs the use of modulators called neuropeptides [2]. These short peptide sequences act either synaptically or extrasynaptically, able to regulate the nervous system ranging from a global scale down to a single paired neuron-neuron connection.

Of over 130 neuropeptide precursor genes [8], physiological roles have been elucidated for under a quarter of them, while even fewer receptors have been uncovered, despite a massive initiative to deorphanize the thousand-plus G protein-coupled receptors in the *C. elegans* genome. The tools available to study peptide signaling in *C. elegans* are young, and the space able to be filled is vast.

Classification of *C. elegans* Neuropeptides

C. elegans employs a vast array of peptides to serve as modulators of the nervous system. With over 130 genes encoding peptide precursors, the final count of individual peptide sequences is approaching 400 [8].

The majority of these fall into one of three classes of neuropeptides: FMRFamide-like peptides (FLP), insulin-like peptides (INS), and non-insulin/non-FMRFamide-related peptides (NLP) [2]. However, in recent years the number of peptides falling within this later class have grown, and the designation of NLP has not been employed for newly discovered peptides [9,10].

FMRFamide-like Peptides

The FMRFamide-like peptides (FLPs), or FMRF-amide-related peptides (FaRPs), constitute a major class of neuropeptides encoded by the *C. elegans* genome. The 31 *flp* genes encode for over 70 unique peptides [2]. cDNAs from all 31 genes have been isolated, confirming that all *flp* genes are expressed [11]. Expression studies have shown that the *flp* expression patterns overlap extensively, making elucidations as to their individual function difficult [11].

These genes are organized into four categories: Category I contains ten genes that encode a single, unique FLP peptide; Category II contains six genes that encode multiple copies of a single peptide sequence: Category III contains ten genes that encode multiple unique peptides, while Category IV contains five genes that encode not only multiple peptides, but multiple copies of some of those peptides (**Table 3, Figure 21**) [12]. That most *flp* genes encode more than one peptide sequence, understanding the function of individual peptides is extremely difficult, as it can be tedious to tease apart roles and interactions of components of genes such as *flp-13*, which encodes seven unique peptides – two of which are encoded twice [2].

Insulin-Like Peptides

The genome of *C. elegans* encodes 40 insulin-like peptides, or *ins* genes [2] (with the exception of *daf-28*, which had been previously named for its role in dauer formation [13]). While initial studies suggested that only 37 of these genes were expressed, recent studies have examined the effects of expressing all 40 genes [14]. As insulin-like peptides, each gene encodes a precursor which, post-peptide cleavage, results in an A-peptide and B-peptide, held together by disulfide bonds, as in the human insulin protein[15].

The insulin genes are organized into four classes, based on the arrangement of their disulfide bonds [16]. The eleven type-γ peptides contain the canonical three disulfide bonds found in vertebrate homologs, while the ten type-β peptides contain a fourth disulfide

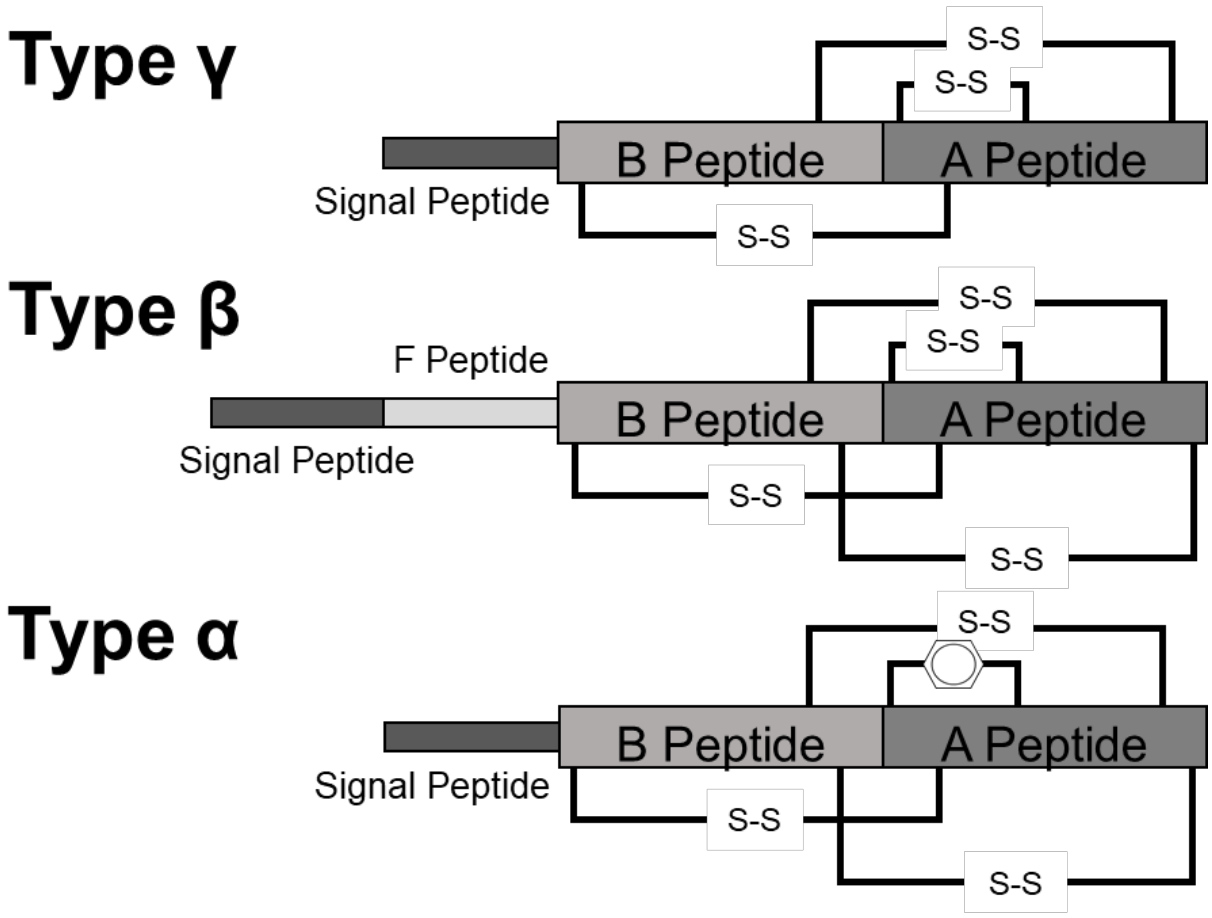

Figure 20. The structures of INS peptides.
Type γ and Type β INS proteins contain both an A-peptide and B-peptide, linked by three or four disulfide bonds, respectively. Type β proteins also contain an F-peptide. Type α proteins replace the A6/A11 bond with aromatic amino acids.

bond; the fifteen type-α peptides lack a specific disulfide bonds, the A6/A11 bond (**Figure 20, Table 3**) [17]. Within eight of the type-β precursors is the F-peptide (**Figure 20**), a novel domain in *C. elegans ins* genes, which is cleaved by *bli-4* (see ***Peptidergic Maturation***) [17].

Non-Insulin/Non-FLP Peptides

The remaining *C. elegans* neuropeptide genes are categorized simply as non-insulin/non-FLP peptide, or *nlp*, genes. Other than their inability to be classified as *ins* or *flp* genes, there is little linking one *nlp* gene to another [2].

Table 3. Classes of C. elegans Neuropeptides.

Family	Class	Gene
FMRFamide-Like Peptides (FLP) FMRFamide-Related Peptides (FaRPs)	Category I	*flp-10, -12, -21, -23, -24, -27, -28, -32, -33, -34*
	Category II	*flp-6, -8, -9, -14*
	Category III	*flp-1, -2, -3, -4, -5, -11, -15, -19, -25, -26*
	Category IV	*flp-7, -13, -16, -17, -18*
Insulin-Like Peptides (INS)	Type-γ	*ins-11, -12, -13, -14, -15, -16, -17, -18, -19, ins-32, ins-37*
	Type-β	*ins-1, -2, -3, -4, -5, -6, -7, -8, -9, -10, daf-28*
	Type-α	*ins-20, -21, -22, -23, -24, -25, -26, -27, -28, 29, -30, -33, -34, -35, -36, -38, -39*
	Three repeats*	*ins-31**
	Former Gene Name	**Current Gene Name**
non-insulin/non-FaRP peptides (NLP) #	*nlp-37*	*pdf-2*[18]
	nlp-54	*trh-1*[10]
	nlp-72	*lury-1*[9]
	nlp-74	*pdf-1*[19]
	nlp-75	*ntc-1*[20]

(*****) among the INS peptides, *ins-31* does not fall into any of the three broader classes, as it contains three repeats of the A- and B- peptide chains. (**#**) The NLP peptides exhibit little similarity between genes, and therefore are not classified in any meaningful way, as in the *ins* and *flp* gene families. Instead, *nlp* genes that have been renamed upon further functional elucidations are shown (Janssen et al., 2008; Van Sinay et al., 2017; Ohno et al., 2017; Barrios et al., 2012; Garrison et al., 2012).

Further, as the roles and more detailed identities of the *nlp* genes are elucidated, even the naming conventions of *nlp* genes have changed. Five genes have been renamed from their original designation (**Table 3**). Formerly *nlp-54*, the gene is now known to be the thyrotropin-releasing hormone gene, *trh-1* [10]. The genes *nlp-74* and *nlp-37* are now *pdf-1*

and *pdf-2*, respectively – as they encode for a pigment dispersal factor peptides [18,19]. Likewise, *nlp-75* has become the vasopressin-like peptide (nematocin), *ntc-1* [20,21]. Recently, a two novel peptides, the RYamide neuropeptides – both encoded by the *lury-1* gene (formerly *nlp-72*), have been elucidated in *C. elegans* [9].

Prior to 2018, the count of *nlp* genes remained at around fifty, which recent predictions increasing that number slightly. Recent deep and stringent analyses of the genome have uncovered novel neuropeptides which exhibit strong conservation among related nematode species [8]. Currently, there are now 82 *nlp* genes annotated in *C. elegans* [8].

Current strategies for peptide elucidation must be taken into consideration when analyzing the gene count of peptide encoding genes. For example, the peptides encoded by *trh-1* (*nlp-54*) are smaller than 700 Da in size at only five to six amino acids in processed length, thereby missing the mass cut-off employed in novel peptide isolation [8,22], suggesting that there may yet remain further peptides that have not yet been elucidated do so their small size.

Peptidergic Maturation

Neuropeptide genes encode larger precursors, or pre-proteins, which are then cleaved and modified to generate mature neuropeptides ready for packing and signaling. There are four proprotein convertases in *C. elegans* which are responsible for endoproteolytic cleavage at dibasic residues within the precursor peptides [2]. These enzymes are derived from the kex2/substilin-like proprotein convertase (kpc) family [23], and act upon the proteins within the Golgi and dense core vesicle (DCVs) [11], following removal of a signal peptide within the endoplasmic reticulum [2] (**Figure 21**).

The convertase most widely distributed in the nervous system is *egl-3* (*kpc-2*), named after its phenotype of defective **egg** **l**aying [24]. The targets of *egl-3* have diverse functions[23], and many FLP precursors are processed via *egl-3* activity [25]; although NLP precursors are also targeted by the enzyme [23]. EGL-3 targets dibasic residues (generally lysine-arginine

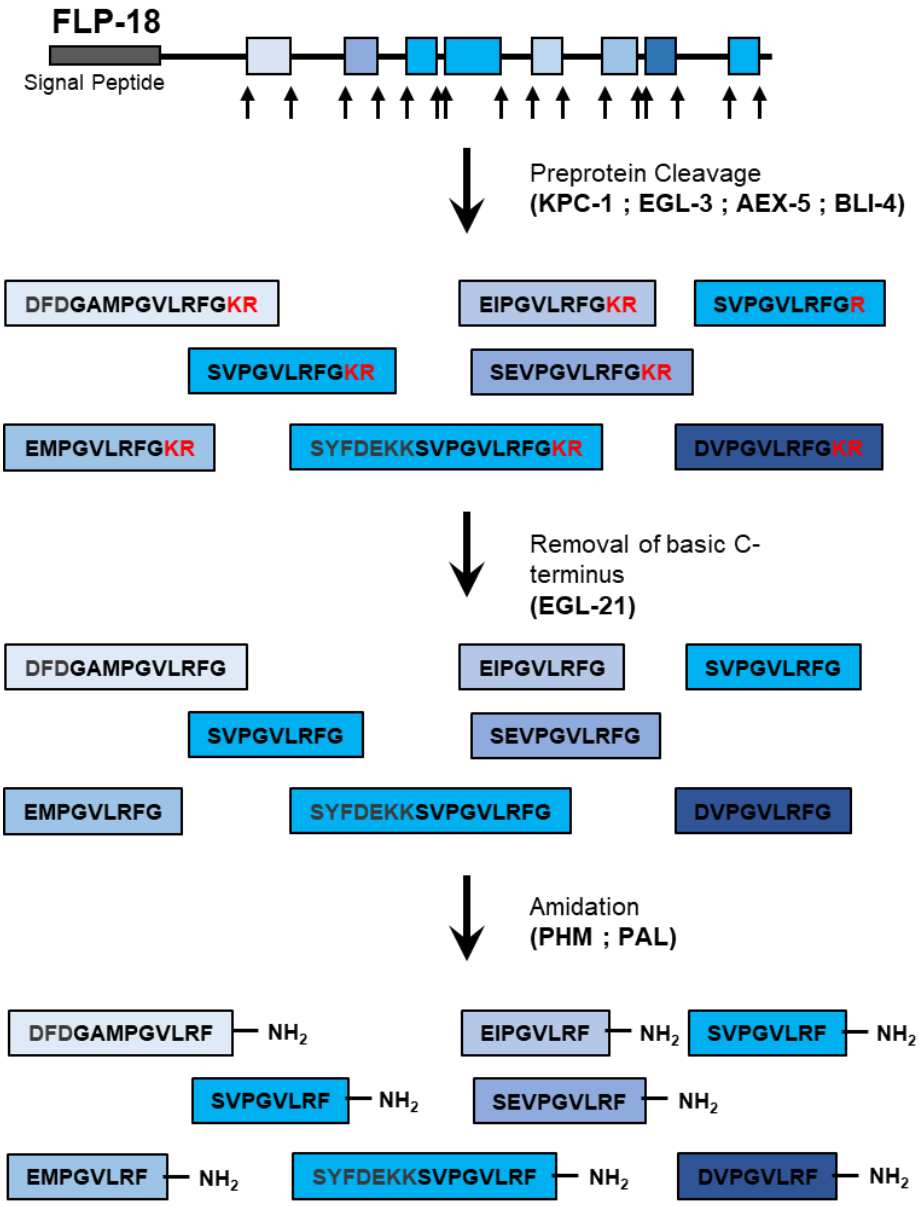

Figure 21. Peptide Maturation of FLP-18.
Preproteins are translated with a signal peptide and appropriate peptide sequences that are flanked by cleavage sites. Dibasic cleavage sites are processed by the KPC enzymes KPC-1, EGL-3, AEX-5, or BLI-4. The basic C-terminus is then removed via EGL-21. Finally, the peptides are amidated by peptidylglycine-α-hydroxylating monooxygenase (PHM) and peptidyl-α-hydroxyglycine α-amidating lyase (PAL).

[KR] or arginine-arginine [RR]): 83% of FLP peptides are flanked by KR or RR sites, while 70% of the remaining are flanked by monobasic resides (often arginine) (**Figure 21**)[11].

The *kpc-1* enzyme has been shown to be involved in growth and movement, although little else has been elucidated as to its function [26]. Meanwhile, *aex-5* (*kpc-3*) is expressed in muscle tissue and is likely involved in regulating exocytosis [26]. Loss of *aex-5* has been shown to result in the loss nearly half of the detectable FLP and NLP processed peptides [23]. The final convertase, *bli-4* (*kpc-4*), while expressed in the nervous system, plays a major role in collagen maturation and cuticle integrity [27]. The gene is remarkably complex, encoding nine separate isoforms of the enzyme [28]. Still, there are neuropeptides that have been found to be processed via *bli-4* in the nervous system [29].

Following cleavage of the precursor protein into its constituent peptides, further processing occurs in the form of basic residue removal from the C-terminus via Carboxypeptidase E (*egl-21*) (**Figure 21**) [30]. To protect against degradation, these peptides are further modified, most commonly through amidation via peptidylglycine-α-hydroxylating monooxygenase (PHM) [31], followed by the action of peptidyl-α-hydroxyglycine α-amidating lyase (PAL) (**Figure 21**) [32].

Roles of Neuropeptides

The roles of individual neuropeptides are being continually elucidated. However, due to the extensive overlap among these modulators of neuronal activity, it is often difficult to attribute a phenotype to a single neuropeptide. In the case where multiple peptides are coded by a single gene, this can be even more tedious.

Locomotion

The first role elucidated for a neuropeptide in *C. elegans* was in 1998, when the FMRFamide-like peptide, *flp-1*, was shown to play a role in locomotion [33]. Animals deficient in *flp-1* are uncoordinated, with an exaggerated sinusoidal waveform when moving [33]. The peptides encoded by *flp-1* were also shown to be necessary for proper nose touch and osmolarity responses [33]. The activity of many *flp* genes have followed similar

methodologies as that used to determine the role of *flp-1*: deletion mutations. However, later analyses determined that the osmolarity defects in *flp-1* mutants were due to a disruption in a neighboring gene, *daf-10* [34]. In this study, the effect of *flp-1* peptides on egg-laying was determined to occur through extra-synaptic signaling, as *flp-1* expressing neurons do not synapse onto the egg-laying circuitry [34]. Recently *flp-2, flp-18,* and *nlp-49* have been shown to regulate locomotion as well [35-38].

Reproduction

The egg-laying machinery is extensively modulated by neuropeptide signaling. Multiple FLPs (*flp-10*, *flp-11*, and *flp-19*) [39-41], as well as NLPs (*nlp-3*, *nlp-7*, *nlp-49*, and *ntc-1* [formerly *nlp-75*]) [20,37,39,42] have been shown to modulate egg-laying behavior and activity.

Similarly, multiple neuropeptides have been shown to be involved in the physical aspects of mating (*flp-7, flp-8, flp-12,* and *flp-20*) [43,44] and mate searching behaviors (*pdf-1* [formerly *nlp-74*]) [19,37,45,46].

Animals defective in *flp-7, -8, -12, and -20* exhibit aberrant "male turning behavior". Males will turn around the tail of a hermaphrodite during mating while attempting to locate the vulva in a stereotyped sequence of motor comments. In these *flp* mutants, however, they exhibit repetitive turning during their mating attempt [44].

Males will leave a food source in the goal of finding a mate at a set "leaving rate". Male lacking the *pdf-1* neuropeptide more readily leave a found source already containing a mate at a significantly increased leaving rate compared to wild-type males [19]. PDF-1 not only controls this behavior but plays a role in setting locomotory states and determining the sexual identity of neurons [45,46]. Little is known about the related *pdf-2* neuropeptide, although it is posed to function in a similar manner as *pdf-1* [45]. **Chapter 3B** of this thesis dissertation provides that that *flp-3* functions in controlling the behavioral valence of males to a mating cue.

Gas Sensation

In order to survive in their natural habitat, *C. elegans* must navigate environments with varying levels of oxygen and carbon dioxide. Multiple neurons have been dedicated to sensing these gases, such as the BAG and URX neurons [47-50]. It stands to reason that peptidergic signaling also plays an integral role in the sensing, processing, and response to changes in oxygen and carbon dioxide levels. The FLP genes, *flp-10, -17,* and *-19* act via the BAG neurons, linking gas sensation to egg-laying [50-52]. The *flp-27* gene has recently been shown to function in "sensitivity to CO_2", while *flp-16* functions to promote attraction to carbon dioxide [53]. In a related facet, *nlp-40* contributes to survival under anoxic conditions [54].

Stress-Induced Sleep and Quiescence

A major class of modulators of stress-induced sleep are neuropeptides. This quiescent behavior is employed by animals in response to stressful environments, allowing themselves to recover cellular stress. The FLP neuropeptide, *flp-13*, is released from the ALA interneuron to signal to wake-promoting neurons to inhibit their activity [55]. This activity has been shown to function in conjunction with *flp-24* and *nlp-8* [56,57]. Similarly, *nlp-22* is released from the RIA neurons to promote normal lethargus – overexpression of this gene results in anachronistic quiescence [58].

Lipid Metabolism and other Facets of Life

Interesting, body fat and lipid metabolism are also regulated by peptidergic signaling. Namely, *flp-7*, *flp-17*, and *nlp-12* all contribute to proper fat storage and lipid metabolism within *C. elegans* [53,59-63].

Multiple neuropeptides also exhibit antimicrobial potential, including *nlp-20* and *nlp-31*[64,65]. Growth and longevity are shown to be modulated by the presence of *trh-1* [formerly *nlp-54*] [10] and *nlp-29* [66], respectively. Even thermosensation is regulated by peptidergic signaling, via *flp-6* [67].

Previously referred to as *nlp-72*, the *lury-1* neuropeptides have recently been shown to function in multiple food-related responses, including feeding, lifespan, egg-laying, and locomotion [9].

The INS Peptides Modulate Neuronal Activity

The INS peptides play as many various roles as the FLP and NLP peptides. As insulin-like peptides, INS proteins often act as either DAF-2 agonists or antagonists [68]. DAF-2/IGFR receptor signaling to suppress *daf-16* signaling, and thereby inhibiting dauer formation [69]. Many of the INS proteins act in this fashion, including *ins-1*, *isn-7*, *ins-18*, *ins-23*, and *ins-35* [17,68,70,71].

INS-1, the structure of which was first determined in 1998 [72], is expressed in multiple amphid neurons, including ASH, ASI, ASJ, and NSM [17]. More recently, it has been shown that AWC^{ON} releases INS-1 to allow ASEL to respond properly to benzaldehyde [73]. AIA also releases INS-1 to affect search behaviors [74].

Expressed in the intestines, INS-18 has been shown to inhibit ADL::*daf-2* signaling. This in turn inhibits ascr#3-mediated avoidance: as *ins-18* expression decreases, ascr#3 avoidance increases (**Figure 22A**) [75]. *ins-18* is also co-expressed alongside *ins-23*, which act as synergistic DAF-2 antagonists [68]. When expressed in the HSN neurons, *ins-18* inhibition of DAF-2 disinhibits *daf-16* signaling, activating a positive-feedback look in which *daf-16* turns on *ins-18* expression (**Figure 22D**) [70].

INS-4 often functions in synergy with other INS peptides [76,77]. When released from AWA, INS-4 acts to antagonize ADL/INS-16 signaling, disinhibiting learning (**Figure 22B**) [77]. When pheromones are sensed by ADL, however, ADL::INS-16 expression is increased, resulting in inhibition of AWA::INS-4 [77]. However, when INS-4 is released alongside INS-6 from ASI, acts upon motor neurons, serving to inhibit synapse formation (**Figure 22C**) [76].

The ASI neuron processes its INS proteins via the EGL-3 protein [76]. However, when INS-6 matures within ASEL, it is cleaved by BLI-4 [29,78]. ASEL uses this specific maturation

of INS-6 to allow AWC^{ON} to respond properly to changes in salt concentrations. Together, ASEL and AWC^{ON} form a circuit of mutual agonism, wherein AWC^{ON} gates ASEL activity via *ins-1*, and ASEL gates AWC^{ON} activity via *ins-6* (**Figure 22E**).

INS-11 functions to inhibit the sensory neurons that drive avoidance in response to pathogenic bacteria. Released from the intestines, INS-11 inhibits ASI::*ins-6* expression

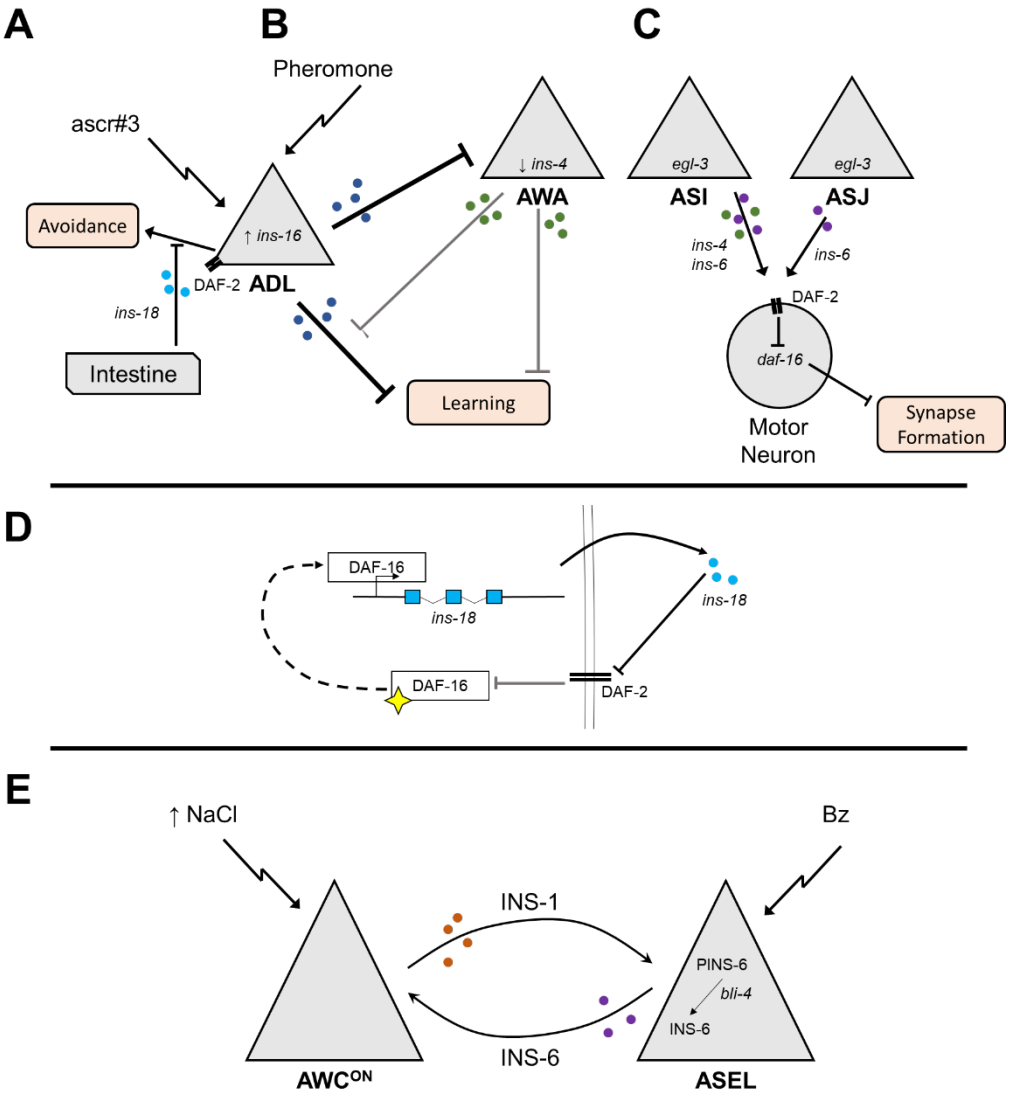

Figure 22. The INS Neuropeptides Modulate Neural Circuit Activity.
(A-C) Sensory neurons employ INS peptides to affect multiple outcomes. **(A)** Release of *ins-18* from the intestine inhibits ADL::DAF-2 signaling from promoting ascr#3-mediated avoidance. **(B)** ADL::*ins-16* modulates AWA::*ins-4* inhibition of learning. **(C)** EGL-3 processing of INS-4 and INS-6 in the ASI and ASJ sensory neurons modulates synapse formation in motor neurons. **(D)** The HSN neurons employ a positive feedback look of *ins-18* signaling resulting in increased *ins-18* expression. **(E)** AWC^{ON} and ASEL function in a feedback look wherein each neuron gates the activity of the other to either increases in salt or benzaldehyde, respectively, through INS signaling. (PINS-6 denotes pre-processed INS-6).

(**Figure 22C**), along with ADF::*tph-1* [79]. These decreases in expression result in decreases of aversive behaviors, preventing proper response to pathogens.

Neuropeptide Receptors

Despite the vast number of neuropeptides active within the *C. elegans* nervous system, only a handful of receptors have been identified. All of the known INS peptide-receptor interactions elucidated to date occur via the DAF-2 receptor, including INS-1 [17], INS-4 [76], INS-6 [78], INS-7 [71], INS-18 [68,70], INS-23 [68], and INS-35 [71]. However, linking receptors and neuropeptide ligands for FLP and NLP peptides has proven more elusive.

Neuropeptides encoded by FLP genes often activate multiple receptors, as seen in FLP-13 activate of both FRPR-4 and DMSR-1 to regulate sleep [55,80]. FLP-18 encodes seven unique peptides, which are sensed by NPR-1, NPR-4, and NPR-5 [35,38,81]. Likewise, FLP-21 peptides have been shown to activate a host of GPCRs, including NPR-1, NPR-3, NPR-6, and NPR-11 [40,82-85]. Conversely, only one receptor has been identified for FLP-2 (FPRR-18), [86], FLP-4 (NPR-4) [87], FLP-15 (NPR-13) [88], and FLP-20 (FRPR-16) [43]. The peptides encoded by FLP-7 and FLP-11 are sensed by NPR-22, along with the LURY-1 peptides [9,61,89]. Also employing convergent ligand-receptor activation, FLP-10 and FLP-17 both activate the EGL-6 receptor [50,90]. **Chapter 3B** of this dissertation aims to elucidate the receptors of FLP-3, NPR-10 and FRPR-16.

Sensation of NLP peptides appears to be more specific. Ligand-Receptor pairs have been identified on a one-to-one basis to date. Making pairings more reasonable to remember, the receptors for PDF-1 (and PDF-2) and TRH-1 peptides share their respective names: PDFR-1 and TRHR-1[10,19]. The CRF receptor-like GPCR, SEB-3, which plays a role in alcohol tolerance and stress response, also senses NLP-49, to modulate locomotion and egg-laying [37,91,92]. NLP-40 is sensed via AEX-2 to regulate anoxic survival [54], while NLP-12 signaling is processed by CKR-2 [60].

Conclusions

Peptidergic signaling offers the nervous system the ability to fine-tune its responses and gate the activity of other neuromodulators. This signaling paradigm is remarkably conserved across phyla [93], making *C. elegans* a prime candidate for studying the mechanisms underlying neuropeptide functions. With a class of insulin-like peptides that exhibit a host of outputs through a single, conserved receptor – DAF-2 – and an expansive class of FMRFamide-like peptides, the nervous system of *C. elegans* is notably complex. No longer are the synaptic connections the only way in which *C. elegans* can modulate its neuronal activity – extrasynaptic connections expand this network considerably [94-96]. Studying of peptides that modulate this network will increase our understanding of how human neuropeptides, such as neuropeptide Y, affect our own physiology [97].

References

1 Chase, D. L. & Koelle, M. R. Biogenic amine neurotransmitters in *C. elegans*. *WormBook*, 1-15, doi:10.1895/wormbook.1.132.1 (2007).

2 Li, C. & Kim, K. Neuropeptides. *WormBook*, doi:10.1895/workbook.1.142.1 (2008).

3 Kawano, T. *et al.* An Imbalancing Act: Gap Junctions Reduce the Backward Motor Circuit Activity to Bias *C. elegans* for Forward Locomotion. *Neuron* **72**, 572-586, doi:10.1016/j.neuron.2011.09.005 (2011).

4 Jorgensen, E. M. GABA. *WormBook*, 1-13, doi:10.1895/wormbook.1.14.1 (2005).

5 Lee, R. Y., Sawin, E. R., Chalfie, M., Horvitz, H. R. & Avery, L. EAT-4, a homolog of a mammalian sodium-dependent inorganic phosphate cotransporter, is necessary for glutamatergic neurotransmission in *Caenorhabditis elegans*. *J Neurosci* **19**, 159-167 (1999).

6 Rand, J. B. Acetylcholine. *WormBook*, 1-21, doi:10.1895/wormbook.1.131.1 (2007).

7 Koelle, M. R. Neurotransmitter signaling through heterotrimeric G proteins: insights from studies in *C. elegans*. *WormBook*, 1-78, doi:10.1895/wormbook.1.75.2 (2016).

8 Van Bael, S. *et al.* A *Caenorhabditis elegans* Mass Spectrometric Resource for Neuropeptidomics. *Journal of The American Society for Mass Spectrometry*, doi:10.1007/s13361-017-1856-z (2018).

9 Ohno, H. *et al.* Luqin-like RYamide peptides regulate food-evoked responses in *C. elegans*. *eLife* **6**, e28877, doi:10.7554/eLife.28877 (2017).

10 Van Sinay, E. *et al.* Evolutionarily conserved TRH neuropeptide pathway regulates growth in *Caenorhabditis elegans*. *Proc Natl Acad Sci U S A* **114**, E4065-e4074, doi:10.1073/pnas.1617392114 (2017).

11 Li, C. & Kim, K. Family of FLP Peptides in *Caenorhabditis elegans* and Related Nematodes. *Front Endocrinol (Lausanne)* **5**, 150, doi:10.3389/fendo.2014.00150 (2014).

12 Masler, E. P. Free-Living Nematodes. *Handbook of Biologically Active Peptides*, 247-254, doi:10.1016/B978-0-12-385095-9.00036-1 (2013).

13 Malone, E. A. & Thomas, J. H. A screen for nonconditional dauer-constitutive mutations in *Caenorhabditis elegans*. *Genetics* **136**, 879-886 (1994).

14 Zheng, S. *et al.* A functional study of all 40 *Caenorhabditis* elegans insulin-like peptides. *J Biol Chem* **293**, 16912-16922, doi:10.1074/jbc.RA118.004542 (2018).

15 Murray-Rust, J., McLeod, A. N., Blundell, T. L. & Wood, S. P. Structure and evolution of insulins: Implications for receptor binding. *BioEssays* **14**, 325-331, doi:10.1002/bies.950140507 (1992).

16 Duret, L., Guex, N., Peitsch, M. C. & Bairoch, A. New insulin-like proteins with atypical disulfide bond pattern characterized in *Caenorhabditis elegans* by comparative sequence analysis and homology modeling. *Genome Res* **8**, 348-353, doi:10.1101/gr.8.4.348 (1998).

17 Pierce, S. B. *et al.* Regulation of DAF-2 receptor signaling by human insulin and *ins-1*, a member of the unusually large and diverse *C. elegans* insulin gene family. *Genes & Development* **15**, 672-686, doi:10.1101/gad.867301 (2001).

18 Janssen, T. *et al.* Functional characterization of three G protein-coupled receptors for pigment dispersing factors in *Caenorhabditis elegans*. *J Biol Chem* **283**, 15241-15249, doi:10.1074/jbc.M709060200 (2008).

19 Barrios, A., Ghosh, R., Fang, C., Emmons, S. W. & Barr, M. M. PDF-1 neuropeptide signaling modulates a neural circuit for mate-searching behavior in *C. elegans*. *Nature Neuroscience* **15**, 1675-1684, doi:10.1038/nn.3253 (2012).

20 Garrison, J. L. *et al.* Oxytocin/vasopressin-related peptides have an ancient role in reproductive behavior. *Science* **338**, 540-543, doi:10.1126/science.1226201 (2012).

21 Beets, I. *et al.* Vasopressin/oxytocin-related signaling regulates gustatory associative learning in *C. elegans*. *Science* **338**, 543-545, doi:10.1126/science.1226860 (2012).

22 Van Bael, S., Edwards, S. L., Husson, S. J. & Temmerman, L. Identification of Endogenous Neuropeptides in the Nematode *C. elegans* Using Mass Spectrometry. *Methods Mol Biol* **1719**, 271-291, doi:10.1007/978-1-4939-7537-2_18 (2018).

23 Husson, S. J., Clynen, E., Baggerman, G., Janssen, T. & Schoofs, L. Defective processing of neuropeptide precursors in *Caenorhabditis elegans* lacking proprotein convertase 2 (KPC-2/EGL-3): mutant analysis by mass spectrometry. *J Neurochem* **98**, 1999-2012, doi:10.1111/j.1471-4159.2006.04014.x (2006).

24 Trent, C., Tsung, N. & Horvitz, H. R. Egg-laying defective mutants of the nematode *Caenorhabditis elegans*. *Genetics* **104** (1983).

25 Salem, J. B., Nkambeu, B., Arvanitis, D. N. & Beaudry, F. Deciphering the Role of EGL-3 for Neuropeptides Processing in *Caenorhabditis elegans* Using High-Resolution Quadrupole-Orbitrap Mass Spectrometry. *Neurochem Res* **43**, 2121-2131, doi:10.1007/s11064-018-2636-2 (2018).

26 Thacker, C. & Rose, A. M. A look at the *Caenorhabditis elegans* Kex2/Subtilisin-like proprotein convertase family. *BioEssays : news and reviews in molecular, cellular and developmental biology* **22**, 545-553, doi:10.1002/(SICI)1521-1878(200006)22:6<545::AID-BIES7>3.0.CO;2-F (2000).

27 Thacker, C., Srayko, M. & Rose, A. M. Mutational analysis of *bli-4/kpc-4* reveals critical residues required for proprotein convertase function in *C. elegans*. *Gene* **252**, 15-25, doi:10.1016/s0378-1119(00)00211-0 (2000).

28 Thacker, C., Marra, M. A., Jones, A., Baillie, D. L. & Rose, A. M. Functional genomics in *Caenorhabditis elegans*: An approach involving comparisons of sequences from related nematodes. *Genome research* **9**, 348-359 (1999).

29 Leinwand, S. G. & Chalasani, S. H. From genes to circuits and behaviors: Neuropeptides expand the coding potential of the nervous system. *Worm* **3**, e27730, doi:10.4161/worm.27730 (2014).

30 Husson, S. J. *et al.* Impaired processing of FLP and NLP peptides in carboxypeptidase E (EGL-21)-deficient *Caenorhabditis elegans* as analyzed by mass spectrometry. *Journal of neurochemistry* **102**, 246-260, doi:10.1111/j.1471-4159.2007.04474.x (2007).

31 Eipper, B. A., Milgram, S. L., Jean Husten, E., Yun, H.-Y. & Mains, R. E. Peptidylglycine α-amidating monooxygenase: A multifunctional protein with catalytic, processing, and routing domains. *Protein Science* **2**, 489-497, doi:10.1002/pro.5560020401 (1993).

32 Eipper, B. A. *et al.* Peptidyl-alpha-hydroxyglycine alpha-amidating lyase. Purification, characterization, and expression. *J Biol Chem* **266**, 7827-7833 (1991).

33 Nelson, L. S., Rosoff, M. L. & Li, C. Disruption of a neuropeptide gene, *flp-1*, causes multiple behavioral defects in *Caenorhabditis elegans*. *Science* **281**, doi:10.1126/science.281.5383.1686 (1998).

34 Buntschuh, I. *et al.* FLP-1 neuropeptides modulate sensory and motor circuits in the nematode *Caenorhabditis elegans*. *PLoS One* **13**, e0189320, doi:10.1371/journal.pone.0189320 (2018).

35 Bhardwaj, A., Pandey, P. & Babu, K. Control of Locomotory Behavior of *Caenorhabditis elegans* by the Immunoglobulin Superfamily Protein RIG-3. *Genetics*, genetics.302872.302019, doi:10.1534/genetics.119.302872 (2019).

36 Chen, D., Taylor, K. P., Hall, Q. & Kaplan, J. M. The Neuropeptides FLP-2 and PDF-1 Act in Concert To Arouse *Caenorhabditis elegans* Locomotion. *Genetics* **204**, 1151-1159, doi:10.1534/genetics.116.192898 (2016).

37 Chew, Y. L., Grundy, L. J., Brown, A. E. X., Beets, I. & Schafer, W. R. Neuropeptides encoded by *nlp-49* modulate locomotion, arousal and egg-laying behaviours in C*aenorhabditis elegans* via the receptor SEB-3. *Philos Trans R Soc Lond B Biol Sci* **373**, doi:10.1098/rstb.2017.0368 (2018).

38 Cohen, M. *et al.* Coordinated regulation of foraging and metabolism in *C. elegans* by RFamide neuropeptide signaling. *Cell metabolism* **9**, 375-385, doi:10.1016/j.cmet.2009.02.003 (2009).

39 Banerjee, N., Bhattacharya, R., Gorczyca, M., Collins, K. M. & Francis, M. M. Local neuropeptide signaling modulates serotonergic transmission to shape the temporal organization of *C. elegans* egg-laying behavior. *PLoS Genet* **13**, e1006697, doi:10.1371/journal.pgen.1006697 (2017).

40 Chang, Y.-J. *et al.* Modulation of Locomotion and Reproduction by FLP Neuropeptides in the Nematode *Caenorhabditis elegans*. *PLoS ONE* **10**, e0135164, doi:10.1371/journal.pone.0135164 (2015).

41 Park, J., Choi, W., Dar, A. R., Butcher, R. A. & Kim, K. Neuropeptide Signaling Regulates Pheromone-Mediated Gene Expression of a Chemoreceptor Gene in *C. elegans*. *Mol Cells* **42**, 28-35, doi:10.14348/molcells.2018.0380 (2019).

42 Brewer, J. C., Olson, A. C., Collins, K. M. & Koelle, M. R. Serotonin and neuropeptides are both released by the HSN command neuron to initiate *Caenorhabditis elegans* egg laying. *PLoS genetics* **15**, e1007896-e1007896, doi:10.1371/journal.pgen.1007896 (2019).

43 Chew, Y. L. *et al.* An Afferent Neuropeptide System Transmits Mechanosensory Signals Triggering Sensitization and Arousal in *C. elegans*. *Neuron* **99**, 1233-1246.e1236, doi:10.1016/j.neuron.2018.08.003 (2018).

44 Liu, T., Kim, K., Li, C. & Barr, M. M. FMRFamide-like neuropeptides and mechanosensory touch receptor neurons regulate male sexual turning behavior in *Caenorhabditis elegans*. *J Neurosci* **27**, 7174-7182, doi:10.1523/JNEUROSCI.1405-07.2007 (2007).

45 Flavell, S. W. *et al.* Serotonin and the neuropeptide PDF initiate and extend opposing behavioral states in *C. elegans*. *Cell* **154**, 1023-1035, doi:10.1016/j.cell.2013.08.001 (2013).

46 Hilbert, Z. A. & Kim, D. H. PDF-1 neuropeptide signaling regulates sexually dimorphic gene expression in shared sensory neurons of *C. elegans*. *eLife* **7**, e36547, doi:10.7554/eLife.36547 (2018).

47 Bretscher, Andrew J. *et al.* Temperature, Oxygen, and Salt-Sensing Neurons in *C. elegans* Are Carbon Dioxide Sensors that Control Avoidance Behavior. *Neuron* **69**, 1099-1113, doi:10.1016/j.neuron.2011.02.023 (2011).

48 Chang, A. J., Chronis, N., Karow, D. S., Marletta, M. A. & Bargmann, C. I. A Distributed Chemosensory Circuit for Oxygen Preference in *C. elegans*. *PLOS Biology* **4**, e274, doi:10.1371/journal.pbio.0040274 (2006).

49 Guillermin, M. L., Castelletto, M. L. & Hallem, E. A. Differentiation of carbon dioxide-sensing neurons in *Caenorhabditis elegans* requires the ETS-5 transcription factor. *Genetics* **189**, 1327-1339, doi:10.1534/genetics.111.133835 (2011).

50 Hussey, R. *et al.* Oxygen-sensing neurons reciprocally regulate peripheral lipid metabolism via neuropeptide signaling in *Caenorhabditis elegans*. *PLoS genetics* **14**, e1007305-e1007305, doi:10.1371/journal.pgen.1007305 (2018).

51 Beets, I. *et al.* Natural Variation in a Dendritic Scaffold Protein Remodels Experience-Dependent Plasticity by Altering Neuropeptide Expression. *Neuron*, S0896-6273(0819)30849-30849, doi:10.1016/j.neuron.2019.10.001 (2019).

52 Ringstad, N. & Horvitz, H. R. FMRFamide neuropeptides and acetylcholine synergistically inhibit egg-laying by *C. elegans*. *Nat Neurosci* **11**, 1168-1176, doi:10.1038/nn.2186 (2008).

53 Guillermin, M. L., Carrillo, M. A. & Hallem, E. A. A Single Set of Interneurons Drives Opposite Behaviors in *C. elegans*. *Current biology : CB* **27**, 2630-2639.e2636, doi:10.1016/j.cub.2017.07.023 (2017).

54 Doshi, S. *et al.* Neuropeptide signaling regulates the susceptibility of developing *C. elegans* to anoxia. *Free Radic Biol Med* **131**, 197-208, doi:10.1016/j.freeradbiomed.2018.12.006 (2019).

55 Iannacone, M. J. *et al.* The RFamide receptor DMSR-1 regulates stress-induced sleep in *C. elegans*. *Elife* **6**, doi:10.7554/eLife.19837 (2017).

56 Cianciulli, A. *et al.* Interneurons Regulate Locomotion Quiescence via Cyclic Adenosine Monophosphate Signaling During Stress-Induced Sleep in *Caenorhabditis elegans*. *Genetics* **213**, 267-279, doi:10.1534/genetics.119.302293 (2019).

57 Nath, R. D., Chow, E. S., Wang, H., Schwarz, E. M. & Sternberg, P. W. *C. elegans* Stress-Induced Sleep Emerges from the Collective Action of Multiple Neuropeptides. *Current biology* **26**, 2446-2455, doi:10.1016/j.cub.2016.07.048 (2016).

58 Nelson, M. D. *et al.* The neuropeptide NLP-22 regulates a sleep-like state in *Caenorhabditis elegans*. *Nature communications* **4**, 2846-2846, doi:10.1038/ncomms3846 (2013).

59 Bhattacharya, R. *et al.* A conserved dopamine-cholecystokinin signaling pathway shapes context-dependent *Caenorhabditis elegans* behavior. *PLoS genetics* **10**, e1004584-e1004584, doi:10.1371/journal.pgen.1004584 (2014).

60 Hu, Z., Vashlishan-Murray, A. B. & Kaplan, J. M. NLP-12 engages different UNC-13 proteins to potentiate tonic and evoked release. *The Journal of neuroscience : the official journal of the Society for Neuroscience* **35**, 1038-1042, doi:10.1523/JNEUROSCI.2825-14.2015 (2015).

61 Palamiuc, L. *et al.* A tachykinin-like neuroendocrine signalling axis couples central serotonin action and nutrient sensing with peripheral lipid metabolism. *Nature communications* **8**, 14237-14237, doi:10.1038/ncomms14237 (2017).

62 Peeters, L. *et al.* A pharmacological study of NLP-12 neuropeptide signaling in free-living and parasitic nematodes. *Peptides* **34**, 82-87, doi:10.1016/j.peptides.2011.10.014 (2012).

63 Tao, L. *et al.* Parallel Processing of Two Mechanosensory Modalities by a Single Neuron in *C. elegans*. *Developmental cell*, S1534-5807(1519)30852-30854, doi:10.1016/j.devcel.2019.10.008 (2019).

64 Scorzoni, L. *et al.* Evaluation of *Caenorhabditis elegans* as a host model for *Paracoccidioides brasiliensis* and *Paracoccidioides lutzii*. *Pathog Dis* **76**, 10.1093/femspd/fty1004, doi:10.1093/femspd/fty004 (2018).

65 Zhang, X. M., Gao, J., Chen, C. H. & Tu, H. J. Progress in the mechanisms of neural modulation of innate immunity in *Caenorhabditis elegans*. *Yi Chuan* **40**, 1066-1074, doi:10.16288/j.yczz.18-133 (2018).

66 Marudhupandiyan, S., Prithika, U., Balasubramaniam, B. & Balamurugan, K. RACK-1, a multifaceted regulator is required for *C. elegans* innate immunity against *S. flexneri* M9OT infection. *Developmental and comparative immunology* **74**, 227-236, doi:10.1016/j.dci.2017.05.008 (2017).

67 Chen, Y. C. *et al.* A *C. elegans* Thermosensory Circuit Regulates Longevity through *crh-1*/CREB-Dependent *flp-6* Neuropeptide Signaling. *Dev Cell* **39**, 209-223, doi:10.1016/j.devcel.2016.08.021 (2016).

68 Matsunaga, Y., Matsukawa, T., Iwasaki, T., Nagata, K. & Kawano, T. Comparison of physiological functions of antagonistic insulin-like peptides, INS-23 and INS-18, in *Caenorhabditis elegans*. *Biosci Biotechnol Biochem* **82**, 90-96, doi:10.1080/09168451.2017.1415749 (2018).

69 Murphy, C. T. & Hu, P. J. Insulin/insulin-like growth factor signaling in *C. elegans*. *WormBook*, 1-43, doi:10.1895/wormbook.1.164.1 (2013).

70 Matsunaga, Y., Gengyo-Ando, K., Mitani, S., Iwasaki, T. & Kawano, T. Physiological function, expression pattern, and transcriptional regulation of a *Caenorhabditis elegans* insulin-like peptide, INS-18. *Biochemical and biophysical research communications* **423**, 478-483, doi:10.1016/j.bbrc.2012.05.145 (2012).

71 Matsunaga, Y. *et al.* Diapause is associated with a change in the polarity of secretion of insulin-like peptides. *Nat Commun* **7**, 10573, doi:10.1038/ncomms10573 (2016).

72 Gregoire, F. M., Chomiki, N., Kachinskas, D. & Warden, C. H. Cloning and Developmental Regulation of a Novel Member of the Insulin-like Gene Family in *Caenorhabditis elegans*. *Biochemical and Biophysical Research Communications* **249**, 385-390, doi:10.1006/bbrc.1998.9164 (1998).

73 Leinwand, S. G. *et al.* Circuit mechanisms encoding odors and driving aging-associated behavioral declines in *Caenorhabditis elegans*. *eLife* **4**, e10181-e10181, doi:10.7554/eLife.10181 (2015).

74 Chalasani, S. H. *et al.* Neuropeptide feedback modifies odor-evoked dynamics in *Caenorhabditis elegans* olfactory neurons. *Nat Neurosci* **13**, 615-621, doi:10.1038/nn.2526 (2010).

75 Ryu, L. *et al.* Feeding state regulates pheromone-mediated avoidance behavior via the insulin signaling pathway in *Caenorhabditis elegans*. *The EMBO journal* **37**, e98402, doi:10.15252/embj.201798402 (2018).

76 Hung, W. L. *et al.* Attenuation of insulin signalling contributes to FSN-1-mediated regulation of synapse development. *The EMBO Journal* **32**, 1745-1760, doi:10.1038/emboj.2013.91 (2013).

77 Wu, T. *et al.* Pheromones Modulate Learning by Regulating the Balanced Signals of Two Insulin-like Peptides. *Neuron*, doi:10.1016/j.neuron.2019.09.006 (2019).

78 Leinwand, S. G. & Chalasani, S. H. Neuropeptide signaling remodels chemosensory circuit composition in *Caenorhabditis elegans*. *Nature neuroscience* **16**, 1461-1467, doi:10.1038/nn.3511 (2013).

79 Lee, K. & Mylonakis, E. An Intestine-Derived Neuropeptide Controls Avoidance Behavior in *Caenorhabditis elegans*. *Cell Rep* **20**, 2501-2512, doi:10.1016/j.celrep.2017.08.053 (2017).

80 Nelson, M. D. *et al.* FRPR-4 Is a G-Protein Coupled Neuropeptide Receptor That Regulates Behavioral Quiescence and Posture in *Caenorhabditis elegans*. *PLoS One* **10**, e0142938, doi:10.1371/journal.pone.0142938 (2015).

81 McGrath, P. T. *et al.* Quantitative mapping of a digenic behavioral trait implicates globin variation in *C. elegans* sensory behaviors. **61**, 692-699 (2009).

82 Andersen, E. C., Bloom, J. S., Gerke, J. P. & Kruglyak, L. A Variant in the Neuropeptide Receptor *npr-1* is a Major Determinant of *Caenorhabditis elegans* Growth and Physiology. *PLOS Genetics* **10**, e1004156, doi:10.1371/journal.pgen.1004156 (2014).

83 de Bono, M. & Bargmann, C. I. Natural variation in a neuropeptide Y receptor homolog modifies social behavior and food response in *C. elegans*. *Cell* **94**, doi:10.1016/s0092-8674(00)81609-8 (1998).

84 Keating, C. D. *et al.* Whole-genome analysis of 60 G protein-coupled receptors in *Caenorhabditis elegans* by gene knockout with RNAi. *Current biology : CB* **13**, 1715-1720, doi:10.1016/j.cub.2003.09.003 (2003).

85 Rogers, C. *et al.* Inhibition of *Caenorhabditis elegans* social feeding by FMRFamide-related peptide activation of NPR-1. **6**, 1178-1185 (2003).

86 Larsen, M. J. *et al.* Functional expression and characterization of the *C. elegans* G-protein-coupled FLP-2 Receptor (T19F4.1) in mammalian cells and yeast. *International Journal for Parasitology: Drugs and Drug Resistance* **3**, 1-7, doi:10.1016/j.ijpddr.2012.10.002 (2013).

87 Yu, Y., Zhi, L., Guan, X., Wang, D. & Wang, D. FLP-4 neuropeptide and its receptor in a neuronal circuit regulate preference choice through functions of ASH-2 trithorax complex in *Caenorhabditis elegans*. *Sci Rep* **6**, 21485, doi:10.1038/srep21485 (2016).

88 Kubiak, T. M. *et al.* Functional Annotation of the Putative Orphan *Caenorhabditis elegans* G-protein-coupled Receptor C10C6.2 as a FLP15 Peptide Receptor. *Journal of Biological Chemistry* **278**, 42115-42120, doi:10.1074/jbc.M304056200 (2003).

89 Turek, M., Besseling, J., Spies, J.-P., König, S. & Bringmann, H. Sleep-active neuron specification and sleep induction require FLP-11 neuropeptides to systemically induce sleep. *eLife* **5**, e12499, doi:10.7554/eLife.12499 (2016).

90 Zang, K. E., Ho, E. & Ringstad, N. Inhibitory peptidergic modulation of *C. elegans* serotonin neurons is gated by T-type calcium channels. *eLife* **6**, e22771, doi:10.7554/eLife.22771 (2017).

91 Jee, C., Goncalves, J. F., LeBoeuf, B. & Garcia, L. R. CRF-like receptor SEB-3 in sex-common interneurons potentiates stress handling and reproductive drive in *C. elegans*. *Nature communications* **7**, 11957-11957, doi:10.1038/ncomms11957 (2016).

92 Jee, C. *et al.* SEB-3, a CRF receptor-like GPCR, regulates locomotor activity states, stress responses, and ethanol tolerance in *C. elegans*. *Genes, brain, and behavior* **12**, 10.1111/j.1601-1183X.2012.00829.x, doi:10.1111/j.1601-183X.2012.00829.x (2013).

93 Elphick, M. R., Mirabeau, O. & Larhammar, D. Evolution of neuropeptide signalling systems. *J Exp Biol* **221**, doi:10.1242/jeb.151092 (2018).

94 Azulay, A., Itskovits, E. & Zaslaver, A. The *C. elegans* Connectome Consists of Homogenous Circuits with Defined Functional Roles. *PLoS computational biology* **12**, e1005021, doi:10.1371/journal.pcbi.1005021 (2016).

95 Bentley, B. *et al.* The Multilayer Connectome of *Caenorhabditis elegans*. *PLoS computational biology* **12**, e1005283, doi:10.1371/journal.pcbi.1005283 (2016).

96 DiLoreto, E. M., Chute, C. D., Bryce, S. & Srinivasan, J. Novel Technological Advances in Functional Connectomics in *C. elegans*. *Journal of Developmental Biology* **7**, doi:10.3390/jdb7020008 (2019).

97 Stephens, T. W. *et al.* The role of neuropeptide Y in the antiobesity action of the obese gene product. **377**, 530-532 (1995).

Chapter 3B A Single Neuropeptide Controls the Sex-Specific Behavioral Valence to a Mating Pheromone in *Caenorhabditis elegans*

In Preparation as:

Reilly DK[1], McGlame EJ[1,6], Vandewyer E[2], Robidoux AM[1,3], Northcott HT[1,4], Alkema MJ[5], Gegear RJ[7], Beets I[2], Srinivasan J[1,4,*]. A Single Neuropeptide Controls the Sex-Specific Behavioral Valence to a Mating Pheromone in *Caenorhabditis elegans*.

[1] Department of Biology and Biotechnology, Worcester Polytechnic Institute, Worcester, MA 01605, USA
[2] Neural Signaling and Circuit Plasticity Group, Department of Biology, KU Leuven, Leuven, BEL
[3] Department of Chemistry and Biochemistry, Worcester Polytechnic Institute, Worcester, MA 01605, USA
[4] Program of Bioinformatics and Computational Biology, Worcester Polytechnic Institute, Worcester, MA 01605, USA
[5] Neurobiology Department, University of Massachusetts Medical School, Worcester, MA 01605, USA
[6] Present address: AbbVie Foundational Neuroscience Center, Cambridge, MA 02139, USA
[7] Department of Biology, University of Massachusetts Dartmouth, Dartmouth, MA 02747, USA
* Corresponding author: Jagan Srinivasan, jsrinivasan@wpi.edu

Abstract

Proper neuromodulation of chemical cues is paramount to the execution of adaptive behavior in many contexts, including foraging, predator avoidance and reproduction. In the nematode *Caenorhabditis elegans*, a library of small molecules called ascarosides aid in mate recognition and reproduction. Here we show that the attractive behavioral valence observed in male *C. elegans* to the mating pheromone ascr#8 is dependent on the neuropeptide-encoding gene, *flp-3*. Combining behavioral analyses of loss of function neuropeptide receptor mutants with biochemical receptor activation assays, we show that the two G protein-coupled receptors, NPR-10 and FRPR-16, are required for FLP-3 signaling *in vivo*, and for execution of the behavioral response of males to ascr#8. In developing a novel peptide rescue-by-feeding paradigm to rescue individual FLP-3 peptides, we show that FLP-3 is a complex neuropeptide precursor that acts in a peptide- and sex-specific manner to regulate mate recognition.

Introduction

The ability of an organism to sense and respond to environmental stimuli in a timely fashion is critical to survival – at both the individual and species levels. The nematode, *Caenorhabditis elegans*, which feeds on rotting vegetation [2], must navigate a constantly changing environment, and decode olfactory cues communicating information on food availability, population density, and mate availability [3-5]. Given its conserved cellular developmental lineage [6], *C. elegans* provides a prime tool for studying the neural bases of these social behaviors.

Nematodes communicate this information through a large and growing class of small-molecule pheromones termed ascarosides [3,5,7]. These pheromones convey social as well as developmental information [8], and the assays used to understand the roles of these cues have varied [4,9]. There are multiple ascarosides found to communicate attractive behaviors, specifically in a sex-specific manner, including: ascr#1, ascr#2, ascr#3, ascr#4, and ascr#8 [10-12]. Unique among ascaroside structure is the presence of a *p*-aminobenzoate group at the terminus of ascr#8: a folate precursor that *C. elegans* cannot synthesize yet are able to obtain from bacterial food sources [13-15]. This pheromone has previously been shown to act as an extremely potent male attractant, being sensed via a chemosensory pathway shared with ascr#3: the male specific CEM neurons [10]. However, whereas ascr#3 is also sensed by over half a dozen chemosensory neurons [10,16-18], ascr#8 is only sensed by the male-specific CEM [10].

In order to better understand the neuronal mechanisms governing the behavioral response of male *C. elegans* to ascr#8 [19], we questioned whether neuropeptides play a role in the neural network. Males exhibit a unique behavioral tuning curve to ascr#8 (preferring concentrations in the 1 μM range, no longer being attracted to higher concentrations [10]. Multiple FMRFamide-like peptide (*flp*) genes have been shown to play roles in setting physiological state [20-22], as well as linking sensation to physiology and

behavior [23-25]: We therefore reasoned that peptidergic signaling may play a role in the ascr#8 behavioral response.

The attraction of *C. elegans* to the attractive social ascarosides employed a Spot Retention Assay (SRA) [10-12]. However, we found that the SRA contains several drawbacks, including male-male contact and the inability to track individual animals through the course of an assay. To address these issues, we have developed a single worm assay (SWA): a more robust assay that determines variables on a per-worm basis, and not solely at the population level. We utilized our novel SWA to examine the responses of *him-8* males defective in *flp* neuropeptide genes expressed strongly in male-specific neurons; *flp-3*, *flp-6*, *flp-12*, and *flp-19* [26]. In doing so, we discovered that *flp-3* plays a role in determining the sex-specific behavioral valence: i.e., determining whether the response to ascr#8 is attractive or aversive [17,27,28].

In order to identify the site and pathway of action of FLP-3, we then sought to identify the receptors responsible for sensing the processed neuropeptides. Receptor activation studies elucidated that the previously identified *flp-3*-sensing G protein-coupled receptor, NPR-10 [1], and the novel receptor, FRPR-16, are both activated by FLP-3 peptides at nanomolar affinities. Similarly, loss of function mutants resulted in behavioral defects in the male attraction to ascr#8 that parallel those observed in *flp-3* mutants.

To more completely understand *flp-3*'s role in mediating the ascr#8 behavioral response, we adapted a peptide feeding protocol [29]. Using this method, we were able to rescue individual peptides in *flp-3* mutant animals without the need for transgenics and showed that a specific subset of FLP-3 peptides responsible for suppressing the avoidance differs from those responsible for driving male attraction to ascr#8. Interestingly, we were able to elucidate that not all of the peptides encoded by the pro-peptide are involved in the functional circuit [1].

To our knowledge, this study is the first instance in which individual neuropeptides encoded by a single gene have been found to: (1) have *specific* biological activity, (2) bind

multiple receptors, and (3) drive the behavioral valence to a cue in (4) a sex-specific manner. Given the complexity of the *flp-3* gene (which encodes 10 unique peptides) [30], and its expression in male-specific neurons, this gene serves as a powerful platform for future studies investigating sex-specific neuronal regulation.

Results

Spot Retention Assay vs. Single Worm Assay

In order to determine the attractiveness of 1 μM ascr#8 (**Figure *23*, inset**) in multiple strains of *C. elegans*, the historical Spot Retention Assay (SRA) was utilized (**Supplementary Figure 1A**) [10,19,31]. The average dwell time of both males and hermaphrodites in either 1 μM ascr#8 or a vehicle control (dH_2O) was calculated over 20-minute assay intervals (**Supplementary Figure 1B-E**). Male *C. elegans* exhibited a significant increase in the amount of time spent in ascr#8 over the vehicle control, as shown in previous studies [10].

The male specific cephalic sensory CEM neurons are required for ascr#8 sensation [10]. To test whether sensory cilia are required for mediating attractive responses to this chemical, we tested mutants that have defective cilia formation. The *osm-3* gene encodes a kinesin protein required in the proper development of chemosensory cilia and thereby chemosensory behaviors [32]. In the SRA, *osm-3;him-5* animals did not exhibit the increase in ascr#8 dwell time observed in wild type animals, instead showing no difference in dwell time compared to the vehicle, and a significant defect compared to him-5 dwell time (**Supplementary Figure 1B, C**). Hermaphrodites did not exhibit this same trend, instead exhibiting no observed difference in dwell time between vehicle and ascr#8 in any strain (**Supplementary Figure 1D, E**). In the N2 strain, there is a decrease in the amount of times spent in ascr#8, which while statistically significant, is not replicated across any other strain (**Supplementary Figure 1D, E**).

While the SRA allows for worm attraction to be measured, it does so with a large amount of room for variability in the results obtained. Given that ascarosides are not volatile compounds, *C. elegans* are unable to sense the cue until they contact the cue. With nothing driving them to the location of the cue – other than diffusion of the compound through the agar over time – the worms do not always visit the vehicle control or the male-attracting ascaroside, ascr#8. This cue has been shown to function as a male attractant, and slight hermaphrodite repellant [19]. In the experiments testing these compounds, many males will be in contact with the ascaroside at the same time (**Supplementary Video 1**). This can skew the dwell time values, as: 1) it becomes impossible to track individual worms and determine the correct order of departure from the cue, and 2) raises the concern that it is instead male-male contact that is driving the perceived "attractive response" to the ascaroside.

To circumvent these issues, we have developed a novel behavioral assay which we have called the single worm assay (SWA) (**Figure 23A**), which tests the response of *C. elegans* to ascarosides on a per-worm basis (see ***Materials and Methods*** section for a more detailed description of the assay). By placing a single animal per well directly in the cue, the SWA forces contact with the cue and removes any potential of male-male contact. The results of this assay show that males are indeed attracted to the cue itself, and not the male-male contact, while also showing that it is a minority of the animals (30%-45%) that exhibit attractive visits to the cue (**Supplementary Figure 2B**). These results are also able to shed light on discrepancies seen between the SRA results, which imply consistent attractive responses, and calcium imaging experiments, with only 30-40% of the CEM neurons exhibiting calcium transients, now corroborate them [10,33].

Within the SWA, male *C. elegans* again exhibited a significant increase in the amount of time spent within ascr#8 compared to the vehicle control (**Figure 23B,C**), in all strains tested. Normalized increased in dwell time, calculated as log(fold-change) [i.e., ascaroside dwell time over vehicle dwell time], allow for comparison across strains and

conditions while accounting for baseline variability in vehicle dwell times. Using this log(fold-change) metric, we can see that that increase in attraction to ascr#8 is consistent across all "wild-type" strains: N2, *him-5*, and *him-8* (**Figure 23C**).

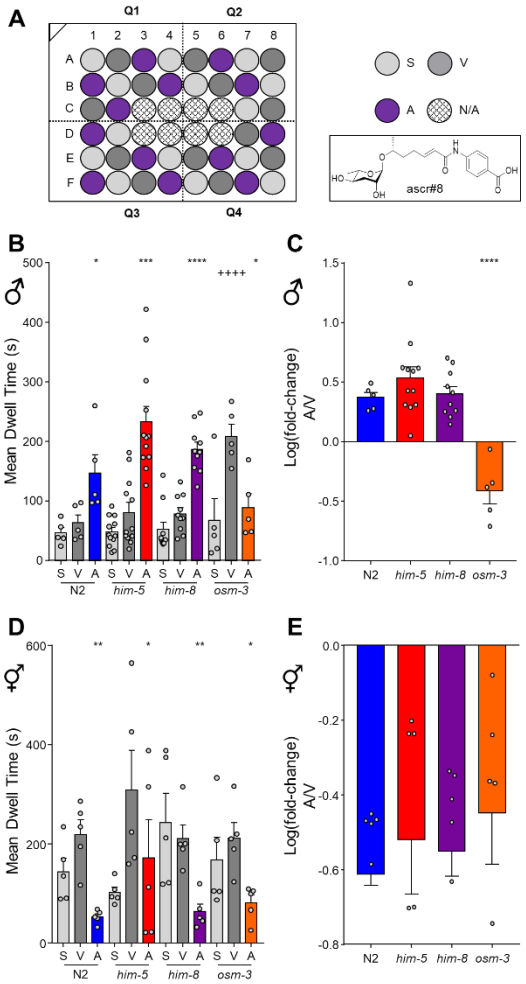

Figure 23. Attraction to ascr#8 is Sex-Specific.
(A) The Single Worm Assay (SWA). The outer 40 wells of a 48-well suspension cell culture plate are seeded with NGM agar and a thin lawn of OP50 *E. coli*. A random block design results in spatial control (light grey), vehicle control (dark grey), and ascaroside (purple) containing wells. Quadrants are recorded for 15 minutes. **(Inset)** The structure of ascr#8. **(B)** Raw dwell times of males of control lines in SWA. The wild-type strains spend more time in ascr#8 than the vehicle control, while *osm-3;him-5* animals are defective in response to both vehicle and ascr#8. **(C)** Transformed log(fold-change) of male dwell time data. Wild-type strains are similar, while *osm-3;him-5* worms exhibit aberrant attraction. **(D)** Raw dwell time and **(E)** log(fold-change) of hermaphrodites shows no difference across strains. Light grey denotes spatial controls (when applicable), dark grey denotes vehicle controls, colors denote ascr#8 values (N2, blue; *him-5*, red; *him-8*, purple; *osm-3;him-5*, orange). **(B, D)** RM-ANOVA comparing vehicle to both spatial control and ascr#8 values, followed by Bonferroni Correction. **(C, E)** One-Way ANOVA followed by Dunnett's Correction. Error bars denote SEM. $n \geq 5$. * $p < 0.05$, ** $p < 0.01$, *** $p < 0.001$, **** $p < 0.0001$. ++++ $p < 0.0001$, vehicle vs. spatial control.

This assay also allows us to determine the number of visits per worm (**Supplementary Figure 2A,C**), as well as the percentage of attractive visits to the cue, and we found that there was no difference between any control strains (**Supplementary Figure 2B**). While *osm-3;him-5* males again exhibited a defect in their response to ascr#8, this result was not as expected. Instead of simply not responding to ascr#8, as seen in our SRA data (**Supplementary Figure 2B, C**), these males exhibited a significant *decrease* in the amount of time spent in ascr#8 compared to the vehicle, although they exhibited no difference in their dwell times in ascr#8 (A) and spatial control (S) (**Figure 23B**), suggesting a defect in the response the vehicle itself. Further supporting the hypothesis that the behavioral change in *osm-3* mutants was not due to a change in ascr#8 response, there was no difference in the number of times the animals visited either cue (**Supplementary Figure 2A**), nor in the percent of attractive visits to either vehicle or ascr#8, as would be expected in a chemosensory defective mutant (**Supplementary Figure 2B**).

Unlike the SRA, wherein hermaphrodites did not exhibit any difference in dwell time between vehicle and ascr#8 (**Supplementary Figure 1D,E**), the SWA revealed that hermaphrodites from all strains consistently spent significantly less time in ascr#8 than the vehicle, with no difference between the spatial and vehicle control dwell times (**Figure 23D,E**). Hermaphrodites also visited the ascaroside cue less than they did vehicle or spatial control well centers and exhibited little to no attractive visits **Supplementary Figure 2C,D**).

Together, these data validated the SWA as a robust assay to measure the attractiveness of a cue on a single animal basis in both sexes. It also provides data on visit count and the percent of attractive visits that was previously impossible utilizing the SRA. Interestingly, attractive visits were only observed 30%-45% of the time (**Supplementary Figure 2B**), suggesting that the individual physiological state of the animal plays a critical role in determining the behavioral response to the ascaroside, as seen in other ascaroside behavioral responses [34-36].

Peptidergic Signaling Contributes to Proper ascr#8 Response

The SWA revealed that individual males are only attracted in 30%-45% of their visits to ascr#8 (**Supplementary Figure 2B**). In order to understand why an attractive concentration of a mating pheromone does not result in consistent attraction (**Supplementary Figure 2B**), we sought to investigate potential peptidergic signaling pathways that function in the sensation of ascr#8.

Several neuropeptides of the FMRFamide-like-peptide (FLP) family have been implicated in the mechanosensory regulation of male-mating behavior [37]. The genes encoding the neuropeptides *flp-8*, *flp-10*, *flp-12*, and *flp-20* all suppress the number of turns around a hermaphrodite executed by a male prior to mating [37]. Despite this enrichment of *flp* genes functioning in the mechanosensation of these male specific behaviors [37], there has been no neuropeptide found to regulate the chemosensation of mating ascarosides.

We therefore focused our initial screening of neuropeptides on the FLPs, excluding INS and NLP peptides. We generated *him-8* lines of *flp* genes expressed in male-specific neurons, specifically *flp-3*, *flp-6*, *flp-12*, and *flp-19* [26]. In order to avoid confounding variables, our criteria for selection stipulated that outside of male-specific neurons, expression profiles would be limited to a small number of neurons (*flp-5* was therefore excluded as it exhibits expression in the pharyngeal muscle; while *flp-21* and *flp-22* are expressed in a large number of neurons outside of the male-specific expression profiles).

We found that loss of *flp-3* strongly affected the ability of male *C. elegans* to respond to ascr#8, (**Figure 24A,B, Supplementary Figure 3A,B**). The log(fold-change) of *flp-3* was the only value significantly different than that seen in the wild-type (**Figure 24B**). Interestingly, there was no defect seen in *flp-3* hermaphrodites, nor in any other strain (**Figure 24D,E, Supplementary Figure 3C,D**).

Because the defect in male response to ascr#8 was so significant, and the SWA was designed to detect attractive behaviors, we sought to determine if *flp-3* loss-of-function (*lof*) animals were in fact avoiding ascr#8. Using a previously described drop avoidance

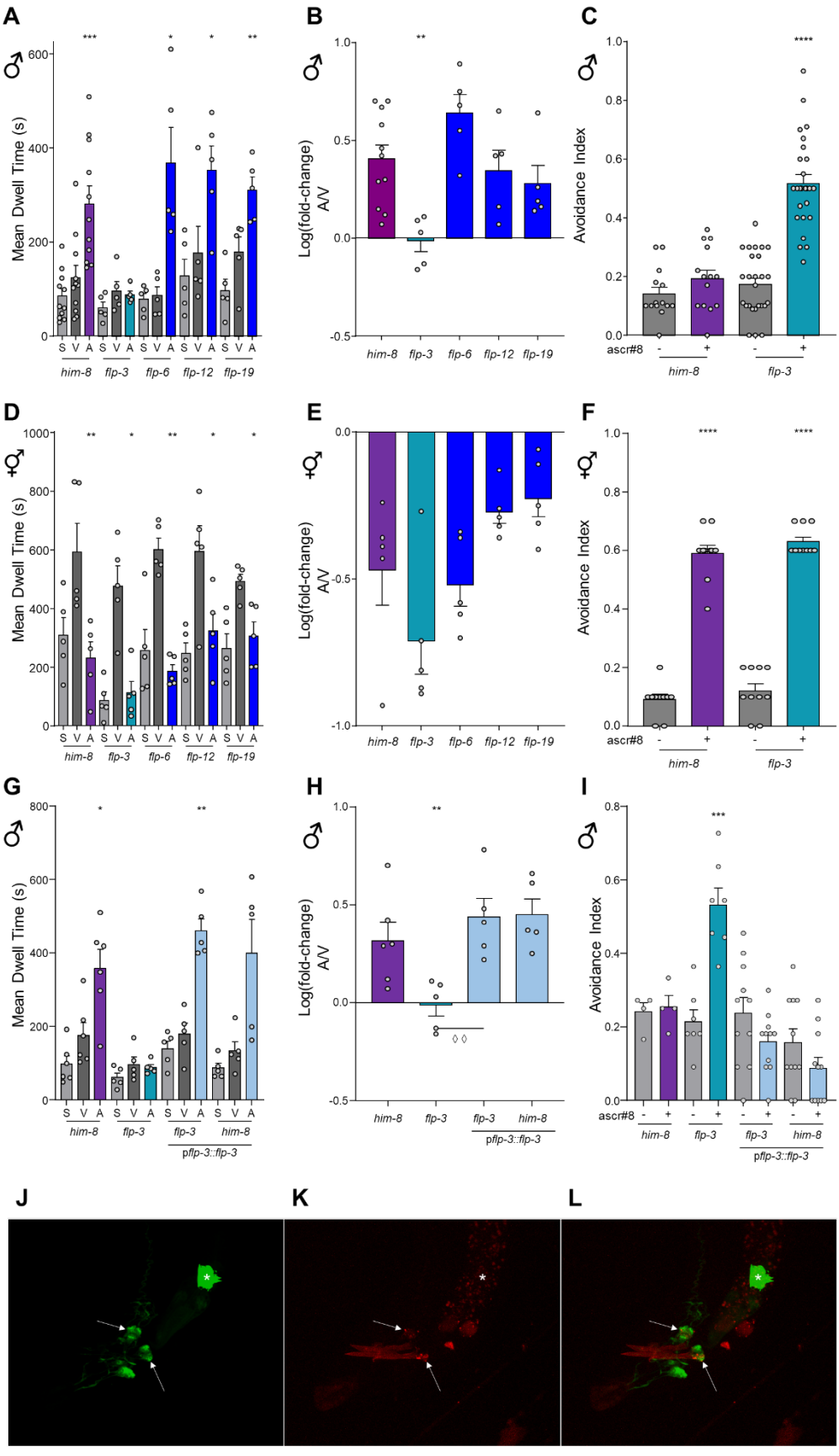
A
B
C
D
E
F
G
H
I
J
K
L
Mean Dwell Time (s)
Log(fold-change) A/V
Avoidance Index
S V A
him-8
flp-3
flp-6
flp-12
flp-19
ascr#8
pflp-3::flp-3

Figure 24. Peptidergic Regulation of the Male Behavioral Response to ascr#8.
(A, B) A screen of neuropeptide defective mutants revealed that *flp-3* males are not attracted to ascr#8. **(A)** Raw dwell time and **(B)** log(fold-change) values. **(C)** *him-8* males do not avoid ascr#8, although *flp-3* males do. **(D)** Hermaphroditic raw dwell time and **(E)** log(fold-change) values show no defective response to ascr#8. **(F)** both *him-8* and *flp-3* hermaphrodites avoid ascr#8. **(G-I)** Expression of *flp-3* under its endogenous promoter rescues both attractive behavior **(G)** raw dwell times and **(H)** log(fold-change) values, as well as **(I)** the avoidance phenotype. Overexpression does not affect the wild-type behavior. **(J-L)** Expression of *pflp-3*::*flp-3*::mCherry is localized to the male tail, co-localizing with *gpa-1*::GFP in the SPD spicule neurons (arrows). **(J)** GFP, **(K)** mCherry, **(L)** merged image at 63X magnification. **(A, D, G)** RM-ANOVA comparing vehicle to both spatial control and ascr#8 values, followed by Bonferroni Correction. **(B, E, H)** One-Way ANOVA followed by Dunnett's Correction. **(C, F, I)** Paired t-tests of vehicle vs. ascr#8 avoidance indexes. Error bars denote SEM. $n \geq 5$. * $p < 0.05$, ** $p < 0.01$, *** $p < 0.001$, **** $p < 0.0001$.

assay [34,38], we exposed forward moving animals to a drop of either vehicle control or ascr#8 and scored the avoidance index (see ***Materials and Methods***). Wild-type males did not avoid the cue, as expected for an attractive cue, although *flp-3* males strongly avoided the pheromone (**Figure 24C**). Again, the hermaphroditic behavior was unaffected (**Figure 24F**).

Together, these results suggest that *flp-3* functions to drive the attractive behavioral valence to ascr#8 in males. In doing so, the neuropeptide suppresses the non-sex-specific avoidance behavior that is observed in hermaphrodites (**Figure 24F**). Rescue of *flp-3* under a 4kb region of its endogenous promoter was able to restore the behavioral valence of males to wild-type levels (**Figure 2G-I, Supplementary Figure 3E,F**). Given that overexpression of neuropeptides has resulted in dominant negative phenotypes [39-43], we investigated whether that would be the case for *flp-3*. However, we merely found that overexpression of the *flp-3* resulted in normal behavior (**Figure 24G-I, Supplementary Figure 3E,F**).In order to rule out an allele-specific effect of *flp-3(pk361)*, which results in deletion of the entire coding sequence as well as 439 bp of upstream and 1493 bp of downstream genomic sequence [44], we also generated and assayed *him-8* mutants of *flp-3(ok3265)*, an in-frame deletion of the coding sequence that retains expression of two peptides produced by the *flp-3* gene FLP-3-1 (SPLGTMRFamide) and FLP-3-4 (NPLGTMRFamide) [45] (**Supplementary Figure 5A**). The mutant phenotype we observed

in *pk361* was consistent across both alleles (**Supplementary Figure 5B-F**), confirming that the deletion in the *pk361* allele did not cause any off-target effects, and that the peptides FLP-3-1 and FLP-3-4 encoded by the *ok3625* allele were not sufficient to rescue the mutant phenotype.

FLP-3 Functions Specifically to Modulate the ascr#8 Behavioral Response

While ascr#8 is a male-attracting pheromone, it is not the only one [11,17,19]. Previous studies have shown that ascr#2, ascr#3, ascr#4, and ascr#8 function synergistically to attract males [11]. The CEM neurons that are required for ascr#8 sensation also function in ascr#3 sensation [10,11,19]. While ascr#3 signal propagation is processed through the hub-and-spoke circuit centered around RMG [10,17,18,46], little is none about the mechanics of ascr#8 sensation outside of the involved of the CEM neurons [10]. In order to determine if *flp-3* functions to regulate pheromone-mediated male attraction and avoidance in a general manner, or rather one specific to ascr#8, we assayed the response of wild-type and *flp-3 lof* males to ascr#3, a cue for which behavioral valence has also recently been shown to be regulated in a sex-specific manner [17]. We found that *flp-3 lof* males exhibited no defect in their attractive response to ascr#3 (**Supplementary Figure 6**), suggesting that its role is indeed specific to that of ascr#8 sensation.

Expression analysis of a FLP-3 translational fusion (p*flp-3*::*flp-3*::mCherry) confirmed previous expression of the neuropeptide within the male-specific spicule [26,47] (**Figure 24J-L, Supplementary Figure 4A-C**). Transcriptional reporters have shown robust *flp-3* expression in the head IL1 neurons, as well as the phasmid sensory neuron, PQR and the male-specific interneuron, CP9. Our translational fusion exhibited no PQR or CP9 expression (**Figure 24J-L, Supplementary Figure 4A-C**). Previous studies employed 1-2 kb regions of promoter sequence driving GFP expression, while our construct employs a 4 kb region, thereby incorporating further regulatory elements that may restrict

expression patterns. By including the full coding sequence in our translational fusion, we have also incorporated the regulatory elements found within the introns of the gene [48].

Interestingly, we observed localization of mCherry within sensory cilia of the dorsal and ventral IL1 neurons, as well as in puncta spanning their dendrites (**Supplementary Figure 4D-F**), consistent with peptide packing into dense core vesicles [49]. Recent single-cell RNA-sequencing of the adult nervous system has again found more prolific expression of *flp-3* within the nervous system including most of the VC neurons [50]. However, these studies were performed only in hermaphrodites, and were therefore unable to examine any male-specific expression changes. Still, a *flp-3* construct which exhibits spicule- and IL1D/V-specific expression completely rescued wild-type behavior (**Figure 24G-I, Supplementary Figure 3E, F**).

Because the spicule neurons are exposed to the environment, we wanted to see if they played a direct role in the sensation of ascr#8. To test this, we assayed *ceh-30 lof* males for their ability to avoid ascr#8. Male *ceh-30 lof* animals lack the male-specific CEM neurons responsible for ascr#8 sensation in the head region of the animal [10,51]. *him-5* males did not avoid ascr#8 (**Supplementary Figure 7**), supporting the lack of *him-8* male avoidance (**Figure 24C**). Males lacking their CEM neurons also did not avoid ascr#8 **Supplementary Figure 7**). However, with *flp-3* still present in these animals, it may be that they are still able to sense the cue, but do not avoid it due to the presence of the neuropeptide. We therefore generated a *ceh-30;flp-3* double mutant, and found that these animals still do not avoid the pheromone (**Supplementary Figure 7**), confirming that the CEM neurons are the sole source of ascr#8 chemosensation in male *C. elegans* [10].

FLP-3 Regulates Attractive Behavior to ascr#8 by Activation of Two G Protein-Coupled Receptors

The *flp-3* gene encodes multiple peptides [1]. Recent studies have uncovered a tenth peptide encoded by the gene; although this peptide does not contain the conserved RFamide

motif found in the remainder of *flp-3* peptides (**Figure 25A**) [30]. We determined that the lysine-arginine sites flanking the individual peptides are processed specifically by the proprotein convertase encoded by the *egl-3* gene, and not by *aex-5* or *bli-4* [37,52,53] (**Supplementary Figure 8**), similar to this enzyme being the sole required enzyme in the physical act of mating [37].

To better understand where the fully processed peptides act within the male-specific circuit, we tested known FLP-3 peptide receptor mutants for their ability to respond properly to ascr#8. While activation of NPR-4 has been reported for two peptides encoded by *flp-3*, NPR-5 and NPR-10 have been shown to respond to four and six peptides, respectively (**Figure 25A**) [1]. Testing *him-8*-crossed lines of these mutants using our SWA, we found that *npr-4* and *npr-5* males respond similarly to *him-8* males (**Figure 25B-D**). However, *npr-10 lof* animals exhibited a complete loss of attraction to the cue, as well as a partial avoidance phenotype matching that of *flp-3* (**Figure 25B-D, Supplementary Figure 9**).

Transgenic rescue by an NPR-10::GFP translation fusion construct expressed under 1.6 kb of the endogenous promoter [54] was able to restore wild-type levels of attraction in an *npr-10 lof* mutant background (**Figure 25C**). This construct was also able to suppress the

avoidance phenotype of *npr-10* (**Figure 25D, Supplementary Figure 9C**). Expression analysis of NPR-10::GFP revealed expression in both head and tail regions of the animals (**Figure 25E-F**). Among these head neurons is the command interneuron, AVF (**Figure 25, arrowhead**), which contributes to the reversal locomotory circuit.

Using Chinese hamster ovarian (CHO) cell cultures stably expressing the promiscuous Gα16 subunit and the calcium reporter, aequorin [55], we found that both isoforms of NPR-10 are in fact activated by seven of the ten FLP-3 peptides (**Supplementary Figure 10A,B)**, with half-maximal effective concentrations (EC_{50}) in the nM range (**Figure 26**). Peptide FLP-3-6 (EDGNAPFGTMKFamide) did not activate NPR-

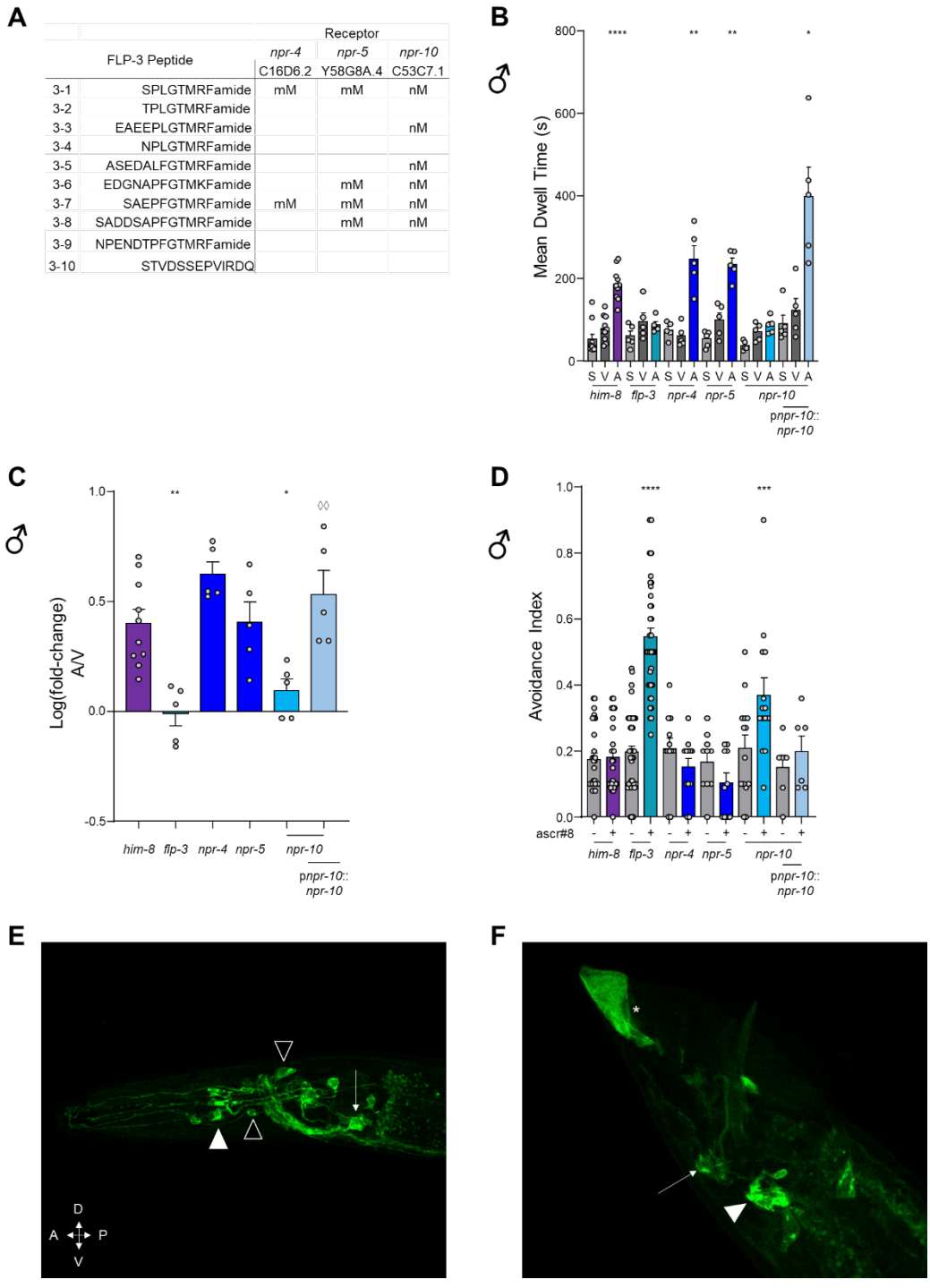

Figure 25. The G Protein-Coupled Receptor, NPR-10, is Required for Male Behavioral Response to ascr#8.

(A) Previously identified FLP-3 peptide affinities for known receptors. NPR-4 and NPR-5 exhibit millimolar affinities for some peptides, while NPR-10 has nanomolar affinities for the majority of the FLP-3 peptides. Adapted from Li and Kim, 2014 [1]. **(B)** Raw dwell time and **(C)** log(fold-change) values for *npr* receptor mutants and *npr-10* rescue in the SWA. **(D)** Avoidance indexes of *npr* receptor mutants and rescue. **(B)** RM-ANOVA comparing vehicle to both spatial control and ascr#8 values, followed by Bonferroni Correction. **(C)** One-Way ANOVA followed by Dunnett's Correction. **(D)** Paired t-tests of vehicle vs. ascr#8 avoidance

indexes. Error bars denote SEM. $n \geq 5$. * $p < 0.05$, ** $p < 0.01$, *** $p < 0.001$, **** $p < 0.0001$. **(E)** Localization of p*npr-10*::*npr-10*::GFP in the amphid region of the male head. Localization includes a set of inner labial (IL) neurons (arrowhead), the male specific CEM neurons (open arrowhead), and the command interneuron, AVF (arrow). **(F)** Expression of p*npr-10*::*npr-10*::GFP in the mail tail. Localization is observed in a ray neuron (arrow), as well as a posterior ganglia (arrowhead).

10 in our assay. This peptide contains an R-to-K mutation within the C-terminal motif which may explain the lack of receptor activation. Likewise, peptide FLP-3-10 (STVDSSEPVIRDQ), which contains no sequence homology with any RFamide peptide (**Figure 26I**) also failed to activate the receptor. Interestingly, FLP-3-8 (SADDSAPFGTMRFamide) did not activate either NPR-10A or NPR-10B, despite its conserved terminal amino acid sequence.

The lack of full avoidance phenotype observed in *npr-10 lof* mutants suggests that there are other *flp-3* receptors involved in regulating the ascr#8 avoidance behavior [56]. The neuropeptide receptor FRPR-16 was found to be reliably activated by FLP-3 peptides *in vitro* (**Supplementary Figure 10C**), exhibiting higher potencies to FLP-3 peptides than either NPR-10 isoform. Potencies were in the 10-nanomolar range for seven of the FLP-3 peptides, and sub-micromolar for an eighth peptide (**Figure 26**). Again, FLP-3-6 and FLP-3-10 did not activate FRPR-16, supporting the notion that the terminal motif conserved in the remaining FLP-3 peptides is critical for receptor activation. Cells transfected with a control vector did not exhibit any activation following exposure to FLP-3 peptides, confirming that the activation observed is specific to receptor-ligand interactions with NPR-10 and FRPR-16 (**Supplementary Figure 10D**).

A full-gene deletion of *frpr-16* was generated using CRISPR mutagenesis [57]. Following incorporation of the *him-8* locus into homozygous *frpr-16 lof* animals, we assayed males for their ability to respond to ascr#8. Males lacking *frpr-16* exhibited a loss of attraction to the cue, as well as a partial avoidance phenotype, like that observed in *npr-10* mutant animals (**Figure 27, Supplementary Figure 11A,B**). However, a double mutant containing both *npr-10* and *frpr-16* null alleles did not result in an additive effect in the

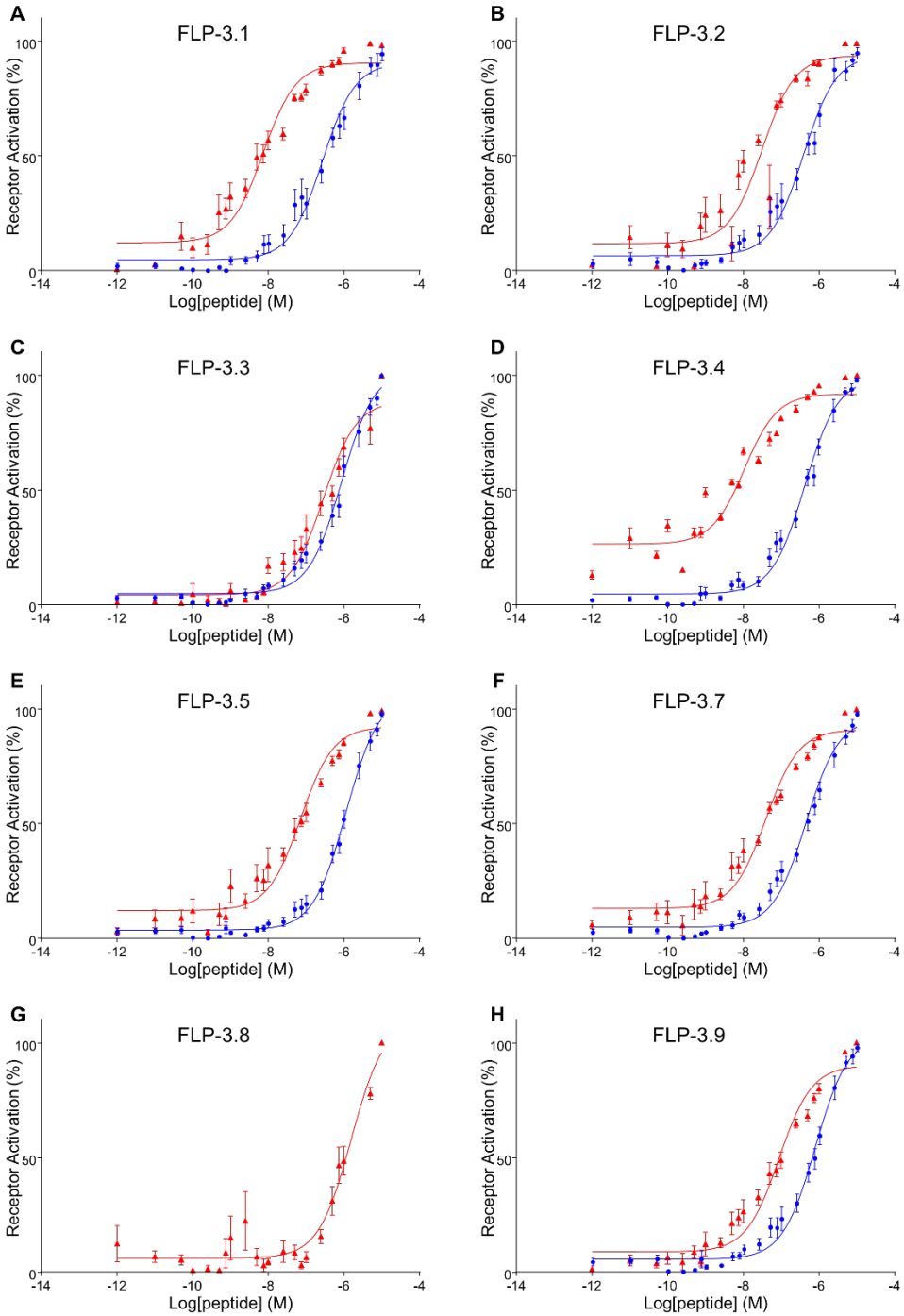

I

	FLP-3 Peptide	NPR-10 EC_{50}	NPR-10 95% CI	FRPR-16 EC_{50}	FRPR-16 95% CI
3-1	SPLGTMRFamide	262.1 nM	189.7 nM to 359.8 nM	7.4 nM	5.2 nM to 10.6 nM
3-2	TPLGTMRFamide	366.5 nM	270.4 nM to 491.3 nM	31.7 nM	19.0 nM to 51.2 nM
3-3	EAEEPLGTMRFamide	866.7 nM	706.6 nM to 1.1 µM	288.3 nM	203.7 nM to 402.3 nM
3-4	NPLGTMRFamide	427.1 nM	351.7 nM to 516.3 nM	10.7 nM	7.6 nM to 15.3 nM
3-5	ASEDALFGTMRFamide	1.1 µM	946.2 nM to 1.4 µM	72.1 nM	51.1 nM to 101.3 nM
3-7	SAEPFGTMRFamide	438.6 nM	351.3 nM to 530.1 nM	39.5 nM	28.5 nM to 54.0 nM
3-8	SADDSAPFGTMRFamide	N/A	N/A	1.6 µM	1.1 µM to 2.4 µM
3-9	NPENDTPFGTMRFamide	760.1 nM	624.1 nM to 923.3 nM	88.3 nM	65.2 nM to 119.6 nM

Figure 26. FLP-3 Peptides Activate G Protein-Coupled Receptors NPR-10 and FRPR-16 *in vitro*.
Dose response curves of **(A)** FLP-3-1, **(B)** FLP-3-2, **(C)** FLP-3-3, **(D)** FLP-3-4, **(E)** FLP-3-5, **(F)** FLP-3-7, **(G)**

FLP-3-8, (**H**) and FLP-3-9 for activation of NPR-10B (blue circles) and FRPR-16 (red triangles). Peptides FLP-3-6 and FLP-3-10 did not activate either receptor. **(I)** EC_{50} values and 95% Confidence Intervals for FLP-3 peptide activating NPR-10B and FRPR-16. (**A-H**) Error bars denoting SEM. $n \geq 6$.

avoidance phenotype, suggesting that these receptors are non-redundant in their functions (**Figure 27C, Supplementary Figure 11C**).

Rescue of FRPR-16 under 1.9 kb of its endogenous promoter was able to rescue wild-type attractive behavior (**Figure 27, Supplementary Figure 11A,B**), as well as suppress the avoidance phenotype (**Figure 27C, Supplementary Figure 11C**). Together, these data show that NPR-10 and FRPR-16 function as receptors for FLP-3 peptides and contribute to the proper behavioral response to ascr#8.

Rescue of Individual FLP-3 Peptides by Feeding Reveals a Specific Subset of Peptides Required for Attractive Behavior

In order to identify which FLP-3 peptides are required for male avoidance of ascr#8, we adopted a peptide feeding approach, similar to RNAi feeding, as initially described previously [29]. Using Gateway Cloning technology, we inserted the peptide sequences for FLP-3 peptides. These sequences were flanked by EGL-3 processing sites (MRFGKR was placed upstream, and KRK-STOP was placed immediate downstream (**Figure 28A**)) to allow for proper processing of the rescue peptides (**Supplementary Figure 8**) [52]. Peptide DNA sequences were eventually placed into the expression vector pDEST527 (a gift from Dominic Esposito (Addgene plasmid # 11518)), which contains a 6x-His tag upstream of the target peptide. *flp-3 lof* animals were grown on lawns of bacteria expressing the rescue peptides, and their progeny were tested by both SWA and avoidance assays (**Figure 28B-D, Supplementary Figure 12**). The *flp-3* mutant phenotype was maintained in in the *ok3625* allele (**Supplementary Figure 5**), suggesting that FLP-3-1 (SPLGTMRFamide) and FLP-3-4 (NPLGTMRFamide) are not involved in suppressing the avoidance behavior. We therefore tested these peptides and found that they indeed did not rescue the avoidance phenotype in *flp-3* mutants (**Figure 28B-D, Supplementary Figure 12**). Not surprisingly, given its lack of consensus sequence and inability to activate either NPR-10 or FRPR-16,

the non-RFamide-like peptide FLP-3-10 (STVDSSEPVIRDQ), was also unable to rescue the avoidance phenotype (**Figure 28B, Supplementary Figure 12A**).

FLP-3-1 and FLP-3-4 differ in sequence only in their N-terminal amino acid. Similarly, a single amino acid change is all that distinguishes them from FLP-3-2 (TPLGTMRFamide), which we then tested for its ability to rescue the *flp-3* phenotype. Surprisingly, this peptide was able to completely abolish the avoidance phenotype observed in *flp-3 lof* animals (**Figure 28B, Supplementary Figure 12A**). However, it was not able to restore the animal's ability to be attracted to ascr#8 (**Figure 28C,D, Supplementary Figure 12C**). The only difference being the presence of a threonine in the ninth position from the C-terminus of the peptide, we hypothesized that this may be the required component to suppress the avoidance behavior. Peptide FLP-3-9 (NPENDTPFGTMRFamide) also contains a threonine in the same location, although the N-terminus is capped with a NPEND sequence and the lysine conserved in FLP-3-1, FLP-

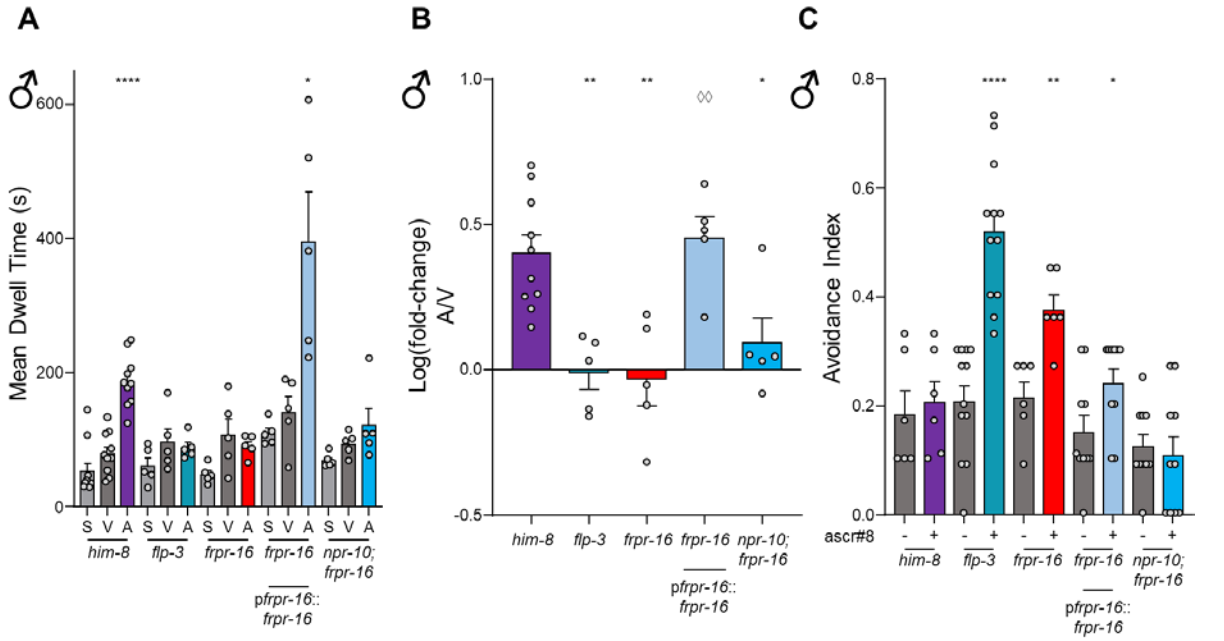

Figure 27. FRPR-16 is Required for Male Behavioral Response to ascr#8.
(A) Raw dwell time and **(B)** log(fold-change) values for *frpr-16 lof* animals, transgenic rescues, and *frpr-16;npr-10* double mutant animals. **(C)** Avoidance indexes of *frpr-16 lof* animals, transgenic rescues, and *frpr-16;npr-10* double mutant animals. **(A)** RM-ANOVA comparing vehicle to both spatial control and ascr#8 values, followed by Bonferroni Correction. **(B)** One-Way ANOVA followed by Dunnett's Correction. **(C)** Paired t-tests of vehicle vs. ascr#8 avoidance indexes. Error bars denote SEM. $n \geq 5$. * $p < 0.05$, ** $p < 0.01$, *** $p < 0.001$, **** $p < 0.0001$. ◊◊, $p < 0.01$ for *frpr-16 lof* mutant versus transgenic rescue.

3-2, and FLP-3-4 is replaced by a phenylalanine. When *flp-3* animals were fed NPENDTPFGTMRFamide, they not only displayed lack of avoidance to ascr#8, but also a full rescue of their ability to be attracted to the cue (**Figure 28, Supplementary Figure 12**).

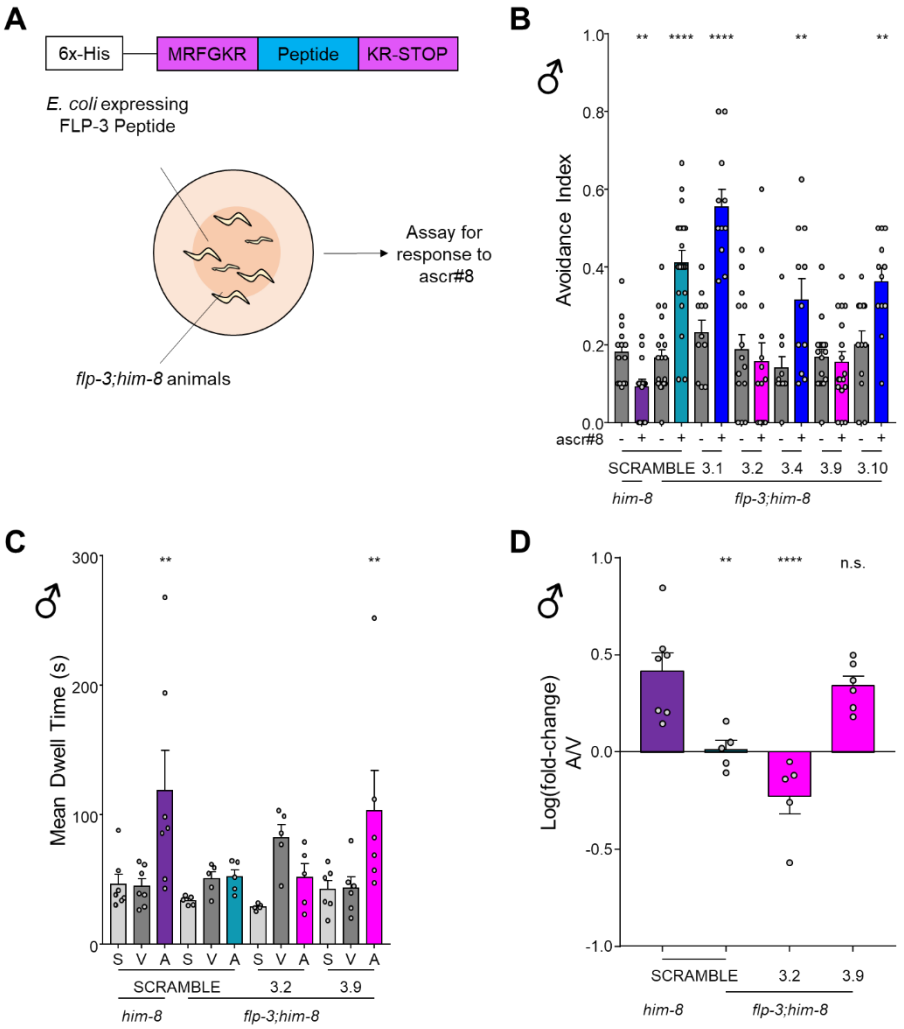

Figure 28. Peptide Feeding Rescues Wild-Type Behavior and Reveals Two Active Peptides Within the FLP-3 Precursor.

(A) Overview of rescue-by-feeding paradigm. Top: the peptide of interest is flanked by EGL-3 cleavage sites, with a 6x-His tag upstream. Bottom: *flp-3 lof* animals are raised on bacteria expressing a FLP-3 peptide of interest and are assayed when young adults. **(B)** Avoidance Indexes of *him-8* and *flp-3* animals raised on SCRAMBLE peptide, FLP-3-1, FLP-3-2, FLP-3-4, FLP-3-9, and FLP-3-10 peptides. FLP-3-2 and FLP-3-9 (pink) are able to suppress the avoidance phenotype. **(C)** Raw dwell time and **(D)** log(fold-change) values for *him-8* and *flp-3* animals raised on SCRAMBLE peptide, FLP-3-2 and FLP-3-9 peptides. Only FLP-3-9 can restore attraction on its own. **(B)** Paired t-tests of vehicle vs. ascr#8 avoidance indexes. **(C)** RM-ANOVA comparing vehicle to both spatial control and ascr#8 values, followed by Bonferroni Correction. **(D)** One-Way ANOVA followed by Dunnett's Correction. Error bars denote SEM. $n \geq 5$. * $p < 0.05$, ** $p < 0.01$, *** $p < 0.001$, **** $p < 0.0001$.

Together, these ***data drive us to pose that the threonine in the ninth position from the C-terminus is critical*** for suppression of the basal avoidance response, as FLP-3-2 and FLP-3-9 are the capable of doing so, while FLP-3-1 and FLP-3-4 are not (**Figure 28, Supplementary Figure 12**). Likewise, the NPEND sequence in FLP-3-9 likely conveys specificity to the peptide to drive attraction to the pheromone, flipping the behavioral valence of the ascr#8 response. Interestingly, however, FLP-3.9 is not the peptide with the highest potency to either NPR-10 or FRPR-16 *in vitro* (**Figure 26**).

Discussion

Our results support the hypothesis that *flp-3* serves, in part, to set the male state of the nervous system required for sensing and responding to asr#8. The physiological state of an animal can determine how an individual may respond to an olfactory cue. For example, starved *C. elegans* will avoid a starvation cue, while animals that have fed recently can choose to ignore that cue [34]. The state of sleep alters the ability of the animals to respond to its environment [58,59]. Responses to pheromones can be regulated by the current physiological state of the animal [18], and neuromodulators help set these states [60,61]. The pheromone ascr#3 serves to elicit similar behavioral outputs as ascr#8; although these responses have been shown to be dependent on the sexual identity of the sensory neuron, ADF [17].

Here, we show that the RFamide-like neuropeptide gene, *flp-3*, helps set a male behavioral state to drive attraction to the male attracting pheromone, ascr#8 [10,19] (**Figure 24**). Hermaphrodites avoid the pheromone, regardless of the presence of *flp-3* (**Figure 24F**), while males lacking the neuromodulator "revert" to the hermaphroditic response (**Figure 24C**). In the male, *flp-3* is only expressed in the SPD spicule neurons and head IL1 neurons (**Figure 24, Supplementary Figure 4**), suggesting that it plays a sex-specific role in modulating this behavior.

The *flp-3* gene falls within the remarkably expansive class of RFamide-related peptide (FLP) genes in *C. elegans*, of which there are 31 encoding over 70 unique peptides [44]. FLPs have been identified as regulators of a variety of behavioral and sensory mechanisms, including locomotion [62-65], egg-laying [44,66], gas sensing [67,68], sleep [20-22,69,70], and mating [37,71,72]. Here, we show that *flp-3* plays a role linking these two: the male sensation of ascr#8 to the resulting attractive behavior. However, not every male is attracted to ascr#8 – only 30-45% of males are attracted (**Supplementary Figure 2B**). Interestingly though, this rate of attraction matches well with the rate of CEM chemosensory neuron calcium transient activity upon exposure to mating ascarosides [33].

Neuropeptides can function both synaptically and extrasynaptically [44]. Here, we identify two G protein-coupled receptors for FLP-3 peptides that function in the response to ascr#8: the previously identified NPR-10, and the novel FRPR-16 (**Figure 25, Figure 26, Figure 27**). Both exhibit high potencies for multiple FLP-3 peptides, although our single peptide rescues have shown that FLP-3-2 and FLP-3-9 are required for the wild-type response to ascr#8 (**Figure 28**). Given that FLP-3 is a complex neuropeptide precursor encoding ten unique peptides [30], and is expressed in a sex-specific manner (**Figure 24J-L, Supplementary Figure 4**), it is likely that the remaining peptides function in some other male-specific manner.

Presence of NPR-10 in the AVF neuron suggests that its activation by FLP-3 peptides may suppress reversals upon sensation of ascr#8 (**Figure 25**). Similarly, the receptor seems to be expressed in chemosensory neurons, including the IL1 neurons and the male specific CEM (**Figure 25E**). Coupled with the expression of the receptor in the dorsorectal ganglia (**Figure 25**), NPR-10 may function in both chemosensory processing areas of the male to drive an appropriate sex-specific response to ascr#8. Loss of either the ligand, FLP-3, or the receptor, NPR-10, resulting in avoidance of ascr#8 suggests that within AVF, NPR-10 sensation of FLP-3 may suppress reversals upon pheromone sensation.

We have employed a peptide feeding assay to rescue the individual FLP-3 peptides of interest [29]. Following the design of RNAi feeding protocols, this assay employs IPTG induction of protein expression with the food source of the worm, allowing the nematodes to eat the peptides. A previous study used this method to examine the effect of scorpion venom on *C. elegans* lifespan and fecundity, finding that it increased both [29]. However, scorpion venom is a non-physiologically relevant peptide for *C. elegans* to encounter. We therefore adapted the protocol to feed neuropeptides, which we flanked by endogenous cleavage sites (targeted by the proprotein convertase, EGL-3) (**Figure 28, Supplementary Figure 8, Supplementary Figure 12**).

To our knowledge, this is the first instance in which an endogenous peptide has been fed to *C. elegans* when expressed in the food source. While "feeding" of peptides through soaking is a valid approach, there are many constraints on such approaches, such as the ability to acquire purified peptides [21,41,69,73,74]. Using this new approach, we are able to bypass that need, providing the peptide to the worms directly through their food source.

By combining biochemical receptor activation studies with behavioral feeding assays, we have been able to link individual peptides encoded by a neuropeptide gene to an output through a specific receptor. In the past, the behavioral and physiological outputs have been linked to the entire catalog of peptides encoded by precursor molecules and their receptors through biochemical studies and full transgenic rescue [21,69,75]. Future studies can now combine these biochemical approaches with behavioral or developmental assays to link peptide activities to their functions.

In summary, we have shown that the neuropeptide gene, *flp-3*, expressed in neurons of both the male head and tail, and that specific peptides activate the receptors NPR-10 and FRPR-16 to both suppress an avoidance response and drive an attractive response (**Figure 29A-C**). Interestingly, the entirety of the gene is not required to recapitulate wild-type behavior, leading to the question: what is the rest of the *flp-3* gene doing? Mutants containing lesions in *flp-3* have been found to exhibit changes in locomotion, body shape,

foraging, and the rate of pharyngeal action potentials[45,76]. Using our peptide feeding paradigm, the individual peptides that affect these phenotypes can be rapidly elucidated.

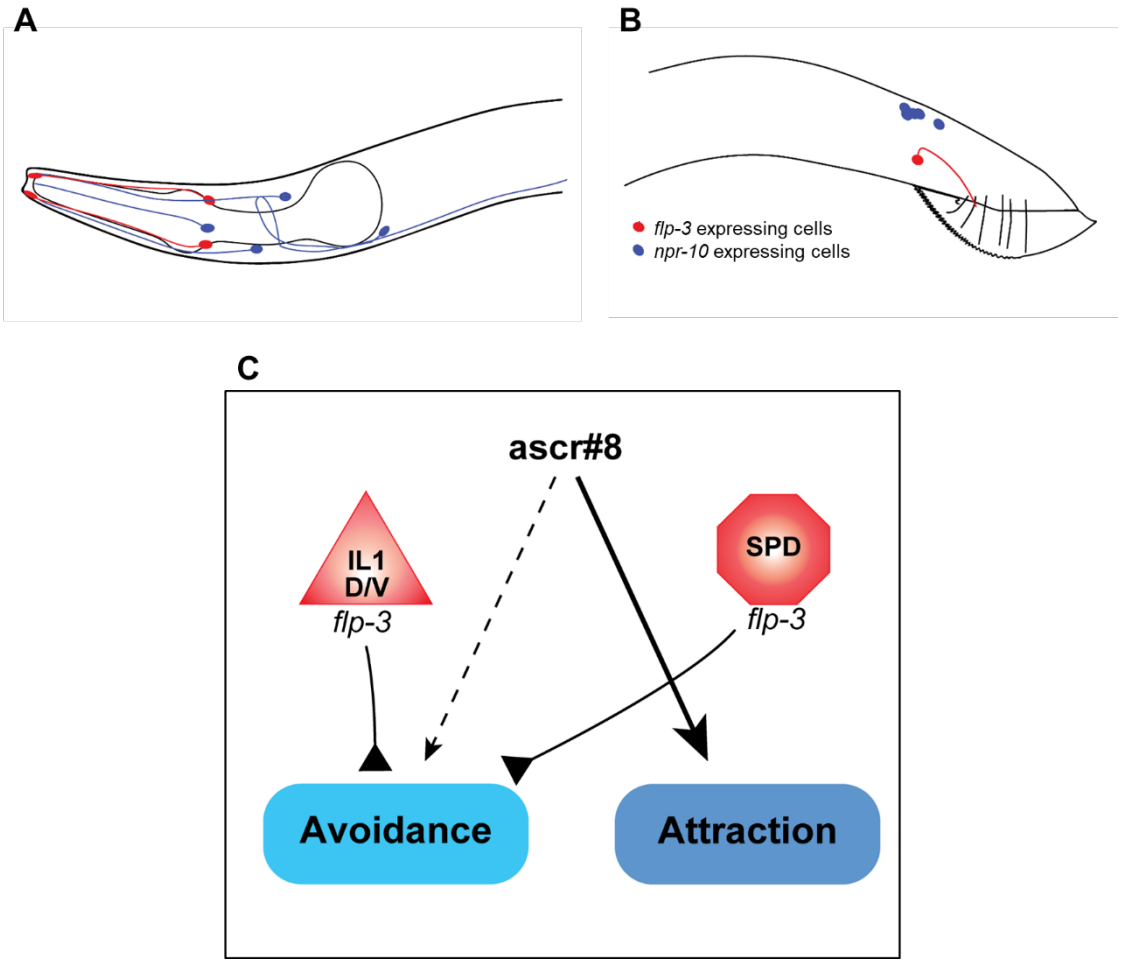

Figure 29. The Role of FLP-3 in Mediating the Male Behavioral Response to ascr#8.
(A) The CEM neurons in the male head sense ascr#8. NPR-10 expressing cells (CEM, AVF, and IL1D/L/V) sense *flp-3* released from IL1D/V to suppress avoidance and drive attractive behaviors. **(B)** In the male tail, the spicule neurons SPD release *flp-3* to mediate the physiological response of Ray 7 and the dorsorectal ganglia to drive similar behavioral responses. **(C)** A model of the *flp-3* ascr#8 circuit. Red bars denote inhibitory signals, while blue arrows denote excitatory pathways.

Materials and Methods

Strains

Strains were obtained from the *Caenorhabditis* Genetics Center (University of Minnesota, MN), the National BioResource Project (Tokyo Women's Medical University, Tokyo, Jagan), Chris Li at City University of New York, Paul Sternberg at the California Institute of Technology, Ding Xue at University of Colorado Boulder, and Maureen Barr at Rutgers University. The novel allele of *frpr-16* was generated via CRISPR editing using previously discussed methods [57]. Strains were crossed with either *him-5* or *him-8* worms to generate stable males prior to testing. See **Supplementary Table 1** for a comprehensive list of strains used in this study.

Vector Generation

Peptide constructs: DNA oligos containing the sequence for the peptides of interest were generated using Integrated DNA Technologies' Ultramer synthesis service. The DNA sequence encoding the peptide sequence was flanked with sequences encoding EGL-3 cut sites (MRFGKR upstream, and KRK-STOP) downstream. These sites were then flanked with Gateway Cloning sites attB1 and attB2. Annealed oligos were then used to perform a BP reaction with pDONR p1-p2 to generate the pENTRY clones. These vectors where then recombined with pDEST-527 (a gift from Dominic Esposito (Addgene plasmid # 11518)) in LR reactions to generate the expression clones. The SCRAMBLE control was generated in an identical manner, with the sequence between the cut sites being amplified from pL4440 (provided by Victor Ambros, University of Massachusetts Medical School, MA).

Fusion constructs: DNA for the *flp-3, npr-10,* and *frpr-16* promoter and coding regions were isolated from *C. elegans* genomic DNA via PCR.

In generating the *flp-3* fusion product, PstI and BamHI restriction sites added onto the isolated fragments were introduced through primer design. PCR amplicons and the Fire

GFP Vector, pPD95.75 (kindly provided by Josh Hawk, Yale University, CT), were digested with PstI and BamHI enzymes. Products were ligated together to generate JSR#DKR18 (p*flp-3*::*flp-3*::GFP).

The promoter-gene fragments of *npr-10* and *frpr-16* were fused to GFP (pPD95.75) or dsRed (isolated from DACR1342; a gift from Dr. Josh Hawk, Yale University), respectively, following the PCR fusion protocol previously described [54]. Prior to the second PCR reaction, fragments were annealed by Gibson Assembly.

See **Supplementary Table 2** for a complete plasmid list, and **Supplementary Table 3** for primer and Ultramer sequences.

Transgenic Animals

CB1489 animals were injected with JSR#DKR18 (p*flp-3*::*flp-3*::GFP at 20 ng/μL), using p*unc-122*::RFP (at 20 ng/μL) (kindly provided by Sreekanth Chalasani at the Salk Institute, CA) as a co-injection marker to generate JSR81 (*him-8*(e1489);worEx17[p*flp-3*::*flp-3*::GFP; p*unc-122*::RFP]). JSR81 was then crossed with JSR99 to generate JSR109 (*flp-3*(pk361);*him-8*(e1489);worEx17[p*flp-3*::*flp-3*::GFP; p*unc-122*::RFP]).

PS2218 animals were injected with JSR#DKR34 (p*flp-3*::*flp-3*::SL2::mCherry at 25 ng/μL), using p*unc-122*::GFP (at 50 ng/μL) as a co-injection marker to generate JSR119 (*dpy-20*(e1362);*him-5*(e1490);syls33[HS.C3(50ng/uL) + pMH86(11ng/uL)];worEx21[*pflp-3*::*flp-3*::SL2::mCherry; *punc-122*::GFP]).

JSR102 animals were injected with a linear fusion product (p*npr-10*::*npr-10*::GFP at 25 ng/μL), alongside p*unc-122*::RFP (at 50 ng/μL) as a co-injection marker to generate JSR126 (*npr-10*(tm8982);*him-8*(e1489);worEx22[p*npr-10*::*npr-10*::GFP, p*unc-122*::RFP]). JSR103 animals were injected with a linear fusion product (p*frpr-16*::*frpr-16*::dsRed at 25 ng/μL), alongside p*unc-122*::GFP (at 50 ng/μL) as a co-injection marker to generate JSR111 (*frpr-16*(gk5305[loxP + p*myo-2*::GFP::*unc-54* 3' UTR + p*rps-27*::neoR::*unc-54* 3' UTR + loxP]);*him-8*(e1489);worEx23[p*frpr-16*::*frpr-16*::dsRed, p*unc-122*::GFP]).

Injections for JSR119, JSR126, and JSR111 were performed by NemaMetrix.

Chemical Compounds

The ascarosides ascr#3 and ascr#8 were synthesized as described previously [11,19]. Peptides used in *in vitro* GPCR activation assays were synthesized by GL Biochem Ltd.

Spot Retention Assay

Assays were performed as described previously [10,11]. 50-60 larval-stage 4 (L4) males were segregated by sex and stored at 20 °C for 5 hours to overnight to be assayed as young adults. For hermaphrodite trials, young adult hermaphrodites were segregated 1.5 hours prior to testing. 0.6 μL of vehicle control or ascaroside #8 was placed in each scoring region (**Supplementary Figure 1A**). As the working stock of ascaroside #8 was made in MilliQ-purified ultrapure H_2O, this was used as the vehicle control. Five animals were placed on each "X" the assay plate (**Supplementary Figure 1A**), which was then transferred to a microscope containing a camera and recorded for 20 minutes. Each strain and sex were assayed over five plates per day on at least three different days.

Single Worm Assay

The outer forty wells of a 48-well suspension culture plate (Olympus Plastics, Cat #: 25-103) were seeded with 200 μL of standard NGM agar [77]. In order to prepare the plates for the assay, they were acclimated to room temperature, at which point each well was seeded with 65 μL of OP50 *E. coli*. The assay plates were then transferred to a 37 °C incubator with the lid tilted for 4 hours to allow the bacterial culture to dry on the agar. Once the bacterial culture dried, the lid was replaced the plate was stored at 20 °C until used in the assay. 50-60 L4 worms were segregated by sex and stored at 20 °C for 5 hours to overnight to be assayed as young adults. 0.8 μL of either vehicle control or ascaroside #8 was placed in the center of the well corresponding to that condition within the quadrant being tested, following a random block design (**Figure 23A**). A single worm was placed in each of the 10 wells to be assayed, and the plate was transferred to a light

source and camera and recorded for 15 minutes. This process was repeated for all four quadrants. Each strain and sex were assayed over five plates assayed on at least three different days.

Raw Dwell Time

Raw dwell time values were calculated by subtracting the time a worm exited the cue (center of the well in spatial controls), from the time it entered, as in the SRA [10]. This was determined per visit, and the average dwell time was calculated for each animal in the quadrant. Averages of the four-quadrant means were determined per plate, and a minimum of five plates were assayed per strain/condition. The mean raw dwell time across five plates was calculated and used for statistical analyses and graphical display.

Log(fold-change)

The average dwell time in the ascaroside was divided by the average dwell time within the vehicle control per plate to generate a fold-change. To transform the data, the log of this fold-change was taken, and the average log(fold-change) was used for statistical analyses and graphical display.

Visit Count

The number of visits per worm was calculated, and the average visit count determined per quadrant, and per plate. The average visit count across five plates was calculated and used for statistical analyses and graphical display.

Percent Attractive Visits

An "attractive visit" was first determined for each plate as any visit greater than two standard deviations above the mean dwell time within the vehicle control for that plate. Any individual visit meeting this threshold was scored as a "1", and any below was scored a "0". The percent visits per worm that were attractive was determined, and the average of each quadrant taken. The four quadrant values were then averaged to generate

plate averages. The average percent of attractive visits across five plates was calculated and used for statistical analyses and graphical display.

Avoidance Assay

Assays were performed as described previously [4,34,38]. 50-60 L4 worms were segregated by sex and stored at 20 °C for 5 hours to overnight to be assayed as young adults. 1-4 hours prior to the assay, the lids of unseeded plates were tilted to allow any excess moisture to evaporate off the plates. At the time of the assay, 10 or more animals were transferred onto each of the dried, unseeded plates. A drop of either water or 1 μM ascr#8 was placed on the tail of forward moving animals, and their response was scored as either an avoidance response, or no response. The total number of avoidances was divided by the total number of drops to generate an avoidance index for that plate. This was repeated for at least 10 plates over at least three different days.

Statistical Analyses

Spot Retention Assay

Statistical comparisons within each strain were made by Paired t-tests. For comparisons between strains/conditions, the data was transformed as described previously [31,78]. In short, the data was transformed in order to have only non-zero data for the calculation of fold-changes. This was done using a Base 2 Exponentiation (2^n, where n is equal to the dwell time). The log (base 2) of the fold-changes of these transformed values was used to allow for direct comparisons between strains of the same background (i.e., *him-5* and *osm-3;him-5*) using a Student's t-test. *p*-values are defined in respective figure captions, with thresholds set as: * $p < 0.05$, ** $p < 0.01$, *** $p < 0.001$, **** $p < 0.0001$.

Single Worm Assay

Statistical comparisons within each strain/sex (spatial, vehicle, ascaroside) were made by Repeated Measured ANOVA with the significance level set at 0.05, followed by multiple comparisons using Bonferroni correction. For comparisons between strains/sexes, the

spatial control dwell times were compared using a one-way ANOVA followed by a Dunnett's correction to confirm that mutations of interest had no effect on the amount of time animals naturally spent in the center of the well. To directly compare strains, a fold-change was calculated by dividing the ascaroside by vehicle dwell times for each assay. This was then transformed by taking the log (base 10) of the fold-change. Comparisons were then made by One-Way ANOVA followed by multiple comparisons using Dunnett's correction. *p*-values are defined in respective figure captions, with thresholds set as: * $p < 0.05$, ** $p < 0.01$, *** $p < 0.001$, **** $p < 0.0001$.

Avoidance Assay

Statistical comparisons within each strain were made by paired t-test against a significance level set at 0.05. For comparisons between strains/conditions, comparisons were made by One-Way ANOVA, followed by multiple comparisons using Bonferroni correction. *p*-values are defined in respective figure captions, with thresholds set as: * $p < 0.05$, ** $p < 0.01$, *** $p < 0.001$, **** $p < 0.0001$.

In vitro GPCR activation assay

The GPCR activation assay was performed as previously described [75,79]. Briefly, *npr-10* and *frpr-16* cDNAs were cloned into the pcDNA3.1 TOPO expression vector (Thermo Fisher Scientific). A CHO-K1 cell line (PerkinElmer, ES-000-A24) stably expressing apo-aequorin targeted to the mitochondria (mtAEQ) and human Gα16 was transiently transfected with the receptor cDNA construct or the empty pcDNA3.1 vector using Lipofectamine LTX and Plus reagent (Thermo Fisher Scientific). Cells were shifted to 28°C one day later and allowed to incubate for 24 h. On the day of the assay, cells were collected in BSA medium (DMEM/Ham's F12 with 15 mM HEPES, without phenol red, 0.1% BSA) and loaded with 5 mM coelenterazine h (Thermo Fisher Scientific) for 4 h at room temperature. The incubated cells were then added to synthetic peptides dissolved in DMEM/BSA, and luminescence was measured for 30 s at 496 nm using a Mithras LB940

(Berthold Technologies) or MicroBeta LumiJet luminometer (PerkinElmer). After 30 s of readout, 0.1 % triton X-100 was added to lyse the cells, resulting in a maximal calcium response that was measured for 10 s. After initial screening, concentration-response curves were constructed for HPLC-purified FLP-3 peptides by subjecting the transfected cells to each peptide in a concentration range from 1 pM to 10 μM. Cells transfected with an empty vector were used as a negative control. Assays were performed in triplicate on at least two independent days. Concentration-response curves were fitted using Prism v. 7 (nonlinear regression analysis with a sigmoidal concentration-response equation).

Generation of a Null frpr-16 Mutant by CRISPR Mutagenesis

The *frpr-16* CRISPR/Cas9 knockout was provided by the Vancouver node of the International *C. elegans* Consortium. The mutation was generated following previously described techniques [57]. In short, a 1702 bp region containing the coding sequence, 52 bp upstream and 58 bp downstream, was removed from the genome, and replaced with a trackable cassette containing p*myo-2*::GFP and a neomycin resistance gene.

Peptide Rescue

SCRAMBLE control or FLP-3 peptide constructs were grown overnight in LB media containing 50 μg/μL ampicillin at 37 °C and diluted to an OD_{600} of 1.0 prior to seeding on NGM plates containing 50 μg/μL ampicillin and 1 mM IPTG. The 75 μL lawn was left to dry and grow overnight at room temperature before 3 L4 animals were placed on the plates. Males were selected for testing in the same manner as described above but were isolated onto plates also seeded with the same peptide on which they had been reared. Animals were then assayed using either the Avoidance Assay or Single Worm Assay.

Imaging

Animals were mounted on a 5% agar pad with 1 M sodium azide on a microscope slide as described previously [34]. DIC, GFP, and RFP images were acquired at 40x magnification using a Zeiss Apotome microscope.

References

1 Li, C. & Kim, K. Family of FLP Peptides in *Caenorhabditis elegans* and Related Nematodes. *Front Endocrinol (Lausanne)* **5**, 150, doi:10.3389/fendo.2014.00150 (2014).

2 Félix, M.-A., Braendle, C. & Cutter, A. D. A Streamlined System for Species Diagnosis in *Caenorhabditis* (Nematoda: Rhabditidae) with Name Designations for 15 Distinct Biological Species. *PLOS ONE* **9**, e94723, doi:10.1371/journal.pone.0094723 (2014).

3 Butcher, R. A. Decoding chemical communication in nematodes. *Natural product reports* **34**, 472-477, doi:10.1039/c7np00007c (2017).

4 Chute, C. D. & Srinivasan, J. Chemical mating cues in *C. elegans*. *Semin Cell Dev Biol* **33**, 18-24, doi:10.1016/j.semcdb.2014.06.002 (2014).

5 Ludewig, A. H. & Schroeder, F. C. Ascaroside signaling in *C. elegans*. *WormBook*, 1-22, doi:10.1895/wormbook.1.155.1 (2013).

6 Sulston, J. E., Schierenberg, E., White, J. G. & Thomson, J. N. The embryonic cell lineage of the nematode *Caenorhabditis elegans*. *Dev Biol* **100**, doi:10.1016/0012-1606(83)90201-4 (1983).

7 Choe, A. *et al.* Ascaroside Signaling is Widely Conserved Among Nematodes. *Current Biology* **22**, 772-780, doi:10.1016/j.cub.2012.03.024 (2012).

8 Butcher, R. A. Small-molecule pheromones and hormones controlling nematode development. *Nat Chem Biol* **13**, 577-586, doi:10.1038/nchembio.2356d (2017).

9 Reilly, D. K. & Srinivasan, J. *Caenorhabditis elegans* Olfaction. doi:10.1093/acrefore/9780190264086.013.191 (2017).

10 Narayan, A. *et al.* Contrasting responses within a single neuron class enable sex-specific attraction in *Caenorhabditis elegans*. *Proc Natl Acad Sci U S A* **113**, E1392-1401, doi:10.1073/pnas.1600786113 (2016).

11 Srinivasan, J. *et al.* A blend of small molecules regulates both mating and development in *Caenorhabditis elegans*. *Nature* **454**, 1115-1118, doi:10.1038/nature07168 (2008).

12 Srinivasan, J. *et al.* A modular library of small molecule signals regulates social behaviors in *Caenorhabditis elegans*. *PLoS Biol* **10**, e1001237, doi:10.1371/journal.pbio.1001237 (2012).

13 Maynard, C., Cummins, I., Green, J. & Weinkove, D. A bacterial route for folic acid supplementation. *BMC Biol* **16**, 67, doi:10.1186/s12915-018-0534-3 (2018).

14 Virk, B. *et al.* Excessive folate synthesis limits lifespan in the C. elegans: E. coli aging model. *BMC Biol* **10**, 67, doi:10.1186/1741-7007-10-67 (2012).

15 Virk, B. *et al.* Folate Acts in E. coli to Accelerate C. elegans Aging Independently of Bacterial Biosynthesis. *Cell Rep* **14**, 1611-1620, doi:10.1016/j.celrep.2016.01.051 (2016).

16 Aprison, E. Z. & Ruvinsky, I. Counteracting Ascarosides Act through Distinct Neurons to Determine the Sexual Identity of *C. elegans* Pheromones. *Curr Biol* **27**, 2589-2599.e2583, doi:10.1016/j.cub.2017.07.034 (2017).

17 Fagan, K. A. *et al.* A Single-Neuron Chemosensory Switch Determines the Valence of a Sexually Dimorphic Sensory Behavior. *Curr Biol* **28**, 902-914.e905, doi:10.1016/j.cub.2018.02.029 (2018).

18 Jang, H. *et al.* Neuromodulatory state and sex specify alternative behaviors through antagonistic synaptic pathways in *C. elegans*. *Neuron* **75**, 585-592, doi:10.1016/j.neuron.2012.06.034 (2012).

19 Pungaliya, C. *et al.* A shortcut to identifying small molecule signals that regulate behavior and development in *Caenorhabditis elegans*. *Proceedings of the National Academy of Sciences of the United States of America* **106**, 7708-7713, doi:10.1073/pnas.0811918106 (2009).

20 Cianciulli, A. *et al.* Interneurons Regulate Locomotion Quiescence via Cyclic Adenosine Monophosphate Signaling During Stress-Induced Sleep in *Caenorhabditis elegans*. *Genetics* **213**, 267-279, doi:10.1534/genetics.119.302293 (2019).

21 Iannacone, M. J. *et al.* The RFamide receptor DMSR-1 regulates stress-induced sleep in *C. elegans*. *Elife* **6**, doi:10.7554/eLife.19837 (2017).

22 Nath, R. D., Chow, E. S., Wang, H., Schwarz, E. M. & Sternberg, P. W. *C. elegans* Stress-Induced Sleep Emerges from the Collective Action of Multiple Neuropeptides. *Current biology* **26**, 2446-2455, doi:10.1016/j.cub.2016.07.048 (2016).

23 Beets, I. *et al.* Natural Variation in a Dendritic Scaffold Protein Remodels Experience-Dependent Plasticity by Altering Neuropeptide Expression. *Neuron*, S0896-6273(0819)30849-30849, doi:10.1016/j.neuron.2019.10.001 (2019).

24 Hussey, R. *et al.* Oxygen-sensing neurons reciprocally regulate peripheral lipid metabolism via neuropeptide signaling in *Caenorhabditis elegans*. *PLoS genetics* **14**, e1007305-e1007305, doi:10.1371/journal.pgen.1007305 (2018).

25 Ringstad, N. & Horvitz, H. R. FMRFamide neuropeptides and acetylcholine synergistically inhibit egg-laying by *C. elegans*. *Nat Neurosci* **11**, 1168-1176, doi:10.1038/nn.2186 (2008).

26 Kim, K. & Li, C. Expression and regulation of an FMRFamide-related neuropeptide gene family in *Caenorhabditis elegans*. *J Comp Neurol* **475**, 540-550, doi:10.1002/cne.20189 (2004).

27 Fenk, L. A. & de Bono, M. Memory of recent oxygen experience switches pheromone valence in <em>Caenorhabditis elegans</em&gt. *Proceedings of the National Academy of Sciences* **114**, 4195, doi:10.1073/pnas.1618934114 (2017).

28 Rengarajan, S., Yankura, K. A., Guillermin, M. L., Fung, W. & Hallem, E. A. Feeding state sculpts a circuit for sensory valence in <em>Caenorhabditis elegans</em&gt. *Proceedings of the National Academy of Sciences* **116**, 1776, doi:10.1073/pnas.1807454116 (2019).

29 Xu, J. *et al.* Feeding recombinant *E. coli* with GST-mBmKTX fusion protein increases the fecundity and lifespan of *Caenorhabditis elegans*. *Peptides* **89**, 1-8, doi:10.1016/j.peptides.2017.01.003 (2017).

30 Van Bael, S. *et al.* A *Caenorhabditis elegans* Mass Spectrometric Resource for Neuropeptidomics. *Journal of The American Society for Mass Spectrometry*, doi:10.1007/s13361-017-1856-z (2018).

31 Zhang, Y. K., Reilly, D. K., Yu, J., Srinivasan, J. & Schroeder, F. C. Photoaffinity probes for nematode pheromone receptor identification. *Journal of Organic & Biomolecular Chemistry*, 10.1039/c1039ob02099c, doi:10.1039/c9ob02099c (2019).

32 Shakir, M. A., Fukushige, T., Yasuda, H., Miwa, J. & Siddiqui, S. S. *C. elegans osm-3* gene mediating osmotic avoidance behaviour encodes a kinesin-like protein. *Neuroreport* **4**, 891-894 (1993).

33 Reilly, D. K., Lawler, D. E., Albrecht, D. R. & Srinivasan, J. Using an Adapted Microfluidic Olfactory Chip for the Imaging of Neuronal Activity in Response to Pheromones in Male *C. Elegans* Head Neurons. *Journal of Visualized Experiments*, e56026, doi:doi:10.3791/56026 (2017).

34 Chute, C. D. *et al.* Co-option of neurotransmitter signaling for inter-organismal communication in *C. elegans*. *Nat Commun* **10**, 3186, doi:10.1038/s41467-019-11240-7 (2019).

35 Greene, J. S. *et al.* Balancing selection shapes density-dependent foraging behaviour. *Nature* **539**, 254-258, doi:10.1038/nature19848 (2016b).

36 Greene, J. S., Dobosiewicz, M., Butcher, R. A., McGrath, P. T. & Bargmann, C. I. Regulatory changes in two chemoreceptor genes contribute to a *Caenorhabditis elegans* QTL for foraging behavior. *Elife* **5**, doi:10.7554/eLife.21454 (2016a).

37 Liu, T., Kim, K., Li, C. & Barr, M. M. FMRFamide-like neuropeptides and mechanosensory touch receptor neurons regulate male sexual turning behavior in

Caenorhabditis elegans. *J Neurosci* **27**, 7174-7182, doi:10.1523/JNEUROSCI.1405-07.2007 (2007).

38 Hilliard, M. A., Bergamasco, C., Arbucci, S., Plasterk, R. H. A. & Bazzicalupo, P. Worms taste bitter: ASH neurons, QUI-1, GPA-3 and ODR-3 mediate quinine avoidance in *Caenorhabditis elegans*. *The EMBO Journal* **23**, 1101-1111, doi:10.1038/sj.emboj.7600107 (2004).

39 Barrios, A., Ghosh, R., Fang, C., Emmons, S. W. & Barr, M. M. PDF-1 neuropeptide signaling modulates a neural circuit for mate-searching behavior in *C. elegans*. *Nature Neuroscience* **15**, 1675-1684, doi:10.1038/nn.3253 (2012).

40 Brewer, J. C., Olson, A. C., Collins, K. M. & Koelle, M. R. Serotonin and neuropeptides are both released by the HSN command neuron to initiate *Caenorhabditis elegans* egg laying. *PLoS genetics* **15**, e1007896-e1007896, doi:10.1371/journal.pgen.1007896 (2019).

41 Davis, R. E. & Stretton, A. O. The motornervous system of *Ascaris*: electrophysiology and anatomy of the neurons and their control by neuromodulators. *Parasitology* **113 Suppl**, S97-117, doi:10.1017/s0031182000077921 (1996).

42 Kao, G. *et al.* ASNA-1 positively regulates insulin secretion in *C. elegans* and mammalian cells. *Cell* **128**, 577-587, doi:10.1016/j.cell.2006.12.031 (2007).

43 Pierce, S. B. *et al.* Regulation of DAF-2 receptor signaling by human insulin and *ins-1*, a member of the unusually large and diverse *C. elegans* insulin gene family. *Genes & Development* **15**, 672-686, doi:10.1101/gad.867301 (2001).

44 Chang, Y.-J. *et al.* Modulation of Locomotion and Reproduction by FLP Neuropeptides in the Nematode *Caenorhabditis elegans*. *PLoS ONE* **10**, e0135164, doi:10.1371/journal.pone.0135164 (2015).

45 Yemini, E., Jucikas, T., Grundy, L. J., Brown, A. E. X. & Schafer, W. R. A database of *Caenorhabditis elegans* behavioral phenotypes. *Nature Methods* **10**, 877-879, doi:10.1038/nmeth.2560 (2013).

46 Macosko, E. Z. *et al.* A Hub-and-Spoke Circuit Drives Pheromone Attraction and Social Behavior in *C. elegans*. *Nature* **458**, 1171-1175, doi:10.1038/nature07886 (2009).

47 Jiang, L. I. & Sternberg, P. W. An HMG1-like protein facilitates Wnt signaling in *Caenorhabditis elegans*. *Genes Dev* **13**, 877-889 (1999).

48 Puckett Robinson, C., Schwarz, E. M. & Sternberg, P. W. Identification of DVA interneuron regulatory sequences in *Caenorhabditis elegans*. *PLoS One* **8**, e54971, doi:10.1371/journal.pone.0054971 (2013).

49 Laurent, P. *et al.* Genetic dissection of neuropeptide cell biology at high and low activity in a defined sensory neuron. *Proceedings of the National Academy of Sciences* **115**, E6890, doi:10.1073/pnas.1714610115 (2018).

50 Taylor, S. R. *et al.* Expression profiling of the mature *C. elegans* nervous system by single-cell RNA-Sequencing. *bioRxiv*, 737577, doi:10.1101/737577 (2019).

51 Peden, E., Kimberly, E., Gengyo-Ando, K., Mitani, S. & Xue, D. Control of sex-specific apoptosis in *C. elegans* by the BarH homeodomain protein CEH-30 and the transcriptional repressor UNC-37/Groucho. *Genes Dev* **21**, 3195-3207, doi:10.1101/gad.1607807 (2007).

52 Husson, S. J., Clynen, E., Baggerman, G., Janssen, T. & Schoofs, L. Defective processing of neuropeptide precursors in *Caenorhabditis elegans* lacking proprotein convertase 2 (KPC-2/EGL-3): mutant analysis by mass spectrometry. *J Neurochem* **98**, 1999-2012, doi:10.1111/j.1471-4159.2006.04014.x (2006).

53 Thacker, C., Srayko, M. & Rose, A. M. Mutational analysis of *bli-4/kpc-4* reveals critical residues required for proprotein convertase function in *C. elegans*. *Gene* **252**, 15-25, doi:10.1016/s0378-1119(00)00211-0 (2000).

54 Boulin, T., Etchberger, J. F. & Hobert, O. Reporter gene fusions. *WormBook*, 1-23, doi:10.1895/wormbook.1.106.1 (2006).

55 Beets, I., Lindemans, M., Janssen, T. & Verleyen, P. Deorphanizing G protein-coupled receptors by a calcium mobilization assay. *Methods Mol Biol* **789**, 377-391, doi:10.1007/978-1-61779-310-3_25 (2011).

56 Oranth, A. *et al.* Food Sensation Modulates Locomotion by Dopamine and Neuropeptide Signaling in a Distributed Neuronal Network. *Neuron* **100**, 1414-1428.e1410, doi:10.1016/j.neuron.2018.10.024 (2018).

57 Au, V. *et al.* CRISPR/Cas9 Methodology for the Generation of Knockout Deletions in *Caenorhabditis elegans*. *G3 (Bethesda, Md.)* **9**, 135-144, doi:10.1534/g3.118.200778 (2019).

58 Nichols, A. L. A., Eichler, T., Latham, R. & Zimmer, M. A global brain state underlies *C. elegans* sleep behavior. *Science* **356**, doi:10.1126/science.aam6851 (2017).

59 Skora, S., Mende, F. & Zimmer, M. Energy Scarcity Promotes a Brain-wide Sleep State Modulated by Insulin Signaling in *C. elegans*. *Cell Rep* **22**, 953-966, doi:10.1016/j.celrep.2017.12.091 (2018).

60 Flavell, S. W. *et al.* Serotonin and the neuropeptide PDF initiate and extend opposing behavioral states in *C. elegans*. *Cell* **154**, 1023-1035, doi:10.1016/j.cell.2013.08.001 (2013).

61 Waggoner, L. E., Zhou, G. T., Schafer, R. W. & Schafer, W. R. Control of alternative behavioral states by serotonin in *Caenorhabditis elegans*. *Neuron* **21**, 203-214 (1998).

62 Bhardwaj, A., Pandey, P. & Babu, K. Control of Locomotory Behavior of *Caenorhabditis elegans* by the Immunoglobulin Superfamily Protein RIG-3. *Genetics*, genetics.302872.302019, doi:10.1534/genetics.119.302872 (2019).

63 Buntschuh, I. *et al.* FLP-1 neuropeptides modulate sensory and motor circuits in the nematode *Caenorhabditis elegans*. *PLoS One* **13**, e0189320, doi:10.1371/journal.pone.0189320 (2018).

64 Chen, D., Taylor, K. P., Hall, Q. & Kaplan, J. M. The Neuropeptides FLP-2 and PDF-1 Act in Concert To Arouse *Caenorhabditis elegans* Locomotion. *Genetics* **204**, 1151-1159, doi:10.1534/genetics.116.192898 (2016).

65 Cohen, M. *et al.* Coordinated regulation of foraging and metabolism in *C. elegans* by RFamide neuropeptide signaling. *Cell metabolism* **9**, 375-385, doi:10.1016/j.cmet.2009.02.003 (2009).

66 Banerjee, N., Bhattacharya, R., Gorczyca, M., Collins, K. M. & Francis, M. M. Local neuropeptide signaling modulates serotonergic transmission to shape the temporal organization of *C. elegans* egg-laying behavior. *PLoS Genet* **13**, e1006697, doi:10.1371/journal.pgen.1006697 (2017).

67 Guillermin, M. L., Carrillo, M. A. & Hallem, E. A. A Single Set of Interneurons Drives Opposite Behaviors in *C. elegans*. *Curr Biol* **27**, 2630-2639.e2636, doi:10.1016/j.cub.2017.07.023 (2017).

68 Rojo Romanos, T., Petersen, J. G., Riveiro, A. R. & Pocock, R. A novel role for the zinc-finger transcription factor EGL-46 in the differentiation of gas-sensing neurons in *Caenorhabditis elegans*. *Genetics* **199**, 157-163, doi:10.1534/genetics.114.172049 (2015).

69 Nelson, M. D. *et al.* FRPR-4 Is a G-Protein Coupled Neuropeptide Receptor That Regulates Behavioral Quiescence and Posture in *Caenorhabditis elegans*. *PLoS One* **10**, e0142938, doi:10.1371/journal.pone.0142938 (2015).

70 Palamiuc, L. *et al.* A tachykinin-like neuroendocrine signalling axis couples central serotonin action and nutrient sensing with peripheral lipid metabolism. *Nature communications* **8**, 14237-14237, doi:10.1038/ncomms14237 (2017).

71 Chew, Y. L., Grundy, L. J., Brown, A. E. X., Beets, I. & Schafer, W. R. Neuropeptides encoded by *nlp-49* modulate locomotion, arousal and egg-laying behaviours in C*aenorhabditis elegans* via the receptor SEB-3. *Philos Trans R Soc Lond B Biol Sci* **373**, doi:10.1098/rstb.2017.0368 (2018).

72 Zang, K. E., Ho, E. & Ringstad, N. Inhibitory peptidergic modulation of *C. elegans* serotonin neurons is gated by T-type calcium channels. *eLife* **6**, e22771, doi:10.7554/eLife.22771 (2017).

73 Husson, S. J. & Schoofs, L. Altered neuropeptide profile of *Caenorhabditis elegans* lacking the chaperone protein 7B2 as analyzed by mass spectrometry. **581**, 4288-4292 (2007).

74 Rosoff, M. L., Doble, K. E., Price, D. A. & Li, C. The *flp-1* propeptide is processed into multiple, highly similar FMRFamide-like peptides in *Caenorhabditis elegans*. *Peptides* **14**, 331-338, doi:10.1016/0196-9781(93)90049-M (1993).

75 Van Sinay, E. *et al.* Evolutionarily conserved TRH neuropeptide pathway regulates growth in *Caenorhabditis elegans*. *Proc Natl Acad Sci U S A* **114**, E4065-e4074, doi:10.1073/pnas.1617392114 (2017).

76 Rogers, C. M., Franks, C. J., Walker, R. J., Burke, J. F. & Holden-Dye, L. Regulation of the pharynx of Caenorhabditis elegans by 5-HT, octopamine, and FMRFamide-like neuropeptides. *Journal of Neurobiology* **49**, 235-244, doi:10.1002/neu.1078 (2001).

77 Brenner, S. The Genetics of *Caenorhabditis elegans*. *Genetics* **77**, 71-94 (1974).

78 Reilly, D. K., Randle, L. J. & Srinivasan, J. Evolution of hermaphroditism decreases efficacy of Ascaroside#8-mediated mate attraction in *Caenorhabditis* nematodes. *microPublication Biology*, doi:10.17912/micropub.biology.000134 (2019).

79 Peymen, K. *et al.* Myoinhibitory peptide signaling modulates aversive gustatory learning in *Caenorhabditis elegans*. *PLoS Genet* **15**, e1007945, doi:10.1371/journal.pgen.1007945 (2019).

Acknowledgements

We thank the *Caenorhabditis* Genetics Center, which is funded by the NIH Office of Research Infrastructure Programs (P40 OD01044), as well as Dr. Paul Sternberg (CalTech), Dr. Chris Li (CUNY), the National BioResource Project, Dr. Ding Xue (UC Boulder), and Dr. Maureen Barr (Rutgers) for providing strains. We want to thank Dr. Don Moerman (UBC; *C. elegans* Knockout Facility) for providing the *frpr-16* knockout. We thank Nemametrix for generating transgenic animals by injection. We also would like to thank Dr. Victor Ambros (UMass Medical School), Dr. Shreekanth Chalasani (Salk Institute), Dr. Josh Hawk (Yale), and Dr. Dominic Esposito (Addgene) for providing us with the necessary plasmids. Funding for this work was provided under the Research foundation Flanders (FWO) project grant G0C0618N (I.B.), and the National Institutes of Health grant, 1R01DC016058-01 (J.S.).

Competing interests

No competing interests are declared.

Author contributions

D.K.R. performed behavioral assays, contributed to the single worm assay design, performed all molecular biology, performed and designed peptide rescue experiments, performed the statistical analyses, and led manuscript writing and revision. E.J.M., H.T.N., and A.N.R contributed to the behavioral assays and as well as manuscript revisions. E.V. and I.B. performed the GPCR activation assays, as well as contributed to manuscript revisions. M.J.A. contributed to injections of the flp-3 rescue, expression imaging, and manuscript revisions. R.J.G. assisted in the single worm assay design and manuscript revisions. J.S. contributed to the single worm assay design, manuscript writing and revisions, as well as provided the funding for this work.

Chapter 4 Linking Sensation to Behavior

Chapter 4A Ascaroside #8, Neural Imaging, and the Evolution of *C. elegans* GPCRs

Summary

Small molecule signaling is the sole means of nematode communication. The vast majority of these signals are ascarosides – ascarylose based pheromones. The ascaroside ascr#8 functions as a male-attractant and is unique in the inclusion of a *p*-aminobenzoate moiety. The neuronal profile of ascr#8 sensation is also unique in that it varies from animal to animal, making conclusive findings difficult. In this chapter, we develop a male-adapted microfluidic device to aid in these experiments (**Chapter 4B**). We also identify candidate G protein-coupled receptors responsible for the sensation of ascr#8 in the male-specific CEM neurons using single-cell transcriptomic analyses (**Chapter 4C**). The findings in **Chapter 4C** motivate the work presented in the following chapters, wherein we develop a trifunctional probe for identifying ascr#8 receptors (**Chapter 5**) and determine the effects of evolutionary pheromone receptor loss on behavior (**Chapter 6**).

Ascaroside #8

As discussed in **Chapter 2** of this dissertation, *C. elegans* communicate with conspecifics using a class of small-molecule pheromones called ascarosides. Among these is the mating pheromone, ascaroside #8 (ascr#8) (Pungaliya et al., 2009). This ascaroside is unique in that it contains a *p*-aminobenzoate attached to the terminus of the fatty-acid derived side chain. Since the initial discovery of ascr#8, two new ascarosides containing this moiety have been elucidated in *C. elegans* extracts – though they are derivatives of ascr#8 (Artyukhin et al., 2018).

Released by sexually mature hermaphrodites, ascr#8 functions as a male-attracting mating pheromone. Males spend significantly more time in 1 μM ascr#8 compared to a vehicle control (Narayan et al., 2016; Pungaliya et al., 2009). We have previously shown that the male-specific amphid sensory CEM neurons are required and sufficient for the behavioral and physiological responses to ascr#8 (Narayan et al., 2016).

While **Chapter 3** of this dissertation focused on the mechanisms controlling the neuromodulation of the behavioral response to ascr#8, the sensory components remain unknown. In this and subsequent chapter(s), we work towards the identification of CEM sensory machinery responsible for sensation of ascr#8.

Asymmetric Calcium Activity in *C. elegans*

The dynamics of neural activity in response to ascr#8 are unique. While most amphid chemosensory neurons are bilateral in structure (e.g. ASI is present in a left/right pair), they are identical in their function. There are two known pairs of developmentally and functionally asymmetric neurons; the AWC and ASE neurons (Cochella et al., 2014; Pierce-Shimomura, Morse, & Lockery, 1999).

AWC neurons sense the removal of volatile odorants (Chalasani et al., 2007; Chalasani et al., 2010; Cochella et al., 2014), and are present as an -ON/-OFF pair. The AWC^{ON} neurons exhibit a lower basal intracellular calcium concentration, while the AWC^{OFF}

maintains a higher concentration (Alqadah, Hsieh, Xiong, & Chuang, 2016). The AWC^{OFF} "state" being the natural state, the AWC^{ON} "state" is stochastically induced during development – every *C. elegans* has both an AWC^{ON} and AWC^{OFF} neuron, though the location of each on either the left or right side of the animal is random (Cochella et al., 2014).

The asymmetry observed in ASE neurons is conserved, unlike the stochastic AWC asymmetry. The left ASE (ASEL) reliably responds to Na^+, while ASER (right) responds to changes in Cl^- and K^+ (Bargmann, 2006; Pierce-Shimomura et al., 1999). Interestingly, opposite calcium transients are observed in ASEL vs. ASER in respond to changes in salt concentration.

Despite these asymmetries and stochastic natures, these phenomena are conserved from animal to animal. While the AWC^{ON} neuron might be on the left side of one animal, and the right side of another, the role is identical.

This has not been found to be true for the male specific CEM neurons. There are four CEM neurons, as opposed to two, resulting in a radially symmetric neuronal class. The CEM neurons exhibit three responses to ascr#8 (as well as the ascaroside, ascr#3) (Narayan et al., 2016): depolarization, hyperpolarization, and no-response. The distribution of these responses is variable from animal to animal, while the behavioral affect remains the same (Narayan et al., 2016). Due to complexities surrounding nematode retrieval following neuronal imaging, there have been no studies to date in which an animal is imaged, and the same animal then assayed for behavioral activity. Future studies could instead assay the behavior of animals first, and correlate this to the neuronal physiology in following calcium imaging studies on the same animals.

Similarly, the transcription factors controlling CEM development are largely understudied. While some developmental controls are known, such as the transcription factor, *ceh-30* (Peden, Kimberly, Gengyo-Ando, Mitani, & Xue, 2007; Schwartz & Horvitz,

2007), the identities of molecular players controlling variable CEM neurophysiologies remain a mystery.

Male *C. elegans* are smaller than hermaphrodites, resulting in difficulties imaging olfactory neural activity using the canonical "olfactory chip" microfluidic device. To address this issue and others that arise with the presence of four neurons in the CEM class, **Chapter 4B** of this dissertation aims to develop a male-adapted chip for neural imaging of amphid activity in male *C. elegans* (Reilly, Lawler, Albrecht, & Srinivasan, 2017).

Ascaroside Receptor Identification

Aside from general neuronal calcium activity and developmental transcription factors, many components contribute to the chemosensation of ligands in the environment of an animals. To date, there are over 230 structurally elucidated ascarosides and other small-molecule signals ("*C. elegans* Small Molecule Identifier Database (SMID DB),"). However, only a handful of receptors have been linked to sensation of these pheromones (**Table 4**) (Chute et al., 2019; Greene et al., 2016b; Greene, Dobosiewicz, Butcher, McGrath, & Bargmann, 2016a; Kim et al., 2009; McGrath et al., 2011; Park et al., 2012).

Genetic Avenues of Approach in Identifying Ascaroside Receptors

Multiple approaches have been used to elucidate receptors responsible for ascaroside sensation. To date, all identified receptors have been G protein-coupled receptors (GPCRs).

The first identified receptors were responsible for the sensation of the dauer-inducing pheromones: ascr#1, ascr#2, and ascr#3 (Kim et al., 2009). These two receptors, SRBC-64 and SRBC-66, were found to be expressed in the ASK neurons. Following a similar, reverse genetic screen-based approach, our lab has recently shown that the tyraminergic receptor, TYRA-2, has been co-opted into a role as a receptor for the octopamine-derived, osas#9 (Chute et al., 2019).

Using quantitative trace locus analyses, the Bargmann lab has elucidated four GPCRs responsible for ascaroside sensation. First, they uncovered a pair of receptors responsible for the sensation of ascr#5 – SRG-36 and SRG-37, both expressed in the ASI neurons (McGrath et al., 2011). More recently, they have uncovered SRX-43 in the ASI neurons, and SRX-44 in either ASJ or ADL (Greene et al., 2016b; Greene et al., 2016a). The expression pattern of SRX-44 either promotes (ASJ) or suppresses (ADL) roaming and is dependent on proximal promoter sequence (Greene et al., 2016a).

Table 4. Known Ascaroside Receptors.

Receptor	Neurons	Ascaroside	Identification Method	Year	Lab
SRBC-64	ASK	ascr#1, #2, #3	Revere Genetic Screen	2009	Sengupta
SRBC-66	ASK	ascr#1, #2, #3			
DAF-37	ASI, ASK, CEM	ascr#2	Photo-affinity Probe	2012	Riddle
DAF-38	ASI, ASK	ascr#2, #3, #5			
SRG-36	ASI	ascr#5	Quantitative Trace Locus (QTL) Analysis	2012	Bargmann
SRG-37	ASI				
SRX-43*	ASI	icas#9	QTL Analysis	2016	
SRX-44*	ASJ, ADL		QTL Analysis	2016	
TYRA-2*	ASH	osas#9	Reverse Genetic Screen	2019	Srinivasan

G protein-coupled receptors linked to sensation of ascarosides, the neuron of expression, ascaroside sensed, as well as method, year, and lab of identification. Most ascaroside receptors are linked with developmental changes (i.e., dauer), but the more recent discoveries have also been linked to behavior (denoted with *).

In **Chapter 4C** of this dissertation, we employ transcriptomic analyses of the CEM neurons to identify candidate receptors for ascr#8. Confirmation of receptor roles in sensation are then performed using RNAi knockdown and CRISPR-mediated knockouts.

A Biochemical Approach to Receptor Identification

A more targeted approach has been employed by the Riddle lab in their elucidation of ascr#2 receptors. In this method, a biochemical probe was constructed, based on the structure of ascr#2, and supplemented with photo-crosslinking and click-chemistry components (Park et al., 2012). A donor-acceptor bead system was used to elicit

fluorescence after covalently binding the ascr#2-probe to its receptor. In this manner, the identify of DAF-37 as an ascr#2 receptor was elucidated. Via ascr#2 pull-down experiments, a heterodimeric component of the DAF-37 sensation machinery was identified in DAF-38 (Park et al., 2012). Whereas DAF-37 is expressed in ASI, ASK, and the male specific CEM neurons, DAF-38 is only expressed in ASI and ASK. More interestingly, while DAF-37 is specific to ascr#2, DAF-38 also participates in ascr#3 and ascr#5 sensation (Park et al., 2012).

In **Chapter 5** of this dissertation, we develop a novel probe for identifying ascr#8 receptors (Zhang, Reilly, Yu, Srinivasan, & Schroeder, 2019). During the development of this probe, we uncover multiple sites of moiety attachment that do not detrimentally affect probe activity (Zhang et al., 2019).

The Evolution of Receptors in Small-Molecule Signaling

While examining the transcriptomic profiles of the male specific CEM neurons (see **Chapter 4C**), we uncovered an interesting finding in the phylogeny of one the candidate ascr#8 receptors. Following up on these findings, we assayed an array of male *Caenorhabditis* nematodes for their ability to be attracted to ascr#8 (**Chapter 6**) (Reilly, Randle, & Srinivasan, 2019). Hermaphroditic nematodes seem to exhibit a loss of mating pheromone receptor paralogs, while gonochoristic sibling species retain the receptors, and attract mates via ascr#8 signaling.

Conclusions

The CEM neurons pose an interesting platform of questions. First, they allow us to ask how male-specific chemosensory neurons different in function compared to hermaphroditic (or non-sex-specific) neurons. Second, they offer a third, novel set of asymmetric neurons in an organism that is remarkably conserved and symmetric. Third, by performing comparative studies with neurons such as ASE or AWC, the CEM neurons

can help us understand the link between sex-specific cellular asymmetry and receptor expression and function.

To begin addressing these questions, this thesis first aims to identify receptors that are expressed within the CEM neurons (**Chapter 4C**). While the receptors identified and studied also relate directly to a function (mate attraction), our transcriptomic data set makes many more receptors and genes available for study that exhibit asymmetric expression profiles within the CEM neurons.

As a targeted, non-biased approach to identifying CEM-expressed receptors, we worked alongside the Schroeder lab at Cornell University to develop a novel biochemical probe that will allow us to pull-down direct binders of ascr#8 (**Chapter 5**) (Zhang et al., 2019).

Finally, our examination of the ascr#8 receptor candidates identified in **Chapter 4C** led us to an interesting phenomenon wherein hermaphroditic species have variable levels of mating pheromone receptors compared to closely related male-female sister species. Our investigation into the behavioral response resulted in an interesting finding that hermaphroditism seems to result a loss of mate-attraction ability (**Chapter 6**) (Reilly et al., 2019).

Together, these following chapters build a strong foundation for understanding the role of the male specific CEM neurons in their sensation of the male attracting pheromone, ascr#8.

References

Alqadah, A., Hsieh, Y.-W., Xiong, R., & Chuang, C.-F. (2016). Stochastic left-right neuronal asymmetry in Caenorhabditis elegans. *Philosophical transactions of the Royal Society of London. Series B, Biological sciences, 371*(1710), 20150407. doi:10.1098/rstb.2015.0407

Artyukhin, A. B., Zhang, Y. K., Akagi, A. E., Panda, O., Sternberg, P. W., & Schroeder, F. C. (2018). Metabolomic "Dark Matter" Dependent on Peroxisomal beta-Oxidation in *Caenorhabditis elegans*. *J Am Chem Soc, 140*(8), 2841-2852. doi:10.1021/jacs.7b11811

Bargmann, C. I. (2006). Chemosensation in *C. elegans*. *WormBook*, 1-29. doi:10.1895/wormbook.1.123.1

C. elegans Small Molecule Identifier Database (SMID DB). (27 Oct. 2011). Retrieved 27 Oct. 2011, from Boyce Thompson Institute, Cornell University

Chalasani, S. H., Chronis, N., Tsunozaki, M., Gray, J. M., Ramot, D., Goodman, M. B., & Bargmann, C. I. (2007). Dissecting a circuit for olfactory behaviour in Caenorhabditis elegans. *Nature, 450*(7166), 63-70. doi:10.1038/nature06292

Chalasani, S. H., Kato, S., Albrecht, D. R., Nakagawa, T., Abbott, L. F., & Bargmann, C. I. (2010). Neuropeptide feedback modifies odor-evoked dynamics in *Caenorhabditis elegans* olfactory neurons. *Nat Neurosci, 13*(5), 615-621. doi:10.1038/nn.2526

Chute, C. D., DiLoreto, E. M., Zhang, Y. K., Reilly, D. K., Rayes, D., Coyle, V. L., . . . Srinivasan, J. (2019). Co-option of neurotransmitter signaling for inter-organismal communication in *C. elegans*. *Nat Commun, 10*(1), 3186. doi:10.1038/s41467-019-11240-7

Cochella, L., Tursun, B., Hsieh, Y. W., Galindo, S., Johnston, R. J., Chuang, C. F., & Hobert, O. (2014). Two distinct types of neuronal asymmetries are controlled by the *Caenorhabditis elegans* zinc finger transcription factor die-1. *Genes Dev, 28*(1), 34-43. doi:10.1101/gad.233643.113

Greene, J. S., Brown, M., Dobosiewicz, M., Ishida, I. G., Macosko, E. Z., Zhang, X., . . . Bargmann, C. I. (2016b). Balancing selection shapes density-dependent foraging behaviour. *Nature, 539*(7628), 254-258. doi:10.1038/nature19848

Greene, J. S., Dobosiewicz, M., Butcher, R. A., McGrath, P. T., & Bargmann, C. I. (2016a). Regulatory changes in two chemoreceptor genes contribute to a *Caenorhabditis elegans* QTL for foraging behavior. *eLife, 5*. doi:10.7554/eLife.21454

Kim, K., Sato, K., Shibuya, M., Zeiger, D. M., Butcher, R. A., Ragains, J. R., . . . Sengupta, P. (2009). Two Chemoreceptors Mediate Developmental Effects of Dauer Pheromone in *C. elegans*. *Science, 326*(5955), 994-998. doi:10.1126/science.1176331

McGrath, P. T., Xu, Y., Ailion, M., Garrison, J. L., Butcher, R. A., & Bargmann, C. I. (2011). Parallel evolution of domesticated *Caenorhabditis* species targets pheromone receptor genes. *Nature, 477*(7364), 321-325. doi:10.1038/nature10378

Narayan, A., Venkatachalam, V., Durak, O., Reilly, D. K., Bose, N., Schroeder, F. C., . . . Sternberg, P. W. (2016). Contrasting responses within a single neuron class enable sex-specific attraction in *Caenorhabditis elegans*. *Proc Natl Acad Sci U S A, 113*(10), E1392-1401. doi:10.1073/pnas.1600786113

Park, D., O'Doherty, I., Somvanshi, R. K., Bethke, A., Schroeder, F. C., Kumar, U., & Riddle, D. L. (2012). Interaction of structure-specific and promiscuous G-protein-coupled receptors mediates small-molecule signaling in *Caenorhabditis elegans*. *PNAS, 109*(25), 9917-9922. doi:10.1073/pnas.1202216109

Peden, E., Kimberly, E., Gengyo-Ando, K., Mitani, S., & Xue, D. (2007). Control of sex-specific apoptosis in *C. elegans* by the BarH homeodomain protein CEH-30 and the transcriptional repressor UNC-37/Groucho. *Genes Dev, 21*(23), 3195-3207. doi:10.1101/gad.1607807

Pierce-Shimomura, J. T., Morse, T. M., & Lockery, S. R. (1999). The fundamental role of pirouettes in Caenorhabditis elegans chemotaxis. *J Neurosci, 19*(21), 9557-9569.

Pungaliya, C., Srinivasan, J., Fox, B. W., Malik, R. U., Ludewig, A. H., Sternberg, P. W., & Schroeder, F. C. (2009). A shortcut to identifying small molecule signals that regulate behavior and development in *Caenorhabditis elegans*. *Proceedings of the National Academy of Sciences of the United States of America, 106*(19), 7708-7713. doi:10.1073/pnas.0811918106

Reilly, D. K., Lawler, D. E., Albrecht, D. R., & Srinivasan, J. (2017). Using an Adapted Microfluidic Olfactory Chip for the Imaging of Neuronal Activity in Response to Pheromones in Male *C. Elegans* Head Neurons. *Journal of Visualized Experiments*(127), e56026. doi:doi:10.3791/56026

Reilly, D. K., Randle, L. J., & Srinivasan, J. (2019). Evolution of hermaphroditism decreases efficacy of Ascaroside#8-mediated mate attraction in *Caenorhabditis* nematodes. *microPublication Biology*. doi:10.17912/micropub.biology.000134

Schwartz, H. T., & Horvitz, H. R. (2007). The *C. elegans* protein CEH-30 protects male-specific neurons from apoptosis independently of the Bcl-2 homolog CED-9. *Genes Dev, 21*(23), 3181-3194. doi:10.1101/gad.1607007

Zhang, Y. K., Reilly, D. K., Yu, J., Srinivasan, J., & Schroeder, F. C. (2019). Photoaffinity probes for nematode pheromone receptor identification. *Journal of Organic & Biomolecular Chemistry*, 10.1039/c1039ob02099c. doi:10.1039/c9ob02099c

Chapter 4B Using an Adapted Microfluidic Olfactory Chip for the Imaging of Neuronal Activity in Response to Pheromones in Male *C. elegans* Head Neurons

Published as:

Reilly DK[1,] Lawler DE[2], Albrecht DR[1,2], Srinivasan J[1] (2017). Using an Adapted Microfluidic Olfactory Chip for the Imaging of Neuronal Activity in Response to Pheromones in Male *C. elegans* Head Neurons. J. Vis. Exp. (127), E56026, doi:10.3791/56026

[1] Department of Biology and Biotechnology
Worcester Polytechnic Institute
[2] Department of Biomedical Engineering
Worcester Polytechnic Institute

Abstract

The use of calcium indicators has greatly enhanced our understanding of neural dynamics and regulation. The nematode *Caenorhabditis elegans*, with its completely mapped nervous system and transparent anatomy, presents an ideal model for understanding real-time neural dynamics using calcium indicators. In combination with microfluidic technologies and experimental designs, calcium-imaging studies using these indicators are performed in both free-moving and trapped animals. However, most previous studies utilizing trapping devices, such as the olfactory chip described in Chronis et al., have devices designed for use in the more common hermaphrodite, as the less common male is both morphologically and structurally dissimilar. An adapted olfactory chip was designed and fabricated for increased efficiency in male neuronal imaging with using young adult animals. A turn was incorporated into the worm loading port to rotate the animals and to allow for the separation of the individual neurons within a bilateral pair in 2D imaging. Worms are exposed to a controlled flow of odorant within the microfluidic device, as described in previous hermaphrodite studies. Calcium transients are then analyzed using the open-source software ImageJ. The procedure described herein should allow for an increased amount of male-based *C. elegans* calcium imaging studies, deepening our understanding of the mechanisms of sex-specific neuronal signaling.

Introduction

Microfluidic devices provide increased access to precisely controlled environments, wherein animals, such as the nematode *C. elegans*, can be experimentally manipulated[1]. These studies include behavioral assays, calcium imaging studies, or even screenings for specific phenotypes, resulting in more exact measurements of experimental outcomes[1-6]. Microfluidics provide small-scale liquid conditions through which detailed experiments can be run while utilizing minimal amounts of reagents. There is a constant production of new microfluidic device designs, and the use of each varies, from arenas that allow for the natural sinusoidal motion of *C. elegans* in behavioral assays and neural imaging studies, to trap devices used in neural imaging and olfactory studies, to devices that allow for high-throughput phenotypic analysis in genetic screens[4-7]. Following the fabrication of a master mold, microfluidic devices are inexpensive to construct—given the reusability of the master—and easy to use, allowing for rapid data generation via high-throughput studies. The fabrication of devices using polymers such as polydimethylsiloxane (PDMS) allows for the creation of new devices within hours.

Calcium imaging studies use genetically encoded calcium indicators (GECIs) expressed in target cells to measure the neural dynamics of those cells in real time[8-11]. The transparent nature of *C. elegans* allows for the recording of the fluorescent levels of these proteins in live animals. Traditionally, GECIs rely on the green fluorescent protein (GFP)-based sensor GFP-Calmodulin-M13 Peptide (GCaMP), although more recent studies have adapted these sensors to allow for better signal-to-noise ratios and red-shifted excitation profiles. Following the development of GCaMP3, proteins with these specifications have varied, including sensors such as GCaMP6s and GCaMP6f (slow and fast fluorescence offrates, respectively), as well as RFP-Calmodulin-M13 Peptide (RCaMP), which has a red-shifted activation profile. The combination of these GECIs with *C. elegans* cell-specific gene promoter sequences can target cells of interest, particularly sensory neurons[12-16].

While the ease of *C. elegans* use in microfluidic studies is apparent, almost all studies have focused on hermaphrodites. Despite males only accounting for 0.01-0.02% of the wild type population, invaluable findings can arise from their characterization. While the physical connectome of the hermaphrodite nervous system has been fully mapped for decades[17], the male connectome remains incomplete, especially in the head region of the animal[18]. The use of calcium imaging in males will help to generate an understanding of the male nervous system and the differences that arise between the two sexes. The smaller size of *C. elegans* adult males prevents effective and reliable trapping in the loading ports of traditional olfactory devices designed for larger hermaphrodites. To address this, a modified version of the Chronis Olfactory Chip[19] was developed with a narrower loading port, a lower channel height, and turns in the worm loading port (which rotate the animal), allowing for the visualization of bilateral left/right neuronal pairs. This design permits: (1) the effective trapping of young adult males, (2) a more reliable orientation of the animal for the visualization of both members of bilateral paired neurons, and (3) the precise imaging of neural activity in male neurons.

Increasingly, studies show that *C. elegans* males respond differently than hermaphrodites to a variety of ascarosides (ascr), or nematode pheromones[20-24]. Therefore, developing an understanding of the neural dynamics and representations within the male connectome has become even more pertinent. Male *C. elegans* contain 87 sex-specific neurons not present in the hermaphrodite[25,26], altering the connectome in as-yet undetermined ways. Being able to image these unique neural dynamics will allow us to better understand sex-specific responses and neural representations.

This protocol describes the use of a male-adapted olfactory chip for the neural imaging of male *C. elegans* chemosensation. The nociceptive neuron ASH responds reliably to 1 M glycerol in males, consistent with previous hermaphroditic studies[27]. Exposure to ascarosides may elicit responses that are variable from animal to animal, requiring a larger number of animals to be tested. The response of the male-specific CEM neurons

has previously been shown, through both electrophysiology and calcium imaging studies, to respond variably to ascaroside #3[23].

Device Fabrication

NOTE: See reference[1].

NOTE: Silicon master molds were fabricated using standard photolithographic techniques for patterning SU-8 photoresist on a silicon master[1,7]. Photomasks for wafer patterning were printed at 25,000 dpi. The male-adapted device features a Chronis Olfactory Chip design[19] with a change in the worm loading port, adapting a design obtained from M. Zimmer (personal correspondence, 2016). A turn is included to control the rotation of the animals. The width of the worm loading port channel is narrowed to 50 μm. All channels are 32 μm tall. Once a silicon master mold is available to the user, the user can follow the subsequent protocol, as described previously[1].

1. Mix PDMS base and curing agent at a 10:1 ratio by weight.
2. Mix thoroughly with transfer pipettes.
3. Degas the mixture in a vacuum desiccator for 1 h, until all visible bubbles are removed.
4. Pour the mixture onto a silicon mold master in a 150 mm diameter dish until it is 5 mm thick (100 g). Use a Pasteur pipette to remove any bubbles or dust that have been introduced to the mixture.
5. Bake at 65 °C for at least 3 h, or overnight.
6. Cut the PDMS away from the mold using a scalpel and cut the separate devices apart using a razor blade.
7. Punch inlet and outlet holes with a 1 mm dermal punch.
8. Flush the holes with dH_2O, ethanol, and again with dH_2O to remove particles from the punches. Dry the device in an air stream pulse.

9. Clean both channel sides and the top side of the device with adhesive tape, removing any dust or debris remaining on the device to allow for successful bonding.
10. **Plasma-bond the device, channel-side down, to a no. 1 cover glass.**
    a. Expose cover glass and device (channel-side up) to air plasma using conditions that allow for proper bonding, such as 100 W for 30 s or 24 W for 60 s.

       NOTE: Settings can be adjusted to improve the bonding efficiency. The plasma-bonding conditions are not as critical as proper cleaning when attempting to improve the bonding efficiency. An insufficiently cleaned device will not bond, even under ideal plasma conditions.
    b. Invert the cover glass onto the channel side of the device and press down with the thumb for 5 s.

Buffer Preparation

1. Dilute 1x S Basal (100 mM NaCl and 0.05 M KPO_4, pH 6.0) from a sterile 10x stock.
2. Dilute 1 M tetramisole stock to a final concentration of 1 mM in 1x S Basal for all buffer solutions.
3. **Add fluorescein to both the "flow control" and "buffer" reservoirs.**
    1. Create a 100-mg/mL stock of fluorescein in 1x S Basal.
    2. Dilute the stock to final concentrations of 1 μg/mL in the flow control and 0.1 μg/mL in the buffer.
4. **Create the stimuli.**
    1. Dilute glycerol to a final concentration of 1 M in 1X S Basal.
    2. Dilute ascaroside #3 (ascr#3) to a final concentration of 1 μM into 1X S Basal.

Device Setup

NOTE: See[1].

1. Prepare three fluid reservoirs by attaching a 30 or 60 mL syringe to 3-way Luer valve, with a 3 mL syringe and needle attached to the Luer valve as well (as in **Figure 30A**).

Connect the needle to tubing that extends to the microfluidic device (as in **Figure 30A-B**).

2. Remove the air bubbles from the reservoir and tubing.
3. Fill the 3 mL syringe with attached tubing with 1x S Basal and insert it into the outlet port.
4. Gently apply pressure to the syringe until the buffer appears at the top of the inlet holes.
5. Connect the flow control, buffer, and stimulus tubing to appropriate inlet holes (as in **Figure 30B-C**), ensuring that liquid drops are present on both the loading port hole and the buffer tubing to be attached.
6. Again, gently apply pressure to the syringe that is connected to the outlet port until droplets appear in the worm loading port inlet.
7. Insert a solid blocking pin into the worm loading port.
8. Remove the syringe from the outlet port and attach the outlet line connected to the house vacuum (-670 Torr).
9. **Inspect the device for any bubbles in the flow channels, visually and through video confirmation via a software compatible with the camera used, such as the open-source software Micro-Manger. See step 6 for tips on using Micro-Manager.**
    a. If any bubbles are present, wait for them to dislodge or be absorbed into the PDMS wall prior to loading any animals; the presence of bubbles will disturb the proper flow of fluids through the device.
10. **Using a GFP filter, confirm proper flow dynamics within the device prior to worm loading by actuating the 3-way valve and observing the switching of buffers.**
    a. Determine the proper flow dynamics: observe the fluorescein present in the flow control and buffer solutions (**Figure 31D-2E**) changing when the flow control value is changed by pressing the control button corresponding to the 3-way valve on the valve link (**Figure 30B**).

b. After opening Micro-Manager, click on "Live" to observe a live image of the device. Turn on the fluorescent light source to observe the flow of buffers in the device (**Figure 31D-E**).

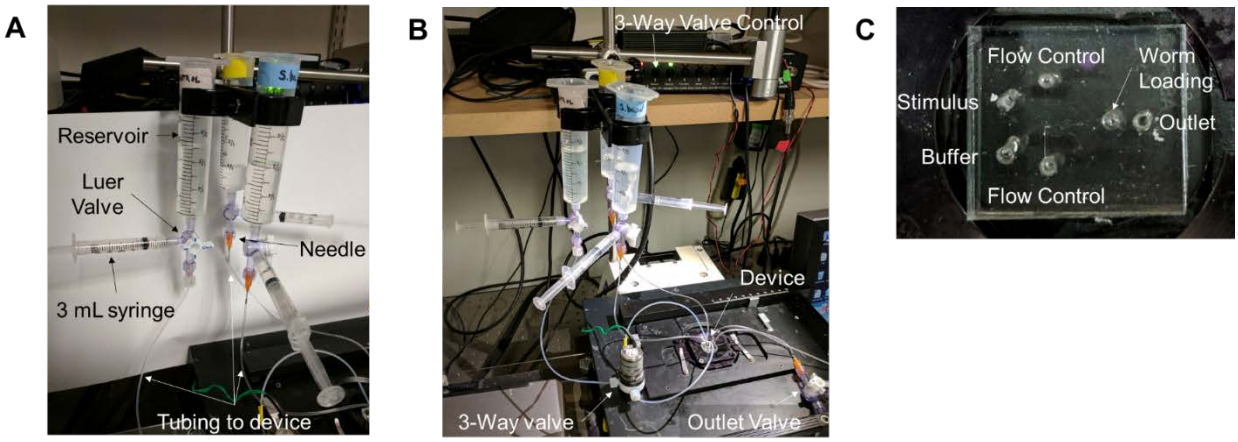

Figure 30. Microfluidic device setup.
(**A**) Reservoirs and tubing. A 30 mL syringe without a plunger serves as the "reservoir." This is attached to a Luer valve with three flow options. One outlet is connected to a 3 mL syringe with a plunger, while the other is connected to a needle (orange) that is inserted into the tubing that connects to the microfluidic device. (**B**) The overall setup of the microfluidic imaging experiment. The device is placed on a stage of an inverted epifluorescence microscope, above the objective lenses. The "flow control" buffer travels through a 3-way valve that is controlled by a unit on the shelf above the setup. Lines containing buffers are then inserted into the appropriate device ports. (**C**) The ports of the microfluidic device. The "flow control" ports flank the other inlet ports: the "stimulus" and "buffer" ports. The "outlet" port is the right-most port. Due to the location of the worm loading arena, the "worm loading" port is the central-most port on the device.

Animal Preparation

NOTE: See reference[23].

1. Imaging ASH responses to 1 M glycerol.

a. Place approximately 20 *C. elegans* males that are positive for p*sra-6*::GCaMP3 array expression onto a nematode growth medium (NGM) agar plate seeded with a lawn of OP50 *E. coli*. Use the expression of fluorescent GECI and/or a co-injection marker for the identification of array-positive animals.

NOTE: Array positive animals will fluoresce according to the GECI used (i.e., animals expressing GCaMP will fluoresce green under blue-light stimulation, while RCaMP animals will fluoresce red under green-light stimulation). Co-injection markers can range from other fluorescent proteins, such as GFP and RFP,

to phenotypic markers, such as *rol-6*, or can rescue a dominant phenotype, such as the *pha-1* mutation[28].

i. If picking immediately prior to the assay, pick young adult males. If picking the day prior to the assay, pick L4 larval males.

2. Imaging the CEM responses to 1 μM ascr#3.

a. Pick approximately 20 L4 *C. elegans* males (fkEx98[p*pkd-2*::GCaMP::SL2::dsRED + pBX-1]; *pha-1*(e2123ts); *him-5*(e1490); *lite-1*(ce314)) that are positive for dsRed co-injection marker expression.

NOTE: dsRed expression within the ray neurons of the male tale is easier to observe and confirm than GCaMP expression within the four CEM neurons.

b. Isolate these males from hermaphrodites on an NGM agar plate seeded with a lawn of OP50 *E. coli* for 5-14 h before performing the imaging experiment.

NOTE: Males not isolated for a minimum of 5 h do not behaviorally respond to ascr#3 and therefore may exhibit even fewer calcium transients to the ascaroside than observed here.

Animal Loading

NOTE: See reference[1].

1. **Pick one worm onto an unseeded NGM agar plate using standard worm maintenance techniques.**
   a. Pick worms by flaming a pick (made of flattened platinum wire), picking bacteria onto the pick, and "dabbing" a worm to pick it up. Gently place the worm onto the new plate, allowing it to crawl off on its own.
2. Add approximately 5 mL of 1x S Basal to the unseeded plate, such that plate is flooded.
3. **Draw the worm into a loading syringe (*i.e.*, 3 mL syringe with attached tubing) that has been pre-filled with 1x S Basal.**

   a. Be sure to suck the worm only into the tubing, not all the way into the syringe.
   b. NOTE: If the worm travels into the syringe, it is near impossible to get it back into the tubing.
4. Turn off the vacuum to stop the flow by turning the outlet Luer valve.
5. Remove the solid pin blocking the worm loading port.
6. Turn the Luer valve connected to the outlet port (**Figure 30B**) so that it is venting.
7. NOTE: Use a live video feed while loading the worm to confirm the location and orientation of the animal (steps 5.8-5.13).
8. Insert the worm loading tube into the worm loading port.
9. Gently apply pressure to the syringe until the worm appears in the loading channel.
10. If the worm starts to enter the channel tail-first, pull on the syringe plunger to prevent the worm from entering the channel.
11. Switch between applying and reversing pressure until the head enters the channel first.
12. Open the vacuum by turning the 3-way Luer valve connected to the outlet port to open it to vacuum instead of atmosphere.
13. Manually apply pressure by depressing the syringe plunger to orient and place the worm head such that it is exposed to the buffer flow channel, but not so far that the head can move around freely (**Figure 31D-E**).

Stimulus and Acquisition

1. Using an open-source microscopy software, such as Micro-Manager, record by capturing images as a TIFF stack at 10 frames/s using bluelight excitation (470 nm) for 30 s.
2. **Set the exposure on the main menu to 100 ms.**
   a. Open "Multi-D Acq." from the main menu of the software. Set the "number" to "300," and the "interval" to "0." Click "Acquire!" to acquire the video.

3. **Apply a 10 s pulse of the stimulus 5 s after initiating acquisition. Adjust the duration of stimulus application as desired.**
    a. After acquiring 5 s of video, change the 3-way valve controlling the flow control buffer to apply the stimulus to the animal being tested. Click the left-most button on the valve link (**Figure 30B**).
    b. After 10 s of stimulus exposure (this time can be adjusted as desired by the user), alter the flow of buffers by again pressing the leftmost button on the valve link.
4. Record under buffer only until the 30-s window is complete to allow the GECI fluorescence to return to baseline.
5. Repeat as desired. Wait 30 s between the end of acquisition and the initiation of the next trial.

Image Analysis

1. Open the TIFF stack with the open-source software, ImageJ, by dragging file into the ImageJ window.
2. Click using the cursor and drag to set the region of interest (ROI) around the neuron of interest. Set the region to include the soma of the neuron of interest (as in **Figure 32A**).
3. Plot the z-stack of the fluorescence intensity of the ROI across stacks by clicking Open -> Image -> Stacks -> Plot Z-axis Profile.
4. Click "List" in the window that opens. Click Edit -> Copy to copy the values. Paste the values into a spreadsheet program.
5. Analyze the background fluorescence for each pulse by dragging the ROI to a region of the worm that does not contain GCaMP expression.
6. Perform background subtraction for each pulse by subtracting the background fluorescence value from the neuron fluorescence intensity value.
7. **Calculate $\Delta F/F_0$ for each frame of each pulse.**

a. Calculate F_0 as the average intensity value of the ROI for first 1 s of acquisition (*e.g.*, frames 1-10).
b. Calculate $\Delta F/F_0$ by dividing the background-subtracted value for the frame of interest by the calculated F_0 value.

8. Repeat for every neuron imaged and every stimulus pulse.
9. For neurons with consistent response profiles, such as ASH, average all pulses for each neuron and calculate the SEM (as in **Figure 31F**).
10. Plot the average $\Delta F/F_0$ with SEM over time for each neuron.

    NOTE: In this instance, it is common practice to include heatmaps of the individual neuronal responses of each trial as well. In neurons that do not exhibit consistent changes in calcium transients upon exposure to stimuli across repeated stimulations, or in different individuals[23], it may be more applicable to show individual pulse traces (as in **Figure 33**). See the **Discussion** for details on determining how to display the data.

Representative Results

An example of the overall device setup can be seen in **Figure 30A-B**. **Figure 30A** depicts the proper reservoir construction and setup. **Figure 30B** shows the connections of the reservoirs to the microfluidic device. **Figure 30C** depicts a microfluidic device with individual ports labeled for clarity.

The design of the male-adapted microfluidic device contains a curve in the loading port, but flow dynamics are identical to the device designed by Chronis *et al.*[19](**Figure 31A-C**). The flow of buffers can be controlled by altering which flow control valve is open (**Figure 31A-B**). The measurements of the device as fabricated vary from the designed file. The measurements provided in **Figure 31C** are "as fabricated" measurements.

After loading male *C. elegans* into the male-adapted olfactory device, their placement and orientation, as well as channel flow dynamics, can be verified via both bright-field and fluorescent imaging (**Figure 31D-E**). The exposure of worms expressing GCaMP3 in the nociceptive neuron, ASH, to 1 M glycerol results in visible changes in fluorescence within

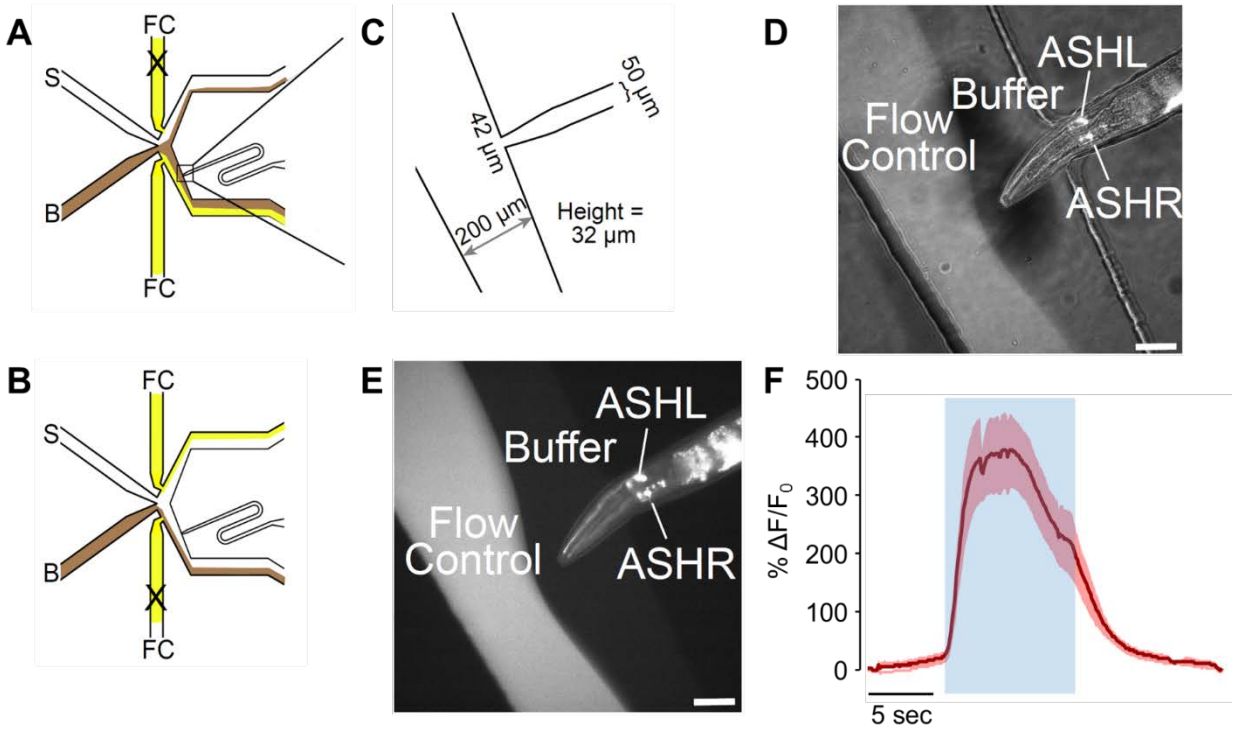

Figure 31. A male-adapted microfluidic olfactory chip.
(**A**) The flow patterns of the device when the worm is exposed to buffer. Buffer (B) is shown in brown, and flow control (FC) is shown in yellow, with stimulus (S) in white. The worm loading port has been adapted to include a curve, which allows for better control of worm orientation. (**B**) The flow patterns of the device when the worm is exposed to stimulus. Buffer (B) is shown in brown, and flow control (FC) is shown in yellow, with stimulus (S) in white. (**C**) Measurements of the adapted device as fabricated. The worm loading port ends in a 42 µm opening, with a 50 µm channel designed for the male width. The measured height of the channels is 32 µm, despite a target of 25 µm in the design. (**D-E**) A trapped male expressing p*sra-6*::GCaMP3. The *sra-6* promoter is not ASH-specific, and some expression may be observed in the ASI neuron, although no calcium transients were observed in ASI. The image is (**D**) a combination of bright-field and fluorescent illumination, while (**E**) is fluorescent only. The scale bars denote 42 µm. (**F**) The ASH neuron responds to 1 M glycerol stimulation with robust neural activity. The blue area denotes the time of the 1 M glycerol stimulus. The shaded region denotes the standard error, with n = 20 pulses from seven worms. The red traces denote depolarizing responses. The Y-axes show $\Delta F/F_0$. The scale bar denotes 5 s.

the ASH neuron, indicative of neural activity (**Figure 31F**). Subtle changes in fluorescence may not be visible by eye, but software can be used to quantify these changes. The free ImageJ software can be used to analyze and quantify the fluorescent intensity of ASH

neurons upon exposure to 1 M glycerol over time (**Figure 31F**). This is similar to what is observed in hermaphrodites[27] and, due to the robustness of the ASH neuronal response to glycerol, this is observed in all animals tested.

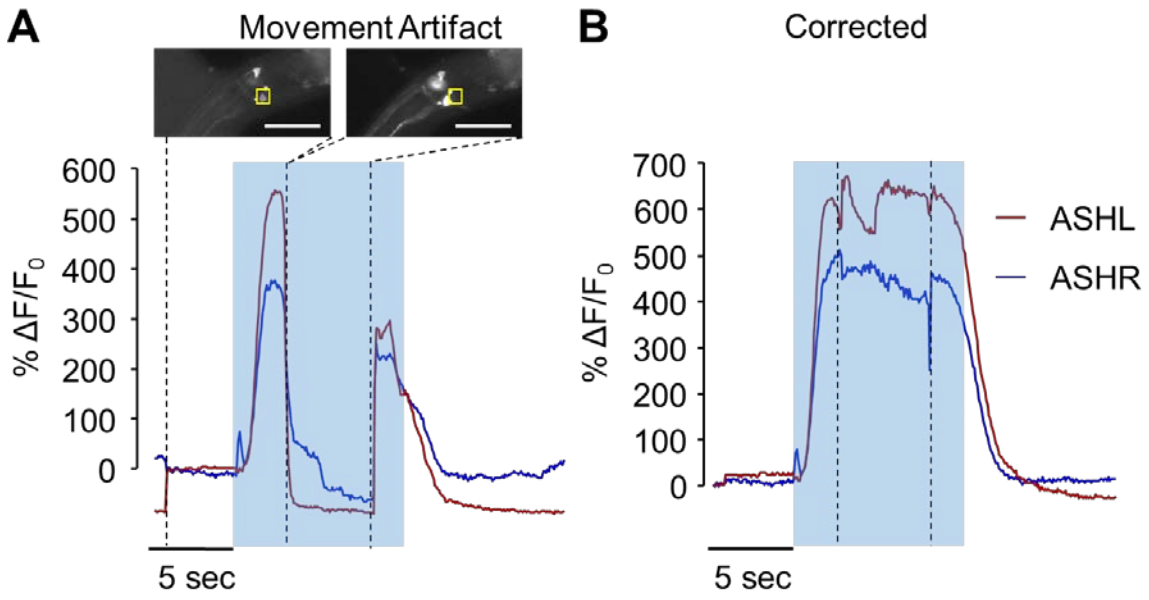

Figure 32. Addressing worm movement during the image acquisition period.
(**A**) $\Delta F/F_0$ (change in fluorescent intensity divided by the average background fluorescent intensity for first 1 s of acquisition) was calculated using ImageJ by defining an area where the neuron of interest was reliably static for 1 s. During the stimulus pulse (blue area), the animal moved, as seen in the images above the calcium trace, resulting in the neuron no longer being contained within the analyzed area (yellow box). The scale bars denote 42 μm. the dashed lines show the region of the trace that corresponds to the location of the worm in each image. (**B**) If the area of analysis is moved to follow the neuron during the trial and the individual traces are rebuilt to convey the actual neural dynamics, the trace appears as if the animal did not move. The dashed lines show the region of the trace that was corrected for worm movement. Traces for both ASH neurons, left and right (ASHL (red) and ASHR (blue), respectively) are shown. The Y-axes show $\Delta F/F_0$. The scale bar denotes 5 s.

A small amount of axial or rotational movement is expected in unparalyzed animals, often necessitating a neuron-tracking algorithm during video analysis (**Figure 32A**). The addition of a paralytic in the buffers (*e.g.*, 1 mM tetramisole) nearly eliminates this effect, although some animals (~10%) still move during the trials. This can be circumvented by: (a) using older males, which are more efficiently trapped; (b) decreasing the width or thickness of the worm loading port even further; or (c) either increasing the concentration of the paralytic used or using another paralytic. This will also ensure that there is not too

much of the head past the end of the trap and exposed to the odor channel. If a trial with worm movement occurs, the area of analysis can be moved and reread from the new neuronal location, starting at the frame after which the movement occurs (**Figure 32B**). Manual reconstruction of the neural traces by the user is required in this instance. Scripts that analyze the fluorescent changes within the neuron and that follow the neuron's center as it moves can also be written[19].

Male *C. elegans* sense attractive biogenic pheromones called ascarosides via the four sex-specific CEM neurons[23]. When calcium transients are observed in males, the responses

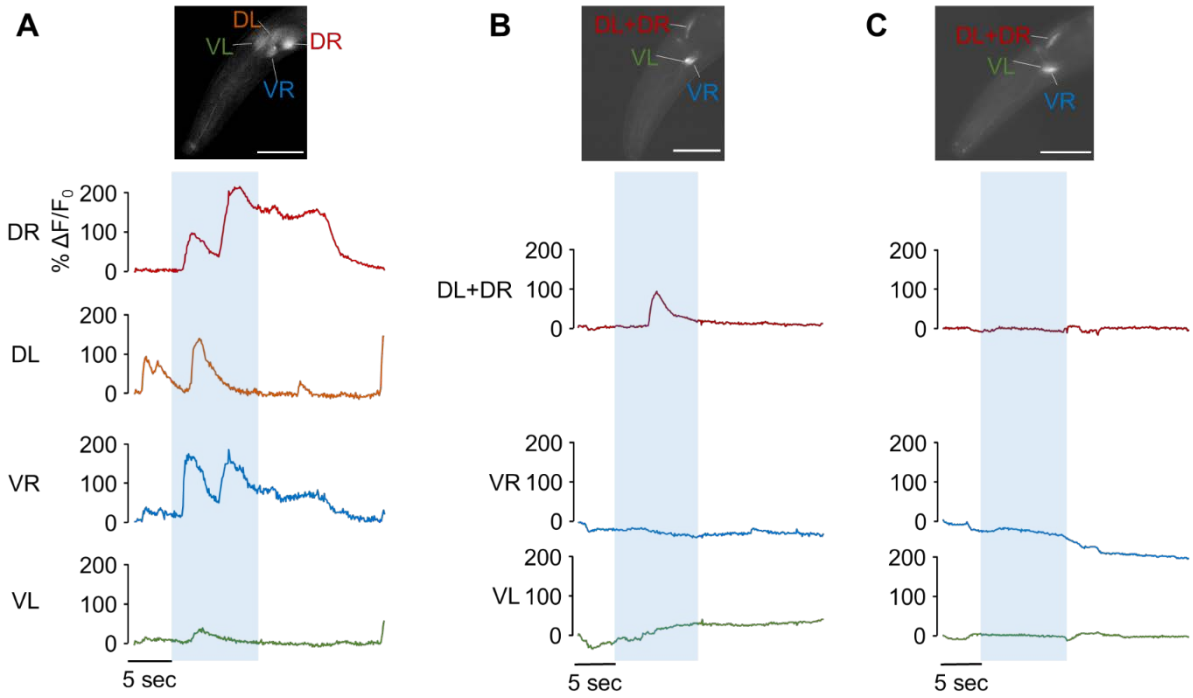

Figure 33. Male *C. elegans* CEM response to 1 μM ascr#3 is variable.
The male-specific CEM neurons display unique patterns of response to biogenic pheromones. (**A**) The responses observed in each CEM neuron for one pulse in one responsive animal are shown. There are four CEM neurons: dorsal right (CEM DR), dorsal left (CEM DL), ventral right (CEM VR), and ventral left (CEM VL). Three of the four neurons respond with depolarizations of varying shape and magnitude, with the fourth not responding to the ascaroside. (**B**) Approximately one-third of the trapped animals (2/7 tested in this study) result in only three neurons able to be imaged. The responses of a worm in this orientation resulted in CEM calcium transients that were different than those observed in the first worm. This was not due to the change in orientation of the worm, as CEM DR is visible in both orientations and exhibits variable response between animals. (**C**) Many worms do not respond with any detectable calcium transients (5/7 tested in this study). Individual traces shown are representative of the single animals shown in the images above the plots. The scale bars denote 42 μm. Traces: The blue area denotes the time of 1 μM ascr#3 exposure. The red traces denote the depolarizing response. The black traces denote no observed response. The Y-axes show $\Delta F/F_0$. The scale bar denotes 5 s.

are variable in shape, sign, and magnitude between both neurons and animals (**Figure 33A-B**). However, male response to pheromones is not as reliably observed as calcium transients in many animals (**Figure 33C**). This is not discouraging, as most ascarosides do not elicit calcium transients upon sensation[13-15].

Discussion

The male-adapted olfactory chip incorporates a turn into a narrower loading port, which allows for more control of the orientation and for the efficient trapping of male *C. elegans*. This allows for the visualization of both the left and right members of neuronal bilateral pairs, without the need for z-stacking. This curve leads to an orientation away from vertical 100% of the time in worms where only one bilateral pair is targeted with a fluorescent marker, such as ASH (**Figure 31D-E**)[29,30]. However, in neuronal classes with four radially symmetric neurons, such as CEM, all four neurons are visible only one-third of the time. Another third of worms tested have only three of the four neurons visible, and for the remaining third, the only distinguishable difference is between the dorsal and ventral cell bodies, not the left-right asymmetry (data not shown). The narrower port is combined with a lower channel height to prevent worm fluctuation across the z-axis. This design allows for the imaging of males in future studies, which, when combined with the constantly increasing knowledge of the male connectome[25,31], will allow for a better understanding of sex-specific neural function.

The analysis performed in this protocol uses the free software ImageJ to measure changes in fluorescence in the neuron of interest. With the current design, 1 mM tetramisole in the buffer effectively paralyzes the worms and prevents movement of the neurons being imaged. If movement is not preventable, or if the user wishes to avoid the use of a paralytic, more complex tracking scripts must be written that track the neurons as they move[7]. However, in this protocol, male worms only move when they were too small to be effectively constrained by the loading port and when presented with an extremely

aversive stimulus, such as glycerol. Even in these instances, the movement is brief and does not require large amounts of tracking adjustments—setting an ROI around the new neuron location alleviates the incorrect fluorescent readouts (**Figure 31**).

A limitation of single-worm, trap-based imaging is that only one worm can be imaged at a time[1]. Another limitation of these traps is that worms can get stuck within the device, causing devices to be clogged and "used up" after imaging only a few worms. However, the quick turnaround time for the fabrication of new devices from a master mold alleviates this downside. Extended blue-light illumination has also been shown to induce photodamage in *C. elegans*[32,33]. The relatively short experimental time frame of this protocol (30 s) allows for imaging without measurable photobleaching. However, to avoid photobleaching and photodamage in longer experiments, the light source can be pulsed[7]. For example, during each 100-ms exposure, the light can be pulsed for 10 ms. This has been shown to eliminate increased body autofluorescence over time[7].

In order to properly test males for their responses to ascarosides, larval-stage 4 (L4) males must first be isolated from hermaphrodites, for at least 5 h, in order to achieve a near-naïve response to the pheromones[23]. Isolation for less than this length of time may cause animals to fail to respond to the ascarosides. However, this isolation is not necessary when testing non-ascaroside cues, such as glycerol. For the sake of consistency, however, animals were always isolated at least 5 h prior to calcium imaging. In some neurons, such as the CEM, not every stimulation will elicit a neuronal response, and each CEM that does responds does so to generate a certain "code" of neural representation. This phenomenon in CEM has been observed via electrophysiology studies, as well as with calcium imaging studies like the ones described here[23]. Thus, measurable calcium transients in CEM neurons in every ascaroside-exposed animal are not guaranteed[23]. In fact, many of the ascarosides investigated to date do not elicit measurable calcium transients[13,15,34,35]. The successful elicitation of measurable transients was observed during only one of three pulses of pheromone in two of the five animals exposed to the

ascaroside of interest (**Figure 32**). This matches the rate of success previously observed in other labs[23]. This variability is a limitation when studying pheromone response and is not due to the male-based focus of this protocol.

When investigating calcium transients elicited in response to ascarosides, one should not dismiss a lack of consistent response without further investigation. This can be tested through experiments such as electrophysiology studies to confirm the variable response within a neuronal class. For neurons, such as ASH, that respond reliably, a lack of consistent response could be indicative of larger experimental problems, such as errors in stimulus control. The peak intensity of the responses can also be investigated if variability is expected in the response. The traces can be plotted with the standard deviation or standard error (as in **Figure 31F**). If the standard deviation is small, the traces can be plotted and analyzed as such. If there is noticeable amount of variation leading to moderate standard deviations, the data can be plotted the same, with accompanying heatmaps sorted by response "type" to show the response-by-response variation. If there is significant variation (**Figure 32**), wherein the peaks cannot be distributed in a Gaussian manner, responses can be categorized into response "types" (*e.g.*, depolarizing, hyperpolarizing, or non-polarizing)[23]. Responses that fall into a certain "type" can be plotted and analyzed together. Similarly, heatmaps should accompany this analysis as well.

Moving forward, this device can be adapted to allow for the imaging of larval-staged nematodes by narrowing the loading port even further. Further narrowing of the end of the loading port will allow for the constraint of the animal to allow for imaging of just the cilia of the sensory neurons, as opposed to the cell body. While other devices are designed for the more commonly studied hermaphrodite, this adapted olfactory chip allows for the imaging of neural activity in male neural circuits. As the connectome of the male is still being elucidated, being able to measure neural dynamics in sex-specific networks is

critical to fully understanding neuronal signaling. Differences between hermaphroditic and male responses can now be tested and measured using this device.

Acknowledgements

We would like to thank Manuel Zimmer for providing us with the initial design file that was adapted for use with males; Frank Schroeder for the synthesis and supply of ascr#3; Ross Lagoy for the insight and assistance with imaging and analysis; and Laura Aurilio for the master fabrication and who, alongside Christopher Chute, contributed to the review of this manuscript. Funding for this work was provided under the National Institutes of Health grant 1R01DC016058-01 (J.S.), the National Science Foundation grant CBET 1605679 (D.R.A.), and the Burroughs Wellcome Career Award at the Scientific Interface (D.R.A.).

References

1 Lagoy, R. C. & Albrecht, D. R. Microfluidic Devices for Behavioral Analysis, Microscopy, and Neuronal Imaging in Caenorhabditis elegans. *Methods Mol Biol.* **1327** 159-179, doi:10.1007/978-1-4939-2842-2_12, (2015).

2 Ben-Yakar, A., Chronis, N. & Lu, H. Microfluidics for the analysis of behavior, nerve regeneration, and neural cell biology in C. elegans. *Curr Opin Neurobiol.* **19** (5), 561-567, doi:10.1016/j.conb.2009.10.010, (2009).

3 Chronis, N. Worm chips: Microtools for C. elegans biology. *Lab on a Chip.* **10** (4), 432-437, doi:10.1039/B919983G, (2010).

4 Lee, H., Crane, M. M., Zhang, Y. & Lu, H. Quantitative screening of genes regulating tryptophan hydroxylase transcription in Caenorhabditis elegans using microfluidics and an adaptive algorithm. *Integr Biol (Camb).* **5** (2), 372-380, doi:10.1039/c2ib20078c, (2013).

5 Lockery, S. R. *et al.* A microfluidic device for whole-animal drug screening using electrophysiological measures in the nematode C. elegans. *Lab Chip.* **12** (12), 2211-2220, doi:10.1039/c2lc00001f, (2012).

6 Mondal, S. *et al.* Large-scale microfluidics providing high-resolution and high-throughput screening of Caenorhabditis elegans poly-glutamine aggregation model. *Nat Commun.* **7** 13023, doi:10.1038/ncomms13023, (2016).

7 Larsch, J., Ventimiglia, D., Bargmann, C. I. & Albrecht, D. R. High-throughput imaging of neuronal activity in Caenorhabditis elegans. *Proc Natl Acad Sci U S A.* **110** (45), E4266-4273, doi:10.1073/pnas.1318325110, (2013).

8 Akerboom, J. *et al.* Genetically encoded calcium indicators for multi-color neural activity imaging and combination with optogenetics. *Front Mol Neuro.* **6** 2, doi:10.3389/fnmol.2013.00002, (2013).

9 Badura, A., Sun, X. R., Giovannucci, A., Lynch, L. A. & Wang, S. S. H. Fast calcium sensor proteins for monitoring neural activity. *Neurophotonics.* **1** (2), 025008, doi:10.1117/1.NPh.1.2.025008, (2014).

10 Tatro, E. T. Brain-wide imaging of neurons in action. *Front Neural Circuits.* **8** 31, doi:10.3389/fncir.2014.00031, (2014).

11 Tian, L. *et al.* Imaging neural activity in worms, flies and mice with improved GCaMP calcium indicators. *Nat Methods.* **6** (12), 875-881, doi:10.1038/nmeth.1398, (2009).

12 Greene, J. S. *et al.* Balancing selection shapes density-dependent foraging behaviour. *Nature.* **539** (7628), 254-258, doi:10.1038/nature19848, (2016).

13 Greene, J. S., Dobosiewicz, M., Butcher, R. A., McGrath, P. T. & Bargmann, C. I. Regulatory changes in two chemoreceptor genes contribute to a *Caenorhabditis elegans* QTL for foraging behavior. *Elife.* **5**, doi:10.7554/eLife.21454, (2016).

14 Kim, K. *et al.* Two Chemoreceptors Mediate Developmental Effects of Dauer Pheromone in *C. elegans*. *Science.* **326** (5955), 994-998, doi:10.1126/science.1176331, (2009).

15 McGrath, P. T. *et al.* Parallel evolution of domesticated *Caenorhabditis* species targets pheromone receptor genes. *Nature.* **477** (7364), 321-325, doi:10.1038/nature10378, (2011).

16 Schmitt, C., Schultheis, C., Husson, S. J., Liewald, J. F. & Gottschalk, A. Specific Expression of Channelrhodopsin-2 in Single Neurons of Caenorhabditis elegans. *PLoS ONE.* **7** (8), e43164, doi:10.1371/journal.pone.0043164, (2012).

17 White, J. G., Southgate, E., Thomson, J. N. & Brenner, S. The Structure of the Nervous System of the Nematode Caenorhabditis elegans. *Phil Trans of the Royal Soc of Lon.* **314** (1165), 1 (1986).

18 White, J. Q. *et al.* The sensory circuitry for sexual attraction in C. elegans males. *Curr Biol.* **17** (21), 1847-1857, doi:10.1016/j.cub.2007.09.011, (2007).

19 Chronis, N., Zimmer, M. & Bargmann, C. I. Microfluidics for in vivo imaging of neuronal and behavioral activity in Caenorhabditis elegans. *Nat Meth.* **4** (9), 727-731, doi:http://www.nature.com/nmeth/journal/v4/n9/suppinfo/nmeth1075_S1.html, (2007).

20 Chute, C. D. & Srinivasan, J. Chemical mating cues in *C. elegans*. *Semin Cell Dev Biol.* **33** 18-24, doi:10.1016/j.semcdb.2014.06.002, (2014).

21 Izrayelit, Y. *et al.* Targeted metabolomics reveals a male pheromone and sex-specific ascaroside biosynthesis in *Caenorhabditis elegans*. *ACS Chem Biol.* **7** (8), 1321-1325, doi:10.1021/cb300169c, (2012).

22 Ludewig, A. H. & Schroeder, F. C. Ascaroside signaling in *C. elegans*. *WormBook.* 1-22, doi:10.1895/wormbook.1.155.1, (2013).

23 Narayan, A. *et al.* Contrasting responses within a single neuron class enable sex-specific attraction in Caenorhabditis elegans. *Proc Natl Acad Sci U S A.* **113** (10), E1392-1401, doi:10.1073/pnas.1600786113, (2016).

24 Srinivasan, J. *et al.* A blend of small molecules regulates both mating and development in *Caenorhabditis elegans*. *Nature.* **454** (7208), 1115-1118, doi:10.1038/nature07168, (2008).

25 Sammut, M. *et al.* Glia-derived neurons are required for sex-specific learning in C. elegans. *Nature.* **526** (7573), 385-390, doi:10.1038/nature15700, (2015).

26 Sulston, J. E., Albertson, D. G. & Thomson, J. N. The Caenorhabditis elegans male: postembryonic development of nongonadal structures. *Dev Biol.* **78** (2), 542-576 (1980).

27 Hilliard, M. A. *et al.* In vivo imaging of C. elegans ASH neurons: cellular response and adaptation to chemical repellents. *The EMBO Journal.* **24** (1), 63-72, doi:10.1038/sj.emboj.7600493, (2005).

28 Evans, T. C. Transformation and microinjection. *WormBook.* doi:doi/10.1895/wormbook.1.108.1, (2006).

29 Cáceres, I. d. C., Valmas, N., Hilliard, M. A. & Lu, H. Laterally Orienting C. elegans Using Geometry at Microscale for High-Throughput Visual Screens in Neurodegeneration and Neuronal Development Studies. *PLOS ONE.* **7** (4), e35037, doi:10.1371/journal.pone.0035037, (2012).

30 Schrodel, T., Prevedel, R., Aumayr, K., Zimmer, M. & Vaziri, A. Brain-wide 3D imaging of neuronal activity in Caenorhabditis elegans with sculpted light. *Nat Methods.* **10** (10), 1013-1020, doi:10.1038/nmeth.2637, (2013).

31 García, L. R. & Portman, D. S. Neural circuits for sexually dimorphic and sexually divergent behaviors in Caenorhabditis elegans. *Curr Opin Neurobiol.* **38** 46-52, doi:http://dx.doi.org/10.1016/j.conb.2016.02.002, (2016).

32 Clokey, G. V. & Jacobson, L. A. The autofluorescent "lipofuscin granules" in the intestinal cells of Caenorhabditis elegans are secondary lysosomes. *Mech Ageing Dev.* **35** (1), 79-94 (1986).

33 Coburn, C. *et al.* Anthranilate Fluorescence Marks a Calcium-Propagated Necrotic Wave That Promotes Organismal Death in C. elegans. *PLOS Biology.* **11** (7), e1001613, doi:10.1371/journal.pbio.1001613, (2013).

34 Macosko, E. Z. *et al.* A Hub-and-Spoke Circuit Drives Pheromone Attraction and Social Behavior in C. elegans. *Nature.* **458** (7242), 1171-1175, doi:10.1038/nature07886, (2009).

35 Park, D. *et al.* Interaction of structure-specific and promiscuous G-protein-coupled receptors mediates small-molecule signaling in *Caenorhabditis elegans*. *Proc Natl Acad Sci U S A.* **109** (25), 9917-9922, doi:10.1073/pnas.1202216109, (2012).

Chapter 4C Multiple G Protein-Coupled Receptors Mediate ascr#8 Sensation

Summary

The ability of animals to sense their environment is critical to their survival. The nematode, *Caenorhabditis elegans*, relies on chemosensation to interpret their surroundings, which includes pheromones released by conspecifics. Sensed by male-specific neurons, the pheromone ascr#8 elicits an attractive response. Here, we show that this sensation is meditated by a group of G protein-coupled receptors enriched in the male-specific CEM neurons. Promoter-fusion analysis reveals expression in non-overlapping subsets of the sensory neurons, while RNAi-mediated knockdown and CRISPR/Cas9 gene editing confirm the role of *dmsr-12*, *srw-97*, and *srr-7* in the sensation of ascr#8. Phylogenetic analyses reveal conservation of these genes across the *Caenorhabditis* genus, with *srw-97* exhibiting species-specific enrichment of a closely related ortholog, *srw-98*, in a related species. Together these results increase our understanding of the mechanisms, and – along with the work in **Chapter 6** – the evolution of sex-specific pheromone sensation.

Introduction

The ability of an organism to find a mate is critical to the survival of a species. Many species utilize small molecule pheromones to signal mate location [1,2], sexual maturity [3,4], and receptivity [5,6]. The nematode, *Caenorhabditis elegans*, communicates with conspecifics almost exclusively through the use of pheromones called ascarosides [7,8]. Ascarosides signal a host of environmental and developmental information, including the sexual maturity and location of potential mates [1,4].

Ascaroside #8 (ascr#8) is unique among the ever-growing class of small molecule pheromones, in that it contains a *p*-aminobenzoic acid moiety on its terminus [2,9]. Released by sexually mature hermaphrodites, ascr#8 serves to attract males as a mating pheromone[1]. Previous studies have shown through both laser and genetic ablation experiments that the sensation of ascr#8 occurs solely through the CEM neurons located in the head region of the male nervous system [1]. These male-specific neurons pose an interesting model in the *C. elegans* nervous system, as they are one of the few radially symmetric classes of sensory neurons (IL1 and IL2 being the other sets) [10-12]. Both electrophysiology and calcium imaging studies have shown that the neural dynamics of the CEM neurons in sensing ascr#8 (and another mating pheromone, ascr#3) are extremely variable from animal to animal [1,13]. However, unlike the stochastic asymmetry observed in the AWC chemosensory neurons [14], the genetic regulators of the CEM variability have yet to be uncovered.

In order to more fully understand the genetic mechanisms, we performed single-cell RNAseq on the male-specific CEM neurons. Within this dataset, we uncovered enriched genes encoding G protein-coupled receptors (GPCRs). Given that all ascaroside receptors identified to date have been GPCRs [15-20], we investigated whether any of these enriched genes play a role in male *C. elegans* sensation of ascr#8. We identified two previously uncharacterized GPCRs, *srw-97* and *dmsr-12*, expressed in non-overlapping subsets of the CEM neurons, which contribute to proper ascr#8 sensation. Further phylogenetic

analyses suggest that *srw-97* may be unique to *C. elegans,* as a result of a gene duplication within the species evolutionary history.

Results

The Transcriptomic Landscape of the CEM Neuron is Variable

Individual CEM neurons were isolated from *C. elegans* expressing an integrated GFP labeling extracellular vesicle-releasing neurons (EVNs, p*pkd-2*::GFP), as previously described [1,21,22]. Cells were separated by anatomical identity (i.e., CEM dorsal left (DL), dorsal right (DR), ventral left (VL), and ventral right (VR)), and cDNA libraries were constructed.

Table 5. Unique Gene Counts Per CEM Cell

Cell Type	Gene Count
CEM DL	105
CEM DR	98
CEM VL	20
CEM VR	639

Counts per CEM cell type of genes expressed at least two times higher in a given CEM cell types than other CEM cell types

Enriched genes in each CEM neuron were identified (see ***Methods***), and genes expressed at least two times higher in a given CEM type were isolated and annotated for GO terms. A variety of gene counts were identified between the CEM neurons, ranging from 20 genes enriched in CEM VL to over 600 in CEM VR (**Table 5, Supplementary Table 8, Supplementary Table 9**). The dorsal CEM were more consistent, expressing 98 and 105 enriched genes in the right and left neurons, respectively (**Table 5, Supplementary Table 10, Supplementary Table 11**). Although uniquely mapped reads ranged from 1.9 to 3.8 million, and the alignment rates with each CEM neuron, the two were not correlated (**Supplementary Table 4**). The alignment rates ranged from 19.73%

to 48.01%, with an average of 10,554 genes being detected in each neuron (**Supplementary Table 5**).

Five genes encoding G protein-coupled receptors were expressed at enrichment levels of four times greater than the other CEM neurons. Of these (*seb-3*, *srr-7*, *srw-97*, *dmsr-12*, *srd-32*), four remained uncharacterized. SEB-3 has previously been shown to play roles in locomotion, stress response, and ethanol tolerance [23]. DMSR-12 is related to DAF-37 [24], a previously identified ascaroside receptor [20], although it is more closely related to DMSR-1, a neuropeptide receptor – and distantly, SRW-97 [24]. SRD-32 belongs to the edge of the SRD phylogeny – which is in and of itself a basal and divergent family of the STR superfamily – [24], while SRR-7 belongs to the one of the smallest families of *C. elegans* chemoreceptors (outside of the single family member, *srn-1*, and the *srm* family, which encodes 5 chemoreceptor genes [24]).

Table 6. Enrichment levels of candidate GPCR genes in CEM neurons.

Gene	CEM DL	CEM DR	CEM VL	CEM VR	Max CEM
pkd-2	1.30	0.09	0.25	0.77	143
seb-3	0.15	0.31	0.23	**3.25**	6.50
dmsr-12	**4.96**	0.06	0.04	0.11	4.96
srd-32	**1.62**	0.38	0.23	0.62	4.33
srw-97	0.14	0.27	0.18	**3.67**	5.50
srw-98	0.27	0.64	0.45	**1.57**	2.75
srr-7	0.16	0.26	**1.90**	0.53	6.33
trf-1	0.00	0.00	0.00	226.28	226.28

Enrichment levels displayed as normalized count within a single CEM cell type over the normalized count in the remaining three CEM neurons. Max CEM is the enrichment in all four CEM neurons over the remainder of the animal. The CEM with highest enrichment of each GPCR gene are denoted by bolded-underlined values.

seb-3 and *srw-97* exhibited similar enrich profiles across the CEM, displaying similar enrichment levels in CEM VR (approximately 3.5-fold enrichment) (**Table 6, Figure 34B**). The gene *dmsr-12* was nearly five-fold enriched in CEM DL, while *srd-32* was only 1.62-fold enriched (**Table 6, Figure 34A**). The distantly related *srr-7* was enriched only in the CEM VL neurons, and only 2-fold enriched (**Table 6, Figure 34B**). Similarly, other labs have found *srr-7* to be enriched in *C. elegans* ciliated neurons by transcriptomic analyses [11].

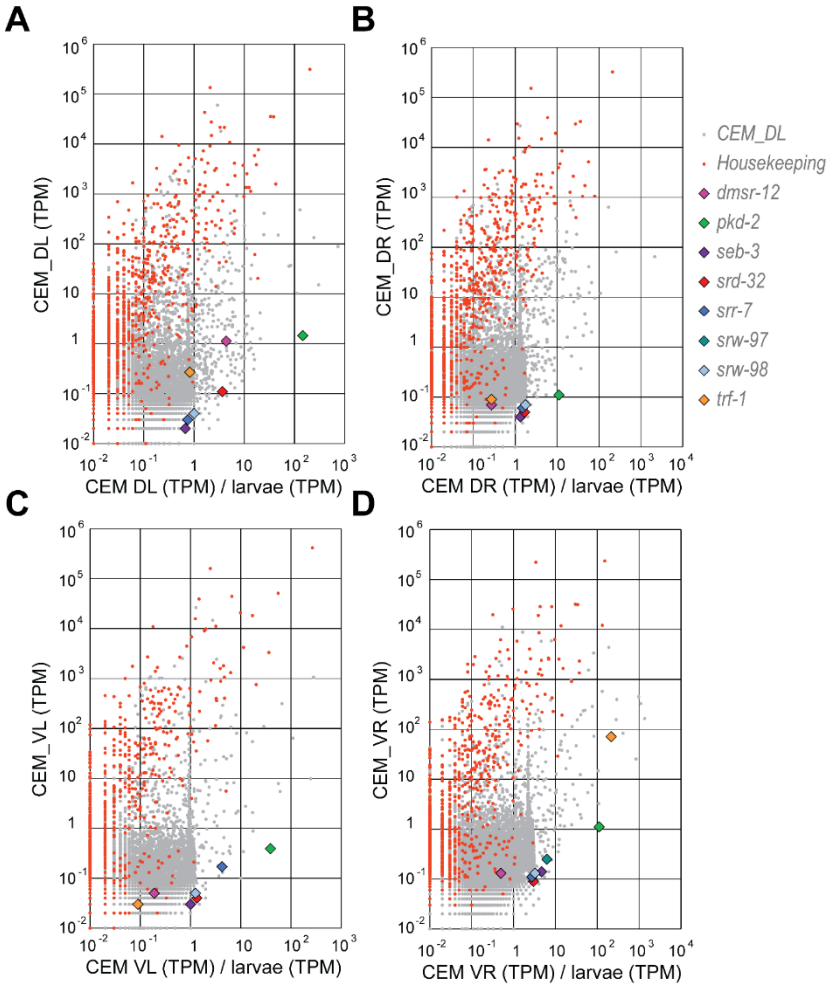

Figure 34. Transcriptomic landscapes of the CEM neurons.
(A-D) TPKM plots of individual CEM DL **(A)**, CEM DR **(B)**, CEM VL **(C)**, and CEM VR **(D)** neurons. X-axes display enrichment in individual CEM neurons compared to whole larvae, while the Y-axes display total transcript counts (TPM). Genes of interest are denoted by colored symbols, defined in the legend.

CEM-specific Receptor Expression Patterns

In order to confirm the transcriptomic data, GFP fusions were generated for the five receptor genes [25]. Approximately 3 kb of promoter region upstream of the start codon was included in the constructs, along with the majority of the coding sequence (**Supplementary Table 12**) containing GFP extracted from the Fire Kit vector pPD95.75 [25]. *pha-1;lite-1;him-5* animals were injected with reporter constructs and a co-injection marker of pBX (*pha-1*(+)). Strains were generated, and GFP positive males were imaged

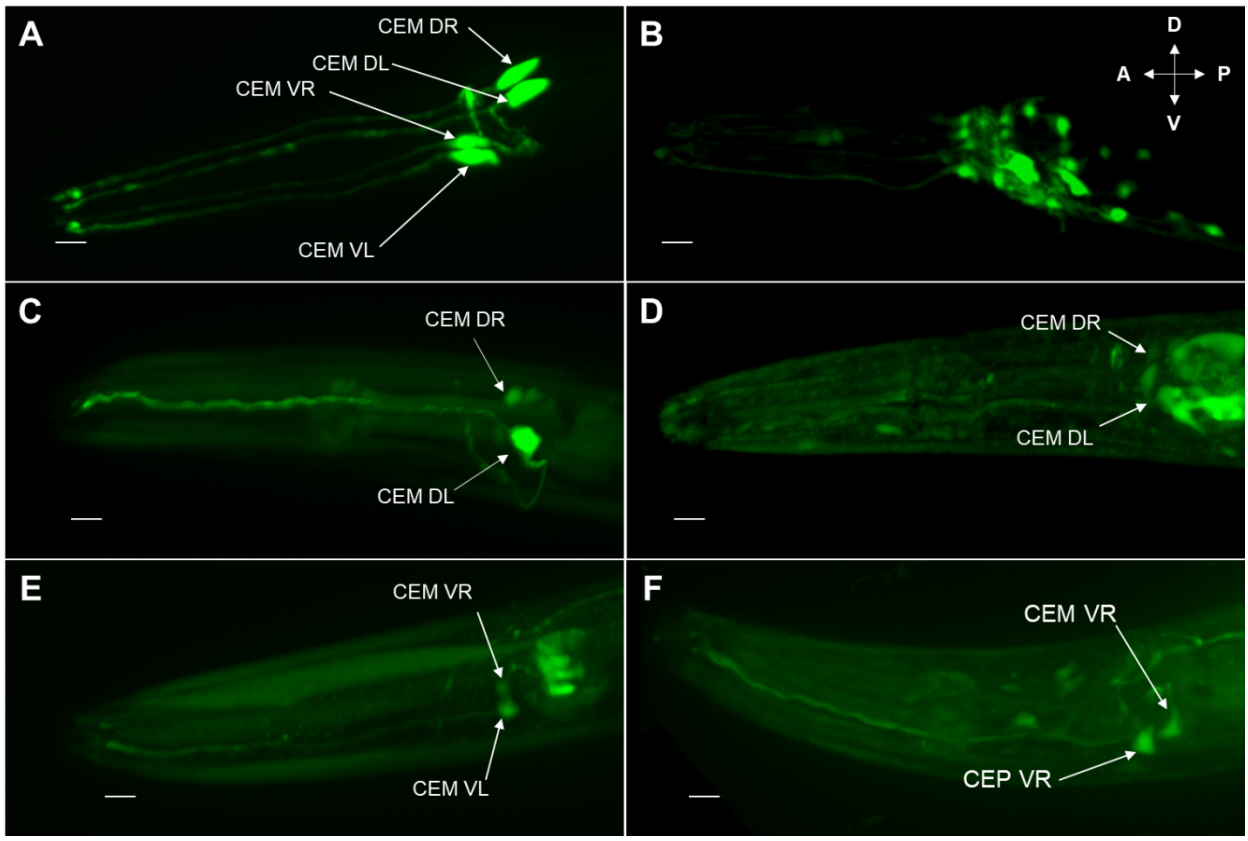

Figure 35. Expression profiles of CEM-enriched G protein-coupled receptor genes of interest.
GFP fusions of GPCR genes enriched in the CEM neurons. **(A)** A previously published CEM reporter, p*pkd-2*::GFP. **(B)** p*seb-3*::GFP, matching previously published expression, with no discernable enrichment in the CEM. **(C)** *dmsr-12*::GFP is strongly expressed in the CEM DL neuron, as well as the CEM DR soma. **(D)** *srd-32*::GFP is weakly expressed in the somas of CEM DR and DL. **(E)** *srw-97*::GFP is expressed in both CEM VR and VL, with localization in the cilia as well as the soma. **(F)** *srr-7*::GFP is expressed in CEM VR, both the soma and cilia, as well the cilia of a neighboring neuron, presumably CEP VR. White bars denote cilia region of CEM dendrites. Dorsal/ventral axes and anterior/posterior directions shown in **(B)**. Scale bars denote distal, cilia region.

for expression at 63x (**Figure 35**). An integrated p*pkd-2*::GFP line was used a CEM-specific control (**Figure 35A**).

The previously characterized GPCR, *seb-3*, displayed a non-CEM specific expression pattern matching that previously described (**Figure 35B**) [23]. The remainder of the receptors investigated displayed expression patterns similar to their transcriptomic enrichment: *dmsr-12* was heavily enriched in CEM DL (**Figure 35C**), but also exhibited CEM DR expression; *srd-32* was found faintly in both dorsal CEM neurons (**Figure 35D**); *srw-97* was found in both ventral CEM, with slightly higher expression in CEM VL (**Figure 35E**); and *srr-7* was found in only CEM VR (and one other neuron, tentatively CEP VR) (**Figure 35F**). With the exception of *srd-32*, all of the receptors displayed sub-cellular localization profiles that included the sensory cilia (**Figure 35, white bars**). However, this may be an artifact of the *srd-32*::GFP construct, as only 52% of the *srd-32* coding sequence was included in the transgene (**Methods, Supplementary Table 12**).

Non-GPCR genes were also found to be heavily enriched in single CEM neurons, such as *trf-1*, a TNF Receptor homolog with predicted zinc ion binding activity (wormbase.org) and EVN-specific promoter [11], offering an option outside of the canonical *pkd-2* and *klp-6* promoters (**Supplementary Figure 13**) [26,27]. This is supported by previous work which found *trf-1*::GFP expression in the CEM, HOB, and RnB neurons [11].

Further elucidation of CEM-enriched expression patterns will likely uncover novel promoter profiles, allowing for targeted interrogation of CEM transcriptomic profiles. However, given the unique expression profiles of the most enriched CEM-specific GPCRs, we then chose to interrogate the functions of these receptors in relate to the sensation of CEM-sensed mating pheromone, ascaroside #8 [1].

RNAi-mediated knockdown of CEM Receptors

To investigate the role of CEM enriched receptors in ascr#8 sensation, we utilized RNAi to knockdown target receptors in a strain hypersensitive to neuronal RNA interference,

nre-1;lin-15B [28,29]. This strain was first crossed into a *him-5* background, to allow for male phenotyping, as the attraction to ascr#8 is sex-specific. Young adults were then grown on NGM agar plates containing 1 mM IPTG to induce expression of the dsRNA. Young adult males of the subsequent generation were then assayed for their response to ascr#8 after developing on either a control vector (pL4440) or targeted dsRNA vector.

In order to first confirm that RNAi knockdown could affect behavioral phenotypes, we first fed animals M02B7.3 (*α-osm-3*) and B0212.5 (*α-osm-9*) RNAi clones from the Ahringer Library [30,31]. Using a previously described Spot Retention Assay, we then assayed *osm-3* and *osm-9* knockdown animals for their behavioral dwell time in ascr#8 (**Figure 36A**). Animals fed *osm-3* dsRNA exhibited a significant defect in their response to ascr#8, similar to that seen in genetic knockouts (**Figure 36B**). Meanwhile, animals fed *osm-9* exhibited only a slight defect in their ability to respond to ascr#8. Given *osm-9*'s lack of defect, this suggests that the calcium channel subunit does not play a role in ascr#8 signaling. Conversely, the RNAi clone used in these experiments may result in insufficient knockdown of the *osm-9* mRNA. The successful abrogation seen in *osm-3* knockdown however suggests that RNAi can be utilized to affect behavioral effects related to gene expression.

We then proceeded to feed animals dsRNA clones targeting receptors of interest, namely: T18H12.5 (*α-srd-32*), H34P18.1 (*α-dmsr-12*), ZC204.15 (*α-srw-97*), and T01G5.4 (*α-srr-7*). The *α-srd-32* clone is the only one not available, and therefore a clone from the Vidal Library was utilized [32]. These clones are in the same backbone vector, allowing for the same control vector to be used. We did not target *seb-3*, despite its enrichment in CEM transcriptomes, as it is expressed in a number of other cells outside of the CEM (**Figure 35B**), and any defect could not be definitely confirmed as a CEM-specific defect in SEB-3.

Knockdown of *srd-32* resulted in no defect of ascr#8 behavioral response (**Figure 36C**). The GFP fusion only incorporated half of the protein product codons **Supplementary Table 12**). While *srd-32* was not observed in the cilia of the CEM neurons, this truncation

which may affect the localization of the gene (**Figure 35D**). *dmsr-12* feeding resulted in a visual decrease, but no significant defect was observed (**Figure 36C**). Meanwhile,

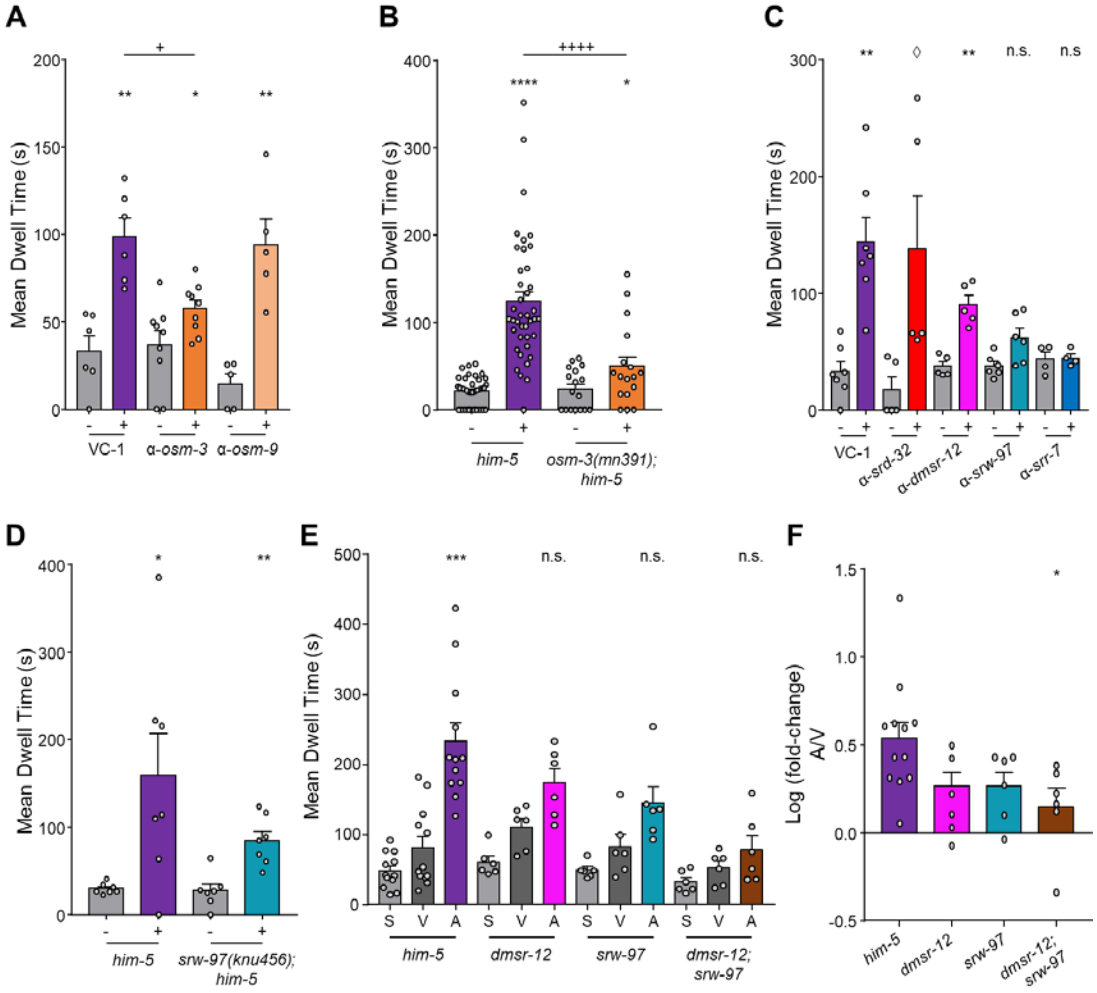

Figure 36. DMSR-12 and SRW-97 are involved in ascr#8 sensation.
(A-C) RNAi-meditated knockdown of chemosensory genes affects behavior. **(A)** RNAi knockdown of the kinesin motor, *osm-3*, and the TRPV channel, *osm-9*. $n \geq 5$. **(B)** Genetic null *osm-3* mutants are unable to respond to ascr#8. $n \geq 17$. **(C)** RNAi knockdown of GPCRs of interest (*srd-32*, *dmsr*-12, *srw-97*, and *srr-7*), as well as an empty vector control (VC-1). $n \geq 4$. **(D-F)** CRISPR-generated knockouts of *dmsr-12* and *srw-97* result in defective ascr#8 response. **(D)** *srw-97(knu456);him-5(e1490)* animals exhibit a visual, yet not statistically significant decrease in ascr#8 dwell time, using the Spot Retention Assay. n =7. **(E, F)** Single Worm Assay of *him-5*, *dmsr-12*, *srw-97*, and *dmsr-12;srw-97* animals; **(E)** Raw mean dwell time and **(F)** Log(fold-change) A/V. The double mutant results in complete loss of ascr#8 response. $n \geq 6$. Error bars denote SEM. **(A-D)** Vehicle (-) vs. ascr#8 (+) comparisons performed via paired t-tests or Wilcoxon Matched Pairs Ranked Sign Tests, dependent on a Shapiro-Wilk Normality Test. **(C)** ◊ $p = 0.0625$. **(E)** Internal strain comparisons performed by Repeated Measures ANOVA ($p < 0.05$), followed by a Bonferroni's multiple corrections test. n.s, $p > 0.05$, not significant; * $p < 0.05$, ** $p < 0.01$, *** $p < 0.001$, **** $p < 0.0001$. **(A-F)** Comparison across strains, One-Way ANOVA ($p < 0.05$) followed by a Dunnett's multiple corrections test. **(A, B)** + $p < 0.05$, ++++ $p < 0.0001$, **(F)** * $p < 0.05$.

knockdowns of *srw-97*, and *srr-7* all exhibited abrogated ascr#8 responses (**Figure 36C**).

We then utilized CRISPR genome editing to generate null mutants for *srw-97* and *srr-7* via Knudra Transgenics (See **Methods** for more details on generation of the null mutants). A null mutant for *dmsr-12,* (tm8706), was available from the National BioResource Program in Japan. The novel null mutations were generated in *him-5* animals, to allow for males to be tested, while the *dmsr-12(tm8706)* allele was first crossed into a *him-5* background. Difficulties in backcrossing *srr-7(knu507)* prevented accurate assaying of behavioral defects (**Supplementary Figure 14**), although a similar defect to that observed in the RNAi knockdown is likely recapitulated.

The spot retention assay was then used to test backcrossed *srw-97(knu456);him-5(e1490)* animals for their ability to respond to ascr#8 (**Figure 36D**). The defect was similar to that observed via RNAi-mediated knockdown.

CRIPSR-generated Null Mutants of Candidate Receptors

In order to better understand the roles of these GPCRs in ascr#8 sensation, we then utilized a novel assay developed in our lab in which single worms are assayed for their responses to ascr#8 (**Chapter 3B**). Worms were raised and prepared in an identical manner to the spot retention assay but were assayed in single wells of a 48-well tissue culture. See *Methods* for more detailed description of the assay and effects on statistical power.

As a wild-type control, *him-5* animals respond attractively to ascr#8 in the new assay, just as they did in the spot retention assay (**Figure 36D, E, Supplementary Figure 15**). Individual mutants of *dmsr-12* and *srw-97* displayed partial defects in their ascr#8 attraction: *(1)* their ascr#8 dwell time was no different than that of vehicle (**Figure 36E, Supplementary Figure 15**), while *(2)* their increase over the vehicle was no different than that of *him-5* (**Figure 36F, Supplementary Figure 15**).

Given that *dmsr-12* is expressed in the dorsal CEM, and *srw-97* is found in the ventral CEM (**Figure 35**), we hypothesized that some activity may be retained in single mutants, with the opposing CEM pair "saving" the ability to respond to ascr#8. We then generated a double mutant for *dmsr12* and *srw-97*, and assayed animals for their ability to respond to ascr#8. These animals exhibited a full loss of ascr#8 activity, both in their ability to be attracted (**Figure 36E, Supplementary Figure 15**) and the increase in time spent in ascr#8 compared to vehicle (**Figure 36F, Supplementary Figure 15**).The receptors were found to be specific to ascr#8 sensation, as there was no defect observed in response of the double mutants to ascr#3 (**Supplementary Figure 16**).

Together, these data suggest that multiple GPCR receptors are present in the CEM that contribute to sensation of ascr#8. The two candidate receptors, *dmsr-12* and *srw-97* are present in non-overlapping subsets of the CEM neurons, and therefore may be functioning as a members of heterodimeric receptor pairs. It is possible that the heterodimeric partner will be expressed in all four CEM, as more promiscuous CEM-ascaroside sensor to the specific ascr#8 sensors, *dmsr-12* and *srw-97* [20].

Phylogenetic Analyses of ascr#8 Receptors Reveals Likely Gene Duplication Events

Pheromone-mediated mate attraction machinery is critical for species survival. However, *C. elegans* is a self-fertile hermaphrodite: male involvement in mating is useful in creating genetic diversity but is not required for species propagation. In order to further understand why *C. elegans* hermaphrodites have retains such a robust ability to attract potential mates, we investigated the evolution of the receptor, *srw-97*, which is necessary for proper ascr#8 sensation (**Figure 36**).

The *C. elegans srw-97* (*Cel-srw-97*) coding sequence was compared across the genomes of other *Caenorhabditis* genome assemblies for the presence of paralogs using OrthoFinder (**Figure 37A**). The closely related gene, *Cel-srw-98*, underwent a species-specific expansion within *C inopinata*. However, more closely related species to C. elegans (such

as *C. briggsae* or *C nigoni*) have closely related paralogs to the *Cel-srw-97* gene. The cDNA sequences of both *srw-97* and *srw-98* are 66.2% identical, while their amino acid sequences are 73.9% similar (only 57.1% identical) [33].

In contrast, the other candidate ascr#8 receptor, *dmsr-12*, has not undergone any species-specific expansion (**Figure 37B**). Outside of the *C. elegans* genome, a slight reduction in gene paralogs is seen. Meanwhile, the *srr-7* family is remarkably conserved

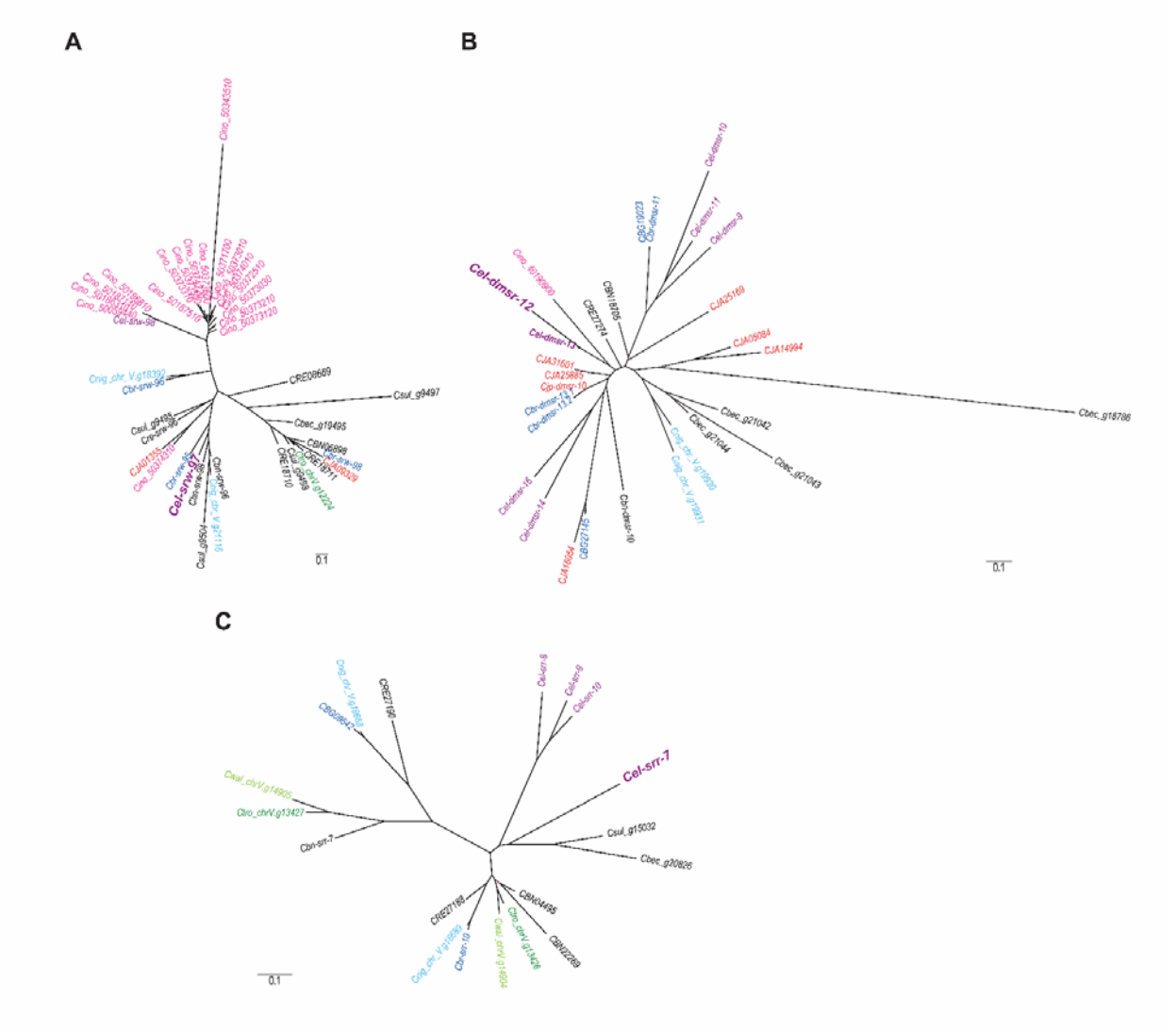

Figure 37. Phylogenetic analyses of ascr#8 Receptors.
Phylogenetic analysis of ascr#8-receptor candidate paralogs across the *Caenorhabditis* genus. **(A)** The phylogeny of *srw-97* reveals a *C. inopinata*-specific amplification of *srw-98*. The phylogenies of **(B)** *dmsr-12* and **(C)** *srr-7* show conserved counts of orthologs across the genus. Genes for *C. elegans* denoted in purple; *C. inopinata* in pink, *C. nigoni* in light blue, *C. briggsae* in dark blue, *C. japonica* in red, *C. wallacei* in light green, and *C. tropicalis* in dark green. Distance reference bars (0.1) depict substitutions per site.

across the genus, with only a handful of paralogs present in any species analyzed (**Figure 37C**).

Discussion

Mating pheromones play a major role in the mating motifs of many animals. Hermaphrodites of the nematode, *C. elegans*, utilize a small molecule pheromone, ascaroside #8 to attract potential male mates [1,2]. While this the ascaroside class of small molecule pheromones utilized by nematodes is rapidly being elucidated (currently there are over 230 known ascaroside structures (http://smid-db.org/)), the sensory machineries regulating these signals remains largely unknown, although the sensory components for a select few ascarosides have been elucidated at the cellular [15-17], receptor [18-20], and/or sub-cellular levels [34].

dmsr-12 and srw-97 are likely CEM-Specific Receptors of ascr#8

Here, we identify two novel G protein-coupled receptors as active, required components in the sensation and behavioral response to the mating pheromone, ascr#8. Transcripts for the two GPCRs, *dmsr-12* and *srw-97*, are enriched in single CEM neurons (**Table 6)**, and they express in non-overlapping subsets of the male-specific chemosensory neurons (**Figure 35**). This is similar, but not identical to the one-neuron-one-receptor rule adhered to by mammals. There are other receptors present in these same neurons that must navigate a vast and ever-changing array of environmental cues, such as the widely expressed *seb-3* (**Figure 35B**) [23].

Previous work by the Riddle lab identified two receptors for ascr#2 in the ASK neuron: DAF-37 and DAF-38. While both are required for proper ascr#2 response, only DAF-38 is involved in the sensation of other ascarosides [20]. This heterodimeric complex of a structure specific receptor coupled with a more promiscuous receptor may be a system utilized by *C. elegans* to allow for broad, yet accurate detection of a vast array of ascaroside compounds. Multiple ascarosides are sensed by the male specific CEM neurons,

including ascr#8 and ascr#3 [1]. The two receptors identified here may function as ascr#8-specific receptors, as *dmsr-12; srw-97* double mutant animals do not exhibit defective responses to ascr#3 (**Supplementary Figure 16**). and dimerize with a more "CEM-specific" receptor that senses both ascr#8 and ascr#3, such as is seen in DAF-38's ability response to ascr#2, ascr#3, and ascr#5 [20].

The role of DAF-37 as an ascr#2-specific receptor further supports our hypothesis, as the dorsally expressed *dmsr-12* is related to DAF-37 [24]. The ventral CEM-receptor, *srw-97* falls within the same large falling GPCRs as well [35], while the promiscuous DAF-38 does not [24].

Confirmation of the roles of these receptors in ascr#8 sensation will require rescue via generation of transgenic animals. Given the loss of *srw-97* (*srw-98*) paralogs in the genome of another hermaphroditic species, *C. tropicalis*, its lack of ascr#8 behavioral response [36] (**Chapter 6**), and the conserved genomic regulatory elements within *Caenorhabditis* [37,38], it would be interesting to express a *Cel-srw-97* construct in *C. tropicalis* to see if it confers ascr#8 behavioral activity.

Further dissection of the ascr#8-receptor interaction can then be carried out using a biochemical ascr#8 probe (as in **Chapter 5**) [39]. Following confirmation that a probe retains bioactivity in wild-type animals, as well as *dmsr-12;srw-97* mutant animals, a co-immunoprecipitation experiment can be performed to validate the binding partner of ascr#8 [20].

C. elegans evolved its robust behavioral response to ascr#8 through gene duplication events

C. elegans exhibits the most robust attractive response to ascr#8 among *Caenorhabditis* nematodes [36] (**Chapter 6)**, despite well-conserved gene sequences for *srw-97*, *dmsr-12*, and *srr-7* (**Figure 37**).

Approximately 90% of *srw* receptors in the *C. elegans* genome are present in clusters on the chromosomal arms of chromosome V [24] (including *srw-98*, as well as the non-srw receptor candidates *dmsr-12*, *srr-7*, and *srj-27*), reminiscent of the functional clustering observed in the organization of reproductive genes [40]. The coding sequence for *srw-98* is flanked upstream by the coding sequence for the GPCR *srw-91*, and downstream by the pseudogene *srw-96*.

Meanwhile, *srw-97* is preset on Chromosome II, flanked by an ion transporter gene (*nhx-6*), an uncharacterized protein coding gene, and a DNA binding protein (*duxl-1*), adding further credence to the likelihood that it arose from a duplication event, as these genes are not functionally related to *srw-97* activity. Given that the other receptors active in the ascr#8 behavioral response (*dmsr-12* and *srr-7*) are present on Chromosome V, a role of functional clustering is likely. The placement of *srw-97* on Chromosome II would then have nothing to do with functional placement, instead having resulted as a byproduct of duplication.

Similar to *srw-97*, *srr-7* appears to be the result of a *C. elegans*-specific gene duplication event, along with *srr-8* and *srr-9* (**Figure 37C**). *srr-10* would appear to be the ancestral gene, with paralogs present in related species. All four *C. elegans* receptors are present on Chromosome V, in various clusters. Four of the ten *srr* genes (*srr-3*, *-5* [a pseudogene], *-6*, and *-8*) are sequentially placed on one of the chromosomal arms. Similarly, *srr-9* (a *C. elegans*-specific gene), is located immediately downstream of *srr-10*. The remaining four *srr* genes are "scattered" across the Chromosome, although only *srr-7* is clustered among other GPCR-encoding genes. It is flanked on the opposing strand by the likewise ventral CEM-enriched GCPRs, *srj-27* and *str-171*, with less than 1000 nucleotides between the coding sequences (**Supplementary Figure 17**).

Given a partially defective phenotype matching that of *srw-97*, and its expression in both dorsal CEM neurons compared to *srw-97*'s ventral expression, it is likely that *dmsr-12* serves a similar role as an ascr#8-specific CEM receptor. Also located on Chromosome

V, *dmsr-12* is flanked by three other *dmsr* genes: *dmsr-16* upstream, and *dmsr-11* and *dmsr-10* downstream. Other than sequence homologies, there is little else known about these related receptors, although the downstream pair of genes (*dmsr-11* and *dmsr-10*) exhibited slight enrichment in the ventral CEM in our RNAseq dataset (**Supplementary Table 8, Supplementary Table 9**).

Related to *dmsr-12*, DAF-37 has been shown to play a role in the sensation of another ascaroside, ascr#2 [20]. However, another *dmsr* receptor, *dmsr-1*, has been shown to bind an internally expressed and released neuropeptide, the FMRFamide-like peptide, FLP-13 [41]. However, given that other recently discovered ascaroside receptors have been shown to be the results of co-option on internal ligand receptors [15], *dmsr-12* may be yet another receptor that fits this paradigm.

SRR-7: A Receptor Regulating the Neural Activity of a Sensory Network

The gene coding the GPCR is expressed in a single CEM neuron, CEM VR. However, RNAi knockdown of this gene completely abolishes the ability of male *C. elegans* to respond (**Figure 36C**). However, we have previously shown ablation of the remaining three CEM neurons, with only CEM VR remaining to sense ascr#8 does not result in as robust an ablation of behavioral response [1]. In fact, when CEM VR was the only neuron present, males exhibited enhanced attraction to extreme concentrations of ascr#8.

This suggests that *srr-7* is not acting as the sole binder of ascr#8. As well as being expressed only in CEM VR, it is expressed in a neighboring, non-CEM neuron, which we currently hypothesize as CEP VR (**Figure 35F**). In this neuron, *srr-7* is localized strictly to the soma, suggesting a role in neuron-to-neuron signaling, as opposed to cilia-mediated sensation. If *srr-7* does indeed play a role in synaptic signaling, this may explain the complete loss of ascr#8 behavioral response in knockdown studies. The two genes adjacent to *srr-7*, *srj-27* and *str-171*, show similar enrichment profiles in CEM VL (**Supplementary Figure 17**). It will be extremely interesting to confirm the expression

profiles of these two genes, and to see if similar phenomena are observed: both in terms neighboring CEP expression, and CEM-network regulation (observed via complete loss of ascr#8 response).

The CEM Sensory Network is a Complex System of Four Neurons

Together, the data presented in this chapter pose a model of ascr#8 sensation through GPCR signaling in the CEM sensory neuron network. Through study of the transcriptomes of the four CEM neurons, we have identified candidate receptors of ascr#8, in the forms of *srw-97* and *dmsr-12*.

Each of these receptors is present in non-overlapping CEM neurons (**Figure 35C, E**), granting the ventral and dorsal CEM neurons the ability to sense ascr#8, respectively. Each of these likely acts as an ascr#8-specific receptor (**Figure 36E, F; Supplementary Figure 16**), potentially work in concert with a "general CEM-ascaroside receptor" – similar to the DAF-37-DAF-38 heterodimeric ascr#2 sensation machinery [20].

Other species have retained the ability to respond attractively to ascr#8, albeit at must lower levels [36] (see **Chapter 6**). This is likely due to the ancestral *srw-97* gene, *srw-98* (**Figure 37A**). Whether *srw-98* also plays a role in ascr#8 sensation however – or whether it forms a heterodimer with *srw-97* – remains to be elucidated.

Adding complexity to this sensory network is the GPCR *srr-7*, which, while able to be seen in the cilia of CEM VR, does not seem to be playing a direct role in ascr#8. Knockdown of the receptor results in a different phenotype than ablation of the CEM VR neuron (**Figure 36**) [1]. It is possible, therefore, that *srr-7* is acting as an internal CEM-network-regulator, priming the CEM network to be able to respond to ascr#8. The as-yet untested receptors, *srj-27* and *str-171*, may be playing similar roles in CEM VL. Should this be the case, there will likely be dorsal CEM network regulators as well. Calcium imaging of *srr-7 lof* animals will reveal critical information into the role of the receptor.

In all, the CEM network is therefore comprised of four, radially symmetric neurons, with dorsal and ventral GPCRs sensing ascaroside #8, and yet another receptor regulating the CEM network closer to the soma (**Figure 38**). Understanding this network will be furthered through continued dissection into the expression and function of CEM enriched receptors, as well as calcium imaging studies. However, the network will likely grow increasingly complex as other ascarosides which are not sensed by *dmsr-12* or *srw-97* (such as ascr#3, **Supplementary Figure 16**) are investigated.

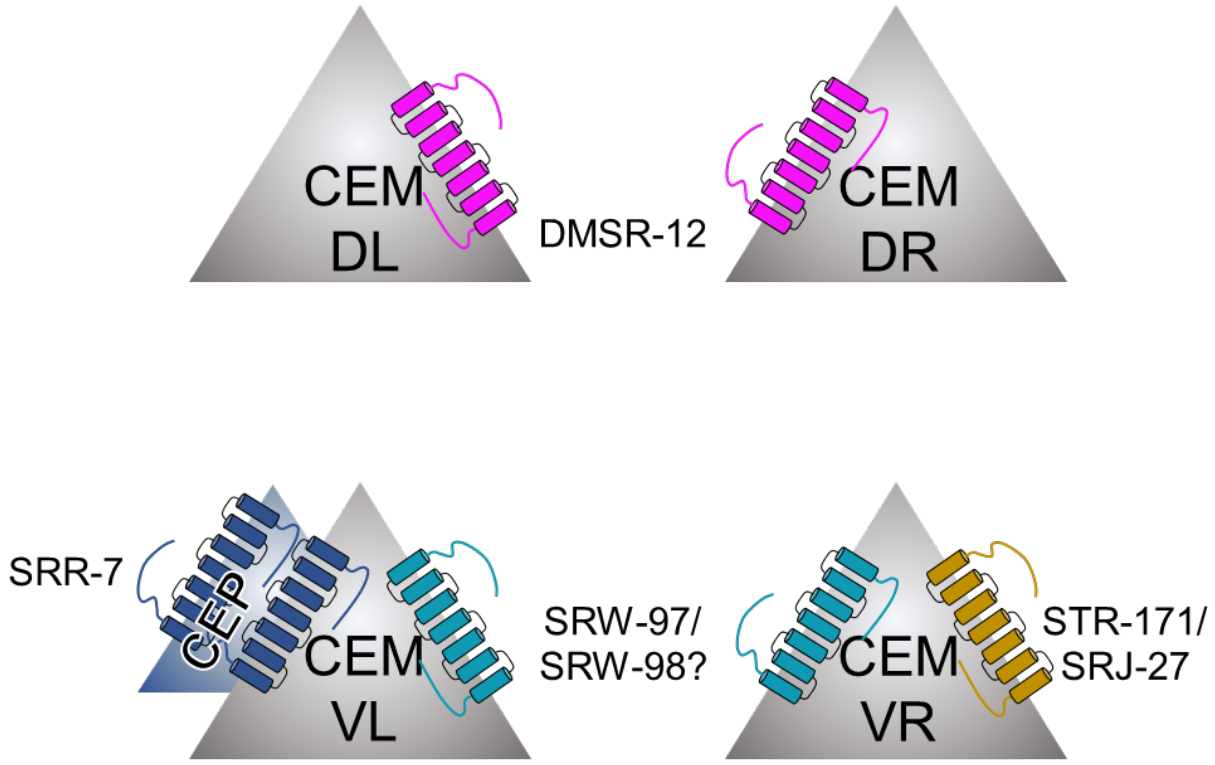

Figure 38. The CEM sensory network is complex
The four CEM neurons express many receptors, some of which function in the cilia of only the dorsal or ventral CEM, while others are functional in the soma. The machineries depicted in this circuit are specific to ascr#8 and are not shown to be involved in ascr#3 sensation.

Acknowledgements.

Science does not occur in a vacuum. Many of these studies would have been impossible without the help of collaborators. This project began with the isolation of individual CEM neurons from living *C. elegans* animals. Therefore, I must also thank Dr. Meenakshi Doma for isolating those neurons and generating the RNA/cDNA libraries that Erich was able to use and analyze for this work. I would like to thank Dr. Erich Schwarz, at Cornell University, for his contributions, including analysis of the RNAseq data, generation of the TPKM plots, and the phylogenetic analyses of the receptors. Dr. Hee June Choi's assistance was critical in being able to obtain the GFP images. I would also like to thank Knudra Transgenics (now part of NemaMetric Inc.) for their part in injecting the promoter-GFP fusions and generation of homozygotic strains for the CRISPR edited *srw-97*, *srr-7*, and *srw-98* alleles. I also thank the Walhout Lab at UMass Medical School (UMMS) for supplying the Ahringer Library RNAi clones, and the Ambros Lab 9also at UMMS) for the Vidal Library clone. I also need to thank Dr. Paul Sternberg (CalTech) for letting my PI, Dr. Jagan Srinivasan, take this work with him to WPI when he left his post-doctoral training for a faculty position. Annalise Robidoux, and undergraduate in the lab, generated the *dmsr-12;srw-97* double mutant, and performed the behavioral assays and analysis for those data. The strains used were provided by the CGC (which is funded by NIH Office of Research Infrastructure Programs (P40 OD010440), the National BioResource Project, Knudra Transgenics, Erich Schwarz, and Rene Garcia. This work was supported in part by the NIH (R01DC016058 to JS) and startup funds from WPI to JS.

Methods

Single Cell Isolation and cDNA Library Construction

Microdissection and single-cell RT-PCR of individual CEM_DL, CEM_DR, CEM_VL, and CEM_DR neurons was performed essentially as described [42]. For all four neuronal types, single-end 50-nucleotide (nt) RNA-seq was performed on an Illumina HiSeq 2000. To identify so-called housekeeping genes and genes primarily active outside the nervous system, we compared results from CEM_DL, CEM_DR, CEM_VL, and CEM_DR to published single-end 38-nt RNA-seq data from mixed-stage whole *C. elegans* hermaphrodite larvae [42].

TPKM Analysis

Reads were quality-filtered as follows: neuronal reads that failed Chastity filtering were discarded (Chastity filtering had not been available for the larval reads); raw 38-nt larval reads were trimmed 1 nt to 37 nt; all reads were trimmed to remove any indeterminate ("N") residues or residues with a quality score of less than 3; and larval reads that had been trimmed below 37 nt were deleted, as were neuronal reads that had been trimmed below 50 nt. This left a total of 21,554,964 to 24,546,096 filtered reads for analysis of each neuronal type, versus 23,369,056 filtered reads for whole larvae (**Supplementary Table 4**).

We used RSEM version 1.2.17 [43] with bowtie2 version 2.2.3 [44] and SAMTools version 1.0 [45] to map filtered reads to a *C. elegans* gene index and generate read counts and gene expression levels in transcripts per million (TPM). To create the *C. elegans* gene index, we ran RSEM's *rsem-prepare-reference* with the arguments '*--bowtie2 --transcript-to-gene-map*' upon a collection of coding DNA sequences (CDSes) from both protein-coding and non-protein-coding *C. elegans* genes in WormBase release WS245 [46]. The CDS sequences were obtained from *ftp://ftp.sanger.ac.uk/pub2/wormbase/releases/WS245/species/c_elegans/PRJNA13758/c_elegans.PRJNA13758.WS245.mRNA_transcripts.fa.gz* and *ftp://*

ftp.sanger.ac.uk/pub2/wormbase/releases/WS245/species/c_elegans/PRJNA13758/c_elegans.PRJNA13758.WS245.ncRNA_transcripts.fa.gz. For each RNA-seq data set of interest, we computed mapped reads and expression levels per gene by running RSEM's *rsem-calculate-expression* with the arguments '*--bowtie2 -p 8 --no-bam-output --calc-pme --calc-ci --ci-credibility-level 0.99 --fragment-length-mean 200 --fragment-length-sd 20 --estimate-rspd --ci-memory 30000*'. These arguments, in particular '*--estimate-rspd*', were aimed at dealing with single-end data from 3'-biased RT-PCR reactions; the arguments '*--phred33-quals*' and '*--phred64-quals*' were also used for the neuronal and larval reads, respectively. We computed posterior mean estimates (PMEs) both for read counts and for gene expression levels, and rounded PMEs of read counts down to the nearest lesser integer. We also computed 99% credibility intervals (CIs) for expression data, so that we could use the minimum value in the 99% CI for TPM as a robust minimum estimate of a gene's expression (minTPM).

We observed the following overall alignment rates of the reads to the WS245 *C. elegans* gene index: 48.01% for the CEM_DL read set, 28.19% for the CEM_DR read set, 40.75% for the CEM_VL read set, 19.73% for the CEM_VR read set, and 76.41% for the larval read set (**Supplementary Table 4**). A similar discrepancy between lower alignment rates for hand-dissected linker cell RNA-seq reads versus higher alignment rates for whole larval RNA-seq reads was previously observed and found to be due to a much higher rate of human contaminant RNA sequences in the hand-dissected linker cells [42]. We defined detectable expression for a gene in a given RNA-seq data set by that gene having an expression level of 0.1 TPM; we defined robust expression by that gene having a minimum estimated expression level (termed minTPM) of at least 0.1 TPM in a credibility interval of 99% (i.e., ≥ 0.1 minTPM). The numbers of genes being scored as expressed in a given neuronal type above background levels, for various data sets, are given in **Supplementary Table 5**. Other results from RSEM analysis are given in **Supplementary Table 6**.

We annotated *C. elegans* genes and the encoded gene products in several ways (**Supplementary Table 6**). For the products of protein-coding genes, we predicted classical signal and transmembrane sequences with Phobius 1.01 [47], regions of low sequence complexity with pseg (SEG for proteins, from *ftp://ftp.ncbi.nlm.nih.gov/pub/seg/pseg*) [48], and coiled-coil domains with ncoils (from *http://www.russell.embl-heidelberg.de/coils/coils.tar.gz*) [49]. PFAM 27.0 protein domains from PFAM [50] were detected with HMMER 3.0/hmmsearch [51] at a threshold of $E \leq 10^{-5}$. The memberships of genes in orthology groups from eggNOG 3.0 [52] were extracted from WormBase WS245 with the TableMaker function of ACEDB 4.3.39. Genes with likely housekeeping status (based on ubiquitous expression in both larvae and linker cells) were as identified in our previous work [42]. Genes were predicted to encode GPCRs on the basis of their encoding a product containing one or more of the following Pfam-A protein domains: 7tm_1 [PF00001.16], 7tm_2 [PF00002.19], 7tm_3 [PF00003.17], 7tm_7 [PF08395.7], 7TM_GPCR_Srab [PF10292.4], 7TM_GPCR_Sra [PF02117.11], 7TM_GPCR_Srbc [PF10316.4], 7TM_GPCR_Srb [PF02175.11], 7TM_GPCR_Srd [PF10317.4], 7TM_GPCR_Srh [PF10318.4], 7TM_GPCR_Sri [PF10327.4], 7TM_GPCR_Srj [PF10319.4], 7TM_GPCR_Srsx [PF10320.4], 7TM_GPCR_Srt [PF10321.4], 7TM_GPCR_Sru [PF10322.4], 7TM_GPCR_Srv [PF10323.4], 7TM_GPCR_Srw [PF10324.4], 7TM_GPCR_Srx [PF10328.4], 7TM_GPCR_Srz [PF10325.4], 7TM_GPCR_Str [PF10326.4], ABA_GPCR [PF12430.3], Sre [PF03125.13], and Srg [PF02118.16]. By this criterion, we identified 1,615 genes encoding GPCRs in the WS245 version of the *C. elegans* genome; this resembles a previous estimate of ~1,470 *C. elegans* genes encoding chemoreceptors and other GPCRs, identified through extensive computational and manual analysis [53]. The memberships of genes in orthology groups from eggNOG 3.0 [52] were extracted directly from WormBase WS245 with the TableMaker function of ACEDB 4.3.39. Genes with likely housekeeping status (based on ubiquitous expression in both larvae and linker cells) were as identified in our previous work [42]. Gene Ontology (GO) annotations for *C. elegans* genes were extracted from WormBase-

computed annotations in *ftp://ftp.wormbase.org/pub/wormbase/releases/WS245/ONTOLOGY/gene_association.WS245.wb.c_elegans*; human-readable text descriptions for GO term IDs were extracted from *term.txt* in the Gene Ontology archive *http://archive.geneontology.org/full/2014-07-01/go_201407-termdb-tables.tar.gz*.

GFP Reporter Construction

Reporter fusion constructs were generated using previously described techniques [25]. Approximately 2-3 kb of upstream promoter region of each gene was included in construct generation, as well as a portion of the coding sequence **Supplementary Table 12**). This was then fused to GFP (from the Fire Vector Kit plasmid, pPD95.75), via PCR fusion [25]. Primers were designed using Primer 3 and ordered from IDT (Integrated DNA Technologies). Primer sequences available in **Supplementary Table 14**. Successful fusion was confirmed via gel electrophoresis prior to injection.

Reporter fusion constructs were injected into the gonads of *pha-1(e2123ts);lite-1(ce314);him-5(e1490)* animals, along with a co-injection marker of pBX (*pha-1* (+)). In this manner, positive array animals will propagate normally at 20 °C. Strains were confirmed via GFP expression, with multiple array lines being generated per injection (See **Supplementary Table 13**). Injections were performed by Knudra Transgenics (now part of NemaMetrix), with strain isolation being performed in house.

Imaging

Animals were imaged for GFP expression using previously described techniques. In short, positive array young adult male animals were mounted on a 1% agarose pad and immobilized with sodium azide. Animals were then imaged on a spinning disk confocal microscope at 63x magnification. Z-stack imaging was performed, generating 3D reconstructions of the heads of the imaged animals. Central/optimal z-plane images were used to generate the images used to verify expression (**Figure 35**).

RNAi Feeding

VH624 (rhIs13 [*unc-119*::GFP + *dpy-20*(+)];*nre-1(hd20);lin-15B(hd126)*) animals [28,29] (provided by Dr. Erich Schwarz) were crossed with *him-5(e1490)* animals to integrate male production into a strain hypersensitive to neuronal RNAi-knockdown, generating JSR44 (*nre-1(hd20);lin-15B(hd126);him-5(e1490)*). During the cross, insertion of the *him-5(e1490)* allele displaced the integrated array (rhIs13), suggesting location of the array on Chromosome V. Presence of *lin-15B(hd126)* in JSR44 was confirmed via sequencing. The non-annotated *nre-1 (hd20)* is linked with *lin-15B*, being retained alongside *lin-15B* [28,29].

RNAi clones were grown overnight in cultures of LB containing 50 μg/mL ampicillin. Cultures were then diluted to an OD_{600} of 1.0 before plating on NGM agar plates containing 50 μg/mL ampicillin and 1 mM IPTG (Isopropyl-β-D-thiogalactoside) to select for RNAi clones and induce expression. Lawns were allowed to grow at room temperature for 8-16 hours, before JSR44 young adult hermaphrodites were placed on the plates and left to propagate at 16 °C. Young adult males of the F1 progeny were then selected for behavioral testing (see ***Spot Retention Behavioral Assay***). Empty vector controls (VC-1 clone) were run alongside every targeted knockdown experiment.

Spot Retention Behavioral Assay

Following previously described methods, young adult males were isolated from hermaphrodites 5-16 hours prior to testing [1,2]. In short, at the time of the assay, 0.6 μL of either vehicle control (-) or ascaroside #8 (+) was added to the NGM plates covered in a thin lawn of OP50 *E. coli*. Ten males were then divided between two pre-marked spots on the agar, equidistant from the cues. The plate was then recorded for 20 minutes. The time spent of each visit in either vehicle or ascaroside #8 (if greater than 10 seconds) was scored, and averaged. Plates in which the average was greater than two standard deviations removed from the population average were removed from the final analysis as outliers. To compare between strains or conditions, the vehicle was subtracted from

the ascaroside dwell time for each plate. The average of these differences was then compared statistically.

Single Worm Behavioral Assay

Following previously described methods (**Chapter 3B**), animals were isolated and prepared in an identical manner to the Spot Retention Assay. The two outside rings of wells in a 48-well tissue culture plate were filled with 200 μL of NGM agar, which was then seeded with 65 μL of OP50 *E. coli*. The plates and lawns were then dried at 37 °C for 4 hours. Alternating wells were then prepared as spatial controls (nothing done), vehicle controls (0.85 μL of dH_2O was placed in the center of the well), or ascaroside well (0.85 μL of ascaroside was placed in the center of the well). This was performed over four quadrants (see **Chapter 3B** for a more detailed description of plate preparation and recording). Animals were scored for their visits and duration to the center of the well and/or the cue.

The average duration of each worm's visits was calculated, and these values were again averaged together to generate a Mean Dwell Time in seconds for each plate. When comparing across strains or conditions, the Spatial controls were then compared for statistical difference. If none was observed, the Log(fold-change) A/V was then calculated by taking the log of the ascaroside mean dwell time divided by the vehicle mean dwell time for each plate. The amount of times each worm visited the center was averaged to generate the Visit Counts.

The Percent Attraction values were calculated by first determining the "attractive" cut off as two standard deviations above the vehicle average. Any visit longer than this was deemed "attractive" and scored as a "1"; non-attractive visits were scored as "0". The percent attraction was then calculated for each worm was the percent of visits scored a "1". The average was then calculated across the plate to determine Percent Attraction.

CRISPR Design and Strain Generation

Null mutations were generated for *srw-97* and *srr-7* by Knudra Transgenics (now part of NemaMetrix). The *srw-97(knu456)* allele was generated in a *him-5(e1490)* strain using the sgRNAs, TTTAGTAGAGCAGAAATTAA and TACAGCTTTAACTTTCAAC, to generate a 1620 base pair deletion which removed the start codon and left only the terminal exon intact. The *srr-7(knu506)* allele was generated in a *him-5(e1490)* strain using the sgRNAs, CAGAAAAAGTCACACAATAC and CCATTCTCAATCAAAACTTT to generate a 1899 base pair deletion, removing the start codon and all but three terminal codons. Following generation of homozygous deletions by Knudra Transgenics, the lines were then backcrossed twice.

The *dmsr-12(tm8706)* allele, provided by the National BioResource Group (NRBP) contains a 118 base pair deletion was generated by Dr. Mitani of the NRBP. The allele was crossed into a *him-5(e1490)* background prior to testing. The deletion spans intron 2 and exon 3 of the coding sequence. Whether this results in a correctly spliced gene remains unknown, although the expected coding sequence remains in frame.

Phylogenetic Analyses

For phylogenetic analysis of selected CEM genes, we downloaded proteomes for *C. elegans* and related *Caenorhabditis* nematodes from WormBase (release WS275), the Blaxter *Caenorhabditis* database (release 1), or our unpublished work, as listed in **Supplementary Table 6**. From each proteome, we extracted the longest predicted isoform for each gene with *get_largest_isoforms.pl* (*https://github.com/SchwarzEM/ems_perl/blob/master/fasta/get_largest_isoforms.pl*). We observed that the predicted isoform for *dmsr-12* in the WormBase WS275 release of *C. elegans*' proteome was shorter than past versions of *dmsr-12*, and that the WS275 isoform omitted exons that our transgenic expression data (based on older gene models for *dmsr-12*) indicated were likely to be real. We therefore manually replaced the WS275 version of *dmsr-12* with an older version (extracted from

the *C. elegans* proteome in the WS250 release of WormBase). We then computed orthology groups for *C. elegans* and its related species with OrthoFinder version 2.3.11 [54,55], using the arguments '*-a 1 -S diamond -og*'. We identified which orthology groups contained the *C. elegans* genes *srr-7*, *srw-97*, and *dmsr-12*, and extracted their sequences from a concatenation of all 11 proteomes via *extract_fasta_subset.pl* (*https://github.com/SchwarzEM/ems_perl/blob/master/fasta/extract_fasta_subset.pl*). For each orthogroup's member sequences, we aligned the sequences with MAFFT version 7.455 [56] and filtered the alignments twice with trimAl version 1.4.rev15 [57], using first the argument '*-automated1*' and then the arguments '*-resoverlap 0.50 -seqoverlap 50*'. From the filtered alignments, we computed maximum-likelihood protein phylogenies with IQ-TREE version 2.0-rc1 [58,59], using the arguments '*-m MFP -b 100 --tbe*'. In particular, we used transfer bootstrap expectation ('*--tbe*') which provides more reliable confidence values than classic bootstrapping [60]. We visualized the resulting phylogenies with FigTree version 1.4.4 (*http://tree.bio.ed.ac.uk/software/figtree*).

Statistical Analyses

Prior to any statistical analyses, outliers were identified and removed. Outliers were defined as any data points greater than two standard deviations removed from the average. All data were then tested for normality using a Shapiro-Wilk Normality Test. This test was chosen over the more conventional D'Agostino-Pearson Normality Test as many data sets were below 10 in number (due to the statistical power offered by the Single Worm Behavioral Assay (see **Chapter 3B**).

The Spot Retention Assay data was analyzed using two-tailed, paired *t*-tests or Wilcoxon Matched-Pairs Signed Rank tests to compare vehicle control and ascaroside dwell times (**Figure 36A-D**). When comparing the values of multiple conditions or strains, the data was first normalized to account for vehicle dwell time variation between plates by subtracted each plates vehicle dwell time from the ascaroside dwell time. These

normalized values were then compared using a Student's *t*-test or a Mann-Whitney test (**Figure 36B, D**) or a One-Way ANOVA followed by a Dunnett's multiple comparisons test if more than two strains or conditions were compared (**Figure 36A, C**).

The Single Worm Behavioral Assay was first analyzed by performing a Repeated-Measures ANOVA followed by a Bonferroni's multiple comparisons test within each strain, comparing the Spatial control and Ascaroside dwell times to the Vehicle Control. Then, the Spatial Control values for each strain or condition were compared to account for any baseline differences in worm speed of time spent in the center or edges of wells. Once no differences were observed, the log(fold-change) A/V values were calculated and compared using a One-Way ANOVA followed by a Dunnett's multiple corrections test (**Figure 36F, Supplementary Figure 14B, Supplementary Figure 16B**). Visit Counts were analyzed in the same manner as the Mean Dwell Time data. The Percent Attraction data was analyzed using paired t-tests to compare the attractive values of the vehicle and ascaroside (**Supplementary Figure 14D, Supplementary Figure 15B, Supplementary Figure 16D**).

References

1 Narayan, A. *et al.* Contrasting responses within a single neuron class enable sex-specific attraction in *Caenorhabditis elegans*. *Proc Natl Acad Sci U S A* **113**, E1392-1401, doi:10.1073/pnas.1600786113 (2016).

2 Pungaliya, C. *et al.* A shortcut to identifying small molecule signals that regulate behavior and development in *Caenorhabditis elegans*. *Proceedings of the National Academy of Sciences of the United States of America* **106**, 7708-7713, doi:10.1073/pnas.0811918106 (2009).

3 Aprison, E. Z. & Ruvinsky, I. Sex Pheromones of *C. elegans* Males Prime the Female Reproductive System and Ameliorate the Effects of Heat Stress. *PLoS Genet* **11**, e1005729, doi:10.1371/journal.pgen.1005729 (2015).

4 Aprison, E. Z. & Ruvinsky, I. Counteracting Ascarosides Act through Distinct Neurons to Determine the Sexual Identity of *C. elegans* Pheromones. *Curr Biol* **27**, 2589-2599.e2583, doi:10.1016/j.cub.2017.07.034 (2017).

5 Houck, L. *et al.* A new vertebrate courtship pheromone, PMF, affects female receptivity in a terrestrial salamander. *Animal Behaviour* **73**, 315-320 (2007).

6 Jang, Y. H., Chae, H. S. & Kim, Y. J. Female-specific myoinhibitory peptide neurons regulate mating receptivity in *Drosophila melanogaster*. *Nat Commun* **8**, 1630, doi:10.1038/s41467-017-01794-9 (2017).

7 Ludewig, A. H. *et al.* An excreted small molecule promotes *C. elegans* reproductive development and aging. *Nat Chem Biol* **15**, 838-845, doi:10.1038/s41589-019-0321-7 (2019).

8 McGrath, P. T. & Ruvinsky, I. A primer on pheromone signaling in *Caenorhabditis elegans* for systems biologists. *Current opinion in systems biology* **13**, 23-30, doi:10.1016/j.coisb.2018.08.012 (2019).

9 Artyukhin, A. B. *et al.* Metabolomic "Dark Matter" Dependent on Peroxisomal beta-Oxidation in *Caenorhabditis elegans*. *J Am Chem Soc* **140**, 2841-2852, doi:10.1021/jacs.7b11811 (2018).

10 Hrus, A. *et al. C. elegans* Agrin Is Expressed in Pharynx, IL1 Neurons and Distal Tip Cells and Does Not Genetically Interact with Genes Involved in Synaptogenesis or Muscle Function. *PLOS ONE* **2**, e731, doi:10.1371/journal.pone.0000731 (2007).

11 Wang, J. *et al.* Cell-Specific Transcriptional Profiling of Ciliated Sensory Neurons Reveals Regulators of Behavior and Extracellular Vesicle Biogenesis. *Curr Biol* **25**, 3232-3238, doi:10.1016/j.cub.2015.10.057 (2015).

12 Wang, J. *et al. C. elegans* Ciliated Sensory Neurons Release Extracellular Vesicles that Function in Animal Communication. *Current Biology* **24**, 518-525 (2014).

13 Reilly, D. K., Lawler, D. E., Albrecht, D. R. & Srinivasan, J. Using an Adapted Microfluidic Olfactory Chip for the Imaging of Neuronal Activity in Response to Pheromones in Male *C. Elegans* Head Neurons. *Journal of Visualized Experiments*, e56026, doi:doi:10.3791/56026 (2017).

14 Cochella, L. *et al.* Two distinct types of neuronal asymmetries are controlled by the *Caenorhabditis elegans* zinc finger transcription factor die-1. *Genes Dev* **28**, 34-43, doi:10.1101/gad.233643.113 (2014).

15 Chute, C. D. *et al.* Co-option of neurotransmitter signaling for inter-organismal communication in *C. elegans*. *Nat Commun* **10**, 3186, doi:10.1038/s41467-019-11240-7 (2019).

16 Greene, J. S. *et al.* Balancing selection shapes density-dependent foraging behaviour. *Nature* **539**, 254-258, doi:10.1038/nature19848 (2016b).

17 Greene, J. S., Dobosiewicz, M., Butcher, R. A., McGrath, P. T. & Bargmann, C. I. Regulatory changes in two chemoreceptor genes contribute to a *Caenorhabditis elegans* QTL for foraging behavior. *Elife* **5**, doi:10.7554/eLife.21454 (2016a).

18 Kim, K. *et al.* Two Chemoreceptors Mediate Developmental Effects of Dauer Pheromone in *C. elegans*. *Science* **326**, 994-998, doi:10.1126/science.1176331 (2009).

19 McGrath, P. T. *et al.* Parallel evolution of domesticated *Caenorhabditis* species targets pheromone receptor genes. *Nature* **477**, 321-325, doi:10.1038/nature10378 (2011).

20 Park, D. *et al.* Interaction of structure-specific and promiscuous G-protein-coupled receptors mediates small-molecule signaling in *Caenorhabditis elegans*. *PNAS* **109**, 9917-9922, doi:10.1073/pnas.1202216109 (2012).

21 Goodman, M. B., Hall, D. H., Avery, L. & Lockery, S. R. Active currents regulate sensitivity and dynamic range in *C. elegans* neurons. *Neuron* **20**, 763-772, doi:10.1016/s0896-6273(00)81014-4 (1998).

22 Narayan, A., Laurent, G. & Sternberg, P. W. Transfer characteristics of a thermosensory synapse in *Caenorhabditis elegans*. *Proceedings of the National Academy of Sciences of the United States of America* **108**, 9667-9672, doi:10.1073/pnas.1106617108 (2011).

23 Jee, C. *et al.* SEB-3, a CRF receptor-like GPCR, regulates locomotor activity states, stress responses, and ethanol tolerance in *C. elegans*. *Genes, brain, and behavior* **12**, 10.1111/j.1601-1183X.2012.00829.x, doi:10.1111/j.1601-183X.2012.00829.x (2013).

24 Robertson, H. M. & Thomas, J. H. The putative chemoreceptor families of *C. elegans*. *WormBook*, 1-12, doi:10.1895/wormbook.1.66.1 (2006).

25 Boulin, T., Etchberger, J. F. & Hobert, O. Reporter gene fusions. *WormBook*, 1-23, doi:10.1895/wormbook.1.106.1 (2006).

26 Bae, Y. K. *et al.* General and cell-type specific mechanisms target TRPP2/PKD-2 to cilia. *Development* **133**, 3859-3870, doi:10.1242/dev.02555 (2006).

27 Peden, E. M. & Barr, M. M. The KLP-6 kinesin is required for male mating behaviors and polycystin localization in *Caenorhabditis elegans*. *Curr Biol* **15**, doi:10.1016/j.cub.2004.12.073 (2005).

28 Poole, R. J., Bashllari, E., Cochella, L., Flowers, E. B. & Hobert, O. A Genome-Wide RNAi Screen for Factors Involved in Neuronal Specification in *Caenorhabditis elegans*. *PLoS Genet* **7**, e1002109, doi:10.1371/journal.pgen.1002109 (2011).

29 Schmitz, C., Kinge, P. & Hutter, H. Axon guidance genes identified in a large-scale RNAi screen using the RNAi-hypersensitive *Caenorhabditis elegans* strain *nre-1(hd20) lin-15b(hd126). Proceedings of the National Academy of Sciences* **104**, 834-839, doi:10.1073/pnas.0510527104 (2007).

30 Fraser, A. G. *et al.* Functional genomic analysis of *C. elegans* chromosome I by systematic RNA interference. *Nature* **408**, 325-330, doi:10.1038/35042517 (2000).

31 Kamath, R. S. *et al.* Systematic functional analysis of the *Caenorhabditis elegans* genome using RNAi. *Nature* **421**, 231-237, doi:10.1038/nature01278 (2003).

32 Rual, J. F. *et al.* Toward improving *Caenorhabditis elegans* phenome mapping with an ORFeome-based RNAi library. *Genome Res* **14**, 2162-2168, doi:10.1101/gr.2505604 (2004).

33 Madeira, F. *et al.* The EMBL-EBI search and sequence analysis tools APIs in 2019. *Nucleic acids research* **47**, W636-W641, doi:10.1093/nar/gkz268 (2019).

34 Zwaal, R. R., Mendel, J. E., Sternberg, P. W. & Plasterk, R. H. Two neuronal G proteins are involved in chemosensation of the *Caenorhabditis* elegans Dauer-inducing pheromone. *Genetics* **145**, 715-727 (1997).

35 Krishnan, A., Almén, M. S., Fredriksson, R. & Schiöth, H. B. Insights into the Origin of Nematode Chemosensory GPCRs: Putative Orthologs of the Srw Family Are Found across Several Phyla of Protostomes. *PLoS ONE* **9**, e93048, doi:10.1371/journal.pone.0093048 (2014).

36 Reilly, D. K., Randle, L. J. & Srinivasan, J. Evolution of hermaphroditism decreases efficacy of Ascaroside#8-mediated mate attraction in *Caenorhabditis* nematodes. *microPublication Biology*, doi:10.17912/micropub.biology.000134 (2019).

37 Gordon, K. L., Arthur, R. K. & Ruvinsky, I. Phylum-Level Conservation of Regulatory Information in Nematodes despite Extensive Non-coding Sequence Divergence. *PLoS genetics* **11**, e1005268-e1005268, doi:10.1371/journal.pgen.1005268 (2015).

38 Wang, X., Greenberg, J. F. & Chamberlin, H. M. Evolution of regulatory elements producing a conserved gene expression pattern in *Caenorhabditis*. *Evolution & Development* **6**, 237-245, doi:10.1111/j.1525-142X.2004.04029.x (2004).

39 Zhang, Y. K., Reilly, D. K., Yu, J., Srinivasan, J. & Schroeder, F. C. Photoaffinity probes for nematode pheromone receptor identification. *Journal of Organic & Biomolecular Chemistry*, 10.1039/c1039ob02099c, doi:10.1039/c9ob02099c (2019).

40 Miller, M. A., Cutter, A. D., Yamamoto, I., Ward, S. & Greenstein, D. Clustered Organization of Reproductive Genes in the *C. elegans* Genome. *Current Biology* **14**, 1284-1290, doi:10.1016/j.cub.2004.07.025 (2004).

41 Iannacone, M. J. *et al.* The RFamide receptor DMSR-1 regulates stress-induced sleep in *C. elegans*. *Elife* **6**, doi:10.7554/eLife.19837 (2017).

42 Schwarz, E. M., Kato, M. & Sternberg, P. W. Functional transcriptomics of a migrating cell in Caenorhabditis elegans. *Proceedings of the National Academy of Sciences of the United States of America* **109**, 16246-16251, doi:10.1073/pnas.1203045109 (2012).

43 Li, B. & Dewey, C. N. RSEM: accurate transcript quantification from RNA-Seq data with or without a reference genome. *BMC bioinformatics* **12**, 323-323, doi:10.1186/1471-2105-12-323 (2011).

44 Langmead, B. & Salzberg, S. L. Fast gapped-read alignment with Bowtie 2. *Nature methods* **9**, 357-359, doi:10.1038/nmeth.1923 (2012).

45 Li, H. *et al.* The Sequence Alignment/Map format and SAMtools. *Bioinformatics (Oxford, England)* **25**, 2078-2079, doi:10.1093/bioinformatics/btp352 (2009).

46 Howe, K. L. *et al.* WormBase 2016: expanding to enable helminth genomic research. *Nucleic acids research* **44**, D774-D780, doi:10.1093/nar/gkv1217 (2016).

47 Käll, L., Krogh, A. & Sonnhammer, E. L. L. A combined transmembrane topology and signal peptide prediction method. *Journal of molecular biology* **338**, 1027-1036, doi:10.1016/j.jmb.2004.03.016 (2004).

48 Wootton, J. C. Non-globular domains in protein sequences: automated segmentation using complexity measures. *Comput Chem* **18**, 269-285, doi:10.1016/0097-8485(94)85023-2 (1994).

49 Lupas, A. Prediction and analysis of coiled-coil structures. *Methods in enzymology* **266**, 513-525, doi:10.1016/s0076-6879(96)66032-7 (1996).

50 Finn, R. D. *et al.* The Pfam protein families database: towards a more sustainable future. *Nucleic acids research* **44**, D279-D285, doi:10.1093/nar/gkv1344 (2016).

51 Eddy, S. R. A new generation of homology search tools based on probabilistic inference. *Genome Inform* **23**, 205-211 (2009).

52 Powell, S. *et al.* eggNOG v3.0: orthologous groups covering 1133 organisms at 41 different taxonomic ranges. *Nucleic acids research* **40**, D284-D289, doi:10.1093/nar/gkr1060 (2012).

53 Hobert, O. The neuronal genome of Caenorhabditis elegans. *WormBook : the online review of C. elegans biology*, 1-106, doi:10.1895/wormbook.1.161.1 (2013).

54 Emms, D. M. & Kelly, S. OrthoFinder: solving fundamental biases in whole genome comparisons dramatically improves orthogroup inference accuracy. *Genome Biology* **16**, 157, doi:10.1186/s13059-015-0721-2 (2015).

55 Emms, D. M. & Kelly, S. OrthoFinder: phylogenetic orthology inference for comparative genomics. *Genome Biology* **20**, 238, doi:10.1186/s13059-019-1832-y (2019).

56 Katoh, K. & Standley, D. M. MAFFT multiple sequence alignment software version 7: improvements in performance and usability. *Molecular biology and evolution* **30**, 772-780, doi:10.1093/molbev/mst010 (2013).

57 Capella-Gutiérrez, S., Silla-Martínez, J. M. & Gabaldón, T. trimAl: a tool for automated alignment trimming in large-scale phylogenetic analyses. *Bioinformatics (Oxford, England)* **25**, 1972-1973, doi:10.1093/bioinformatics/btp348 (2009).

58 Kalyaanamoorthy, S., Minh, B. Q., Wong, T. K. F., von Haeseler, A. & Jermiin, L. S. ModelFinder: fast model selection for accurate phylogenetic estimates. *Nature methods* **14**, 587-589, doi:10.1038/nmeth.4285 (2017).

59 Nguyen, L.-T., Schmidt, H. A., von Haeseler, A. & Minh, B. Q. IQ-TREE: a fast and effective stochastic algorithm for estimating maximum-likelihood phylogenies. *Molecular biology and evolution* **32**, 268-274, doi:10.1093/molbev/msu300 (2015).

60 Lemoine, F. *et al.* Renewing Felsenstein's phylogenetic bootstrap in the era of big data. *Nature* **556**, 452-456, doi:10.1038/s41586-018-0043-0 (2018).

61 Stevens, L. *et al.* The Genome of Caenorhabditis bovis. *Current biology : CB*, S0960-9822(0920)30118-30114, doi:10.1016/j.cub.2020.01.074 (2020).

62 Harris, T. W. *et al.* WormBase: a comprehensive resource for nematode research. *Nucleic acids research* **38**, D463-D467, doi:10.1093/nar/gkp952 (2010).

63 Gene Ontology, C. Gene Ontology Consortium: going forward. *Nucleic acids research* **43**, D1049-D1056, doi:10.1093/nar/gku1179 (2015).

Chapter 5 Photoaffinity probes for nematode pheromone receptor identification

Chapter 5A Photoaffinity probes for nematode pheromone receptor identification

Published as:

Zhang YK,‡[a] Reilly DK,‡[b] Yu, J,[a] Srinivasan J,*[b] Schroeder FC*[a] (2019). *Photoaffinity probes for nematode pheromone receptor identification*. Journal of Organic and Biomolecular Chemistry. doi: 10.1093/c9ob02099c

[a] Boyce Thompson Institute and Department of Chemistry and Chemical Biology, Cornell University, Ithaca, NY, USA. E-mail: fs31@cornell.edu

[b] Department of Biology and Biotechnology, Worcester Polytechnic Institute, Worcester, MA, USA. E-mail: jsrinivasan@wpi.edu

‡These authors contributed equally

Summary

Identification of pheromone receptors plays a central role for uncovering signaling pathways that underlie chemical communication in animals. Here, we describe the synthesis and bioactivity of photoaffinity probes for the ascaroside ascr#8, a sex-pheromone of the model nematode, *Caenorhabditis elegans*. Structure–activity studies guided incorporation of alkyne- and diazirine- moieties and revealed that addition of functionality in the sidechain of ascr#8 was well tolerated, whereas modifications to the ascarylose moiety resulted in loss of biological activity. Our study will guide future probe design and provides a basis for pheromone receptor identification *via* photoaffinity labeling in *C. elegans*.

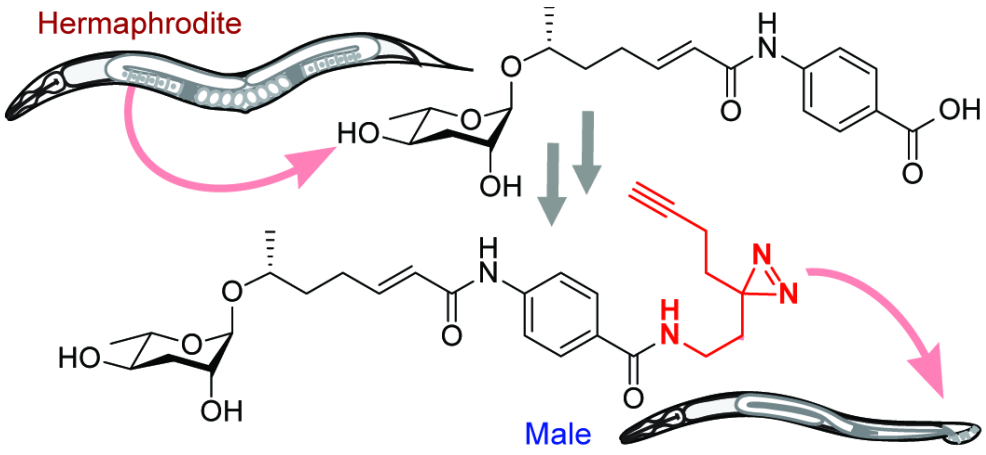

Introduction

The nematode *Caenorhabditis elegans* has become an important model for inter-organismal signaling *via* pheromones. *C. elegans* and other nematode species communicate with conspecifics *via* ascarosides, a family of small-molecule pheromones based on the 3,6-dideoxysugar, L-ascarylose, linked to fatty acid-like side chains (**Figure 39**). Ascarosides can be further decorated with building blocks from diverse primary metabolic pathways, *e.g.* the likely folate-derived *p*-aminobenzoic acid in ascr#8[1] (**1**), or the neurotransmitter octopamine in osas#9[2] (**5**). Ascarosides are involved in almost every aspect of the life history of *C. elegans*, including developmental changes,[3-5] aging,[6, 7] and diverse behaviors *e.g.* dispersal,[8] aggregation,[9, 10] and mating.[11, 12] Ascarosides are typically sensed as

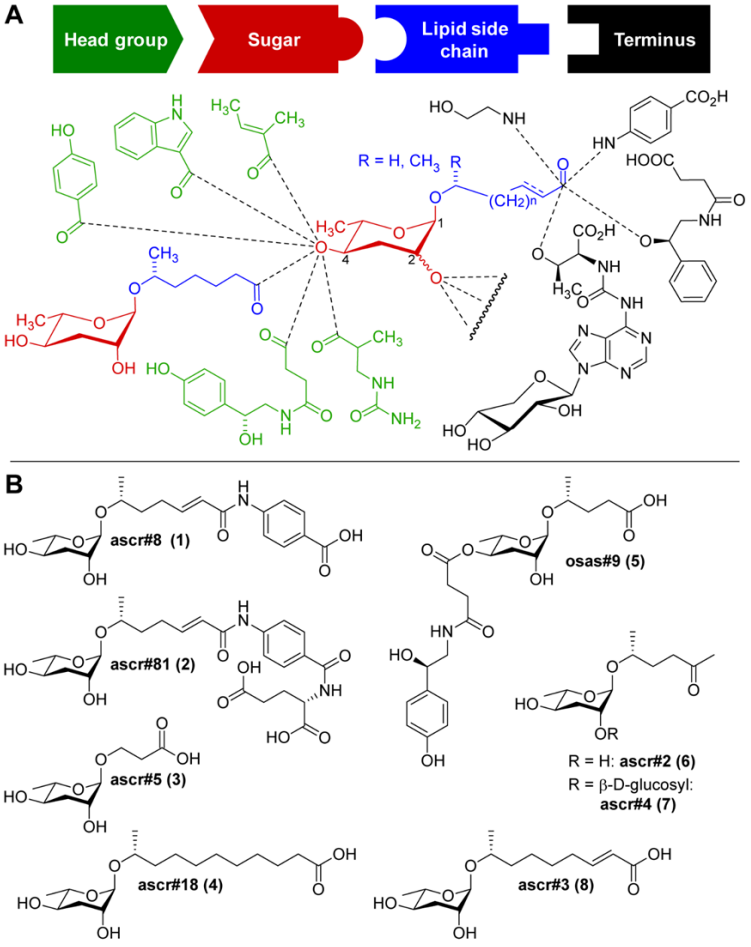

Figure 39. Structures of ascaroside pheromones from *C. elegans* and other nematodes.
(A) Overview of structural diversity of ascaroside pheromones. Building blocks from diverse metabolic pathways are combined to furnish a modular library of signaling molecules, with specific examples shown in **(B)**.

cocktails of compounds,[13] often functioning in synergy.[1, 8, 12] Notably, even small changes in ascaroside structures can result in dramatic differences in biological responses.[6]

Three ascarosides (ascr#2 (**6**), ascr#3 (**8**), and ascr#4 (**7**)) have been shown to synergistically attract males,[12] whereas the structurally distinct ascr#8 (**1**) acts as a potent male attractant even in the absence of other ascarosides.[1, 11] ascr#8 (**1**) and the related ascr#81 (**2**) are unique among identified ascaroside pheromones in that they incorporate a *p*-aminobenzoate moiety.[5, 14]

Identification of ascaroside receptors has not kept pace with the discovery of new ascarosides and activities, and it appears that multiple G protein-coupled receptors (GPCRs) are involved in sensing individual compounds.[15, 16] Receptor identification has been hampered in part by the large number of GPCRs in *C. elegans*, which likely exceeds 1000.[17] In order to identify ascaroside receptors, previous studies have employed reverse genetics screens,[15, 18] as well as quantitative trace locus analyses.[19-21] The use of ascaroside-based photoaffinity probes could enable targeted receptor identification and, importantly, has the advantage to demonstrate direct ascaroside-receptor binding. In a previous study, an ascr#2-based photoaffinity probe was used to confirm binding to the GPCR DAF-37, which was originally identified *via* immunoprecipitation;[16] however, the ascr#2 probe used in this study featured extensive structural modifications and correspondingly was much less biologically active than unmodified ascr#2 and thus unlikely to facilitate *de novo* receptor identification.

Toward identification of receptor(s) of the sex pheromone ascr#8, we aimed to design a photoaffinity probe that would enable covalent linking and receptor pull-down, yet retain most bioactivity. We synthesized four ascr#8 probe designs, two of which retained potent activity. The inactive probes provide insight into structure–activity relationships and may help guide design for probes of other ascaroside pheromones.

Results

Previous studies showed that ascr#8 elicits a robust attractive response in young adult male *C. elegans*. We confirmed attraction to ascr#8 (**1**) using a spot retention assay, in which the dwell time of worms in areas treated either with vehicle control or the chemical of interest is measured (**Figure 40A**).[1, 11, 12]

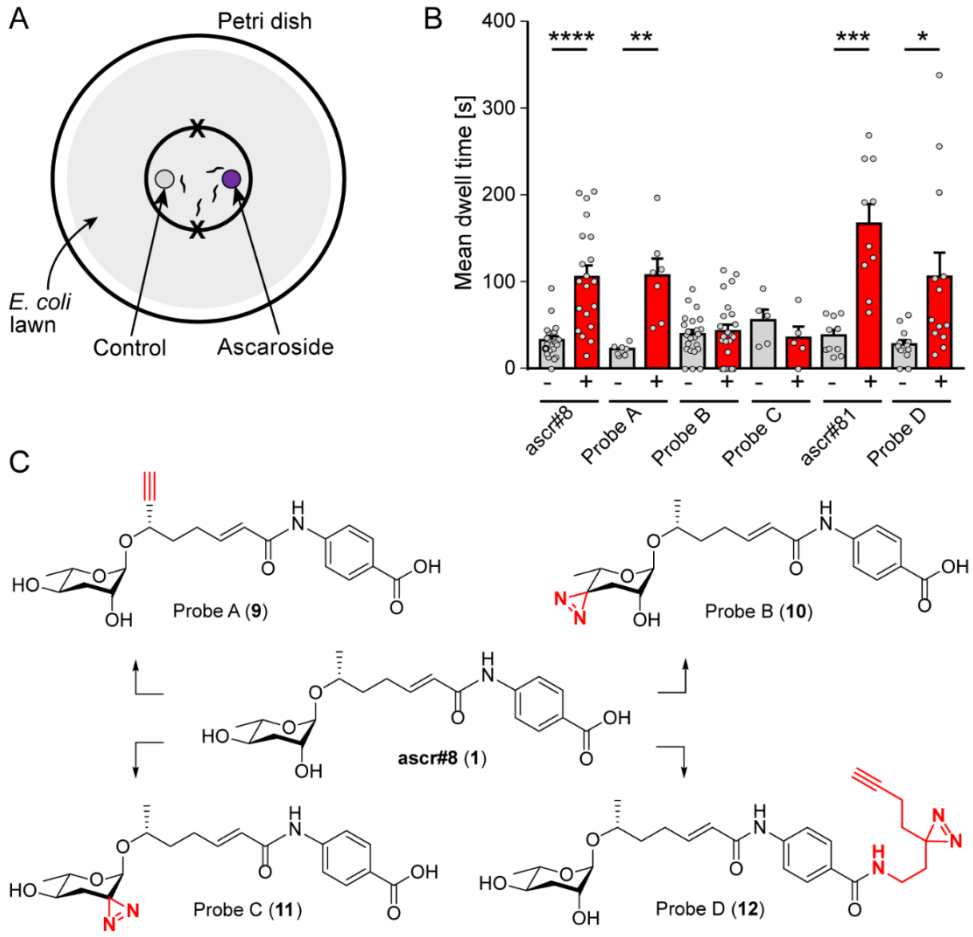

Figure 40. Response of *C. elegans* males to ascr#8 and derivatives.
(A) Schematic of the spot retention assay. Males are placed on each "X" and scored for time spent in each of the smallest circles. **(B)** Dwell times of *C. elegans* males in vehicle controls (−) and ascaroside-treated (+) circles. Data presented as mean ± SEM. * $p < 0.05$, ** $p < 0.01$, *** $p < 0.001$, **** $p < 0.0001$. **(C)** Structures of ascr#8 (**1**) and four probe designs (**9–12**).

For photoaffinity labeling, the installation of two types of groups into ascr#8 is required, a photoreactive group and a bioorthogonal reactive group for affinity purification. Since large photoreactive groups may interfere with binding between the ligand and its receptor,[22] we focused on diazirine derivatives, which have additional

advantages including short lifetime following UV irradiation and subsequent high reactivity.[23, 24] As a click-chemistry handle for affinity purification, we chose an alkyne, since azides may become subject to metabolic reduction.[25] To assess whether additional functional groups affect the biological activity of ascr#8, chemical modifications were introduced one at a time, followed by testing the bioactivity of the resulting ascr#8 derivatives.

In the initial probe designs, we planned to integrate the click-chemistry moiety as part of the fatty acid side-chain (**9**). Replacing the ω-methyl group in the side chain with a terminal alkyne seemed most straightforward and least likely to perturb receptor binding. For introduction of the diazirine moiety, we envisioned replacing one of the two hydroxyl groups of the ascarylose, as we felt such modification may cause only minimal changes to the overall size and shape of ascr#8 (**1**) (**Figure 40**). For the synthesis of the alkyne-integrating side chain (**Scheme 1**), metathesis of 4-pentenoic acid (**13**) with ethyl acrylate produced intermediate **14**, which was converted into the TMS-protected alkyne

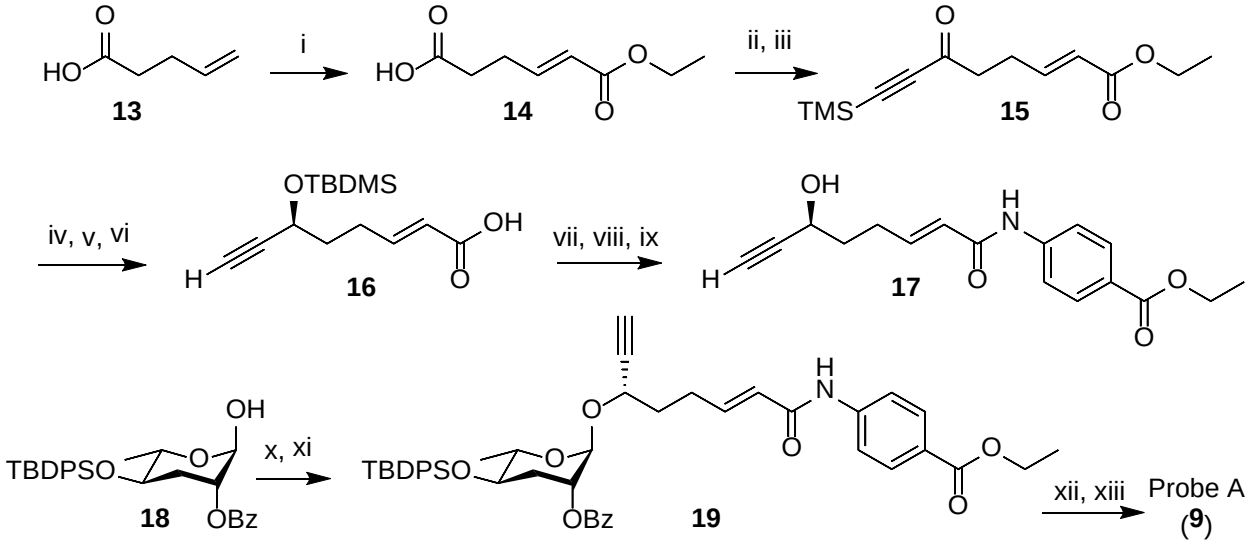

Scheme 1. Synthesis of probe A (9).

(i) ethyl acrylate, Grubb's second generation catalyst, DCM, 25 °C, 10 h, 75%; (ii) oxalyl chloride, cat. DMF, DCM, 0 °C, 20 min; (iii) bis(trimethylsilyl)acetylene, AlCl3, DCM, 0 °C, 3 h, 26% ~2 steps; (iv) freshly prepared Terashima reagent (see Experimental section), −78 °C, 98%, ee 80%; (v) TBDMSCl, imidazole, DMF, 25 °C, 2.5 h, 94%; (vi) LiOH·H2O, dioxane, H2O, 60 °C, 12 h, 50%; (vii) oxalyl chloride, cat DMF, DCM, 0 °C, 20 min; (viii) benzocaine, DIEA, DCM, 0 °C, 1 h, 87% ~2 steps; (ix) HF in H2O, MeCN, 25 °C, 1 h, 85%; (x) CCl3CN, DBU, DCM, 25 °C, 2 h; (xi) 17, TMSOTf, DCM, 0 °C, 1 h, 50% ~2 steps; (xii) TBAF, THF, 25 °C, 12 h, 93%; (xiii) LiOH·H2O, dioxane, H2O, 60 °C, 12 h, 62%.

15. Following reduction of the ketone, TBDMS protection of the resulting alcohol and hydrolysis of the ester, the acid **16** was coupled t o ethyl *p*-aminobenzoate, followed by TBDMS deprotection. The alkyne-containing side chain **17** was then coupled to protected ascarylose using established procedures, furnishing probe A (**9**). Given that the alkyne moiety in Probe A is sterically somewhat encumbered, we confirmed the ability of such

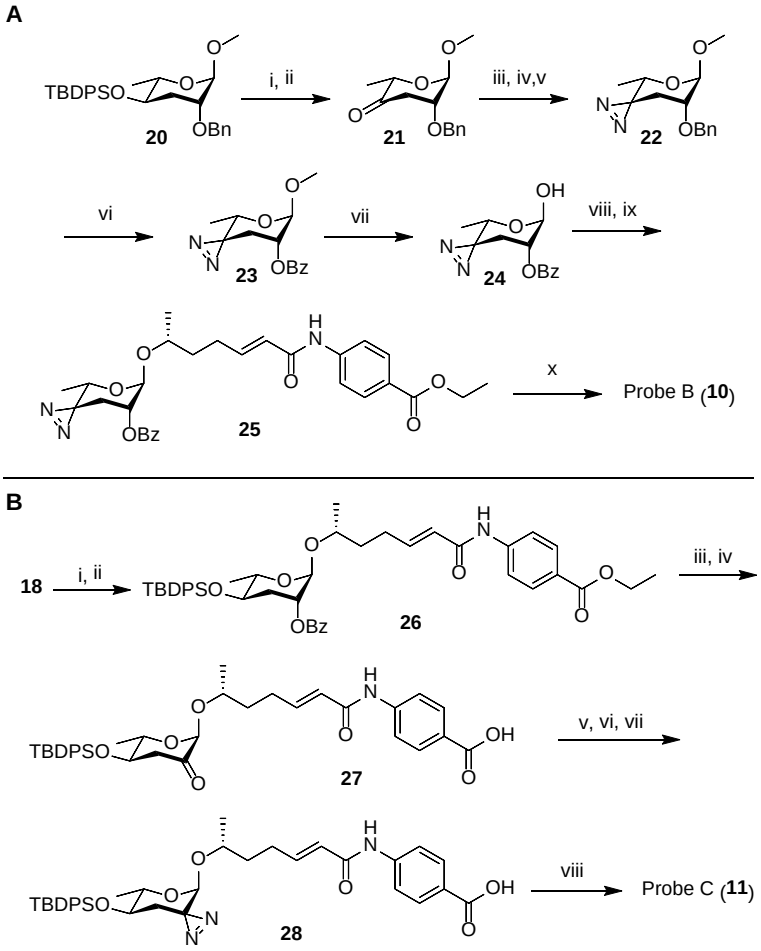

Scheme 2. (A) Synthesis of probe B (**10**).
(i) TBAF, THF, 25 °C, 8 h, 95%; (ii) PCC, 4 Å molecular sieves, DCM, 25 °C, 4 h, 74%; (iii) 7N NH3 in MeOH, pTsOH, MeOH, 0 °C, 3 h; (iv) NH2OSO3H, 0 °C → rt, 16 h; (v) NEt3, I2 in MeOH titration, 25 °C, 39% ~3 steps; (vi) RuCl3·H2O, NaIO4, DCM : MeCN : H2O = 1 : 1 : 1, 25 °C, 5 h, 72%; (vii) BBr3, DCM, −78 °C, 30 min, 71% BRSM; (viii) CCl3CN, DBU, DCM, 25 °C, 2 h; (ix) N-(6′Rhydroxy- 2′E-heptenoyl)-4-aminobenzoic acid ethyl ester (prepared following previous reported method1), TMSOTf, DCM, 0 °C, 2 h, 57%~2 steps; (x) LiOH·H2O, dioxane, H2O, 60 °C, 3 h, 79%.
(**B**) **Synthesis of probe C** (**11**).: (i) CCl3CN, DBU, DCM, 25 °C, 2 h; (ii) N-(6′R-hydroxy-2′Eheptenoyl)- 4-aminobenzoic acid ethyl ester (prepared following previous reported method1), TMSOTf, DCM, 0 °C, 2 h, 15% ~2 steps; (iii) LiOH·H2O, dioxane, H2O, 60 °C, 12 h, 42%; (iv) Dess-Martin periodinane, DCM, 25 °C, 12 h, 51%; (v) 7 N NH3 in MeOH, pTsOH, MeOH, 0 °C, 3 h; (vi) NH2OSO3H, 0 °C → rt, 16 h; (vii) NEt3, I2 in MeOH titration, 25 °C; (viii) TBAF, THF, 25 °C, 8 h, 13% ~4 steps.

alkynes to undergo click chemistry using the analogous alkyne derivative of ascr#18 (**4**) (see **ESI†**). Probe A was found to elicit levels of attraction comparable to unmodified ascr#8 (**Figure 40B** and **ESI†**), indicating the integration of an alkyne moiety in place of the ω-methyl in the side chain does not significantly perturb activity of ascr#8 and may represent a useful entry for the design of other ascaroside receptor probes.

Next, we developed syntheses for introduction of the diazirine at the 2′ and 4′ carbons of ascarylose. Starting from key intermediate (**20)**,[26] a diazirine moiety was installed in position 4 in 10 steps, furnishing probe B (**10, Scheme 2A**). Our approach to probe B necessitated late-stage introduction of benzoyl protection in position 2, since the 2-O-benzoyl-protected derivative of ketone **21** had a strong tendency to eliminate and would not survive under the conditions required to install the diazirine. The 2-O-benzoyl moiety is required for stereochemical control of the subsequent glycosylation step *via* neighboring group participation (NGP). Conversion of the benzyl ether (Bn) into the benzoyl ester (Bz) after installment of the diazirine group in **22** was achieved through ruthenium(III) chloridecatalyzed oxidation (**Scheme 2A**). Following a different synthetic strategy, we inserted the diazirine at the 2′ carbon of the ascarylose, furnishing probe C (**11**, **Scheme 2B**). In the probe C synthesis, we opted to first establish the glycosidic linkage, followed by benzoyl deprotection, oxidation, and introduction of the diazirine moiety. Desilylation of **28** furnished probe C.

Testing probes B and C in the spot retention assay, we found that both probes had no activity (**Figure 40B** and **ESI†**). In fact, males spent less time in the probe C-treated spot compared to control, although the difference did not reach significance. Loss of biological activity with probe B (**10**) and probe C (**11**) suggests that both 2′ and 4′ hydroxyl groups of ascarylose participate in essential interactions during receptor binding. These data support previous studies that demonstrate the importance of these hydroxyl groups in determining the identity of individual ascarosides.[8, 12]

These results led us to reevaluate our design strategy, based on a biological evaluation of naturally occurring ascr#8 derivatives. Recent expansion of the known family of ascarosides has uncovered two derivatives of ascr#8, named ascr#81 and ascr#82.[14] In these ascr#8 derivatives, L-glutamic acid or L-glutamyl-L-glutamic acid is attached to the *p*-aminobenzoate *via* amide linkages. We asked whether these alterations of the carboxy terminus affect biological activity and tested a synthetic sample of ascr#81 (**2**) in the spot retention assay. We found that ascr#81 is at least as active as ascr#8 (**1**) in this assay (**Figure 40B** and **ESI†**). In fact, dwell times elicited by ascr#81 were higher than those measured for ascr#8, though the difference did not reach statistical significance.

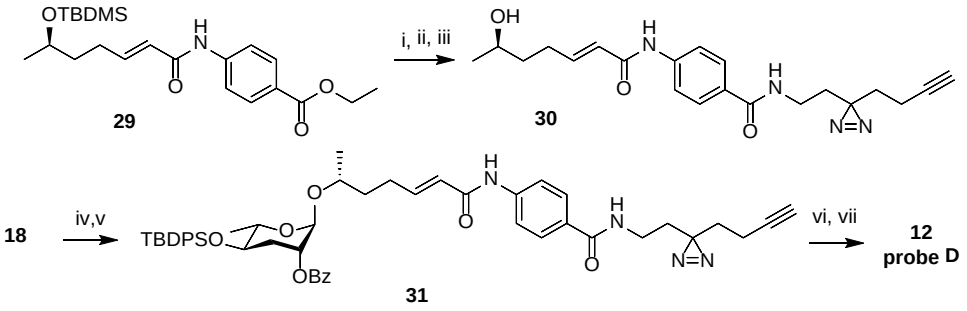

Scheme 3. Synthesis of probe D (12).
Reagents and conditions: (i) LiOH·H2O, dioxane, H2O, 60 °C, 12 h, 72%; (ii) 2-(3-(but-3-yn-1-yl)-3Hdiazirin-3-yl)ethan-1-amine, EDC·HCl, DMAP, DCM/DMF, 25 °C, 8 h, 53%; (iii) HF in H2O, MeCN, 25 °C, 1 h, 92%; (iv) CCl3CN, DBU, DCM, 25 °C, 2 h; (v) **30**, TMSOTf, DCM, 0 °C, 1 h, 8% ~2 steps; (vi) TBAF, THF, 25 °C, 12 h, 77%; (vii) LiOH·H2O, dioxane, H2O, 60 °C, 12 h, 60%.

This result suggested that modification of ascr#8 at the carboxy terminus may be well tolerated. Therefore, we revised our probe design to incorporate both the diazirine and alkyne handle into a single moiety linked *via* an amide to the *p*-aminobenzoic acid in ascr#8 (probe D (**12**), **Scheme 3**). Commercially available 2-(3-(but-3-yn-1-yl)-3H-diazirin-3-yl)ethan-1-amine was incorporated at the terminal carboxylic acid, analogous to the previously described synthesis of ascr#81 (**2**).[14] Gratuitously, bioassays demonstrated that probe D retained biological activity matching that of unmodified ascr#8 (**Figure 40B** and **ESI†**).

Discussion

Together, these results suggest multiple avenues for testing and development of ascaroside receptor probes. The presence of the hydroxyl groups on the ascarylose sugar appears to be essential for maintaining ascaroside activity (**Figure 40**, **10, 11**).[3, 14] Introduction of an alkyne moiety at the ω-position of the side chain is well tolerated in the case of ascr#8. Except for ascr#5 (**3**), all ascarosides for which biological activity has been demonstrated in *C. elegans* feature an ω-methyl group in the side chain, suggesting that alkyne introduction at this position could be used for probing receptor interactions of biosynthesis of diverse ascarosides in *C. elegans*. However, in other nematode species, modification of the ω-methyl may be less well tolerated; for example, in *Caenorhabditis nigoni*, hydroxylation of the ω-side chain carbon was found to abolish the attraction of *C. nigoni* males to ascr#3 (**8**).[27]

In the case of ascr#8, use of commercially available 2-(3- (but-3-yn-1-yl)-3H-diazirin-3-yl)ethan-1-amine, as in probe D (**12**), allowed for inclusion of both the photo-reactive group and bioorthogonal reactive group with relative ease. However, activity of many other ascarosides requires the presence of an unmodified carboxy terminus, and therefore installation of the alkyne at the ω-position of the side chain may be preferable, though a suitable location for the diazirine moiety remains to be found. For the identification of the receptor of ascr#8, our efforts are directed at crosslinking probe D with putative receptor candidates in heterologous expression systems.

Conflicts of interest

There are no conflicts to declare.

Acknowledgements

The strain of *C. elegans* used in this study, CB4088 (*him-5 (e1490)*), was provided by the CGC, which is funded by NIH Office of Research Infrastructure Programs (P40 OD010440). This work was supported in part by the NIH (R01GM113692 and

R01GM088290 to F.C.S., and R01DC016058 to JS) and startup funds from WPI to JS. We would also like to thank Elizabeth DiLoreto in the Srinivasan Lab for providing comments and edits to early versions of this manuscript.

Notes and References

1. C. Pungaliya, J. Srinivasan, B. W. Fox, R. U. Malik, A. H. Ludewig, P. W. Sternberg and F. C. Schroeder, *Proceedings of the National Academy of Sciences of the United States of America*, 2009, **106**, 7708-7713.
2. A. B. Artyukhin, J. J. Yim, J. Srinivasan, Y. Izrayelit, N. Bose, S. H. von Reuss, Y. Jo, J. M. Jordan, L. R. Baugh, M. Cheong, P. W. Sternberg, L. Avery and F. C. Schroeder, *J Biol Chem*, 2013, **288**, 18778-18783.
3. R. A. Butcher, *Natural product reports*, 2017, **34**, 472-477.
4. P.-Y. Jeong, M. Jung, Y.-H. Yim, H. Kim, M. Park, E. Hong, W. Lee, Y. H. Kim, K. Kim and Y.-K. Paik, *Nature*, 2005, **433**, 541-545.
5. S. H. von Reuss and F. C. Schroeder, *Natural product reports*, 2015, **32**, 994-1006.
6. A. H. Ludewig, A. B. Artyukhin, E. Z. Aprison, P. R. Rodrigues, D. C. Pulido, R. N. Burkhardt, O. Panda, Y. K. Zhang, P. Gudibanda, I. Ruvinsky and F. C. Schroeder, *Nat Chem Biol*, 2019, **15**, 838-845.
7. A. H. Ludewig, Y. Izrayelit, D. Park, R. U. Malik, A. Zimmermann, P. Mahanti, B. W. Fox, A. Bethke, F. Doering, D. L. Riddle and F. C. Schroeder, *Proceedings of the National Academy of Sciences*, 2013, **110**, 5522.
8. J. Srinivasan, S. H. von Reuss, N. Bose, A. Zaslaver, P. Mahanti, M. C. Ho, O. G. O'Doherty, A. S. Edison, P. W. Sternberg and F. C. Schroeder, *PLoS Biol*, 2012, **10**, e1001237.
9. A. Choe, S. H. von Reuss, D. Kogan, R. B. Gasser, E. G. Platzer, F. C. Schroeder and P. W. Sternberg, *Current Biology*, 2012, **22**, 772-780.
10. C. D. Chute and J. Srinivasan, *Semin Cell Dev Biol*, 2014, **33**, 18-24.

11. A. Narayan, V. Venkatachalam, O. Durak, D. K. Reilly, N. Bose, F. C. Schroeder, A. D. Samuel, J. Srinivasan and P. W. Sternberg, *Proc Natl Acad Sci U S A*, 2016, **113**, E1392-1401.

12. J. Srinivasan, F. Kaplan, R. Ajredini, C. Zachariah, H. T. Alborn, P. E. Teal, R. U. Malik, A. S. Edison, P. W. Sternberg and F. C. Schroeder, *Nature*, 2008, **454**, 1115-1118.

13. A. H. Ludewig and F. C. Schroeder, *WormBook*, 2013, DOI: 10.1895/wormbook.1.155.1, 1-22.

14. A. B. Artyukhin, Y. K. Zhang, A. E. Akagi, O. Panda, P. W. Sternberg and F. C. Schroeder, *J Am Chem Soc*, 2018, **140**, 2841-2852.

15. K. Kim, K. Sato, M. Shibuya, D. M. Zeiger, R. A. Butcher, J. R. Ragains, J. Clardy, K. Touhara and P. Sengupta, *Science*, 2009, **326**, 994-998.

16. D. Park, I. O'Doherty, R. K. Somvanshi, A. Bethke, F. C. Schroeder, U. Kumar and D. L. Riddle, *PNAS*, 2012, **109**, 9917-9922.

17. C. I. Bargmann, *Science*, 1998, **282**, 2028.

18. C. D. Chute, E. M. DiLoreto, Y. K. Zhang, D. K. Reilly, D. Rayes, V. L. Coyle, H. J. Choi, M. J. Alkema, F. C. Schroeder and J. Srinivasan, *Nat Commun*, 2019, **10**, 3186.

19. J. S. Greene, M. Brown, M. Dobosiewicz, I. G. Ishida, E. Z. Macosko, X. Zhang, R. A. Butcher, D. J. Cline, P. T. McGrath and C. I. Bargmann, *Nature*, 2016b, **539**, 254-258.

20. J. S. Greene, M. Dobosiewicz, R. A. Butcher, P. T. McGrath and C. I. Bargmann, *Elife*, 2016a, **5**.

21. P. T. McGrath, Y. Xu, M. Ailion, J. L. Garrison, R. A. Butcher and C. I. Bargmann, *Nature*, 2011, **477**, 321-325.

22. T. Yang, Z. Liu and X. D. Li, *Chemical science*, 2015, **6**, 1011-1017.

23. L. Dubinsky, B. P. Krom and M. M. Meijler, *Bioorganic & medicinal chemistry*, 2012, **20**, 554-570.

24. E. Smith and I. Collins, *Future Med Chem*, 2015, **7**, 159-183.

25. P. K. Sasmal, S. Carregal-Romero, A. A. Han, C. N. Streu, Z. Lin, K. Namikawa, S. L. Elliott, R. W. Köster, W. J. Parak and E. Meggers, *ChemBioChem*, 2012, **13**, 1116-1120.

26. Y. K. Zhang, M. A. Sanchez-Ayala, P. W. Sternberg, J. Srinivasan and F. C. Schroeder, *Org Lett*, 2017, **19**, 2837-2840.

27. C. Dong, D. K. Reilly, C. Bergame, F. Dolke, J. Srinivasan and S. H. von Reuss, *J Org Chem*, 2018, DOI: 10.1021/acs.joc.8b00094.

Chapter 6 Evolution of Hermaphroditism Decreases Efficacy of Ascaroside#8-Mediated Mate Attraction in *Caenorhabditis* Nematodes

Chapter 6A Evolution of Hermaphroditism Decreases Efficacy of Ascaroside#8-Mediated Mate Attraction in *Caenorhabditis* Nematodes

Published as:

Reilly DK[1†], Randle LJ[2,3,†], Srinivasan J[1*] (2019). Evolution of Hermaphroditism Decreases Efficacy of Ascaroside#8-Mediated Mate Attraction in *Caenorhabditis* Nematodes. microPublication Biology. doi: 10.17912/micropub.biology.000134

[1]Department of Biology and Biotechnology, Worcester Polytechnic Institute, Worcester, MA

[2]Department of Chemistry and Biochemistry, Worcester Polytechnic Institute, Worcester, MA

[3]Current Address: SBH Sciences, Natick, MA

†. These authors contributed equally to this work

*. corresponding author: jsrinivasan@wpi.edu

Description

Nematodes, such as the model organism *Caenorhabditis elegans*, communicate environmental and developmental information with conspecifics through a class of small-molecule pheromones termed ascarosides (1-3). Nematodes share ascaroside signaling pathways (4) but are also capable of eavesdropping on chemical signals of predatory species (5). Ascarosides signal vast arrays of information, either individually or as blends, based on concentration, sex, physiological state, and other ascarosides sensed (6-9). For instance, octopamine-succinylated ascaroside #9 (osas#9) is able to signal starvation conditions in the absence of other ascarosides (10).

C. elegans (*Cel*) is an androdiecious species, with the majority of the natural population comprised of self-fertilizing hermaphrodites, and a small proportion (<0.2%) being male (11). There are two other similarly androdiecious species in the genus, *C. briggsae* (*Cbr*) and *C. tropicalis* (*Ctr*). All three species evolved their hermaphroditism separately and uniquely (12). Of the male-attracting ascarosides secreted by *C. elegans* (ascr#2, ascr#3, ascr#4, and ascr#8), ascr#8 is the most potent (7). Since ascr#8 is a male attractant in this hermaphroditic species, we asked if other hermaphroditic species retained the ability to attract males using this cue. Males from the gonochoristic (male-female) sister species to *C. briggsae* and *C. tropicalis* – *C. nigoni* (*Cni*) and *C. wallacei* (*Cwa*), respectively – were also assayed for their ability to respond to ascr#8. The closest relative of *C. elegans*, the gonochoristic *C. inopinata* (*Cin*, formerly *C. sp. 34*), which has been recently characterized (13), was also tested, along with the *Japonica* Group gonochoristic species *C. japonica* (*Cja*) and *C. afra* (*Caf*).

Dwell times were analyzed as previously described using a Spot Retention Assay (14). Dwell times were transformed using a Base 2 Exponentiation (2^n, wherein n is equal to the raw dwell time value) to generate only non-zero data in order to calculated fold-changes. The Logbase2 of the fold-changes was then calculated to normalize the data. All

data sets were first checked for normality using a D'Agostino & Pearson normality test before comparisons were performed. Species in which both vehicle and ascr#8 dwell times were normally distributed were compared using a paired *t*-test, while those in which one or both data sets were not normally distributed were compared using a Wilcoxon matched-pairs signed rank test (GraphPad Prism 7.03). Transformed values were compared between related species via an unpaired *t*-test.

C. elegans responded strongly to ascr#8, supporting our previously published results using the Spot Retention Assay (7, 14). The other well studied hermaphroditic model species, *C. briggsae*, responded significantly, although not robustly as *C. elegans*, spending approximately 40 seconds in ascr#8 compared to *C. elegans*' dwell time of nearly 150 seconds. (**Figure 41A**). Surprisingly, the sister-species of *C. briggsae*, *C. nigoni*, responded in a more robust manner (**Figure 41A, B**). Similarly, while *C. tropicalis* exhibited no response to ascr#8 – its dwell time in ascr#8 being no different than that of the vehicle control (**Figure 41A**) – *C. wallacei* spent significantly more time in ascr#8 than the vehicle (**Figure 41A**), and therefore exhibited significantly more attraction than *C. tropicalis* (**Figure 41B**). These data suggest that females of gonochoristic species have retained their ability to attract males via ascr#8 signaling, while in androdiecious species, this communicatory mechanism is lost, potentially due to a lack of selective evolutionary pressure. However, neither *Japonica* Group member responded to ascr#8, nor did the closest *C. elegans* relative, *C. inopinata* (**Figure 41A**). This lack of attraction to ascr#8 may be due to the highly specialized insect-commensal life-cycle of *C. inopinata*. This species may have lost the necessary olfactory receptors to sense ascr#8 within its reduced genome (13), in a manner similar to *Trichinella* (15).

Given that hermaphroditism evolved multiple times during nematode evolution, it is plausible that *C. briggsae* and *C. nigoni* both inherited mechanisms to sense ascr#8. However, given the recent evolution of *C. briggsae* (between 100,000 to 1 million years ago) (16, 17), the reduced response compared to *C. nigoni* indicates less selective pressure

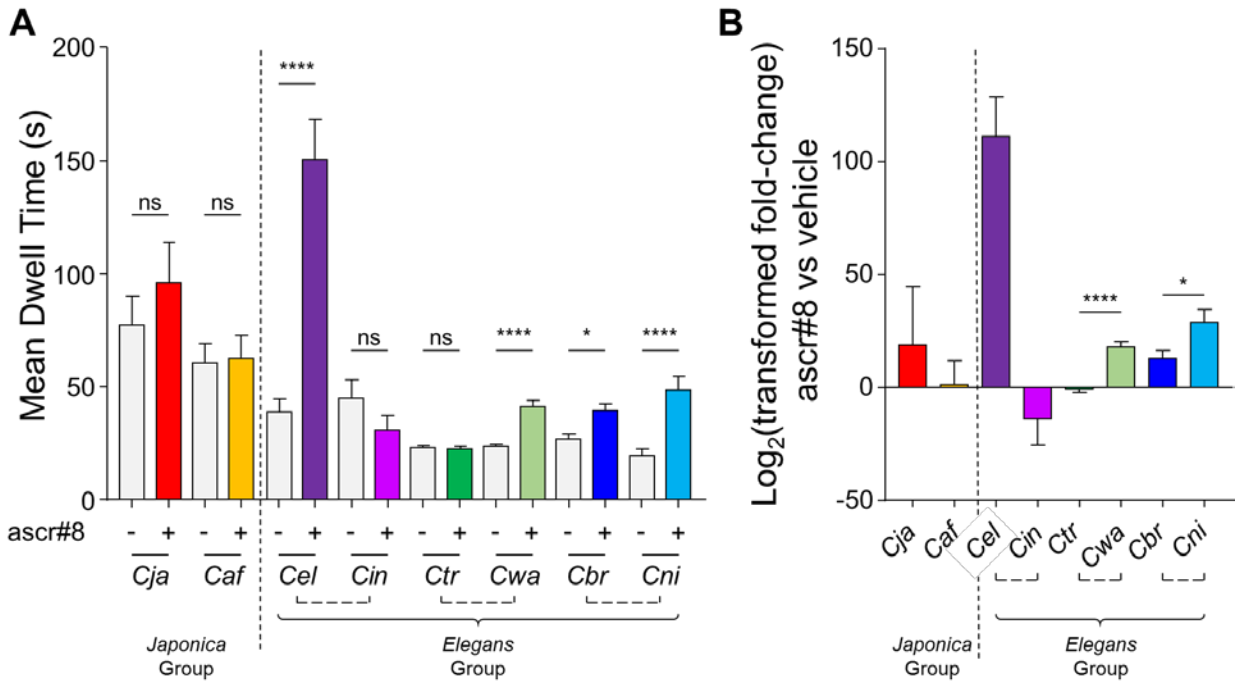

Figure 41. *Caenorhabditis* species males respond differentially to ascr#8.
(A) Dwell times of *Caenorhabditis* males in vehicle control (-) and ascr#8 (+), respectively. Hermaphroditic species were tested alongside their gonochoristic sister-species (denoted by dotted horizontal brackets: *C. elegans* vs. *C. inopinata, C. briggsae* vs. *C. nigoni*, *C. tropicalis* vs. *C. wallacei*). The *Japonica* Group species, *C. japonica* and *C. afra*, (left of vertical dotted line) were also tested for their attractive response. Species are displayed according to the most recent phylogenetic analysis of the *Caenorhabditis* genus (18). No species were as attracted to ascr#8 as *C. elegans*, although *C. briggsae*, *C. nigoni*, and *C. wallacei* did spend significantly more time in ascr#8 compared to the vehicle. Error bars denote SEM. n ≥ 12. Paired t-tests or Wilcoxon test (dependent on Normality test) of ascr#8 vs. vehicle control. **(B)** The Log_2 of Transformed fold-change of ascr#8 vs vehicle dwell times. See *Description* for transformation calculations. Among the sister-species pairs, gonochoristic species exhibited a significant increase in ascaroside dwell time. Student's t-test. Brackets linking species denote sister-species pairs, with androdiecious species on the left, gonochoristic on the right. * $p < 0.05$, **** $p < 0.0001$.

to retain ascr#8 sensing mechanisms. Similarly, *C. tropicalis* likely evolved the ability to self-fertilize even before the *nigoni-briggsae* split (18), leading to its inability to respond attractively to ascr#8. Together, these data suggest that ascr#8 functions as a *C. elegans* species-specific male attractant, with other species having lost the necessary mechanisms to sense and respond to this chemical. As different neurons and receptors may play roles in the ascr#8-mediated dauer development pathways, the comprehensive ability to sense this pheromone in the species tested is yet to be determined.

Reagents

The *C. elegans* strain CB1489 (*him-8(e1489)*) was obtained from Maureen Barr at Rutgers University. RE980 (*C. briggsae him-8(v188)*) and RE1017 (*C. tropicalis (him-8(v287)*) were generously provided by Ronald Ellis at Rowan University. The *C. wallacei* (JU1873), *C. nigoni* (JU1422), *C. afra* (JU1286), and *C. japonica* (DR5081) wild isolates were obtained from the *Caenorhabditis* Genetics Center. *C. inopinata* (NK74SC) was generously provided by the Forestry and Forest Products Research Institute in Japan.

Acknowledgements

We would like the thank Dr. Erich Schwarz (Cornell University) for valuable insights in interpreting our results. We would like to thank the Forestry and Forest Products Research Institute in Japan for providing the *C. inopinata* strain even before publication. We also like to thank Dr. Ronald Ellis (Rowan University) for protocols regarding maintenance of *C. briggsae him-8* and *C. tropicalis him-8* strains.

Funding

This work was supported by a grant from the NIH (R01DC016058 to J.S.).

Author Contributions

D.K.R.: Conceptualization, data curation, formal analysis, visualization, writing – original draft, writing – review & editing. L.J.R.: Data curation, writing – review & editing. J.S.: Funding acquisition, resources, writing – review & editing.

References

1. Butcher RA. Decoding chemical communication in nematodes. Natural product reports. 2017;34(5):472-7. Epub 2017/04/08. doi: 10.1039/c7np00007c. PubMed PMID: 28386618.

2. Chute CD, Srinivasan J. Chemical mating cues in *C. elegans*. Semin Cell Dev Biol. 2014;33:18-24. doi: 10.1016/j.semcdb.2014.06.002. PubMed PMID: 24977334.

3. Ludewig AH, Schroeder FC. Ascaroside signaling in *C. elegans*. WormBook. 2013:1-22. doi: 10.1895/wormbook.1.155.1. PubMed PMID: 23355522; PMCID: 3758900.

4. Choe A, von Reuss SH, Kogan D, Gasser RB, Platzer EG, Schroeder FC, Sternberg PW. Ascaroside signaling is widely conserved among nematodes. Curr Biol. 2012;22(9):772-80. doi: 10.1016/j.cub.2012.03.024. PubMed PMID: 22503501; PMCID: 3360977.

5. Liu Z, Kariya MJ, Chute CD, Pribadi AK, Leinwand SG, Tong A, Curran KP, Bose N, Schroeder FC, Srinivasan J, Chalasani SH. Predator-secreted sulfolipids induce defensive responses in *C. elegans*. Nature communications. 2018;9(1):1128. Epub 2018/03/21. doi: 10.1038/s41467-018-03333-6. PubMed PMID: 29555902; PMCID: PMC5859177.

6. McGrath PT, Ruvinsky I. A primer on pheromone signaling in *Caenorhabditis elegans* for systems biologists. Current opinion in systems biology. 2019;13:23-30. Epub 2019/04/16. doi: 10.1016/j.coisb.2018.08.012. PubMed PMID: 30984890; PMCID: PMC6456899.

7. Pungaliya C, Srinivasan J, Fox BW, Malik RU, Ludewig AH, Sternberg PW, Schroeder FC. A shortcut to identifying small molecule signals that regulate behavior and development in *Caenorhabditis elegans*. Proceedings of the National Academy of Sciences of the United States of America. 2009;106(19):7708-13. doi: 10.1073/pnas.0811918106; PMCID: 2683085.

8. Srinivasan J, Kaplan F, Ajredini R, Zachariah C, Alborn HT, Teal PE, Malik RU, Edison AS, Sternberg PW, Schroeder FC. A blend of small molecules regulates both mating and development in *Caenorhabditis elegans*. Nature. 2008;454(7208):1115-8. doi: 10.1038/nature07168. PubMed PMID: 18650807; PMCID: 2774729.

9. Srinivasan J, von Reuss SH, Bose N, Zaslaver A, Mahanti P, Ho MC, O'Doherty OG, Edison AS, Sternberg PW, Schroeder FC. A modular library of small molecule signals regulates social behaviors in *Caenorhabditis elegans*. PLoS Biol. 2012;10(1):e1001237. doi: 10.1371/journal.pbio.1001237. PubMed PMID: 22253572; PMCID: 3254649.

10. Artyukhin AB, Yim JJ, Srinivasan J, Izrayelit Y, Bose N, von Reuss SH, Jo Y, Jordan JM, Baugh LR, Cheong M, Sternberg PW, Avery L, Schroeder FC. Succinylated octopamine ascarosides and a new pathway of biogenic amine metabolism in Caenorhabditis elegans. The Journal of biological chemistry. 2013;288(26):18778-83. doi: 10.1074/jbc.C113.477000. PubMed PMID: 23689506; PMCID: 3696653.

11. Hodgkin J, Horvitz HR, Brenner S. Nondisjunction Mutants of the Nematode *Caenorhabditis elegans*. Genetics. 1979;91(1):67-94; PMCID: 1213932.

12. Ellis RE, Lin SY. The evolutionary origins and consequences of self-fertility in nematodes. F1000prime reports. 2014;6:62. Epub 2014/08/29. doi: 10.12703/p6-62. PubMed PMID: 25165561; PMCID: PMC4126538.

13. Kanzaki N, Tsai IJ, Tanaka R, Hunt VL, Liu D, Tsuyama K, Maeda Y, Namai S, Kumagai R, Tracey A, Holroyd N, Doyle SR, Woodruff GC, Murase K, Kitazume H, Chai C, Akagi A, Panda O, Ke H-M, Schroeder FC, Wang J, Berriman M, Sternberg PW, Sugimoto A, Kikuchi T. Biology and genome of a newly discovered sibling species of *Caenorhabditis elegans*. Nature communications. 2018;9(1):3216-. doi: 10.1038/s41467-018-05712-5. PubMed PMID: 30097582.

14. Narayan A, Venkatachalam V, Durak O, Reilly DK, Bose N, Schroeder FC, Samuel AD, Srinivasan J, Sternberg PW. Contrasting responses within a single neuron class enable sex-specific attraction in *Caenorhabditis elegans*. Proc Natl Acad Sci U S A.

2016;113(10):E1392-401. doi: 10.1073/pnas.1600786113. PubMed PMID: 26903633; PMCID: PMC4791020.

15. Srinivasan J, Dillman AR, Macchietto MG, Heikkinen L, Lakso M, Fracchia KM, Antoshechkin I, Mortazavi A, Wong G, Sternberg PW. The Draft Genome and Transcriptome of *Panagrellus redivivus* Are Shaped by the Harsh Demands of a Free-Living Lifestyle. Genetics. 2013;193(4):1279. doi: 10.1534/genetics.112.148809; PMCID: PMC3606103

16. Cutter AD, Yan W, Tsvetkov N, Sunil S, Felix MA. Molecular population genetics and phenotypic sensitivity to ethanol for a globally diverse sample of the nematode *Caenorhabditis briggsae*. Mol Ecol. 2010;19(4):798-809. Epub 2010/01/22. doi: 10.1111/j.1365-294X.2009.04491.x. PubMed PMID: 20088888.

17. Thomas CG, Wang W, Jovelin R, Ghosh R, Lomasko T, Trinh Q, Kruglyak L, Stein LD, Cutter AD. Full-genome evolutionary histories of selfing, splitting, and selection in *Caenorhabditis*. Genome Res. 2015;25(5):667-78. Epub 2015/03/19. doi: 10.1101/gr.187237.114. PubMed PMID: 25783854; PMCID: PMC4417115.

18. Stevens L, Félix M-A, Beltran T, Braendle C, Caurcel C, Fausett S, Fitch D, Frézal L, Gosse C, Kaur T, Kiontke K, Newton MD, Noble LM, Richaud A, Rockman MV, Sudhaus W, Blaxter M. Comparative genomics of 10 new *Caenorhabditis* species. Evolution Letters. 2019;3(2):217-36. doi: 10.1002/evl3.110. PubMed PMID: 31007946.

Chapter 7 Conclusions

Chapter 7A Conclusions

Summary

The work presented in this dissertation examines the molecular mechanisms involved in sex-specific processing of social cues. Using the roundworm, *Caenorhabditis elegans*, the machinery involved in sensation of mating cues, and the neuromodulation of the resulting behavioral responses, were studied. Preliminary data were generated for novel pheromones in **Chapter 2A**, while **Chapter 2B** focused on the differences in machinery regulating the responses to ascr#3 and ascr#8. Later chapters then worked to elucidate the identity of ascr#8 receptors, through both transcriptomic and genetic screens (**Chapter 4C)**, as well as directed, biochemical approaches (**Chapter 5**). A neuromodulator that controls the valence of the male behavioral response to ascr#8 was identified as *flp-3* (**Chapter 3B**). New technologies were developed as part of these studies, including a male-adapted microfluidic device (**Chapter 4B**), the behavioral Single Worm Assay (**Chapter 3B**), and a peptide rescue by feeding paradigm (**Chapter 3B**). Together, the results of this dissertation deepen our understand of sex-specific sensation and processing of social cues, allowing us to better understand just how the brain works.

Nematode Social Signaling is Modular and Complex

Worms employ small molecules called ascarosides as pheromones and an alphabet of social communication signals (1-3). As discussed in **Chapter 2A**, these structures are extremely modular in structure, with various moieties being incorporated onto the ends of a sugar core or fatty-acid derived side chain (4, 5).

Small changes in ascaroside structure can elicit vast differences in output. This is most readily observed in the differences between ascr#3 and ascr#10, which differ only in the saturation of their fatty acid side chain. However, they elicit opposite, sex-specific responses, and more recently have been shown to not only regulate germ line proliferation and development but serve to link the behavioral and physiological outputs of their signaling (**Chapter 2B**) (7-12).

While the molecule studied in depth in this dissertation, ascaroside #8 (ascr#8), has been a known, potent male attractant (13), recent in-depth analyses of *C. elegans* exometabolome identified modified ascr#8 derivates, ascr#81 and ascr#82, with glutamic acid and glutamyl-glutamic acid moieties being attached to the *p*-aminobenzoate group respectively (14). In **Chapter 5**, as part of our development of a photoaffinity probe, we have shown that ascr#81 maintains the male attractant ability of ascr#8 (15). These results suggest that the *p*-aminobenzoate group, the initial building block in the ascr#8-#81-#82 chain, is the functional unit for attracting males, and that the glutamic acid groups serve to signal other information about either the environment, or physiological state of the hermaphrodite producing the pheromone. What these other cues may be have yet to be elucidated.

Recent studies have uncovered a growing body of non-ascaroside signals employed by nematodes for signaling. While some of these are species-specific, such as the paratose-derived molecules employed by *Pristionchus pacificus* (16), or the *C. nigoni*-specific caenorhabdose-based epimers (17), this work details the first study of the effects of a *C. elegans*-specific sugar-derivative of ascr#3, which we have named ascr#3-sd for this

body of work (**Chapter 2A**). Interestingly, males exhibit a flip in behavioral valence to this cue compared to the ascarylose-based relative ascr#3, avoiding the cue instead of being attracted to it. Hermaphrodites do not experience a similar valence change: they lose their avoidance of the cue, but do not gain an attraction to it. Does this suggest that a male-specific receptor for ascr#3-sd exists? If so, what is ascr#3-sd signaling, and why is its role different so different, when the only change is the normally conserved sugar, and not the more often variable side chain?

We also began to generate preliminary data into the behavioral effects of the glutamine-based signaling molecule, nacq#1. This molecule was recently shown to alter the rate of reproductive development (18), and in this dissertation, we show that low concentrations (within the nanomolar range) of nacq#1 result in slight, yet significant attraction of hermaphrodites (**Chapter 2A**). However, these data are preliminary, and an expansion of the dose-response curve into the sub-nanomolar range is required for a more complete understanding of the social implications of this molecule.

These studies add to the depth of understanding of the modularity of nematode social signaling. While most pheromones are based on ascarylose-derived molecules, working this generation has contributed preliminary data adding to our knowledge of the modularity of signals.

***Caenorhabditis* Social Signals Exhibit Conserved Activity Across Species**

Ascaroside signaling has been shown to be conserved across nematode species (19). We have shown that ascr#3 is among the ascarosides that has conserved signaling, but interestingly, the species-specific (ω)-hydroxylation observed in *C. nigoni* ascr#3 molecules removes the ability of males to respond attractively to the pheromone (**Chapter 2A**) (20). Similar to the mystery of what the glutamic acid moieties in ascr#81 and ascr#82 add to the ascr#8 signal (14, 15), the role of the *C. nigoni*-hydroxylation remains unknown (20).

The majority of this dissertation focused on ascr#8 as a male attracting pheromone. In **Chapter 6**, we investigated the conserved ability of male *Caenorhabditis* nematodes to respond attractively to ascr#8 (21). Males of the two non-*elegans* hermaphroditic species, *C. tropicalis* and *C. briggsae*, exhibited decreased attraction to ascr#8 compared to their gonochoristic sister species. While none of the species tested exhibited an attraction close to the level of *C. elegans* bioactivity, they did exhibit significant attraction over vehicle. The two species that exhibited no attraction within the *Elegans* group were *C. tropicalis* – the most ancient hermaphrodite within the genus – and the recently characterized gonochoristic sister species to *C. elegans*, *C. inopinata* (**Chapter 6**) (21, 22).

C. inpoinata is unique in that it is twice the length of *C. elegans*, and despite its status as a "sister species", it is as divergent from *C. elegans* as the remainder of the *Elegans* group (22). Interestingly, *C. inopinata* has experiences a remarkable reduction in olfactory receptor gene count, likely contributing to its inability to respond attractively to ascr#8.

Together, these data add to the growing base of knowledge that ascaroside signaling is not only complex, but extremely conserved across Nematoda. Elucidation of how these signals function, and how they are processed, will increase our understanding of social communication.

Ascaroside #8 Utilizes Unique Neuronal Pathways Compared to Ascaroside #3

The ascarosides, ascr#3 and ascr#8, both elicit attractive behavior in males (23). These cues are both sensed via the male specific CEM neurons, although ascr#3 sensation is more promiscuous (11, 23-25) (**Figure 42**). In focusing on the physiology of the male specific CEM neurons, we have previously shown that the sensation of these ascarosides does not elicit reliable nor stereotyped calcium transients (23). This is not an ascaroside-specific phenomenon, as the ADF neurons generate robust calcium transients upon ascr#3 sensation (24).

In order to more reliably record calcium transients in the amphid chemosensory neurons of males, which are narrower than their hermaphroditic counterparts, in **Chapter 4B** we developed an adapted microfluidic device. This olfactory chip incorporates a narrower channel to more efficient trap males, a pinch in the loading port to prevent reversals upon sensation of aversive cues, and a turn in the loading port. This turn allows for the imaging of both neurons of a bilateral pair – although in neuronal classes such as the radially symmetric CEM, all four neurons are only distinguishable a third of a time (**Chapter 4B**) (26).

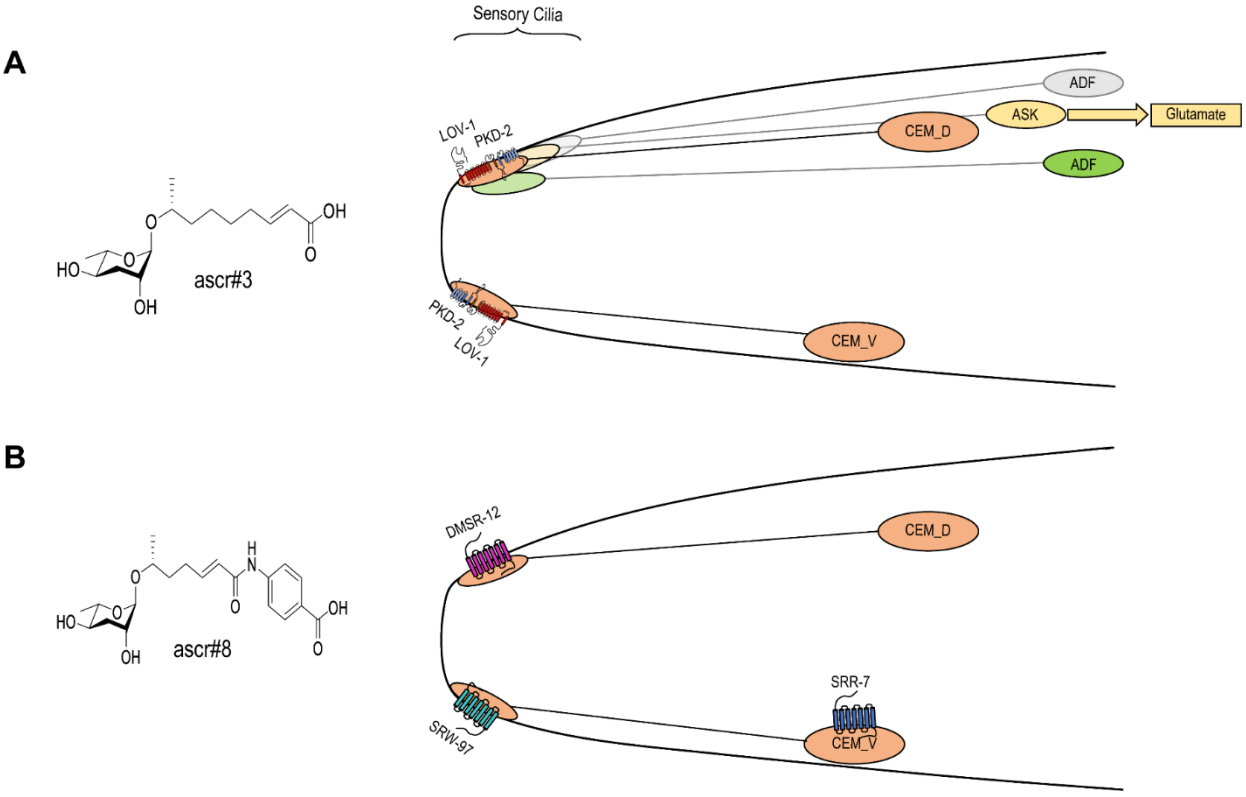

Figure 42. Separate machinery governs the neuronal and behavioral responses to ascr#3 and ascr#8. The sensory pathways for **(A)** ascr#3 and **(B)** ascr#8 are discrete. **(A)** ascr#3 is sensed by multiple neurons, including ADL (grey), ADF (green), ASK (yellow), and the male specific CEM neurons. ASK likely releases glutamate upon sensation of ascr#3 (arrow and box). Within the sensory cilia of the CEM neurons, the mechanosensory proteins LOV-1 and PKD-2 are localized, although only LOV-1 plays a role in the sensation of ascr#3 (**Chapter 2A**). Structures of LOV-1 and PKD-2 adapted from (6). **(B)** ascr#8 is sensed only by the CEM neurons, via the receptors, DMSR-12 and SRW-97 (**Chapter 4C**). Within the soma of CEM_VL, SRR-7 plays a role in the regulation of the CEM sensory circuit.

While both ascr#3 and ascr#8 are sensed via the CEM neurons, our data suggest that that is limit of their shared circuitry (**Figure 42**). In **Chapter 2C**, we show that the polycystin, *pkd-2*, which is expressed in extracellular vesicle-releasing neurons (27, 28) of the male tail and CEM neurons (29-31), does not play a role in the sensation of either ascaroside. Interestingly, *lov-1*, which function as heterodimers with *pkd-2* in mechanosensory pathways and to date has been phenotypically indistinguishable from the other polycystin (30, 32), shows an increase in attraction to ascr#3 (**Chapter 2C**). This response was specific to ascr#3, suggesting a role of *lov-1* in sensation of the ascaroside that is separate from *pkd-2* function (**Figure 42A**).

It has previously been shown that the ASK neurons contribute to ascr#3 sensation (13, 23). ASK expresses the glutamate transporter gene, *eat-4* (33). We show in **Chapter 2C** that animals defective in *eat-4* production are dysfunctional in their response to ascr#3, exhibited an increase in attraction to the pheromone (**Figure 42A**). Interestingly, this phenotype is the opposite of removal the ASK neuron itself (23). Decoupling the role of glutamatergic signaling and ASK function will provide valuable insights into sensory integration.

Together, these data support the notion that while the CEM neurons themselves are responsible for sensation of both ascr#3 and ascr#8, the machinery involved is unique to each pheromone (**Figure 42**).

Multiple ascr#8 Receptors Function Within the CEM Sensory Network

Given the stochastic and non-stereotyped calcium physiology of the CEM network, we generated a set of single-cell transcriptomes of the male-specific chemosensory neurons (**Chapter 4C**). We showed that each CEM neuron exhibits its own transcriptomic landscape, with unique enrichment profiles of G protein-coupled receptors (GPCRs) in each cell.

Promoter-GFP Fusions Suggest the Presence of Sub-Class of CEM Neurons

Our subsequent GFP-fusion expression profiling revealed that expression of GPCRs enriched in CEM are segregated by an apparent dorsal-ventral split (**Chapter 4C**). This was seen most prominently in the expression profiles of *srw-97* and *dmsr-12*, which drove GFP expression in the ventral and dorsal CEM neurons, respectively. However, principle component analysis of the CEM transcriptomic landscape did not reveal and significant evidence supporting such a split into two possible neuronal subclasses (**Figure 43**). However, given the low mapping rate of our transcriptomic data set (**Chapter 4C/Appendix 2**), it is difficult to make any solid conclusions regarding this hypothesis. Deeper sequencing depth with a higher mapping rate will allow for a more useful determination as to the presence of ventral/dorsal sub-classes of the CEM neurons.

Phylogenetic Analyses of srw-97 Reveals an Ancestral Gene

We showed in **Chapter 4C,** through both RNAi-mediated knockdown and CRISPR/Cas-mediated gene editing, that the two GPCRs, *srw-97* and *dmsr-12*, are involved in the ascr#8 response (**Figure 42B**). Again, these two receptors are expressed in non-overlapping subsets of the CEM neurons, suggesting that they are specific to ventral and dorsal function, respectively.

The gene encoding *srw-97* is only present in the genome of *C. elegans* (**Chapter 4C**). Paralogs of the gene do exist across the *Caenorhabditis* genus, but they are more closely related to the gene encoding *srw-98*. In fact, the *srw-97* gene appears to be the product of an ancient gene duplication of *srw-98*.

We provide evidence in **Chapter 4C** to support this claim, mainly that the *C. elegans*-specific gene (*srw-97*) is present on Chromosome II, in a region devoid of GPCR genes. Meanwhile, *srw-98* is located on Chromosome V, in an area dense in GPCR coding genes. This translocation likely occurred simultaneously with the gene duplication event and – given the presence of *srw-97* only in the *C. elegans* genome – occurred following the speciation of *C. elegans*.

Analysis of CEM transcriptomes reveals a slight enrichment of *srw-98* in an expression pattern matching that of *srw-97*, although at a much lower level (**Chapter 4C**). Testing of *srw-98* null and rescue animals will provide further evidence of srw-98 as a related, and ancestral, gene to *srw-97*.

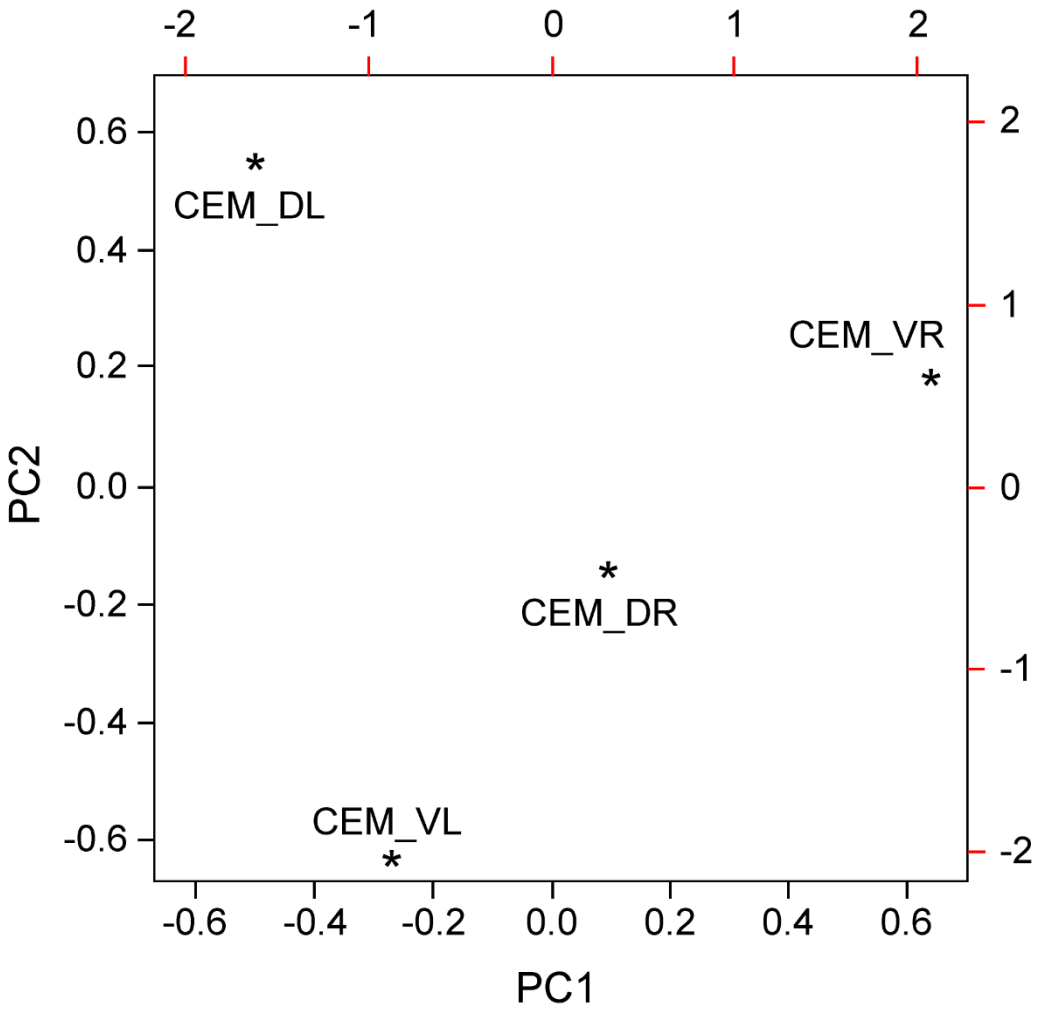

Figure 43. PCA Analysis of the CEM neurons does not reveal any sub-class on a dorsal-ventral axis. Principle component analysis of the CEM transcriptomes did not reveal any segregation of the neuronal class into sub-classes of neurons based on anatomical position. While dorsal and ventral CEM neurons express non-overlapping receptors (**Chapter 4C**), their transcriptomic profiles do not segregate in any meaningful way. A left-right split is more visible, although not statistically significant.

SRR-7 Acts as a Soma-Localized Regulator of CEM Activity

The GPCR coding gene, *srr-7*, was also found to be enriched in our transcriptomic data set. Interestingly, despite its lack of localization to the sensory cilia of the CEM neurons, knockdown of *srr-7* resulted in a complete loss of behavioral response to ascr#8.

The location of the *srr-7* gene between two other CEM-enriched GPCRs makes elucidation of the role of the receptor difficult. While knockdown of *srr-7* is specific to the receptor, it is closely related to three other *srr* genes (-8, -9, and -10), and there can be no guarantee that the dsRNA does not target these genes as well. However, generation of a gene deletion of *srr-7* will also affect the function and expression of the neighboring *srj-27* and *str-171* genes (**Chapter 4C**).

However, given the stark and significant defect upon *srr-7* knockdown, it is likely that the receptor plays a role in the ascr#8 response (**Figure 42B**). Combined with the localization data, we pose that *srr-7* functions within the soma of CEM VL, possibly synaptically, to regulate the CEM sensory network (**Chapter 4C**).

Development of A Bioactive Probe Allows for Targeted Identification of Pheromone Binders

These avenues of receptor identification lack one crucial facet: they do not show that these GPCRs *bind* the pheromone they are involved in sensing. While they are clearly involved in the response and sensation of ascr#8, they may be merely function in the signaling cascade, or as a heterodimeric component of the ascr#8 sensory machinery.

In order to definitively show that receptors bind their proposed ligands, they are often expressed in a heterologous system, such as Xenopus oocytes (34), or Chinese hamster ovarian cells expressing aequorin (35). However, not all receptors remain functional expressed in these systems. For example, with the GPCR involved in osas#9 sensation, TYRA-2 (36), only low level of expression within in transfected *Xenopus* oocytes is

achieved and yields little-to-no currents even in response to its native ligand, tyramine (*unpublished data*).

To avoid the complications that can arise during such cell-based assays, we developed a bioactive ascr#8 probe (**Chapter 5**) (15). This molecule maintains the core structure of ascr#8, although whereas ascr#81 incorporates a glutamic acid to the terminus of the *p*-aminobenzoate moiety (14), the ascr#8 probe contains a photo-crosslinking group (15). This modified ascr#8 is still able to elicit male attraction, suggesting that it is still sensed properly by the CEM neurons.

C. elegans males can be exposed to this pheromone, and the probe crosslinked to the receptor using a UV light during the exposure. Worms would then be lysed to free the bound probe-receptor molecules from the mass of the animal. Using the other moieties in the cross-linking group, the rec can be pulled down in an immunoprecipitation experiment. The binding pocket of the receptor can then be sequences via proteomics and mass spectroscopy, confirming the identity of the GPCR sensing ascr#8 (**Figure 44**).

This study primes the field for the development of bioactive ascaroside probes and should result in expedited identification of ascaroside-sensing GPCRs - a field that unfortunately experiences a growing lag in regard to the expansion of known ascaroside molecules.

A Neuropeptide Gene Controls the Valence of Male Behavioral Responses to ascr#8

A reverse genetic screen of male-specific neuron-enriched neuropeptides (37-39) identified *flp-3* as a key player in regulating the behavioral response to ascr#8 (**Chapter 3B**). Using our novel Single Worm Assay, *flp-3 lof* males were found to exhibit a defect in their attractive behavior to ascr#8. Interestingly, they also exhibited a behavioral phenotype of ascr#8 avoidance, a behavior normal reserved for hermaphroditic response (**Chapter 3B**) (13). The notion that the *flp-3* phenotype is sex-specific was further

confirmed by a translational fusion exhibiting expression of the neuropeptide in the male-specific SPD spicule neurons.

Employing cell culture techniques, the binding affinity of FLP-3 peptides to their cognate receptors were identified. The previously identified FLP-3 receptor, NPR-10 (38), was confirmed as a potent binder of FLP-3 peptides, with sub-micromolar affinities for

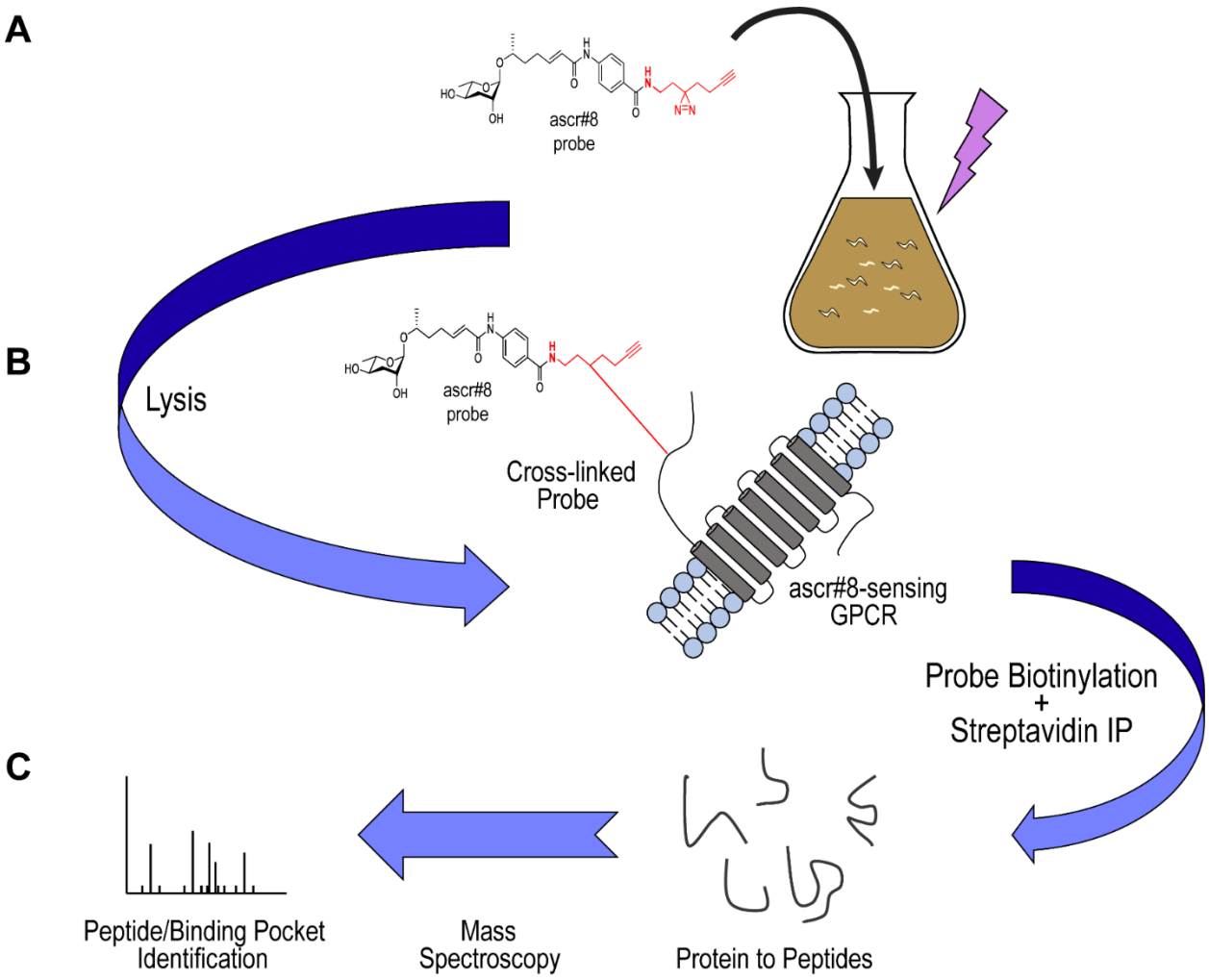

Figure 44. Experimental paradigm for utilization of ascr#8 photoaffinity probe for receptor identification.
(A) A male-enriched liquid culture of *him-5 C. elegans* will be grown and exposed to the ascr#8 photoaffinity probe developed in **Chapter 5**. During exposure to the pheromone probe, animals will be treated with UV-light (lightning bolt) to cross-link the probe to the receptor. **(B)** Following worm lysis, the receptor-bound probes will be biotinylated, and purified via Streptavidin immunoprecipitation. **(C)** The receptors will be broken down into smaller peptide sequences to remove the hydrophobic, transmembrane domains of the receptors, and binding pocket sequences will be eluted, analyzed and characterized via mass spectroscopy.

the majority of the peptides. A novel receptor, FRPR-16, was also discovered as having even higher affinities for FLP-3 peptides (**Chapter 3B**). Expression pattern analysis of revealed that NPR-10 is promiscuously expressed in the male head, suggesting that *flp-3* may serve to regulate the integration of ascr#8 sensory integration (**Chapter 3B**).

A Novel Mode of Peptide Rescue: Feeding

Adapting a feeding protocol that mirrors RNAi-knockdown by feeding (40, 41), we developed a system that allows us to rescue individual neuropeptides in mutant animals by feeding them *E. coli* expressing the peptide of interest (**Chapter 3B**).

E. coli expressing individual FLP-3 peptides were fed to *flp-3 lof* animals. In this manner, we were able to identify active components of the FLP-3 propeptide. Namely, TPLGTMRFamide (FLP-3.2) and NPENDTPFGTMRFamide (FLP-3.9) are the two necessary and sufficient peptides for maintaining wild-type response to ascr#8 (**Chapter 3B**). Feeding of TPLGTMRFamide alone is able to suppress the avoidance phenotype present in *flp-3 lof* males. However, it cannot restore the attractive behavior of wild-type males. NPENDTPFGTMRFamide feeding, however, not only suppressing the avoidance behavior, but drives normal levels of attraction to ascr#8. (**Chapter 3B**).

This feeding paradigm offers a robust technology for rescue of individual neuropeptides in *C. elegans* studies. Given the large number of neuropeptide genes and final peptide products (**Chapter 3A**) (42, 43), this will allow for a more rapid generation of rescue constructs, by bypassing the need for transgenic generation.

Overall Conclusions

Together, the data presented in this dissertation serve to strengthen and deepen our understanding of sex-specific neuronal regulation of social behaviors. Using the nematode, *C. elegans*, these studies not only elucidate mechanisms governing these principles, but develop technologies that will assist future studies in their endeavors (26).

The pheromone, ascr#8, while resulting in a sex-specific response only seen in males, nevertheless stands poised to serve as a reliable and robust model of study. It generates stochastic calcium transients in the sensory neurons of an animal that is famous for its stereotypy (23); elicits a robust behavioral response regulated by a single, yet complex neuropeptide gene (**Chapter 3A**); is sensed by a host of GPCRs (**Chapter 4C**); and elicits conserved outputs across the phylogeny (**Chapter 6**) (21).

Future studies investigating the neuronal processes activated by ascr#8 and the mechanisms governing those phenomena will result in a complex network of cellular, molecular, and genetic interactions. These findings will deepen our understanding of not only functional connectomics, but sex-specificity and neuronal networks as a whole.

References

1. Butcher RA. Decoding chemical communication in nematodes. Natural product reports. 2017;34(5):472-7. Epub 2017/04/08. doi: 10.1039/c7np00007c. PubMed PMID: 28386618.

2. Butcher RA. Natural products as chemical tools to dissect complex biology in *C. elegans*. Current Opinion in Chemical Biology. 2019;50:138-44. doi: 10.1016/j.cbpa.2019.03.005.

3. McGrath PT, Ruvinsky I. A primer on pheromone signaling in *Caenorhabditis elegans* for systems biologists. Current opinion in systems biology. 2019;13:23-30. Epub 2019/04/16. doi: 10.1016/j.coisb.2018.08.012. PubMed PMID: 30984890; PMCID: PMC6456899.

4. von Reuss SH, Schroeder FC. Combinatorial chemistry in nematodes: modular assembly of primary metabolism-derived building blocks. Natural product reports. 2015;32(7):994-1006. doi: 10.1039/c5np00042d. PubMed PMID: 26059053.

5. Zhang YK, Sanchez-Ayala MA, Sternberg PW, Srinivasan J, Schroeder FC. Improved Synthesis for Modular Ascarosides Uncovers Biological Activity. Org Lett. 2017;19(11):2837-40. Epub 2017/05/18. doi: 10.1021/acs.orglett.7b01009. PubMed PMID: 28513161; PMCID: PMC5533076.

6. Kahn-Kirby AH, Bargmann CI. TRP CHANNELS IN C. ELEGANS. Annual Review of Physiology. 2006;68(1):719-36. doi: 10.1146/annurev.physiol.68.040204.100715.

7. Apirson EZ, Ruvinsky I. Coordinated behavioral and physiological responses to a social signal are regulated by a shared neuronal circuit. Curr Biol. 2019(THIS ISSUE).

8. Apirson EZ, Ruvinsky I. Dynamic regulation of adult-specific functions of the nervous system by signaling from the reproductive system. Curr Biol. 2019(THIS ISSUE).

9. Aprison EZ, Ruvinsky I. Sex Pheromones of *C. elegans* Males Prime the Female Reproductive System and Ameliorate the Effects of Heat Stress. PLoS Genet.

2015;11(12):e1005729. Epub 2015/12/10. doi: 10.1371/journal.pgen.1005729. PubMed PMID: 26645097; PMCID: PMC4672928.

10. Aprison EZ, Ruvinsky I. Sexually Antagonistic Male Signals Manipulate Germline and Soma of *C. elegans* Hermaphrodites. Curr Biol. 2016;26(20):2827-33. Epub 2016/10/26. doi: 10.1016/j.cub.2016.08.024. PubMed PMID: 27618262.

11. Aprison EZ, Ruvinsky I. Counteracting Ascarosides Act through Distinct Neurons to Determine the Sexual Identity of *C. elegans* Pheromones. Curr Biol. 2017;27(17):2589-99.e3. Epub 2017/08/29. doi: 10.1016/j.cub.2017.07.034. PubMed PMID: 28844646.

12. Reilly DK, Srinivasan J. Chemical Communication: Linking Behavior and Physiology. Current Biology. 2019;29(23):R1226-R8. doi: 10.1016/j.cub.2019.10.031. PubMed PMID: 31794752.

13. Pungaliya C, Srinivasan J, Fox BW, Malik RU, Ludewig AH, Sternberg PW, Schroeder FC. A shortcut to identifying small molecule signals that regulate behavior and development in *Caenorhabditis elegans*. Proceedings of the National Academy of Sciences of the United States of America. 2009;106(19):7708-13. doi: 10.1073/pnas.0811918106; PMCID: 2683085.

14. Artyukhin AB, Zhang YK, Akagi AE, Panda O, Sternberg PW, Schroeder FC. Metabolomic "Dark Matter" Dependent on Peroxisomal beta-Oxidation in *Caenorhabditis elegans*. J Am Chem Soc. 2018;140(8):2841-52. Epub 2018/02/06. doi: 10.1021/jacs.7b11811. PubMed PMID: 29401383; PMCID: PMC5890438.

15. Zhang YK, Reilly DK, Yu J, Srinivasan J, Schroeder FC. Photoaffinity probes for nematode pheromone receptor identification. Journal of Organic & Biomolecular Chemistry. 2019:10.1039/c9ob02099c. doi: 10.1039/c9ob02099c. PubMed PMID: 31781713.

16. Bose N, Ogawa A, von Reuss SH, Yim JJ, Ragsdale EJ, Sommer RJ, Schroeder FC. Complex small-molecule architectures regulate phenotypic plasticity in a nematode. Angew Chem Int Ed Engl. 2012;51(50):12438-43. Epub 2012/11/20. doi: 10.1002/anie.201206797. PubMed PMID: 23161728; PMCID: PMC3733369.

17. Bergame CP, Dong C, Sutour S, von Reuss SH. Epimerization of an Ascaroside-Type Glycolipid Downstream of the Canonical β-Oxidation Cycle in the Nematode *Caenorhabditis nigoni*. Organic Letters. 2019. doi: 10.1021/acs.orglett.9b03808.

18. Ludewig AH, Artyukhin AB, Aprison EZ, Rodrigues PR, Pulido DC, Burkhardt RN, Panda O, Zhang YK, Gudibanda P, Ruvinsky I, Schroeder FC. An excreted small molecule promotes *C. elegans* reproductive development and aging. Nat Chem Biol. 2019;15(8):838-45. Epub 2019/07/20. doi: 10.1038/s41589-019-0321-7. PubMed PMID: 31320757; PMCID: PMC6650165.

19. Choe A, von Reuss SH, Kogan D, Gasser RB, Platzer EG, Schroeder FC, Sternberg PW. Ascaroside Signaling is Widely Conserved Among Nematodes. Current Biology. 2012;22(9):772-80. doi: 10.1016/j.cub.2012.03.024. PubMed PMID: PMC3360977.

20. Dong C, Reilly DK, Bergame C, Dolke F, Srinivasan J, von Reuss SH. Comparative Ascaroside Profiling of *Caenorhabditis* Exometabolomes Reveals Species-Specific (ω) and (ω - 2)-Hydroxylation Downstream of Peroxisomal beta-Oxidation. J Org Chem. 2018. Epub 2018/02/27. doi: 10.1021/acs.joc.8b00094. PubMed PMID: 29480728.

21. Reilly DK, Randle LJ, Srinivasan J. Evolution of hermaphroditism decreases efficacy of Ascaroside#8-mediated mate attraction in *Caenorhabditis* nematodes. microPublication Biology. 2019. doi: 10.17912/micropub.biology.000134.

22. Kanzaki N, Tsai IJ, Tanaka R, Hunt VL, Liu D, Tsuyama K, Maeda Y, Namai S, Kumagai R, Tracey A, Holroyd N, Doyle SR, Woodruff GC, Murase K, Kitazume H, Chai C, Akagi A, Panda O, Ke H-M, Schroeder FC, Wang J, Berriman M, Sternberg PW, Sugimoto A, Kikuchi T. Biology and genome of a newly discovered sibling species of *Caenorhabditis elegans*. Nature communications. 2018;9(1):3216-. doi: 10.1038/s41467-018-05712-5. PubMed PMID: 30097582.

23. Narayan A, Venkatachalam V, Durak O, Reilly DK, Bose N, Schroeder FC, Samuel AD, Srinivasan J, Sternberg PW. Contrasting responses within a single neuron class enable sex-specific attraction in *Caenorhabditis elegans*. Proc Natl Acad Sci U S A.

2016;113(10):E1392-401. doi: 10.1073/pnas.1600786113. PubMed PMID: 26903633; PMCID: 4791020.

24. Fagan KA, Luo J, Lagoy RC, Schroeder FC, Albrecht DR, Portman DS. A Single-Neuron Chemosensory Switch Determines the Valence of a Sexually Dimorphic Sensory Behavior. Curr Biol. 2018;28(6):902-14.e5. Epub 2018/03/13. doi: 10.1016/j.cub.2018.02.029. PubMed PMID: 29526590; PMCID: PMC5862148.

25. Jang H, Kim K, Neal SJ, Macosko E, Kim D, Butcher RA, Zeiger DM, Bargmann CI, Sengupta P. Neuromodulatory state and sex specify alternative behaviors through antagonistic synaptic pathways in *C. elegans*. Neuron. 2012;75(4):585-92. doi: 10.1016/j.neuron.2012.06.034. PubMed PMID: 22920251; PMCID: PMC3462069.

26. Reilly DK, Lawler DE, Albrecht DR, Srinivasan J. Using an Adapted Microfluidic Olfactory Chip for the Imaging of Neuronal Activity in Response to Pheromones in Male *C. Elegans* Head Neurons. Journal of Visualized Experiments. 2017(127):e56026. doi: doi:10.3791/56026.

27. Wang J, Kaletsky R, Silva M, Williams A, Haas LA, Androwski RJ, Landis JN, Patrick C, Rashid A, Santiago-Martinez D, Gravato-Nobre M, Hodgkin J, Hall DH, Murphy CT, Barr MM. Cell-Specific Transcriptional Profiling of Ciliated Sensory Neurons Reveals Regulators of Behavior and Extracellular Vesicle Biogenesis. Curr Biol. 2015;25(24):3232-8. Epub 2015/12/22. doi: 10.1016/j.cub.2015.10.057. PubMed PMID: 26687621; PMCID: PMC4698341.

28. Wang J, Silva M, Haas LA, Morsci NS, Nguyen KCQ, Hall DH, Barr MM. *C. elegans* Ciliated Sensory Neurons Release Extracellular Vesicles that Function in Animal Communication. Current Biology. 2014;24:518-25.

29. Bae YK, Qin H, Knobel KM, Hu J, Rosenbaum JL, Barr MM. General and cell-type specific mechanisms target TRPP2/PKD-2 to cilia. Development. 2006;133(19):3859-70. doi: 10.1242/dev.02555. PubMed PMID: 16943275.

30. Barr MM, DeModena J, Braun D, Nguyen CQ, Hall DH, Sternberg PW. The *Caenorhabditis elegans* autosomal dominant polycystic kidney disease gene homologs *lov-1* and *pkd-2* act in the same pathway. Curr Biol. 2001;11. doi: 10.1016/S0960-9822(01)00423-7.

31. Knobel KM, Peden EM, Barr MM. Distinct protein domains regulate ciliary targeting and function of *C. elegans* PKD-2. Experimental Cell Research. 2008;314(4):825-33. doi: 10.1016/j.yexcr.2007.10.017.

32. Hu J, Barr MM. ATP-2 Interacts with the PLAT Domain of LOV-1 and Is Involved in *Caenorhabditis elegans* Polycystin Signaling. Molecular Biology of the Cell. 2005;16(2):458-69. doi: 10.1091/mbc.E04-09-0851. PubMed PMID: PMC545878.

33. Lee RY, Sawin ER, Chalfie M, Horvitz HR, Avery L. EAT-4, a homolog of a mammalian sodium-dependent inorganic phosphate cotransporter, is necessary for glutamatergic neurotransmission in *Caenorhabditis elegans*. J Neurosci. 1999;19(1):159-67. Epub 1998/12/31. PubMed PMID: 9870947; PMCID: PMC3759158.

34. Bianchi L, Driscoll M. Heterologous expression of *C. elegans* ion channels in *Xenopus* oocytes. WormBook. 2006:1-16. doi: 10.1895/wormbook.1.117.1. PubMed PMID: 18050441; PMCID: PMC4781024.

35. Beets I, Lindemans M, Janssen T, Verleyen P. Deorphanizing G protein-coupled receptors by a calcium mobilization assay. Methods Mol Biol. 2011;789:377-91. Epub 2011/09/17. doi: 10.1007/978-1-61779-310-3_25. PubMed PMID: 21922422.

36. Chute CD, DiLoreto EM, Zhang YK, Reilly DK, Rayes D, Coyle VL, Choi HJ, Alkema MJ, Schroeder FC, Srinivasan J. Co-option of neurotransmitter signaling for inter-organismal communication in *C. elegans*. Nat Commun. 2019;10(1):3186. Epub 2019/07/20. doi: 10.1038/s41467-019-11240-7. PubMed PMID: 31320626; PMCID: PMC6639374.

37. Kim K, Li C. Expression and regulation of an FMRFamide-related neuropeptide gene family in *Caenorhabditis elegans*. J Comp Neurol. 2004;475(4):540-50. doi: 10.1002/cne.20189. PubMed PMID: 15236235.

38. Li C, Kim K. Neuropeptides. WormBook. 2008. Epub 2008. doi: 10.1895/workbook.1.142.1.

39. Li C, Kim K. Family of FLP Peptides in *Caenorhabditis elegans* and Related Nematodes. Front Endocrinol (Lausanne). 2014;5:150. doi: 10.3389/fendo.2014.00150. PubMed PMID: 25352828; PMCID: 4196577.

40. Fraser AG, Kamath RS, Zipperlen P, Martinez-Campos M, Sohrmann M, Ahringer J. Functional genomic analysis of *C. elegans* chromosome I by systematic RNA interference. Nature. 2000;408(6810):325-30. doi: 10.1038/35042517.

41. Xu J, Jiang Y, Wan L, Wang Q, Huang Z, Liu Y, Wu Y, Chen Z, Liu X. Feeding recombinant *E. coli* with GST-mBmKTX fusion protein increases the fecundity and lifespan of *Caenorhabditis elegans*. Peptides. 2017;89:1-8. doi: 10.1016/j.peptides.2017.01.003.

42. Van Bael S, Edwards SL, Husson SJ, Temmerman L. Identification of Endogenous Neuropeptides in the Nematode *C. elegans* Using Mass Spectrometry. Methods Mol Biol. 2018;1719:271-91. Epub 2018/02/25. doi: 10.1007/978-1-4939-7537-2_18. PubMed PMID: 29476518.

43. Van Bael S, Zels S, Boonen K, Beets I, Schoofs L, Temmerman L. A *Caenorhabditis elegans* Mass Spectrometric Resource for Neuropeptidomics. Journal of The American Society for Mass Spectrometry. 2018. doi: 10.1007/s13361-017-1856-z.

Chapter 7B Future Directions

Summary

A host of new avenues of research arise when answering any line of scientific questioning. Here, potential paths of inquiry are posed, in addition to how unpublished findings can influence this questioning. The mate recognition pheromone, ascr#8, allows for research within a wide area of study, ranging from chemosensation (**Chapter 4**), neuromodulation (**Chapter 3**), biochemistry (**Chapter 5**), evolution (**Chapter 6**), and potentially epigenetics (**this chapter**). The sex-specific nature of the ascr#8 response adds a layer of complexity to these problems that will add to our understanding of neuronal function and variation between the sexes.

Decoding Nematode Chemical Communication

C. elegans employ an ever-growing library of ascaroside pheromones to communicate on almost every aspect of their current physiological state and life history (3-5). However, our understanding of this alphabet has recently expanded beyond strictly ascaroside pheromones, with molecules employing other sugars (6, 7) or glutamine-based pheromones (8).

Deciphering the Role of Sugars in Pheromone Signaling

In this dissertation, we began to analyze the roles of the ascr#3 based sugar derivative, ascr#3-sd (**Chapter 2A**). This molecule utilizes the same fatty acid-derived side chain as ascaroside #3 but employs a different sugar. Whether this change occurs pre-assembly or is the result of a direct modification of ascr#3 remains unknown.

The pheromone ascr#3 serves to attract males and repel hermaphrodites (9, 10) (**Chapter 2A**). In this dissertation, it was shown that the change in sugar reverses the valence of the male behavioral response. This preliminary data poses the groundwork for an interesting set of questions regarding the role of L-ascarylose in the function of ascarosides.

Laser ablations offer a simple and useful tool for elucidating the chemosensory neurons involved in cue response (11). Given the change in ascr#3-sd behavior compared to ascr#3, it will be interesting to uncover if the same neurons play a role in sensation of the two cues. Should the neurons differ, it would more easily explain the difference in behavior. However, should the neurons required remain the same, it may be that different receptors within those neurons are involved in sensing the two sugar cores.

Attraction and avoidance of ascr#3-sd is but one metric of the information encoded by the pheromone. Native ascr#3 is also involved in dauer formation. Does ascr#3-sd play a similar – or even opposing – role in dauer development? Dauer assays, in which worms are reared on an NGM agar plate containing the ascaroside of interest, can be rapidly run

(**Chapter 1C**) to determine if the role of ascr#3-sd's in dauer development is conserved, despite the change in sugar.

Glutamine-Based Pheromones

The glutamine-derived pheromone, nacq#1, lacks any structural similarity to the main pheromone employed by nematodes: ascarosides (8). Despite that, it plays a significant role in reproductive development and aging. In **Chapter 2A**, the ability of nacq#1 to attract hermaphrodites at nanomolar concentrations was elucidated. However, the attraction was still faint, begging the question of how attractive are sub-nanomolar concentrations of nacq#1. Certain ascarosides, such as osas#9, have been shown to retain activity even down to femtomolar concentrations (12). The developmental effects of nacq#1 are also known to function in the pM range (8).

Following the generation of a full dose-response curve, laser ablations can be performed on amphid chemosensory neurons to elucidate the neurons involved in sensing the concentration eliciting the most robust behavioral response (11-13). ASI, ASK, and ASJ have been shown to play a role in the development signaling pathways activated by nacq#1 (8), suggesting that they may also play a role in behavioral pathways. The novel pheromone nacq#1 will then pose an extremely interesting model for non-ascaroside based communication in nematodes.

Sex-Specific Modulation of Pheromone Mediated Responses

The neuropeptide encoding gene, *flp-3*, is responsible for setting the valence of the male behavioral response to ascr#8 (**Chapter 3B**). In this dissertation, it was also shown that the GPCRs, NPR-10 and FRPR-16, act as downstream receptors for the *flp-3* peptides. Interestingly, of the ten peptides encoded by *flp-3*, only FLP-3.2 and FLP-3.9 are necessary for affecting the mutant phenotype.

Determining if flp-3 is Involved in Setting a "Male Physiological State"

Our translational fusion of *flp-3* exhibited specific and repeated expression in the male tail: in particular, the spicule neurons. Despite other studies showing expression in other neurons (14, 15), our specific expression was able to rescue the male behavioral response to ascr#8 (**Chapter 3B**).

What is the role of *flp-3* in the male tail? The spicule neuron plays no chemosensory role (16-18) (**Chapter 3B**). A model thereby arises in which *flp-3* serves to set the state of the animal's nervous system as a male. In order to test this theory, the neurons activated by *flp-3* should be investigated.

Using single-cell RNAseq, the transcriptomes of *frpr-16* or *npr-10* expressing neurons can be determined in wild-type animals (15). Comparisons with the same neurons harvested in *flp-3 lof* animals will determine which genes are differentially expressed in the two states. Should transcription factors be enriched in the upregulated gene clusters, *flp-3* could then be said to set the state of these neurons.

It is unlikely that the spicule neuron experiences any graded potential or neuromodulator release upon on ascr#8 sensation. Calcium imaging of neurons is difficult, and the calcium transients at the sensory level, which are usually robust, are unreliable in CEM sensation of ascarosides (19) (**Chapter 4B**). Therefore, confirming neural activity of the spicule neuron under ascr#8 exposure would be difficult.

The *flp-3* receptor, *npr-10*, is expressed in neurons of the male head (**Chapter 3B**). Potentially included among these neurons is the male specific CEM. Crossing the p*npr-10*::*npr-10*::GFP transgenics with a strain that exhibits red-tagged CEM neurons (i.e., p*pkd-2*::DsRed2 (20)) will confirm if *npr-10* is indeed expressed in the male-specific chemosensory neurons.

Should this be the case, in the absence of *flp-3*, the *npr-10* positive CEM neurons should therefore exhibit a defect in their ability to respond to ascr#8. If *npr-10* acts as a gate

during CEM activation by ascr#8, then both *flp-3* and *npr-10* animals should have CEM neurons unable to generate calcium transients upon ascr#8 exposure.

Determine Why FLP-3 Activity is Sex-Specific

Our *flp-3* rescue construct is expressed in the male-specific Spicule neurons (SPD) of the tail and the non-sex-specific IL1 head neurons. However, previous studies have shown also expression in the PQR neuron and male-specific interneuron, CP9 (14). Does *flp-3* expression play a role in hermaphroditic behavior? Expressing *flp-3* under a hermaphroditic promoter would determine if *flp-3* does indeed impact hermaphroditic behavior. However, given the lack of aberrant phenotype in *flp-3* hermaphrodites, this remains unlikely.

An Unconfirmed FLP-3 Receptor?

Unpublished data suggests that the neuropeptide receptor gene, *npr-13*, which is closely related to *npr-4*, *npr-5*, and *npr-10*, (2) may play a role in sensing FLP-3 peptides. Phylogenetic analyses of genes related to NPR-1 clusters these for genes together in a single clade, with *npr-13* the only receptor to not play any known role (**Figure 45A**).

Given that the receptor is related to three other FLP-3 receptors, we have generated a *him-8* strain of *npr-13*(tm1504). The tm1504 allele results in a 1104 bp removing exons 10 and 11 (and the terminus of exon 9) (21). We assayed the strain for the ability to respond attractively to ascr#8 and found that *npr-13 lof* animals were no longer attracted to ascr#8 (**Figure 45B,C**). However, they lacked the avoidance phenotype characteristic of *flp-3* and FLP-3 receptor mutants (**Figure 45D; Chapter 3B**).

A few possibilities arise that should be investigated as to the cause of these partial phenotype. Firstly, a new null allele of *npr-13* should be assayed. The tm1504 allele encodes a truncated protein, with the C-terminus and intracellular tail being delated (21). This maintains the possibility that *npr-13* is still partially functional, with only a reduced capacity to signal through its associative G proteins. A similar phenotype was observed

in the initial testing of *npr-10*, using the ok1442 allele, which encodes a similar truncation – wherein half of the animals responded as wild-type worms, while the remaining worms exhibited a defective response (**Figure 46**). In testing a full null allele, the phenotype observed – loss of attraction to, but no avoidance of ascr#8 – can be confirmed.

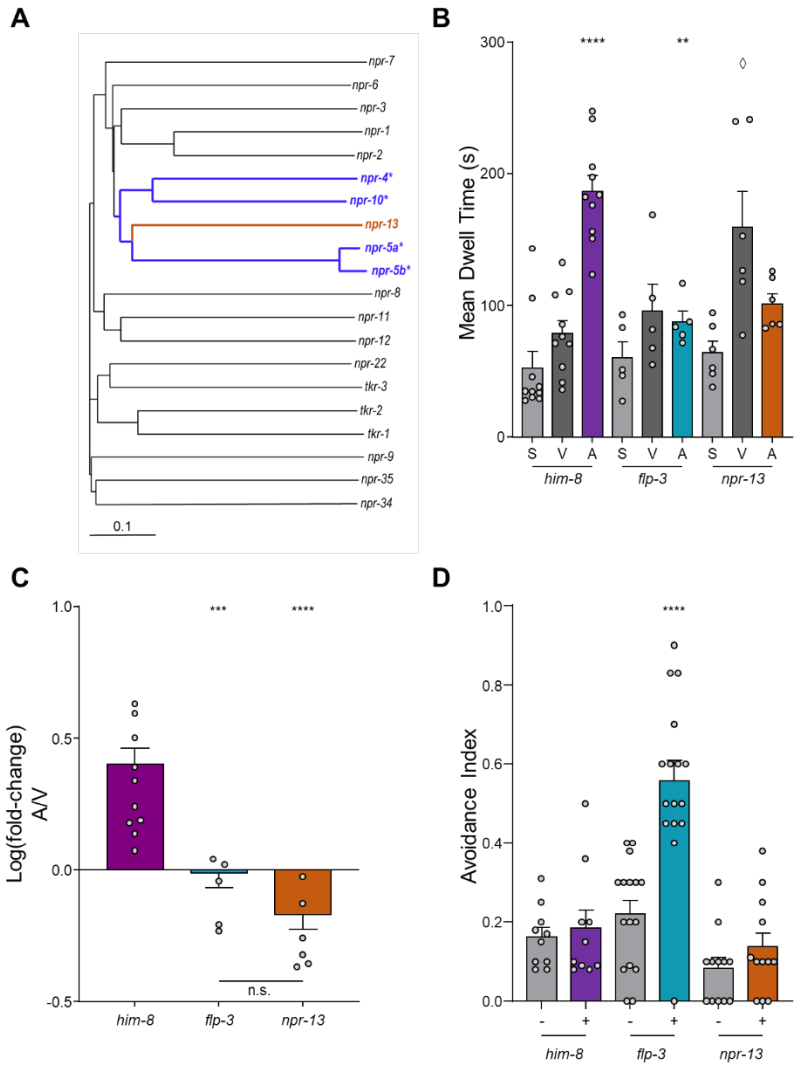

Figure 45. The neuropeptide receptor, NPR-13, is deficient in the male behavioral response to ascr#8.

(A) The NPR phylogeny places NPR-13 within a FLP-3 receptor clade. Receptors known to bind FLP-3 *in vitro* are shown in blue with asterisks. Adapted from Kubiak et al. (1, 2). **(B)** Raw dwell times and **(C)** log(fold-changes) of *npr-13*(tm1504) males show a loss of attraction to ascr#8. **(D)** The *flp-3* avoidance phenotype is not observed in *npr-13*(tm1504) males. **(B)** RM-ANOVA comparing vehicle to both spatial control and ascr#8 values, followed by Bonferroni Correction**. (C)** One-Way ANOVA followed by Dunnett's Correction. **(D)** Paired t-tests of vehicle vs. ascr#8 avoidance indexes. Error bars denote SEM. $n \geq 5$. * $p < 0.05$, ** $p < 0.01$, *** $p < 0.001$, **** $p < 0.0001$. ◊ $p < 0.05$ V vs A.

Secondly, NPR-13 may function as an obligate heterodimer, dimerizing with another FLP-3 receptor, such as NPR-10 or FRPR-16, to improve sensation of FLP-3 peptides. Given that *npr-13* mutants are only defective in their attraction, and do not exhibit avoidance to ascr#8, it is likely that NPR-13 contributes to sensation of FLP-3.2. This peptide is able to suppress avoidance but cannot rescue attraction in *flp-3* mutants (**Chapter 3B**) – similar to the phenotype observed in *npr-13 lof* animals (**Figure 45**).

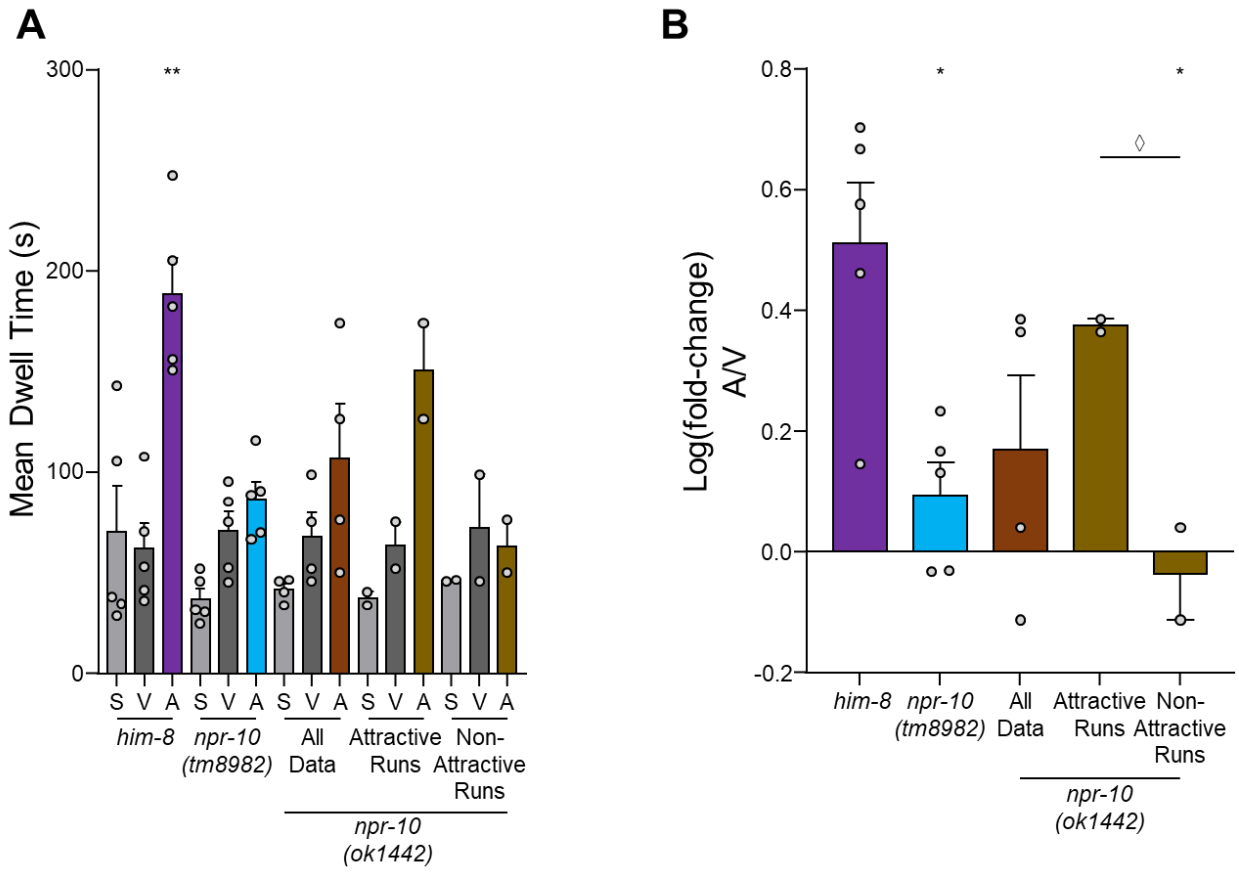

Figure 46. The *npr-10(ok1442)* allele encodes a truncated, partially functional protein.
(A) Raw dwell times and **(B)** log(fold-change) values for *npr-10* mutant animal responses to ascr#8. *npr-10*(ok1442) animals are partially defective: some animals maintain their ability to respond to ascr#8 ("attractive runs"), while others do not ("non-attractive runs"). *npr-10*(tm8982) animals contain a complete gene deletion and exhibit a complete loss of ascr#8 response (data from **Chapter 3B**). **(A)** RM-ANOVA comparing vehicle to both spatial control and ascr#8 values, followed by Bonferroni Correction**. (B)** One-Way ANOVA followed by Dunnett's Correction. Error bars denote SEM. $n \geq 2$. * $p < 0.05$, ** $p < 0.01$, *** $p < 0.001$, **** $p < 0.0001$. ◊ $p < 0.05$, t-test of attractive versus non-attractive run log(fold-change) values.

Expression of NPR-13 in CHO cells expressing aequorin and Gα16 (22, 23) are not activated by any FLP or NLP peptides (*personal communication, Isabel Beets*). The only peptide capable of resulting in receptor activation was FLP-18 (*personal communication, Isabel Beets*). Interesting, the FLP-18 peptides activate the same receptors that sense many of the FLP-3 receptors (i.e., NPR-4, NPR-5, and NPR-10) (24). However, the activation by FLP-18 required a nearly 10 μM concentration of the peptide, suggesting that this interaction is not physiologically relevant.

It is unlikely that NPR-13 sensing no neuropeptide. It is more likely that the receptor is merely not expressed functionally in the CHO cell system. Instead, the receptor could be expressed in yet another heterologous system, such as *Xenopus* oocytes (25).

Conversely, NPR-13 could also be ectopically expressed within the muscle cells (26). The cuticle could then be resected prior to performing electrophysiology recordings at the neuromuscular junctions of these cells upon exposure to a bath of FLP-3 peptides. However, this unconventional method does rely on receptors utilizing the Go intracellular cascade (26, 27).

Finally, elucidating the expression pattern of *npr-13* is vital in determining its role in FLP-3 sensation. Should it indeed co-localize in neurons expressing *npr-10* or *frpr-16* (**Chapter 3B**), *npr-13* would be shown to function as a heterodimer for the peptides. Double mutants of *npr-13* and co-expressed receptors should therefore result in full *flp-3* mutant phenotypes (i.e., increased avoidance compared to single mutants of *npr-10* and/or *frpr-16*; **Chapter 3B**).

Sensation of Ascaroside #8

This dissertation has worked to elucidate the molecular mechanisms governing the behavioral response to the *C. elegans* mating pheromone, ascr#8. Previous studies have confirmed the required role of the male specific CEM chemosensory neurons in sensing ascr#8 (28, 29). Here, we developed a male-adapted microfluidic device to better allow

for calcium imaging studies of these amphid neurons (**Chapter 4B**; (19)), as well identified a set of G protein-coupled receptors (GPCRs) that are involved in the biochemical sensation of the cue (**Chapter 4C**).

Further Understanding the CEM Sensory Network

The initial confirmation of the male-adapted device used the male attractive pheromone, ascr#3, as a control for the study (**Chapter 4B**; (19)). The same device and transgenic animals should first be imaged upon exposure to ascr#8. This should replicate the data previously published (Narayan), but should also provide more data. This data should include: **(1)** the response rate of animals to the cue; **(2)** the trend of neurons to respond to repeated exposure of the pheromone; and **(3)** a large enough data set to generate accurate and effective models.

The rate of CEM neuron calcium transient generation upon exposure to ascr#3 was shown to be approximately 25-30% (**Chapter 4B**; (19)). While the behavioral response of males and the stochastic response of the CEMs to both ascr#3 and ascr#8 is similar (28) (**Chapter 3B**), the rate of ascr#8 has not been confirmed. Given that ascr#3 elicits a 25-30% physiological response (**Chapter 4B**), and an attractive behavioral response of 50% (**Chapter 3B**), it would interesting to see if the rate of calcium transient generation within the CEM neurons upon ascr#8, which attracts approximately 30-45% of males (**Chapter 3B**), would exhibit a similar trend to that of ascr#3.

Repeated exposure of the CEM neurons to ascr#3 elicits calcium transients only during the first exposure to the cue (*unpublished observation*). This is not the case for other pheromone calcium transient activity, as in the case of osas#9 (12). These experiments can determine if ascr#8 follows the trend of ascr#3, or the more general physiological response of the osas#9 pheromone or abiotic cues such as glycerol (12, 19).

The physiological response of the CEM neurons to both ascr#3 and acsr#8 is stochastic. However, the behavioral response is relatively consistent, in that males are attracted (28).

This gives rise to the question: how does stochastic neuronal activity generate reliable behavioral outputs?

Recent studies have begun to generate neuronal models which incorporate stochasticity in the generation of behavioral outputs (30). These models incorporate entire neuronal networks and connectomes, while the ascr#8 sensory network is comprised of only four non-synaptically connected neurons. In order to begin building a model which integrates enough information about the CEM network, a larger number of animals would have to be imaged.

Relating Receptor Function to Sensory Activity

Chapter 4C of this dissertation uncovered a set of GPCRs which are involved in the sensation of ascr#8. The next steps required in confirmed the involvement of these receptors in the sensation of ascr#8 (i.e., generation of transgenic rescues) are already underway at the time of this thesis submission.

The lowest hanging fruit of the receptors presented in **Chapter 4C** is *srw-97*. This receptor seems to have arisen as the product of a gene duplication event somewhere in the *C. elegans*-specific evolutionary history (**Chapter 4C**). Following successful rescue of the GPCR in null mutants, the receptor could then be expressed in a *Caenorhabditis* species that lacks **(1)** an attractive behavioral response to the pheromone, and **(2)** conserved paralogs of the receptor within its own genome.

C. tropicalis provides a number of reasons that is will serve as an ideal model for these experiments. Firstly, like *C. elegans*, *C. tropicalis* is an androdiecious species, which likely adapted a hermaphroditic lifestyle prior to *C. briggsae* (31). The speciation event separating *C. briggsae* and *C. nigoni* is among the most recent within the genus, having occurred 100,000 to 1 million years ago (32, 33). There are male mutants available that correspond to *C. elegans* mutants (i.e., *him-8*) (34, 35) (**Chapter 6**), allowing for easier study of males without the need for male maintenance through mating plates.

Secondly, *C. tropicalis* exhibits no behavioral response to ascr#8, despite its role as a mating pheromone. It has been shown that ascarosides exhibit conserved, cross-reactivity across nematode species (36, 37). For example, ascr#3, which also attracts *C. elegans* males, elicits a similar phenotype in the gonochoristic species, *C. nigoni* (35, 37). Similarly, icas#9/ascr#9 (check) maintains its function across *Caenorhabditis* species as well (Choe). In the work of this dissertation, ascr#8 was shown to have a conserved – if not reduced – function across the genus (35) (**Chapter 6**). Recent work has recapitulated a portion of this data using the new single worm assay (**Chapter 3B**) (38). That *C. wallacei*, the gonochoristic sister-species to *C. tropicalis*, responds attractively to ascr#8 suggests that the loss of ability to respond to ascr#8 lies in changes between the genomes. Interestingly,

Table 7. Paralog counts of ascr#8 Receptors within the *Caenorhabditis* genus.

	Paralog Count		
Species	*srw-97/srw-98*	*dmsr-12*	*srr-7*
C. elegans	2	7	4
C. inopinata	18	2	0
C. wallacei	0	0	2
C. tropicalis	1	0	2
C. briggsae	3	4	2
C. nigoni	2	2	2
C. remanei	4	1	2
C. brenneri	3	2	3
C. japonica	2	7	0
C. becei	1	4	1
C. sulstoni	4	0	1

Genes of ascr#8 receptors are well preserved across *Caenorhabditis*, with *dmsr-12* and *srr-7* exhibiting similar gene counts across species. Meanwhile, a species-specific expansion of the *srw-97* related *srw-98* occurred at some point in the evolutionary history of *C. inopinata*. Data generated from the dataset presented in Chapter 4C.

the genome of *C. wallacei* has contains no *srw-97* paralogs (**Table 7**).

Finally, the regulatory elements driving gene expression in *C. elegans* have been shown to be conserved across the genus (39). Therefore, expressing *srw-97* under the *C. elegans* promoter should drive similar expression within the *C. tropicalis* CEM neurons (40-43). Using a translational GFP fusion, proper expression of the receptor can be confirmed prior to behavioral analyses. Should a *Cel-srw-97* construct cause *C. tropicalis* males to be attracted to ascr#8, it would serve as an ectopic expression confirming the role of the GCPR in ascr#8 sensation.

Similar experiments could be performed using *dmsr-12*. However, given the more conserved phylogeny of this receptor across the genus, this may prove more difficult to determine.

Determining the Different Roles of srw-97 and srw-98

As stated throughout this dissertation, the gene *srw-97* appears to be the result of a gene duplication event – in particular, of the gene *srw-98* (**Chapter 4C**). Currently, a null mutation for *srw-98* has been generated using CRISPR/Cas genome editing. This allele *(knu698)*, generated by Knudra Transgenics (now Nemametrix), is comprised of a 2047 bp deletion, which results in a truncated translated protein product of only 21 amino acids (the full-length protein is 365 amino acids in length).

Despite its remarkable accuracy, CRISPR editing can still generate off-target mutations (44-47). Anecdotally, there is likely an off-target effect in the *srw-98(knu698)* parental strain, as these animals develop noticeably slower than their *him-5* background counterparts. To remove as many off-target effects as possible, the *srw-98(knu698)* strain is being backcrossed with *him-5* to also maintain the presence of males within the strain. Following a successful series of four backcrosses, this strain will be assayed using the single worm assay for its ability to respond behaviorally to ascr#8. Should *srw-98* mutants

display a similar partial loss-of-function phenotype, it would serve to bolster our claim that these genes are indeed ancestrally related.

Transcriptional and translational fluorescent fusions of *srw-98* will serve to confirm the expression pattern of the receptor within the CEM neurons. Given its similar enrichment to *srw-97* within the CEM VR neurons by transcriptomic analyses (**Chapter 4C**), it is likely that the gene will also be expressed within the ventral CEM neurons.

Should they both indeed exhibit identical expression profiles, they may function as heterodimers. This would explain why *C. elegans* males exhibit such a profound attraction to ascr#8 in comparison to other species that lack the *srw-97* receptor (**Chapter 6**). In order to test this theory, each receptor could be expressed in a heterologous cell system, such as *Xenopus* oocytes (25), or Chinese hamster ovarian (CHO) cells (22, 23). Following confirmation that both receptors bind to the cue (in the form of either electrophysiological changes (25) or bioluminescent readout (22, 23), respectively), subsequent co-expression of the receptors can be evaluated for increased affinity to ascr#8. Should co-expression indeed result in increased affinity, the two receptors could then be said to function as heterodimers for ascr#8. A precedent for this has been set, as the receptors for ascr#2, DAF-37 and DAF-38, heterodimerize to sense the cue (48).

Understanding the functions of *srw-97* and *srw-98* will greatly increase our understanding of how sensory receptors regulate behavioral activity. Given the profound strength of evolutionary data for these two receptors (**Chapter 4C**), these experiments will also shed light on evolutionary selection and mate recognition following the advent of hermaphroditism (34).

Dissecting the Enigmatic SRR-7 Receptor

Our transcriptomic and promoter-fusion analyses, as well as RNAi knockdown studies, have confirmed a role of the GPCR encoding gene, *srr-7*, in regulating the acsr#8 response. Enriched only in a single CEM neuron (CEM VL, **Chapter 4C**), knockdown of this

receptor results in complete loss of behavioral response to ascr#8. Previous transcriptomic analyses of extracellular vesicle neurons (EVNs) (49, 50) have also uncovered *srr-7* as a significantly enriched gene, supporting our findings.

However, while GFP fusions of receptors such as *srw-97* and *dmsr-12* exhibited localization to the sensory cilia as well as the soma (**Chapter 4C, Figure 35**), *srr-7* seems to be localized to the soma, raising the possibility that the receptor functions synaptically, and not as a chemosensor. However, the question remains: if loss of a receptor that is present in a single CEM neuron complete ablates the behavioral response, what is it doing? Its localization to the soma suggests it plays a role in the modulation of the sensory circuit.

Generation of a null mutant for *srr-7* has proven difficult. Initial attempts resulted in deletions of the *srr-7* gene, although confirmation of the deletion by sequencing proved difficult, due to the AT-richness of the region (~68%, with the average genome content being ~64%) (51). Subsequent attempts likewise proved problematic. Using the current high throughput method for CRISPR/Cas gene editing (52), two alleles were generated via the same guide RNAs. However, while one is a stable homozygote, the other is a heterozygote (*unpublished results, personal communication, Mark Edgely*).

Compounding the difficulty of deleting *srr-7* is the fact that is located in a gene-dense region of Chromosome V (**Chapter 4C**). Less than 1000 bp in either direction of the coding sequence of *srr-7*, are *str-171* and *srj-27*. They are located on the opposite strand, and in deleting the entire coding region of *srr-7*, the proximal 1200 bp of the *srj-27* promoter are also deleted – in effect removing two genes with one deletion.

In order to separate the effects of *srr-7* from *srj-27*, instead of a full gene deletion of *srr-7*, a premature stop codon should be insert at the start of the first exon. Alternatively, a frameshift mutation could be generated early within the *srr-7* coding sequence, although this would likely adversely affect *srj-27* as well.

Whereas *srr-7* is enriched in CEM VL, *srj-27* is likewise enriched solely in CEM VR. The *C. elegans* genome is organized so that genes that play related functions are often grouped together (53, 54). Does *srj-27* play a similar role to *srr-7*, albeit in CEM VR instead of CEM VL (**Figure 47**)?

Identification of further GPCRs that are enriched in single CEM neurons will increase our understanding of the role of *srr-7* (and potentially *srj-27*). However, given the density of genes in the vicinity of *srr-7*, generation of true, useful null mutants will be difficult, and will rely heavily on precise mutations introduction premature stop codons, and not on gross, full-gene deletions.

Relating Sensation to Physiological Changes

Following the generation of a baseline of calcium transient activity, as well as stable null mutations of all GPCRs of interest, the two approaches should be combined. A host of questions sit poised to be answered by this simple, yet informative combination of techniques and data sets.

- If ascr#8 elicits calcium transients in ~30% of wild-type male CEM neurons, how does removing a GPCR expressed in a subset of the CEM neurons change the response?
- Does this percentage change?
- Do the neurons retain their ability to generate stochastic calcium transient profiles?
- Does removing a receptor expressed only the dorsal CEM remove the ability of those neurons to respond to acsr#8?

Confirming ascr#8 Receptor Identity: A Biochemical Approach

These transcriptomic avenues of ascr#8 receptor identification are useful. They are driven by expression profiles and behavioral activity. However, they do not provide the ability to confirm direct sensation of ascr#8 by the receptors.

In this dissertation, we worked to generate a biochemical probe that would alleviate these concerns (**Chapter 5**, (55)). This ascr#8-probe ("probe D") maintains its ability to attract males and given that modifications to the ascr#8 structure followed the suit of

ascr#81, it is likely that these modifications do not alter the receptors involved in sensation of the molecule.

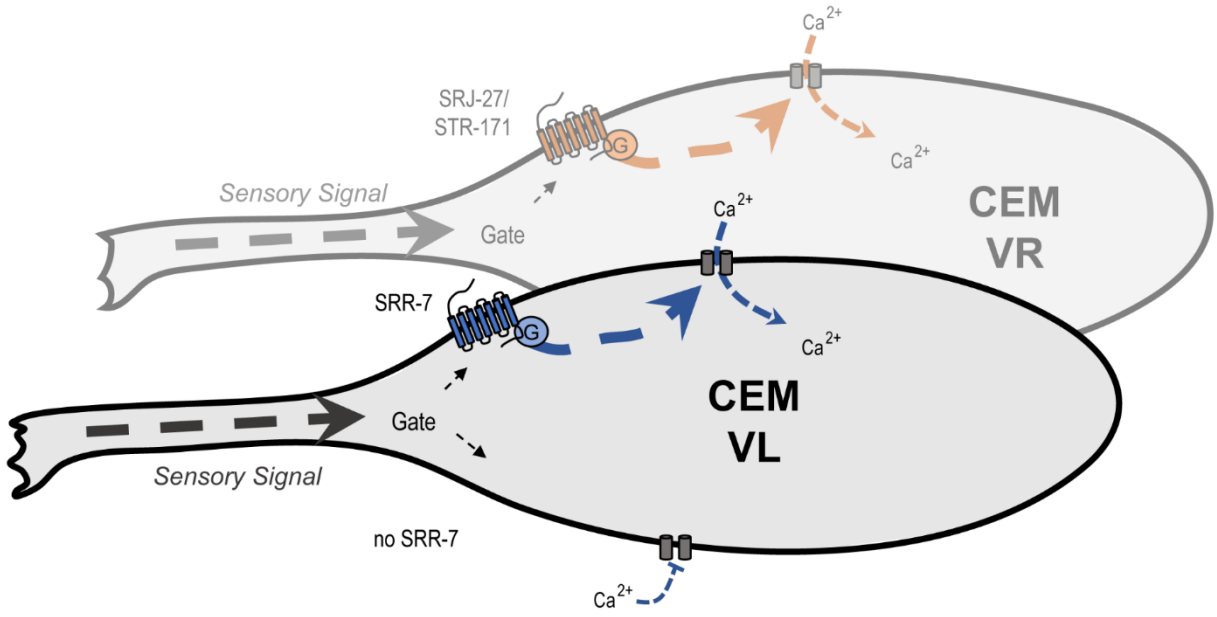

Figure 47. A model of CEM sensory network gating by single CEMs enriched GPCRs.
The G protein-coupled receptor *srr-7* is enriched within CEM VL, while *srj-27* and *str-171* are enriched in the adjacent CEM VR. *srr-7* exhibits localization to the soma, but not the cilia, suggesting a synaptic role in regulating CEM activity. *srr-7* knockdown ("no SRR-7") results in complete loss of ascr#8 response. A similar effect is predicted for *srj-27* (and potentially *str-171*).

This approach will allow us to covalently bind the ascr#8-probe to the receptors by activating the photo-crosslinking moiety on the probe addition (56). Following this binding, worms can be lysed, freeing the probe and bound receptor to be pulled down in a subsequent biotin-streptavidin purification. Proteomic analysis of pull-down eluates will allow for the direct identification of the ascr#8 receptor(s).

Given the strong data that *srw-97* and *dmsr-12* play roles in the ascr#8 response (**Chapter 4C**), it is likely that they will be among the proteins pulled down in the purification step. However, given that receptors are membrane bound, should they instead function as heterodimeric partners and not direct ascr#8 binders, they may not be present in purification eluates.

Nematodes as a Model for Evolutionary Ethology

We have shown that the bioactivity of ascr#8 is conserved across a handful of *Caenorhabditis* species (**Chapter 6**, (35)). However, the ability of ascr#8 to attract males was statistically significant, it remained markedly reduced. The only males tested were from the remaining two hermaphroditic (androdiecious) species, *C. tropicalis* and *C. briggsae*, as well as their gonochoristic sister species, *C. wallacei* and *C. nigoni*, respectively. The newly discovered sister species of *C. elegans*, *C. inopinata* (formerly *C. sp. 34* (57)) was also tested.

Testing of the *Caenorhabditis japonica* outgroup revealed that the ability to respond is not conserved across the entire genus. The question remains however, how conserved is this response within the *Elegans* group? How well do males from species such as *C. brenneri* and *C. remanei* respond to acsr#8, given the conservation of ascr#8 receptor genes in their genomes (**Chapter 4C**)?

We have also previously shown that other ascarosides, such as ascr#3, retain their bioactivity in other *Caenorhabditis* species (37). A similar comparative ethological study could be performed on *Caenorhabditis* nematodes using ascr#3. This would generate interesting insights into the evolution of mating pheromones and behavioral responses. These findings would be extremely informative, especially given that the three instances of hermaphroditism within the genus arose separately, and uniquely (34).

The same study could be undertaken using a non-sex-specific mating cue, but instead an ecologically relevant starvation cue, such as osas#9. Do *C. elegans* only alert conspecifics to the lack of food? Or do they warn all nematodes in the vicinity?

Together, these data can be used to generate a genus-wide "behavioral activity conservation" heat map for how well related species respond to the variety of pheromone cues.

Epigenetic Effects of ascr#8 Sensation and Exposure

Ascarosides mediate a plethora of biological functions (3). Even pheromones that elicit behavioral outcomes can affect development (58, 59) (**Chapter 2B**). It is not surprising, therefore, that prior exposure to a pheromone can alter the outcome later in life – or even in future generations.

The mating pheromone, ascr#3, has been shown to elicit avoidance in adult hermaphrodites (10, 60-63). Recently, Hong et al. showed that even a brief exposure (0-14 hours of L1 larval stage) can imprint the presence of ascr#3 in the life-history of the animal (64). These animals exhibited increased avoidance to the ascaroside as adults compared to naïve animals.

Our lab has shown that similar exposure to the starvation cue, osas#9, under a similar exposure and imprinting paradigm (65). Juxtaposing the effect of ascr#3 imprinting, animals exposed to the pheromone lose their ability to avoid osas#9. This effect is transferred to progeny for over seven generations (66).

A handful of questions can be applied to ascr#8 attraction through the filter of epigenetic regulation:

- Does this phenomenon also occur in the presence of ascr#8?
- Do males that are pre-exposed to the mating pheromone exhibit increased or defected attraction later in life?
- Are progeny affected?
- How to *flp-3 lof* animals respond to ascr#8 imprinting?

Development of Neuropeptide-Rescue-by-Feeding Paradigm

The peptide feeding paradigm presented in **Chapter 3B** offers a powerful and robust novel tool for rescuing neuropeptides in *C. elegans*. The phenotypes exhibited by neuropeptide mutants are vast (Chapter 3A), and there is a startling lack of tools for studying the effects of these neuromodulators outside of transgenic rescues.

This rescue paradigm, adapted from RNAi feeding protocols (67, 68), allows for the rapid rescue of animals without the need for generation of transgenics. Many neuropeptides are expressed in complex genes that produce pro-proteins that are eventually cleaved into more than one peptide (24). Combinatorial studies, which would be a considerable burden in transgenic studies, are now achievable – a simple mixture of *E. coli* cultures prior to plate seeding is all that is required.

In order to develop a more accessible form of peptide feeding for the public, the SCRAMBLE vector used in Chapter 3B should be removed from the DH5α strain and transferred to HT115(DE3) (69). This RNAase III-deficient strain is widely used in RNA interference feeding protocols (67, 69) and will provide a more comparable food source than DH5α cells.

Rescue constructs are generated using GATEWAY cloning technology (68, 70). The initial donor vector is the p1-p2 vector available in most cloning kits, and the destination vector, pDEST527, is currently available on Addgene (generated by Dominic Esposito). This destination vector results in an IPTG-inducible *E. coli* expression vector. A 6x-histidine tag is added to the N-terminus of the translated product (**Chapter 3B**). Incorporation of EGL-3 cleavage sites (KR) flanking the peptide of interest removes this tag from the final product, preventing any functional interference. Rescue design instructions, as well as a macro-like Excel sheet have been generated, and should be made available to the public – along with the SCRAMBLE and pDEST527 vectors. These kits will allow labs to investigate the role of neuropeptides using this feeding system.

The rescue of three neuropeptides previously characterized and rescued by transgenics via peptide feeding will serve as a proof-of-principle and methods dissemination. Three areas of study affected by neuropeptide signaling will be rescued.

Firstly, the mate-search controlling neuropeptide, PDF-1 (71) (which plays a role in many other facets of *C. elegans* biology as well) (72, 73), will be rescued by feeding. This gene encodes two peptides, which will be rescued in combination and singularly. Males

lacking PDF-1 leave a food patch in search of a mate significantly less than wild-type animals (71). Transgenic rescue of the peptide rescues the rate of leaving.

Secondly, the thyrotropic-releasing hormone paralog, TRH-1, affects the growth of animals (74). Animals lacking the peptide grow slower and less than their wild-type counterparts. Rescue of both peptides by transgenics has restored this phenotype, and like the rescue of PDF-1, TRH-1 will be rescued by feeding the two peptides separately, and in combination.

The neuropeptide gene, *ins-6*, has a robust effect on the ability of the AWC^{ON} chemosensory neuron to generation calcium transients in response to increases in salt concentration (75, 76). Only one peptide is encoded within the pro-protein, as with other INS encoding genes (**Chapter 3A**). Considerably longer than FLP or NLP peptides, it will be interesting to see if our novel peptide feeding protocol is able to rescue INS phenotypes. Transgenic rescue of INS-6 was only able to restore the peak change of calcium fluorescence approximately halfway to wild-type levels (75, 76). The ability of feeding rescue to restore peak calcium changes should correlate to this change.

Conclusions

Together, the data presented in this dissertation build a strong foundation for future studies into the sex-specific neuromodulation of pheromone response in *C. elegans*. With ascarosides no longer the only form of chemical social communication utilized by nematodes (**Chapter 2A**), the field is primed for elucidation of specific, or broad, conserved pathways.

With only twelve pairs of chemosensory neurons, how conserved and redundant are *C. elegans* sensory mechanisms? Recent studies have shown that the abiotic lab molecule, SDS, which elicits a strong avoidance phenotype, is sensed by the same four pairs of neurons that sense predator cues secreted by *Pristionchus pacificus* (13). It has also been shown that the neurons that sense dauer inducing pheromones, such as ASI, also

contribute to the sensation of non-ascaroside, development influencing nacq pheromones (8).

The work in this dissertation provides another layer of intricacy to these questions: the male-specific chemosensory system. In the case of ascr#8, the cephalic male, CEM neurons are the sole source of male sensation (**Chapter 3B**). However, the neurons that sense the cue in the hermaphroditic nervous system remain unknown. With neurons having sex-specific responses to pheromones regardless of the sex-specificity of their presence (77), any of the twelve remaining amphid chemosensory neurons could play a role.

Whereas mammalian studies suffer from an overriding focus on male biology (78), *C. elegans* studies are inherently driven towards hermaphroditic studies. Despite the occurrence of only 0.1-0.2% male progeny (79), the *him-5* and *him-8* mutants available for study are wild-type in nearly every way tested to date (**Chapter 1B**).

Understanding chemosensory mechanisms must first start at how neurons sense their ligands. This work has identified candidates for likely ascr#8 receptors (in the forms of *srw-97*, *dmsr-12*, and potentially *srw-98*) (**Chapter 4C**). However, the role of GPCRs, such as *srr-7*, in the soma of these chemosensory neurons, which are able to completely gate the ability of an animal to respond behaviorally (**Chapter 4C, this chapter**), offer intriguing and complex avenues of study.

The development of a bioactive ascr#8 photoaffinity probe not only opens the door for rapid biochemical confirmation of receptors but makes development of ascaroside probes in general more feasible. Only nine receptors have been identified to date (**Chapter 4A**), yet the library of known ascarosides continues to grow rapidly, making identification of native receptors all the more prescient.

Finally, the elucidation of a conserved behavioral phenotype across the *Caenorhabditis* genus (**Chapter 6**) proves comparative studies a prime starting point in understand nematode social biology.

C. elegans does not exist in isolation in its native habit (80). It, along with a host of competing nematode species (81), must navigate an ever changing, often harsh environment, in the hopes finding food (82, 83) and a mate (28), while avoiding predators (13) and other harmful microbes (84). Proper functioning of the machinery involved in how these nematodes sense their environment, process multiple stimuli, and enact proper behaviors is critical for their survival. These studies further our understanding of these mechanisms and offer directed questions for the next stages of study.

References

1. Kubiak TM, Larsen MJ, Bowman JW, Geary TG, Lowery DE. FMRFamide-like peptides encoded on the *flp-18* precursor gene activate two isoforms of the orphan *Caenorhabditis elegans* G-protein-coupled receptor Y58G8A.4 heterologously expressed in mammalian cells. Biopolymers. 2008;90(3):339-48. Epub 2007/09/20. doi: 10.1002/bip.20850. PubMed PMID: 17879267.

2. Kubiak TM, Larsen MJ, Zantello MR, Bowman JW, Nulf SC, Lowery DE. Functional Annotation of the Putative Orphan *Caenorhabditis elegans* G-protein-coupled Receptor C10C6.2 as a FLP15 Peptide Receptor. Journal of Biological Chemistry. 2003;278(43):42115-20. doi: 10.1074/jbc.M304056200.

3. Butcher RA. Decoding chemical communication in nematodes. Natural product reports. 2017;34(5):472-7. Epub 2017/04/08. doi: 10.1039/c7np00007c. PubMed PMID: 28386618.

4. Butcher RA. Small-molecule pheromones and hormones controlling nematode development. Nat Chem Biol. 2017;13(6):577-86. Epub 2017/05/18. doi: 10.1038/nchembio.2356d. PubMed PMID: 28514418.

5. McGrath PT, Ruvinsky I. A primer on pheromone signaling in *Caenorhabditis elegans* for systems biologists. Current opinion in systems biology. 2019;13:23-30. Epub 2019/04/16. doi: 10.1016/j.coisb.2018.08.012. PubMed PMID: 30984890; PMCID: PMC6456899.

6. Bergame CP, Dong C, Sutour S, von Reuss SH. Epimerization of an Ascaroside-Type Glycolipid Downstream of the Canonical β-Oxidation Cycle in the Nematode *Caenorhabditis nigoni*. Organic Letters. 2019. doi: 10.1021/acs.orglett.9b03808.

7. Bose N, Ogawa A, von Reuss SH, Yim JJ, Ragsdale EJ, Sommer RJ, Schroeder FC. Complex small-molecule architectures regulate phenotypic plasticity in a nematode. Angew Chem Int Ed Engl. 2012;51(50):12438-43. Epub 2012/11/20. doi: 10.1002/anie.201206797. PubMed PMID: 23161728; PMCID: PMC3733369.

8. Ludewig AH, Artyukhin AB, Aprison EZ, Rodrigues PR, Pulido DC, Burkhardt RN, Panda O, Zhang YK, Gudibanda P, Ruvinsky I, Schroeder FC. An excreted small molecule promotes *C. elegans* reproductive development and aging. Nat Chem Biol. 2019;15(8):838-45. Epub 2019/07/20. doi: 10.1038/s41589-019-0321-7. PubMed PMID: 31320757; PMCID: PMC6650165.

9. Aprison EZ, Ruvinsky I. Counteracting Ascarosides Act through Distinct Neurons to Determine the Sexual Identity of *C. elegans* Pheromones. Curr Biol. 2017;27(17):2589-99.e3. Epub 2017/08/29. doi: 10.1016/j.cub.2017.07.034. PubMed PMID: 28844646.

10. Jang H, Kim K, Neal SJ, Macosko E, Kim D, Butcher RA, Zeiger DM, Bargmann CI, Sengupta P. Neuromodulatory state and sex specify alternative behaviors through antagonistic synaptic pathways in *C. elegans*. Neuron. 2012;75(4):585-92. doi: 10.1016/j.neuron.2012.06.034. PubMed PMID: 22920251; PMCID: PMC3462069.

11. Fang-Yen C, Gabel CV, Samuel AD, Bargmann CI, Avery L. Laser microsurgery in *Caenorhabditis elegans*. Methods Cell Biol. 2012;107:177-206. doi: 10.1016/B978-0-12-394620-1.00006-0. PubMed PMID: 22226524; PMCID: PMC3617498.

12. Chute CD, DiLoreto EM, Zhang YK, Reilly DK, Rayes D, Coyle VL, Choi HJ, Alkema MJ, Schroeder FC, Srinivasan J. Co-option of neurotransmitter signaling for inter-organismal communication in *C. elegans*. Nat Commun. 2019;10(1):3186. Epub 2019/07/20. doi: 10.1038/s41467-019-11240-7. PubMed PMID: 31320626; PMCID: PMC6639374.

13. Liu Z, Kariya MJ, Chute CD, Pribadi AK, Leinwand SG, Tong A, Curran KP, Bose N, Schroeder FC, Srinivasan J, Chalasani SH. Predator-secreted sulfolipids induce defensive responses in *C. elegans*. Nature communications. 2018;9(1):1128. Epub 2018/03/21. doi: 10.1038/s41467-018-03333-6. PubMed PMID: 29555902; PMCID: PMC5859177.

14. Kim K, Li C. Expression and regulation of an FMRFamide-related neuropeptide gene family in *Caenorhabditis elegans*. J Comp Neurol. 2004;475(4):540-50. doi: 10.1002/cne.20189. PubMed PMID: 15236235.

15. Taylor SR, Santpere G, Reilly M, Glenwinkel L, Poff A, McWhirter R, Xu C, Weinreb A, Basavaraju M, Cook SJ, Barrett A, Abrams A, Vidal B, Cros C, Rafi I, Sestan N, Hammarlund M, Hobert O, Miller DM. Expression profiling of the mature *C. elegans* nervous system by single-cell RNA-Sequencing. bioRxiv. 2019:737577. doi: 10.1101/737577.

16. LeBoeuf B, Correa P, Jee C, García LR. *Caenorhabditis elegans* male sensory-motor neurons and dopaminergic support cells couple ejaculation and post-ejaculatory behaviors. eLife. 2014;3:e02938. doi: 10.7554/eLife.02938.

17. Liu K, Sternberg, P. Sensory Regulation of Male Mating Behavior. Neuron. 1995.

18. Schindelman G, Whittaker AJ, Thum JY, Gharib S, Sternberg PW. Initiation of male sperm-transfer behavior in *Caenorhabditis elegans* requires input from the ventral nerve cord. BMC Biology. 2006;4(1):26. doi: 10.1186/1741-7007-4-26.

19. Reilly DK, Lawler DE, Albrecht DR, Srinivasan J. Using an Adapted Microfluidic Olfactory Chip for the Imaging of Neuronal Activity in Response to Pheromones in Male *C. Elegans* Head Neurons. Journal of Visualized Experiments. 2017(127):e56026. doi: doi:10.3791/56026.

20. Peden EM, Barr MM. The KLP-6 kinesin is required for male mating behaviors and polycystin localization in *Caenorhabditis elegans*. Curr Biol. 2005;15. doi: 10.1016/j.cub.2004.12.073.

21. Yemini E, Jucikas T, Grundy LJ, Brown AEX, Schafer WR. A database of *Caenorhabditis elegans* behavioral phenotypes. Nature Methods. 2013;10(9):877-9. doi: 10.1038/nmeth.2560.

22. Iannacone MJ, Beets I, Lopes LE, Churgin MA, Fang-Yen C, Nelson MD, Schoofs L, Raizen DM. The RFamide receptor DMSR-1 regulates stress-induced sleep in *C. elegans*. Elife. 2017;6. Epub 2017/01/18. doi: 10.7554/eLife.19837. PubMed PMID: 28094002; PMCID: PMC5241116.

23. Peymen K, Watteyne J, Borghgraef C, Van Sinay E, Beets I, Schoofs L. Myoinhibitory peptide signaling modulates aversive gustatory learning in *Caenorhabditis elegans*. PLoS Genet. 2019;15(2):e1007945. Epub 2019/02/20. doi: 10.1371/journal.pgen.1007945. PubMed PMID: 30779740; PMCID: PMC6380545.

24. Li C, Kim K. Neuropeptides. WormBook. 2008. Epub 2008. doi: 10.1895/workbook.1.142.1.

25. Bianchi L, Driscoll M. Heterologous expression of *C. elegans* ion channels in *Xenopus* oocytes. WormBook. 2006:1-16. doi: 10.1895/wormbook.1.117.1. PubMed PMID: 18050441; PMCID: PMC4781024.

26. Law W, Wuescher LM, Ortega A, Hapiak VM, Komuniecki PR, Komuniecki R. Heterologous Expression in Remodeled *C. elegans*: A Platform for Monoaminergic Agonist Identification and Anthelmintic Screening. PLoS Pathog. 2015;11(4):e1004794. Epub 2015/05/01. doi: 10.1371/journal.ppat.1004794. PubMed PMID: 25928899; PMCID: PMC4415803.

27. Oakes MD, Law WJ, Clark T, Bamber BA, Komuniecki R. Cannabinoids Activate Monoaminergic Signaling to Modulate Key *C. elegans* Behaviors. The Journal of neuroscience : the official journal of the Society for Neuroscience. 2017;37(11):2859-69. Epub 2017/02/10. doi: 10.1523/JNEUROSCI.3151-16.2017. PubMed PMID: 28188220.

28. Narayan A, Venkatachalam V, Durak O, Reilly DK, Bose N, Schroeder FC, Samuel AD, Srinivasan J, Sternberg PW. Contrasting responses within a single neuron class enable sex-specific attraction in *Caenorhabditis elegans*. Proc Natl Acad Sci U S A. 2016;113(10):E1392-401. doi: 10.1073/pnas.1600786113. PubMed PMID: 26903633; PMCID: 4791020.

29. Pungaliya C, Srinivasan J, Fox BW, Malik RU, Ludewig AH, Sternberg PW, Schroeder FC. A shortcut to identifying small molecule signals that regulate behavior and development in *Caenorhabditis elegans*. Proceedings of the National Academy of Sciences

of the United States of America. 2009;106(19):7708-13. doi: 10.1073/pnas.0811918106; PMCID: 2683085.

30. Roberts WM, Augustine SB, Lawton KJ, Lindsay TH, Thiele TR, Izquierdo EJ, Faumont S, Lindsay RA, Britton MC, Pokala N, Bargmann CI, Lockery SR. A stochastic neuronal model predicts random search behaviors at multiple spatial scales in *C. elegans*. eLife. 2016;5:e12572. doi: 10.7554/eLife.12572.

31. Stevens L, Félix M-A, Beltran T, Braendle C, Caurcel C, Fausett S, Fitch D, Frézal L, Gosse C, Kaur T, Kiontke K, Newton MD, Noble LM, Richaud A, Rockman MV, Sudhaus W, Blaxter M. Comparative genomics of 10 new *Caenorhabditis* species. Evolution Letters. 2019;3(2):217-36. doi: 10.1002/evl3.110. PubMed PMID: 31007946.

32. Cutter AD. Molecular evolution inferences from the *C. elegans* genome. WormBook. 2010:1-14. doi: 10.1895/wormbook.1.149.1. PubMed PMID: 20213859.

33. Thomas CG, Wang W, Jovelin R, Ghosh R, Lomasko T, Trinh Q, Kruglyak L, Stein LD, Cutter AD. Full-genome evolutionary histories of selfing, splitting, and selection in *Caenorhabditis*. Genome Res. 2015;25(5):667-78. Epub 2015/03/19. doi: 10.1101/gr.187237.114. PubMed PMID: 25783854; PMCID: PMC4417115.

34. Ellis RE, Lin SY. The evolutionary origins and consequences of self-fertility in nematodes. F1000prime reports. 2014;6:62. Epub 2014/08/29. doi: 10.12703/p6-62. PubMed PMID: 25165561; PMCID: PMC4126538.

35. Reilly DK, Randle LJ, Srinivasan J. Evolution of hermaphroditism decreases efficacy of Ascaroside#8-mediated mate attraction in *Caenorhabditis* nematodes. microPublication Biology. 2019. doi: 10.17912/micropub.biology.000134.

36. Choe A, von Reuss SH, Kogan D, Gasser RB, Platzer EG, Schroeder FC, Sternberg PW. Ascaroside Signaling is Widely Conserved Among Nematodes. Current Biology. 2012;22(9):772-80. doi: 10.1016/j.cub.2012.03.024. PubMed PMID: PMC3360977.

37. Dong C, Reilly DK, Bergame C, Dolke F, Srinivasan J, von Reuss SH. Comparative Ascaroside Profiling of *Caenorhabditis* Exometabolomes Reveals Species-Specific (ω) and

(ω - 2)-Hydroxylation Downstream of Peroxisomal beta-Oxidation. J Org Chem. 2018. Epub 2018/02/27. doi: 10.1021/acs.joc.8b00094. PubMed PMID: 29480728.

38. Lockery JA. Sex Pheromone Attractive Response in *C. elegans* and Related Species [MQP]. https://digitalcommons.wpi.edu/mqp-all/7051/: Worcester Polytechnic Institute; 2019.

39. Kuntz SG, Schwarz EM, DeModena JA, De Buysscher T, Trout D, Shizuya H, Sternberg PW, Wold BJ. Multigenome DNA sequence conservation identifies Hox cis-regulatory elements. Genome Res. 2008;18(12):1955-68. Epub 2008/11/05. doi: 10.1101/gr.085472.108. PubMed PMID: 18981268; PMCID: PMC2593573.

40. Fitch DHA. Evolution of Male Tail Development in Rhabditid Nematodes Related to *Caenorhabditis elegans*. Systematic Biology. 1997;46(1):145-79. doi: 10.1093/sysbio/46.1.145 %J Systematic Biology.

41. Jansen G, Thijssen KL, Werner P, van derHorst M, Hazendonk E, Plasterk RHA. The complete family of genes encoding G proteins of *Caenorhabditis elegans*. Nat Genet. 1999;21(4):414-9. doi: 10.1038/7753.

42. Lok JB. *Strongyloides stercoralis*: a model for translational research on parasitic nematode biology. WormBook. 2007:1-18. doi: 10.1895/wormbook.1.134.1. PubMed PMID: 18050500; PMCID: PMC3092380.

43. Stein LD, Bao Z, Blasiar D, Blumenthal T, Brent MR, Chen N, Chinwalla A, Clarke L, Clee C, Coghlan A, Coulson A, D'Eustachio P, Fitch DHA, Fulton LA, Fulton RE, Griffiths-Jones S, Harris TW, Hillier LW, Kamath R, Kuwabara PE, Mardis ER, Marra MA, Miner TL, Minx P, Mullikin JC, Plumb RW, Rogers J, Schein JE, Sohrmann M, Spieth J, Stajich JE, Wei C, Willey D, Wilson RK, Durbin R, Waterston RH. The Genome Sequence of *Caenorhabditis briggsae*: A Platform for Comparative Genomics. PLOS Biology. 2003;1(2):e45. doi: 10.1371/journal.pbio.0000045.

44. Cho SW, Kim S, Kim Y, Kweon J, Kim HS, Bae S, Kim JS. Analysis of off-target effects of CRISPR/Cas-derived RNA-guided endonucleases and nickases. Genome Res.

2014;24(1):132-41. Epub 2013/11/21. doi: 10.1101/gr.162339.113. PubMed PMID: 24253446; PMCID: PMC3875854.

45. Doench JG, Fusi N, Sullender M, Hegde M, Vaimberg EW, Donovan KF, Smith I, Tothova Z, Wilen C, Orchard R, Virgin HW, Listgarten J, Root DE. Optimized sgRNA design to maximize activity and minimize off-target effects of CRISPR-Cas9. Nature biotechnology. 2016;34(2):184-91. doi: 10.1038/nbt.3437.

46. Kleinstiver BP, Pattanayak V, Prew MS, Tsai SQ, Nguyen NT, Zheng Z, Joung JK. High-fidelity CRISPR–Cas9 nucleases with no detectable genome-wide off-target effects. Nature. 2016;529(7587):490-5. doi: 10.1038/nature16526.

47. Shen B, Zhang W, Zhang J, Zhou J, Wang J, Chen L, Wang L, Hodgkins A, Iyer V, Huang X, Skarnes WC. Efficient genome modification by CRISPR-Cas9 nickase with minimal off-target effects. Nature Methods. 2014;11(4):399-402. doi: 10.1038/nmeth.2857.

48. Park D, O'Doherty I, Somvanshi RK, Bethke A, Schroeder FC, Kumar U, Riddle DL. Interaction of structure-specific and promiscuous G-protein-coupled receptors mediates small-molecule signaling in *Caenorhabditis elegans*. PNAS. 2012;109(25):9917-22. doi: 10.1073/pnas.1202216109. PubMed PMID: 22665789; PMCID: 3382479.

49. Wang J, Kaletsky R, Silva M, Williams A, Haas LA, Androwski RJ, Landis JN, Patrick C, Rashid A, Santiago-Martinez D, Gravato-Nobre M, Hodgkin J, Hall DH, Murphy CT, Barr MM. Cell-Specific Transcriptional Profiling of Ciliated Sensory Neurons Reveals Regulators of Behavior and Extracellular Vesicle Biogenesis. Curr Biol. 2015;25(24):3232-8. Epub 2015/12/22. doi: 10.1016/j.cub.2015.10.057. PubMed PMID: 26687621; PMCID: PMC4698341.

50. Wang J, Silva M, Haas LA, Morsci NS, Nguyen KCQ, Hall DH, Barr MM. *C. elegans* Ciliated Sensory Neurons Release Extracellular Vesicles that Function in Animal Communication. Current Biology. 2014;24:518-25.

51. Sulston JE, Brenner S. The DNA of *Caenorhabditis elegans*. Genetics. 1974;77(1):95-104. Epub 1974/05/01. PubMed PMID: 4858229; PMCID: PMC1213121.

52. Au V, Li-Leger E, Raymant G, Flibotte S, Chen G, Martin K, Fernando L, Doell C, Rosell FI, Wang S, Edgley ML, Rougvie AE, Hutter H, Moerman DG. CRISPR/Cas9 Methodology for the Generation of Knockout Deletions in *Caenorhabditis elegans*. G3 (Bethesda, Md). 2019;9(1):135-44. Epub 2018/11/14. doi: 10.1534/g3.118.200778. PubMed PMID: 30420468; PMCID: PMC6325907.

53. Miller MA, Cutter AD, Yamamoto I, Ward S, Greenstein D. Clustered Organization of Reproductive Genes in the *C. elegans* Genome. Current Biology. 2004;14(14):1284-90. doi: 10.1016/j.cub.2004.07.025.

54. Robertson HM, Thomas JH. The putative chemoreceptor families of *C. elegans*. WormBook. 2006:1-12. doi: 10.1895/wormbook.1.66.1. PubMed PMID: 18050473; PMCID: PMC4781013.

55. Zhang YK, Reilly DK, Yu J, Srinivasan J, Schroeder FC. Photoaffinity probes for nematode pheromone receptor identification. Journal of Organic & Biomolecular Chemistry. 2019:10.1039/c9ob02099c. doi: 10.1039/c9ob02099c. PubMed PMID: 31781713.

56. Grunbeck A, Huber T, Sachdev P, Sakmar TP. Mapping the Ligand-binding Site on a GPCR Using Genetically-encoded Photocrosslinkers. Biochemistry. 2011;50(17):3411-3. doi: 10.1021/bi200214r. PubMed PMID: PMC3099303.

57. Kanzaki N, Tsai IJ, Tanaka R, Hunt VL, Liu D, Tsuyama K, Maeda Y, Namai S, Kumagai R, Tracey A, Holroyd N, Doyle SR, Woodruff GC, Murase K, Kitazume H, Chai C, Akagi A, Panda O, Ke H-M, Schroeder FC, Wang J, Berriman M, Sternberg PW, Sugimoto A, Kikuchi T. Biology and genome of a newly discovered sibling species of *Caenorhabditis elegans*. Nature communications. 2018;9(1):3216-. doi: 10.1038/s41467-018-05712-5. PubMed PMID: 30097582.

58. Apirson EZ, Ruvinsky I. Coordinated behavioral and physiological responses to a social signal are regulated by a shared neuronal circuit. Curr Biol. 2019(THIS ISSUE).

59. Apirson EZ, Ruvinsky I. Dynamic regulation of adult-specific functions of the nervous system by signaling from the reproductive system. Curr Biol. 2019(THIS ISSUE).

60. Butcher RA, Fujita M, Schroeder FC, Clardy J. Small-molecule pheromones that control dauer development in *Caenorhabditis elegans*. Nat Chem Biol. 2007;3(7):420-2. doi: 10.1038/nchembio.2007.3.

61. Edison AS. *Caenorhabditis elegans* pheromones regulate multiple complex behaviors. Curr Opin Neurobiol. 2009;19(4):378-88. Epub 2009/08/12. doi: 10.1016/j.conb.2009.07.007. PubMed PMID: 19665885; PMCID: PMC2779695.

62. Jeong P-Y, Jung M, Yim Y-H, Kim H, Park M, Hong E, Lee W, Kim YH, Kim K, Paik Y-K. Chemical structure and biological activity of the *Caenorhabditis elegans* dauer-inducing pheromone. Nature. 2005;433(7025):541-5. doi: 10.1038/nature03201.

63. Macosko EZ, Pokala N, Feinberg EH, Chalasani SH, Butcher RA, Clardy J, Bargmann CI. A Hub-and-Spoke Circuit Drives Pheromone Attraction and Social Behavior in *C. elegans*. Nature. 2009;458(7242):1171-5. doi: 10.1038/nature07886. PubMed PMID: PMC2760495.

64. Hong M, Ryu L, Ow MC, Kim J, Je AR, Chinta S, Huh YH, Lee KJ, Butcher RA, Choi H, Sengupta P, Hall SE, Kim K. Early Pheromone Experience Modifies a Synaptic Activity to Influence Adult Pheromone Responses of *C. elegans*. Current Biology. 2017;43(9):667-95. Epub 2017 Oct 5. doi: 10.1016/j.cub.2017.08.068. PubMed PMID: 28988862.

65. McGlame E, Garver I, Srinivasan J. *Caenorhabditis elegans* experiences leave behavioral modifications on great-grandchildren [Major Qualifying Project]. https://digitalcommons.wpi.edu/mqp-all/3942/: Worcester Polytechnic Institute; 2018.

66. Robidoux AN. Epigenetic Reprogramming Prompts Hereditable Behavioral and Genetic Changes in *C. elegans* [Major Qualifying Project]: Worcester Polytechnic Institute; 2020.

67. Fraser AG, Kamath RS, Zipperlen P, Martinez-Campos M, Sohrmann M, Ahringer J. Functional genomic analysis of *C. elegans* chromosome I by systematic RNA interference. Nature. 2000;408(6810):325-30. doi: 10.1038/35042517.

68. Xu J, Jiang Y, Wan L, Wang Q, Huang Z, Liu Y, Wu Y, Chen Z, Liu X. Feeding recombinant *E. coli* with GST-mBmKTX fusion protein increases the fecundity and lifespan of *Caenorhabditis elegans*. Peptides. 2017;89:1-8. doi: 10.1016/j.peptides.2017.01.003.

69. Papic L, Rivas J, Toledo S, Romero J. Double-stranded RNA production and the kinetics of recombinant *Escherichia coli* HT115 in fed-batch culture. Biotechnology reports (Amsterdam, Netherlands). 2018;20:e00292. Epub 2018/12/21. doi: 10.1016/j.btre.2018.e00292. PubMed PMID: 30568886; PMCID: PMC6288044.

70. Petersen LK, Stowers RS. A Gateway MultiSite recombination cloning toolkit. PLoS One. 2011;6(9):e24531. Epub 2011/09/21. doi: 10.1371/journal.pone.0024531. PubMed PMID: 21931740; PMCID: PMC3170369.

71. Barrios A, Ghosh R, Fang C, Emmons SW, Barr MM. PDF-1 neuropeptide signaling modulates a neural circuit for mate-searching behavior in *C. elegans*. Nature Neuroscience. 2012;15(12):1675-84. doi: 10.1038/nn.3253.

72. Chen D, Taylor KP, Hall Q, Kaplan JM. The Neuropeptides FLP-2 and PDF-1 Act in Concert To Arouse *Caenorhabditis elegans* Locomotion. Genetics. 2016;204(3):1151-9. Epub 2016/09/03. doi: 10.1534/genetics.116.192898. PubMed PMID: 27585848; PMCID: PMC5105848.

73. Hilbert ZA, Kim DH. PDF-1 neuropeptide signaling regulates sexually dimorphic gene expression in shared sensory neurons of *C. elegans*. eLife. 2018;7:e36547. doi: 10.7554/eLife.36547. PubMed PMID: 30024377.

74. Van Sinay E, Mirabeau O, Depuydt G, Van Hiel MB, Peymen K, Watteyne J, Zels S, Schoofs L, Beets I. Evolutionarily conserved TRH neuropeptide pathway regulates growth in *Caenorhabditis elegans*. Proc Natl Acad Sci U S A. 2017;114(20):E4065-e74. Epub 2017/05/04. doi: 10.1073/pnas.1617392114. PubMed PMID: 28461507; PMCID: PMC5441806.

75. Chalasani SH, Kato S, Albrecht DR, Nakagawa T, Abbott LF, Bargmann CI. Neuropeptide feedback modifies odor-evoked dynamics in *Caenorhabditis elegans* olfactory neurons. Nat Neurosci. 2010;13(5):615-21. doi: 10.1038/nn.2526.

76. Leinwand SG, Chalasani SH. Neuropeptide signaling remodels chemosensory circuit composition in *Caenorhabditis elegans*. Nature neuroscience. 2013;16(10):1461-7. Epub 2013/09/08. doi: 10.1038/nn.3511. PubMed PMID: 24013594.

77. Fagan KA, Luo J, Lagoy RC, Schroeder FC, Albrecht DR, Portman DS. A Single-Neuron Chemosensory Switch Determines the Valence of a Sexually Dimorphic Sensory Behavior. Curr Biol. 2018;28(6):902-14.e5. Epub 2018/03/13. doi: 10.1016/j.cub.2018.02.029. PubMed PMID: 29526590; PMCID: PMC5862148.

78. McCarthy MM, Arnold AP, Ball GF, Blaustein JD, De Vries GJ. Sex differences in the brain: the not so inconvenient truth. J Neurosci. 2012;32(7):2241-7. doi: 10.1523/JNEUROSCI.5372-11.2012. PubMed PMID: 22396398; PMCID: 3295598.

79. Brenner S. The Genetics of *Caenorhabditis elegans*. Genetics. 1974;77(1):71-94. PubMed PMID: 4366476; PMCID: PMC1213120.

80. Barriere A, Felix MA. Isolation of *C. elegans* and related nematodes. WormBook. 2014:1-19. doi: 10.1895/wormbook.1.115.2. PubMed PMID: 24803426.

81. Félix M-A, Braendle C, Cutter AD. A Streamlined System for Species Diagnosis in *Caenorhabditis* (Nematoda: Rhabditidae) with Name Designations for 15 Distinct Biological Species. PLOS ONE. 2014;9(4):e94723. doi: 10.1371/journal.pone.0094723.

82. Bretscher AJ, Busch KE, de Bono M. A carbon dioxide avoidance behavior is integrated with responses to ambient oxygen and food in *Caenorhabditis elegans*. Proceedings of the National Academy of Sciences. 2008;105(23):8044-9. doi: 10.1073/pnas.0707607105.

83. Harris G, Korchnak A, Summers P, Hapiak V, Law WJ, Stein AM, Komuniecki P, Komuniecki R. Dissecting the Serotonergic Food Signal Stimulating Sensory-Mediated

Aversive Behavior in *C. elegans*. PLoS ONE. 2011;6(7):e21897. doi: 10.1371/journal.pone.0021897. PubMed PMID: PMC3140990.

84. Maguire SM, Clark CM, Nunnari J, Pirri JK, Alkema MJ. The *C. elegans* touch response facilitates escape from predacious fungi. Current biology. 2011;21(15):1326-30. Epub 2011/07/28. doi: 10.1016/j.cub.2011.06.063. PubMed PMID: 21802299.

Chapter 8 Appendices

Appendix II

Chapter 8A Appendix 1

Supplemental Figure and Table Legends for Chapter 3B:

A Single Neuropeptide Controls the Sex-Specific Behavioral Valence to a Mating Pheromone in *Caenorhabditis elegans*

In Preparation as:

Reilly DK[1], McGlame EJ[1,6], Vandewyer E[2], Robidoux AM[1,3], Northcott HT[1,4], Alkema MJ[5], Gegear RJ[7], Beets I[2], Srinivasan J[1,4,*]. A Single Neuropeptide Controls the Sex-Specific Behavioral Valence to a Mating Pheromone in *Caenorhabditis elegans*.

[1] Department of Biology and Biotechnology, Worcester Polytechnic Institute, Worcester, MA 01605, USA
[2] Neural Signaling and Circuit Plasticity Group, Department of Biology, KU Leuven, Leuven, BEL
[3] Department of Chemistry and Biochemistry, Worcester Polytechnic Institute, Worcester, MA 01605, USA
[4] Program of Bioinformatics and Computational Biology, Worcester Polytechnic Institute, Worcester, MA 01605, USA
[5] Neurobiology Department, University of Massachusetts Medical School, Worcester, MA 01605, USA
[6] Present address: AbbVie Foundational Neuroscience Center, Cambridge, MA 02139, USA
[7] Department of Biology, University of Massachusetts Dartmouth, Dartmouth, MA 02747, USA
* Corresponding author: Jagan Srinivasan, jsrinivasan@wpi.edu

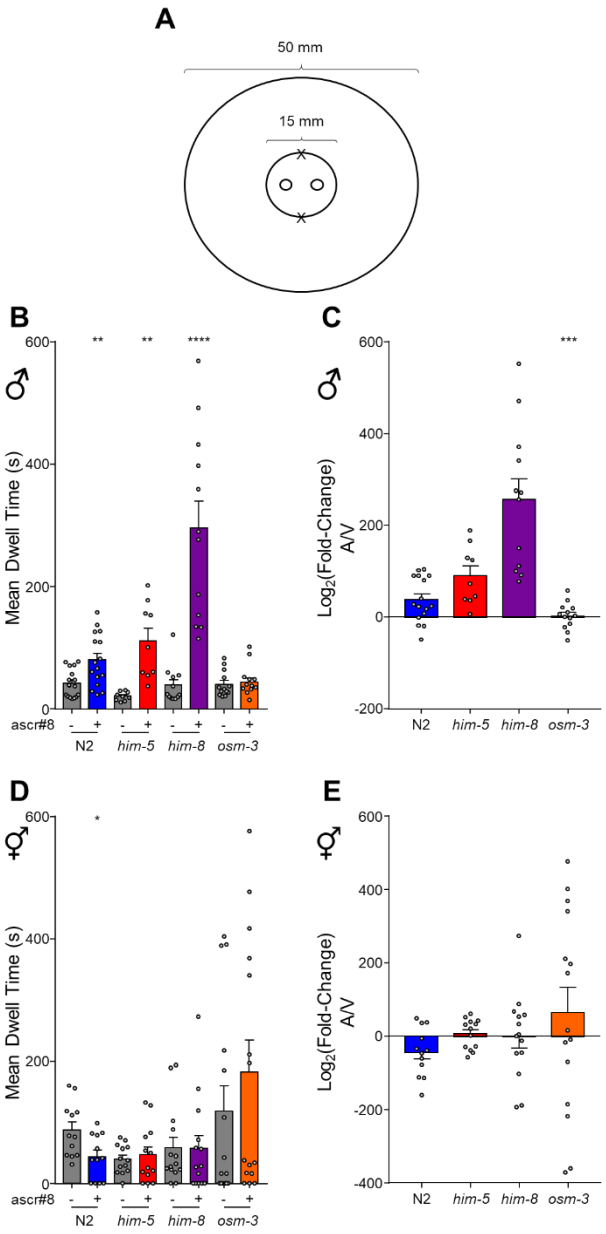

Supplementary Figure 1. Canonical Spot Retention Assay.
(A) The Spot Retention Assay (SRA), as described previously. **(B)** Male *C. elegans* are attracted to ascr#8 in all wild-type strains (N2, *him-5*, *him-8*), but not chemosensory mutants (*osm-3;him-5*). **(C)** Transformed attraction data, logbase2(fold-change), of the raw data shown in B. *osm-3;him-5* animals are less attracted to ascr#8 than *him-5* controls. **(D)** Hermaphroditic *C. elegans* are not attracted to ascr#8. The responses are variable across strains, with N2 exhibiting a slight decrease in ascr#8 dwell time compared to the vehicle control. **(E)** Transformed logbase2(fold-change) data of hermaphrodite SRA data. There is not difference in the attraction across strains. **(B, D)** Paired t-tests of vehicle vs. ascr#8 dwell time. **(C, E)** One-Way ANOVA followed by Dunnett's Correction. Error bars denote SEM. $n \geq 5$. * $p < 0.05$, ** $p < 0.01$, *** $p < 0.001$, **** $p < 0.0001$.

Appendix V

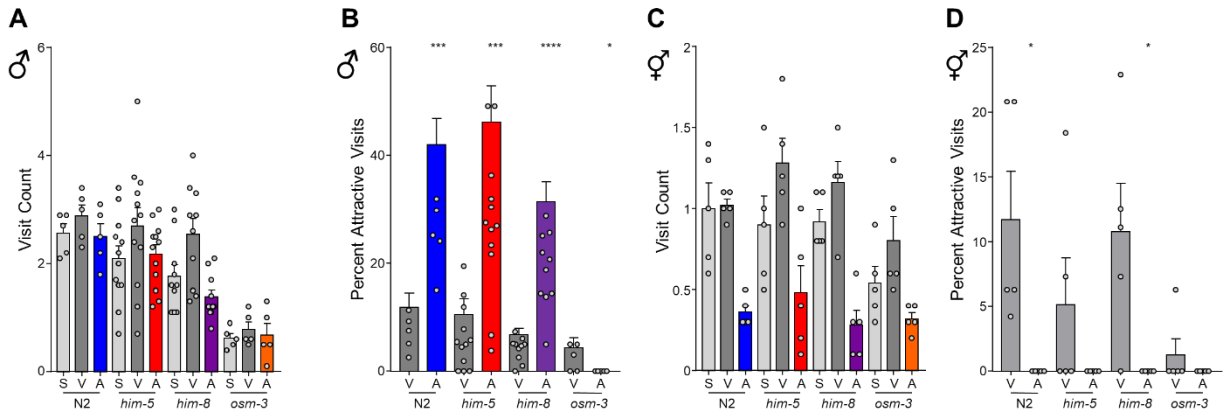

Supplementary Figure 2. Control Strain Single Worm Assay Visit Count and Percent Attractiveness.

(A) Male visit count of control strains. **(B)** Percent of attractive visits per worm for males of control strains. **(C)** Hermaphrodite visit count of control strains. **(D)** Percent of attractive visits per worm of control strains. **(A, C)** RM-ANOVA followed by Bonferroni correction comparing vehicle control to spatial control and ascaroside values. **(B, D)** Paired t-tests comparing vehicle and ascaroside values. Error bars denote SEM values. $n \geq 5$. * $p < 0.05$, ** $p < 0.01$, *** $p < 0.001$, **** $p < 0.0001$.

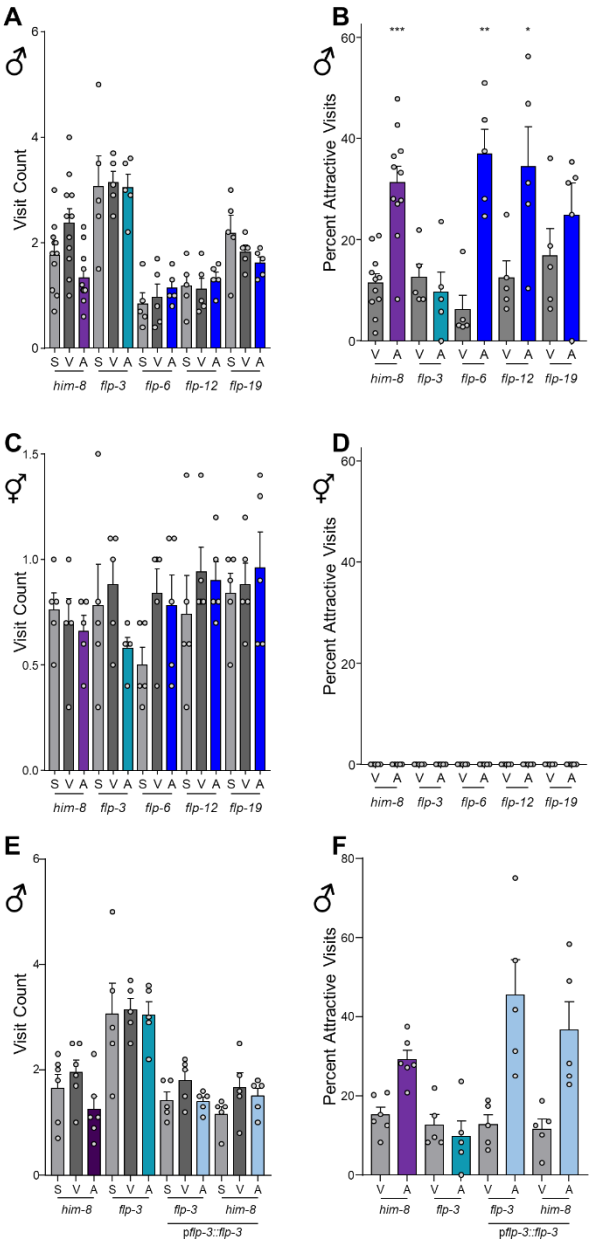

Supplementary Figure 3. Neuropeptide Null Mutant Screen SWA Supplementary Information.

(A) Visit counts for males defective in neuropeptide genes. **(B)** Percent of attractive visits per worm of males defective in neuropeptide genes. **(C)** Visit counts for hermaphrodites defective in neuropeptide genes. **(D)** Percent of attractive visits per worm of hermaphrodites defective in neuropeptide genes. **(E)** Visit counts for males of *flp-3* rescue and overexpression transgenics. **(F)** Percent of attractive visits per worm of *flp-3* rescue and overexpression transgenics. **(A, C, E)** RM-ANOVA followed by Bonferroni correction comparing vehicle control to spatial control and ascaroside values. **(B, D, F)** Paired t-tests comparing vehicle and ascaroside values. Error bars denote SEM values. $n \geq 5$. * $p < 0.05$, ** $p < 0.01$, *** $p < 0.001$, **** $p < 0.0001$.

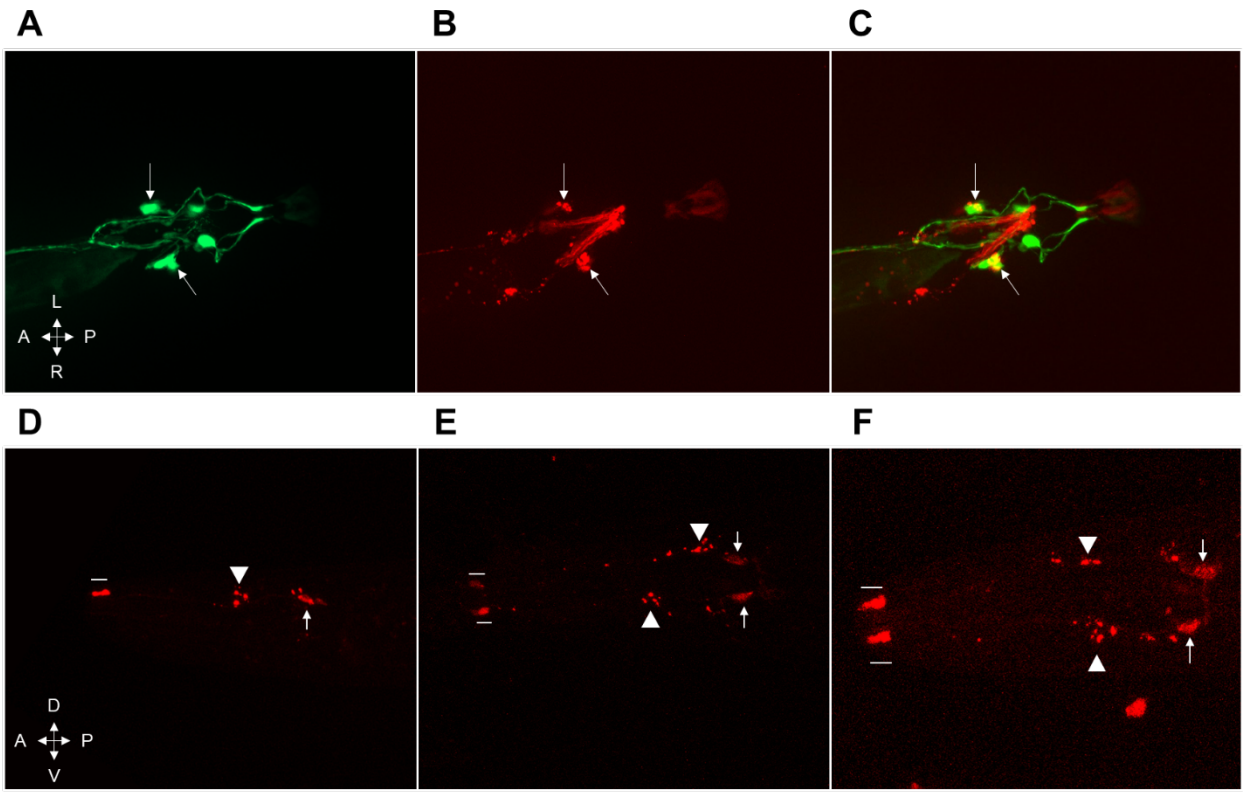

Supplementary Figure 4. Expression Pattern Analysis of *flp-3*::mCherry.
(A-C) 40x magnification of a mail tail expressing **(A)** *gpa-1*::GFP and **(B)** p*flp-3*::*flp-3*::mCherry. **(C)** The two reporters co-localize in the SPD neuronal soma (arrows). **(D-F)** IL1 expression of p*flp-3*::*flp-3*::mCherry. mCherry is faintly observed in the IL1 soma (arrows). The fluorescent protein is also observed in the dendritic cilia of the IL1 neurons (bars), as well as in punctate vesicles along the dendrites (arrowheads).

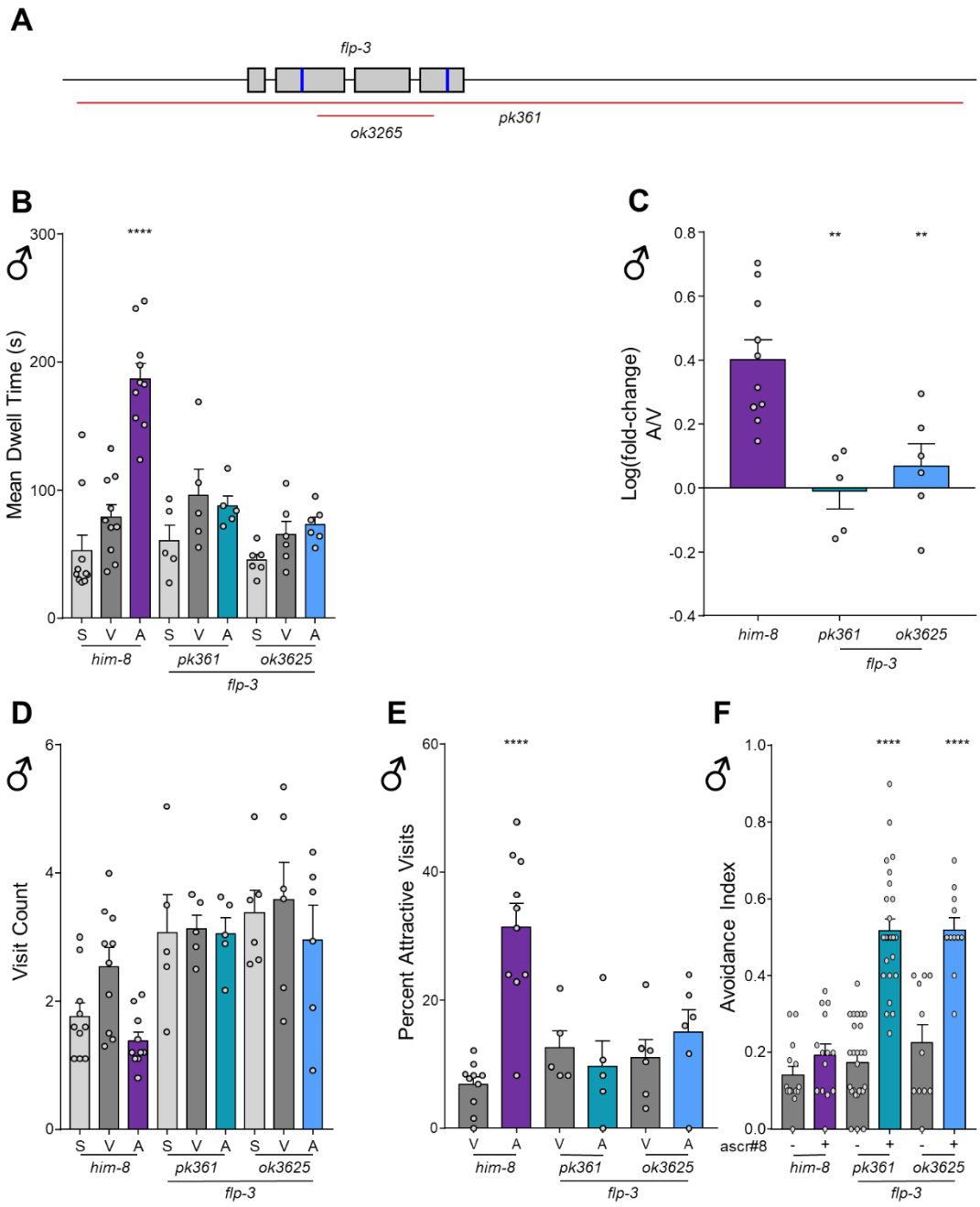

Supplementary Figure 5. The *flp-3* Phenotype is Consistent Across Alleles.
(A) Schematic of *flp-3* deletion alleles *pk361* and *ok3625*, which result in a full gene deletion and in-frame partial gene deletion, respectively. **(B)** Raw dwell time, **(C)** log(fold-change) values, **(D)** visit count, and **(E)** percent of attractive visits of both *flp-3* alleles, *pk361* and *ok3625*. **(F)** Avoidance indexes of both *flp-3* alleles. **(B, D)** RM-ANOVA followed by Bonferroni correction comparing vehicle control to spatial control and ascaroside values. **(C, F)** One-Way ANOVA followed by Dunnett's correction. **(E, F)** Paired t-tests comparing vehicle and ascaroside values. Error bars denote SEM values. $n \geq 5$. * $p < 0.05$, ** $p < 0.01$, *** $p < 0.001$, **** $p < 0.0001$.

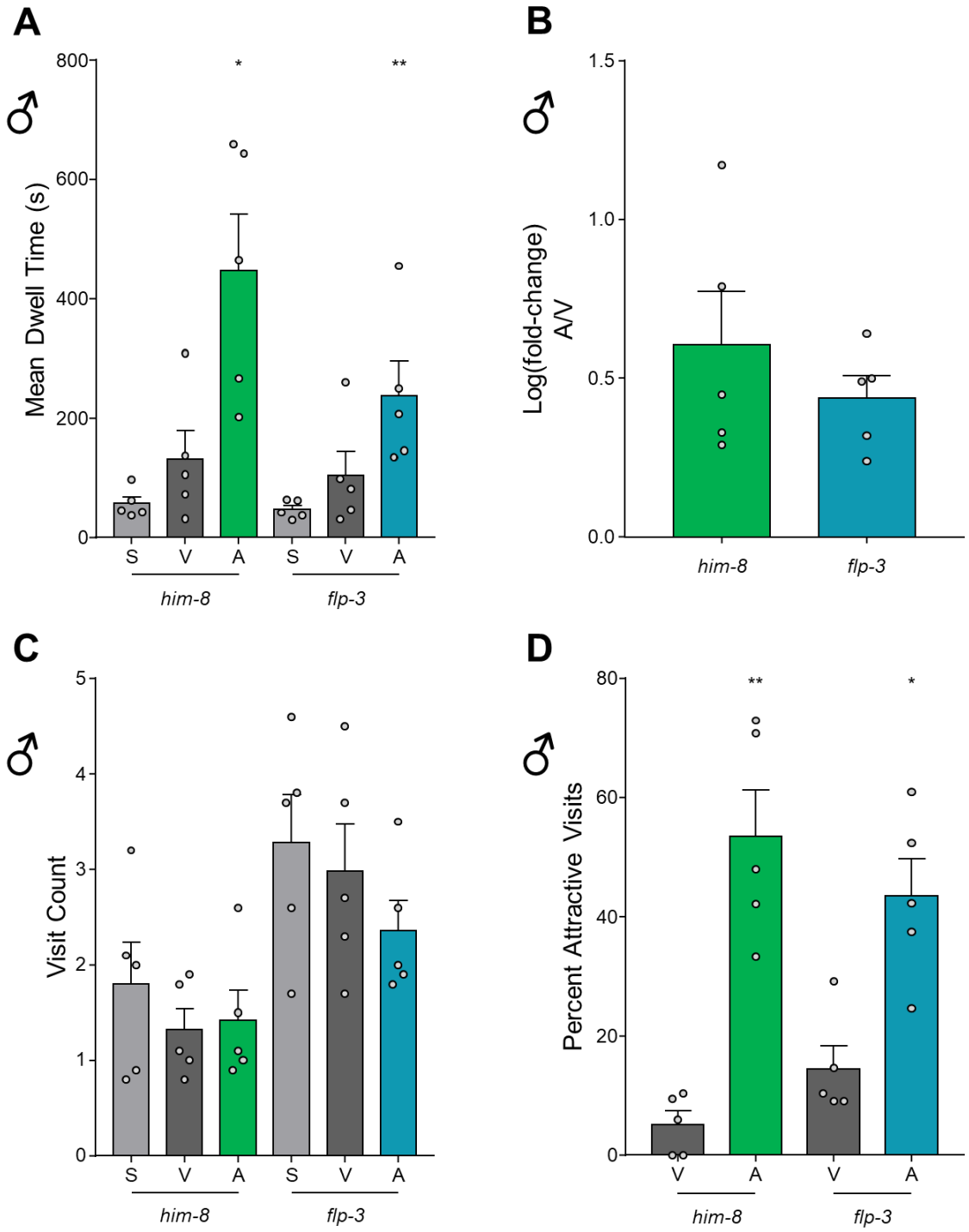

Supplementary Figure 6. The Role of *flp-3* is Specific to ascr#8.
(A) Raw dwell time, **(B)** log(fold-change) values, **(C)** visit count, and **(D)** percent of attractive visits of *flp-3*(pk361) to two attractive ascarosides, ascr#8 and ascr#3. **(A, C)** RM-ANOVA followed by Bonferroni correction comparing vehicle control to spatial control and ascaroside values. **(B, D)** Paired t-tests comparing vehicle and ascaroside values. Error bars denote SEM values. $n \geq 5$. * $p < 0.05$, ** $p < 0.01$, *** $p < 0.001$, **** $p < 0.0001$.

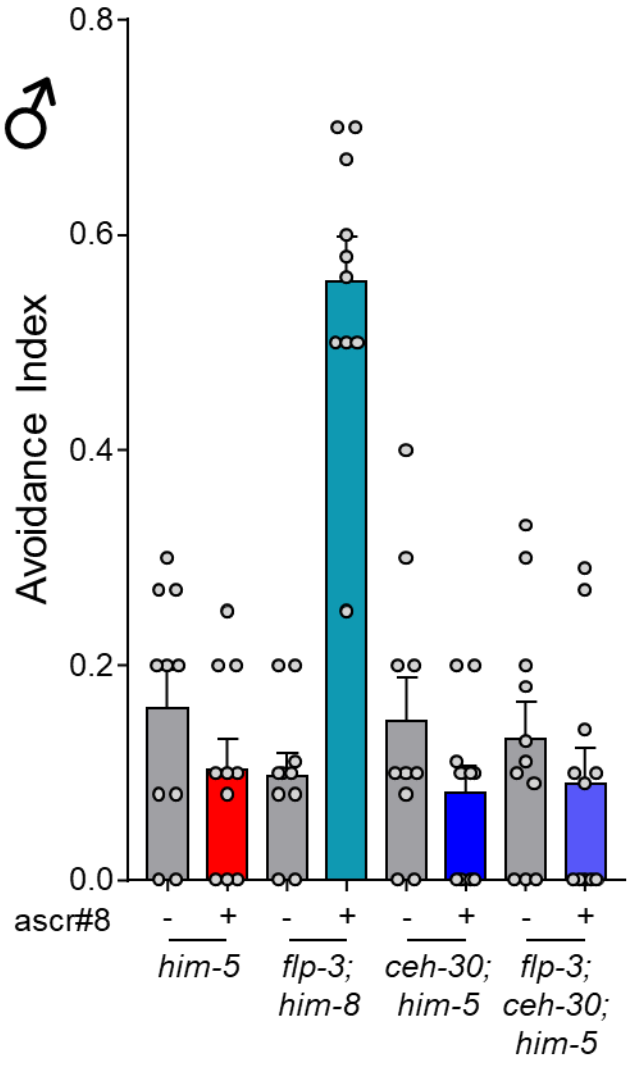

Supplementary Figure 7. The CEM Neurons are the Sole Chemosensory Pathway Detecting ascr#8.

Avoidance index values of *him-5* and *flp-3;him-8* control males, as well as *ceh-30;him-5* and *ceh-30;flp-3;him-5* males. Paired t-tests comparing vehicle and ascaroside values. Error bars denote SEM values. $n \geq 10$. * $p < 0.05$, ** $p < 0.01$, *** $p < 0.001$, **** $p < 0.0001$.

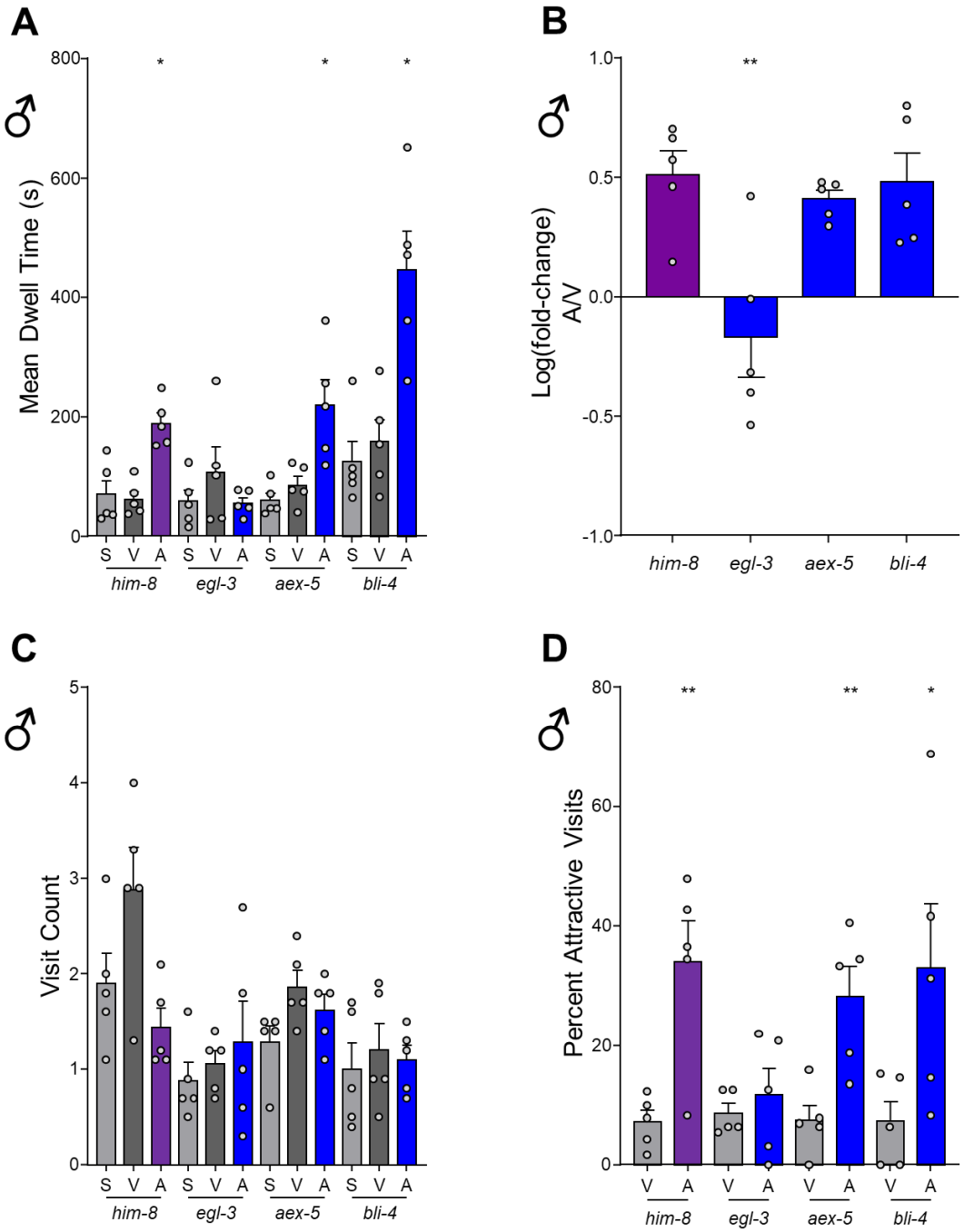

Supplementary Figure 8. EGL-3 is the Proprotein Cleavage Enzyme Involved in FLP-3 Maturation.

(A) Raw dwell time, **(B)** log(fold-change) values, **(C)** visit count, and **(D)** percent of attractive visits per worm of propeptide convertase enzymes involved in neuropeptide maturation: *egl-3*, *aex-5*, and *bli-4*. **(A, C)** RM-ANOVA followed by Bonferroni correction comparing vehicle control to spatial control and ascaroside values. **(B, D)** Paired t-tests comparing vehicle and ascaroside values. Error bars denote SEM values. $n \geq 5$. * $p < 0.05$, ** $p < 0.01$, *** $p < 0.001$, **** $p < 0.0001$.

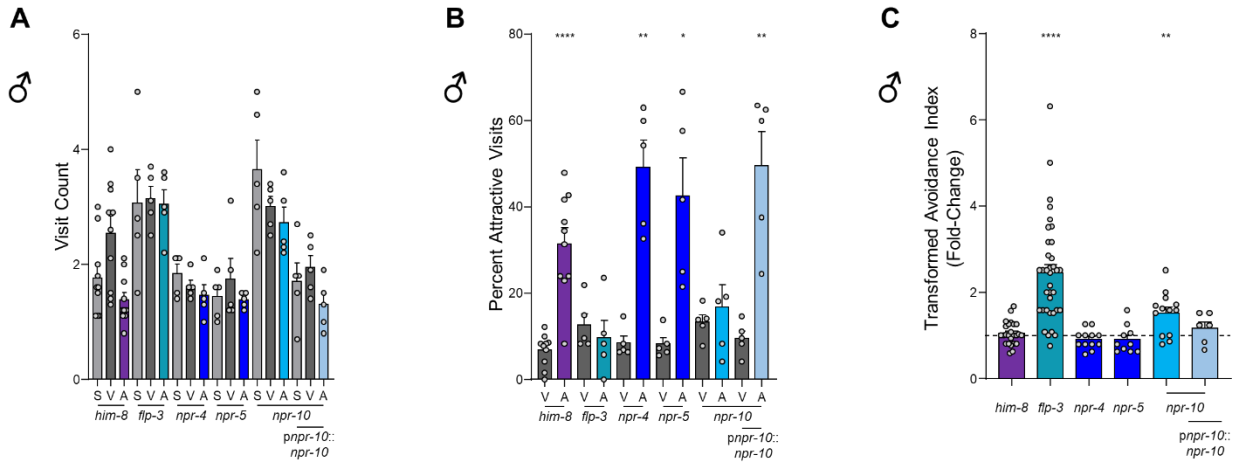

Supplementary Figure 9. NPR SWA Supplementary Information.
(A) Visit count and **(B)** percent of attractive visits per worm of *npr* receptor mutants and *npr-10* rescue. **(C)** Transformed avoidance of *npr* mutants and *npr-10* rescue. **(A)** RM-ANOVA followed by Bonferroni correction comparing vehicle control to spatial control and ascaroside values. **(B)** Paired t-tests comparing vehicle and ascaroside values. **(C)** One-Way ANOVA followed by Dunnett's correction. Error bars denote SEM values. $n \geq 5$. * $p < 0.05$, ** $p < 0.01$, *** $p < 0.001$, **** $p < 0.0001$.

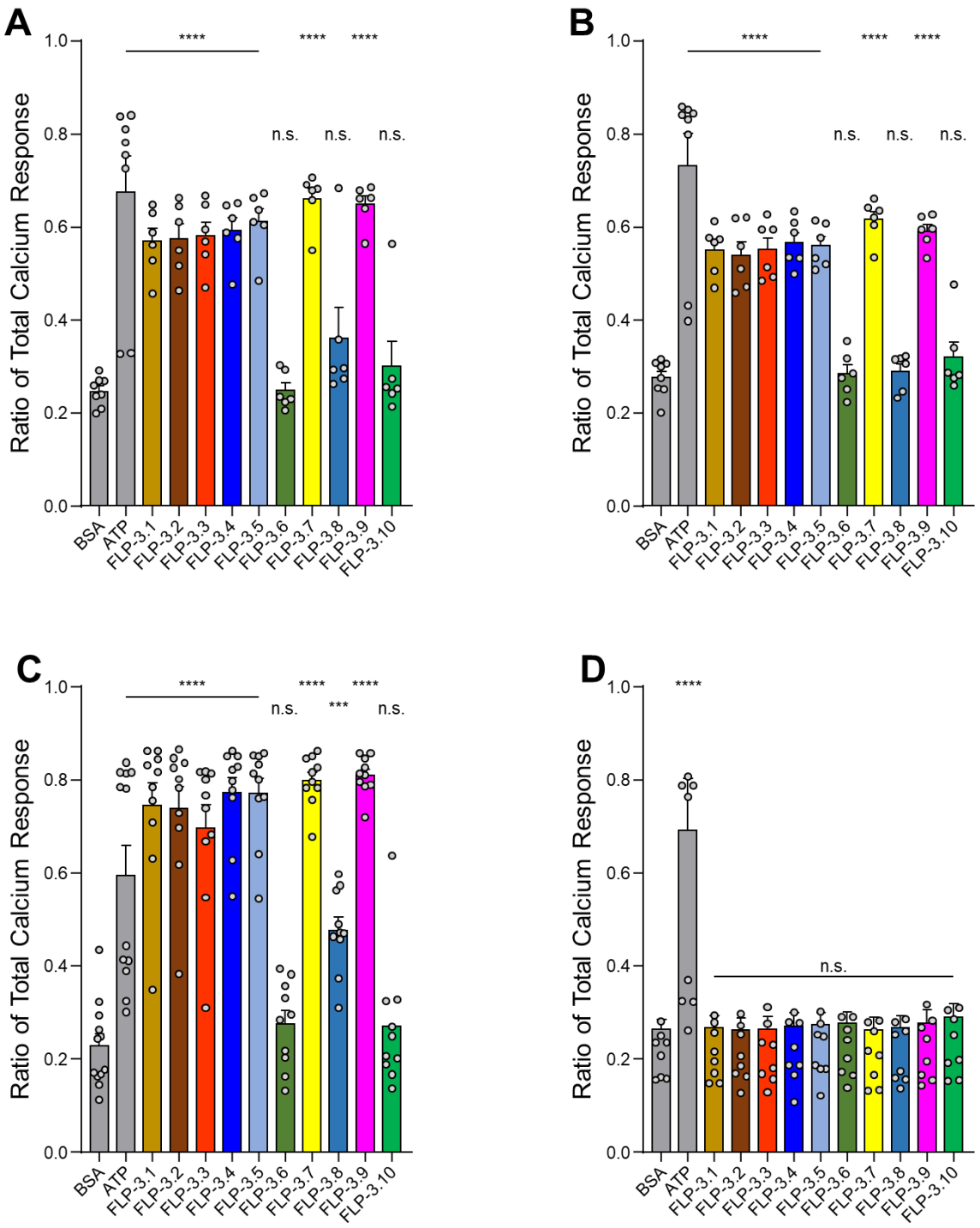

Supplementary Figure 10. FLP-3 Peptides Activate NPR-10 and FRPR-16 *in vitro*. Ratios of Total Calcium Response for cells transfected with **(A)** NPR-10A, **(B)** NPR-10B, **(C)** FRPR-16, and **(D)** empty vector control. Peptides FLP-3-6 and FLP-3-10 activated no receptors, likely due to lack of sequence homology. No peptides activated cells transfected with empty vector control. Error bars denote SEM values. $n \geq 6$. One-Way ANOVA compared to BSA control. *** $p < 0.001$, **** $p < 0.0001$.

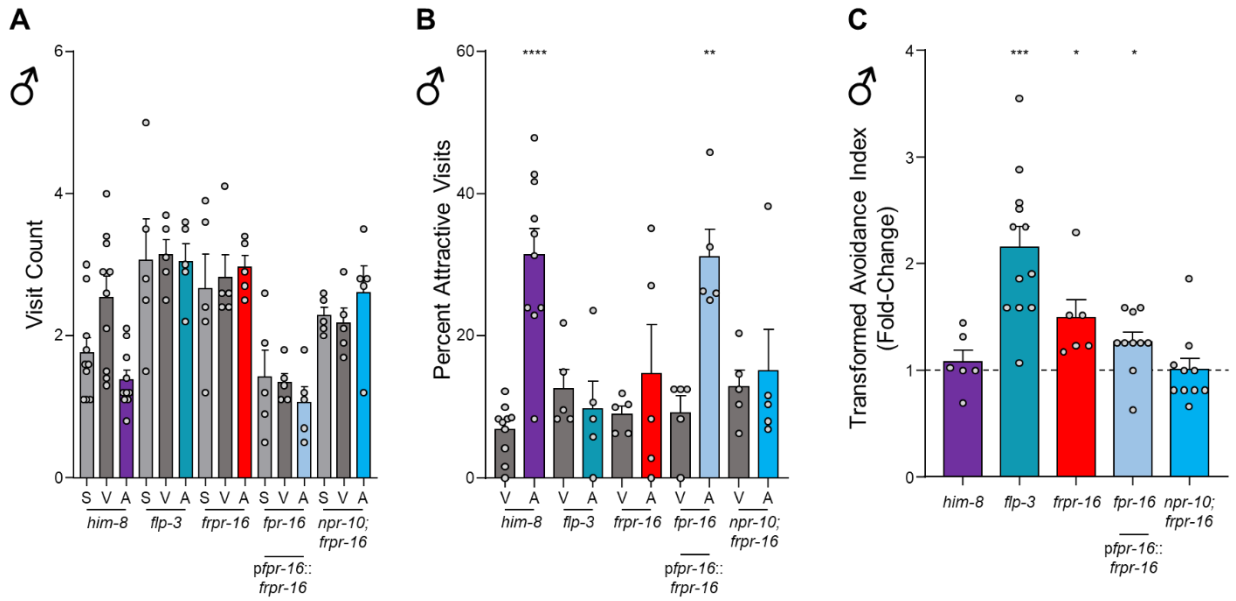

Supplementary Figure 11. FRPR-16 Supplementary Information.
(A) Visit count and **(B)** percent of attractive visits per worm of *frpr-16 lof* animals, transgenic rescues, and *frpr-16;npr-10* double mutant animals. **(C)** Transformed avoidance values for *frpr-16 lof* animals, transgenic rescues, and *frpr-16;npr-10* double mutant animals. **(A)** RM-ANOVA followed by Bonferroni correction comparing vehicle control to spatial control and ascaroside values. **(B)** Paired t-tests comparing vehicle and ascaroside values. **(C)** One-Way ANOVA followed by Dunnett's correction. Error bars denote SEM values. $n \geq 5$. * $p < 0.05$, ** $p < 0.01$, *** $p < 0.001$, **** $p < 0.0001$.

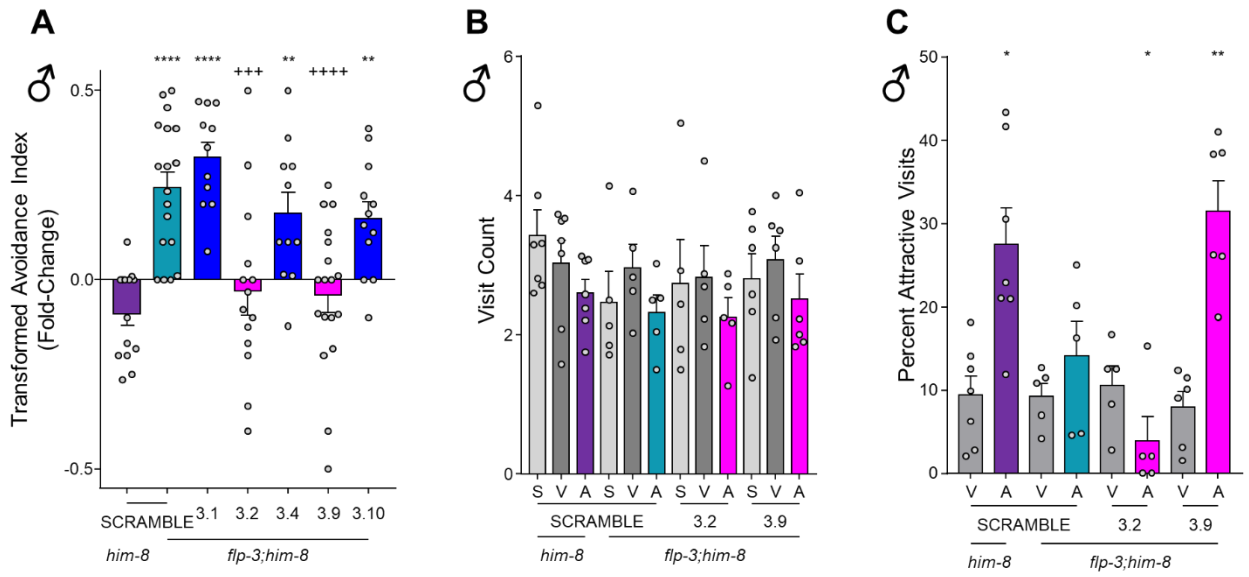

Supplementary Figure 12. FLP-3 Peptide Feeding Rescue Supplementary Information. **(A)** Transformed avoidance of *flp-3* animals fed SCRAMBLE and FLP-3 peptides. **(B)** Visit counts, and **(C)** percent of attractive visits per worm of *flp-3* animals fed peptides. **(A)** One-Way ANOVA followed by Dunnett's correction. **(B)** RM-ANOVA followed by Bonferroni correction comparing vehicle control to spatial control and ascaroside values. **(C)** Paired t-tests comparing vehicle and ascaroside values. Error bars denote SEM values. $n \geq 5$. * $p < 0.05$, ** $p < 0.01$, *** $p < 0.001$, **** $p < 0.0001$.

Supplementary Video 1. Spot Retention Assay of *him-8* males.
Scoring region on left contains 0.6 μL vehicle control, while the scoring region on the right contains 0.6 μL 1 μM ascr#8. Males enter the ascaroside and spend a large portion of their time therein in contact with other males. Video at 20X speed.

**** This video is saved on the Srinivasan Lab drive within WPI servers and will be made available upon request. ****

Supplementary Table 1. Strains used in this study.

Strain	Genotype	Received From
N2	wild-type, Bristol	*Caenorhabditis* Genetics Center (CGC)
CB4088	*him-5*(e1490)	CGC
CB1489	*him-8*(e1489)	CGC
PT690	*osm-3*(mn391);*him-5*(e1490)	Paul Sternberg (CalTech)
pk361	*flp-3*(pk361)	Chris Li (CUNY)
NY183	*flp-6*(pk1593)	Chris Li (CUNY)
NY106	*flp-12*(n4902)	Chris Li (CUNY)
NY193	*flp-19*(pk1594)	Chris Li (CUNY)
JSR99	*flp-3*(pk361);*him-8*(e1489)	This Study
JSR1	*flp-6*(pk1593);*him-8*(e1489)	This Study
JSR4	*flp-12*(n4902);*him-8*(e1489)	This Study
JSR2	*flp-19*(pk1594);*him-8*(e1489)	This Study
VC2497	*flp-3*(ok3265)	CGC
JSR84	*flp-3*(ok3265); *him-8*(e1489)	This Study
JSR109	*him-8*(e1489);worEx17[p*flp-3*::*flp-3*::GFP; p*unc-122*::RFP];*flp-3*(pk361)	This Study
JSR81	*him-8*(e1489);worEx17[p*flp-3*::*flp-3*::GFP; p*unc-122*::RFP]	This Study
PS2218	*dpy-20*(e1362);*him-5*(e1490);syls33[HS.C3(50ng/uL) + pMH86(11ng/uL)]	Paul Sternberg (CalTech)
JSR113	*dpy-20*(e1362);*him-5*(e1490);syls33[HS.C3(50ng/uL) + pMH86(11ng/uL)];worEx21[p*flp-3*::*flp-3*::SL2::mCherry; p*unc-122*::GFP]	This Study
tm1782	*npr-4*(tm1782))	National BioResource Project (NBRP)
CX14393	*npr-5*(ok1583)	CGC
tm8982	*npr-10*(tm8982)	NBRP
VC4220	*frpr-16*(gk5305[loxP + p*myo-2*::GFP::*unc-54* 3' UTR + p*rps-27*::neoR::*unc-54* 3' UTR + loxP])	This Study
JSR91	*npr-4*(tm1782);*him-8*(e1489)	This Study
JSR97	*npr-5*(ok1583);*him-8*(e1849)	This Study
JSR102	*npr-10*(tm8982);*him-8*(e1489)	This Study

JSR103	*frpr-16*(gk5305[loxP + p*myo-2*::GFP::*unc-54* 3' UTR + p*rps-27*::neoR::*unc-54* 3' UTR + loxP])*;him-8*(e1489)	Vancouver Node of International *C. elegans* Knockout Consortium
JSR107	*npr-10(tm8982);frpr-16*(gk5305[loxP + p*myo-2*::GFP::*unc-54* 3' UTR + p*rps-27*::neoR::*unc-54* 3' UTR + loxP])*;him-8*(e1489)	This Study
JSR126	*npr-10*(tm8982);*him-8*(e1489);worEx22[p*npr-10*::*npr-10*::GFP, p*unc-122*::RFP]	This Study
JSR111	*frpr-16*(gk5305[loxP + p*myo-2*::GFP::unc-54 3' UTR + p*rps-27*::neoR::*unc-54* 3' UTR + loxP])*;him-8*(e1489);worEx23[p*frpr-16*::frpr-16::dsRed, punc-122::GFP]	This Study
CU5248	*ceh-30*(tm272);*him-5*(e1490);smIs26[p*pkd-2*::GFP]	Ding Xue (UC Boulder)
JSR98	*flp-3*(pk361);*ceh-30*(tm272);*him-5*(e1490);smIs26[p*pkd-2*::GFP]	This Study
PT315	*egl-3*(n150);*him-8*(e1489)	Maureen Barr (Rutgers)
PT440	*aex-5*(sa23);*him-8*(e1489)	Maureen Barr (Rutgers)
PT436	*bli-4*(e937);*him-8*(e1489)	Maureen Barr (Rutgers)

Supplementary Table 2. Plasmids used and generated in this study.

Plasmid ID	Function	Component	Received From
pDONR p1-p2	DONR Vector	L1-L2 sites	
pL4440	-	Scramble Sequence	Victor Ambors, UMass Medical School
JSR#DKR20	ENTRY Clone	6xHis-MRFGKR-SCRAMBLE_KRK_STOP	
JSR#DKR27	ENTRY Clone	6xHis-MRFGKR-FLP3.1-KRK-STOP	
JSR#DKR22	ENTRY Clone	6xHis-MRFGKR-FLP3.2-KRK-STOP	
JSR#DKR12	ENTRY Clone	6xHis-MRFGKR-FLP3.4-KRK-STOP	
JSR#DKR13	ENTRY Clone	6xHis-MRFGKR-FLP3.9-KRK-STOP	
JSR#DKR23	ENTRY Clone	6xHis-MRFGKR-FLP3.10-KRK-STOP	
pDEST-527	DEST Vector	*E. coli* Expression Vector	Dominic Esposito (Addgene plasmid # 11518)
JSR#DKR21	*E. coli* Expession	6xHis-MRFGKR-SCRAMBLE_KRK_STOP	
JSR#DKR28	*E. coli* Expession	6xHis-MRFGKR-FLP3.1-KRK-STOP	
JSR#DKR25	*E. coli* Expession	6xHis-MRFGKR-FLP3.2-KRK-STOP	
JSR#DKR15	*E. coli* Expession	6xHis-MRFGKR-FLP3.4-KRK-STOP	
JSR#DKR16	*E. coli* Expession	6xHis-MRFGKR-FLP3.9-KRK-STOP	
JSR#DKR26	*E. coli* Expession	6xHis-MRFGKR-FLP3.10-KRK-STOP	
JSR#DKR18	Translational Fusion	p*flp-3*::*flp-3*::GFP	
JSR#DKR34	Translational Fusion	p*flp-3*::*flp-3*::SL2::mCherry	

-	Co-Injection Marker	p*unc-122*::GFP	Mark Alkema, UMass Medical School
-	Co-Injection Marker	p*unc-122*::RFP	Shreekanth Chalasani, Salk Institute
DACR1432	DONR Vector	L2-L3 SL2::dsRed::*unc-54* 3' UTR	Josh Hawk, Yale University
pPD95.75	GFP Fire Vector	GFP	

Supplementary Table 3. Primer and Ultramer sequences.

Primer/Ultramer Name	Primer/Ultramer Sequence	References
p*flp-3* Forward	GACTCTGCAGcatttccaagacacatttgacg	
flp-3 Reverse	GACTGGATCCttttccaaagcgcatggtt	
p*npr-10* Forward	gtttgttttccggcactttc	
npr-10 Reverse_overhang	AGTCGACCTGCAGGCATGCAAGCTaattgaactggaatcgtggtagt	
p*npr-10* Forward#2	cggcactttcctcatttttc	
p*frpr-16* Forward	accgatttctgatcgacgtg	
frpr-16 Reverse_overhang	CAGCAGTTTCCCTGAATTAAAATTAaacaattgccggagctttc	
pfrpr-16 Forward#2	ttctgatcgacgtgttggtt	
GFP_C	AGCTTGCATGCCTGCAGGTCGACT	Boulin et al.
GFP_D	AAGGGCCCGTACGGCCGACTAGTAG	Boulin et al.
GFP/dsRed_D#2	GGAAACAGTTATGTTTGGTATATTGGG	Boulin et al.
dsRed_E	TAATTTTAATTCAGGGAAACTGCTG	
dsRed_F	AAAGTTGgaaacagttatgtttgg	
SCRAMBLE Forward	GGGGACAAGTTTGTACAAAAAAGCAGGCTGGATGCGCTTTGGAAAACGTaattcgaagctccaccgcggtggcggccgctctagaactagtggatccaccggttccatggctagccacgcgcgtggatcccccgggctgcaggAAACGTaaataaCACCCAGCTTTCTTGTACAAAGTGGTCCCC	
FLP-3.1 Forward	GGGGACAAGTTTGTACAAAAAAGCAGGCTGGATGCGCTTTGGAAAACGTtctccactgggaacaatgcgctttggcAAACGTaaataaCACCCAGCTTTCTTGTACAAAGTGGTCCCC	
FLP-3.2 Forward	GGGGACAAGTTTGTACAAAAAAGCAGGCTGGATGCGCTTTGGAAAACGTactccattgggaactatgcgttttggaAAACGTaaataaCACCCAGCTTTCTTGTACAAAGTGGTCCCC	
FLP-3.4 Forward	GGGGACAAGTTTGTACAAAAAAGCAGGCTGGATGCGCTTTGGAAAACGTaaccctcttggaacc	

	atgcgctttggaAAACGTaaataaCACCCAGCTTTC TTGTACAAAGTGGTCCCC	
FLP-3.9 Forward	GGGGACAAGTTTGTACAAAAAAGCAGGCT GGATGCGCTTTGGAAAACGTaatcctgagaacgac acaccattcggaacaatgagatttggaAAACGTaaataaCA CCCAGCTTTCTTGTACAAAGTGGTCCCC	
FLP-3.10 Forward	GGGGACAAGTTTGTACAAAAAAGCAGGCT GGATGCGCTTTGGAAAACGTctactgttgattcttc ggagcccgtcattcgtgatcagAAACGTaaataaCACCC AGCTTTCTTGTACAAAGTGGTCCCC	

Chapter 8B Appendix 2

Supplemental Figure and Table Legends for Chapter 4C:

Multiple G Protein-Coupled Receptors Mediate ascr#8 Sensation

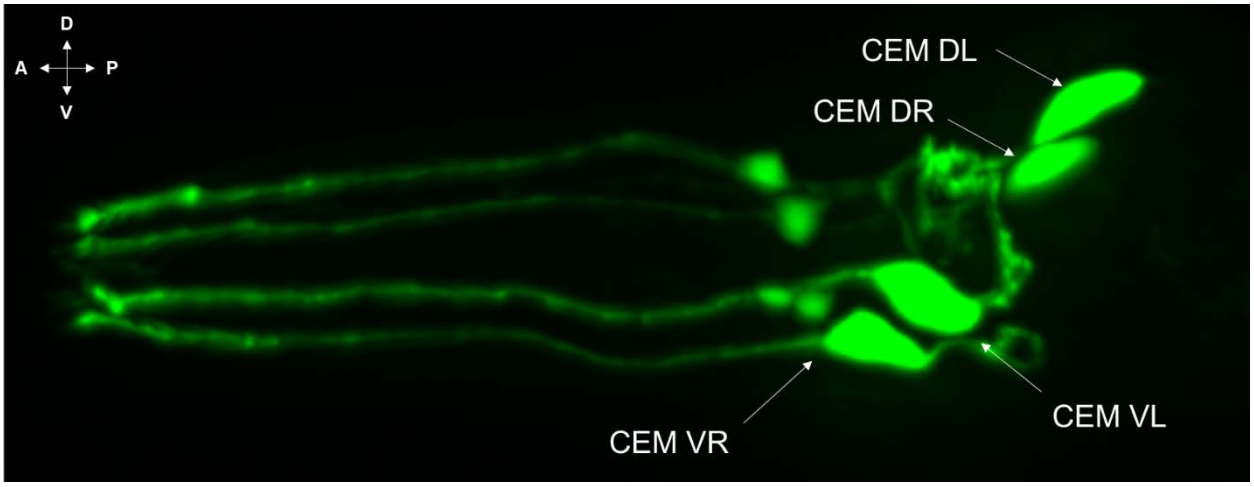

Supplementary Figure 13. Expression of GFP under a *trf-1* promoter.
While *trf-1* shows strong enrichment in CEM VR via transcriptomic analysis, promoter-GFP fusion expression resulted in strong expression in all four CEM neurons.

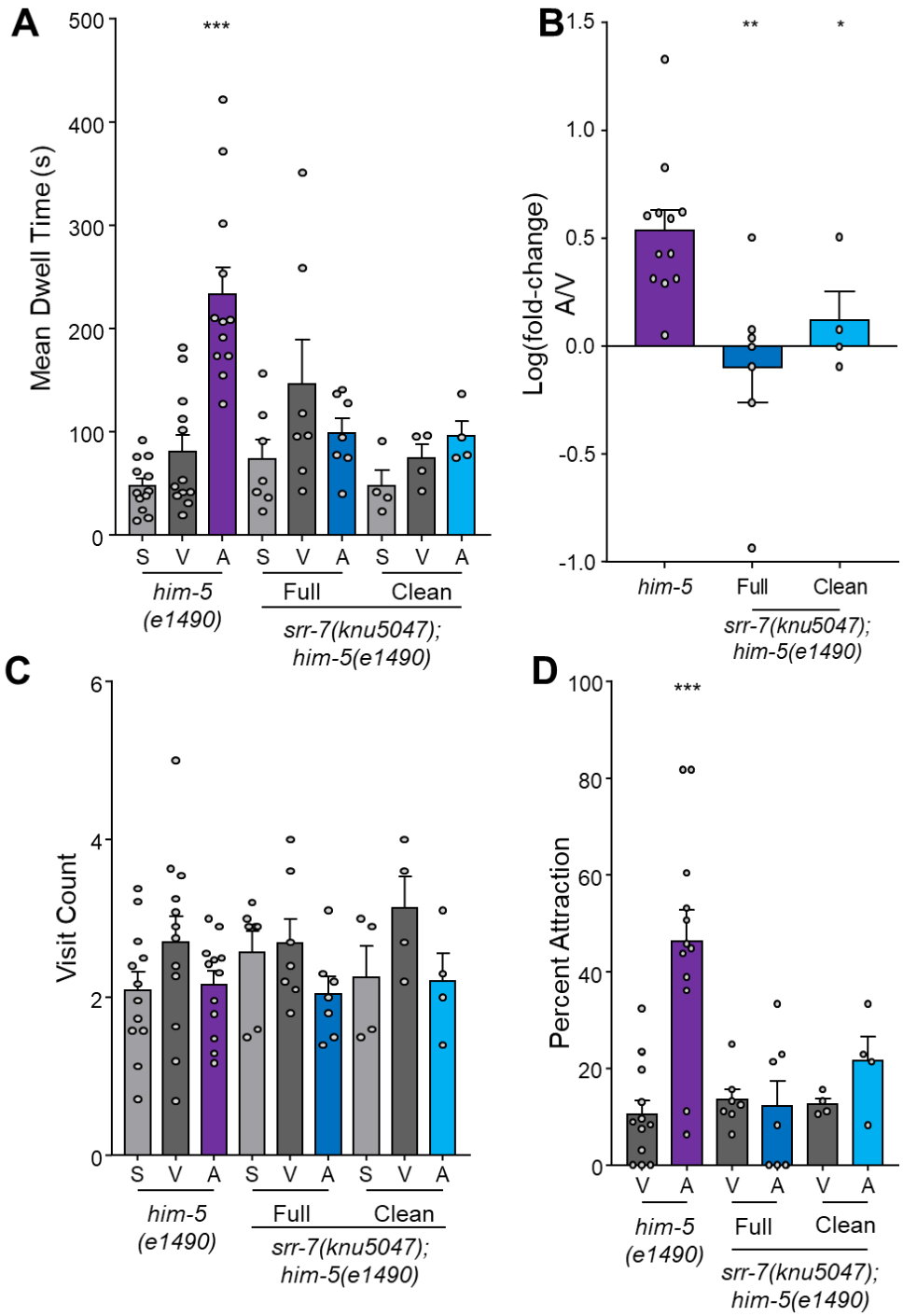

Supplementary Figure 14. Unbackcrossed *srr-7* knockouts mutants exhibit variable responses to ascr#8. **(A)** Raw dwell time data, **(B)** Log(fold-change) A/V values, **(C)** Visit Counts, and **(D)** Perfect Attraction of *him-5(e1490)* and unbackcrossed *srr-7(knu507);him-5(e1490*) [divided into a "full" data set, and one "clean" data set with Spatial and Vehicle control outliers removed]. Error bars denote SEM. n = 12, 7, and 4, respectively. **(A)** Internal strain comparisons performed by Repeated Measures ANOVA ($p < 0.05$), followed by a Bonferroni's multiple corrections test. **(B)** Comparison across strains and conditions, One-Way ANOVA ($p < 0.05$) followed by a Dunnett's multiple corrections test. **(D)** Vehicle vs. ascaroside #8 percent attractions compared via a paired t-test. * $p < 0.05$, ** $p < 0.01$, *** $p < 0.001$, **** $p < 0.0001$.

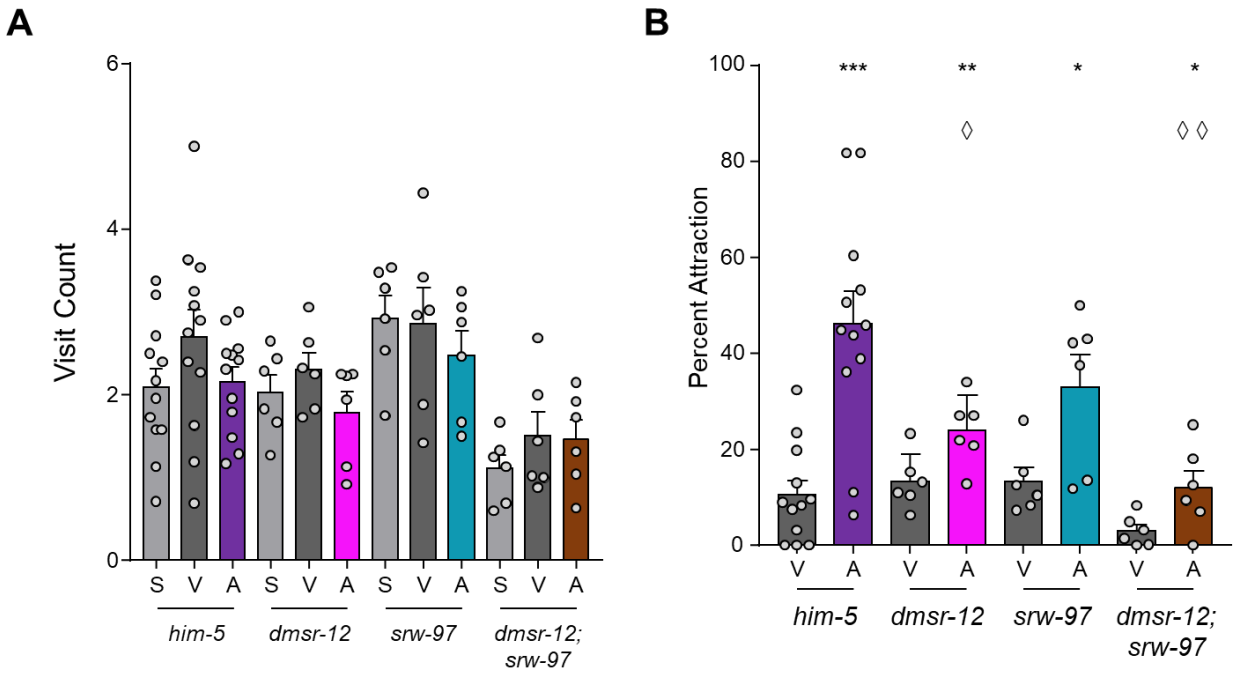

Supplementary Figure 15. Supplemental information for GPCR knockouts tested using Single Worm Assay.

(A) Visit counts of *him-5*, *dmsr-12*, *srw-97*, and *dmsr-12;srw-97* mutant animals. **(B)** Percent Attraction values for the same strains. Error bars denote SEM. $n \geq 6$. paired t-tests of vehicle vs ascr#8 percent attraction values. * $p < 0.05$, *** $p < 0.001$.

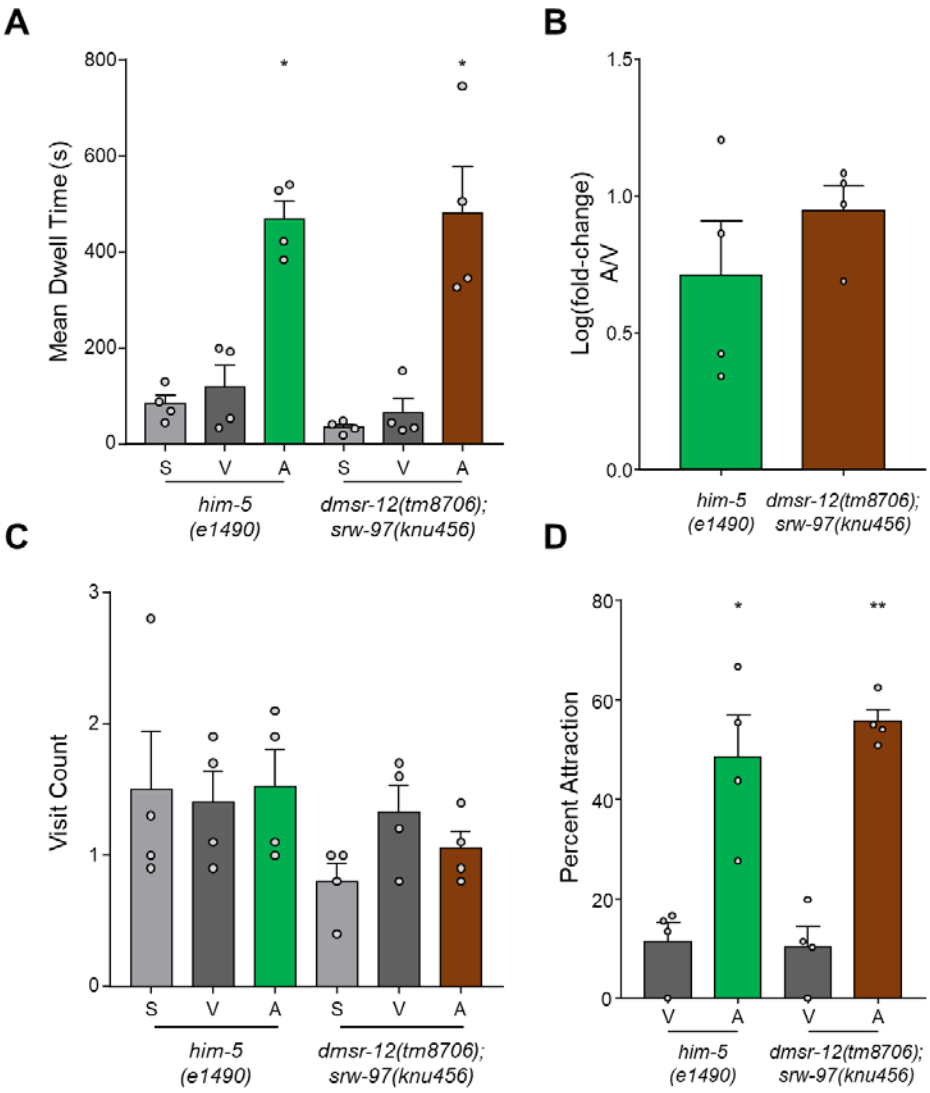

Supplementary Figure 16. ***dmsr-12;srw-97*** **double mutant males are not defective in their behavioral response to ascr#3.**

Single Worm Assay of double mutant animals in response to ascr#3. **(A)** Raw dwell time data, **(B)** Log(fold-change) A/V values, **(C)** Visit Counts, and **(D)** Perfect Attraction of *him-5(e1490)* and *dmsr-12(tm8706);srw-97(knu456);him-5(e1490)* males in response to 1 μM ascr#3. Error bars denote SEM. n = 4. **(A)** Internal strain comparisons performed by Repeated Measures ANOVA ($p < 0.05$), followed by a Bonferroni's multiple corrections test. **(B)** Comparison across strains and conditions, One-Way ANOVA ($p < 0.05$) followed by a Dunnett's multiple corrections test. **(D)** Vehicle vs. ascaroside #8 percent attractions compared via a paired *t*-test. * $p < 0.05$, ** $p < 0.01$, *** $p < 0.001$, **** $p < 0.0001$.

A

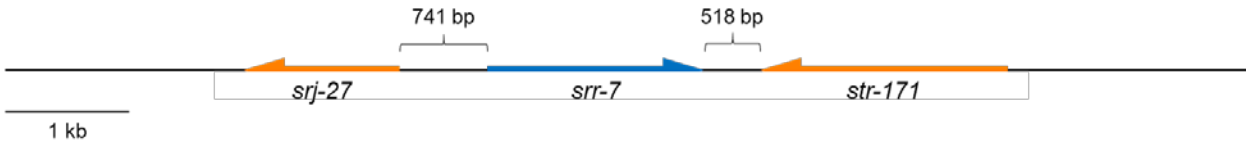

B

Gene	CEM Enrichment	CEM Cell	Enrichment
srr-7	6.33	CEM VL	1.90
srj-27	3.25	CEM VR	1.86
str-171	3.00	CEM VR	1.71

Supplementary Figure 17. Within Chromosome V, *srr-7* is flanked closely by GPCRs.
(A) A 10 kb genomic map of the *srr-7* locus. Bar denotes 1 kb. On the opposite strand from *srr-7*, *srj-27* is located 741 nucleotides upstream, while *str-171* is only 518 nucleotides downstream. **(B)** All three receptors exhibit transcript enrichment in the CEM, with *srr-7* being most enriched in CEM VL, while *srj-27* and *str-171* are enriched in CEM VR.

Supplementary Table 4. Numbers of filtered and mapped reads in RNA-seq data sets.
"Total reads" denotes the complete set of quality-filtered reads for a given data set that were mapped with RSEM to a *C. elegans* gene index (from WormBase release WS245) in order to compute gene expression values. With RSEM, a read can be mapped to the gene index either 0 times (i.e., it can fail to map at all); it can map exactly 1 time (i.e., it can map to a unique site in the gene index); or it can map 2+ times. For each RNA-seq data set, the numbers and percentages of reads with each status are given, as is the overall percentage of reads that mapped to the gene index. Whole larval RNA-seq data were originally generated by Schwarz et al [42]. Both CEM and larval reads were quality-filtered and mapped as described in **Methods**.

Input data (post-filter)	**Total reads**	**Aligned 0 times**	**Aligned exactly 1 time**	**Aligned 2+ times**	**Overall alignment rate**
CEM_DL	24,546,096	12,762,090 (51.99%)	3,815,458 (15.54%)	7,968,548 (32.46%)	48.01%
CEM_DR	23,927,441	17,182,697 (71.81%)	2,340,764 (9.78%)	4,403,980 (18.41%)	28.19%
CEM_VL	21,554,964	12,770,253 (59.25%)	2,623,239 (12.17%)	6,161,472 (28.58%)	40.75%
CEM_VR	23,682,948	19,009,725 (80.27%)	1,851,672 (7.82%)	2,821,551 (11.91%)	19.73%
Larvae	23,369,056	5,513,350 (23.59%)	7,422,251 (31.76%)	10,433,455 (44.65%)	76.41%

Supplementary Table 5. Numbers of genes with above-background expression in CEM neuronal and larval RNA-seq data.
Protein-coding and ncRNA-coding genes were counted as detectably expressed if, in a given RSEM analysis of a given data set, the gene had an expression value of ≥ 0.1 transcripts per million (i.e., ≥ 0.1 TPM); they were counted as robustly expressed if the gene had an expression value of ≥ 0.1 TPM in a 99% credibility interval (i.e., ≥ 0.1 minTPM). All gene annotations (including those used here, such as coding status) are given in **Supplementary Table 6**.

Data set	Protein-coding, detectably expressed	Protein-coding, robustly expressed	ncRNA-coding, detectably expressed	ncRNA-coding, robustly expressed
CEM_DL	7,688	2,011	9,145	4
CEM_DR	10,745	1,482	9,191	7
CEM_VL	7,844	917	9,165	5
CEM_VR	15,940	1,232	9,222	15
Larvae	15,022	9,918	9,151	6

Supplementary Table 6. Proteomes used for phylogenetic analysis of select CEM-expressed genes.
A phylogeny of the *Caenorhabditis* genus that includes these species and that defines the Elegans and Japonica groups within *Caenorhabditis* has been published [61], updating previous phylogenetic analyses. Genome assemblies for *C. remanei*, *C. brenneri*, and *C. japonica* were generated by the Washington University Genome Center (WashU) and made publicly available by 2010 [62]. Other genomes have been published as noted.

Organism	Features	URL	Reference
C. elegans	Hermaphrodite	[For almost all of the proteome:] *ftp://ftp.wormbase.org/pub/wormbase/releases/WS275/species/c_elegans/PRJNA13758/c_elegans.PRJNA13758.WS275.protein.fa.gz* [For an earlier long isoform of *dmsr-12*:] *ftp://ftp.wormbase.org/pub/wormbase/releases/WS250/species/c_elegans/PRJNA13758/c_elegans.PRJNA13758.WS250.protein.fa.gz*	64
C. inopinata	Male-female sibling species of *C. elegans*	*ftp://ftp.wormbase.org/pub/wormbase/releases/WS275/species/c_inopinata/PRJDB5687/c_inopinata.PRJDB5687.WS275.protein.fa.gz*	65
C. briggsae	Hermaphrodite	*ftp://ftp.wormbase.org/pub/wormbase/releases/WS275/species/c_briggsae/PRJNA10731/c_briggsae.PRJNA10731.WS275.protein.fa.gz*	66
C. nigoni	Male-female sibling species of *C. briggsae*	*ftp://ftp.wormbase.org/pub/wormbase/releases/WS275/species/c_nigoni/PRJNA384657/c_nigoni.PRJNA384657.WS275.protein.fa.gz*	67
C. tropicalis	Hermaphrodite	n/a	Unpublished
C. wallacei	Male-female sibling species of *C. tropicalis*	n/a	Unpublished
C. remanei	Male-female, Elegans group	*ftp://ftp.wormbase.org/pub/wormbase/releases/WS275/species/c_remanei/PRJNA53967/c_remanei.PRJNA53967.WS275.protein.fa.gz*	62
C. brenneri	Male-female, Elegans group	*ftp://ftp.wormbase.org/pub/wormbase/releases/WS275/species/c_brenneri/PRJNA20035/c_brenneri.PRJNA20035.WS275.protein.fa.gz*	62
C. japonica	Male-female, Japonica group	*ftp://ftp.wormbase.org/pub/wormbase/releases/WS275/species/c_japonica/PRJNA12591/c_japonica.PRJNA12591.WS275.protein.fa.gz*	62
C. becei	Male-female, Japonica group	*http://download.caenorhabditis.org/v1/sequence/Caenorhabditis_sp29_QG2083_v1.proteins.fa.gz*	68
C. sulstoni	Male-female, Japonica group	*http://download.caenorhabditis.org/v1/sequence/Caenorhabditis_sp32_JU2788_v1.proteins.fa.gz*	68

Supplementary Table 7. Traits of *C. elegans* genes expressed in CEM neurons (CEM_DL, CEM_DR, CEM_VL, and CEM_VR) and whole larvae.

See the Excel spreadsheet CEM_RNAseq_annots_2020.02.28.01.xlsx. Its data columns are as follows:

Gene: a given predicted protein-coding or ncRNA-coding gene in the *C. elegans* genome, from WormBase release WS245, for which we observed non-zero gene activity in CEM neurons. All further data columns are pertinent to that particular gene.

[*CEM RNA-seq read set*]_TPM: for a given RNA-seq data set from a particular CEM neuron type (CEM_DL, CEM_DR, CEM_VL, or CEM_VR; **Supplementary Table 4**), this denotes the expression level for a given gene, determined with RNA-seq reads from single-cell RT-PCR products (**Supplementary Table 4**), measured in transcripts per million (TPM).

Larvae_TPM: the expression level for a given gene in whole larvae, generated from a pooled set of all larval RNA-seq reads (**Supplementary Table 4**), measured in TPM.

[*RNA-seq read set*]_TPM_nz: for a given RNA-seq data set from either a particular CEM neuron type or from larvae, this denotes the same expression level for a given gene as in [*RNA-seq read set*]_TPM above, but with any zero gene expression values in a given RNA-seq data set replaced with empirical non-zero pseudominimum values. We computed these values because replacing zero values with empirical non-zero pseudominima allows logarithmic plotting and comparison of expression ratios for all genes. For a given RNA-seq data set, we define its empirical non-zero pseudominimum as being the smallest non-zero expression value observed in our RNA-seq analysis; we reason that the smallest such non-zero value is effectively equivalent to noise. For relatively small RNA-seq data sets, the smallest observed non-zero expression value will tend to be larger because the reads have less granularity, so an empirical pseudominimum will approach zero as the raw data set grows in size.

[*CEM RNA-seq read set*]/larvae: the ratio of gene expression (measured in TPM) between a given CEM neuron type and whole *C. elegans* larvae.

Coding: the nature of a given gene's coding potential, as annotated in WormBase WS245. Most genes are either solely protein-coding or solely ncRNA-coding and are noted as such in this data column. For 301 genes in *C. elegans*, WS245 predicts both protein-coding and non-protein-coding transcripts; in this table, such genes are denoted with "protein; ncRNA". However, for purposes of gene analysis, we assume that any gene with dual predicted nature is solely protein-coding.

Prot_size: the full range of sizes for all protein products from a gene's predicted isoforms.

Max_prot_size: the size of the largest predicted protein product.

Housekeeping: a set of genes that were previously observed, by single-cell RNA-seq, to be constitutively active both in whole *C. elegans* larvae and in three different developmental stages/ genotypes of migrating *C. elegans* linker cells [42].

TF: genes annotated as encoding transcription factors by one or more of three different censuses by Gupta, Thomas, or Walhout, as previously compiled [42].

7TM_GPCRs: 7TM_GPCRs: a set of genes encoding G-protein coupled receptors (GPCRs), a class of genes of particular biological interest in deciphering CEM function [53].

PFAM-A: for protein-coding genes, predicted domains from the annotated (PFAM-A) subdivision of PFAM 27 [50], with an E-value of $\leq 10^{-5}$.

GO_term: Gene Ontology terms [63] for which a gene was annotated in WormBase release WS245.

eggNOG: for protein-coding genes, predicted orthology groups from the eggNOG 3.0 database [52].

Phobius: predictions of signal and transmembrane sequences made with Phobius [47]. 'SigP' indicates a predicted signal sequence, and 'TM' indicates one or more transmembrane-spanning helices, with N helices indicated with '(Nx)'. Varying predictions from different isoforms are listed.

NCoils: coiled-coil domains, predicted by ncoils [49]. As with Psegs, the relative and absolute fractions of each protein's coiled-coil residues are shown.

Psegs: this shows what fraction of a protein is low-complexity sequence, as detected by pseg [48]. Both the proportion of such sequence (ranging from 0.01 to 1.00) and the exact ratio of low-complexity residues to total residues are given. Proteins with no predicted low-complexity residues are blank.

[*RNA-seq read set*]_reads: for the gene in question, and for a given RNA-seq data set, this denotes a posterior mean estimate of the number of RNA-seq reads mapping to that gene as computed by RSEM, and with decimal fractions rounded off. All cell types are as with "[*RNA-seq read set*]_TPM" above.

[*RNA-seq read set*]_minTPM: for the gene in question, and for a given RNA-seq data set, this denotes the minimum estimate of that gene's activity as measured in that RNA-seq data set and computed by RSEM with a 99% confidence interval in Transcripts Per Million (minTPM). All cell types are as with "[*RNA-seq read set*]_TPM" above.

Supplementary Table 8. List of genes enriched 2-fold the CEM VL over non-VL CEM neurons.
20 genes were enriched at least 2-fold, while *srr-7* was only enriched 1.9-fold. Genes discussed in paper are added or bolded in the table.

Gene	CEM_VL	CEM_VL/ max_non_ CEM_VL	max_CEM / larvae
WBGene00011105|R07E3.4	81.02	1350.33	8.45
WBGene00006786|Y60A3A.1|unc-51	5.64	564.00	1.56
WBGene00022690|ZK250.7|math-49	10.10	252.50	252.50
WBGene00011460|T05A10.3|ttr-14	4.96	124.00	0.24
WBGene00013269|Y57A10A.29	27.06	112.75	4.59
WBGene00004111|C37A2.5|pqn-21	6.13	87.57	1.50
WBGene00015208|B0495.9	14.13	83.12	0.23
WBGene00022288|Y75B7B.1	4.62	77.00	0.94
WBGene00021763|Y51F10.2	43.28	58.49	0.18
WBGene00020216|T04G9.5|trap-2	4.04	50.50	0.03
WBGene00003661|K11E4.5|nhr-71	2.31	46.20	1.16
WBGene00021010|W03G1.2	2.52	42.00	0.60
WBGene00009006|F21D5.1	0.62	31.00	0.10
WBGene00011680|T10B10.3	1.17	29.25	0.33
WBGene00022076|Y69A2AR.5|daao-1	1.36	27.20	0.24
WBGene00006959|R74.3|xbp-1	2.85	25.91	0.18
WBGene00008575|F08E10.7|scl-24	2.41	24.10	0.30
WBGene00020612|T20D4.6|arrd-22	0.67	22.33	0.35
WBGene00020687|T22D1.10|ruvb-2	1.02	20.40	0.03
WBGene00001748|F56C9.1|gsp-2	6.94	19.28	1.33
WBGene00009048|F22B8.6|cth-1	2.20	18.33	0.02
WBGene00001065|EGAP7.1|dpy-3	19.71	15.52	1.66
WBGene00001372|R09B3.1|exo-3	5.19	15.26	0.32
WBGene00003576|W01B6.9|ndc-80	0.29	14.50	0.02
WBGene00013446|Y66D12A.21	9.35	13.36	0.09
WBGene00017574|F18F11.1	2.38	13.22	0.13
WBGene00017137|EEED8.9|pink-1	0.26	13.00	0.02
WBGene00006720|F25H2.8|ubc-25	6.95	12.64	0.11
WBGene00004700|Y111B2A.18|rsp-3	69.64	12.50	0.59
WBGene00019351|K03A1.2|lron-7	0.73	12.17	0.21

Appendix XXXV

WBGene00017084|E01A2.1	187.71	12.12	4.28
WBGene00017885|F28B3.4|dip-2	1.06	11.78	3.21
WBGene00003891|F11C7.5|osm-11	67.82	11.77	116.93
WBGene00018239|F40G9.1|sec-20	0.69	11.50	13.80
WBGene00020358|T08E11.2|math-39	1.34	11.17	0.27
WBGene00018811|F54D11.1|pmt-2	3.77	11.09	0.01
WBGene00015744|C13F10.5	95.50	10.93	1.67
WBGene00000671|Y41C4A.19|col-96	104.73	10.05	2.57
WBGene00007710|C25A1.9|rsa-1	14.85	9.97	0.18
WBGene00011449|T04H1.2	0.39	9.75	0.04
WBGene00011966|T23G7.3	0.39	9.75	0.01
WBGene00021801|Y53G8AL.3	0.76	9.50	10.86
WBGene00008912|F17C8.7	16.71	9.08	0.52
WBGene00013242|Y56A3A.30	0.18	9.00	0.86
WBGene00011918|T22C1.8	0.71	8.88	0.11
WBGene00004338|F58F6.4|rfc-2	0.43	8.60	0.01
WBGene00012530|Y32F6A.5	2.52	8.40	0.03
WBGene00007278|C03D6.6|lab-1	0.99	8.25	0.04
WBGene00019986|R09F10.1	3.16	8.10	0.33
WBGene00000040|ZK455.1|aco-1	2.68	7.44	0.11
WBGene00006706|F29B9.6|ubc-9	29.96	6.79	0.17
WBGene00007948|C35A5.4	0.33	6.60	0.12
WBGene00003149|T04C10.1|mbk-1	0.13	6.50	0.01
WBGene00015056|B0222.5	0.19	6.33	0.03
WBGene00003660|Y51A2D.17|nhr-70	0.25	6.25	0.18
WBGene00002997|B0454.1|lin-8	0.36	6.00	12.00
WBGene00009367|F33H2.3	0.41	5.86	1.03
WBGene00015391|C03G5.1|sdha-1	0.58	5.80	0.01
WBGene00019612|K10B3.6|gpcp-1	9.83	5.75	2.16
WBGene00015693|C10H11.4|ugt-28	0.17	5.67	0.06
WBGene00019455|K06H7.1	0.34	5.67	6.80
WBGene00044169|C06C3.10	0.75	5.36	0.87
WBGene00010265|F58G1.3	0.37	5.29	0.06
WBGene00022034|Y65B4BL.2|deps-1	7.74	5.23	0.33
WBGene00006415|F38H4.7|tag-30	0.26	5.20	0.03
WBGene00018605|F48E3.4	4.49	5.04	0.03

WBGene00019666|K12B6.1|sago-1	0.05	5.00	0.01
WBGene00022244|Y73B6BL.23	0.95	5.00	0.01
WBGene00010061|F54E12.2	8.16	4.83	0.22
WBGene00011276|R53.7|aakg-5	0.33	4.71	0.01
WBGene00004953|F32H2.3|spd-2	0.14	4.67	0.01
WBGene00008516|F02C12.2	0.27	4.50	0.12
WBGene00015977|C18F10.2	0.09	4.50	4.50
WBGene00013030|Y49E10.4	0.18	4.50	0.05
WBGene00011746|T13F2.6	0.61	4.36	0.06
WBGene00011917|T22C1.6	0.13	4.33	0.03
WBGene00005658|T01G5.4|srr-7	**0.17**	**4.25**	**4.25**
WBGene00000741|T10E10.1|col-168	106.25	4.22	0.23
WBGene00011773|T14G10.3|ttr-53	0.58	4.14	0.01
WBGene00014075|ZK757.4|dhhc-4	1.36	4.12	0.44
WBGene00001907|F17E9.13|his-33	1.78	4.05	7.12
WBGene00000298|F32G8.6|cat-4	3.05	4.01	0.03
WBGene00015698|C10H11.10|kca-1	0.16	4.00	0.30
WBGene00001904|F35H10.1|his-30	1.66	3.86	6.64
WBGene00009740|F45H10.3	221.25	3.84	0.50
WBGene00006051|T28H11.5|ssq-2	300.81	3.81	4.56
WBGene00018803|F54D10.2|fbxa-24	0.80	3.81	0.20
WBGene00008802|F14E5.4|acp-2	0.30	3.75	0.04
WBGene00020531|T15B12.2	0.15	3.75	0.07
WBGene00007010|R10E12.1|alx-1	0.26	3.71	0.06
WBGene00007192|B0491.5	8.53	3.71	0.02
WBGene00016738|C47D2.1	25.03	3.69	5.28
WBGene00009114|F25D7.5	0.11	3.67	11.00
WBGene00009776|F46B6.12	0.40	3.64	0.01
WBGene00016033|C24A3.2	2.86	3.62	0.03
WBGene00004807|F46A9.5|skr-1	30.93	3.57	0.14
WBGene00014259|ZK1320.11	0.50	3.57	0.07
WBGene00020912|W01A11.7	0.85	3.54	0.82
WBGene00022435|Y108G3AL.3	0.07	3.50	0.25
WBGene00016142|C26E6.6|mrps-18C	0.14	3.50	0.00
WBGene00016788|C49G7.10	0.21	3.50	0.12
WBGene00019738|M02F4.7|clec-265	13.52	3.49	0.07

Appendix XXXVII

WBGene00002985|C29A12.3|lig-1	1.63	3.47	0.06
WBGene00021552|Y44E3B.1|zip-4	0.83	3.46	0.07
WBGene00022672|ZK177.4	109.78	3.39	1.04
WBGene00004148|T13H2.4|pqn-65	0.10	3.33	0.01
WBGene00001000|C18A11.7|dim-1	0.23	3.29	0.00
WBGene00013391|Y62H9A.3	0.59	3.28	0.02
WBGene00011743|T13F2.2	186.10	3.26	0.23
WBGene00000223|C07G2.2|atf-7	0.39	3.25	0.04
WBGene00009147|F26C11.3	0.29	3.22	4.14
WBGene00017067|D2092.6	0.16	3.20	0.73
WBGene00044535|K11D12.13	0.64	3.20	0.04
WBGene00011708|T11B7.5	0.67	3.19	0.10
WBGene00017776|F25B5.5	6.77	3.15	0.22
WBGene00007758|C27A7.8	114.06	3.06	30.34
WBGene00018134|F37A4.4	0.03	3.00	0.03
WBGene00016202|C29E4.2|kle-2	0.06	3.00	0.86
WBGene00012351|W09C5.1	13.42	2.87	0.13
WBGene00017990|F32E10.2|cec-4	0.17	2.83	0.00
WBGene00006793|W09C5.2|unc-59	0.14	2.80	0.01
WBGene00016845|C50F7.5	0.25	2.78	1.00
WBGene00019767|M04F3.1|rpa-2	3.52	2.77	0.02
WBGene00021993|Y59E9AL.3	0.93	2.74	0.01
WBGene00017039|D1073.1|trk-1	0.08	2.67	2.00
WBGene00006994|F22B5.7|zyg-9	0.58	2.64	0.08
WBGene00017016|D1014.3|snap-1	0.21	2.63	0.01
WBGene00012201|W02B12.1	4.99	2.60	0.19
WBGene00007574|C14B1.3	3.64	2.53	0.23
WBGene00013425|Y66A7A.5|ceh-91	0.05	2.50	0.06
WBGene00010354|H02I12.8|cyp-31A2	0.15	2.50	0.02
WBGene00003178|F57H12.7|mec-17	12.17	2.41	0.24
WBGene00012339|W07G4.5	0.12	2.40	0.00
WBGene00000726|F17C11.3|col-153	5.11	2.38	1.11
WBGene00011507|T05H10.1	0.07	2.33	0.21
WBGene00012099|T27E9.9|acc-4	0.07	2.33	0.26
WBGene00019013|F57C9.7|tofu-4	0.07	2.33	2.33
WBGene00008956|F19H6.1|nekl-3	0.23	2.30	0.62

WBGene00001685|K10B3.7|gpd-3	3.54	2.30	0.02
WBGene00004796|ZK520.2|sid-2	0.16	2.29	0.03
WBGene00008453|E02A10.3	0.70	2.26	0.10
WBGene00015641|C09E7.7	0.09	2.25	0.01
WBGene00022584|ZC266.1	0.09	2.25	0.02
WBGene00010087|F55B11.5	0.36	2.25	0.22
WBGene00018302|F41G3.6	0.11	2.20	0.00
WBGene00001919|B0035.10|his-45	0.22	2.20	0.73
WBGene00012546|Y37D8A.4	0.13	2.17	0.01
WBGene00020330|T07H6.1	0.30	2.14	1.11
WBGene00011247|R11D1.9|mrpl-49	0.21	2.10	0.01
WBGene00011564|T07C5.1|ugt-50	0.23	2.09	0.01

Supplementary Table 9. List of genes enriched 2-fold the CEM VR over non-VR CEM neurons.
639 genes were enriched at least 2-fold, with *srw-97* and *seb-3* were enriched 3.67-fold, and 3.25-fol, respectively. Genes discussed in paper are added or bolded in the table.

Gene	CEM_VR	CEM_VR/ max_non_ CEM_VR	max_CEM /larvae
WBGene00008382|D1081.4	427.19	4271.90	316.44
WBGene00009498|F36H2.1|tat-5	32.16	1608.00	12.71
WBGene00044917|F40F8.12	97.52	812.67	487.60
WBGene00017567|F18E3.11	188.86	786.92	40.79
WBGene00020070|R13H9.1|rmd-6	105.05	750.36	5.62
WBGene00019972|R09A1.2	225.88	352.94	46.67
WBGene00006612|F45G2.6|trf-1	**78.02**	**339.22**	**236.42**
WBGene00019805|R01B10.3	84.06	300.21	96.62
WBGene00022002|Y59E9AR.7	664.73	295.44	152.81
WBGene00021327|Y34D9A.1|mrpl-38	24.37	243.70	2.47
WBGene00000970|C17G10.8|dhs-6	14.19	236.50	11.73
WBGene00019808|R01B10.6	6.22	207.33	0.98
WBGene00011467|T05C12.3|decr-1.3	8.05	201.25	1.73
WBGene00008750|F13E9.1	5.61	187.00	5.29
WBGene00017215|F07F6.1	5.49	183.00	4.16
WBGene00016424|C34H4.1	38.51	148.12	1.39
WBGene00009671|F43G9.10|mfap-1	2.27	113.50	0.16
WBGene00018721|F53A3.2|polh-1	2.22	111.00	0.52
WBGene00002978|Y105E8B.1|lev-11	73.22	110.94	0.40
WBGene00013477|Y69E1A.5	6.61	110.17	73.44
WBGene00016680|C45G9.9	3628.99	97.92	89.23
WBGene00003369|C36E6.3|mlc-1	49.65	95.48	0.55
WBGene00017803|F26A1.4	122.60	93.59	27.43
WBGene00011888|T21B10.6|cutl-15	1.83	91.50	0.07
WBGene00022410|Y97E10C.1	10.75	89.58	2.92
WBGene00016746|C48B6.10	14.33	84.29	15.75
WBGene00007082|AH10.1|acs-10	2.49	83.00	1.15
WBGene00010596|K06A4.6	19.70	82.08	4.25
WBGene00003421|F09E8.3|msh-5	1.62	81.00	6.23
WBGene00020187|T03F1.5|gsp-4	58.21	72.76	15.86

WBGene00004050|E02H1.4|pme-2	0.67	67.00	0.09
WBGene00010946|M176.10	28.62	59.63	954.00
WBGene00017106|E02H9.9	5.09	56.56	36.36
WBGene00009126|F25H5.3|pyk-1	62.19	54.08	1.42
WBGene00012475|Y18D10A.2	3.17	52.83	19.81
WBGene00008002|C38C10.6	8.68	51.06	28.93
WBGene00000107|F54D8.3|alh-1	5.40	49.09	0.03
WBGene00013956|ZK265.3	2.90	48.33	0.26
WBGene00009154|F26D2.16	0.45	45.00	0.94
WBGene00012258|W04G3.5	156.78	43.55	4.70
WBGene00019490|K07E3.1	2.08	41.60	1.59
WBGene00003543|F20G2.4|nas-24	1.22	40.67	0.78
WBGene00000872|F11H8.4|cyk-1	0.40	40.00	0.14
WBGene00000288|T07G12.1|cal-4	3.99	39.90	1.32
WBGene00021625|Y47D7A.13	342.55	39.60	0.29
WBGene00016195|C28H8.4	417.92	39.09	8.46
WBGene00017547|F18A1.6|alfa-1	5.44	38.86	0.55
WBGene00016684|C45G9.13	2.62	37.43	0.19
WBGene00016990|CD4.4|vps-37	1.86	37.20	0.08
WBGene00022707|ZK354.6	2.22	37.00	0.92
WBGene00007777|C27D8.1	1674.30	35.34	68.03
WBGene00001781|C02A12.1|gst-33	359.19	34.27	1197.30
WBGene00010290|F58H1.7	2.95	32.78	0.35
WBGene00003901|F48E8.5|paa-1	46.05	31.11	0.42
WBGene00020826|T26A8.3	2.78	30.89	1.97
WBGene00044366|F34D6.9	10.70	30.57	34.52
WBGene00017415|F13A2.6	2.13	30.43	42.60
WBGene00001172|C51E3.7|egl-3	3.95	30.38	0.73
WBGene00015484|C05D11.7|atgl-1	6.24	29.71	0.45
WBGene00015427|C04E6.13	4.75	29.69	5.79
WBGene00000975|K08F4.9|dhs-12	4.34	28.93	0.24
WBGene00006585|T20B3.2|tni-3	1.87	26.71	0.13
WBGene00006048|ZK1225.6|ssp-31	3.13	26.08	10.10
WBGene00014088|ZK809.8	1.82	26.00	0.37
WBGene00000216|H22K11.1|asp-3	1262.71	25.92	0.79
WBGene00021997|Y59E9AR.1	265.37	25.89	4.21

Appendix XLI

WBGene00017712|F22E5.17	0.95	23.75	19.00
WBGene00010625|K07C5.2	0.68	22.67	1.70
WBGene00014214|ZK1073.2	0.68	22.67	0.71
WBGene00004208|ZK675.1|ptc-1	0.22	22.00	0.18
WBGene00003589|T07C4.9|nex-2	4.12	20.60	0.60
WBGene00017280|F09D1.1|usp-39	2.26	20.55	1.00
WBGene00008748|F13E6.4|yap-1	0.80	20.00	0.03
WBGene00009529|F38B2.2	265.01	19.97	52.58
WBGene00017880|F28A12.3	37.66	19.61	20.47
WBGene00009173|F26H9.1|prom-1	0.19	19.00	0.10
WBGene00016032|C24A3.1	0.19	19.00	3.80
WBGene00016404|C34D4.13|mutd-1	1.48	18.50	0.38
WBGene00022874|ZK1248.1|nep-25	0.36	18.00	0.51
WBGene00009888|F49E2.5	6.97	17.87	0.37
WBGene00008386|D1081.8	2.46	17.57	0.17
WBGene00007142|B0334.1|ttr-18	2.63	17.53	0.05
WBGene00004192|ZK809.7|prx-2	0.70	17.50	0.48
WBGene00002027|T05F1.6|hsr-9	1.52	16.89	0.16
WBGene00014213|ZK1073.1	0.65	16.25	0.45
WBGene00006802|T07A5.6|unc-69	224.91	16.18	4.92
WBGene00000738|F14H12.1|col-165	0.48	16.00	0.06
WBGene00004136|K11D12.2|pqn-51	67.63	15.66	0.82
WBGene00020143|T01C8.2	1.85	15.42	0.30
WBGene00020808|T25F10.6	730.18	15.39	1.19
WBGene00013503|Y71A12B.6|clec-112	0.61	15.25	12.20
WBGene00016792|C49H3.6	0.61	15.25	0.44
WBGene00010848|M04B2.6	5.65	14.49	1.81
WBGene00017673|F21F3.3	2.15	14.33	0.84
WBGene00000860|C37H5.11|cwp-2	518.39	14.04	1126.93
WBGene00001458|ZK525.1|flp-15	9.69	14.04	3.73
WBGene00011975|T24B1.1	0.14	14.00	0.01
WBGene00006587|F53A9.10|tnt-2	439.86	13.96	0.65
WBGene00013647|Y105C5B.5	3.16	13.74	0.43
WBGene00001485|Y113G7A.8|fre-1	0.41	13.67	8.20
WBGene00007778|C27D8.2	0.27	13.50	0.05
WBGene00018378|F43C11.1	2.14	13.38	8.92

WBGene00018294|F41E6.13|atg-18	0.93	13.29	0.02
WBGene00008052|C41C4.7|ctns-1	12.05	13.10	0.47
WBGene00009951|F53A2.3	0.39	13.00	3.00
WBGene00007793|C28D4.5	2.33	12.94	0.12
WBGene00016194|C28H8.3	29.63	12.94	0.27
WBGene00000101|D1022.7|aka-1	1.28	12.80	0.09
WBGene00015942|C18A3.4|osta-2	3.17	12.68	0.10
WBGene00018837|F54G2.1	0.38	12.67	5.43
WBGene00019672|K12B6.8	0.25	12.50	0.51
WBGene00013047|Y50E8A.2	1.73	12.36	4.68
WBGene00018702|F52E4.5	0.37	12.33	9.25
WBGene00016151|C27A2.1|smc-5	0.12	12.00	0.01
WBGene00009294|F31D4.9	1480.40	11.97	40.91
WBGene00008852|F15C11.2|ubql-1	27.98	11.91	0.06
WBGene00003868|B0334.11|ooc-3	53.22	11.54	0.55
WBGene00006833|F53F10.4|unc-108	32.95	11.40	0.38
WBGene00009143|F26A3.5	0.34	11.33	0.03
WBGene00022400|Y97E10AR.5|rpb-9	13.79	11.03	0.27
WBGene00022761|ZK546.4	1.76	11.00	0.19
WBGene00017328|F10C5.2	2.59	10.36	0.06
WBGene00011392|T03D8.3|sbt-1	1.32	10.15	0.03
WBGene00003906|W03G9.6|paf-1	0.20	10.00	0.34
WBGene00018714|F52H2.1	1.00	10.00	7.69
WBGene00015505|C06A5.8	26.59	9.26	0.39
WBGene00006831|C52E12.2|unc-104	0.09	9.00	4.50
WBGene00020084|R105.1	0.62	8.86	0.03
WBGene00001248|F38A6.2|elp-1	0.95	8.64	0.10
WBGene00007880|C33A12.1	0.60	8.57	0.05
WBGene00016442|C35D10.5	0.34	8.50	0.01
WBGene00017791|F25E5.10|try-8	0.17	8.50	0.27
WBGene00019085|F59A6.3	0.17	8.50	8.50
WBGene00013347|Y59A8B.10	1.68	8.40	2.37
WBGene00021644|Y47G6A.18	0.42	8.40	0.01
WBGene00007883|C33A12.4	4789.59	8.26	207.70
WBGene00009562|F39H2.1|flp-22	81.49	8.25	17.83
WBGene00020628|T20F5.6	0.08	8.00	0.80

Appendix XLIII

WBGene00003068|T27C10.6|lrk-1	0.72	8.00	0.45
WBGene00010911|M106.3	0.64	8.00	0.69
WBGene00011886|T21B10.4	0.16	8.00	0.03
WBGene00010736|K10C8.3|istr-1	8.81	7.87	0.13
WBGene00003370|C36E6.5|mlc-2	1111.65	7.79	0.81
WBGene00001452|C36H8.3|flp-9	1.21	7.56	0.06
WBGene00000066|M03F4.2|act-4	10.14	7.40	0.05
WBGene00012004|T24H10.6|dyrb-1	87.00	7.29	2.64
WBGene00021283|Y24D9A.5	0.36	7.20	3.27
WBGene00011834|T19B10.6|dvc-1	10.42	7.14	0.34
WBGene00016675|C45G9.4	1.24	6.89	0.03
WBGene00008514|F02A9.4	22.78	6.82	0.16
WBGene00018777|F53H1.3	1.22	6.78	4.88
WBGene00006856|C13B4.2|usp-14	411.68	6.77	0.46
WBGene00022011|Y59H11AR.3	0.81	6.75	4.05
WBGene00003183|T01G9.5|mei-1	177.07	6.66	1.07
WBGene00001031|F54D5.8|dnj-13	0.53	6.63	0.06
WBGene00010114|F55D12.6	0.46	6.57	0.09
WBGene00020679|T22B11.5|ogdh-1	0.45	6.43	0.01
WBGene00008707|F11E6.3	19.45	6.42	2.45
WBGene00003450|R13H9.2|msp-57	116.01	6.27	1.66
WBGene00022329|Y82E9BL.13|fbxa-79	0.74	6.17	0.39
WBGene00002047|Y39G10AR.13|icp-1	1.78	6.14	0.16
WBGene00020211|T04C9.3	1.90	6.13	2.88
WBGene00021154|Y4C6A.4	2.32	6.11	2.17
WBGene00011557|T07A5.4|ostf-4	15.19	6.08	0.97
WBGene00018841|F54H5.5	0.06	6.00	0.02
WBGene00006441|Y73F8A.19|cpna-4	0.06	6.00	0.46
WBGene00007993|C37E2.1|idhb-1	0.18	6.00	0.16
WBGene00020298|T07A9.10	0.12	6.00	0.04
WBGene00022497|Y119D3B.21	5.75	5.99	0.23
WBGene00003444|ZK354.5|msp-51	149.24	5.80	2.58
WBGene00003052|DY3.2|lmn-1	1.09	5.74	0.03
WBGene00003902|Y106G6H.2|pab-1	15.11	5.68	0.05
WBGene00010419|H28O16.1	501.78	5.67	0.10
WBGene00007646|C17E4.9|nkb-1	0.17	5.67	0.03

WBGene00017926|F29C4.2	468.05	5.59	9.21
WBGene00000474|M01E11.5|cey-3	6259.28	5.54	4.98
WBGene00003465|T13F2.11|msp-78	6.34	5.51	1.23
WBGene00011120|R07E5.15	0.22	5.50	0.01
WBGene00015244|B0524.5	0.49	5.44	0.08
WBGene00001713|F42C5.7|grl-4	1687.42	5.41	1.43
WBGene00019410|K05F1.9	0.27	5.40	0.01
WBGene00008464|E02H4.6	19.32	5.40	0.22
WBGene00001840|C26D10.2|hel-1	1.27	5.29	0.01
WBGene00008442|E01B7.2	0.63	5.25	2.74
WBGene00000370|Y73F8A.6|ccg-1	0.31	5.17	0.02
WBGene00016101|C25E10.12	1.80	5.14	0.14
WBGene00015529|C06E2.5	24.92	5.11	0.19
WBGene00009482|F36G3.1	0.61	5.08	1.03
WBGene00007091|B0001.6|eri-12	0.10	5.00	0.01
WBGene00019327|K02F3.4|zip-2	0.20	5.00	0.05
WBGene00018813|F54D11.3	0.15	5.00	0.24
WBGene00016394|C34B2.9	0.25	5.00	0.06
WBGene00014121|ZK858.8	0.25	5.00	0.05
WBGene00018117|F36H12.1|nlp-47	4.71	4.96	0.46
WBGene00010066|F54F7.6	2.13	4.95	0.81
WBGene00012456|Y17D7C.2	1.38	4.93	7.67
WBGene00013892|ZC434.4	244.35	4.86	0.80
WBGene00008229|C50F4.1	0.24	4.80	0.01
WBGene00010871|M05B5.3	0.19	4.75	0.63
WBGene00009256|F29F11.3|tut-2	0.14	4.67	0.02
WBGene00010260|F58E10.3|ddx-17	0.97	4.62	0.04
WBGene00008921|F17C11.10	3.85	4.58	0.10
WBGene00003085|Y37A1B.1|lst-3	0.59	4.54	0.95
WBGene00015146|B0336.6|abi-1	4.75	4.52	0.08
WBGene00004076|W09B6.1|pod-2	0.09	4.50	0.03
WBGene00016594|C42D4.1	0.18	4.50	0.03
WBGene00044916|F40F8.11	0.35	4.38	0.02
WBGene00021595|Y46E12BL.2	0.83	4.37	0.23
WBGene00020507|T14F9.1|vha-15	0.26	4.33	0.01
WBGene00003000|ZC247.3|lin-11	1.56	4.33	0.25

Appendix XLV

WBGene00009547|F38H4.3	0.17	4.25	0.18
WBGene00004435|B0336.10|rpl-23	13050.53	4.24	15.15
WBGene00022765|ZK546.14	0.21	4.20	0.00
WBGene00003371|F09F7.2|mlc-3	4535.03	4.19	2.73
WBGene00001878|T10C6.11|his-4	1.20	4.14	5.71
WBGene00017548|F18A1.7	4.74	4.12	0.01
WBGene00018782|F54A3.3|cct-3	0.41	4.10	0.12
WBGene00001209|C27D11.1|egl-45	0.61	4.07	0.02
WBGene00017948|F31D5.5|mth-1	0.04	4.00	0.18
WBGene00020511|T14G11.3|immt-1	0.04	4.00	0.00
WBGene00007846|C31E10.5	0.04	4.00	0.07
WBGene00021703|Y48G9A.10|cpt-3	0.04	4.00	1.00
WBGene00004906|ZK1010.9|snf-7	0.04	4.00	0.06
WBGene00017010|D1007.15	0.04	4.00	2.00
WBGene00000509|C28D4.2|cka-1	0.20	4.00	0.87
WBGene00021906|Y55B1AR.2	0.12	4.00	0.60
WBGene00006580|T23G4.1|tlp-1	0.08	4.00	0.07
WBGene00006820|C09D1.1|unc-89	0.08	4.00	0.23
WBGene00008439|DY3.6|mfb-1	0.08	4.00	0.03
WBGene00001562|B0513.1|lin-66	0.44	4.00	0.71
WBGene00000981|C45B11.3|dhs-18	2.45	3.95	0.25
WBGene00004419|Y24D9A.4|rpl-7A	323.96	3.93	0.07
WBGene00006920|Y38F2AL.3|vha-11	0.35	3.89	0.17
WBGene00011122|R07H5.2|cpt-2	0.31	3.88	0.10
WBGene00001911|C50F4.7|his-37	1.12	3.86	0.11
WBGene00014938|Y62E10A.11|mdt-9	21.88	3.78	0.17
WBGene00009992|F53F4.10	0.49	3.77	0.03
WBGene00006923|F08B1.1|vhp-1	0.30	3.75	2.14
WBGene00007964|C36A4.2|cyp-25A2	0.11	3.67	0.15
WBGene00003990|F35C8.6|pfn-2	0.33	3.67	0.00
WBGene00022219|Y73B3A.18	35.04	3.60	1.44
WBGene00022116|Y71F9AL.11	0.25	3.57	0.50
WBGene00020820|T26A5.4	2.45	3.55	0.12
WBGene00007725|C25F9.5	0.07	3.50	0.07
WBGene00008121|C46F11.6	0.14	3.50	0.33
WBGene00018250|F40H3.2	0.14	3.50	0.06

WBGene00007171|B0393.6	0.07	3.50	0.02
WBGene00015219|B0507.2	0.07	3.50	0.01
WBGene00001664|F38E1.5|gpa-2	0.07	3.50	0.35
WBGene00004172|Y75B8A.27|pqn-92	0.07	3.50	0.05
WBGene00006764|ZK721.2|unc-27	881.41	3.46	0.23
WBGene00021294|Y25C1A.7	0.76	3.45	0.08
WBGene00004357|Y51H4A.3|rho-1	0.31	3.44	0.25
WBGene00000535|K08B4.6|cpi-1	0.82	3.42	0.08
WBGene00003756|F33A8.2|nlp-18	0.95	3.39	0.05
WBGene00020840|T27A3.4	1.73	3.39	0.10
WBGene00008234|C50F4.9	0.27	3.38	0.12
WBGene00015246|B0545.3|scl-23	0.10	3.33	0.02
WBGene00021979|Y58A7A.5	0.10	3.33	0.07
WBGene00044058|F17B5.6	0.10	3.33	2.50
WBGene00011017|R04F11.5	0.20	3.33	0.00
WBGene00005844|ZC204.15|srw-97	**0.10**	**3.33**	**2.50**
WBGene00005026|ZK1307.5|sqv-8	0.10	3.33	0.04
WBGene00001076|F54D8.1|dpy-17	0.10	3.33	0.00
WBGene00003048|W06F12.1|lit-1	0.80	3.33	1.16
WBGene00019355|K03B4.4	0.73	3.32	0.84
WBGene00012862|Y45F3A.5	0.66	3.30	1.83
WBGene00001678|Y95B8A.5|gpa-16	1.57	3.27	5.41
WBGene00000625|Y54E10BL.2|col-48	0.13	3.25	0.00
WBGene00009692|F44E5.5	0.13	3.25	0.30
WBGene00010098|F55C5.10	0.32	3.20	1.07
WBGene00001754|F11G11.3|gst-6	0.16	3.20	0.05
WBGene00007190|B0491.3|rmd-3	0.16	3.20	0.01
WBGene00003451|ZK354.10|msp-58	1.42	3.16	1.51
WBGene00001451|F31F6.4|flp-8	1.32	3.14	0.06
WBGene00003078|F32A5.7|lsm-4	0.22	3.14	0.14
WBGene00021345|Y37B11A.3	2.92	3.11	8.11
WBGene00009306|F32A7.5	0.40	3.08	0.85
WBGene00004298|W06D4.6|rad-54	0.03	3.00	0.04
WBGene00000771|C30B5.3|cpb-2	0.03	3.00	0.01
WBGene00007100|B0024.10	0.03	3.00	0.01
WBGene00017577|F18F11.4	0.03	3.00	0.05

Appendix XLVII

WBGene00016780|C49G7.1	0.03	3.00	0.30
WBGene00018778|F53H1.4	0.03	3.00	0.09
WBGene00015333|C02C2.4|slc-17.3	0.03	3.00	0.38
WBGene00008005|C38D4.4	0.03	3.00	1.00
WBGene00001484|T07D1.4|fox-1	0.03	3.00	0.02
WBGene00020793|T25D1.1	0.03	3.00	0.60
WBGene00001202|R07A4.1|egl-36	0.03	3.00	0.30
WBGene00013198|Y54E5A.2	0.03	3.00	0.09
WBGene00002694|C10H11.9|let-502	0.03	3.00	0.02
WBGene00017681|F21F8.11|slc-17.5	0.03	3.00	1.00
WBGene00006807|C17D12.2|unc-75	0.03	3.00	1.00
WBGene00009185|F27C8.5	0.03	3.00	0.01
WBGene00011990|T24D5.2	0.03	3.00	0.60
WBGene00003882|F59E10.1|orc-2	0.03	3.00	0.00
WBGene00004878|Y69A2AR.4|smf-3	0.03	3.00	1.00
WBGene00011189|R10D12.8	0.03	3.00	1.00
WBGene00016063|C24G7.1|delm-2	0.03	3.00	0.17
WBGene00007070|AC3.2|ugt-49	0.03	3.00	0.38
WBGene00006483|F42A9.1|dgk-4	0.03	3.00	0.60
WBGene00003571|C07A9.4|ncx-6	0.03	3.00	1.00
WBGene00017747|F23F1.6	0.03	3.00	0.30
WBGene00021501|Y40C7B.5	0.03	3.00	1.00
WBGene00011928|T22C8.7|cutl-12	0.03	3.00	0.03
WBGene00016314|C32D5.6	0.03	3.00	0.04
WBGene00004045|K10F12.3|pll-1	0.03	3.00	0.15
WBGene00000161|T20B5.1|apa-2	0.03	3.00	1.00
WBGene00003246|R06B9.6|mig-14	0.03	3.00	0.03
WBGene00003905|Y18D10A.13|pad-1	0.03	3.00	0.04
WBGene00000090|B0334.8|age-1	0.03	3.00	0.01
WBGene00005164|T12A2.13|srg-6	0.12	3.00	2.40
WBGene00009798|F46G10.4	0.06	3.00	0.05
WBGene00007664|C18B12.2|seb-3	**0.06**	**3.00**	**2.00**
WBGene00019407|K05F1.5	0.06	3.00	0.40
WBGene00000966|F55A12.4|dhs-2	0.21	3.00	0.02
WBGene00004728|F21H11.2|sax-2	0.50	2.94	0.12
WBGene00022856|ZK1127.10|cth-2	0.26	2.89	0.00

WBGene00001835|C08B11.2|hda-2	3.01	2.84	0.18
WBGene00000229|C34E10.6|atp-2	26.97	2.83	0.05
WBGene00017788|F25E5.7	0.65	2.83	1.02
WBGene00010264|F58G1.2	11.48	2.81	0.56
WBGene00003479|Y39H10A.3|mtm-9	0.39	2.79	0.19
WBGene00004132|F56F3.1|ifet-1	3.20	2.78	0.23
WBGene00022748|ZK484.1	3.24	2.77	0.08
WBGene00015313|C01G8.6|hpo-32	25.36	2.73	0.26
WBGene00004305|R05D11.3|ran-4	2.34	2.72	0.02
WBGene00019620|K10C2.4|fah-1	814.23	2.70	2.60
WBGene00003446|R13H9.4|msp-53	274.02	2.68	1.25
WBGene00007352|C06A1.1|cdc-48.1	9.01	2.67	0.03
WBGene00021469|Y39G10AR.11	0.08	2.67	1.00
WBGene00010456|K01C8.1	0.08	2.67	0.02
WBGene00016644|C44C1.5	0.32	2.67	0.43
WBGene00010263|F58G1.1|wago-4	0.16	2.67	0.00
WBGene00017114|E03H12.7	0.24	2.67	0.02
WBGene00000534|R01B10.1|cpi-2	43.70	2.66	0.25
WBGene00010136|F55H12.5	19.12	2.66	0.51
WBGene00022402|Y97E10AR.7	239.24	2.65	1.01
WBGene00010700|K09A9.1|nipi-3	1.19	2.64	0.02
WBGene00022705|ZK354.2	0.21	2.63	0.01
WBGene00004466|B0205.3|rpn-10	80.92	2.62	0.34
WBGene00015191|B0432.10	0.13	2.60	0.01
WBGene00005025|C52E12.3|sqv-7	1.74	2.60	0.06
WBGene00006789|F11C3.3|unc-54	0.57	2.59	0.05
WBGene00000110|T05H4.13|alh-4	5.35	2.57	0.92
WBGene00003588|ZC155.1|nex-1	1.63	2.55	0.04
WBGene00001555|T04D3.4|gcy-35	1.27	2.54	9.07
WBGene00012602|Y38E10A.24	0.99	2.54	0.93
WBGene00018849|F55A3.3	10.04	2.50	0.10
WBGene00007512|C10C6.3	0.15	2.50	0.05
WBGene00008905|F17B5.1	0.05	2.50	0.71
WBGene00003953|F39H11.5|pbs-7	2.12	2.49	0.01
WBGene00001167|F25H5.4|eef-2	140.38	2.47	0.52
WBGene00021932|Y55F3AR.1	10.70	2.47	107.00

Appendix XLIX

WBGene00015380|C03B1.10	2.71	2.46	1.32
WBGene00044176|C30G7.2	0.27	2.45	1.69
WBGene00012766|Y41E3.8	2.91	2.45	1.90
WBGene00003787|K07F5.13|npp-1	0.22	2.44	0.12
WBGene00003175|C44B11.3|mec-12	12794.94	2.44	140.87
WBGene00011428|T04C12.3	0.39	2.44	0.05
WBGene00001926|F07B7.4|his-52	0.68	2.43	1.94
WBGene00011647|T09E8.1|noca-1	17.22	2.41	0.13
WBGene00004027|Y49E10.14|pie-1	6768.06	2.40	9.23
WBGene00001971|Y48B6A.14|hmg-1.1	2872.07	2.40	0.87
WBGene00018286|F41E6.5	0.12	2.40	0.03
WBGene00017763|F23H11.9|crls-1	0.43	2.39	0.04
WBGene00016669|C45G7.2|ilys-2	17.73	2.38	126.64
WBGene00022376|Y94H6A.3	0.07	2.33	0.07
WBGene00007795|C28D4.8	0.07	2.33	0.47
WBGene00001494|H09G03.2|frm-8	0.07	2.33	0.78
WBGene00017826|F26F4.4|tag-340	0.07	2.33	0.01
WBGene00007792|C28D4.4	0.07	2.33	0.10
WBGene00004895|CC4.3|smu-1	0.07	2.33	0.02
WBGene00009401|F35C11.2	0.07	2.33	0.06
WBGene00010876|M05D6.3	0.07	2.33	0.03
WBGene00001583|M163.4|gfi-3	0.07	2.33	0.04
WBGene00001896|K06C4.12|his-22	0.65	2.32	1.91
WBGene00019011|F57C9.4	0.58	2.32	0.02
WBGene00015971|C18E3.2|swsn-2.2	2.37	2.30	0.05
WBGene00007092|B0001.7	0.23	2.30	0.04
WBGene00002033|Y73B6BL.2|htp-2	2.86	2.29	0.06
WBGene00044338|C03G5.10|nspc-3	0.32	2.29	0.55
WBGene00007018|C55B7.9|mdt-18	0.16	2.29	0.02
WBGene00000522|C09F12.1|clc-1	7.92	2.28	0.11
WBGene00009770|F46B6.5	0.09	2.25	0.64
WBGene00000959|F46H6.2|dgk-2	0.45	2.25	0.02
WBGene00001894|K06C4.4|his-20	0.63	2.25	1.85
WBGene00015913|C17F4.7	3118.62	2.24	0.13
WBGene00008357|D1025.6|nspc-16	0.49	2.23	0.27
WBGene00012126|T28D6.6	0.20	2.22	0.00

WBGene00001928|F07B7.11|his-54	0.51	2.22	1.76
WBGene00022518|ZC123.3|zfh-2	0.11	2.20	1.38
WBGene00004881|Y73B6BL.18|smg-3	0.11	2.20	0.01
WBGene00011524|T06D8.3	0.22	2.20	7.33
WBGene00010405|H19N07.1|erfa-3	0.24	2.18	0.03
WBGene00044364|F34D6.7	0.50	2.17	1.19
WBGene00002214|M7.2|klc-1	0.13	2.17	0.01
WBGene00009187|F27D4.1	4.05	2.14	0.02
WBGene00015976|C18E3.9	0.15	2.14	0.02
WBGene00012764|Y41E3.6	187.09	2.12	1559.08
WBGene00004924|T23H2.2|snt-4	0.72	2.12	0.07
WBGene00001151|F38H4.8|ech-2	49.73	2.11	0.27
WBGene00004175|ZK1236.6|pqn-96	2827.17	2.08	13.61
WBGene00003658|H12C20.3|nhr-68	0.52	2.08	0.05
WBGene00012637|Y38H8A.3	1.13	2.02	0.05
WBGene00010351|H02I12.1|cbd-1	30664.04	2.01	8.81
WBGene00005615|T01G5.3|srj-27	**0.06**	**2.00**	**1.20**
WBGene00022605|ZC404.11|dmsr-11	**0.04**	**2.00**	**0.57**
WBGene00022604|ZC404.10|dmsr-10	**0.07**	**1.75**	**1.17**
WBGene00006215|T01G5.5|str-171	**0.05**	**1.67**	**1.00**
WBGene00194821|T27B2.1|dmsr-16	**0.06**	**1.50**	**0.29**

Supplementary Table 10. List of genes enriched 2-fold the CEM DL over non-DL CEM neurons.
98 genes were enriched at least 2-fold, with no GPCRs of interest being enriched in this cell. Genes discussed in paper are added or bolded in the table.

Gene	CEM_DR	CEM_DR/ max_non_ CEM_DR	max_CEM /larvae
WBGene00021842|Y54E10BR.3	16.74	186.00	3.15
WBGene00006523|F26G5.9|tam-1	1.25	125.00	0.06
WBGene00022706|ZK354.3	6.00	120.00	2.99
WBGene00003391|F52C9.7|mog-3	4.29	107.25	0.63
WBGene00008368|D1053.3	6.22	103.67	9.15
WBGene00004914|Y116A8C.42|snr-1	19.23	101.21	0.29
WBGene00003943|K09C8.1|pbo-4	3.01	100.33	0.70
WBGene00002036|F36D4.3|hum-2	8.34	92.67	0.24
WBGene00000235|B0464.7|baf-1	22.27	89.08	0.22
WBGene00018253|F40H6.1	66.40	86.23	9.37
WBGene00008140|C47D12.8|xpf-1	1.72	86.00	0.67
WBGene00018835|F54F2.7	8.76	79.64	4.06
WBGene00004926|C08G5.4|snt-6	7.66	76.60	23.94
WBGene00001498|F22B5.9|fars-3	2.13	71.00	0.24
WBGene00003829|F53A2.4|nud-1	112.84	67.17	1.58
WBGene00003425|K07F5.2|msp-10	33.27	63.98	16.39
WBGene00017372|F10G7.9	2.54	63.50	1.94
WBGene00015133|B0303.15|mrpl-11	6.30	63.00	0.07
WBGene00007780|C27D8.4	11.54	60.74	0.95
WBGene00016411|C34E10.10	4.71	58.88	0.13
WBGene00015581|C07H6.4	2.32	58.00	0.26
WBGene00000536|ZC395.2|clk-1	18.99	55.85	0.33
WBGene00021857|Y54F10BM.2|iffb-1	1.10	55.00	1.64
WBGene00011306|R186.3	16.15	50.47	0.36
WBGene00000913|T07A9.6|daf-18	2.89	48.17	0.25
WBGene00004303|C29E4.3|ran-2	4.30	47.78	0.61
WBGene00013556|Y75B8A.23	79.29	44.80	255.77
WBGene00017999|F33D4.7|emc-6	8.06	44.78	9.48
WBGene00018784|F54A3.5	7.56	44.47	0.40
WBGene00020154|T01G6.10	3.11	44.43	51.83

WBGene00010054|F54D5.11	10.49	43.71	0.36
WBGene00014016|ZK632.9	24.56	43.09	0.38
WBGene00003510|F40G9.11|mxl-2	11.91	42.54	0.41
WBGene00007683|C18E9.2	6.31	42.07	0.24
WBGene00018298|F41G3.1	8.59	40.90	11.61
WBGene00007108|B0035.5|gspd-1	7.71	40.58	0.42
WBGene00002231|C02F5.1|knl-1	0.40	40.00	0.07
WBGene00014111|ZK856.10|rpc-25	46.90	39.75	1.91
WBGene00007756|C27A7.5	26.33	38.72	2.54
WBGene00002957|F33A8.1|let-858	0.75	37.50	5.36
WBGene00022783|ZK652.2|tomm-7	44.29	36.91	62.38
WBGene00015487|C05D11.10|mrps-17	4.01	36.45	0.09
WBGene00018934|F56B3.11	6.56	36.44	0.23
WBGene00007001|C43E11.4|tufm-2	2.53	36.14	0.20
WBGene00006512|F18E2.2|abcf-1	1.42	35.50	0.04
WBGene00012481|Y18D10A.11	1.75	35.00	0.53
WBGene00002059|F53A2.6|ife-1	27.49	34.80	0.18
WBGene00018904|F55G1.9	1.73	34.60	0.34
WBGene00004187|C50C3.6|prp-8	0.34	34.00	8.50
WBGene00003922|C15H11.7|pas-1	1.69	33.80	0.09
WBGene00022398|Y97E10AR.3	1.67	33.40	0.07
WBGene00007623|C16C10.2	2.98	33.11	0.12
WBGene00016739|C48A7.2|pitr-1	2.91	32.33	0.54
WBGene00003059|C48E7.3|lpd-2	1.60	32.00	0.03
WBGene00000001|Y110A7A.10|aap-1	1.60	32.00	0.88
WBGene00004443|B0513.3|rpl-29	415.62	31.85	29.92
WBGene00007403|C07A9.7|set-3	1.91	31.83	0.35
WBGene00010638|K07F5.14	1.27	31.75	0.06
WBGene00020263|T05E8.3	5.05	31.56	0.64
WBGene00019338|K02F6.4	0.31	31.00	31.00
WBGene00000973|Y32H12A.3|dhs-9	1.55	31.00	1.07
WBGene00017356|F10E9.4	1.84	30.67	0.05
WBGene00009287|F31C3.5|psf-2	3.61	30.08	0.85
WBGene00010305|F59A2.5	5.36	29.78	0.85
WBGene00004888|K12C11.2|smo-1	225.20	29.67	4.42
WBGene00011976|T24B8.2	4.74	29.63	0.37

Appendix LIII

WBGene00019457|K06H7.3|vms-1	1.17	29.25	0.07
WBGene00004916|T28D9.10|snr-3	31.41	28.04	0.31
WBGene00003061|ZK973.10|lpd-5	92.64	27.90	0.36
WBGene00020713|T23B3.5	21.45	27.86	0.77
WBGene00010721|K09E4.3	3.34	27.83	0.69
WBGene00010232|F58B3.6	0.83	27.67	0.06
WBGene00009995|F53F4.13	140.80	27.55	17.69
WBGene00015104|B0280.9	3.79	27.07	0.14
WBGene00003367|M106.1|mix-1	0.27	27.00	0.60
WBGene00016443|C35D10.6	1.88	26.86	1.17
WBGene00021630|Y47D9A.3	2.32	25.78	0.39
WBGene00044388|C27D6.11	1.25	25.00	0.22
WBGene00009180|F26H11.2|nurf-1	7.66	24.71	0.15
WBGene00011936|T22H2.6|pgrn-1	2.21	24.56	0.82
WBGene00012643|Y39A1A.3	2.17	24.11	0.07
WBGene00044746|C53H9.3	18.88	23.60	65.10
WBGene00022463|Y110A7A.16|elpc-1	9.72	23.14	0.79
WBGene00017607|F19F10.11	4.39	23.11	0.55
WBGene00019678|K12H4.3	0.92	23.00	0.06
WBGene00022176|Y71H2AM.11	0.68	22.67	0.09
WBGene00010557|K04D7.2|mspn-1	17.90	22.66	0.18
WBGene00011375|T02E1.2	2.26	22.60	0.40
WBGene00017219|F07F6.7	2.02	22.44	0.48
WBGene00008418|D2030.8	2.85	21.92	1.63
WBGene00004244|C30G12.7|puf-8	2.19	21.90	0.10
WBGene00015329|C02B10.4	17.67	21.81	0.33
WBGene00021466|Y39G10AR.8	0.65	21.67	0.03
WBGene00017119|E04A4.5	4.98	21.65	0.13
WBGene00003955|W03D2.4|pcn-1	1.28	21.33	0.01
WBGene00004969|F47G6.4|spe-15	14.86	20.93	3.19
WBGene00001398|VZK822L.1|fat-6	21.99	20.36	0.14
WBGene00009993|F53F4.11	3.05	20.33	0.08
WBGene00011423|T04B2.5	0.81	20.25	0.84
WBGene00003077|Y62E10A.12|lsm-3	36.54	20.19	1.59
WBGene00021844|Y54E10BR.5	5.64	20.14	0.25
WBGene00003148|H21P03.1|mbf-1	1.60	20.00	0.04

WBGene00002061|B0348.6|ife-3	21.12	19.92	4.22
WBGene00012964|Y48A6B.3	26.26	19.89	0.18
WBGene00015105|B0280.10|pot-1	0.99	19.80	0.22
WBGene00020098|R144.10	1.76	19.56	1.61
WBGene00000976|F36H9.3|dhs-13	1.56	19.50	0.98
WBGene00012187|W01G7.3|rpb-11	6.72	19.20	1.83
WBGene00012342|W08D2.7|mtr-4	0.19	19.00	0.41
WBGene00018064|F35F11.1|cdc-73	0.38	19.00	0.06
WBGene00016412|C34E10.11|mrps-26	0.95	19.00	0.07
WBGene00018341|F42A10.5	3.01	18.81	0.43
WBGene00014014|ZK632.5	0.37	18.50	0.84
WBGene00019472|K07C6.4|cyp-35B1	67.95	18.46	2265.00
WBGene00015128|B0303.7	4.21	18.30	0.90
WBGene00006733|F19B6.2|ufd-1	1.99	18.09	0.17
WBGene00007588|C14C10.5	3.41	17.95	0.45
WBGene00016390|C34B2.5	1.60	17.78	0.04
WBGene00020028|R12C12.8	1.59	17.67	0.58
WBGene00020181|T02H6.11	13.39	17.62	0.05
WBGene00009508|F37D6.2	2.46	17.57	0.22
WBGene00020349|T08B2.11	1.57	17.44	0.29
WBGene00018637|F49E8.6	15.10	17.36	1.64
WBGene00018391|F43E2.2|rpb-4	32.74	17.32	0.57
WBGene00021900|Y54H5A.2	30.99	17.03	0.54
WBGene00018564|F47D12.9	3.05	16.94	1.28
WBGene00003406|Y37D8A.9|mrg-1	16.71	16.88	0.26
WBGene00020710|T23B3.2	29.42	16.62	2.84
WBGene00006321|T22B2.4|sup-12	3.97	16.54	0.91
WBGene00013382|Y62E10A.16|gcl-1	0.33	16.50	4.71
WBGene00013136|Y53C10A.5	20.11	16.48	1.13
WBGene00022719|ZK370.5|pdhk-2	0.49	16.33	0.02
WBGene00004988|T08A9.7|spp-3	50.47	16.28	7.28
WBGene00016360|C33G8.2	5.17	16.16	3.23
WBGene00009492|F36H1.3	1.13	16.14	0.54
WBGene00015307|C01G5.5	3.70	16.09	9.02
WBGene00020843|T27A3.7	0.48	16.00	0.09
WBGene00007048|C16A3.7|nfx-1	1.92	16.00	0.12

Appendix LV

WBGene00020652|T21E3.1|egg-4	0.95	15.83	0.13
WBGene00001600|B0414.6|glh-3	0.31	15.50	2.82
WBGene00044654|Y61B8A.4|fbxa-85	13.31	15.48	121.00
WBGene00003499|K04F10.6|mut-2	1.39	15.44	0.07
WBGene00000206|F35G12.10|asb-1	9.41	15.43	0.09
WBGene00003792|F56A3.3|npp-6	0.46	15.33	0.79
WBGene00003210|C38D4.3|mel-28	0.46	15.33	0.17
WBGene00000784|F44C4.3|cpr-4	21.71	15.18	0.33
WBGene00008394|D1086.7	14.05	15.11	0.71
WBGene00010890|M18.5|ddb-1	0.15	15.00	0.02
WBGene00010905|M88.2|mrps-34	1.20	15.00	0.04
WBGene00016601|C43E11.1|acin-1	3.42	14.87	0.40
WBGene00017827|F26F4.5	3.86	14.85	0.20
WBGene00004179|C01G5.2|prg-2	6.20	14.76	0.25
WBGene00022704|ZK353.9	1.18	14.75	0.05
WBGene00009650|F43D2.1|ccnk-1	4.91	14.44	0.38
WBGene00001856|B0414.3|hil-5	55.54	14.35	0.39
WBGene00009937|F52F12.4|lsl-1	245.30	14.22	2.98
WBGene00021331|Y34D9A.6|glrx-10	4.89	13.97	1.90
WBGene00012888|Y45F10D.9|sas-6	4.33	13.97	0.94
WBGene00019084|F59A6.2	32.56	13.91	9.55
WBGene00018659|F52C6.2	1.11	13.88	0.31
WBGene00019510|K07H8.10	0.83	13.83	0.02
WBGene00013219|Y54G11A.11	15.19	13.81	0.54
WBGene00004491|F53A3.3|rps-22	499.33	13.54	2.10
WBGene00004698|W02B12.3|rsp-1	3.09	13.43	0.19
WBGene00009092|F23H12.2|tomm-20	13.71	13.31	0.23
WBGene00011600|T07G12.10|zim-2	0.26	13.00	0.04
WBGene00000888|C34D4.12|cyn-12	10.02	12.85	0.14
WBGene00012992|Y48C3A.10|mrpl-20	16.30	12.64	0.72
WBGene00009440|F35G12.2|idhg-1	0.88	12.57	0.04
WBGene00021347|Y37E3.3|rpb-10	30.68	12.52	4.50
WBGene00021828|Y54E10A.6	0.25	12.50	6.25
WBGene00000121|F23B2.6|aly-2	1.00	12.50	0.09
WBGene00011142|R08D7.1	0.50	12.50	0.03
WBGene00007235|C01G10.8	23.15	12.45	0.35

WBGene00006528|F26E4.8|tba-1	66.04	12.44	0.19
WBGene00007202|B0564.2	9.97	12.31	0.82
WBGene00011376|T02E1.3|gla-3	0.61	12.20	0.23
WBGene00004510|F10B5.7|rrf-3	0.12	12.00	0.04
WBGene00021420|Y38F2AR.2|trap-3	0.96	12.00	0.02
WBGene00003951|K05C4.1|pbs-5	0.72	12.00	0.04
WBGene00017044|D2007.4|mrpl-18	1.19	11.90	0.06
WBGene00004422|T22F3.4|rpl-11.1	264.33	11.85	0.18
WBGene00019905|R05G9.3	0.71	11.83	0.09
WBGene00000915|C47E8.5|daf-21	14.31	11.54	0.04
WBGene00019247|H27M09.3|syp-4	0.23	11.50	0.02
WBGene00004431|C09D4.5|rpl-19	243.98	11.44	0.09
WBGene00003164|Y57E12AL.5|mdt-6	0.80	11.43	0.07
WBGene00003073|R74.1|lars-1	1.25	11.36	0.11
WBGene00010809|M01F1.3	1.46	11.23	0.05
WBGene00002879|C29E4.8|let-754	1.12	11.20	0.01
WBGene00009680|F44D12.3|msd-1	1.90	11.18	0.38
WBGene00007436|C08B11.9	17.88	11.11	0.36
WBGene00011435|T04D3.8	19.97	10.97	7.21
WBGene00002073|F26B1.3|ima-2	30.23	10.95	0.18
WBGene00001497|T08B2.9|fars-1	4.31	10.78	0.15
WBGene00019859|R03H10.7	0.43	10.75	0.36
WBGene00012206|W02B12.11	9.32	10.71	0.63
WBGene00014017|ZK632.10	5.46	10.71	0.19
WBGene00016010|C23G10.1	1.60	10.67	0.69
WBGene00021202|Y17G9B.5	0.53	10.60	0.05
WBGene00009396|F35C5.8|clec-65	2.86	10.59	0.13
WBGene00004117|F02E9.4|sin-3	0.21	10.50	0.02
WBGene00007387|C06H2.3|jmjd-5	1.05	10.50	0.14
WBGene00002228|C06G3.2|klp-18	1.47	10.50	0.18
WBGene00001716|T02E9.2|grl-7	0.94	10.44	0.02
WBGene00000613|C27H5.5|col-36	13.62	10.40	5.72
WBGene00003735|Y18D10A.6|nhx-8	0.31	10.33	1.35
WBGene00003133|W10C6.1|mat-2	0.31	10.33	0.02
WBGene00009711|F44G4.1	0.41	10.25	0.01
WBGene00020841|T27A3.5	0.41	10.25	0.03

Appendix LVII

WBGene00019631|K10D2.5	5.79	10.16	0.62
WBGene00009237|F28H7.3	2.73	10.11	0.09
WBGene00235102|Y54G2A.75	1.31	10.08	0.31
WBGene00001479|F53F4.5|fmo-4	0.50	10.00	0.03
WBGene00004444|Y106G6H.3|rpl-30	365.48	9.81	3.06
WBGene00010616|K07A1.10	4.88	9.76	0.24
WBGene00001480|H24K24.5|fmo-5	0.39	9.75	1.05
WBGene00002144|Y47G6A.2|inx-22	4.86	9.72	0.38
WBGene00077500|C27H6.9	0.68	9.71	0.05
WBGene00006572|C06G3.11|tin-9.1	5.90	9.67	1.24
WBGene00011730|T12D8.2|drr-2	0.58	9.67	0.33
WBGene00008458|E02H1.6	0.86	9.56	0.02
WBGene00013593|Y87G2A.1	0.19	9.50	0.54
WBGene00002012|F38E11.1|hsp-12.3	37.02	9.47	12.02
WBGene00010560|K04G2.1|iftb-1	8.95	9.42	0.07
WBGene00020662|T21H3.1	250.21	9.28	0.42
WBGene00077453|Y62F5A.12	4.05	9.20	0.63
WBGene00008344|C56A3.5	1.38	9.20	0.05
WBGene00009139|F25H9.7	6.59	9.15	0.27
WBGene00006963|K07G5.2|xpa-1	0.64	9.14	0.02
WBGene00008275|C53B4.6|nstp-1	0.99	9.00	0.06
WBGene00001869|R12B2.4|him-10	0.45	9.00	0.03
WBGene00004477|F42C5.8|rps-8	324.67	8.90	0.07
WBGene00003805|R06F6.5|npp-19	2.83	8.84	0.32
WBGene00015915|C17G10.1	40.23	8.84	1.50
WBGene00009322|F32B6.8|tbc-3	0.61	8.71	0.03
WBGene00008452|E02A10.1|mrps-5	0.26	8.67	0.02
WBGene00015524|C06E1.9	0.26	8.67	0.04
WBGene00021781|Y51H7C.3	112.45	8.64	1.36
WBGene00016446|C35D10.10	0.69	8.63	0.09
WBGene00003132|Y110A7A.17|mat-1	0.60	8.57	0.05
WBGene00007616|C15H11.8|rpoa-12	4.71	8.56	0.26
WBGene00011687|T10C6.5	12.71	8.53	0.16
WBGene00001973|C32F10.5|hmg-3	3.58	8.52	0.18
WBGene00015810|C16A3.5	13.19	8.51	0.02
WBGene00015346|C02F5.3	0.34	8.50	0.01

WBGene00045433|F49D11.10	0.34	8.50	0.08
WBGene00017112|E03H12.5	5.35	8.49	0.26
WBGene00002263|K08H10.1|lea-1	2.63	8.48	0.14
WBGene00009051|F22D6.4|nduf-6	7.80	8.48	0.18
WBGene00004919|Y49E10.15|snr-6	2.70	8.44	0.44
WBGene00016173|C27H5.3|fust-1	2.52	8.40	0.42
WBGene00016674|C45G9.2	0.42	8.40	0.09
WBGene00000547|Y77E11A.11|clp-7	0.75	8.33	0.05
WBGene00002064|T05G5.10|iff-1	686.44	8.31	4.14
WBGene00009112|F25D7.2|tag-353	0.83	8.30	0.06
WBGene00021845|Y54E10BR.6|rpb-7	216.68	8.26	10.34
WBGene00004034|F09E5.1|pkc-3	0.33	8.25	0.09
WBGene00020068|R13F6.10|cra-1	0.33	8.25	0.18
WBGene00020297|T07A9.9	2.45	8.17	0.15
WBGene00007969|C36A4.9|acs-19	14.49	8.14	0.12
WBGene00022583|ZC262.8|mrps-18A	21.64	8.14	0.45
WBGene00007554|C13G3.3|pptr-2	72.04	8.13	1.30
WBGene00015701|C11D2.3	0.73	8.11	10.43
WBGene00012781|Y43C5A.1|nspd-7	8.00	8.08	2.42
WBGene00019543|K08F11.3|cif-1	1.05	8.08	0.05
WBGene00007952|C35A5.8	0.08	8.00	0.01
WBGene00010677|K08F4.2|gtbp-1	0.16	8.00	0.00
WBGene00013550|Y75B8A.14	0.48	8.00	0.02
WBGene00015293|C01C4.3	0.56	8.00	0.07
WBGene00043064|Y59E9AL.7|nbet-1	0.64	8.00	0.54
WBGene00014171|ZK970.1|nep-26	0.24	8.00	3.43
WBGene00016799|C50C3.1	0.56	8.00	0.15
WBGene00000851|C47G2.1|cut-1	1.68	8.00	56.00
WBGene00016653|C44E4.4	1.92	8.00	0.03
WBGene00003041|R06C7.7|lin-61	0.79	7.90	0.05
WBGene00021340|Y34F4.5	5.28	7.88	0.54
WBGene00020954|W02G9.4	0.47	7.83	0.03
WBGene00018361|F42G8.10	9.39	7.83	0.07
WBGene00021945|Y55F3BR.8|lem-4	0.39	7.80	3.25
WBGene00002169|F37A4.8|isw-1	0.31	7.75	0.04
WBGene00019005|F57B10.8	2.00	7.69	0.11

WBGene00002083|F57B9.6|inf-1	113.80	7.67	0.33
WBGene00008413|D2030.3	0.23	7.67	0.01
WBGene00008729|F13B12.1	2.45	7.66	0.04
WBGene00194892|F26H11.6|dsb-2	0.45	7.50	0.10
WBGene00009521|F38A1.8	0.15	7.50	0.19
WBGene00009565|F39H11.1	0.30	7.50	0.02
WBGene00044174|C12D8.18|fipr-5	2.40	7.50	6.67
WBGene00010699|K08H10.9|trpp-6	0.67	7.44	0.17
WBGene00001005|T26A5.9|dlc-1	600.54	7.40	3.18
WBGene00016276|C30G12.4	0.44	7.33	0.46
WBGene00021210|Y18H1A.4	0.95	7.31	0.91
WBGene00021133|W10D9.5|tomm-22	4.15	7.28	0.06
WBGene00013035|Y49E10.16	2.91	7.28	0.13
WBGene00018375|F43C9.1	0.29	7.25	0.46
WBGene00017068|D2092.8	1.01	7.21	4.04
WBGene00000113|F45H10.1|alh-7	12.76	7.21	0.63
WBGene00012484|Y18D10A.17|car-1	22.96	7.20	0.05
WBGene00013670|Y105E8A.10|hpo-13	0.43	7.17	0.02
WBGene00011968|T23G11.1	2.41	7.09	0.04
WBGene00015327|C02B10.2|snpn-1	3.17	7.04	0.06
WBGene00006725|H06I04.4|ubl-1	187.80	7.03	0.19
WBGene00018238|F40F4.7	0.28	7.00	0.02
WBGene00008381|D1081.3	0.14	7.00	7.00
WBGene00018785|F54A3.6	0.21	7.00	0.44
WBGene00016003|C18H9.5	13.61	6.98	36.78
WBGene00004704|D2089.1|rsp-7	2.57	6.95	0.09
WBGene00020094|R144.4|wip-1	0.76	6.91	0.08
WBGene00010094|F55C5.5|tsfm-1	0.55	6.88	0.04
WBGene00014226|ZK1098.11	2.13	6.87	0.64
WBGene00016191|C28G1.6	0.41	6.83	0.10
WBGene00010624|K07A12.7|mrps-15	0.34	6.80	0.01
WBGene00012361|W09D10.3|mrpl-12	0.68	6.80	0.37
WBGene00013967|ZK287.7	0.54	6.75	0.06
WBGene00022347|Y82E9BR.14	0.74	6.73	0.64
WBGene00008572|F08B12.4	31.88	6.73	1.92
WBGene00017347|F10E7.5	9.48	6.72	0.04

WBGene00017503|F16B4.1|nhr-177	6.43	6.70	2.30
WBGene00011367|T02C12.2|snpc-3.4	0.20	6.67	0.34
WBGene00006515|C05D11.3|tag-170	87.06	6.67	1.22
WBGene00016028|C24A1.1|flp-24	0.86	6.62	0.35
WBGene00009459|F36A2.12	1.32	6.60	0.67
WBGene00008432|D2085.7	3.29	6.58	0.77
WBGene00021038|W05F2.6	3.08	6.55	0.16
WBGene00004059|C44B7.9|pmp-2	0.13	6.50	0.08
WBGene00022880|ZK1248.10|tbc-2	0.13	6.50	0.01
WBGene00001599|C55B7.1|glh-2	1.80	6.43	0.15
WBGene00015156|B0361.2	1.34	6.38	0.09
WBGene00003097|C17G10.5|lys-8	0.89	6.36	0.01
WBGene00013442|Y66D12A.16	3.75	6.36	5.68
WBGene00004425|C32E8.2|rpl-13	1086.87	6.35	0.25
WBGene00010279|F58G11.1|letm-1	0.19	6.33	0.05
WBGene00020112|R151.9|pfd-5	10.30	6.28	0.09
WBGene00022115|Y71F9AL.10	0.81	6.23	0.20
WBGene00004015|T24H7.1|phb-2	2.97	6.19	0.06
WBGene00009397|F35C5.9|clec-66	1.36	6.18	0.04
WBGene00045268|H01M10.3|ttr-42	2.47	6.18	0.99
WBGene00020558|T19B4.5	4.75	6.17	3.04
WBGene00014093|ZK829.1	0.43	6.14	0.41
WBGene00010231|F58B3.4	1.35	6.14	0.07
WBGene00012166|W01A8.4|nuo-6	2.57	6.12	0.02
WBGene00045300|C44C8.9|fbxc-10	0.55	6.11	3.93
WBGene00018586|F48A11.5|ubxn-3	24.31	6.08	1.67
WBGene00006648|W03F9.5|ttb-1	0.79	6.08	0.05
WBGene00013854|ZC116.2|cyc-2.2	1.03	6.06	0.14
WBGene00004463|F49C12.8|rpn-7	7.47	6.02	0.05
WBGene00010778|K11H3.1|gpdh-2	3.49	6.02	0.15
WBGene00007216|C01A2.4	253.77	6.01	0.67
WBGene00015184|B0432.2|djr-1.1	0.54	6.00	0.34
WBGene00007028|C47D12.1|trr-1	0.06	6.00	0.09
WBGene00001833|Y110A7A.1|hcp-6	0.12	6.00	0.02
WBGene00012936|Y47D3A.29	0.96	6.00	0.53
WBGene00004502|F29G9.5|rpt-2	0.18	6.00	0.01

Appendix LXI

WBGene00003952|C02F5.9|pbs-6	173.04	5.98	0.94
WBGene00022832|ZK973.3|pdp-1	1.89	5.91	0.06
WBGene00013434|Y66D12A.8	5.12	5.89	0.15
WBGene00021930|Y55F3AM.13	1.23	5.86	0.07
WBGene00006352|F26E4.1|sur-6	0.41	5.86	0.04
WBGene00009274|F30F8.5	0.64	5.82	1.31
WBGene00013168|Y53F4B.22|arp-1	0.87	5.80	0.21
WBGene00002152|R11A8.6|iars-1	0.29	5.80	0.17
WBGene00009277|F30F8.10	1.04	5.78	0.22
WBGene00008628|F09F3.6|ttr-21	12.44	5.76	0.38
WBGene00004096|F40F8.7|pqm-1	19.86	5.76	1.28
WBGene00044644|B0205.13	3.21	5.73	3.28
WBGene00004681|F52G2.2|rsd-2	5.90	5.73	0.70
WBGene00019642|K11C4.1	0.63	5.73	0.12
WBGene00020716|T23B12.1|phf-30	0.40	5.71	0.05
WBGene00001431|F31D4.3|fkb-6	0.57	5.70	0.13
WBGene00001862|ZK381.1|him-3	32.14	5.70	1.03
WBGene00010053|F54D5.9	0.17	5.67	0.02
WBGene00004917|C52E4.3|snr-4	3.32	5.63	0.08
WBGene00009334|F32D8.12	1.35	5.63	0.05
WBGene00045299|C44C8.8|fbxc-11	0.45	5.63	3.21
WBGene00017735|F23C8.6|did-2	5.21	5.60	0.08
WBGene00010115|F55F3.1|aakb-1	12.01	5.56	0.43
WBGene00009444|F35G12.11	6.30	5.53	0.33
WBGene00010174|F56H9.2	1089.96	5.49	82.26
WBGene00004201|F54F2.8|prx-19	0.49	5.44	0.01
WBGene00016450|C35D10.14|clec-5	0.87	5.44	0.05
WBGene00003836|Y71F9AM.5|nxt-1	59.80	5.44	0.52
WBGene00017074|D2096.7	2.12	5.44	0.55
WBGene00000380|C07G2.3|cct-5	1.57	5.41	0.00
WBGene00004496|F56E10.4|rps-27	161.62	5.37	3.09
WBGene00014164|ZK945.1|lact-2	41.18	5.37	0.84
WBGene00007101|B0024.11	1.66	5.35	0.05
WBGene00016011|C23G10.2	4.43	5.34	0.33
WBGene00017300|F09F7.3|rpc-2	0.16	5.33	0.01
WBGene00017850|F27B10.1	0.96	5.33	0.18

WBGene00006724|C08B11.7|ubh-4	0.53	5.30	0.02
WBGene00009084|F23B12.7	18.42	5.23	0.21
WBGene00016393|C34B2.8	1.41	5.22	0.01
WBGene00017620|F20A1.9|tofu-2	1.35	5.19	0.08
WBGene00022456|Y110A7A.6|pfkb-1.1	0.62	5.17	0.03
WBGene00010409|H21P03.2	0.36	5.14	0.02
WBGene00018145|F37C4.5	1.58	5.10	0.37
WBGene00018419|F44E2.6	1.22	5.08	0.21
WBGene00194717|ZC239.22	6.25	5.08	4.77
WBGene00001055|C27C12.7|dpf-2	13.07	5.07	1.59
WBGene00020588|T19H12.2	12.03	5.01	0.04
WBGene00019259|H34C03.2	0.15	5.00	0.02
WBGene00002637|F26F12.7|let-418	0.05	5.00	0.01
WBGene00016812|C50D2.9	0.20	5.00	0.87
WBGene00009479|F36F2.6|fcp-1	0.10	5.00	0.05
WBGene00010333|F59E10.3|copz-1	0.45	5.00	5.63
WBGene00015938|C17H12.13|anat-1	0.45	5.00	0.02
WBGene00022360|Y92H12A.4	16.67	4.99	7.38
WBGene00001227|R08D7.3|eif-3.D	0.94	4.95	0.01
WBGene00012140|T28F4.5	0.98	4.90	0.09
WBGene00010627|K07C5.4	315.12	4.82	0.38
WBGene00006919|F46F11.5|vha-10	1.30	4.81	0.00
WBGene00018285|F41E6.4|smk-1	0.24	4.80	0.02
WBGene00045301|C44C8.10|fbxc-9	0.43	4.78	3.07
WBGene00022042|Y65B4BR.5|icd-2	923.02	4.75	0.29
WBGene00000259|F13H8.10|bpl-1	0.38	4.75	0.06
WBGene00011636|T09A5.8|cec-3	0.19	4.75	0.01
WBGene00004462|F57B9.10|rpn-6.1	2.42	4.75	0.06
WBGene00019537|K08D12.3	95.14	4.74	0.09
WBGene00001058|R11E3.8|dpf-5	0.52	4.73	0.09
WBGene00011722|T11G6.8	2.31	4.71	0.04
WBGene00008443|E01F3.1|pde-3	12.78	4.70	60.86
WBGene00006976|K02B12.8|zhp-3	0.75	4.69	0.05
WBGene00020185|T03F1.3|pgk-1	0.14	4.67	0.01
WBGene00004458|T22D1.9|rpn-1	0.14	4.67	0.00
WBGene00021800|Y53G8AL.2	0.14	4.67	0.01

Appendix LXIII

WBGene00008199|C49C3.9	0.14	4.67	0.02
WBGene00044466|Y48A5A.3	2.00	4.65	0.70
WBGene00011625|T08G5.5|vps-39	4.39	4.62	0.30
WBGene00022853|ZK1127.6	9.98	4.62	0.11
WBGene00015509|C06A6.4	4.99	4.62	0.10
WBGene00018395|F43E2.7|mtch-1	0.92	4.60	0.01
WBGene00010317|F59B8.2|idh-1	20.23	4.60	0.59
WBGene00021015|W03G9.3|enu-3.3	3.08	4.60	6.29
WBGene00004028|Y18H1A.6|pif-1	11.39	4.57	14.99
WBGene00020868|T27F7.3|eif-1	38.72	4.55	0.10
WBGene00007630|C16C10.11|har-1	41.43	4.51	0.05
WBGene00004437|C03D6.8|rpl-24.2	17.24	4.50	0.11
WBGene00021830|Y54E10A.10	0.27	4.50	0.01
WBGene00008399|D2005.4	0.09	4.50	0.02
WBGene00007921|C34C12.2	0.09	4.50	0.02
WBGene00011242|R11D1.1	0.40	4.44	0.19
WBGene00044213|Y102A5C.36	2.04	4.43	2.96
WBGene00002198|F22D6.1|kin-14	21.23	4.42	1.93
WBGene00019719|M01H9.3	13.00	4.41	0.12
WBGene00003796|ZK328.5|npp-10	0.22	4.40	0.03
WBGene00004498|B0412.4|rps-29	1147.96	4.34	44.74
WBGene00008393|D1086.6	102.68	4.33	0.48
WBGene00008682|F11A10.1|lex-1	0.13	4.33	0.01
WBGene00007094|B0019.2	0.13	4.33	0.03
WBGene00021097|W08F4.8|cdc-37	48.04	4.33	1.16
WBGene00019162|H06H21.3|eif-1.A	4.72	4.33	0.04
WBGene00010478|K01G5.5	10.06	4.32	0.02
WBGene00022025|Y65B4A.1	2.41	4.30	0.44
WBGene00011156|R09B3.3	128.24	4.30	2.97
WBGene00016652|C44E4.3|got-2.1	0.60	4.29	0.01
WBGene00007983|C36E8.4	0.60	4.29	0.29
WBGene00007143|B0334.3	72.08	4.27	1.11
WBGene00012966|Y48A6B.5|exos-1	0.34	4.25	0.04
WBGene00018921|F56A6.1|sago-2	0.17	4.25	0.29
WBGene00021899|Y54H5A.1	0.68	4.25	0.02
WBGene00219912|F22H10.10	3.44	4.25	3.74

WBGene00077526|C25A1.16	1.78	4.24	0.02
WBGene00013361|Y60A3A.13|fars-2	66.47	4.23	0.57
WBGene00004915|W08E3.1|snr-2	0.38	4.22	0.41
WBGene00009050|F22D6.2	23.42	4.21	0.16
WBGene00001604|Y105C5B.28|gln-3	4.83	4.20	0.35
WBGene00018151|F37C12.3	3.73	4.19	0.04
WBGene00007786|C27H6.4|rmd-2	8.99	4.18	0.13
WBGene00009880|F49C12.11	91.39	4.17	2.01
WBGene00011299|R107.4|ikke-1	0.25	4.17	0.01
WBGene00003243|F10E9.6|mig-10	1.00	4.17	1.37
WBGene00007617|C15H11.9|rrbs-1	0.50	4.17	0.01
WBGene00018319|F41H10.6|hda-6	0.95	4.13	0.03
WBGene00001756|F11G11.1|gst-8	0.41	4.10	4.56
WBGene00000774|F56A8.6|cpf-2	7.03	4.09	0.83
WBGene00018409|F44B9.8	0.53	4.08	0.13
WBGene00015232|B0511.6	27.62	4.07	0.11
WBGene00044081|D1086.11	242.87	4.07	0.66
WBGene00015460|C05C8.1	44.04	4.03	0.37
WBGene00003980|F09C3.1|pes-7	4.01	4.01	0.91
WBGene00009744|F45H11.3|hpo-35	0.08	4.00	0.06
WBGene00018226|F40B5.2	0.24	4.00	0.73
WBGene00021319|Y34B4A.2	0.16	4.00	0.12
WBGene00007313|C04H5.2|clec-147	0.56	4.00	0.33
WBGene00015450|C04F5.8	0.20	4.00	0.03
WBGene00007564|C14A4.14|mrps-22	0.12	4.00	0.13
WBGene00018416|F44E2.2|retr-1	0.12	4.00	0.33
WBGene00014176|ZK1010.2	5.56	4.00	0.28
WBGene00000277|C23H4.1|cab-1	3.51	3.94	0.40
WBGene00019962|R08E5.2|cysl-3	29.83	3.94	0.50
WBGene00001284|F54C8.3|emb-30	4.62	3.88	0.13
WBGene00004420|R13A5.8|rpl-9	1897.36	3.87	0.19
WBGene00013435|Y66D12A.9	0.23	3.83	0.01
WBGene00023422|F43C1.6|mrpl-21	0.38	3.80	0.03
WBGene00005001|F32D8.9|spp-16	1.63	3.79	0.22
WBGene00022057|Y67D2.7	1.74	3.78	0.70
WBGene00017542|F17E9.5	12.53	3.75	0.30

WBGene00022492|Y119D3B.15|dss-1	0.45	3.75	0.01
WBGene00010280|F58G11.2|rde-12	0.15	3.75	0.42
WBGene00006961|B0041.7|xnp-1	3.10	3.73	1.51
WBGene00013203|Y54E5A.8	2.80	3.73	0.89
WBGene00019768|M04F3.2	0.41	3.73	0.05
WBGene00011720|T11G6.5	2.57	3.72	0.82
WBGene00004042|C14B9.4|plk-1	11.40	3.70	0.19
WBGene00014092|ZK822.5	0.37	3.70	0.04
WBGene00000886|B0252.4|cyn-10	4.09	3.68	0.05
WBGene00012030|T25G3.3	0.11	3.67	0.00
WBGene00000467|F52B5.5|cep-1	2.01	3.65	0.10
WBGene00001021|C01G10.12|dnj-3	0.40	3.64	0.05
WBGene00015386|C03B8.3	8.68	3.63	1.67
WBGene00016333|C32F10.8	0.98	3.63	0.02
WBGene00044188|F28F8.9	1.27	3.63	0.07
WBGene00020736|T23F2.3	2.28	3.62	3.30
WBGene00015920|C17G10.9	0.18	3.60	0.01
WBGene00017780|F25E2.2	0.43	3.58	0.02
WBGene00000894|M110.5|dab-1	1.36	3.58	0.99
WBGene00019163|H06H21.6|ubxn-6	0.68	3.58	0.03
WBGene00002023|C09B8.6|hsp-25	3.92	3.56	0.02
WBGene00004493|T07A9.11|rps-24	2159.80	3.56	1.07
WBGene00011155|R09B3.2	16.92	3.52	0.95
WBGene00021938|Y55F3BR.1	0.07	3.50	0.04
WBGene00001744|T10F2.1|gars-1	0.14	3.50	0.01
WBGene00008878|F16A11.3|ppfr-1	0.14	3.50	0.10
WBGene00002845|F57B9.2|let-711	0.07	3.50	0.23
WBGene00010044|F54C9.9	0.28	3.50	0.01
WBGene00018893|F55F8.5|tag-345	0.21	3.50	0.01
WBGene00000765|ZK652.9|coq-5	0.21	3.50	0.03
WBGene00010428|H38K22.2|dcn-1	0.35	3.50	0.01
WBGene00014083|ZK795.3	0.49	3.50	0.02
WBGene00017358|F10E9.7	21.80	3.50	1.38
WBGene00018612|F48E8.6|disl-2	3.03	3.48	0.38
WBGene00009207|F28C6.8	8.89	3.47	0.04
WBGene00006408|T14G12.3|tag-18	8.22	3.45	0.08

WBGene00020557|T19B4.3	63.36	3.44	3.91
WBGene00010900|M28.9	1.06	3.42	0.07
WBGene00010556|K04D7.1|rack-1	64.89	3.41	0.05
WBGene00009122|F25H2.11|tct-1	273.88	3.41	0.10
WBGene00001017|ZK593.5|dnc-1	0.17	3.40	0.06
WBGene00004490|F37C12.11|rps-21	708.85	3.39	22.09
WBGene00016387|C34B2.2|kbp-5	10.49	3.37	0.11
WBGene00003786|VC5.3|npa-1	1.28	3.37	0.01
WBGene00002980|C32D5.9|lgg-1	4.23	3.36	0.00
WBGene00020388|T10B5.2	40.68	3.35	3.74
WBGene00001946|Y49E10.6|his-72	28.91	3.35	0.12
WBGene00001231|C41D11.2|eif-3.H	0.10	3.33	0.12
WBGene00008331|C55A6.2|ttll-5	0.30	3.33	0.02
WBGene00009372|F34D10.2|evl-18	0.10	3.33	0.08
WBGene00012353|W09C5.7	0.43	3.31	0.02
WBGene00004205|F29B9.4|psr-1	5.82	3.31	0.30
WBGene00000935|F56D1.7|daz-1	2.08	3.30	0.05
WBGene00010891|M18.6	0.92	3.29	0.07
WBGene00021128|W10C8.5	0.49	3.27	0.06
WBGene00009895|F49E11.10|scl-2	96.53	3.25	2.01
WBGene00015820|C16A11.7	0.65	3.25	0.09
WBGene00008642|F10B5.8	0.13	3.25	0.01
WBGene00004798|F43D9.4|sip-1	339.40	3.23	1.69
WBGene00017132|EEED8.1|tofu-6	0.29	3.22	0.02
WBGene00010633|K07F5.5|nspd-2	23.76	3.22	5.77
WBGene00000659|K12D12.3|col-84	0.16	3.20	0.84
WBGene00004993|C28C12.5|spp-8	11.28	3.17	0.15
WBGene00011240|R11A8.7	0.19	3.17	0.02
WBGene00000785|W07B8.5|cpr-5	0.19	3.17	0.01
WBGene00004445|W09C5.6|rpl-31	550.91	3.14	3.24
WBGene00010141|F56A8.5	1.41	3.13	0.09
WBGene00010339|F59F4.4|acl-1	7.77	3.13	0.04
WBGene00016440|C35D10.2|gipc-1	0.28	3.11	0.01
WBGene00006433|F42A8.2|sdhb-1	37.84	3.11	0.35
WBGene00020184|T03F1.1|uba-5	0.87	3.11	2.64
WBGene00007413|C07E3.2|pro-2	0.62	3.10	0.02

WBGene00000376|ZC518.3|ccr-4	3.96	3.09	0.27
WBGene00007429|C08B6.8	1.08	3.09	0.03
WBGene00004093|C18E3.7|ppw-1	8.26	3.06	0.16
WBGene00017613|F20A1.1	64.70	3.04	17.16
WBGene00202000|Y38F1A.13	0.94	3.03	2.76
WBGene00017641|F20D12.1|csr-1	1.51	3.02	0.17
WBGene00002269|Y55B1AR.1|lec-6	3.22	3.01	0.12
WBGene00003794|Y41D4B.19|npp-8	0.27	3.00	1.80
WBGene00001259|T04A8.14|emb-5	0.27	3.00	0.12
WBGene00009159|F26E4.4	0.27	3.00	0.02
WBGene00003418|H26D21.2|msh-2	0.06	3.00	0.05
WBGene00012236|W04A8.1	0.12	3.00	0.20
WBGene00017312|F09G2.3|pitr-5	0.06	3.00	0.04
WBGene00022069|Y67D8C.5|eel-1	0.06	3.00	0.22
WBGene00008062|C41G7.4|set-32	0.09	3.00	0.10
WBGene00019168|H06I04.3	0.15	3.00	0.01
WBGene00006530|F44F4.11|tba-4	0.21	3.00	0.02
WBGene00015703|C11D2.7	9.93	2.98	0.20
WBGene00004138|R07B7.3|pqn-53	273.82	2.95	1.30
WBGene00044924|M106.7	0.47	2.94	0.08
WBGene00000159|F29G9.3|aps-1	0.47	2.94	0.01
WBGene00001464|C26F1.10|flp-21	0.94	2.94	0.14
WBGene00044329|F11A10.8|cpsf-4	3.31	2.93	0.05
WBGene00009575|F40F8.1	0.93	2.91	0.05
WBGene00016591|C42C1.13	3.76	2.89	0.12
WBGene00000102|C12D8.10|akt-1	0.26	2.89	0.01
WBGene00009981|F53F1.3	27.98	2.88	1.28
WBGene00017011|D1007.16|eaf-1	0.20	2.86	0.00
WBGene00004412|Y71F9AL.13|rpl-1	119.41	2.85	0.04
WBGene00016808|C50D2.5	2.68	2.85	0.10
WBGene00021359|Y37E11AL.3	0.91	2.84	0.17
WBGene00004897|T10H9.4|snb-1	3.41	2.84	0.02
WBGene00016630|C44B7.10	0.17	2.83	0.00
WBGene00021208|Y18H1A.2	0.51	2.83	0.02
WBGene00000718|B0222.7|col-145	37.08	2.83	0.22
WBGene00020604|T20B12.7	15.81	2.83	0.05

WBGene00006053|T28H11.1|ssq-4	8.28	2.83	1.61
WBGene00007824|C30H6.7	0.31	2.82	0.01
WBGene00003177|T01E8.4|mec-15	45.80	2.81	0.70
WBGene00018421|F44E2.8	0.14	2.80	0.01
WBGene00004705|C18D11.4|rsp-8	72.35	2.79	1.17
WBGene00013238|Y56A3A.21|trap-4	0.50	2.78	2.08
WBGene00003160|C50F4.11|mdf-1	1.55	2.77	1.50
WBGene00022458|Y110A7A.8|prp-31	0.33	2.75	0.14
WBGene00020389|T10B5.3	0.11	2.75	0.00
WBGene00003156|Y39G10AR.14|mcm-4	0.76	2.71	0.01
WBGene00017907|F28F9.3	10.43	2.69	35.97
WBGene00004434|C27A2.2|rpl-22	3125.14	2.68	4.53
WBGene00012903|Y46G5A.12|vps-2	69.13	2.68	0.77
WBGene00001457|Y37D8A.15|flp-14	0.16	2.67	0.02
WBGene00006595|M01E5.5|top-1	0.08	2.67	0.05
WBGene00003009|K10B2.1|lin-23	0.08	2.67	0.02
WBGene00004339|C39E9.13|rfc-3	3.34	2.65	0.04
WBGene00020027|R12C12.7	14.12	2.64	1.37
WBGene00004474|T05E11.1|rps-5	468.28	2.63	0.07
WBGene00001686|F33H1.2|gpd-4	32.63	2.62	0.25
WBGene00021959|Y57E12AL.6	7.97	2.60	0.16
WBGene00009211|F28D1.1|wdr-46	7.50	2.59	0.33
WBGene00018359|F42G8.8	0.31	2.58	0.02
WBGene00044324|ZK652.3|ufm-1	1.26	2.57	0.09
WBGene00004441|C53H9.1|rpl-27	760.13	2.57	0.86
WBGene00016217|C29F9.2	1.41	2.56	0.12
WBGene00020441|T12A2.7	0.64	2.56	0.02
WBGene00011282|R74.8	0.56	2.55	0.01
WBGene00015759|C14C6.5	1.12	2.55	0.03
WBGene00008143|C47E8.4	419.46	2.50	10.54
WBGene00009526|F38A1.14|clec-169	11.58	2.50	7.38
WBGene00019465|K07B1.5|acl-14	0.15	2.50	0.01
WBGene00012150|VF39H2L.1|syx-17	0.15	2.50	0.01
WBGene00006540|F58A4.8|tbg-1	0.05	2.50	0.01
WBGene00004178|D2030.6|prg-1	0.05	2.50	0.01
WBGene00001601|T12F5.3|glh-4	0.05	2.50	0.01

Appendix LXIX

WBGene00019544|K08F11.5|miro-1	0.05	2.50	0.01
WBGene00003839|T09A12.3|ocr-2	0.05	2.50	1.67
WBGene00017663|F21D12.3	0.05	2.50	0.45
WBGene00020719|T23B12.4	0.05	2.50	0.01
WBGene00019458|K06H7.7	0.10	2.50	0.02
WBGene00002076|R06A4.4|imb-2	0.10	2.50	0.02
WBGene00009921|F52B5.2	0.10	2.50	0.07
WBGene00012002|T24H10.4	0.10	2.50	0.29
WBGene00007708|C25A1.6|nola-3	1.55	2.50	0.07
WBGene00016513|C38C3.4	1.05	2.50	0.30
WBGene00001977|Y17G7A.1|hmg-12	7.05	2.50	0.06
WBGene00004446|T24B8.1|rpl-32	1177.28	2.49	2.27
WBGene00004336|W06A7.3|ret-1	3.35	2.48	0.01
WBGene00003066|ZC410.7|lpl-1	0.37	2.47	0.08
WBGene00015554|C06G3.8	2.71	2.46	1.58
WBGene00009436|F35G2.2|marb-1	39.89	2.46	0.52
WBGene00020886|T28B4.3|ttr-6	0.32	2.46	0.02
WBGene00000098|K07C11.2|air-1	9.95	2.46	0.04
WBGene00009087|F23D12.3	0.22	2.44	0.92
WBGene00017934|F30B5.4	0.22	2.44	0.06
WBGene00011559|T07C4.1|umps-1	80.04	2.44	0.68
WBGene00009123|F25H2.12	0.17	2.43	0.02
WBGene00044633|F54H12.7	0.34	2.43	0.04
WBGene00009385|F35B12.5|sas-5	0.53	2.41	0.01
WBGene00018745|F53C3.1	27.71	2.41	16.40
WBGene00009288|F31C3.6	0.12	2.40	0.19
WBGene00005656|C13D9.2|srr-5	0.12	2.40	3.00
WBGene00007580|C14B1.9	0.24	2.40	0.03
WBGene00021460|Y39G10AR.2|zwl-1	69.89	2.40	0.61
WBGene00021269|Y23H5A.2	2.13	2.39	0.17
WBGene00004486|T08B2.10|rps-17	525.49	2.39	1.01
WBGene00003587|F45H11.2|ned-8	0.98	2.39	0.06
WBGene00017924|F29B9.10|mrps-21	0.45	2.37	0.11
WBGene00022194|Y71H2B.4	0.52	2.36	0.09
WBGene00007689|C18E9.9	0.26	2.36	0.01
WBGene00000593|W01B6.7|col-2	0.92	2.36	0.22

WBGene00020033|R12E2.7	6.24	2.34	0.75
WBGene00022664|ZK121.2	0.07	2.33	0.12
WBGene00000938|C26C6.5|dcp-66	0.07	2.33	0.03
WBGene00010435|JC8.2	0.07	2.33	0.00
WBGene00005719|F53F1.7|srv-8	0.14	2.33	2.80
WBGene00007194|B0491.7	0.14	2.33	0.01
WBGene00012444|Y15E3A.5	0.70	2.33	0.02
WBGene00017597|F19C7.8	26.78	2.33	5.26
WBGene00015619|C08G9.1	3.38	2.33	0.12
WBGene00017053|D2024.5	1.02	2.32	0.02
WBGene00004296|T04H1.4|rad-50	22.59	2.32	2.47
WBGene00014240|ZK1251.1|htas-1	0.37	2.31	0.10
WBGene00009179|F26H11.1|kbp-3	0.37	2.31	0.01
WBGene00000381|F01F1.8|cct-6	0.23	2.30	0.01
WBGene00013958|ZK265.6	0.46	2.30	0.01
WBGene00004286|D2013.1|rab-39	0.16	2.29	0.01
WBGene00001427|Y18D10A.19|fkb-2	0.32	2.29	0.03
WBGene00015160|B0361.6	0.09	2.25	0.01
WBGene00003644|F36D3.2|nhr-54	0.09	2.25	0.82
WBGene00018757|F53E2.1|tag-304	0.09	2.25	0.26
WBGene00007177|B0399.2|oac-1	0.09	2.25	4.50
WBGene00017975|F32B5.1	0.18	2.25	0.10
WBGene00006463|T26A5.3|nduf-2.2	0.09	2.25	0.00
WBGene00001018|C28H8.12|dnc-2	9.56	2.24	0.11
WBGene00012557|Y37D8A.19	72.23	2.24	16.53
WBGene00017675|F21F3.6	9.70	2.24	0.05
WBGene00077771|C41G7.9	61.42	2.23	0.22
WBGene00016508|C37H5.5	36.58	2.23	3.22
WBGene00021882|Y54G2A.17	1.20	2.22	0.43
WBGene00016425|C34H4.2	4.32	2.22	0.61
WBGene00013132|Y52D3.1|strd-1	33.26	2.21	11.67
WBGene00000378|T21B10.7|cct-2	0.77	2.20	0.01
WBGene00011554|T07A5.1	0.11	2.20	0.02
WBGene00007000|Y71H2AM.23|tufm-1	0.11	2.20	0.00
WBGene00012127|T28D6.7	0.11	2.20	2.75
WBGene00007455|C08F11.8|ugt-22	0.11	2.20	0.01

Appendix LXXI

WBGene00010664|K08E3.4|dbn-1	0.11	2.20	0.01
WBGene00011412|T04A8.11|mrpl-16	50.46	2.19	0.77
WBGene00011629|T08G11.1	0.70	2.19	0.18
WBGene00022618|ZC477.3	0.37	2.18	0.03
WBGene00017774|F25B5.2|nop-1	0.15	2.14	0.02
WBGene00013200|Y54E5A.5	11.82	2.14	0.13
WBGene00022751|ZK484.5	3.17	2.13	0.16
WBGene00004920|Y71F9B.4|snr-7	2.19	2.13	0.92
WBGene00011634|T09A5.5	1.40	2.12	0.02
WBGene00004449|ZK652.4|rpl-35	818.03	2.12	2.26
WBGene00004304|C26D10.1|ran-3	4.12	2.09	0.17
WBGene00020110|R151.7	0.23	2.09	0.02
WBGene00007223|C01F6.9	21.02	2.09	0.62
WBGene00008944|F19B2.5	6.59	2.09	0.11
WBGene00003449|K07F5.3|msp-56	13.09	2.08	0.17
WBGene00000876|C52E4.6|cyl-1	14.56	2.08	0.34
WBGene00017982|F32D1.2|hpo-18	39.02	2.06	8.91
WBGene00008515|F02C12.1	12.66	2.05	5.65
WBGene00012375|W09H1.5|mecr-1	171.90	2.04	0.90
WBGene00022775|ZK616.5	1.65	2.04	0.01
WBGene00003184|F57B10.12|mei-2	92.06	2.02	0.16
WBGene00012556|Y37D8A.18|mrps-10	15.88	2.01	0.15
WBGene00050914|T12B5.15	65.12	2.01	6.36
WBGene00012551|Y37D8A.11|cec-7	19.84	2.01	0.29

Supplementary Table 11. List of genes enriched 2-fold the CEM DR over non-DR CEM neurons.
105 genes were enriched at least 2-fold, with *dmsr-12* enriched 4.96-fold, and *srd-32* only 1.62-fold enriched. Genes discussed in paper are added or bolded in the table.

Gene	CEM_DR	CEM_DR/ max_non_ CEM_DR	max_CEM /larvae
WBGene00021842|Y54E10BR.3	16.74	186.00	3.15
WBGene00006523|F26G5.9|tam-1	1.25	125.00	0.06
WBGene00022706|ZK354.3	6.00	120.00	2.99
WBGene00003391|F52C9.7|mog-3	4.29	107.25	0.63
WBGene00008368|D1053.3	6.22	103.67	9.15
WBGene00004914|Y116A8C.42|snr-1	19.23	101.21	0.29
WBGene00003943|K09C8.1|pbo-4	3.01	100.33	0.70
WBGene00002036|F36D4.3|hum-2	8.34	92.67	0.24
WBGene00000235|B0464.7|baf-1	22.27	89.08	0.22
WBGene00018253|F40H6.1	66.40	86.23	9.37
WBGene00008140|C47D12.8|xpf-1	1.72	86.00	0.67
WBGene00018835|F54F2.7	8.76	79.64	4.06
WBGene00004926|C08G5.4|snt-6	7.66	76.60	23.94
WBGene00001498|F22B5.9|fars-3	2.13	71.00	0.24
WBGene00003829|F53A2.4|nud-1	112.84	67.17	1.58
WBGene00003425|K07F5.2|msp-10	33.27	63.98	16.39
WBGene00017372|F10G7.9	2.54	63.50	1.94
WBGene00015133|B0303.15|mrpl-11	6.30	63.00	0.07
WBGene00007780|C27D8.4	11.54	60.74	0.95
WBGene00016411|C34E10.10	4.71	58.88	0.13
WBGene00015581|C07H6.4	2.32	58.00	0.26
WBGene00000536|ZC395.2|clk-1	18.99	55.85	0.33
WBGene00021857|Y54F10BM.2|iffb-1	1.10	55.00	1.64
WBGene00011306|R186.3	16.15	50.47	0.36
WBGene00000913|T07A9.6|daf-18	2.89	48.17	0.25
WBGene00004303|C29E4.3|ran-2	4.30	47.78	0.61
WBGene00013556|Y75B8A.23	79.29	44.80	255.77
WBGene00017999|F33D4.7|emc-6	8.06	44.78	9.48
WBGene00018784|F54A3.5	7.56	44.47	0.40
WBGene00020154|T01G6.10	3.11	44.43	51.83

Appendix LXXIII

WBGene00010054|F54D5.11	10.49	43.71	0.36
WBGene00014016|ZK632.9	24.56	43.09	0.38
WBGene00003510|F40G9.11|mxl-2	11.91	42.54	0.41
WBGene00007683|C18E9.2	6.31	42.07	0.24
WBGene00018298|F41G3.1	8.59	40.90	11.61
WBGene00007108|B0035.5|gspd-1	7.71	40.58	0.42
WBGene00002231|C02F5.1|knl-1	0.40	40.00	0.07
WBGene00014111|ZK856.10|rpc-25	46.90	39.75	1.91
WBGene00007756|C27A7.5	26.33	38.72	2.54
WBGene00002957|F33A8.1|let-858	0.75	37.50	5.36
WBGene00022783|ZK652.2|tomm-7	44.29	36.91	62.38
WBGene00015487|C05D11.10|mrps-17	4.01	36.45	0.09
WBGene00018934|F56B3.11	6.56	36.44	0.23
WBGene00007001|C43E11.4|tufm-2	2.53	36.14	0.20
WBGene00006512|F18E2.2|abcf-1	1.42	35.50	0.04
WBGene00012481|Y18D10A.11	1.75	35.00	0.53
WBGene00002059|F53A2.6|ife-1	27.49	34.80	0.18
WBGene00018904|F55G1.9	1.73	34.60	0.34
WBGene00004187|C50C3.6|prp-8	0.34	34.00	8.50
WBGene00003922|C15H11.7|pas-1	1.69	33.80	0.09
WBGene00022398|Y97E10AR.3	1.67	33.40	0.07
WBGene00007623|C16C10.2	2.98	33.11	0.12
WBGene00016739|C48A7.2|pitr-1	2.91	32.33	0.54
WBGene00003059|C48E7.3|lpd-2	1.60	32.00	0.03
WBGene00000001|Y110A7A.10|aap-1	1.60	32.00	0.88
WBGene00004443|B0513.3|rpl-29	415.62	31.85	29.92
WBGene00007403|C07A9.7|set-3	1.91	31.83	0.35
WBGene00010638|K07F5.14	1.27	31.75	0.06
WBGene00020263|T05E8.3	5.05	31.56	0.64
WBGene00019338|K02F6.4	0.31	31.00	31.00
WBGene00000973|Y32H12A.3|dhs-9	1.55	31.00	1.07
WBGene00017356|F10E9.4	1.84	30.67	0.05
WBGene00009287|F31C3.5|psf-2	3.61	30.08	0.85
WBGene00010305|F59A2.5	5.36	29.78	0.85
WBGene00004888|K12C11.2|smo-1	225.20	29.67	4.42
WBGene00011976|T24B8.2	4.74	29.63	0.37

WBGene00019457|K06H7.3|vms-1	1.17	29.25	0.07
WBGene00004916|T28D9.10|snr-3	31.41	28.04	0.31
WBGene00003061|ZK973.10|lpd-5	92.64	27.90	0.36
WBGene00020713|T23B3.5	21.45	27.86	0.77
WBGene00010721|K09E4.3	3.34	27.83	0.69
WBGene00010232|F58B3.6	0.83	27.67	0.06
WBGene00009995|F53F4.13	140.80	27.55	17.69
WBGene00015104|B0280.9	3.79	27.07	0.14
WBGene00003367|M106.1|mix-1	0.27	27.00	0.60
WBGene00016443|C35D10.6	1.88	26.86	1.17
WBGene00021630|Y47D9A.3	2.32	25.78	0.39
WBGene00044388|C27D6.11	1.25	25.00	0.22
WBGene00009180|F26H11.2|nurf-1	7.66	24.71	0.15
WBGene00011936|T22H2.6|pgrn-1	2.21	24.56	0.82
WBGene00012643|Y39A1A.3	2.17	24.11	0.07
WBGene00044746|C53H9.3	18.88	23.60	65.10
WBGene00022463|Y110A7A.16|elpc-1	9.72	23.14	0.79
WBGene00017607|F19F10.11	4.39	23.11	0.55
WBGene00019678|K12H4.3	0.92	23.00	0.06
WBGene00022176|Y71H2AM.11	0.68	22.67	0.09
WBGene00010557|K04D7.2|mspn-1	17.90	22.66	0.18
WBGene00011375|T02E1.2	2.26	22.60	0.40
WBGene00017219|F07F6.7	2.02	22.44	0.48
WBGene00008418|D2030.8	2.85	21.92	1.63
WBGene00004244|C30G12.7|puf-8	2.19	21.90	0.10
WBGene00015329|C02B10.4	17.67	21.81	0.33
WBGene00021466|Y39G10AR.8	0.65	21.67	0.03
WBGene00017119|E04A4.5	4.98	21.65	0.13
WBGene00003955|W03D2.4|pcn-1	1.28	21.33	0.01
WBGene00004969|F47G6.4|spe-15	14.86	20.93	3.19
WBGene00001398|VZK822L.1|fat-6	21.99	20.36	0.14
WBGene00009993|F53F4.11	3.05	20.33	0.08
WBGene00011423|T04B2.5	0.81	20.25	0.84
WBGene00003077|Y62E10A.12|lsm-3	36.54	20.19	1.59
WBGene00021844|Y54E10BR.5	5.64	20.14	0.25
WBGene00003148|H21P03.1|mbf-1	1.60	20.00	0.04

Appendix LXXV

WBGene00002061|B0348.6|ife-3	21.12	19.92	4.22
WBGene00012964|Y48A6B.3	26.26	19.89	0.18
WBGene00015105|B0280.10|pot-1	0.99	19.80	0.22
WBGene00020098|R144.10	1.76	19.56	1.61
WBGene00000976|F36H9.3|dhs-13	1.56	19.50	0.98
WBGene00012187|W01G7.3|rpb-11	6.72	19.20	1.83
WBGene00012342|W08D2.7|mtr-4	0.19	19.00	0.41
WBGene00018064|F35F11.1|cdc-73	0.38	19.00	0.06
WBGene00016412|C34E10.11|mrps-26	0.95	19.00	0.07
WBGene00018341|F42A10.5	3.01	18.81	0.43
WBGene00014014|ZK632.5	0.37	18.50	0.84
WBGene00019472|K07C6.4|cyp-35B1	67.95	18.46	2265.00
WBGene00015128|B0303.7	4.21	18.30	0.90
WBGene00006733|F19B6.2|ufd-1	1.99	18.09	0.17
WBGene00007588|C14C10.5	3.41	17.95	0.45
WBGene00016390|C34B2.5	1.60	17.78	0.04
WBGene00020028|R12C12.8	1.59	17.67	0.58
WBGene00020181|T02H6.11	13.39	17.62	0.05
WBGene00009508|F37D6.2	2.46	17.57	0.22
WBGene00020349|T08B2.11	1.57	17.44	0.29
WBGene00018637|F49E8.6	15.10	17.36	1.64
WBGene00018391|F43E2.2|rpb-4	32.74	17.32	0.57
WBGene00021900|Y54H5A.2	30.99	17.03	0.54
WBGene00018564|F47D12.9	3.05	16.94	1.28
WBGene00003406|Y37D8A.9|mrg-1	16.71	16.88	0.26
WBGene00020710|T23B3.2	29.42	16.62	2.84
WBGene00006321|T22B2.4|sup-12	3.97	16.54	0.91
WBGene00013382|Y62E10A.16|gcl-1	0.33	16.50	4.71
WBGene00013136|Y53C10A.5	20.11	16.48	1.13
WBGene00022719|ZK370.5|pdhk-2	0.49	16.33	0.02
WBGene00004988|T08A9.7|spp-3	50.47	16.28	7.28
WBGene00016360|C33G8.2	5.17	16.16	3.23
WBGene00009492|F36H1.3	1.13	16.14	0.54
WBGene00015307|C01G5.5	3.70	16.09	9.02
WBGene00020843|T27A3.7	0.48	16.00	0.09
WBGene00007048|C16A3.7|nfx-1	1.92	16.00	0.12

WBGene00020652|T21E3.1|egg-4	0.95	15.83	0.13
WBGene00001600|B0414.6|glh-3	0.31	15.50	2.82
WBGene00044654|Y61B8A.4|fbxa-85	13.31	15.48	121.00
WBGene00003499|K04F10.6|mut-2	1.39	15.44	0.07
WBGene00000206|F35G12.10|asb-1	9.41	15.43	0.09
WBGene00003792|F56A3.3|npp-6	0.46	15.33	0.79
WBGene00003210|C38D4.3|mel-28	0.46	15.33	0.17
WBGene00000784|F44C4.3|cpr-4	21.71	15.18	0.33
WBGene00008394|D1086.7	14.05	15.11	0.71
WBGene00010890|M18.5|ddb-1	0.15	15.00	0.02
WBGene00010905|M88.2|mrps-34	1.20	15.00	0.04
WBGene00016601|C43E11.1|acin-1	3.42	14.87	0.40
WBGene00017827|F26F4.5	3.86	14.85	0.20
WBGene00004179|C01G5.2|prg-2	6.20	14.76	0.25
WBGene00022704|ZK353.9	1.18	14.75	0.05
WBGene00009650|F43D2.1|ccnk-1	4.91	14.44	0.38
WBGene00001856|B0414.3|hil-5	55.54	14.35	0.39
WBGene00009937|F52F12.4|lsl-1	245.30	14.22	2.98
WBGene00021331|Y34D9A.6|glrx-10	4.89	13.97	1.90
WBGene00012888|Y45F10D.9|sas-6	4.33	13.97	0.94
WBGene00019084|F59A6.2	32.56	13.91	9.55
WBGene00018659|F52C6.2	1.11	13.88	0.31
WBGene00019510|K07H8.10	0.83	13.83	0.02
WBGene00013219|Y54G11A.11	15.19	13.81	0.54
WBGene00004491|F53A3.3|rps-22	499.33	13.54	2.10
WBGene00004698|W02B12.3|rsp-1	3.09	13.43	0.19
WBGene00009092|F23H12.2|tomm-20	13.71	13.31	0.23
WBGene00011600|T07G12.10|zim-2	0.26	13.00	0.04
WBGene00000888|C34D4.12|cyn-12	10.02	12.85	0.14
WBGene00012992|Y48C3A.10|mrpl-20	16.30	12.64	0.72
WBGene00009440|F35G12.2|idhg-1	0.88	12.57	0.04
WBGene00021347|Y37E3.3|rpb-10	30.68	12.52	4.50
WBGene00021828|Y54E10A.6	0.25	12.50	6.25
WBGene00000121|F23B2.6|aly-2	1.00	12.50	0.09
WBGene00011142|R08D7.1	0.50	12.50	0.03
WBGene00007235|C01G10.8	23.15	12.45	0.35

Appendix LXXVII

WBGene00006528|F26E4.8|tba-1	66.04	12.44	0.19
WBGene00007202|B0564.2	9.97	12.31	0.82
WBGene00011376|T02E1.3|gla-3	0.61	12.20	0.23
WBGene00004510|F10B5.7|rrf-3	0.12	12.00	0.04
WBGene00021420|Y38F2AR.2|trap-3	0.96	12.00	0.02
WBGene00003951|K05C4.1|pbs-5	0.72	12.00	0.04
WBGene00017044|D2007.4|mrpl-18	1.19	11.90	0.06
WBGene00004422|T22F3.4|rpl-11.1	264.33	11.85	0.18
WBGene00019905|R05G9.3	0.71	11.83	0.09
WBGene00000915|C47E8.5|daf-21	14.31	11.54	0.04
WBGene00019247|H27M09.3|syp-4	0.23	11.50	0.02
WBGene00004431|C09D4.5|rpl-19	243.98	11.44	0.09
WBGene00003164|Y57E12AL.5|mdt-6	0.80	11.43	0.07
WBGene00003073|R74.1|lars-1	1.25	11.36	0.11
WBGene00010809|M01F1.3	1.46	11.23	0.05
WBGene00002879|C29E4.8|let-754	1.12	11.20	0.01
WBGene00009680|F44D12.3|msd-1	1.90	11.18	0.38
WBGene00007436|C08B11.9	17.88	11.11	0.36
WBGene00011435|T04D3.8	19.97	10.97	7.21
WBGene00002073|F26B1.3|ima-2	30.23	10.95	0.18
WBGene00001497|T08B2.9|fars-1	4.31	10.78	0.15
WBGene00019859|R03H10.7	0.43	10.75	0.36
WBGene00012206|W02B12.11	9.32	10.71	0.63
WBGene00014017|ZK632.10	5.46	10.71	0.19
WBGene00016010|C23G10.1	1.60	10.67	0.69
WBGene00021202|Y17G9B.5	0.53	10.60	0.05
WBGene00009396|F35C5.8|clec-65	2.86	10.59	0.13
WBGene00004117|F02E9.4|sin-3	0.21	10.50	0.02
WBGene00007387|C06H2.3|jmjd-5	1.05	10.50	0.14
WBGene00002228|C06G3.2|klp-18	1.47	10.50	0.18
WBGene00001716|T02E9.2|grl-7	0.94	10.44	0.02
WBGene00000613|C27H5.5|col-36	13.62	10.40	5.72
WBGene00003735|Y18D10A.6|nhx-8	0.31	10.33	1.35
WBGene00003133|W10C6.1|mat-2	0.31	10.33	0.02
WBGene00009711|F44G4.1	0.41	10.25	0.01
WBGene00020841|T27A3.5	0.41	10.25	0.03

WBGene00019631|K10D2.5	5.79	10.16	0.62
WBGene00009237|F28H7.3	2.73	10.11	0.09
WBGene00235102|Y54G2A.75	1.31	10.08	0.31
WBGene00001479|F53F4.5|fmo-4	0.50	10.00	0.03
WBGene00004444|Y106G6H.3|rpl-30	365.48	9.81	3.06
WBGene00010616|K07A1.10	4.88	9.76	0.24
WBGene00001480|H24K24.5|fmo-5	0.39	9.75	1.05
WBGene00002144|Y47G6A.2|inx-22	4.86	9.72	0.38
WBGene00077500|C27H6.9	0.68	9.71	0.05
WBGene00006572|C06G3.11|tin-9.1	5.90	9.67	1.24
WBGene00011730|T12D8.2|drr-2	0.58	9.67	0.33
WBGene00008458|E02H1.6	0.86	9.56	0.02
WBGene00013593|Y87G2A.1	0.19	9.50	0.54
WBGene00002012|F38E11.1|hsp-12.3	37.02	9.47	12.02
WBGene00010560|K04G2.1|iftb-1	8.95	9.42	0.07
WBGene00020662|T21H3.1	250.21	9.28	0.42
WBGene00077453|Y62F5A.12	4.05	9.20	0.63
WBGene00008344|C56A3.5	1.38	9.20	0.05
WBGene00009139|F25H9.7	6.59	9.15	0.27
WBGene00006963|K07G5.2|xpa-1	0.64	9.14	0.02
WBGene00008275|C53B4.6|nstp-1	0.99	9.00	0.06
WBGene00001869|R12B2.4|him-10	0.45	9.00	0.03
WBGene00004477|F42C5.8|rps-8	324.67	8.90	0.07
WBGene00003805|R06F6.5|npp-19	2.83	8.84	0.32
WBGene00015915|C17G10.1	40.23	8.84	1.50
WBGene00009322|F32B6.8|tbc-3	0.61	8.71	0.03
WBGene00008452|E02A10.1|mrps-5	0.26	8.67	0.02
WBGene00015524|C06E1.9	0.26	8.67	0.04
WBGene00021781|Y51H7C.3	112.45	8.64	1.36
WBGene00016446|C35D10.10	0.69	8.63	0.09
WBGene00003132|Y110A7A.17|mat-1	0.60	8.57	0.05
WBGene00007616|C15H11.8|rpoa-12	4.71	8.56	0.26
WBGene00011687|T10C6.5	12.71	8.53	0.16
WBGene00001973|C32F10.5|hmg-3	3.58	8.52	0.18
WBGene00015810|C16A3.5	13.19	8.51	0.02
WBGene00015346|C02F5.3	0.34	8.50	0.01

Appendix LXXIX

WBGene00045433|F49D11.10	0.34	8.50	0.08
WBGene00017112|E03H12.5	5.35	8.49	0.26
WBGene00002263|K08H10.1|lea-1	2.63	8.48	0.14
WBGene00009051|F22D6.4|nduf-6	7.80	8.48	0.18
WBGene00004919|Y49E10.15|snr-6	2.70	8.44	0.44
WBGene00016173|C27H5.3|fust-1	2.52	8.40	0.42
WBGene00016674|C45G9.2	0.42	8.40	0.09
WBGene00000547|Y77E11A.11|clp-7	0.75	8.33	0.05
WBGene00002064|T05G5.10|iff-1	686.44	8.31	4.14
WBGene00009112|F25D7.2|tag-353	0.83	8.30	0.06
WBGene00021845|Y54E10BR.6|rpb-7	216.68	8.26	10.34
WBGene00004034|F09E5.1|pkc-3	0.33	8.25	0.09
WBGene00020068|R13F6.10|cra-1	0.33	8.25	0.18
WBGene00020297|T07A9.9	2.45	8.17	0.15
WBGene00007969|C36A4.9|acs-19	14.49	8.14	0.12
WBGene00022583|ZC262.8|mrps-18A	21.64	8.14	0.45
WBGene00007554|C13G3.3|pptr-2	72.04	8.13	1.30
WBGene00015701|C11D2.3	0.73	8.11	10.43
WBGene00012781|Y43C5A.1|nspd-7	8.00	8.08	2.42
WBGene00019543|K08F11.3|cif-1	1.05	8.08	0.05
WBGene00007952|C35A5.8	0.08	8.00	0.01
WBGene00010677|K08F4.2|gtbp-1	0.16	8.00	0.00
WBGene00013550|Y75B8A.14	0.48	8.00	0.02
WBGene00015293|C01C4.3	0.56	8.00	0.07
WBGene00043064|Y59E9AL.7|nbet-1	0.64	8.00	0.54
WBGene00014171|ZK970.1|nep-26	0.24	8.00	3.43
WBGene00016799|C50C3.1	0.56	8.00	0.15
WBGene00000851|C47G2.1|cut-1	1.68	8.00	56.00
WBGene00016653|C44E4.4	1.92	8.00	0.03
WBGene00003041|R06C7.7|lin-61	0.79	7.90	0.05
WBGene00021340|Y34F4.5	5.28	7.88	0.54
WBGene00020954|W02G9.4	0.47	7.83	0.03
WBGene00018361|F42G8.10	9.39	7.83	0.07
WBGene00021945|Y55F3BR.8|lem-4	0.39	7.80	3.25
WBGene00002169|F37A4.8|isw-1	0.31	7.75	0.04
WBGene00019005|F57B10.8	2.00	7.69	0.11

WBGene00002083|F57B9.6|inf-1	113.80	7.67	0.33
WBGene00008413|D2030.3	0.23	7.67	0.01
WBGene00008729|F13B12.1	2.45	7.66	0.04
WBGene00194892|F26H11.6|dsb-2	0.45	7.50	0.10
WBGene00009521|F38A1.8	0.15	7.50	0.19
WBGene00009565|F39H11.1	0.30	7.50	0.02
WBGene00044174|C12D8.18|fipr-5	2.40	7.50	6.67
WBGene00010699|K08H10.9|trpp-6	0.67	7.44	0.17
WBGene00001005|T26A5.9|dlc-1	600.54	7.40	3.18
WBGene00016276|C30G12.4	0.44	7.33	0.46
WBGene00021210|Y18H1A.4	0.95	7.31	0.91
WBGene00021133|W10D9.5|tomm-22	4.15	7.28	0.06
WBGene00013035|Y49E10.16	2.91	7.28	0.13
WBGene00018375|F43C9.1	0.29	7.25	0.46
WBGene00017068|D2092.8	1.01	7.21	4.04
WBGene00000113|F45H10.1|alh-7	12.76	7.21	0.63
WBGene00012484|Y18D10A.17|car-1	22.96	7.20	0.05
WBGene00013670|Y105E8A.10|hpo-13	0.43	7.17	0.02
WBGene00011968|T23G11.1	2.41	7.09	0.04
WBGene00015327|C02B10.2|snpn-1	3.17	7.04	0.06
WBGene00006725|H06I04.4|ubl-1	187.80	7.03	0.19
WBGene00018238|F40F4.7	0.28	7.00	0.02
WBGene00008381|D1081.3	0.14	7.00	7.00
WBGene00018785|F54A3.6	0.21	7.00	0.44
WBGene00016003|C18H9.5	13.61	6.98	36.78
WBGene00004704|D2089.1|rsp-7	2.57	6.95	0.09
WBGene00020094|R144.4|wip-1	0.76	6.91	0.08
WBGene00010094|F55C5.5|tsfm-1	0.55	6.88	0.04
WBGene00014226|ZK1098.11	2.13	6.87	0.64
WBGene00016191|C28G1.6	0.41	6.83	0.10
WBGene00010624|K07A12.7|mrps-15	0.34	6.80	0.01
WBGene00012361|W09D10.3|mrpl-12	0.68	6.80	0.37
WBGene00013967|ZK287.7	0.54	6.75	0.06
WBGene00022347|Y82E9BR.14	0.74	6.73	0.64
WBGene00008572|F08B12.4	31.88	6.73	1.92
WBGene00017347|F10E7.5	9.48	6.72	0.04

Appendix LXXXI

WBGene00017503|F16B4.1|nhr-177	6.43	6.70	2.30
WBGene00011367|T02C12.2|snpc-3.4	0.20	6.67	0.34
WBGene00006515|C05D11.3|tag-170	87.06	6.67	1.22
WBGene00016028|C24A1.1|flp-24	0.86	6.62	0.35
WBGene00009459|F36A2.12	1.32	6.60	0.67
WBGene00008432|D2085.7	3.29	6.58	0.77
WBGene00021038|W05F2.6	3.08	6.55	0.16
WBGene00004059|C44B7.9|pmp-2	0.13	6.50	0.08
WBGene00022880|ZK1248.10|tbc-2	0.13	6.50	0.01
WBGene00001599|C55B7.1|glh-2	1.80	6.43	0.15
WBGene00015156|B0361.2	1.34	6.38	0.09
WBGene00003097|C17G10.5|lys-8	0.89	6.36	0.01
WBGene00013442|Y66D12A.16	3.75	6.36	5.68
WBGene00004425|C32E8.2|rpl-13	1086.87	6.35	0.25
WBGene00010279|F58G11.1|letm-1	0.19	6.33	0.05
WBGene00020112|R151.9|pfd-5	10.30	6.28	0.09
WBGene00022115|Y71F9AL.10	0.81	6.23	0.20
WBGene00004015|T24H7.1|phb-2	2.97	6.19	0.06
WBGene00009397|F35C5.9|clec-66	1.36	6.18	0.04
WBGene00045268|H01M10.3|ttr-42	2.47	6.18	0.99
WBGene00020558|T19B4.5	4.75	6.17	3.04
WBGene00014093|ZK829.1	0.43	6.14	0.41
WBGene00010231|F58B3.4	1.35	6.14	0.07
WBGene00012166|W01A8.4|nuo-6	2.57	6.12	0.02
WBGene00045300|C44C8.9|fbxc-10	0.55	6.11	3.93
WBGene00018586|F48A11.5|ubxn-3	24.31	6.08	1.67
WBGene00006648|W03F9.5|ttb-1	0.79	6.08	0.05
WBGene00013854|ZC116.2|cyc-2.2	1.03	6.06	0.14
WBGene00004463|F49C12.8|rpn-7	7.47	6.02	0.05
WBGene00010778|K11H3.1|gpdh-2	3.49	6.02	0.15
WBGene00007216|C01A2.4	253.77	6.01	0.67
WBGene00015184|B0432.2|djr-1.1	0.54	6.00	0.34
WBGene00007028|C47D12.1|trr-1	0.06	6.00	0.09
WBGene00001833|Y110A7A.1|hcp-6	0.12	6.00	0.02
WBGene00012936|Y47D3A.29	0.96	6.00	0.53
WBGene00004502|F29G9.5|rpt-2	0.18	6.00	0.01

WBGene00003952|C02F5.9|pbs-6	173.04	5.98	0.94
WBGene00022832|ZK973.3|pdp-1	1.89	5.91	0.06
WBGene00013434|Y66D12A.8	5.12	5.89	0.15
WBGene00021930|Y55F3AM.13	1.23	5.86	0.07
WBGene00006352|F26E4.1|sur-6	0.41	5.86	0.04
WBGene00009274|F30F8.5	0.64	5.82	1.31
WBGene00013168|Y53F4B.22|arp-1	0.87	5.80	0.21
WBGene00002152|R11A8.6|iars-1	0.29	5.80	0.17
WBGene00009277|F30F8.10	1.04	5.78	0.22
WBGene00008628|F09F3.6|ttr-21	12.44	5.76	0.38
WBGene00004096|F40F8.7|pqm-1	19.86	5.76	1.28
WBGene00044644|B0205.13	3.21	5.73	3.28
WBGene00004681|F52G2.2|rsd-2	5.90	5.73	0.70
WBGene00019642|K11C4.1	0.63	5.73	0.12
WBGene00020716|T23B12.1|phf-30	0.40	5.71	0.05
WBGene00001431|F31D4.3|fkb-6	0.57	5.70	0.13
WBGene00001862|ZK381.1|him-3	32.14	5.70	1.03
WBGene00010053|F54D5.9	0.17	5.67	0.02
WBGene00004917|C52E4.3|snr-4	3.32	5.63	0.08
WBGene00009334|F32D8.12	1.35	5.63	0.05
WBGene00045299|C44C8.8|fbxc-11	0.45	5.63	3.21
WBGene00017735|F23C8.6|did-2	5.21	5.60	0.08
WBGene00010115|F55F3.1|aakb-1	12.01	5.56	0.43
WBGene00009444|F35G12.11	6.30	5.53	0.33
WBGene00010174|F56H9.2	1089.96	5.49	82.26
WBGene00004201|F54F2.8|prx-19	0.49	5.44	0.01
WBGene00016450|C35D10.14|clec-5	0.87	5.44	0.05
WBGene00003836|Y71F9AM.5|nxt-1	59.80	5.44	0.52
WBGene00017074|D2096.7	2.12	5.44	0.55
WBGene00000380|C07G2.3|cct-5	1.57	5.41	0.00
WBGene00004496|F56E10.4|rps-27	161.62	5.37	3.09
WBGene00014164|ZK945.1|lact-2	41.18	5.37	0.84
WBGene00007101|B0024.11	1.66	5.35	0.05
WBGene00016011|C23G10.2	4.43	5.34	0.33
WBGene00017300|F09F7.3|rpc-2	0.16	5.33	0.01
WBGene00017850|F27B10.1	0.96	5.33	0.18

Appendix LXXXIII

WBGene00006724|C08B11.7|ubh-4	0.53	5.30	0.02
WBGene00009084|F23B12.7	18.42	5.23	0.21
WBGene00016393|C34B2.8	1.41	5.22	0.01
WBGene00017620|F20A1.9|tofu-2	1.35	5.19	0.08
WBGene00022456|Y110A7A.6|pfkb-1.1	0.62	5.17	0.03
WBGene00010409|H21P03.2	0.36	5.14	0.02
WBGene00018145|F37C4.5	1.58	5.10	0.37
WBGene00018419|F44E2.6	1.22	5.08	0.21
WBGene00194717|ZC239.22	6.25	5.08	4.77
WBGene00001055|C27C12.7|dpf-2	13.07	5.07	1.59
WBGene00020588|T19H12.2	12.03	5.01	0.04
WBGene00019259|H34C03.2	0.15	5.00	0.02
WBGene00002637|F26F12.7|let-418	0.05	5.00	0.01
WBGene00016812|C50D2.9	0.20	5.00	0.87
WBGene00009479|F36F2.6|fcp-1	0.10	5.00	0.05
WBGene00010333|F59E10.3|copz-1	0.45	5.00	5.63
WBGene00015938|C17H12.13|anat-1	0.45	5.00	0.02
WBGene00022360|Y92H12A.4	16.67	4.99	7.38
WBGene00001227|R08D7.3|eif-3.D	0.94	4.95	0.01
WBGene00012140|T28F4.5	0.98	4.90	0.09
WBGene00010627|K07C5.4	315.12	4.82	0.38
WBGene00006919|F46F11.5|vha-10	1.30	4.81	0.00
WBGene00018285|F41E6.4|smk-1	0.24	4.80	0.02
WBGene00045301|C44C8.10|fbxc-9	0.43	4.78	3.07
WBGene00022042|Y65B4BR.5|icd-2	923.02	4.75	0.29
WBGene00000259|F13H8.10|bpl-1	0.38	4.75	0.06
WBGene00011636|T09A5.8|cec-3	0.19	4.75	0.01
WBGene00004462|F57B9.10|rpn-6.1	2.42	4.75	0.06
WBGene00019537|K08D12.3	95.14	4.74	0.09
WBGene00001058|R11E3.8|dpf-5	0.52	4.73	0.09
WBGene00011722|T11G6.8	2.31	4.71	0.04
WBGene00008443|E01F3.1|pde-3	12.78	4.70	60.86
WBGene00006976|K02B12.8|zhp-3	0.75	4.69	0.05
WBGene00020185|T03F1.3|pgk-1	0.14	4.67	0.01
WBGene00004458|T22D1.9|rpn-1	0.14	4.67	0.00
WBGene00021800|Y53G8AL.2	0.14	4.67	0.01

WBGene00008199|C49C3.9	0.14	4.67	0.02
WBGene00044466|Y48A5A.3	2.00	4.65	0.70
WBGene00011625|T08G5.5|vps-39	4.39	4.62	0.30
WBGene00022853|ZK1127.6	9.98	4.62	0.11
WBGene00015509|C06A6.4	4.99	4.62	0.10
WBGene00018395|F43E2.7|mtch-1	0.92	4.60	0.01
WBGene00010317|F59B8.2|idh-1	20.23	4.60	0.59
WBGene00021015|W03G9.3|enu-3.3	3.08	4.60	6.29
WBGene00004028|Y18H1A.6|pif-1	11.39	4.57	14.99
WBGene00020868|T27F7.3|eif-1	38.72	4.55	0.10
WBGene00007630|C16C10.11|har-1	41.43	4.51	0.05
WBGene00004437|C03D6.8|rpl-24.2	17.24	4.50	0.11
WBGene00021830|Y54E10A.10	0.27	4.50	0.01
WBGene00008399|D2005.4	0.09	4.50	0.02
WBGene00007921|C34C12.2	0.09	4.50	0.02
WBGene00011242|R11D1.1	0.40	4.44	0.19
WBGene00044213|Y102A5C.36	2.04	4.43	2.96
WBGene00002198|F22D6.1|kin-14	21.23	4.42	1.93
WBGene00019719|M01H9.3	13.00	4.41	0.12
WBGene00003796|ZK328.5|npp-10	0.22	4.40	0.03
WBGene00004498|B0412.4|rps-29	1147.96	4.34	44.74
WBGene00008393|D1086.6	102.68	4.33	0.48
WBGene00008682|F11A10.1|lex-1	0.13	4.33	0.01
WBGene00007094|B0019.2	0.13	4.33	0.03
WBGene00021097|W08F4.8|cdc-37	48.04	4.33	1.16
WBGene00019162|H06H21.3|eif-1.A	4.72	4.33	0.04
WBGene00010478|K01G5.5	10.06	4.32	0.02
WBGene00022025|Y65B4A.1	2.41	4.30	0.44
WBGene00011156|R09B3.3	128.24	4.30	2.97
WBGene00016652|C44E4.3|got-2.1	0.60	4.29	0.01
WBGene00007983|C36E8.4	0.60	4.29	0.29
WBGene00007143|B0334.3	72.08	4.27	1.11
WBGene00012966|Y48A6B.5|exos-1	0.34	4.25	0.04
WBGene00018921|F56A6.1|sago-2	0.17	4.25	0.29
WBGene00021899|Y54H5A.1	0.68	4.25	0.02
WBGene00219912|F22H10.10	3.44	4.25	3.74

WBGene00077526|C25A1.16	1.78	4.24	0.02
WBGene00013361|Y60A3A.13|fars-2	66.47	4.23	0.57
WBGene00004915|W08E3.1|snr-2	0.38	4.22	0.41
WBGene00009050|F22D6.2	23.42	4.21	0.16
WBGene00001604|Y105C5B.28|gln-3	4.83	4.20	0.35
WBGene00018151|F37C12.3	3.73	4.19	0.04
WBGene00007786|C27H6.4|rmd-2	8.99	4.18	0.13
WBGene00009880|F49C12.11	91.39	4.17	2.01
WBGene00011299|R107.4|ikke-1	0.25	4.17	0.01
WBGene00003243|F10E9.6|mig-10	1.00	4.17	1.37
WBGene00007617|C15H11.9|rrbs-1	0.50	4.17	0.01
WBGene00018319|F41H10.6|hda-6	0.95	4.13	0.03
WBGene00001756|F11G11.1|gst-8	0.41	4.10	4.56
WBGene00000774|F56A8.6|cpf-2	7.03	4.09	0.83
WBGene00018409|F44B9.8	0.53	4.08	0.13
WBGene00015232|B0511.6	27.62	4.07	0.11
WBGene00044081|D1086.11	242.87	4.07	0.66
WBGene00015460|C05C8.1	44.04	4.03	0.37
WBGene00003980|F09C3.1|pes-7	4.01	4.01	0.91
WBGene00009744|F45H11.3|hpo-35	0.08	4.00	0.06
WBGene00018226|F40B5.2	0.24	4.00	0.73
WBGene00021319|Y34B4A.2	0.16	4.00	0.12
WBGene00007313|C04H5.2|clec-147	0.56	4.00	0.33
WBGene00015450|C04F5.8	0.20	4.00	0.03
WBGene00007564|C14A4.14|mrps-22	0.12	4.00	0.13
WBGene00018416|F44E2.2|retr-1	0.12	4.00	0.33
WBGene00014176|ZK1010.2	5.56	4.00	0.28
WBGene00000277|C23H4.1|cab-1	3.51	3.94	0.40
WBGene00019962|R08E5.2|cysl-3	29.83	3.94	0.50
WBGene00001284|F54C8.3|emb-30	4.62	3.88	0.13
WBGene00004420|R13A5.8|rpl-9	1897.36	3.87	0.19
WBGene00013435|Y66D12A.9	0.23	3.83	0.01
WBGene00023422|F43C1.6|mrpl-21	0.38	3.80	0.03
WBGene00005001|F32D8.9|spp-16	1.63	3.79	0.22
WBGene00022057|Y67D2.7	1.74	3.78	0.70
WBGene00017542|F17E9.5	12.53	3.75	0.30

WBGene00022492|Y119D3B.15|dss-1	0.45	3.75	0.01
WBGene00010280|F58G11.2|rde-12	0.15	3.75	0.42
WBGene00006961|B0041.7|xnp-1	3.10	3.73	1.51
WBGene00013203|Y54E5A.8	2.80	3.73	0.89
WBGene00019768|M04F3.2	0.41	3.73	0.05
WBGene00011720|T11G6.5	2.57	3.72	0.82
WBGene00004042|C14B9.4|plk-1	11.40	3.70	0.19
WBGene00014092|ZK822.5	0.37	3.70	0.04
WBGene00000886|B0252.4|cyn-10	4.09	3.68	0.05
WBGene00012030|T25G3.3	0.11	3.67	0.00
WBGene00000467|F52B5.5|cep-1	2.01	3.65	0.10
WBGene00001021|C01G10.12|dnj-3	0.40	3.64	0.05
WBGene00015386|C03B8.3	8.68	3.63	1.67
WBGene00016333|C32F10.8	0.98	3.63	0.02
WBGene00044188|F28F8.9	1.27	3.63	0.07
WBGene00020736|T23F2.3	2.28	3.62	3.30
WBGene00015920|C17G10.9	0.18	3.60	0.01
WBGene00017780|F25E2.2	0.43	3.58	0.02
WBGene00000894|M110.5|dab-1	1.36	3.58	0.99
WBGene00019163|H06H21.6|ubxn-6	0.68	3.58	0.03
WBGene00002023|C09B8.6|hsp-25	3.92	3.56	0.02
WBGene00004493|T07A9.11|rps-24	2159.80	3.56	1.07
WBGene00011155|R09B3.2	16.92	3.52	0.95
WBGene00021938|Y55F3BR.1	0.07	3.50	0.04
WBGene00001744|T10F2.1|gars-1	0.14	3.50	0.01
WBGene00008878|F16A11.3|ppfr-1	0.14	3.50	0.10
WBGene00002845|F57B9.2|let-711	0.07	3.50	0.23
WBGene00010044|F54C9.9	0.28	3.50	0.01
WBGene00018893|F55F8.5|tag-345	0.21	3.50	0.01
WBGene00000765|ZK652.9|coq-5	0.21	3.50	0.03
WBGene00010428|H38K22.2|dcn-1	0.35	3.50	0.01
WBGene00014083|ZK795.3	0.49	3.50	0.02
WBGene00017358|F10E9.7	21.80	3.50	1.38
WBGene00018612|F48E8.6|disl-2	3.03	3.48	0.38
WBGene00009207|F28C6.8	8.89	3.47	0.04
WBGene00006408|T14G12.3|tag-18	8.22	3.45	0.08

Appendix LXXXVII

WBGene00020557|T19B4.3	63.36	3.44	3.91
WBGene00010900|M28.9	1.06	3.42	0.07
WBGene00010556|K04D7.1|rack-1	64.89	3.41	0.05
WBGene00009122|F25H2.11|tct-1	273.88	3.41	0.10
WBGene00001017|ZK593.5|dnc-1	0.17	3.40	0.06
WBGene00004490|F37C12.11|rps-21	708.85	3.39	22.09
WBGene00016387|C34B2.2|kbp-5	10.49	3.37	0.11
WBGene00003786|VC5.3|npa-1	1.28	3.37	0.01
WBGene00002980|C32D5.9|lgg-1	4.23	3.36	0.00
WBGene00020388|T10B5.2	40.68	3.35	3.74
WBGene00001946|Y49E10.6|his-72	28.91	3.35	0.12
WBGene00001231|C41D11.2|eif-3.H	0.10	3.33	0.12
WBGene00008331|C55A6.2|ttll-5	0.30	3.33	0.02
WBGene00009372|F34D10.2|evl-18	0.10	3.33	0.08
WBGene00012353|W09C5.7	0.43	3.31	0.02
WBGene00004205|F29B9.4|psr-1	5.82	3.31	0.30
WBGene00000935|F56D1.7|daz-1	2.08	3.30	0.05
WBGene00010891|M18.6	0.92	3.29	0.07
WBGene00021128|W10C8.5	0.49	3.27	0.06
WBGene00009895|F49E11.10|scl-2	96.53	3.25	2.01
WBGene00015820|C16A11.7	0.65	3.25	0.09
WBGene00008642|F10B5.8	0.13	3.25	0.01
WBGene00004798|F43D9.4|sip-1	339.40	3.23	1.69
WBGene00017132|EEED8.1|tofu-6	0.29	3.22	0.02
WBGene00010633|K07F5.5|nspd-2	23.76	3.22	5.77
WBGene00000659|K12D12.3|col-84	0.16	3.20	0.84
WBGene00004993|C28C12.5|spp-8	11.28	3.17	0.15
WBGene00011240|R11A8.7	0.19	3.17	0.02
WBGene00000785|W07B8.5|cpr-5	0.19	3.17	0.01
WBGene00004445|W09C5.6|rpl-31	550.91	3.14	3.24
WBGene00010141|F56A8.5	1.41	3.13	0.09
WBGene00010339|F59F4.4|acl-1	7.77	3.13	0.04
WBGene00016440|C35D10.2|gipc-1	0.28	3.11	0.01
WBGene00006433|F42A8.2|sdhb-1	37.84	3.11	0.35
WBGene00020184|T03F1.1|uba-5	0.87	3.11	2.64
WBGene00007413|C07E3.2|pro-2	0.62	3.10	0.02

WBGene00000376|ZC518.3|ccr-4	3.96	3.09	0.27
WBGene00007429|C08B6.8	1.08	3.09	0.03
WBGene00004093|C18E3.7|ppw-1	8.26	3.06	0.16
WBGene00017613|F20A1.1	64.70	3.04	17.16
WBGene00202000|Y38F1A.13	0.94	3.03	2.76
WBGene00017641|F20D12.1|csr-1	1.51	3.02	0.17
WBGene00002269|Y55B1AR.1|lec-6	3.22	3.01	0.12
WBGene00003794|Y41D4B.19|npp-8	0.27	3.00	1.80
WBGene00001259|T04A8.14|emb-5	0.27	3.00	0.12
WBGene00009159|F26E4.4	0.27	3.00	0.02
WBGene00003418|H26D21.2|msh-2	0.06	3.00	0.05
WBGene00012236|W04A8.1	0.12	3.00	0.20
WBGene00017312|F09G2.3|pitr-5	0.06	3.00	0.04
WBGene00022069|Y67D8C.5|eel-1	0.06	3.00	0.22
WBGene00008062|C41G7.4|set-32	0.09	3.00	0.10
WBGene00019168|H06I04.3	0.15	3.00	0.01
WBGene00006530|F44F4.11|tba-4	0.21	3.00	0.02
WBGene00015703|C11D2.7	9.93	2.98	0.20
WBGene00004138|R07B7.3|pqn-53	273.82	2.95	1.30
WBGene00044924|M106.7	0.47	2.94	0.08
WBGene00000159|F29G9.3|aps-1	0.47	2.94	0.01
WBGene00001464|C26F1.10|flp-21	0.94	2.94	0.14
WBGene00044329|F11A10.8|cpsf-4	3.31	2.93	0.05
WBGene00009575|F40F8.1	0.93	2.91	0.05
WBGene00016591|C42C1.13	3.76	2.89	0.12
WBGene00000102|C12D8.10|akt-1	0.26	2.89	0.01
WBGene00009981|F53F1.3	27.98	2.88	1.28
WBGene00017011|D1007.16|eaf-1	0.20	2.86	0.00
WBGene00004412|Y71F9AL.13|rpl-1	119.41	2.85	0.04
WBGene00016808|C50D2.5	2.68	2.85	0.10
WBGene00021359|Y37E11AL.3	0.91	2.84	0.17
WBGene00004897|T10H9.4|snb-1	3.41	2.84	0.02
WBGene00016630|C44B7.10	0.17	2.83	0.00
WBGene00021208|Y18H1A.2	0.51	2.83	0.02
WBGene00000718|B0222.7|col-145	37.08	2.83	0.22
WBGene00020604|T20B12.7	15.81	2.83	0.05

Appendix LXXXIX

WBGene00006053|T28H11.1|ssq-4	8.28	2.83	1.61
WBGene00007824|C30H6.7	0.31	2.82	0.01
WBGene00003177|T01E8.4|mec-15	45.80	2.81	0.70
WBGene00018421|F44E2.8	0.14	2.80	0.01
WBGene00004705|C18D11.4|rsp-8	72.35	2.79	1.17
WBGene00013238|Y56A3A.21|trap-4	0.50	2.78	2.08
WBGene00003160|C50F4.11|mdf-1	1.55	2.77	1.50
WBGene00022458|Y110A7A.8|prp-31	0.33	2.75	0.14
WBGene00020389|T10B5.3	0.11	2.75	0.00
WBGene00003156|Y39G10AR.14|mcm-4	0.76	2.71	0.01
WBGene00017907|F28F9.3	10.43	2.69	35.97
WBGene00004434|C27A2.2|rpl-22	3125.14	2.68	4.53
WBGene00012903|Y46G5A.12|vps-2	69.13	2.68	0.77
WBGene00001457|Y37D8A.15|flp-14	0.16	2.67	0.02
WBGene00006595|M01E5.5|top-1	0.08	2.67	0.05
WBGene00003009|K10B2.1|lin-23	0.08	2.67	0.02
WBGene00004339|C39E9.13|rfc-3	3.34	2.65	0.04
WBGene00020027|R12C12.7	14.12	2.64	1.37
WBGene00004474|T05E11.1|rps-5	468.28	2.63	0.07
WBGene00001686|F33H1.2|gpd-4	32.63	2.62	0.25
WBGene00021959|Y57E12AL.6	7.97	2.60	0.16
WBGene00009211|F28D1.1|wdr-46	7.50	2.59	0.33
WBGene00018359|F42G8.8	0.31	2.58	0.02
WBGene00044324|ZK652.3|ufm-1	1.26	2.57	0.09
WBGene00004441|C53H9.1|rpl-27	760.13	2.57	0.86
WBGene00016217|C29F9.2	1.41	2.56	0.12
WBGene00020441|T12A2.7	0.64	2.56	0.02
WBGene00011282|R74.8	0.56	2.55	0.01
WBGene00015759|C14C6.5	1.12	2.55	0.03
WBGene00008143|C47E8.4	419.46	2.50	10.54
WBGene00009526|F38A1.14|clec-169	11.58	2.50	7.38
WBGene00019465|K07B1.5|acl-14	0.15	2.50	0.01
WBGene00012150|VF39H2L.1|syx-17	0.15	2.50	0.01
WBGene00006540|F58A4.8|tbg-1	0.05	2.50	0.01
WBGene00004178|D2030.6|prg-1	0.05	2.50	0.01
WBGene00001601|T12F5.3|glh-4	0.05	2.50	0.01

WBGene00019544|K08F11.5|miro-1	0.05	2.50	0.01
WBGene00003839|T09A12.3|ocr-2	0.05	2.50	1.67
WBGene00017663|F21D12.3	0.05	2.50	0.45
WBGene00020719|T23B12.4	0.05	2.50	0.01
WBGene00019458|K06H7.7	0.10	2.50	0.02
WBGene00002076|R06A4.4|imb-2	0.10	2.50	0.02
WBGene00009921|F52B5.2	0.10	2.50	0.07
WBGene00012002|T24H10.4	0.10	2.50	0.29
WBGene00007708|C25A1.6|nola-3	1.55	2.50	0.07
WBGene00016513|C38C3.4	1.05	2.50	0.30
WBGene00001977|Y17G7A.1|hmg-12	7.05	2.50	0.06
WBGene00004446|T24B8.1|rpl-32	1177.28	2.49	2.27
WBGene00004336|W06A7.3|ret-1	3.35	2.48	0.01
WBGene00003066|ZC410.7|lpl-1	0.37	2.47	0.08
WBGene00015554|C06G3.8	2.71	2.46	1.58
WBGene00009436|F35G2.2|marb-1	39.89	2.46	0.52
WBGene00020886|T28B4.3|ttr-6	0.32	2.46	0.02
WBGene00000098|K07C11.2|air-1	9.95	2.46	0.04
WBGene00009087|F23D12.3	0.22	2.44	0.92
WBGene00017934|F30B5.4	0.22	2.44	0.06
WBGene00011559|T07C4.1|umps-1	80.04	2.44	0.68
WBGene00009123|F25H2.12	0.17	2.43	0.02
WBGene00044633|F54H12.7	0.34	2.43	0.04
WBGene00009385|F35B12.5|sas-5	0.53	2.41	0.01
WBGene00018745|F53C3.1	27.71	2.41	16.40
WBGene00009288|F31C3.6	0.12	2.40	0.19
WBGene00005656|C13D9.2|srr-5	0.12	2.40	3.00
WBGene00007580|C14B1.9	0.24	2.40	0.03
WBGene00021460|Y39G10AR.2|zwl-1	69.89	2.40	0.61
WBGene00021269|Y23H5A.2	2.13	2.39	0.17
WBGene00004486|T08B2.10|rps-17	525.49	2.39	1.01
WBGene00003587|F45H11.2|ned-8	0.98	2.39	0.06
WBGene00017924|F29B9.10|mrps-21	0.45	2.37	0.11
WBGene00022194|Y71H2B.4	0.52	2.36	0.09
WBGene00007689|C18E9.9	0.26	2.36	0.01
WBGene00000593|W01B6.7|col-2	0.92	2.36	0.22

Appendix XCI

WBGene00020033|R12E2.7	6.24	2.34	0.75
WBGene00022664|ZK121.2	0.07	2.33	0.12
WBGene00000938|C26C6.5|dcp-66	0.07	2.33	0.03
WBGene00010435|JC8.2	0.07	2.33	0.00
WBGene00005719|F53F1.7|srv-8	0.14	2.33	2.80
WBGene00007194|B0491.7	0.14	2.33	0.01
WBGene00012444|Y15E3A.5	0.70	2.33	0.02
WBGene00017597|F19C7.8	26.78	2.33	5.26
WBGene00015619|C08G9.1	3.38	2.33	0.12
WBGene00017053|D2024.5	1.02	2.32	0.02
WBGene00004296|T04H1.4|rad-50	22.59	2.32	2.47
WBGene00014240|ZK1251.1|htas-1	0.37	2.31	0.10
WBGene00009179|F26H11.1|kbp-3	0.37	2.31	0.01
WBGene00000381|F01F1.8|cct-6	0.23	2.30	0.01
WBGene00013958|ZK265.6	0.46	2.30	0.01
WBGene00004286|D2013.1|rab-39	0.16	2.29	0.01
WBGene00001427|Y18D10A.19|fkb-2	0.32	2.29	0.03
WBGene00015160|B0361.6	0.09	2.25	0.01
WBGene00003644|F36D3.2|nhr-54	0.09	2.25	0.82
WBGene00018757|F53E2.1|tag-304	0.09	2.25	0.26
WBGene00007177|B0399.2|oac-1	0.09	2.25	4.50
WBGene00017975|F32B5.1	0.18	2.25	0.10
WBGene00006463|T26A5.3|nduf-2.2	0.09	2.25	0.00
WBGene00001018|C28H8.12|dnc-2	9.56	2.24	0.11
WBGene00012557|Y37D8A.19	72.23	2.24	16.53
WBGene00017675|F21F3.6	9.70	2.24	0.05
WBGene00077771|C41G7.9	61.42	2.23	0.22
WBGene00016508|C37H5.5	36.58	2.23	3.22
WBGene00021882|Y54G2A.17	1.20	2.22	0.43
WBGene00016425|C34H4.2	4.32	2.22	0.61
WBGene00013132|Y52D3.1|strd-1	33.26	2.21	11.67
WBGene00000378|T21B10.7|cct-2	0.77	2.20	0.01
WBGene00011554|T07A5.1	0.11	2.20	0.02
WBGene00007000|Y71H2AM.23|tufm-1	0.11	2.20	0.00
WBGene00012127|T28D6.7	0.11	2.20	2.75
WBGene00007455|C08F11.8|ugt-22	0.11	2.20	0.01

WBGene00010664|K08E3.4|dbn-1	0.11	2.20	0.01
WBGene00011412|T04A8.11|mrpl-16	50.46	2.19	0.77
WBGene00011629|T08G11.1	0.70	2.19	0.18
WBGene00022618|ZC477.3	0.37	2.18	0.03
WBGene00017774|F25B5.2|nop-1	0.15	2.14	0.02
WBGene00013200|Y54E5A.5	11.82	2.14	0.13
WBGene00022751|ZK484.5	3.17	2.13	0.16
WBGene00004920|Y71F9B.4|snr-7	2.19	2.13	0.92
WBGene00011634|T09A5.5	1.40	2.12	0.02
WBGene00004449|ZK652.4|rpl-35	818.03	2.12	2.26
WBGene00004304|C26D10.1|ran-3	4.12	2.09	0.17
WBGene00020110|R151.7	0.23	2.09	0.02
WBGene00007223|C01F6.9	21.02	2.09	0.62
WBGene00008944|F19B2.5	6.59	2.09	0.11
WBGene00003449|K07F5.3|msp-56	13.09	2.08	0.17
WBGene00000876|C52E4.6|cyl-1	14.56	2.08	0.34
WBGene00017982|F32D1.2|hpo-18	39.02	2.06	8.91
WBGene00008515|F02C12.1	12.66	2.05	5.65
WBGene00012375|W09H1.5|mecr-1	171.90	2.04	0.90
WBGene00022775|ZK616.5	1.65	2.04	0.01
WBGene00003184|F57B10.12|mei-2	92.06	2.02	0.16
WBGene00012556|Y37D8A.18|mrps-10	15.88	2.01	0.15
WBGene00050914|T12B5.15	65.12	2.01	6.36
WBGene00012551|Y37D8A.11|cec-7	19.84	2.01	0.29

Supplementary Table 12. Coding Sequences Included in GPCR-GFP Fusion Constructs.
The percentage of codons from each GPCR gene coding sequence included in the GFP transgenes varied from construct to construct, although the majority was included in each product.

Gene (Transcript)	Promoter Length (bp)	Percentage of Codons Included in GFP Fusion (included/total amino acids)
seb-3 (C18B12.2.1)	3082	100% (454/454)
dmsr-12 (H34P18.1a)	2810	99.1% (360/363)
srw-97 (ZC204.15)	1360	99.7% (371/372)
srd-32 (T19H12.5)	1874	52.8% (179/339)
srr-7 (T01G5.4)	657	69.5% (269/387)
trf-1 (F45G2.6.1)	4044	N/A

Supplementary Table 13. Strains
Strains utilized in this study.

Figure	Strain	Genotype	Source
2A	-	bsIs14 [p*pkd-2*::GFP + pha-1(+)];*him-5(e1490)*	Doug Portman
-	-	*pha-1(e2123ts);lite-1(ce314);him-5(e1490)*	Rene Garcia
2B	JSR40	*pha-1(e2123ts);lite-1(ce314);him-5(e1490);* worEx8 [p*seb-3*::GFP; pha-1(+)]	Knudra/DKR
2C	JSR36	*pha-1(e2123ts);lite-1(ce314);him-5(e1490);* worEx4 [p*dmsr-12*::GFP; pha-1(+)]	Knudra/DKR
2D	JSR13	*pha-1(e2123ts);lite-1(ce314);him-5(e1490);* worEx02 [p*srd-32*::GFP; pha-1(+)]	Knudra/DKR
2E	JSR15	*pha-1(e2123ts);lite-1(ce314);him-5(e1490);* worEx03 [p*srw-97*::GFP; pha-1(+)]	Knudra/DKR
2F	JSR10	*pha-1(e2123ts);lite-1(ce314);him-5(e1490);* worEx01 [p*srr-7*::GFP; pha-1(+)]	Knudra/DKR
Supp. Fig. 1	JSR39	*pha-1(e2123ts);lite-1(ce314);him-5(e1490);* worEx07 [p*trf-1*::GFP; pha-1(+)]	Knudra/DKR
-	VH624	rhIs13 [*unc-119*::GFP + dpy-20(+)];*nre-1(hd20);lin-15B(hd126)*	Erich Schwarz
3A-C, Supp. Fig. 2.	JSR44	rhIs13 [*unc-119*::GFP + dpy-20(+)];*nre-1(hd20);lin-15B(hd126);him-5(e1490)*	DKR
3D-F, Supp. Fig. 3, Supp. Fig. 4	CB4088	*him-5(e1490)*	CGC
3D-F, Supp. Fig. 4	JSR55	*srw-97(knu456);him-5(e1490)*	Kndura/DKR
-	tm8706	*dmsr-12(tm8706)*	National BioResource Project
3E-F, Supp. Fig. 4	JSR68	*dmsr-12(tm8706);him-5(e1490)*	DKR
3E-F, Supp. Fig. 4	JSR70	*srw-97(knu456);dmsr-12(tm8706);him-5(e1490)*	ANM
Supp. Fig. 3	COP1552	*srr-7(knu506);him-5(e1490)*	Knudra

Supplementary Table 14. Primers
Primers used to generate GFP-promoter fusions in **Figure 35** and **Supplementary Figure 13**.

Figure	Primer	
	Name	Sequence
Fig. 2B	seb-3_A	TTGACAGTAACTGGCGCTAC
Fig. 2B	seb-3_B	AGTCGACCTGCAGGCATGCAAGAGATTTCGTAGACACCGAGTAGAT
Fig. 2B	seb-3_Ap	ACAGTAACTGGCGCTACTCCC
Fig. 2C	dmsr-12_A	ATTTCCCCAAGGAGTTTTCA
Fig. 2C	dmsr-12_B	AGTCGACCTGCAGGCATGCAAGGAAGCGTGTGCAACTGAATG
Fig. 2C	dmsr-12_Ap	CCCAAGGAGTTTTCAATCTT
Fig. 2D	srd-32_A	TTTTTGTGGATTTTGTTCCA
Fig. 2D	srd-32_B	AGTCGACCTGCAGGCATGCAAGCTGGTTCCCACCACAGTCCTATA
Fig. 2D	srd-32_Ap	TGTGGATTTTGTTCCAATGA
Fig. 2E	srw-97_A	GTCGGAAAACTCAAAAAGCA
Fig. 2E	srw-97_B	AGTCGACCTGCAGGCATGCAAGCTTCGATTTGACGTGCTGCTGTG
Fig. 2E	srw-97_Ap	GGAAAACTCAAAAAGCAAACA
Fig. 2F	srr-7_A	ACATTTGGAAAGCGTAGAAAA
Fig. 2F	srr-7_B	AGTCGACCTGCAGGCATGCAAGCTGAAGTCAAGTAGACGCCGTTT
Fig. 2F	srr-7_Ap	TTGGAAAGCGTAGAAAATTGA
Fig. 2B-F, Supp. Fig. 1	GFP_C	AGC TTG CAT GCC TGC AGG TCG ACT
Fig. 2B-F, Supp. Fig. 1	GFP_D	AAG GCC CCG TAC GGC CGA CTA GTA GG
Fig. 2B-F, Supp. Fig. 1	GFP_Dp	GGA AAC AGT TAT GTT TGG TAT ATT GGG
Supp. Fig. 1	trf-1_A	ATGGCTGACAAGTTGTTCTCG
Supp. Fig. 1	trf-1_B	AGTCGACCTGCAGGCATGCAAGTTTCTATGGAATTCAGAAATTGCT
Supp. Fig. 1	trf-1_Ap	GGAGAGGCTTTGGTGAGAAA